Understanding the molecular mechanisms underpinning the immunomodulatory function of carbohydrates: focus on levan exopolysaccharide

Ian David Young, BA, BSc (Hons)

A thesis submitted in accordance with the requirements for the degree of Doctor of Philosophy (PhD)

To The University of East Anglia

Quadram Institute Bioscience

Norwich Research Park

Colney, Norwich

NR4 7AU

UK

November 2018

Abstract

Polysaccharides (PS) found in plants, mushrooms, algae and gut microbes have been shown to modulate immune function in animals. However, the mechanisms underpinning their immunomodulatory properties remain unclear. C-type lectin receptors (CLRs) are carbohydrate-binding proteins, expressed by immune cells including dendritic cells (DCs). CLRs SIGNR1, Dectin-1 and Dectin-2 recognise mannose/fucose structures, β-glucans and α-mannans, respectively, which initiates cellular activation and an immune response.

We first hypothesised that the mechanisms underpinning immunomodulatory PS involve their interaction with CLRs. To test this, we established SIGNR1 reporter cells, and used Dectin-1 and Dectin-2 reporter cells to screen a range of food and microbial PS for their binding to CLRs.

We report several novel CLR-PS interactions including the interaction between microbial levan, a high molecular weight β-(2,6) fructofuranose exopolysaccharide from gram-negative bacterium *Erwinia herbicola*, and Dectin-2. Crude *E. herbicola* levan also activated Toll-like receptor 4 (TLR4) reporter cells, suggesting an interaction with lipopolysaccharide (LPS).

Following the development of a robust method to remove LPS in levan, we confirmed that LPS was an important contributor to crude levan's ability to bind to TLR4 and Dectin-2. Further, crude *E. herbicola* levan but not enzymatically synthesised (ES) levan or purified *E. herbicola* levan induced cytokine production in bone marrow-derived DCs. We also tested interaction of purified ES levan and intestinal epithelial cells *in vitro* using Caco-2 cells. We found that purified ES levan did not improve barrier integrity following LPS challenge and did not induce or modulate cytokine production following inflammatory challenge by TNF-α treatment.

Overall, we demonstrated that the immunomodulatory properties of levan *in vitro* were largely dependent on the presence of LPS and we present a novel purification method to remove LPS in levan for future studies.

Acknowledgements

This PhD was funded by a UK Biotechnology and Biological Sciences Research Council (BBSRC) Doctoral Training Partnership grant (Project ID: BB/JO14524/1).

I wish to express my greatest gratitude to my supervisor's Dr Nathalie Juge, Dr Norihito Kawasaki, Professor Rob Field and Professor Richard Mithen for their guidance and support over the last 4 years.

I would like to sincerely thank Dr Nathalie Juge for all her support and advice as well as her time and effort that has gone into helping the preparation of this thesis. I have gained so much from her teaching including presentations, writing and scientific thinking. I have learnt a great deal throughout my PhD from Nathalie and it has been a pleasure to work with her.

I also would like to thank Norihito for the opportunity to undertake a PhD, and for his guidance and support over the years. My life ambition was to do a PhD and enter the world of science and I could not have done this without Norihito. I have thoroughly enjoyed the scientific conversations and the good times.

A big thank you to Rob Field for his guidance – thanks for all the chemistry advice and beyond! It has been a pleasure to work in the Rob Field Lab.

I wish to thank Dr Alexandra Wittmann, particularly for her help in the Lab and her expertise in immunology. I have missed the Science lunch hour discussions with you and Norihito.

I also wish to express my gratitude to Dr Sergey Nepogodiev and Dr Gwenaelle Le Gall for their help with NMR analysis, and for Sergey's guidance on carbohydrate chemistry. I would also like to thank Patrick Gunning. Further, my thanks go to Ian Black from the Complex Carbohydrate Research Centre (CCRC) in Atlanta – it was a tremendous experience to go there and discuss carbohydrate chemistry, and I appreciate all his help and guidance. I wish to also thank Dr Parastoo Azadi from the CCRC.

I also would like to thank members of the Kawasaki Lab, Juge Lab and Field Lab. In particular, my thanks go to Dr Dimitris Latousakis, Jordan Hindes, Becky Winsbury, Adeline Wingertsmann-Cusano and Dr Simone Dedola.

It has been great to get to know many of the scientists at the Quadram Institute and I wish to thank the following scientists for their help, guidance and great

conversations: Dr Stephanie Schuller, Dr Tanja Suligoj, Dr George Savva, Dr Angela Patterson, Dr Aimee Parker and Dr Naiara Beraza.

I have had great opportunities to meet and work with scientists from across the world and I would like to thank my collaborators Mar Vilamiel and Tiina Alamäe.

I also wish to take this opportunity to thank the Quadram Institute and Norwich Biosciences Institutes for additional funding throughout my project.

As part of my PhD, I had an internship in intellectual property at UEA. I would like to sincerely thank Dr Georgina Pope, Dr Joita Dey and Dr Jon Carter for a great internship.

My greatest and sincerest gratitude and thanks goes to my parents, Monica and David Young for the uncountable hours of support and help throughout my career and PhD. I would not be where I am today if it was not for them. Also, a big thank to Dr Andrew Young and Dr Claire Young for their amazing support and lovely trips out to Cambridge. Thanks also goes to my sisters Karen Young and Angela Manson. I would also like to mention a thank you to Dr Steven Manson, and my nieces Jessica and Ellie Manson, and my new niece, only born a few months ago, Hannah Margaret Young.

Finally, yes. My partner and best friend Britt, a person who has always been there for me during my PhD. We met during our PhD's and have shared the most amazing times and wonderful challenges together. I sincerely thank you for your great support over the last few years, and that includes all the science! I am now looking forward to entering a new chapter with you in Basel.

Contents

List of Figures

List of Tables

List of Appendices

Abbreviations

AMP	Antimicrobial peptide
AP-1	Activator protein 1
APC	Antigen presenting cell
APS	Astragalus polysaccharides
Bcl10	B-cell lymphoma/leukaemia 10
BMDC	Bone-marrow-derived dendritic cell
BMDM	Bone-marrow-derived macrophage
Bp	Base pairs
CARD9	Caspase recruitment domain-containing protein 9
CAZy	Carbohydrate-active enzymes
CD	Cluster of differentiation
CLR	C-type lectin receptor
CO2	Carbon dioxide
COMP-PI	Compensated propidium iodide
COSY	Homonuclear correlation spectroscopy
CPRG	Chlorophenol red-β-D-galactopyranoside
CPS	Capsular polysaccharide
CRD	Carbohydrate recognition domain
CTLD	C-type lectin domain
DC	Dendritic cell
DC-SIGN	Dendritic cell-specific intercellular adhesion molecule-3-grabbing non-integrin
Dectin-1	Dendritic cell-associated C-type lectin 1
Dectin-2	Dendritic cell-associated C-type lectin 2
DAG	Diacylglycerol

DMSO	Dimethyl sulfoxide
DNA	Deoxyribonucleic acid
EDTA	Ethylenediaminetetraacetic acid
EPS	Exopolysaccharide
ES	Enzymatically synthesised
FAE	Follicle-associated epithelium
FBS	Fetal bovine serum
FcRγ	Fc receptor γ
FITC	Fluorescein isothiocyanate
FSC-A	Forward scatter area
FSC-W	Forward scatter width
GAG	Galactoaminogalactans
GALT	Gut-associated lymphoid tissue
GalXM	Glucuronoxylomannan
GC-MS	Gas chromatography-mass spectrometry
GFP	Green fluorescent protein
GI	Gastrointestinal
GM-CSF	Granulocyte-macrophage colony-stimulating factor
GOS	Galactooligosaccharides
GPC	Gel permeation chromatography
GXM	Galactoxylomannan
HSQC	Heteronuclear single quantum coherence spectroscopy
IBD	Inflammatory bowel disease
IEC	Intestinal epithelial cell
Ig	Immunoglobulin
IL	Interleukin

ILF	Isolated lymphoid follicle
IP_3	Inositol triphosphate
ISAPP	International and Scientific Association for Probiotics and Prebiotics
ITAM	Immunoreceptor tyrosine-based activation motif
ITIM	Immunoreceptor tyrosine-based inhibitory motif
kDa	Kilodaltons
KO	Knockout
LacZ	Lac operon Z
LB	Lysogeny broth
LDM2	Lactobacillus semi-defined medium II
LI	Large intestine
LP	Lamina propria
LPS	Lipopolysaccharide
LRA	Lipid removal agent
MALT	Mucosal-associated lymphoid tissue
MALT1	Mucosa-associated lymphoid tissue lymphoma translocation protein
MAPK	Mitogen-activated protein kinase
MAMP	Microbe-associated molecular pattern
MR	Mannose receptor
MCP-1	Monocyte chemoattractant protein 1
MD-2	Myeloid differentiation factor 2
MIF	Macrophage migration inhibitory factor
MUC2	Mucin 2
NaOH	Sodium hydroxide
NDP	Non-digestible polysaccharide
NFAT	Nuclear factor of activated T cells

NF-kB	Nuclear factor kappa-light-chain-enhancer of activated B cells
PAMP	Pathogen-associated molecular pattern
PBS	Phosphate-buffered saline
PCR	Polymerase chain reaction
PIP_3	Phosphatidylinositol (3,4,5)-triphosphate
PI	Propidium iodide
PLCy2	Phospholipase Cy2
PP	Peyers patch
PRR	Pathogen recognition receptor
PS	Polysaccharide(s)
PSA	Polysaccharide A
PSK	Polysaccharide K
QPD	Glutamine – Proline – Aspartic acid amino acid sequence
R.T	Room temperature
RA	Retinoic acid
RFC	Recombinant factor C
ROS	Reactive oxygen species
SCFA	Short chain fatty acids
SDS-PAGE	Sodium dodecyl sulphate polyacrylamide gel electrophoresis
SI	Small intestine
SIGNR1	Specific ICAM-3 grabbing non-integrin 1
SSC	Side scatter area
SYK	Spleen tyrosine kinase
Th	T helper
TLC	Thin layer chromatography
TLR	Toll-like receptor

TNF-α	Tumour necrosis factor-α
Treg	T regulatory
WT	Wildtype

Chapter 1: Introduction

1.1 Overview of carbohydrates

1.1.1. Carbohydrates in nature

Carbohydrates are one of the most abundant compounds on earth comprising > 50% of the world's biomass[1,2]. They are highly structurally diverse in nature from plants, microorganisms and mammals; and unlike proteins, they are not encoded but synthesised by a vast range of enzymes[1-4]. The large diversity of polysaccharide (PS) structures reflects the abundance of natural monomeric sugars (e.g. D-glucose, D-mannose, D-fructose, D-xylose, D-galactose, D-fucose, D-glucuronic acid, L-rhamnose, among many others) and pyranose and furanose ring formations that can make up countless assortments of di- tri- and oligo-saccharides as well as low to high molecular weight PS[1,2]. These structures can be linked by α or β glycosidic bonds and may adopt many variations of branching combinations from simple structures to highly complex macromolecules[1,2]. Poly- and oligo-saccharides are found abundantly in dietary plants but are also found in animal tissues and secretions, or microbes[1]. They may also be attached to other macromolecules to form glycoconjugates such as glycolipids and glycoproteins which are found abundantly in microbes[1,2,5,6]. Poly- and oligo-saccharides fulfil many critical functions of living organisms including structural integrity and as storage PS in plants[6,7]; or sustenance, structural support as well as physiological and biochemical processes in animals and microorganisms[1,2,5,6,8,9].

1.1.2. Dietary fibres

Edible PS are found abundantly in food and are important for human nutrition[10] including starch, a common plant-derived storage PS that can be broken down by host-derived enzymes to glucose units for energy[10]. In contrast, dietary fibres typically comprise diverse soluble and non-soluble non-digestible PS (NDP)[11]. NDP along with lignin (a non-PS) and resistant starch are the primary components of dietary fibres[12]. In general, these fibres are not capable of being broken down by human gut enzymes in the upper part of the gastrointestinal (GI) tract but are fermented by trillions of resident commensal microbes found in the large intestine (LI)[13,14]. The definition of dietary fibre is still under debate; however, many adopt the CODEX of Alimetartious Commission[15] that states: "Dietary fibre means carbohydrate polymers with 10 or more monomeric units, which are not hydrolysed by the endogenous enzymes in the small intestine of humans and belong to the following categories: 1. Edible carbohydrates polymers naturally occurring in the food as consumed. 2. Carbohydrate polymers, which have been obtained from food raw

material by physical, enzymatic or chemical means and which have been shown to have a physiological effect or benefit to health as demonstrated by generally accepted scientific literature evidence to competent authorities. 3. Synthetic carbohydrate polymers, which have been shown to have a physiological benefit to health as demonstrated by generally accepted scientific evidence to competent authorities."[15]

Consumption of dietary fibres by humans is linked to several health benefits[13]. For example, a reduced risk of death and mortality from diabetes, cancer, infections, and respiratory disease was recently shown by meta-analysis to be associated with increased whole grain or cereal fibre consumption[13,16]. Intake of dietary fibres can also lead to other physiological benefits including: laxation, decreased blood insulin and glucose levels, reduced food transit time, increased satiety (food-bulking effect), promoting weight loss, cholesterol-lowering effects, improved mineral absorption and reduced blood pressure, among others[10,13]. Notably, dietary β-glucans and fructans are well-known examples of dietary fibres that contribute to many of these effects[17,18].

Modulation of the gut microbial composition by NDPs is emerging as a strategy to impact on human health[8]. NDPs are an important source of energy for the microbiota in the LI[8], where they are fermented, leading to the production of metabolites including short chain fatty acids (SCFAs)[14]. SCFAs are important for the proliferation of intestinal epithelial cells (IECs), as an energy source for colonocytes, conferring benefits to host metabolism and influencing intestinal immune homeostasis[8,19]. A low dietary fibre intake - commonly observed in 'western style' diets typically high in sugar, fat and processed foods, and low in fruits, vegetables and legumes - leads to reduced gut microbial diversity and a reduction in SCFAs[8]. This contributes to the degradation of the protective intestinal mucus layer and a reduction in anti-microbial peptides important for intestinal immune regulation[8,19,20]. Therefore, dietary fibres may influence intestinal immune homeostasis through modulation of gut microbial ecology[8,13]. Notably, some PS are termed prebiotics and are commercially available for human consumption including fructans and galactooligosaccharides (GOS)[21]. Prebiotics are defined by the International and Scientific Association for Probiotics and Prebiotics (ISAPP) as "a substrate that is selectively utilised by host microorganisms conferring a health benefit"[22]. As dietary fibre encompasses mixtures of PS, there is now increasing interest in individual PS for conferring health benefits to humans[3,12].

1.1.3. Polysaccharides

PS are homopolymers or heteropolymers that are typically made up of > 20 monomeric sugar units and can be found in plants, fungi, algae and animal tissues[1]. There are two broad classifications of plant PS (I) PS used as storage including fructans, starch and other oligosaccharides and (II) cell-wall PS such as pectin, cellulose and hemicelluloses that provide structural support[10,23]. Further, microbial PS are commonly found in commensal, opportunistic and pathogenic bacteria[24]. Microbial PS can be also consumed in the diet (e.g. in fermented foods or baker's yeast)[25,26]. Therefore, PS are frequently exposed to the environment of the GI tract. Depending on their origin, PS found in nature can be structurally complex[1,27]. In the following sections, we briefly describe some PS relevant to this thesis with a focus on those derived from plants, mushrooms and algae including edible PS, as well as PS from microbes (see Figure 1).

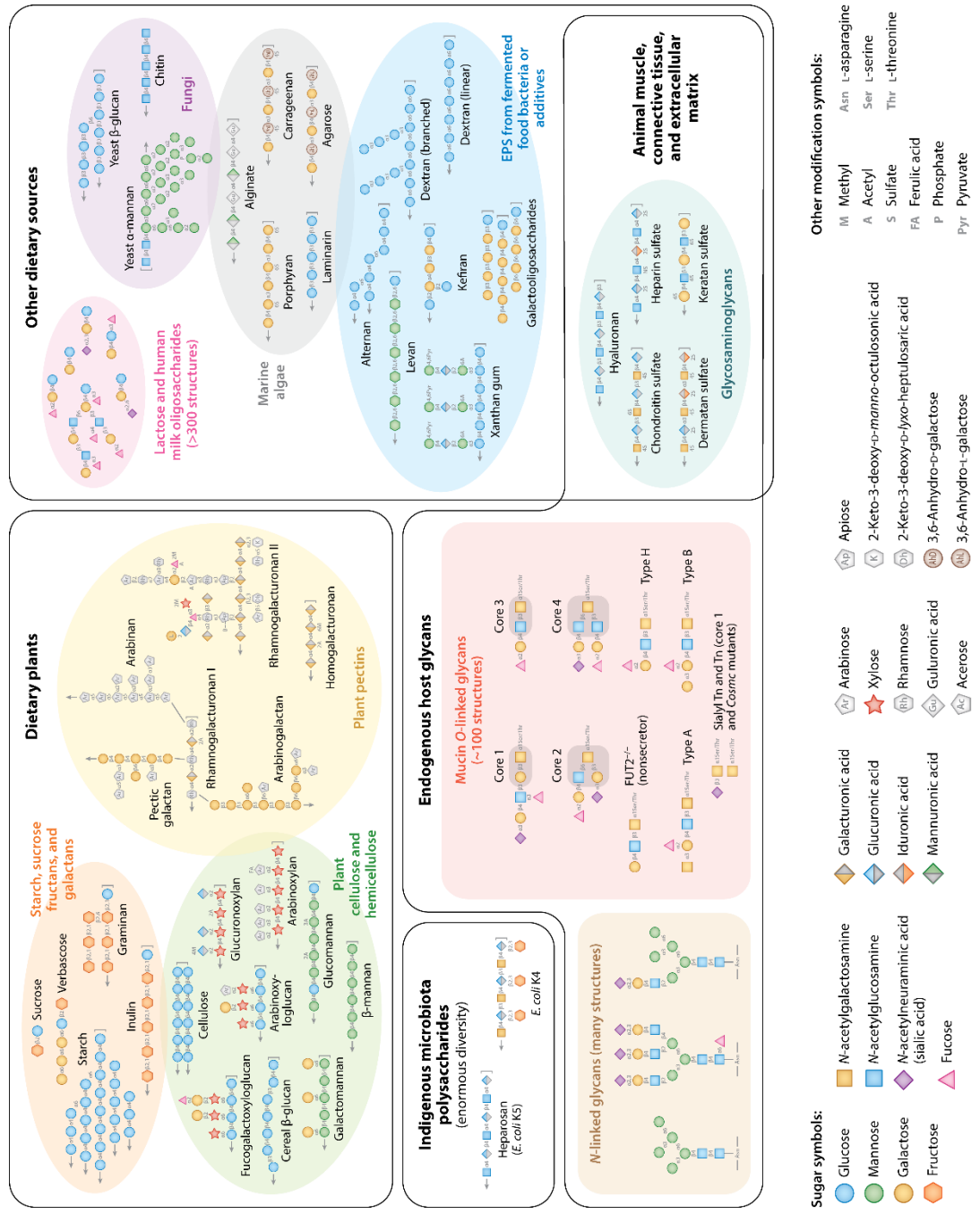

Figure 1. Examples of PS found in nature and their composition

Note: levan should be with fructose label (orange hexagon). Taken from [1] with permission obtained from Annual Reviews and the Copyright Clearance Centre.

1.1.3.1. Polysaccharides from plants and mushrooms

1.1.3.1.1. β-glucans

β-glucans are large polymers of glucose found in many plants and fungi and can vary in size and structure depending on their origin[28]. For example, cereal β-glucans (Figure 1) are heterogenous glucose polymers that typically contain assorted β-(1,3) and/or β-(1,4) linkages[13,18,29]. They are mostly present in the cell-walls of barley and oats but are also found in maize, sorghum and wheat in smaller quantities[13,18,29,30]. The molecular weights of these glucans are origin-specific and can range from 10 to > 1000 kDa[31]. In contrast to plant β-glucans, edible mushrooms such as lentinan (shiitake mushroom) primarily contain large β-(1,3) glucans and are reported to have an average molecular weight of 500 kDa[32]. Further, *Ganoderma lucidium* also harbours a β-(1-3) glucan backbone but with additional β-(1-6) branching points[32]. In addition, the edible mushroom *Agaricus blazei* comprises a number of glucans with β-(1-6) linked glucose backbones that contain either β-(1,3), α-(1,3) or α-(1,4)-linked glucose branching with the latter two being acidic glucans[32]. Dietary β-glucan consumption is associated with several health benefits including cholesterol-lowering properties, improved blood lipid profiles, and reduced postprandial insulin and glucose levels[33].

1.1.3.1.2. Cellulose and hemicelluloses

Cellulose (Figure 1) is a β-1,4-linked linear glucose polymer and found in the cell walls of the majority of plants[13]. This large polymer (up to 10,000 glucose units) is insoluble and an important dietary NDP. Hemicelluloses (Figure 1) are structurally diverse heteropolysaccharides and can comprise xylans, glucomannans (Figure 1), other mannan structures (see 1.1.3.1.4) and xyloglucan[34]. Arabinans, galactans and arabinogalactans have been commonly classified as hemicelluloses but are best described as pectic compounds[12,34]. For a review on hemicellulose structures see [34]. Xyloglucans are hemi-cellulosic polymers consisting of a β-1,4-linked glucose linear chains and comprise α-1,6-linked xylose side units that may be attached to β-1,2-linked galactose units or other sugars depending on the source[35-38]. Xyloglucan is a generic linear β-glucan, as its glucose backbone is linked only to some xylose sugars[39]. Xyloglucans are found in the cell walls of most vascular plants and are commonly extracted from land plants including tamarind seeds, equisetum and cranberry[35,36,38-40].

1.1.3.1.2.1. Arabinoxylan

Arabinoxylans are a major constituent of the cell walls of cereals including barley, millet, maize, rye and oats[41]. Psylium gum is an arabinoxylan (Figure 1) and is primarily sourced from the husk of psyllium seed (*Plantago ovata forsk*)[41]. Psylium gum is generally regarded as a highly branched polymer comprising ~74.6% xylose and 22.6% arabinose typically containing a β-1,4-linked xylose linear chain with arabinose unit side chains[41,42]. Psylium gum from *Plantago spp* has also been proposed to include β-1,3-linked xylose in its linear chain, and may contain xylose and/or aldobiuronic acid disaccharide residues (D-galacturonic acid and L-rhamnose) at its branching points[43]. Psyllium gum has been proposed as a nutraceutical and functional food, for example for its possible cholesterol-lowering properties in humans[41,44].

1.1.3.1.4. β-mannans

Plant-derived mannans (Figure 1) are found as either storage or cell wall PS[27,45]. They can be typically linear or are classed into various subcategories including galactomannans, glucomannans and galactoglucomannan comprising D-galactose or D-glucose units linked to linear mannose chains[45,46]. β-1,4-linked "pure" mannans are generally linear and range in molecular weight from 40 kDa to > 300 kDa[45] and can be found in plant sources such as ivory nut[45,46]. Glucomannan consists of both mannose and glucose and are commonly found in Eastern white pine, Orchid and Higanbana[45]. Further, Konjac glucomannan (Konnyaku root or *Amorphophallus*) is reported as a β-1,4-linked D-glucose and D-mannose polymer which can be partially acetylated. Intake of glucomannans is linked to several health benefits including laxative properties, alleviation of diverticulitis, prebiotic effects, relieving constipation, cholesterol-binding properties and delayed glucose absorption[45]. Galactomannans are found in the endosperm walls of many leguminosae seeds such as guar gum, locust bean gum, fenugreek gum and tara gum[27,39]. They typically consist of β-1,4-linked D-mannose with α-1,6-linked D-galactose side units and are reported as ~1000 kDa in molecular weight[27,45]. Finally, acemannan is a type of glucomannan, a partially acetylated β-1,4-linked D-mannose linear chain containing some D-glucose units and is reported as a bioactive compound found in *aloe vera*[47].

1.1.3.1.4. Pectins

Pectins (Figure 1) are structurally complex PS found in the cell walls of many vegetables and fruits including sweet potatoes, grapefruit, apples, oranges, bananas, beans and carrots[27,48,49]. They are generally heteropolysaccharides and can consist

of a linear chain of α-1,4-linked galacturonic acid which can also be interspersed with individual residues of α-1,2 linked L-rhamnose, and are reported to range from 55 to 4200 kDa in molecular weight[27,50]. However, pectins are highly structurally diverse, which depending on the source, can consist of other sugars or larger PS structures (Figure 1)[27]. Pectins can comprise rhamnogalacturonan type I and II, arabinan, xylogalacturonan and homogalacturonan[1,51-53]. For a review on pectin structure see [53]. Pectins are an important water-soluble dietary NDP that contribute towards gel-formation in the human GI tract[13]. They are also a common dietary fibre and are associated with several promising health benefits including anti-diabetic, anti-cancer, and cholesterol-lowering properties[52,54,55]. For a recent review on the potential health-promoting properties of pectins, see [52].

Gum Karaya is a partly water soluble rhamnogalacturonan pectic polymer that is partially acetylated. It typically contains an alternating α-1,4 L-rhamnose and α-D-galacturonic acid backbone with β-1,4 D galactose or β-1,3 D-glucuronic acid single side units[27]. Gum karaya can be commonly found in gums such as *Sterculia urens* and is used as a food additive[56].

Arabinan is commonly sourced from sugar beet and comprises a α-1,5-linked arabinose backbone branched with α-1,3-linked or α-1,2-linked arabinose units[27]. Arabinan is also found in pectins from vegetables such as cabbage[57]. Pectin-derived arabinan is attached as a side chain to the rhamnose residues of rhamnogalacturonan I (Figure 1).

1.1.3.1.5. Fucoidans

Fucoidans are PS that mostly consist of L-fucose residues and are commonly sulphated. Typically, they consist of α-(1,3)- and α-(1,4)-linked L-fucose linear chains; which may be assorted as linear α-(1,3)-fucans interspersed with single α-(1,3)- and α-(1,4)-linked L-fucose or sulphate ester groups[58,59]. Other sugar units have been reported in fucoidan PS including glucuronic acid, arabinose, mannose xylose and galactose[58,60]. For further information on fucoidan structures see [59] and [60]. Fucoidans are primarily derived from brown seaweeds, however, they can also be found in sea urchin and sea cucumber[59]. Fucoidans can differ in their structure depending on their source and are suggested to have bioactive properties including antitumor, anticoagulant, and antithrombotic effects[59].

1.1.3.1.6. Fructans

Plant fructans are polymers of fructose found as storage PS in ~15 % of higher plants such as forage grasses, cereals and vegetables[61]. Fructooligosaccharides (FOS) or inulins (Figure 1) are described as water soluble linear β-(2,1)-linked fructans where their degree of polymerisation (DOP) is dependent on their source, generally between 3 and 60 DOP[62,63]. Plant levans are typically termed linear β-(2,6) fructans. Fructan PS are termed inulin while fructans with a DOP between 3 and 5 monomers are typically referred to as oligofructose or FOS[63]. Plants including cereal grains utilise fructosyltransferases to synthesise fructans by adding fructose residues onto sucrose (disaccharide of glucose and fructose) leading to the production of different structures including: linear β-(2,1) fructose (1-kestose or inulin); branched structures comprising mixtures of β-(2,1) and β-(2,6) links (bifurcose or graminans); linear β-(2,1) or β-(2,6) fructose as N-kestose or Neoseries; or β-2,6 linear fructans (levan)[62,64-66]. β-(2,1) inulins are a good source of soluble fibre and are found in foods such as banana, garlic, wheat, onions, leeks, barley and rye. It has been also reported that inulin from garlic contains β-(2,6)-linked fructose branching[67]. β-(2,6) levan is produced by several plant species including *Agropyron cristatum*[68], *Pachysandra terminalis*[69] and *Curcuma kwangsiensis*[70]. Plant levans are non-structural storage carbohydrates located in leaf and stem sheaths and are generally low in molecular weight[70-73]. Additionally, high molecular weight (> 500 kDa) β-2,6 levan-type fructans are produced by a diverse range of microbes[72] which is discussed in 1.1.3.2.1.4. Inulin and FOS are linked to a number of health benefits including alleviation of allergy, disease-associated chronic inflammation, or colon cancer, and are suggested to have immunomodulatory properties[74].

1.1.3.1.7. Galactans

Galactans are structurally diverse in nature[75]. From algae and seaweeds, they are primarily linear galactose polymers comprising alternating α-1,4 and β-1,3 linkages and are generally sulphated[75]. Depending on their source, these polymers can also contain mixtures of other sugars including glucose, arabinose, and xylose[75,76]. Galactans are also present in plants such as lupin which are mostly made up of β-1,4-linked linear galactose chains[75,77]. Other plant galactans also contain β-1,3 or β-1,4 galactose chains and may comprise other sugars including arabinose, rhamnose and glucose[75]. For example, arabinogalactan type I is found in some fruits and comprise β-1,4-linked galactose chains attached to α-(1,5)-linked arabinose units[75].

Arabinogalactan type II can also be present[75]. The sources and structures of galactans have been reviewed elsewhere, see [75].

1.1.3.2. Microbial polysaccharides

PS synthesised from pathogenic or commensal microbes are vast and structurally complex[78-80]. Microbial PS can be found in the cytoplasm as storage PS or be present in the cell wall. They also exist as exopolysaccharides (EPS) that are secreted into the extracellular environment or loosely associated with the bacterial cell surface; capsular PS (CPS) that are attached to the microbe's surface; or bacterial lipopolysaccharides (LPS) anchored to the membrane[81,82].

1.1.3.2.1. Exopolysaccharides

EPS are generally high molecular weight carbohydrate polymers that can be subdivided into homopolysaccharides (comprised of one monosaccharide type) or heteropolysaccharides (consisting of 2 or more monosaccharide types). EPS is a general term that describes microbe-derived PS residing outside the cell wall - also referred to as extracellular PS[83]. EPS including dextran, gellan gum, pullulan and levan are used commercially including in the food and pharmaceutical industries[79,84,85]. Here we describe EPS relevant to this thesis that are secreted into the extracellular environment or are loosely attached around the surface of the microbe[79,81] with a focus on levan.

1.1.3.2.1.1. Pullulan

Pullulan is a water-soluble linear EPS primarily consisting of a repeating maltotriose residue (α-1,4-linked trisaccharide of glucose) connected by α-1,6 linkages[84,86,87]. It is produced by fungal microorganisms including *Aureobasidium pullulans*, *Cytaria spp.* and *Telochisttes flavicans*, among others[84,86]. Pullulan is used in the cosmetic, textile, food, and pharmaceutical industries[84,86]. For a recent review, see [86].

1.1.3.2.1.2. Gellan gum

Gellan gum is an EPS made and secreted by *Sphingomonas paucimobilis* (formerly *Pseudomonas elodea*) and comprises a repeating unit of β-D-glucose and β-D-glucuronate, α-L-rhamnose (molar ration 2:1:1) and may be partially acetylated[79,88]. Gellan gum is widely used in the food industry particularly for its gel-forming capability e.g. in milkshakes, jams and jellies[79].

1.1.3.2.1.3. Dextran

Dextran is a high molecular weight glucose polymer and typically contains predominant α-1,6 linkages in its linear chain and can comprise α-1,2, α-1,3, and α-

1,4 branching depending on its source[79,84,89]. It is biosynthesised by many of the bacteria belonging to the Lactobacillaceae family including *Streptobacterium dextranicum, Leuconostoc mesenteroids,* and *Leuconostoc dextranicum*[89]. Dextran is also used extensively in the food industry e.g. as a thickener in ice cream and jam[79].

1.1.3.2.1.4. Levan

Microbial levan is a large β-(2,6) fructofuranose polymer that is linear or can contain β-2,1 branching (Figure 2)[71,72,90]. Many bacteria are capable of synthesising levan including *Lactobacillus reuteri*[91], *Bacillus subtilis*[25,92], *B. amyloliquefaciens*[93], *L. citreum*[94], *Zymomonas mobilis*[95], *Pseudomonas syringae pv*[96], *Erwinia herbicola*[97], *Microbacterium laevaniformans* and *Serratia levanicum*[72,98]. Further, yeast such as *S. cerevisiae* has been used for levan production, although, this is not common[72,99]. Levan's degree of branching depends on the microbial source and the production method used (e.g. culture conditions)[72] and in between ~2 and 13% branching has been reported[72,90]. For example, levan produced from *E. herbicola* is regarded to consist of 5% branching while levan from *M. laevaniformans* produced up to 12.3% or 12.9%[100,101]. Alternatively, low branched levan has shown to be produced by bacteria such as *Serratia levanicum*[98]. Further, some species of acetic acid bacteria produce linear levan[102]. Levan's molecular weight depends on the microbial strain and production method used (e.g. culture conditions)[72]. In general, levans form high molecular weight polymers[72]. For example, levan produced by *Serratia spp*, *B. polymyxa*evan and *E. herbicola* show molecular weights of 4400 kDa, ~2000 kDa, and 1100/1600 kDa, respectively. Interestingly, some bacteria can produce both low and high molecular weight levans. For example, *B. subtilis natto* simultaneously produce levans of 1800 kDa and 11 kDa[103]. The same strain was also reported to produce two levans at 568 kDa and 50 kDa[104].

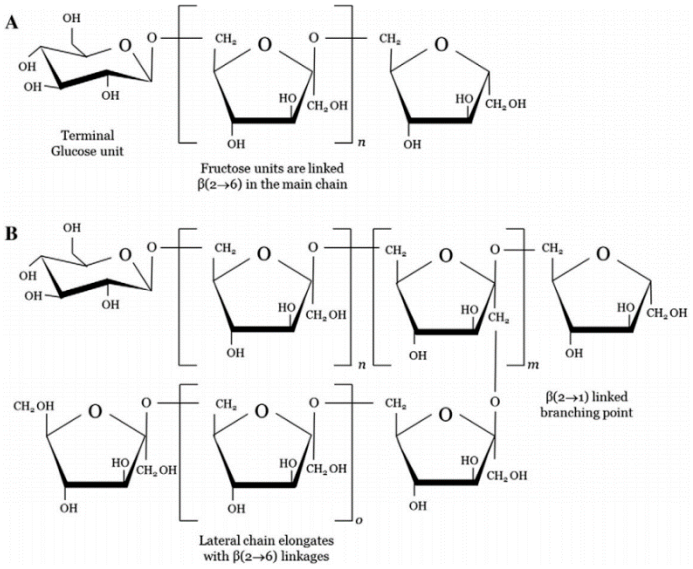

Figure 2. Structural conformations of microbial levan

(a) linear β-(2,6) levan. (b) linear β-(2,6) levan containing β-(2,1) branching points. Taken from [72] with permission obtained from Elsevier, Inc, and the Copyright Clearance Centre.

Levan is synthesised by levansucrase (E.C 2.4.1.10), a fructosyltransferase belonging to family 68 of glycoside hydrolases according to the CAZy (carbohydrate-active enzymes) database (www.cazy.org)[72]. Generally, levansucrases are secreted into the extracellular environment but can also be attached to the bacterial cell surface[71,72]. Levansucrase binds to a substrate, such as sucrose, and adds fructose molecules to a growing fructose chain[71,72]. Typically, this process produces a glucose-capped β-(2,6)-linked fructofuranose polymer containing no or some β-(2,1) branching (Figure 2)[72]. Levan can be produced by bacterial culture methods or *in vitro* using recombinant levansucrase heterologously produced in *Escherichia coli*[72,105-107]. Levan is amphiphilic and known to adopt a spherical conformation in aqueous solution, and, therefore is commonly referred to as a 'nanoparticle'[71,72,90,102,107]. Levan is functionally unique as it has a low intrinsic viscosity, good tensile strength, low toxicity, and is eco-friendly and biodegradable[71]. Levan can be applied in several industries including in aquaculture and biofilm packaging[72]. Further, levan has been proposed for use in the food industry e.g. in dairy products or bread[72,108,109]. It is also present in fermented food such as Natto (fermented soybean)[25,26]. Levan may also be relevant to the pharmaceutical industry, for example, as a nanoparticle for delivering drugs including antibiotics[72,110]. Further, levan is suggested to confer several health benefits including anti-cancer/anti-tumour[95,100], anti-pathogenic[109], anti-diabetic[111], cholesterol-lowering and anti-obesity properties[112], among others[72]. It has also been proposed as a prebiotic[106,113-115]. This

was shown in a recent study where levan supplementation of cultures of faecal microbiota of healthy individuals led to positive changes in microbial composition, including increased *Bacteriodes spp* and *Facalibacterium spp* (a known butyrate-producer). For a recent review on levan as a prebiotic see[106]. Interestingly, isolates of levan-producing strains have been detected in the faeces of healthy humans[116], although due to the limited number of reports, further work is warranted to verify that levan is produced by resident bacteria in the GI tract.

1.1.3.2.2. Cell wall-associated polysaccharides

1.1.3.2.2.1 Microbial glucans and mannans

α- and β-glucans and high-mannose structures are frequently found in pathogenic microbial fungi and mycobacteria (Figure 3)[117,118]. For example, outer layer mannoproteins along with inner layer chitin and β-1,6/β-1,3 glucans are components of *Pneumocystis spp* such as *Pneumocystis jiroveci*[119] (Figure 3). Fungal α-mannans are typically found as O- or N-linked mannoproteins, however, high-mannose structures can also be covalently attached to lipid moieties that form glycolipids such as lipoarabinomannan from *Mycobacterium*[120,121]. In addition, α-(1,3) glucans can be present on the outer surface of *Blastomyces dermatitidis* or *Histoplasma capsulatum* which also consists of an inner layer of β-glucan and chitin (Figure 3)[122,123]. Interestingly, α-(1,3) glucans are thought to help evade immune system recognition by shielding highly immune-responsive β-glucan[117,124]. Other PS found in pathogenic fungi include galactomannans, CPS glucuronoxylomannan (GalXM), CPS galactoxylomannan (GXM) and galactoaminogalactans (GAG) (Figure 3)[117]. Along with mannoproteins, β-glucans and chitin, these PS structures not only uphold structural integrity but also serve as pathogen-associated molecular patterns (PAMPs)[117]. PAMPs are microbial structures recognised by a variety of pathogen recognition receptors (PRRs) found on mammalian immune cells - including C-type lectin receptors (CLRs) and Toll-like receptors (TLRs) (see 1.2.5.2 and 1.2.5.1, respectively) – and help initiate the immune response to help combat infection[24,117,125]. For a review on how the immune system recognises and responds to fungal pathogens see [126] or [117].

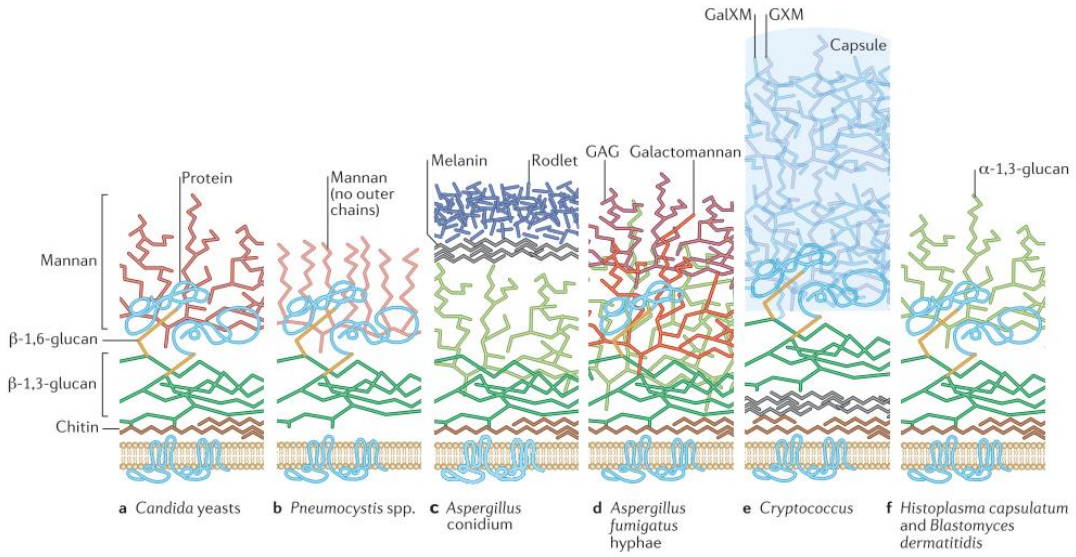

Figure 3. Structure and carbohydrate composition of the cell walls in pathogenic fungi

GAG, galactoaminogalactans. GalXM, Glucuronoxylomannan. GXM, Galactoxylomannan. Taken from [117] with permission obtained from Springer Nature and the Copyright Clearance Centre.

1.1.3.2.2.2. Scleroglucan

Scleroglucan is a high molecular weight β-glucan synthesised by members of the *Sclerotium* genus[127,128]. The plant pathogen *Sclerotium rolfii* is commonly used for the production of scleroglucan in industry[129]. Scleroglucan comprises a linear chain of β-1,3-linked glucose with β-1,6 glucose branching points every 3 residues, and adopts a triple helix formation as a macromolecule[128,130]. Like levan, its average molecular weight depends on the production method used[128]. Scleroglucan's reported molecular weight varies from 130 kDa to 6000 kDa[128]. It is widely used in industry, for example as a drug delivery carrier in the pharmaceutical industry, and as a thickening agent and stabiliser in the food industry[127,128]. For a review on the properties and applications of scleroglucan see [128].

1.1.3.2.2.3. Lipopolysaccharide

LPS is a complex glycolipid which forms the outer membranous layer of gram-negative bacteria (Figure 4a)[82]. LPS can be characterised into 3 main domains as described by Steimle and colleagues (2016) (Figure 4b)[131]. Briefly, (i) lipid A comprises acyl structures - and the length and number of the acyl chains per domain can differ between bacterial species[131] - that are connected to a disaccharide of β-(1,6)-linked glucosamine which are typically phosphorylated (Figure 4b)[131]. (ii) The core saccharide region can consist of up to 15 sugar residues and contains one or more residues of deoxy-D-manno-oct-ulosonic acid (Kdo) that is connected to one of

the sugar moieties on lipid A[131]; (iii) O-antigen or O-specific PS is highly variable among bacterial species and usually comprises repeating oligosaccharide residues consisting of up to 5 different sugar types[82,131,132] (Figure 4 b). The O-antigen fulfils several functions including bacterial motility and protecting against oxidative stress[82,133]. Rough type LPS comprises only lipid A and the core region[131]; the core saccharide being partly responsible for its antigenic potential as no O-antigen is present[131]. In contrast, smooth LPS contains all 3 domains (Figure 4 b)[131]. LPS is important for the immune response against pathogenic gram-negative bacteria (also see 1.2.5.1).

a)

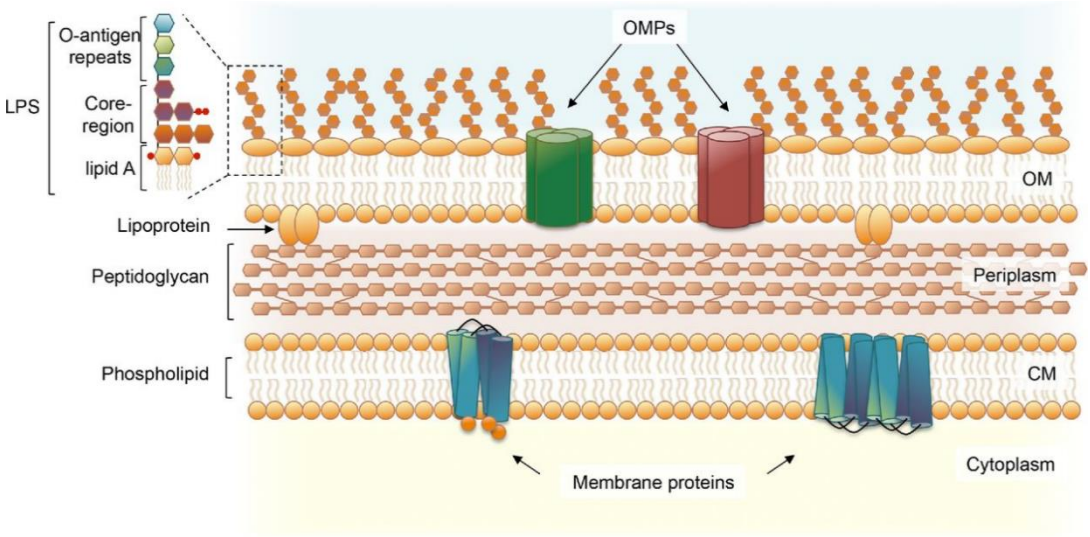

b)

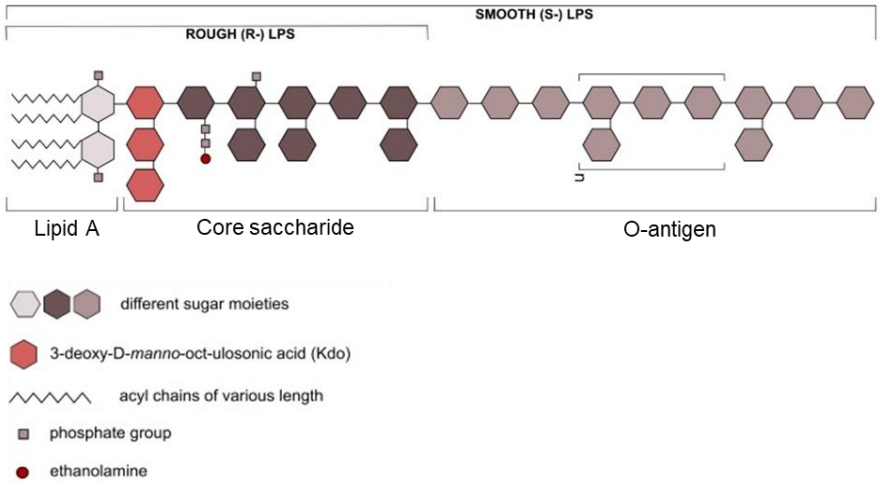

Figure 4. The cell wall of gram-negative bacteria and the structure and composition of LPS

(a)Typical cell wall composition of gram-negative bacteria comprising LPS in the outer lipid bilayer. In the periplasm, a peptidoglycan layer separates the outer membrane from the cytoplasmic region. Taken from [82]. Aritcle is under the Creative Commons CC BY licence. Image licence: https://creativecommons.org/licenses/by/4.0/legalcode. (b) Typical structure of LPS from gram-negative bacteria. Taken with minor adaptions from [131]. Article is under the Creative Commons Attribution-Non-commercial-No Derivatives License (CC BY NC ND). Image licence: https://creativecommons.org/licenses/by-nc-nd/4.0/legalcode. OM, outer membrane. CM Cytoplasmic membrane.

1.1.3.2.2.4. Peptidoglycan

Peptidoglycan (PGN) is a large glycoprotein found in both gram-negative and gram-positive bacteria[134]. It is highly abundant in gram-positive species making up 30 – 70 % of the cell wall[24]. PGN is critical for cell wall structural integrity and helps combat environmental stressors[135]. PGN comprises peptides that link saccharide residues made of β-1,4-linked N-acetylglucosamine and N-acetylmuramic acid[135]. For a review, see [134]. As gram-positive bacteria have no outer membrane, PGN resides on the outer portion. In gram-negative bacteria, PGN is located between the cytoplasmic and outer membrane (Figure 5a)[82,135].

1.1.3.2.3. Capsular polysaccharides

CPS are found on the outer surface of many bacteria[78,80]. They are produced by both pathogenic and non-pathogenic microbes, and the latter use CPS to defend themselves against the host's immune system such as evasion from immune cells[78]. They are large, usually composed of > 200 monosaccharides, and can be found in range of pathogenic microbes[78,117]. For example, *N. meningitidis* W-135 contains the following repeating unit: galactose–[α-(1,4)-]N-acetylneuraminic acid[-α-(2,6)]-[136,137]. Also, microbial fungi *Cryptococcus* contain CPS GalXM and GXM (Figure 3)[117]. Knowledge of the CPS structure from *Neisseria meningitidis* W-135 and other CPS including *Haemophilus influenza* b[138], have helped towards the development of effective vaccines[137]. For a review on pathogenic CPS see [137]. In addition, CPS are present on commensal gut bacteria such as *Bacteroidetes fragilis*, which can be found in the human ileum but mostly in the colon[139]. *B. fragilis* can synthesise up to 8 types of CPS which are thought to help towards colonisation in the gut and possibly immune system evasion[139,140]. These CPS comprise both negative and positive charges (zwitterionic) which are thought to be critical for their immunomodulatory properties[139]. Polysaccharide A (PSA) is the best-characterised zwitterionic CPS from *B. fragilis*[139]. Its structure comprises a repeating oligosaccharide of "[-1,3)-α-D-AAT Galp-(1,4)-[β-D-Galf-(1,3)] α-D-GalpNac (1,3)-[4,6-pyruvate-β-D-Galp-(1,-]"[141,142].

1.1.3.3. Evidence from human clinical studies for immunomodulatory properties of dietary polysaccharides

The health benefits to humans from consuming dietary fibre are well-accepted[8], however, less is known on the molecular mechanisms of individual fibres PS types on the intestinal immune system in humans[3,143]. Interestingly, some oral PS-based products are commercially available for immune health[3,144,145], for example

Yestimum®[145], Cold-FX[3,146] and Resistaid™[147]. The following sections describe some evidence in human studies that reported immunomodulatory properties of oral/dietary PS with a focus on fructans (see Table 1 for a summary).

Table 1. Examples of immunomodulatory PS: human dietary studies.

PS Treatment	Study Design	Relevant immunomodulatory results	Reference
Oral, Wellmune® (β-1,3 and β-1,6 glucans)	DB RCT; 50 – 70 y/o adults; n=49, 250 mg/day or placebo; 90 days.	➢ Trend (p=0.067) for ↓ number of days with symptoms in individuals with urinary tract infections. ➢ ↑ IFN-γ levels from isolated blood after LPS-stimulation compared to control group at 45 days (not at 90 days). Relatively, no notable changes in IL-1β, IL-6, IL-8, TNF-α or MCP-1, among others.	148
lentinula elodes (Shiitake mushrooms; contains β-glucans[149])	4-week parallel group study consuming lentinula elodes mushrooms; daily 5-10g; 52 health male and female adults; 21-41 y/o;	➢ ↑ IL-4, IL-10, TNF-α and IL-1β; ↓ MIP-1a; and no difference with IL-6, IL-1β. IL-17 and MIP-1b in stimulated-PBMCs (ex vivo) after 4 weeks compared to baseline values.	150
Ginseng PS from *Panax ginseng* (reported as rhamnogalacturonan I backbone with arabinogalactan II type side branching[151])	DB RPCT; 72 healthy adults; 50 – 75 y/o; over 14 weeks;	➢ ↑ serum TNF-α compared to placebo at both 8 and 14 weeks. ➢ ↑ NK cell activity (isolated from Peripheral blood measuring % lysis) compared to placebo at both 8 and 14 weeks. ➢ ↑ phagocytosis of peripheral blood macrophages (using pHrodo™ kit) compared to placebo at both 8 and 14 weeks.	152
β-2,1 fructan mix (Orafti® Synergy1 (BENEO)	DB randomised double crossover study; male and female adults; supplemented with inulin or placebo 60 days total; n= 30	➢ ↑ serum IL-4 and GM-CSF. ➢ ↑ $CD282^{+}$/$TLR2^{+}$ circulatory DC. ➢ ↓ serum IL-10. ➢ ↑ IL-10 in Pam3Cys4-induced but not LPS-induced whole blood (ex vivo).	153
Inulin and oligofructose mix (Frutafit IQ)	RPCT; type 2 diabetes females; n = 27 intervention; n = 22 placebo; 2 months supplementation; 10g daily Inulin and oligofructose mix	➢ ↓ serum IL-12 and IFN-γ after 2 months in treatment group and not in placebo group. ➢ ↑ serum IL-4 after 2 months in treatment group and not in placebo group.	154

Legend: DB, double blinded. DC, dendritic cell. GM-CSF, granulocyte-macrophage colony-stimulating factor. IFN, interferon. IL, interleukin. LPS, lipopolysaccharide, MCP-1, monocyte chemoattractant protein. MIP, macrophage inflammatory protein. NK, natural killer. PBMCs, peripheral blood mononuclear cells. PS, polysaccharides. RPCT randomised placebo-controlled trial. TNF-α, tumour necrosis factor-α.

1.1.3.3.1. Glucans

Glucans sourced from mushrooms and yeasts/fungi are one of the best-studied immunomodulatory dietary PS in humans[3,145] (see Table 1 for details). For relevant

reviews, see [3] and [155]. It should be noted that whole mushrooms reported to be immunomodulatory also contain other bioactive compounds in addition to glucans including flavonoids and terpenoids[156].

1.1.3.3.2. Fructans

Dietary inulin is linked to several health benefits in humans and has shown promise in modulating immune system function (Table 1)[74,157,158]. Supporting this, a double-blinded randomised placebo-controlled trial of 60 healthy individuals over 4 weeks receiving a mixture of xylooligosaccharide and inulin not only caused prebiotic effects by positively altering gut microbial composition increasing faecal numbers of Bifidobacterium and butyrate levels but also decreased blood LPS levels, and increased IL-β expression and decreased IL-13 expression in LPS-stimulated whole blood (*ex vivo*)[159]. Another randomised control trial (RCT) of 52 women with type II diabetes given fructans daily (including inulin) showed reduction in circulating TNF-α, IL-6 and LPS and other metabolic parameters when compared to a control group given maltodextrin[160]. Further, a recent systematic review by Fernandes and colleagues[161] investigated the effects of inulin and galacto-oligosaccharides on inflammatory markers in obese individuals including cytokine and LPS levels[162]. They concluded that there was some evidence for immunomodulation in humans by dietary inulin although more well-controlled studies were required[161]. Less explored are the effects of dietary levan on human health. Healthy individuals receiving levan-supplemented juice daily showed no difference in GI symptoms such as bloating/abdominal pain and metabolic measures including blood pressure compared to the control group[163]. Although studies of dietary levan are limited[163], based on the promising health benefits reported in experimental models[71,72], further investigations in humans are warranted including assessment of levan's immunomodulatory and anti-cancer effects[71,72].

1.2. Overview of the gastrointestinal tract

1.2.1. Structure and function of the gastrointestinal tract

The GI tract is a remarkable compartmental and multifunctional system that begins at the mouth and terminates at the anus (Figure 5)[164]. As a long, muscular and tubular structure, its function is to digest food, absorb water and nutrients, maintain electrolyte balance, remove waste, regulate immune function, produce hormones, harbour commensal microorganisms and re-absorb or excrete endogenous or

exogenous biological molecules[165]. This system is broadly categorised into two compartments: the upper GI tract consisting of the oral cavity, oesophagus, stomach and duodenum (part of the small intestine [SI]); and the lower GI tract containing the jejunum and ileum of the small intestine (SI), and the appendix, cecum, colon (ascending, transverse, descending and sigmoid), rectum and anal canal of the large intestine (LI) (Figure 5)[166].

The GI system encounters a continuous bombardment of dietary and environmental exogenous components[166]. The main function of the GI tract is to digest and absorb dietary nutrients, providing energy and support for physiological and cellular processes in the host[166]. Food is encountered and partially degraded in the oral cavity through mastication and secretory digestive enzymes[164]. A dietary-derived bolus then peristaltically descends down the oesophagus entering the stomach where mechanical churning, acidic secretions and local enzymes aid further digestion[164]. The components are passed into the SI and LI where further digestion occurs, macro- and micronutrients are absorbed, and microbial fermentation of non-digestible carbohydrates takes place (in the LI) as well as the absorption of water and ions. Unused components or unwanted biological molecules and secretions are excreted via the anus[164].

In recent years, the GI tract has been the centre of investigation over its role in immune function[165]. The GI tract harbours the largest collection of immune cells in the human body, and is also a habitat for trillions of diverse microorganisms collectively termed the gut microbiota[165]. These organisms have co-evolved with their hosts resulting in a complex and mutualistic relationship that can benefit host health including regulating immune function[165,167].

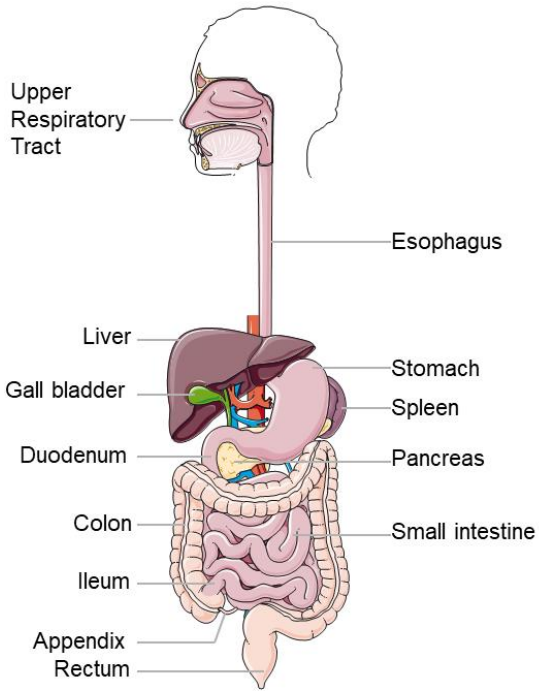

Figure 5. Regions of the gastrointestinal tract.

Adapted from Servicer Medical Art images. Servier Medical Art by Servier is licensed under Creative Commons Attribution 3.0 Unporter License: https://creativecommons.org/licenses/by/3.0/legalcode

1.2.2. The intestinal microbiota

Humans harbour trillions of diverse microorganisms including fungi, bacteria, archaea, viruses, and eukaryotes that are located in or on the host including the skin[168], respiratory[169], urogenital[170] and GI tract[14]. The total microbial DNA associated with humans is collectively known as the microbiome[171]. The number of bacteria to human cells is suggested to be close to 1:1 and not 10:1 as previously reported[172-174]. Further, the microbiome, particularly of the GI tract, is emerging as having profound implications for human health and disease[172-174].

The gut microbiota comprises > 500 species of bacteria[165,175,176]. The majority of these species reside within the LI: ~10^9 - 10^{12} microbes per ml (other estimates suggest 10^{14})[172] which decreases towards the ileum (10^3 – 10^7 [also reported as 10^8][172]) and to the duodenum and jejunum (< 10^5)[165] (Figure 6). These microorganisms have co-evolved with humans to form a mutually beneficial yet complex relationship that contributes to GI function and health[14,167,177]. For example, the gut microbiota plays a role in many intestinal metabolic processes in the gut[14] including the synthesis of vitamins which are important for cellular processes and gut health[178] including folate[179], vitamin B12[180] and vitamin K[181]. Notably, vitamin B12

cannot be synthesised by fungi, animals or plants, however lactic acid bacteria are able to produce[14,182]. Importantly, characterisation of the human intestinal microbiota has benefited from recent technological advances, leading to a better understanding of how microbial composition is influenced by genetic and environmental factors including geographical area, diet and disease[14,183]. Moreover, it is thought that the colonisation of intestinal microbiota starts immediately from birth, however, this is still a matter of debate[14].

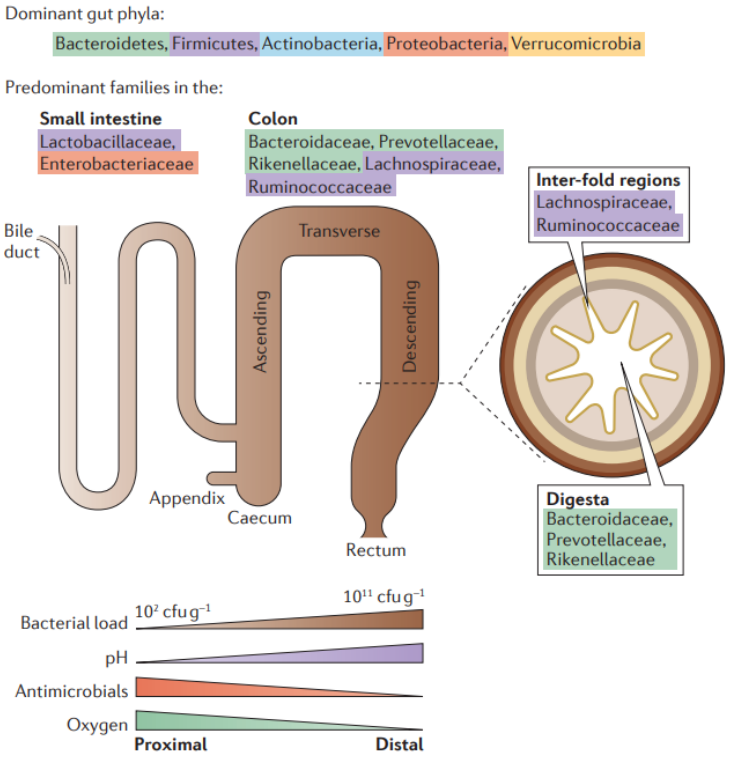

Figure 6. Physiological and biochemical differences across the SI and the LI, and the location of bacteria in the gastrointestinal tract.

Taken from [184] with permission obtained from Springer Nature and the Copyright Clearance Centre.

Commensal bacteria constitute complex microbial communities in the SI and LI and microbial composition and diversity of species not only varies and between individuals but also across specific anatomical regions of the intestine[174]. In this regard, the colon contains a rich diversity of anaerobic species (Figure 6), particularly in the caecum[165]. The phyla that predominate in the LI include Bacteroidetes, Proteobacteria, Actinobacteria, Proteobacteria, Firmicutes and Verrucomicrobia (Figure 6)[165,184]. In contrast, the SI is typically acidic with a higher oxygen content and contains more secreted antimicrobial factors that do not favour bacterial colonisation (Figure 6)[14]. The SI primarily harbours bacteria from Lactobacillaceae as well as

Enterobacteriaceae families (Figure 6)[14,165,185]. Studies in mice have shown that the Lactobacillus genus dominates the SI, reflecting the biochemical and physiological environment of the SI for their colonisation, whereas anerobic families Lachnospiraceae, Bacteroidacea, Prevotellaceasa, Rickenellaceae and Ruminococcacea dominate the LI[186]. In addition, there is transverse spatial distribution of bacteria in the LI (Figure 6) where microbes are kept away from the epithelium due to the presence of the mucus layer[184,187]. In the colon, the mucus is divided into a loose outer layer, which provides a habitat for the gut microbiota, and a more stratified inner layer preventing the majority of bacteria to make contact with the epithelial surface (Figure 7c)[14]. Studies in mice have shown that *B. fragilis* can pass through the mucus layer and reside within intestinal colonic crypts[188-190]. Microbes residing in the outer mucus layer may exert different biological functions than those of the same species located in the lumen[187].

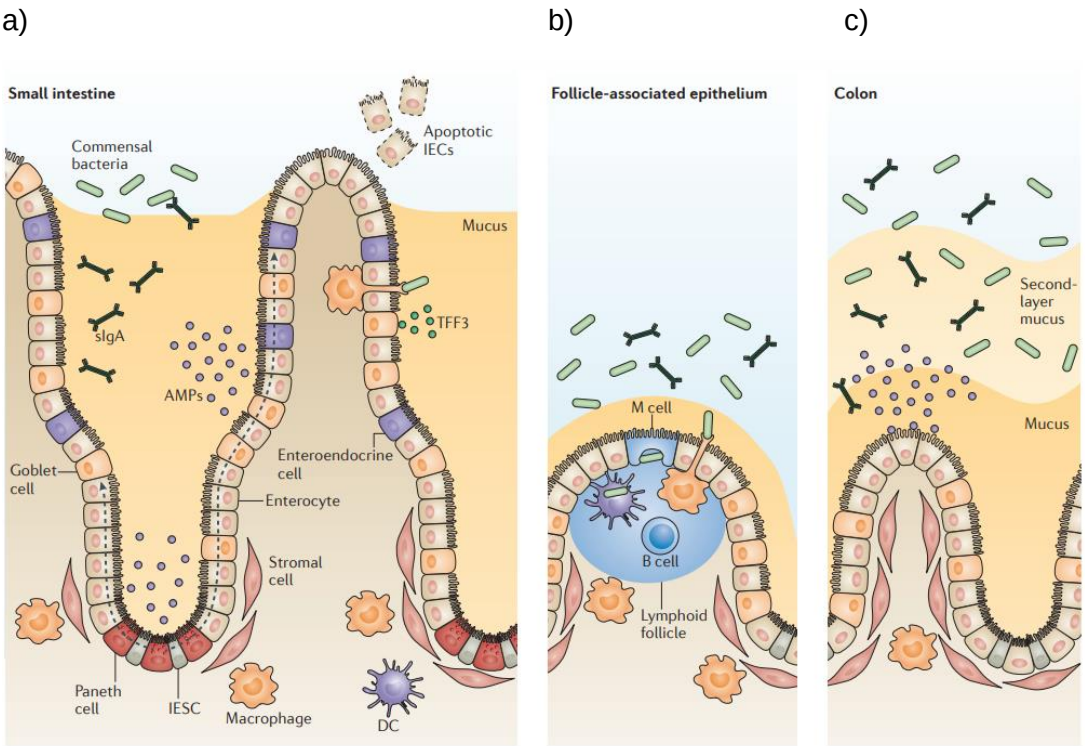

Figure 7. Structure of the epithelial barrier and mucus layers of the SI and LI.

(a) SI containing a loose mucus layer where IEC secrete AMP to limit bacterial numbers in the epithelial region. Intestinal epithelial stem cells (IESC) move up the villi until they are excreted. (b) Example of a lymphoid structure found in gut-associated lymphoid tissue (GALT), such as macroscopically visible peyers patches (PP), that contains a lymphoid follicle harbouring immune cells. The FAE contains microfold cells (M-cells) that aids transportation of antigen from the lumen to underlying innate immune cells including DCs facilitating the sensing of antigen. (c) In contrast to the SI, mucus in the colon is thicker and contains two mucus layers. AMP are also secreted. TFF3, trefoil factor 3. sIgA, secretory IgA. Also see 1.2.3 and 1.2.4. Taken from [191] with permission obtained from Springer Nature and the Copyright Clearance Centre.

Several intrinsic host factors influence microbial composition[191]. In the SI, antimicrobials including α-defensins, REGIIIγ, LPS-binding protein and lysozymes are produced and secreted into the intestinal lumen by Paneth cells (Figure 7)[14,184,192,193]. Many of these molecules are cationic peptides that limit the number of bacteria next to the epithelium through mechanisms such as disruption of the outer bacterial membrane via enzymatic degradation[14,184,192,193]. These secretions are not concentrated in the lumen but typically remain in mucus[14]. Microbes must also resist reactive oxygen species (ROS) including those produced by the host epithelium, however, many bacteria harbour genes for enzymes that contribute to bacterial resistance against ROS[184,194]. Nevertheless, the decrease in secreted AMP from the SI to the LI (Figure 6) influences bacterial diversity and the location of bacteria throughout the intestine[14,190]. Further, IgA secreted into the intestinal lumen resulting from an adaptive immune response also has an influence on microbial composition[14,195]. IgA are found in abundance in the intestinal mucus of mice (Figure 7) which can bind to certain bacteria helping limit their attachment to the epithelium and reducing bacterial motility in the mucus which facilitates their expulsion from the intestine. [196,197].

In addition, the composition of the microbiota[190,198] can be influenced by lifestyle factors[174,184,199-201] including diet and nutrition[171,199]. For example, bacterial diversity in human faecal samples was shown to be significantly altered by both short-term plant and animal-based diets[200]. Human diets high in non-digestible dietary fibre has a major impact on faecal microbial content[14,202]. Further, fibre content as well as galactooligosaccharides have also been shown to modulate bacterial diversity as determined in faecal samples of mice[203]. Moreover, individual dietary components can be important, for example, mice fed dietary emulsifiers led to alterations in bacterial composition in the gut[204]. Other environmental factors including age, smoking, exercise, household conditions are also thought to shape microbial composition in the gut[205,206].

Many bacterial species can break down specific PSs, however, *Bacteroides spp.* have been described as 'generalists' as they harbour the highest number and largest diversity of PS-degrading enzymes[14,184]. The repertoire of enzymes available to bacteria can prove advantageous in times of nutrient depletion, by expanding the range of carbohydrates they can degrade and utilise[14]. Notably, bacterial phyla including Firmicutes and Bacteroides in the LI undergo fermentation of dietary non-digestible carbohydrates that lead to the production of SCFA (including propionate, acetate and butyrate) which are suggested to be important for human health and gut

physiology including immune and/or metabolic functions within the gut [14,207]. For example, butyrate is reported for its anti-cancer properties and its ability to improve gut barrier function[178,208-210].

Further, complex O-linked glycoproteins such as MUC2 found in intestinal mucus are another available carbohydrate source available to bacterial for energy and also function as adhesion sites[14,211]. Adhesion of bacteria to mucus and the epithelium is important for their colonisation and formation of microbial communities[184]. This has been extensively studied in pathogenic bacteria, however, commensals can compete against pathogens for colonisation on the epithelial surface[184]. Studies using *Lactobacillus* species have demonstrated important roles for bacteria-derived molecules such as EPS and cell-surface adhesins (mucus bind proteins [MUB][212]) in their colonisation and adherence to mucus and the epithelium. Therefore, mucus also contributes to shape microbial composition in the intestines.[91,184,212,213].

Alteration of the gut microbiota has been associated with several noncommunicable diseases and physiological conditions including cardiovascular disease, cognitive impairment (e.g. Parkinson's and Alzheimer's), allergy, type II diabetes and some cancers (e.g. colon, prostate or liver)[214]. Moreover, much work has been centred around inflammatory bowel disease (IBD) which is believed to be attributed to a number of factors including genetics[215], environment and lifestyle (e.g. diet)[216] and dysregulation of the immune system[217]. These perturbations or imbalances of the gut microbiota are often referred to as dysbiosis[217]. Dysbiosis is commonly defined as "a compositional and functional alteration in the microbiota that is driven by a set of environmental and host-related factors that perturb the microbial ecosystem to an extent that exceeds its resistance and resilience capabilities"[217]. It is difficult to clearly define a healthy gut microbiota composition across the GI tract due to the heterogeneity between individuals and the methodological limitations in metagenomic studies[14]. However, a healthy microbiota generally incudes a rich bacterial diversity and a capability to regress from a perturbed state back to the original condition[217]. There is clearly inter-individual diversity of the gut microbiome in healthy subjects[174], and age and geographical location can also influence this composition[218]. Further, it is speculated that multiple "states" exist for both healthy individuals and those with dysbiosis, which may be influenced by environmental factors such as diet and antibiotics[201,217]. However, a clear cause and effect for dysbiosis and disease is not yet verified[219].

1.2.3. Structure and function of the intestinal epithelial barrier

The intestinal tissue is made up of the serosa, layers of smooth muscle, submucosa, mucularis mucosa and mucosa (the latter 3 are shown in Figure 8)[165,220]. The mucosa harbours the lamina propria (LP) which is a thin layer of loose areolar connective tissue that provides structural support for villi, blood supply, lymphatic drainage systems and nerve supply[165]. Notably, the LP and epithelium harbour most cells of the innate and adaptive GI immune system including DC (dendritic cells), macrophages, T cells and B cells that are critical for intestinal immunity and homeostasis (Figure 8, also see 1.2.4.2 and 1.2.4.3)[165]. Importantly, the mucosa is covered by a continuous monolayer of several IEC (intestinal epithelial cell) types, mostly enterocytes, constituting the epithelium (Figure 8)[221]. IEC are joined together by tight junction proteins including occludins, claudins and junctional adhesion molecules which maintain monolayer integrity[221]. The epithelium forms a physical and biochemical barrier that helps separate the intestinal mucosal immune system from the luminal contents of the gut including a multitude of commensal microorganisms[191], thereby limiting luminal contents from contact with the intestinal immune system[222].

The epithelium and LP are functionally and compositionally distinct and can differ throughout the intestine (Figure 8)[165]. It was previously proposed that the human intestinal epithelium covered a surface area of 260 - 300 m^2 due to the presence of villi and microvilli, however it is now considered to be 32 m^2 [164,223] where the LI accounts for only 2 m^2 of this area[223]. The intestinal epithelium is characterised by small invaginations known as crypts (crypts of Lieberkühn) which are located between the villi in the SI and distributed between flat areas of the epithelium in the LI (Figure 8)[220]. At the bottom of the crypts, multipotent stem cells differentiate into several types of IEC, including enterocytes that facilitate the absorption of nutrients[164], however, Paneth cells, neuroendocrine cells, and goblet cells, among other cell types are also present (Figure 8)[165]. Goblet cells are mostly responsible for the secretion of mucins as well as production of AMP[191]. Another important IEC are Paneth cells that primarily reside in the ileum also producing antimicrobial peptides (AMPs) that help maintain the crypt sterile[220]. Excluding Paneth cells which migrate downwards, other mature IEC's move upwards towards the tip of the epithelium where they are excreted into the lumen after 4-5 days (Figure 7a)[165]. Notably, IEC play a role in the gastrointestinal immune system which is further discussed in 1.2.4.1.

Supporting the IEC barrier is the mucus layer (Figure 8) comprising > 80% carbohydrates with MUC2 being the most prominent mucin in the intestine[224,225]. In the SI, a loose mucus layer (Figure 8) has been characterised in rodent models[226]. In contrast, the colon has two layers (Figure 8); an inner mucus layer that is attached to IECs and ~50 μm thick (in mice); and an unattached layer ~100 μm thick similar to that in the SI[165,226]. The mucus layer in the colon is substantially thicker compared to the SI[227]. Mucus acts as a strongly charged gel which confers its antimicrobial properties, and aids in the prevention of noxious or toxic substances reaching the epithelium[228]. Mucus also contains AMPs, IgA antibodies and other proteins that protect the epithelium from bacterial colonisation[165,191,229]

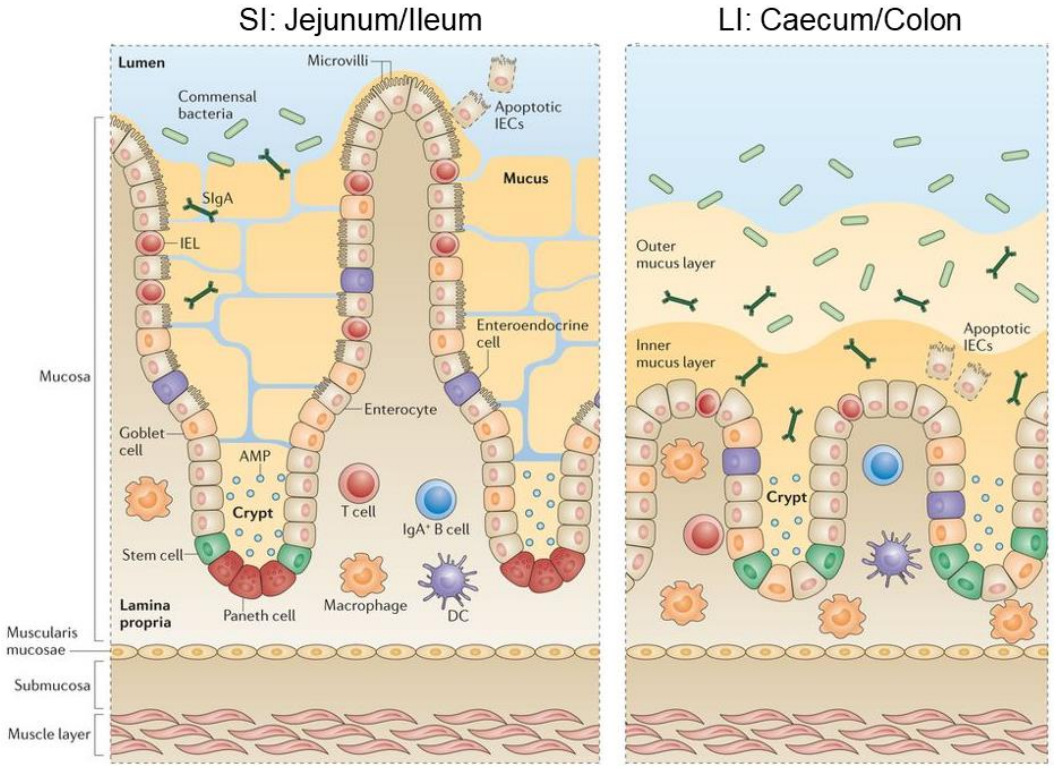

Figure 8. Structure and cellular composition of the epithelium and underlying LP of the small and large intestine

The small and large intestine (SI and LI, respectively) are covered by a single monolayer of intestinal epithelial cells (IECs) including Paneth cells, goblet cells, enteroendocrine cells and micro-villi containing enterocytes. The SI harbour villi but these are not present in the LI. The underlying LP, part of GALT (see 1.2.4.2) harbours many immune cells important for intestinal immunity and gut immune homeostasis. Notably, the LI has 2 layers of mucus whereas the SI has one loose layer. The mucus layer helps limit luminal content from reaching the epithelium and underlying LP. The LP harbours many of the GALT's innate and adaptive immune cells including DC, macrophages, T cells and B cells that are important in intestinal immunity (also see 1.2.4.2 and 1.2.4.3). AMP, antimicrobial peptide. IEL, intraepithelial lymphocyte. Taken from [165] with permission obtained from Springer Nature and the Copyright Clearance Centre.

1.2.4. The gastrointestinal immune system

1.2.4.1. Intestinal epithelial cells

In addition to the epithelium acting as a physical and biochemical barrier, IEC contained within this monolayer also have immunomodulatory roles[191,230]. IEC are capable of secreting immunomodulatory molecules that can interact with the underlying immune cells of LP such as DCs[19,191].

Chemokines and cytokines help control intestinal immune homeostasis and inflammation[231]. For example, chemoattractant molecules such as chemokine monocyte chemoattractant protein 1 (also termed CCL2 [MCP-1]), CXCL8 (IL-8) induce chemoattraction of DCs/macrophages and neutrophils, respectively, and secretion of IL-6 and TNF-α can lead to proinflammatory effects such as inducing the differentiation of T cell subtypes (for further details see 1.2.4.2.)[232,233].

Notably, IECs produce cytokines and chemokines in response to both pathogenic and non-pathogenic bacteria (Figure 9a)[191,231]. This can be through contact with the IEC apical side, internalisation by IEC, breaching the epithelial layer or directly interacting with TLR on IEC either on the apical (facing the lumen) or basolateral side (facing the LP)[19,232]. For example, pathogenic bacteria *Shigella flexneri 2a*/*Shigella dysenteriae*, *Salmonella enterica serovar Thyphinium* or *E. coli shiga* toxin 2 have been reported to induce IL-8, IL-18, and TNF-α expression, respectively, *in vitro*[231,234-236]. In contrast, the study from Wang and colleagues (2014) also showed that the cytotoxin of *E. coli subtilase* reduced IL-8 expression as well as MCP-1, highlighting the differences in immune responses to different bacterial toxins[231,234]. Other molecules derived from bacteria such as LPS have been shown to induce cytokine and chemokine responses of human IEC *in vitro* including IL-6, IL-8, TNF-α, IL-1β, IFN–γ, macrophage migration inhibitory factor (MIF) and MCP-1[237-240]. Further, commensal bacteria have been reported to induce IL-8, as well as TGF-β and TSLP, resulting in the induction of tolerogenic DC subtypes[231,241]. Moreover, the probiotic *Enterococcus facium* HDRsEf1 has also been reported to reduce IL-8 expression following pathogenic challenge *in vitro*[231,242]. These findings suggest that commensals and probiotics also have an immunomodulatory role through modulating IEC cytokine responses[231]. Importantly, cytokines and chemokines secreted by IEC interact with the underlying immune cells of the LP including DC and macrophages, among others, which consequently secrete their own cytokines and chemokines that interact with associated receptors on IEC inducing immunostimulatory effects, for example, AMP production[230]. In this regard, the

epithelial layer and underlying immune cells of the gut-associated lymphoid tissue (GALT) (see Section) have been described as a critical and complex communications network that help direct inflammatory responses to pathogens, inducing tolerance towards non-harmful microbes[230,231].

a)

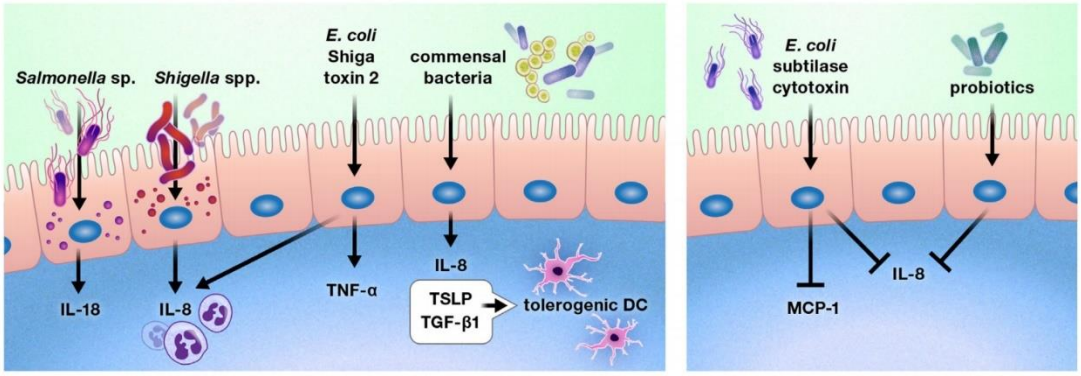

b)

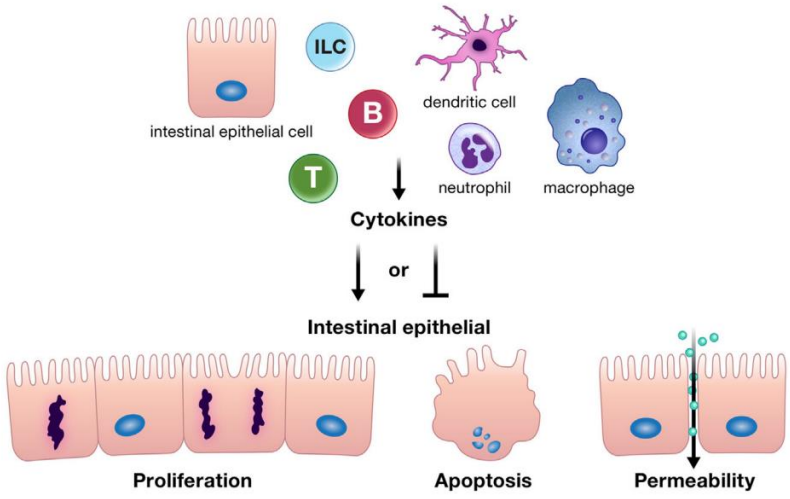

Figure 9. Cytokine and chemokine production by intestinal epithelial cells and their impact on the epithelium.

a) Examples of cytokine and chemokine responses to bacterial stimuli including pathogenic (including their toxins), commensal and probiotic bacteria. b) Effect of cytokine production by intestinal immune cells on IECs and barrier integrity. Taken from [231]. Images are licensed under Creative Commons Attribution 4.0 International: https://creativecommons.org/licenses/by/4.0/legalcode.

1.2.4.2. Gut-associated lymphoid tissue

Underlying the epithelium is the intestinal immune apparatus termed GALT which is formed of numerous lymphoid tissues and home to a dense population of innate and adaptive immune cells including DCs, monocytes, macrophages, T cells, and B cells, among others[243,244] (Figure 10). Importantly, cytokines secreted by these immune cells including DCs, macrophages and T -cells can impact the integrity of the epithelial barrier including through IEC proliferation or apoptosis, or by modulating monolayer permeability between tight junctions (Figure 9b)[231,245-250]. Therefore, this communication network is also responsible for maintaining the integrity of the epithelium[230,231]. For a comprehensive review on cytokine responses of IEC, see [232].

The GALT helps uphold the structural integrity of the GI epithelium and facilitates its immune function including protecting against invasion of exogenous materials and pathogenic or opportunistic microbes[243,244]. The GALT is the largest component of all mucosa-associated lymphoid tissue (MALT), and is regarded as one of the largest lymphoid organs in the body, as it is suggested to harbour ~70% of total lymphoid cells[243,244,251,252]. GALT includes the tonsils, adenoids, aggregates of lymphoid tissues (e.g. in the appendix, colon and oesophagus), and isolated lymphoid follicles (ILF) and peyers patches (PP) of the intestine (Figure 8)[243,253]. GALT in the SI and LI is responsible for many immunoregulatory functions including acting as induction sites for antigen sensing and presentation (PP being important induction sites in the SI)[165], initiating adaptive immune responses against pathogens, maintaining mature and naïve lymphocyte populations, and distinguishing between harmful and non-harmful antigens, for example, inducing tolerance towards commensal microbes[165,243,254,255].

PPs are aggregated lymphoid follicles that can be found in the jejunum but are primarily found in the LP of the ileum and are the most well-characterised structure of GALT (Figure 7b) [165,243,256,257]. Overlying the PPs (and ILfs) is the follicle associated epithelium (FAE)[243]. Here, microfold cells (M cells) have a highly phagocytic capacity and specialise in the uptake and transcytosis of luminal contents and are important in the immunosurveillance of luminal antigen including microbes (Figure 7b)[165,258,259]. Further, murine PPs harbour adaptive immune cell populations including many B cells and smaller amounts of T cells as well as innate immune cells such as DCs, macrophages and neutrophils[256].

T cells are important adaptive immune cells that can also be found in the LP (Figure 8)[165,260]. These cells play a role in inflammatory responses to pathogens, anti-inflammatory responses to non-harmful microbes and maintaining intestinal immune

homeostasis (Figure 10)[165]. Moreover, naïve $CD4^+$ T cells reside in the PP, however they are the most abundant type of T cell in the LP[261-263]. These cells can undergo differentiation into further $CD4^+$ T cell subtypes important for intestinal immunity via the action of DC and macrophages in response to microbial stimuli (Figure 10). $CD4^+$ T helper 17 (Th17) cells play an important role in immunity of the mucosa by producing proinflammatory cytokines IL-17A and IL-22, and among several functions can recruit neutrophils and stimulate production of AMP to help fight pathogens[261,262]. Further, CD4+ Th1 cells are crucial for the immune response to some viruses and pathogenic bacteria[263]. In contrast, CD4+ T regulatory (T reg) cells are critical for intestinal immune regulation, as they have an ability to dampen Th17-mediated inflammation and promote anti-inflammatory responses such as secretion of IL-10 (Figure 10)[261,264,265]. Interestingly, induction of T reg cells are reported to involve the commensal gut microbiota[190,266,267] with Forkhead box P3 (Foxp3) cells being an important T reg cell subset in the intestine for maintaining immune homeostasis[261,265,267].

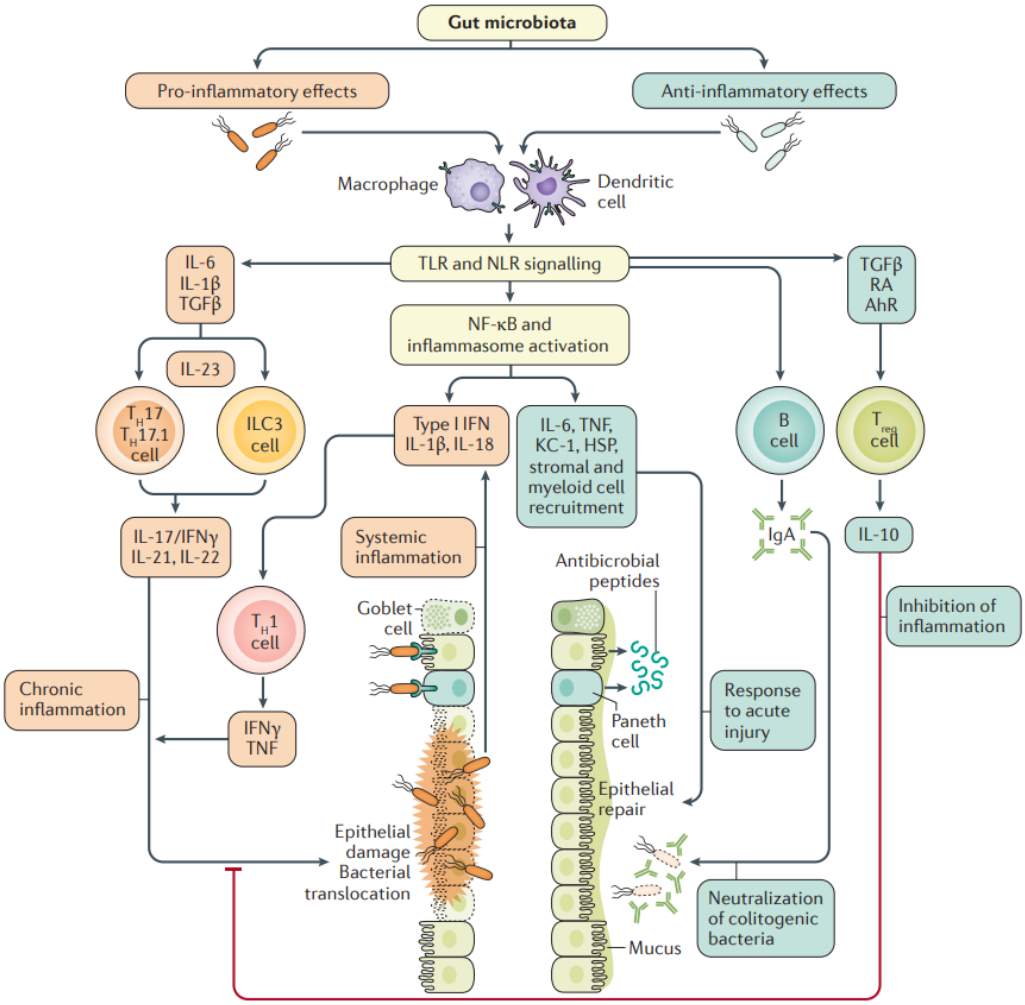

Figure 10. T cell responses induced by the gut microbiota

In the intestine, harmful and non-harmful bacteria can induce proinflammatory or anti-inflammatory responses, respectively. These effects can be via microbial activation of Toll-like receptors (TLRs) (see 1.2.5.1.) or Nod-like receptors (NLRs) on antigen presenting cells (see 1.2.4.3.). This can lead to downstream secretion of immunomodulatory molecules that can induce T helper 17 (Th17) and T helper 1 (Th1) cells which drive inflammation and the clearance of pathogens. This response can also lead to damage to the epithelium and other effects that can lead to chronic inflammation. In contrast, T reg cells can also be induced by certain commensal microbes (e.g. B. fragilis[190]). This leads to T reg cell induction through secretion of immune molecules including TGF-β and retinoic acid (RA) by DCs (see 1.2.4.3.2.) that produces anti-inflammatory cytokine IL-10 leading to suppression of inflammatory responses. Other anti-inflammatory effects include the repair of the epithelial barrier and increased production of antimicrobial peptides. Further, the induction of B cells leads to IgA secretion that positively acts on colitogenic bacteria (capable of inducing colitis). IL, interleukin. Taken from [264] with permission from Springer Nature and Copyright Clearance Center.

1.2.4.3. Antigen presenting cells

Antigen presenting cells (APCs) encompassing DCs and macrophages are found in GALT such as the LP, PPs and IFLs of the intestines[268]. Together, they play a key role in gut immunity, inflammation and tolerance including sampling antigen from the lumen and from M-cells, presenting antigen to T cells and B cells, secreting pro- and

anti-inflammatory cytokines and carrying out phagocytosis of invading microbes[229]. The primary areas for the induction of adaptive immune responses in the intestine - such as T cell and B-cell priming by DCs and macrophages - are the lymphoid structures of the GALT including PP and draining lymph nodes (e.g. mesenteric lymph nodes)[165,259].

Most information on mononuclear phagocyte subsets has been acquired from the study of mouse models[269]. The characterisation of subpopulations of intestinal DCs and macrophages is highly complex partly due to the diverse cell surface markers for their identification and as they share similar phenotypic traits[268]. For a recent review, see [270].

1.2.4.3.1. Intestinal macrophages

Macrophages are an abundant cell type across the LP of the GI tract important for immune homeostasis[271] where they play key functions including the clearance of local bacteria and cell debris, cytokine secretion, and the stimulation and maintenance of T cells[268]. Although similar to DCs, mouse macrophages are best identified by their expression of cell surface markers CX_3CR_1, F4/80 and CD64, however, different subsets can express CD11b or CD11c. The expression profile of macrophages has been shown to be highly diverse across a range of tissues in mice[268,270,272].

In the steady state, macrophages display a strong phagocytic function if invaders breach the epithelial layer despite their well-known anti-inflammatory profile[232,268,273]. Acquisition of their anti-inflammatory characteristics occurs after their differentiation from monocytes in the intestine such as in the LP of the colon, which includes a characteristic IL-10-producing capability[268,274].

Under non-inflammatory conditions and after microbial stimulation, Toll-like receptors (TLRs), a PRR that recognises bacterial LPS (see section 1.2.5.1.)[275], expression by gut macrophages is low, therefore, the production of pro-inflammatory cytokines such as IL-6, TNF-α, IL-1 and IL-23 and nitric oxide is low or non-existent as is their ability to induce an strong oxidative burst[232,273,276]. Alternatively, macrophage-derived IL-10 is suggested to be critical in maintaining T reg cell populations, and immune regulation in the colon heavily relies on IL-10 recognition by macrophages (Figure 11)[268,277]. Moreover, gut macrophages in a TGF-β-rich environment can also induce, maintain, and expand anti-inflammatory FoxP3 T reg cells which can secrete IL-10 which in turn influence macrophage function and this is suggested to partly explain

intestinal macrophages' specific tolerance towards commensal microbes in the gut[232,278,279].

During inflammation, inflammatory-type macrophages arise from Ly6C$^+$ monocytes and become more abundant than resident macrophages with anti-inflammatory profiles[268,280,281]. Ly6C+ monocytes upregulate expression of PRRs [see 1.2.5.]) TLR2 and NOD2 resulting in the development of inflammatory macrophages that induce proinflammatory molecules such as IL-6 and IL-23 and upregulate TNF-α expression[268,280,281]. However, it should be noted that TNF-α has both immunostimulatory and immunosuppressive effects[280,281]. Along with the action of DCs, it is thought that secretion of proinflammatory cytokines by activated macrophages in the inflammatory state can lead to T cell responses to help deal with pathogenic invasion in the event of barrier disruption (Figure 11)[232]. It is unclear which factors influence macrophage differentiation and function across different areas of the gut, however it is suggested that IECs may be involved through their secretion of cytokines and chemokines including thymic stromal lymphopoietin (TSLP) and TGF-β[268,282].

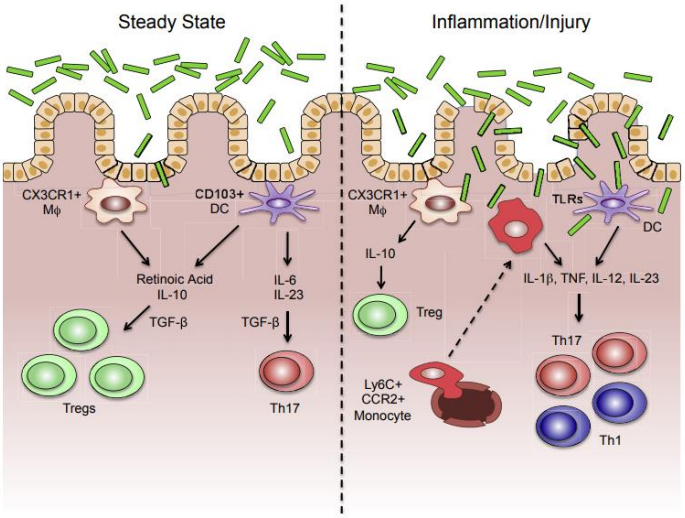

Figure 11. Immune responses of intestinal macrophage and DCs in the steady and inflammatory state.

IL, interleukin. Mϕ, macrophage. Th, T helper. Taken from [232] with permission from Elsevier and Copyright Clearance Center.

It has been proposed that trans-epithelial dendrites (TEDs)[283] on mononuclear phagocytes could reach out through the epithelium of the SI LP into the intestinal lumen and directly sample antigenic content[268,284]. However, often subsets such as CX_3CR1+ macrophages or DCs have been proposed to perform this function[259,285], although more work is required to distinguish between DCs[268,285,286].

Intestinal macrophages expressing CX_3CR_1 have also been implicated with wound healing of the epithelium, and may also influence barrier permeability through their production of nitric oxide and IL-6 that may exacerbate pathogen invasion[268,287]. In line with this, barrier dysfunction by inflammatory macrophages, through their direct communication with IECs has also been reported recently *in vitro*[288].

1.2.4.3.2. Intestinal dendritic cells

In contrast to macrophages, intestinal DCs are the primary innate immune cells in the intestinal LP responsible for inducing adaptive immune responses to foreign antigens through the priming of naïve T cells[268]. They also play a role in immune tolerance towards the microbiota and are capable of secreting both pro- and anti-inflammatory molecules[232,268,289,290]. DCs predominantly express high levels of CD103, CD11c and MHC class II and can express CD11b [165,291-295]. More recently, CD24, among other markers, has been proposed for their discrimination from macrophages[165,268,270,291-295]. Most studies that identify markers on DCs have been performed in mice, however investigation of human DC subsets is more complicated are not always comparable with mice[269,296]. Nevertheless, 3 main murine DCs subsets have been described in the literature: $CD103^+$ $CD11b^-$, $CD103^+CD11b^+$ and $CD103^-$ $CD11b^+$ $CX3CR1^+$ and the distribution of these subsets across the intestines cells are not uniform[198,296]. However, the LP, MLNs and PPs are home to $CD103^+$ DCs where $CD11b^-$ predominantly reside in the PPs and ILFs, and LP of the colon; and $CD11b^+$ are found in the LP of the SI[198].

DCs are important in mediating adaptive immune responses[268]. In the steady state, DCs can be passed antigen from M-cells and goblet cells[259,297,298]. It is also proposed that DCs are able to extend across the epithelium to sense antigen in the lumen but this mechanism remains controversial, as macrophages expressing CD11c, MHCII and CXR_3CR_1 markers may be responsible as previously described[259,268]. However, direct capture of antigenic material across the epithelium by CD103+ DCs has been reported[268,299]. DC uptake of foreign material such as bacteria and food antigens results in their migration to the MLNs leading to antigen presentation to T cells which influence adaptive immune activation or induce tolerance through the generation of inflammatory or regulatory T cells, respectively[198]. The role of DCs in intestinal immune tolerance is critical[268,300]. For example, their secretion of TGF-β and retinoic acid promote proliferation of Foxp3+ T reg cells from naïve $CD4^+$ T cells that helps control intestinal immune homeostasis[300]. In an inflamed gut, DCs residing in intestinal tissue enhance Th17 and Th1 responses that help fight invading microbes through DC (and macrophage) secretion of proinflammatory cytokines such including

TNF-α IL-1β and IL-23 in response to microbial TLR stimulation (Figure 11)[232]. Conversely, in the healthy state, DCs ($CD103^+$) can induce microbial tolerance through T reg cell induction via their production of retinoic acid (RA) and IL-10 yet can still produce proinflammatory cytokines including IL-6 and IL-23 in response to pathogenic microbes, leading to elevated Th17 cell responses dependent on TGF-β (Figure 11)[232,290,301-303].

TGF-β, RA and IL-10 production by DCs can occur in the LP and at the MLNs which leads to proliferation of Foxp3+ T reg cells and help induce plasma B cells leading to secretion of IgA[268,300,304]. Interestingly, it was recently shown that purified mucin induced IL-8 production in human monocyte-derived DCs, suggesting a pro-inflammatory role for intestinal mucins in gut barrier function. Immunomodulation by microbe-associated cell-structures and secreted factors such as PS and SCFAs can also occur through interaction with DCs[141,296,305,306].

The intestine also harbours follicular DCs in the germinal centres and lymphoid follicles of the GALT. These have a unique phenotype manifesting long dendrites which are important in driving IgA responses[261]. Moreover, intestinal plasmacytoid DCs found in the SI[165] can help induce IgA production[261,307]. Further, microbe-stimulated "TNF and inducible nitric oxide synthase (iNOS)-producing (TIP) DCs"[261] can secrete TNF-α/nitric oxide synthase which is thought to influence secretion of IgA by plasma B cells[261,308].

Overall, DCs and macrophages as APCs function in a highly complex environment communicating with other immune cells and act as gut sentinels which help to control the balance between immune activation and tolerance towards the gut microbiota, pathogens and dietary antigens[232,268].

1.2.5. Structure and function of pathogen recognition receptors.

PRRs (Figure 12) are one of the key players in innate immunity and critical for sensing microbes and initiating immune responses[309]. This recognition is mediated by binding to pathogen associated molecular patterns (PAMPs) – typically membrane-associated protein, carbohydrate or lipid-derived structures [309]. PRRs can be found on large variety of innate and adaptive immune cells including macrophages, monocytes, DCs and T cells[309].

The following describes the function of two well-known PRRs: Toll-like receptors (TLRs) and C-type lectin receptors (CLRs) and their association with intestinal immunity.

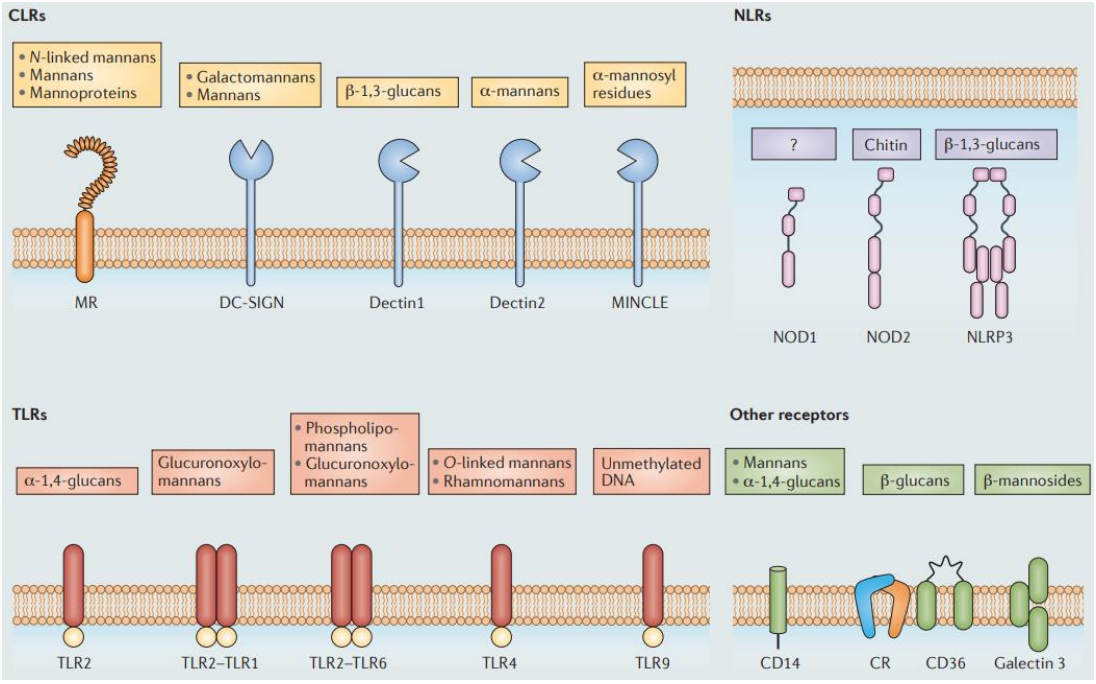

Figure 12. Examples of PRRs found on immune cells and their corresponding carbohydrate ligands from fungi.

TLRs, Toll-like receptors. CLRs, C-type lectin receptors. NLRs, Nod-like receptors. Taken from [117] with permission from Springer Nature and Copyright Clearance Center.

1.2.5.1. Toll-like receptors

TLRs can be classed into 2 categories; intracellular TLRs which include TLR3, TLR7, TLR8, TLR9 TLR11, TLR12 and TLR13; and cell surface TLRs including TLR1, TLR2, TLR4, TLR5, TLR6 and TLR10 (see Figure 12 for examples of cell surface TLRs including TLR2 heterodimeric complexes[310])[311]. TLR1 to TLR9 and TLR11 to TLR13 can be found in mice while humans harbour TLR1 to TLR10[311]. Cell surface TLRs are a family of transmembrane proteins[312] which recognise many PAMPs derived from gram-positive and gram-negative bacteria abundantly present in the gut[198]. Notably, bacterial cell surface structures flagellin and lipoteichoic acid are ligands of TLR5 and TLR2, respectively while LPS is recognised by TLR4. TLRs are the best-characterised PRRs and bind to a diverse range of microbial and host-derived ligands that help initiate and control intestinal immune responses[198,312].

TLR4 is expressed by immune cells including macrophages, monocytes and DCs[312] as well as IECs[313], among others[312]. TLR4 recognises bacterial LPS (Figure 13), among other host-derived and exogenous ligands[312] and is one of the best studied TLRs[314]. LPS is one of the most well-known TLR4 ligands, however its recognition relies on other key factors. Lipid binding protein (LBP) is secreted into the intestinal lumen by Paneth cells (and is found in serum) and interacts with LPS from both

pathogens and commensals and, therefore, plays a role in the maintenance of intestinal immunity[131,315]. Further, LPS is cleaved by from intestinal bacteria by lipid transferase[131]. LBP transfers LPS to CD14 which facilitates binding to myeloid differentiation factor (MD-2) on the cell surface that associates with TLR4 forming a heterooligomeric TLR4/MD-2 complex (Figure 13)[132]. It has been reported that CD14 may not be strictly required for LPS-binding to TLR4/MD-2[316]. Nevertheless, lipid A is primarily responsible for recognition by TLR4/MD-2 on innate immune cells. LPS-binding to TLR4/MD2 leads to the upregulation of > 10^3 genes[132,243,312], and TLR4/MD2 is well-known to associate with adaptor molecules MyD88 or TRIF/TRAM which induces transcription factor NF-κB[132,243,312] resulting in the production of interferons or cytokines including IL-6, TNF-α and IL-1β leading to initiation of an immune response[132,243,314,317,318].

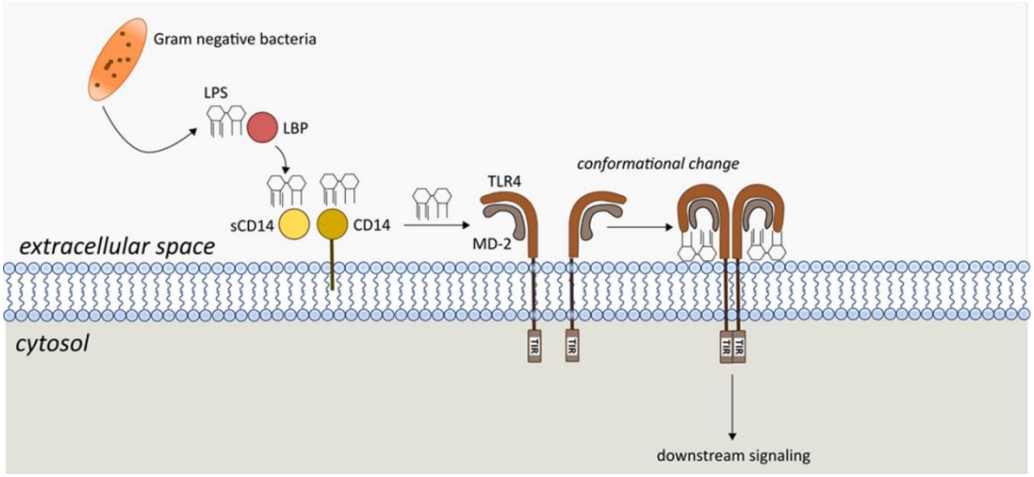

Figure 13. Lipopolysaccharide recognition by the Toll-like receptor-myeloid differentiation protein complex 2.

Taken from [131] Article is under the Creative Commons Attribution-Non-commercial-No Derivatives License (CC BY NC ND). Image licence: https://creativecommons.org/licenses/by-nc-nd/4.0/legalcode. LBP, lipid binding protein. TLR4, Toll-like receptor 4. MD-2, Myeloid differentiation protein.

The low : high ratio of LPS endotoxicity (degree of ability to induce an immune response) can differ between bacteria[131,319]. A large amount of intestinal high-endotoxic LPS may induce Th17 or Th1 responses to enhance inflammation. Alternatively, an abundance of low-endotoxic LPS may induce tolerogenic response including T reg cells or suppress Th17/Th1 responses[131,319], although this needs further work. LPS can be found on both non-pathogenic and pathogenic microbes[243] that are abundant in the gut[198]. The recognition of these molecules by TLRs help in

the fight against pathogenic bacteria, however, they may also play a role in tolerance towards commensal microbes[131,198]. Further, TLR4 has been suggested to play a role in DC tolerance[320-322]. TLR4 is also thought be involved in maintaining intestinal barrier integrity and inflammation particularly in response to bacterial LPS[323-325]. However, very little is known about the role of TLRs in intestinal immune homeostasis with regards to food antigens [221,324].

In addition to TLR expression by immune cells, TLRs are also found on IECs and play a role in the sensing of pathogenic and commensal microbes via their cell surface structures including LPS by TLR4 (further examples from fungal carbohydrate ligands are shown in Figure 12)[19,117]. The control of intestinal immune homeostasis to microbial stimuli is facilitated by the polarised expression of TLRs that can be expressed internally or on the apical or basolateral IECs[19,326]. For example, induction of apical TLR9 can have an overall inhibitory effect on the immune response through IκB stabilisation whereas basolateral TLR activation of IECs activates NF-κB leading to the production of pro-inflammatory cytokines including IL-6, IL-8 and TNF-α as well as chemokines and AMPs[19,326].

A recent study showed TLR expression on IECs across the SI and LI[313]. Apical expression of TLR2, TLR4 and TLR5 was considerable in the colon (Figure 14)[313] whereas there was virtually no expression of TLR2, TLR4, TLR5, TLR7 and TLR9 in the SI, and TLR5 being primarily expressed by Paneth cells[313]. Intracellular TLR4 was also found in colonic IECs[313]. The authors suggested that IECs have a unique ability to sense luminal and transcytosed microbes. Further, upon stimulation of organoids by TLR ligand flagellin, NF-κB-associated proinflammatory cytokine expression was upregulated including TNF-α, however this appeared restrictive to flagellin (a TLR5 ligand[327])[313]. This extensive study provides novel insights into IEC relationships with gut microbes[313], however, the exact role of TLR polarisation and their differential expression across the GI tract as well as their response to different microbial stimuli is not yet fully elucidated.

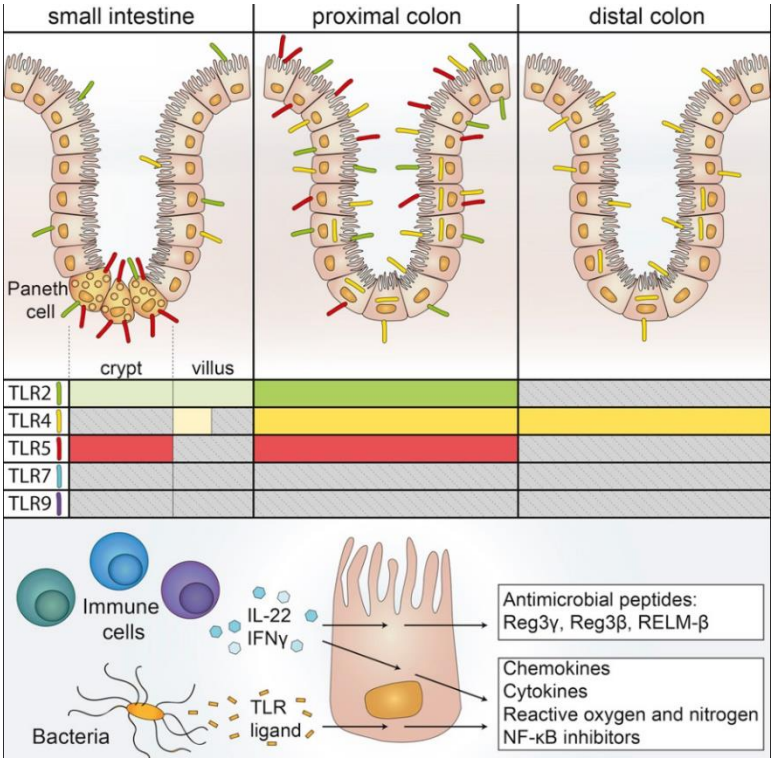

Figure 14. TLR expression in mouse intestine and examples of immune responses by intestinal epithelial cells in response to TLR ligands.

IL, interleukin. TLR, Toll-like receptor. For further details on IECs see 1.2.3. and 1.2.4.1. Taken from [313] with permission from Elsevier and Copyright Clearance Center.

1.2.5.2. C-type lectin receptors

The CLR superfamily covers over 1000 C-type lectin proteins defined by the presence of at least one C-type lectin domain (CTLD)[328,329]. CTLD are conserved protein motifs[330], however fold variability exists including among domains responsible for carbohydrate and Ca^{2+} binding. CLRs are well known for their ability to bind sugars including a broad range of carbohydrate ligands found on pathogens[328,331], however not all CTLD are capable of binding carbohydrates or Ca^{2+} [332]. CLRs are classified into 17 different subgroups based on their domain types and phylogeny. Some examples of CLRs in fungal immunity and their ligand specificities are presented in Figure 12[328,331]. CLRs generally bind carbohydrate ligands including specific amino acid sequences in the carbohydrate recognition domains (CRDs)[328,333]. The EPN (Glutamic acid, proline and asparagine) and QPD (Glutamine, proline and aspartic acid) amino acid motifs recognise mannose and galactose-structures[328,333,334], respectively, in a Ca^{2+}-dependent manner. However, CTLDs can also recognise non-carbohydrate ligands including lipids, inorganic molecules and proteins[328,333]. CLRs exist as secreted and transmembrane-bound

proteins; the latter are particularly important in many biological and cellular processes including immune responses[328]. CLRs are found on innate and adaptive immune cells and are important for the recognition of pathogenic or opportunistic microorganisms[335]. Upon recognition of carbohydrate ligands, CLRs initiate the immune response[335]. Here, we briefly cover CLR ligand binding interactions, intracellular signalling mechanisms, and discuss four well-known classes of CLRs Dectin-1, DC-SIGN, SIGNR1 (mouse homologue of human DC-SIGN) and Dectin-2, and their role in immunity focusing on their possible roles in the intestine.

1.2.5.2.1. Molecular mechanisms of CLR-ligand interactions

CTLD-containing CLRs make up a superfamily of animal proteins with many diverse biological functions[333]. CTLDs contain a double loop structure harbouring, at the bottom of the loop, disulphide bridges to maintain stability and highly conserved polar and hydrophobic interactions[333]. The 'long loop region' forming the second loop is not present in a number of CLRs, however it is responsible for Ca^{2+}-dependent carbohydrate binding to CLRs[333]. The carbohydrate binding ability of CLRs can involve multiple mechanisms including hydrogen bonding and hydrophobic interactions[336].

Ca^{2+}-dependent carbohydrate ligand binding to mannose- or galactose specific CLRs occurs through a highly conserved CRD located in the CTLD[337]. Binding to a carbohydrate structure is facilitated by interaction with a single calcium ion: hydrogen bonds form between carbonyl structures located in the CRD and the calcium ion; and the calcium ion directly forms hydrogen bonds with the carbohydrate ligand[337]. Dectin-2 is an example of a Ca^{2+}-dependent CLR that binds mannose residues[338]. A recent study by Feinberg, et al (2017) showed using competitive solid-phase binding assays that Dectin-2 had a particularly high affinity for mannose disaccharides containing α-(1,2) and α-(1,4) linkages, with mannose monosaccharide and α-(1,6) and α-(1,3) linked mannose disaccharides with modest affinity[339]. Further, analysis by glycan array suggested that the predominant target for mannose oligosaccharide binding by Dectin-2 is the α-(1,2) linkage[339]. Protein crystallisation techniques identified a primary and secondary binding site on the CRD of Dectin-2 that enabled mannose-specific residue binding[339]. At the primary binding site, reducing end-mannose was found to ligate with Ca^{2+} through hydrogen bonding whereas the secondary binding site accommodated the non-reducing mannose of the oligosaccharide[339]. The mannose oligosaccharide used in the crystallisation analysis, which also comprised of two GlcNac units, contained two differing mannose trisaccharides, one containing α-(1,2) linkages only, and the other both α-(1,2) and

α-(1,3) linkages[339]. Both oligosaccharide sub-terminal mannose residues were accommodated by the primary binding site; coordination bonds with Ca^{2+} through their 3- and 4- OH groups as well as hydrogen bonding with four amino acid residues, the latter being also ligated to Ca^{2+} [339]. Interaction of 3- and 4- OH groups of the mannose residue with the CRD is also observed with other mannose-binding CLRs including DC-specific ICAM-grabbing non-integrin (DC-SIGN)[339]. Van der Waals interactions are also present between specific amino acid residues and Carbon 4 and 6 of mannose in the primary binding site [339]. For further details on the molecular interactions of Dectin-2 with its ligands see [339].

In contrast to many mannose-specific CLRs, Dectin-1's ability to bind to β-glucan is independent of Ca^{2+} [337,340]. Dectin-1 possesses one extracellular CTLD, and study insights into the molecular mechanism of β-glucan recognition by Dectin-1 generally considers the glucan binding site to be in a shallow groove of the protein (Histidine 221 and Tryptophan 223) and binding is facilitated by hydrophobic interactions[337,340]. Brown and colleagues (2007) confirmed that the involvement of metal ions was not required for β-glucan binding[340]. However, it has previously been suggested that binding to Dectin-1 required glucans comprising > 10 glucose units[340,341], yet it still may be possible that smaller glucans can bind but with weak affinity[340]. Further, Brown et al (2007) suggested that it was feasible the shallow groove could accommodate glucan binding including chains with > 10 glucose units[340].

1.2.5.2.2. C-type lectin receptor signalling

A diverse array of immune cells including DCs, macrophages and T cells contain cell surface receptors that are coupled to signalling molecules that help regulate signal transduction[329,342]. Many of these receptors harbour a conserved sequence (YxxL/I motifs divided by a distinct interval, YxxL/I-X_{6-8}-YXXL/I[342]) termed the immunoreceptor tyrosine-based activation motif (ITAM), or associate with subunits that contain this sequence[342]. ITAM is crucial for signal transduction in response to ligand binding in many receptors including some CLRs[329,342]. Upon CLR-carbohydrate ligand binding, CLRs elicit intracellular signalling, the context of which depends on their associated intracellular signalling motifs[337,343]. Some CLRs harbour an immunoreceptor tyrosine-based inhibitory motif (ITIM) to inhibit cellular activation, others have ITAM or hemi-ITAM (HemITAM) to initiate cellular activation[337,343]. In addition, some CLRs do not contain these motifs[337,343]. HemITAM CLRs, including Dectin-1, in their cytoplasmic tail, harbour a tyrosine residue within the YxxL sequence[337,344,345]. ITAM-coupled CLRs either associate with ITAM-bearing adapter

proteins, for example the Fc receptor γ (FcRγ) chain; or contain a characteristic ITAM motif as YxxL tandem repeats in their cytoplasmic domain[343,344,346]. Most CLRs in this group interact with FcRγ including Dectin-2, Mincle and the Mannose receptor (MR)[344].

CLR carbohydrate ligand binding induces the phosphorylation of ITAM (via tyrosine residues), which is mediated by Src family kinases, leading to these activatory CLRs with hemi-ITAM or ITAMs associating with spleen tyrosine kinase (SYK) to initiate cellular signalling[343,344,347,348]. SYK is an important intracellular tyrosine kinase involved in proinflammatory cytokine production[345,348]. SYK contains two domains of Src homology 2 (SH2) at the N-terminal and a kinase domain at the C-terminal[348]. The phosphorylated tyrosine residue(s) located in the HemITAM or ITAM motifs serve as docking sites for the SH2 domains of SYK[344,348]. The binding of SYK to the phosphorylated HemITAM or ITAM leads to a conformational change of SYK allowing autophosphorylation, activation and further downstream signalling[344]. For example, upon activation, Mincle (ITAM-coupled) and Dectin-1 (HemITAM) via SYK induce proteins Protein kinase C delta (PKCδ) and Vav which induce caspase recruitment domain-containing protein 9 (CARD9)/B-cell lymphoma/leukaemia 10 (Bcl10)/Mucosa-associated lymphoid tissue lymphoma translocation protein 1 (MALT1) complex and Mitogen-activated protein kinase (MAPK) pathways leading to production of chemokines and cytokines[344,345]. As it is relevant to this thesis, Dectin-1 and Dectin-2 signalling pathways are discussed in sections 1.2.5.2.3 and 1.2.5.2.6, respectively. For a comprehensive review of myeloid CLR signalling including ITAM- and ITIM-associated CLRs see [344].

1.2.5.2.3. Dendritic cell-associated C-type lectin 1

Dendritic cell-associated C-type lectin 1 (Dectin-1) (CLEC7A [human and mouse]) is a type II transmembrane protein in group 5 of the CLR family[328,349]. It is mostly expressed by innate immune cells, particularly of myeloid origin, including DC subsets, macrophages and monocytes[328,349-352]; although it can be expressed on other cell types including langerhans cells, mast cells, kupffer cells, eosinophils, basophils and microglia[328,350,353]. Dectin-1 is important in mediating murine and human anti-fungal immunity, for example against *C. glabrata*[354], and can initiate Th1 and Th17 responses required for host protection at the mucosal surface[349,355].

Isoform A of Dectin-1 contains an CRD connecting to a stalk region, a transmembrane domain, and a cytoplasmic tail comprising an (ITAM)-like motif (Figure 15a). Isoform B does not contain the stalk region[349]. Dectin-1 is generally

known as a β-glucan receptor, as it binds to β-1,3-linked glucans that can be found on fungi, although other ligands have been proposed[341,349,356,357]. Ligand-mediated activation of Dectin-1 leads to the production of cytokines through NF-κB including TNF-α, IL-6 and IL-23 and anti-inflammatory IL-10[349]. Dectin-1 also interacts with other PRRs including TLR2 to modulate cellular responses[349,358].

Dectin-1 recognition of fungal β-glucans initiates cellular activation through SYK-independent or -dependent mechanisms leading to NFAT (Nuclear factor of activated T cells [through dephosphorylation]) and NF-κB activation and the induction of innate and adaptive immune responses, for example cytokine and chemokine production and induction of Th1 or Th17 cells, respectively (Figure 15b)[349,359]. Dectin-1 harbours an ITAM-like motif (HemITAM; see section 1.2.5.2.2.) in its cytoplasmic tail[337]. Receptor clustering and phosphorylation of tyrosine residues on the ITAM region are induced by Dectn-1 ligand binding and activation allowing interaction between SH2 domains of SYK (section 1.2.5.2.2.) and the phosphotyrosine residues of ITAM leading to active SYK[337] (Figure 15b). Active SYK leads to phosphorylation of "downstream substrates" and activation of the enzyme phosphoinositide 3-kinase leading to generation of phosphatidylinositol (3,4,5)-triphosphate (PIP3) that induces the enzyme phospholipase Cy2 (PLCy2) which modulates inositol triphosphate (IP3) and diglycerol (DAG) pathways resulting in endoplasmic reticulum Ca^{2+} release[337,360]. Ca^{2+} release activates PKCδ leading to phosphorylation and induction of CARD9 (signalling adapter protein) resulting in the formation of a complex with Bcl10 and MALT1[337,360,361]. This complex is responsible for upregulation of NFκB pathway, which can upregulate genes associated with chemokine and cytokine production including IL-10, TNF-α and IL-6[337,345,362]. Activated SYK can also interact with the IKK complex through NFκB-inducing kinase (NIK) resulting in activation of NFκB subunits RelB and p52. Notably, SYK-independent activation of Raf by Dectin-1 is able to inhibit these subunits by phosphorylation and acetylation of p65 (Figure 15b)[337]. In addition, activation of PKCδ leads to induction of Calcineurin/NFAT as well as ROS and activation of the NLRP3 inflammasome[337]. NLRP3 is associated with production of the proinflammatory cytokine IL-1β. For a comprehensive review of Dectin-1 signalling and NFκB in immune function see [337] and [362], respectively.

a)

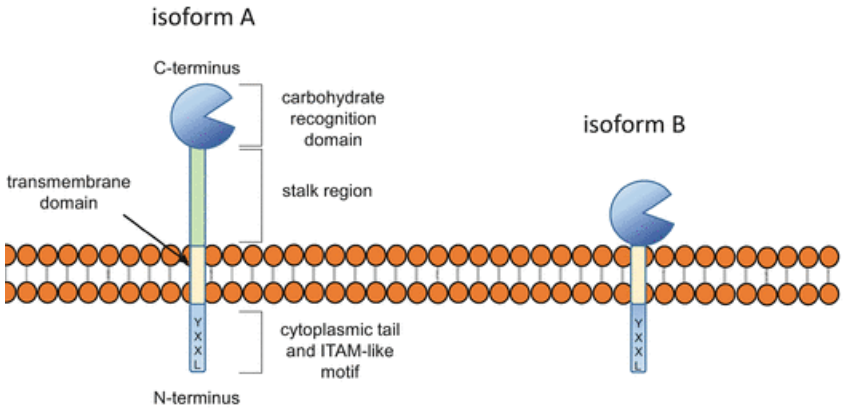

b)

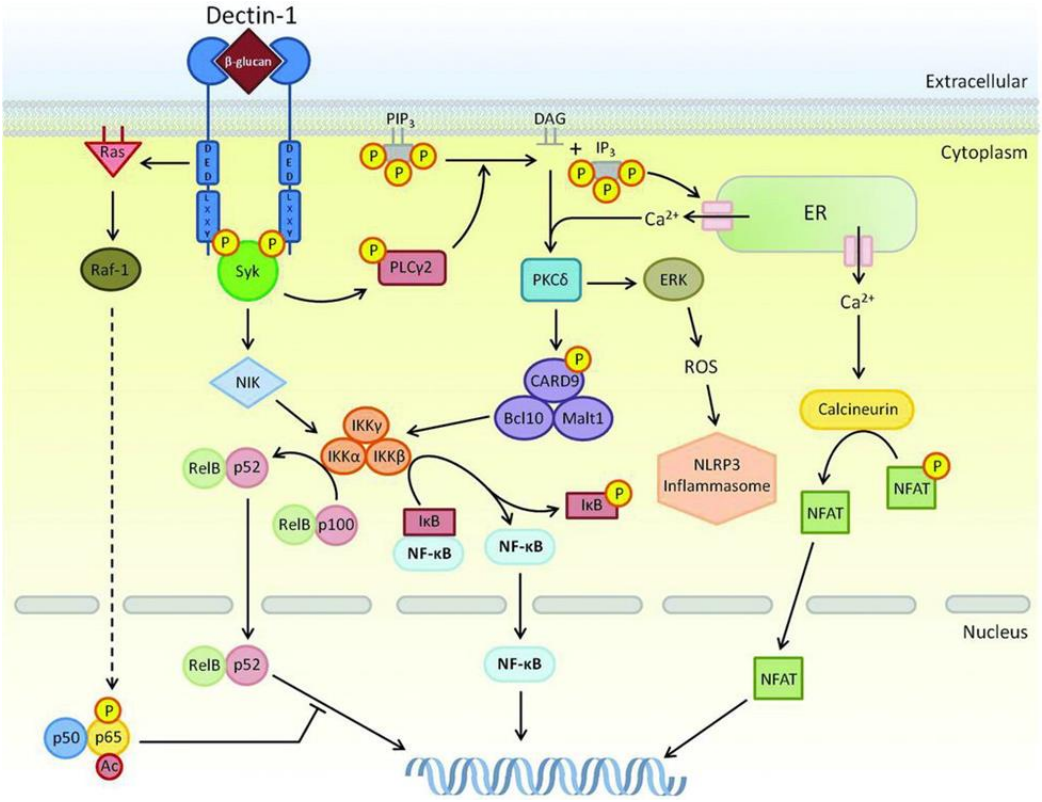

Figure 15. The structure of Dectin-1 and its cell signalling in response to the recognition of β-glucan.

(a) Dendritic cell-associated C-type lectin 1 (Dectin-1) isoforms showing isoform A's CRD, stalk region and immunoreceptor tyrosine-based activation motif (ITAM)-like motif which mediates intracellular signalling. (b) Overview of Dectin-1 signalling upon ligand binding and activation (see section 1.2.5.2.3). CARD9, caspase recruitment domain-containing protein 9. SYK, spleen tyrosine kinase. Th, T helper cell. NF-kB, nuclear factor kappa-light-chain-enhancer of activated B-cells. NFAT, Nuclear factor of activated T cells. ROS, reactive oxygen species. NIK, NFκb-inducing kinase. PKCδ, protein kinase C delta. PLCγ2, Enzyme phospholipase Cy2. IP3, inositol triphosphate. PIP3, phosphatidylinositol-(3,4,5)-triphosphate. DAG, diaglycerol. ER, endoplasmic reticulum. (a) was taken from [349] with permission from Springer Nature and Copyright Clearance Center. (b) was taken from [337] and the article is under the Creative Commons Attribution 3.0 Unported (CC BY 3.0). Image licence: https://creativecommons.org/licenses/by/3.0/legalcode.

It was reported that large particulate glucans (representing multivalent ligands found on a whole microbe) bind to Dectin-1 leading to phagocytosis whereas smaller soluble glucans (a soluble fraction from particulate β-glucan[363,364]) bind but do not induce Dectin-1 signalling[364]. Particulate forms of β-glucans are required for Dectin-1 activation and the induction of cytokines[364,365]. This mechanism may help inform innate immune cells whether a microbe is in direct contact or is at a distance[364]. For a review on PRR clustering and signalling in fungal immunity see [358].

In the past few years, microbiome research has primarily focused on gut bacteria, however, the role of the mycobiome (fungal genetic content) in intestinal immune regulation and disease is gaining more attention[366]. Dectin-1 has been implicated in intestinal immunity, however, the mechanisms are unclear[367]. For example, Rochereau and colleagues (2013) found that Dectin-1 was responsible for reverse transcytosis sIgA uptake by intestinal M-cells and that both systemic and mucosal antibody production against orally-administered HIV p24-SIgA antigen was Dectin-1-dependent[367]. Another study showed that Dectin-1 was expressed by human primary and secondary IEC cell lines and that β-glucan-induced IL-8 and CCL2 production by IECs could be inhibited using a Dectin-1 antagonist[368]. Interestingly, it was recently shown that Dectin-1 was involved in immune regulation of T reg cell responses through changes to microbial content in the gut[369]. CLEC7A deficient mice (Dectin-1 KO) were resistant to experimentally induced colitis[369]. Further, in the colon of Dectin-1 KO mice, *L. murinus* populations were elevated along with T reg cells which was suggested to be attributable to a decrease in AMP levels[369]. These data suggest that Dectin-1 is an important CLR involved in intestinal immune regulation by indirectly impacting T reg cell induction through influencing microbial composition[369].

1.2.5.2.4. DC-specific ICAM-grabbing non-integrin

DC-SIGN (CD209 [human]) is a type II transmembrane CLR consisting of an extracellular domain harbouring a CRD, a transmembrane domain, and a cytoplasmic region (Figure 16)[370,371]. DC-SIGN is found on the cell surface of human myeloid-derived DCs in both lymphoid and peripheral tissues and some macrophages[371-373] as well as in the intestine such as DCs located in the LP and PPs[374,375]. Its CRD contains an EPN amino acid motif which, together with Ca^{2+}, is required for binding to exogenous ligands including mannose or fucose structures, which can be found on a variety of microbes and viruses including HIV, measles virus, dengue virus, *Mycobacterium tuberculosis*, SARS virus, *C. albicans*, *Leishmania spp. Lactobacilli spp, or H. pylori,* among others[345,346,376]. Interestingly, it

was reported that PSA from *B. fragilis* was a ligand for DC-SIGN which was necessary for induction of T cell responses and internalisation of PSA by human DCs[141]; N-acetylglucosamine-high structures were also reported as ligands for DC-SIGN[377]. Ligand-binding of DC-SIGN does not directly result in the immune response, however DC-SIGN modulates signalling from other PRRs such as TLRs that contribute to the production of pro- and anti-inflammatory cytokines including IL-6, IL-23 and IL-10[371]. Further, the intracellular signalling mechanisms of DC-SIGN upon recognition of high mannose or fucose structures are different and lead to differential immune cell responses including cytokine production[371].

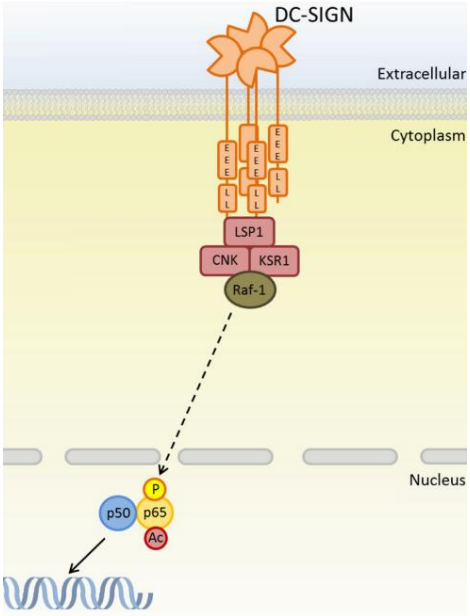

Figure 16. DC-SIGN and its cell signalling.

DC-specific ICAM-grabbing non-integrin (DC-SIGN) does not contain any tyrosine-based motifs, however can signal through Raf1 to activate Nf-κB-associated subunits (p50 and p65) leading to upregulation of inflammatory genes[126]. Taken from [126]. Images are licensed under Creative Commons Attribution 4.0 International: https://creativecommons.org/licenses/by/4.0/legalcode.

1.2.5.2.5. Specific ICAM-3 grabbing non-integrin 1

Type II transmembrane receptor Specific ICAM-3 grabbing non-integrin 1 (SIGNR1) (CD209 [mouse]) are of the murine homologues of DC-SIGN with the CTLD sharing a 59% identical amino acid (70% similarity)[378,379]. Like DC-SIGN, SIGNR1 can bind to high mannose or fucose structures present on microbes and also interacts with N-acetylglucosamine (GlcNAc) residues[380,381]. SIGNR1 is expressed by phagocytic

cells the in the lymph nodes, splenic marginal zone macrophages, and on *in vitro*-generated BMDCs[382-385].

SIGNR1 has been shown to interact with a range of bacterial PS and glycoconjugates. For example, SIGNR1 has been shown to mediate uptake of the glucose polymer dextran by splenic macrophages[383,386]. SIGNR1 can also bind to CPS from *S. pneumoniae*[386]*.* The down-regulation of SIGNR1 (transient KO model) *in vivo* leads to an impaired uptake of both dextran and CPS[383,386]. *In vitro*, core oligosaccharides found on LPS from *Salmonella* were found to be recognised by SIGNR1, and LPS-induced cytokine production was enhanced in SIGNR1-transfected RAW 264.7 macrophages suggesting that SIGNR1 and TLR4 cooperate to enhance innate immune cell responses towards gram-negative bacteria[387]. SIGNR1 has also been shown to be important in reducing susceptibility to LPS-induced experimental colitis[388].

SIGNR1 has also been demonstrated to be important in mediating intestinal immunity and allergic responses[384]. For example, in mice with artificially-induced anaphylaxis using orally-administered BSA, supplementation with multivalent mannoside-conjugated BSA (BSA-man) significantly reduced the allergic response[389]. This was suggested to be due to a direct interaction between BSA-man and LP DCs leading to IL-10 production which was SIGNR1-dependent. Further, BSA-man-SIGNR1 interaction by LP DCs was shown to be responsible for Tr1 regulatory cell responses *in vitro* and *in vivo*[384,389]. This suggests that CLR SIGNR1 has an immunoregulatory effect in intestinal immunity and homeostasis associated with food allergy[384,389]. A proposed model for SIGNR1's role inducing oral tolerance and immune homeostasis to food-induced anaphylaxis is illustrated in Figure 17.

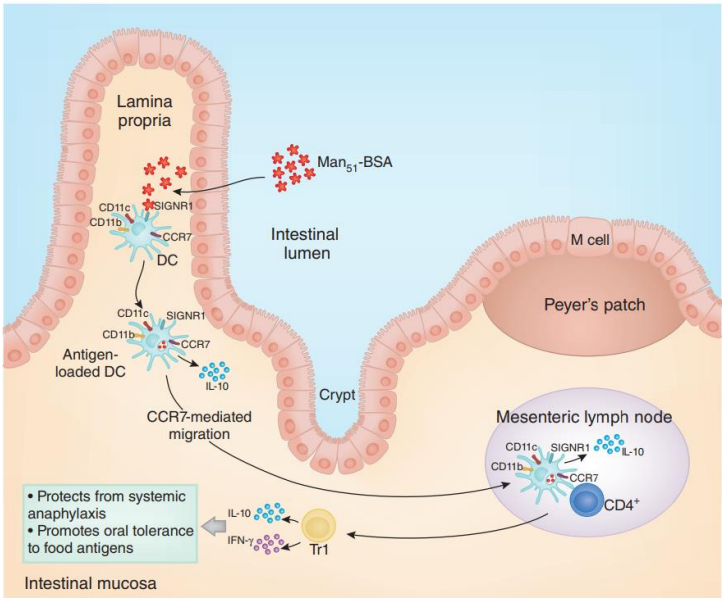

Figure 17. Proposed role of SIGNR1 for inducing oral tolerance and immune homeostasis.

Mannose-conjugated bovine serum albumin (BSA) (Man51-BSA) was suggested to bind to SIGNR1 on LP DCs and upregulate IL-10 production and exerted regulatory responses including induction of T regulatory 1 cells (Tr1)[384,389]. SIGNR1, Specific ICAM-3 grabbing non-integrin 1 (SIGNR1). Taken from [384] with permission from Springer Nature and Copyright Clearance Center.

1.2.5.2.6. Dendritic cell-associated lectin-2

Dendritic cell-associated lectin-2 (Dectin-2) (CLEC6A [human] and CLEC4N [mouse]) is type II transmembrane CLR important for antifungal and anti-mycobacterial immunity[120,121,390]. It is primary expressed on the surface of myeloid-derived cells including DC subsets, monocytes, neutrophils, and macrophages[391-393]. Dectin-2 harbours a cytoplasmic tail, stalk region, transmembrane domain and an extracellular domain comprising a highly conserved CRD containing an EPN amino acid motif responsible for Ca2+-dependent mannose-specific ligand binding[391]. Dectin-2 recognises high mannose-structures on pathogenic and opportunistic microbes including cell surface α-mannan on *C. albicans*, O-linked mannobiose glycoprotein from *Malassezia spp.,* lipoarabinomannan from *Mycobacterium tuberculosis*, α-mannan-linked O-antigen from *Hafnia alvei* and *Klebsiella pneumoniae* O5 ,and α-mannan from *S. cerevisiae,* among others[120,121,339,391,394,395]. Dectin-2 has also been shown to bind to other endogenous mannose-derived ligands such as β-glucuronidase[396]. The binding specificities of human Dectin-2 to α-mannan structures from different sources has recently been described[339]. Dectin-2's role in anti-fungal immunity for *C. albicans*, *Malassezia spp and M. tuberculosis* is well known[391].

A key difference important for understanding the intracellular signalling mechanisms of Dectin-1 and Dectin-2 is that Dectin-1 contains a HemITAM motif within its cytoplasmic tail while Dectin-2 has a shorter tail with no known signalling motif[397]. Instead, Dectin-2 associates with the FcRγ chain with which this interaction is reliant upon the arginine residue located in the cytoplasmic domain[397,398]. The FcRγ chain has shown to be critical for Dectin-2-mediated cellular cytokine production[120]. Dectin-2's SYK-dependent intracellular signalling mechanisms as well as the activation of CARD9/Bcl10/MALT1 complex and induction of ROS and NLRP3 inflammasome is similar to that of Dectin-1 (see section 1.2.5.2.3). Upon ligand recognition, Dectin-2 elicits cellular activation by associating with the ITAM adaptor FcRγ which subsequently recruits phosphorylated SYK kinase leading to activation of the CARD9/Bcl10/MALT1 complex, or ROS production important for activation of the NLRP3 inflammasome and IL-1β production (Figure 18)[391]. Induction of CARD9/Bcl10/MALT1 leads to activation of NF-κB (for a review see [362]) where it translocation into the nucleus leading to the upregulated expression of cytokines including IL-6, TNF-α and IL-23, or IL-1β[391,399,400]. CARD9/Bcl10/MALT1 also activates MAPK signalling cascades (for a review see [401]) leading to cytokine production through another transcription factor activated protein 1 (AP-1)[402 391,403]. The induction of cytokines as a result of Dectin-2 ligand binding and activation leads to Th17 induction and recruitment of neutrophils that aid host protection against pathogens[391,402]. In contrast to Dectin-1, Dectin-2 is not involved with Raf1 signalling[397].

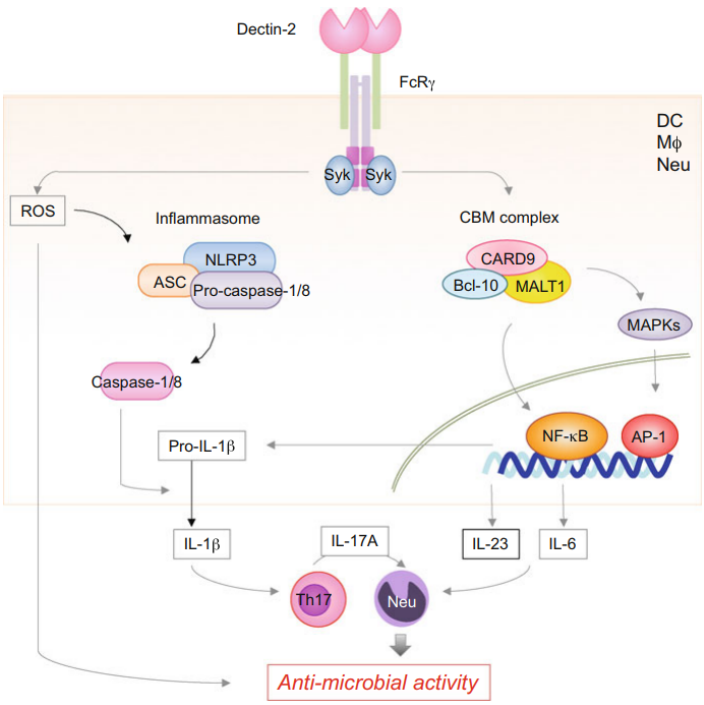

Figure 18. Cell signalling and immune responses of Dectin-2.

Upon carbohydrate recognition by Dectin-2, immune cell activation (for example by DCs or macrophages) is initiated through SYK which leads to downstream signalling and antimicrobial responses including the production of cytokines that are involved with induction of Th17 cells and neutrophils (Neu). For a review, see [391]. AP-1, Activator protein 1. CARD9, caspase recruitment domain-containing protien9. IL, interleukin. ROS, reactive oxygen species. DC, dendritic cell. MAPKs, mitogen-activated protein kinases. Mϕ, macrophage. SYK, spleen tyrosine kinase. Adapted from [391] with permission from Springer Nature and Copyright Clearance Center.

Dectin-2 has also been suggested to have anti-inflammatory properties, as it induced of IL-10 production in BMDCs in response to stimulation by whole yeasts, α-mannan from *C. albicans* and Man-LAM from *Mycobacterium tuberculosis*[121,402].

The role of Dectin-2 in pathogen-mediated immunity is still being investigated, however little evidence exists for its significance in intestinal immunity and homeostasis, despite the growing recognition of the mycobiome[366]. The role of Dectin-2 in the gut and its expression patterns in intestinal immune cells is not clear. However, Dectin-2 was expressed in cells of the mouse LP including $CD11c^+$ and $CD11b^+$ cells suggesting that Dectin-2 is found in macrophage or DC populations[392]. There was also some evidence that Dectin-2 may also be expressed in CD11c+ cells in mouse PPs.

1.3. Mechanisms of the immunomodulatory properties of polysaccharides

1.3.1. Immunomodulatory properties of polysaccharides from plants, mushrooms and algae

PS from plants, algae, mushrooms and microbes have been shown to modulate immune function in animals[1,3,24]. Many studies have been performed *in vitro* (Table 1) or using experimental animal models (Table 2) while studies in humans are more limited[3,12,162].

For orally-administered/dietary PS, the literature mostly describes immunomodulatory properties, including anti-tumour effects, of fungal glucans as well as inulin-type fructans[3,32,74,143,156,157,404]. Nevertheless, there exists a large body of literature investigating dietary and injected immunomodulatory PS which have been extensively reviewed elsewhere[3,12,156,157,162,404-407]. Many of these studies used oral administration or injected PS[3,12], however, there is an abundance of *in vitro/ex vivo* studies investigating many types of PS or crude extracts (for examples see Table 2[156,162]. The term “immunomodulatory” is vague and refers to any stimulatory, inhibitory, or other effect on immune system function. A large heterogeneity observed across many studies due to PS type and origin, characterisation, extraction method, treatment dose, species, cell type, duration of treatment, inflammatory stimulus, immune outcome measures, and purification method, among others[3,162] Further, the use of crude extracts[3,156,162,408-410] renders it difficult to distinguish the immunomodulatory effects of PS from other bioactive consitutents[411-415]. The mechanisms underpinning PS and their immunomodulatory functions remain unclear yet are slowly being unravelled[3,74]. PS accessible to the intestines may modulate the immune system indirectly by altering the gut microbiota and their secretory molecules or through direct interaction with intestinal immune cells and the epithelium[1,24,406].

The following sections describe the immunomodulatory properties of a variety of PS found in plants, mushrooms or algae that have been reported *in vitro* and in experimental animal models.

Table 2. Examples of immunomodulatory PS: in vitro studies.

Polysaccharide/structural analysis*	**Cell type and experiment***	**PS dose**	**Immunomodulatory effects**	**LPS***	
Aqueous extract, crude PS or purified PS from stems of Dendrobium officinale (Dendronan®). PSs reported as acetylated glucomannan[416].	Murine RAW 264.7 macrophages treated with aqueous extract (*Dendrobium officinale*), crude or purified glucomannan.	Up to 160 μg/ml	➢ All treatments ↑ LPS-induced phagocytosis by macrophage (NRU assay) ➢ All treatments ↑ TNF-α, IL-12, IL-6 and NO production compared to unstimulated.	Y; <0.003125 EU per mg.	[409]
β-1,6-glucans extracted from *Agaricus brasiliensis* and *Agaricus bisporus*. Extracts characterised by ^{13}C NMR and GC-MS analysis.	Human THP-1 monocytic cell line cells treated with LPS and/or β-1,6-glucans for 3 or 6 hr; PBS negative control.	Up to 100 μg/ml	➢ Both glucan extracts at either 3 and/or 6 hr incubation ↑ IL-1β and TNF-α gene expression compared to negative control. ➢ Both glucan extracts ↓ IL-1β and COX-2 but not TNF-α gene expression when co-incubated with LPS.	Y; assessed by GC-MS; <5 ng LPS per 100 mg *Agaricus brasiliensis* β-glucan (no LPS detected in other glucan extract; detection sensitivity likely < 5ng)	[417]
PS extract from Pleurotes eryngii (edible mushroom). Constituents: mannose, glucose and galactose in ration of 2.2; 2.0; 3.2 with galactose as the main backbone. Structure assessed by GC-MS, FT-IR and ^{1}H and ^{13}C NMR.	Murine Raw 264.7 macrophages treated with PS extract from Pleurotes eryngii (edible mushroom)	Up to 100 μg/ml	➢ PS ↑ TNF-α, IL-1, IL-6 and NO production by 264.7 macrophages via p38, ERK, JNK MAPKs and NFκB.	N	[410]
5 types of PS extracts from Carrageenans (red algae). Reported primary sugars are Galactose and anhydrogalactose – see [418] for full structural analysis and other references on strucutres.	Human whole blood cells treated with 5 types of carrageenans PS extracts.	Up to 1 μg/ml	➢ All carrageenans ↑ IL-10, TNF-α, IL-6 production by human blood cells compared to control.	N	[418]

Galactomannan from *Antrodia cinnamomea* (pathogenic fungi)	Murine J774A.1 macrophages and isolated peritoneal macrophages, and human DCs were treated with galactomannan from *A. cinnamomea*.	Up to 100 μg/ml	➢ Galactomannan ↑ TNF-α and IL-6 production in all cells. ➢ Immunostimulatory activity was through TLR4 using gene expression analysis of TLR4 shRNA-treated J774A.1 macrophages and TLR4 KO peritoneal macrophages. ➢ Murine cell activity was through protein kinase C-a and MAPK activation ➢ Pre-treatment of murine cells with galactomannan induced LPS tolerance (e.g. ↓TNF-α and IL-6 production)	Y; using polymyxin B (LPS inhibitor)	419
β-mannan PS (partially acetylated) from *Aloe vera.* Two fractions isolated from aloe vera reported primarily as β-1,4-linked mannose chains by ^{13}C and ^{1}H NMR, and GC-MS analysis.	Isolated murine peritoneal macrophages, were treated β-mannan extracts from *Aloe vera*.(*ex-vivo*).		➢ ↑ TNF-α. and IL-1β production by mouse peritoneal macrophages compared to control (media alone).	Y; LAL test, no detectable LPS in samples.	

Legend: *if study accounted for LPS in polysaccharide preparations stating either the method used or LPS concentrations in PS. **if structure was reported in study. COX-2, cyclooxygenase-2. DCs, dendritic cells. ERK, extracellular-signal-regulated-kinase. EU, endotoxin units. GC-MS, gas chromatography-mass spectrometry. JNK, c-jun N-terminal kinases. IL, interleukin. KO, Knockout (animal experimental model). LAL, limulus amebocyte lysate (test for LPS quantification) LPS, lipopolysaccharide. MAPKs, mitogen-activated protein kinases. N, LPS not addressed. NFκB NMR, nuclear magnetic resonance, NO, nitric oxide. PBS, phosphate-buffered saline. TLR, toll-like receptor. TNF, tumour necrosis factor. Y, LPS was considered.

Table 3. Examples of immunomodulatory PS: orally-administered/dietary PS in experimental animal models.

PS/structure*	Experiment	Relevant immunomodulatory results	Reference
Microbial β-glucans: Curdlan (particulate), Zymosan, and glucan phosphate (soluble)	DSS-induced colitis; mice given curdlan (particulate), zymosan, and glucan phosphate (soluble) or vehicle control once daily for 14 days.	➢ ↑ intestinal inflammation by all glucans (observed via colon histology). ➢ ↑ in TNF-α and MCP-1 (CCL-2) in colonic tissue with curdlan (particulate) and zymosan but not glucan phosphate (soluble) compared to controls.	[420]
Seaweed and Yeast (*S. cerevisiae*) β-glucan	Pigs diets supplemented with or without β-glucans for 28 days (experimental as in [421]).	➢ ↑ IL-17a, IL-17F, IL-22 and IL-6 expression in colonic tissue in both glucans compared to control. ➢ No difference to Foxp3 or TGF-β (T reg targets) expression for both glucans in colonic tissue compared to control. ➢ Yeast β-glucan only ↓ IL-10 expression in colonic tissue compared to control.	[422]
Astragalus PS (structure not defined but reported as heteropolysaccharides and largely heterogenous in structure – for a review on APS structure see [423])	*In vivo*: Solid tumour-bearing mice; orally administered APS or control (saline) once daily for 25 days. *In vitro*: raw 264.7 macrophages.	➢ ↑ serum TNF-α, IL-6 and IL-1β but not IL-12p70 in LPS- and APS-treated tumour-bearing mice. ➢ APS ↑ TNF-α, IL-6 and IL-1β by raw 264.7 macrophages. ➢ APS ↑ NO production by raw 264.7 macrophages. ➢ LPS in APS ruled out (by CE TAL assay – no level stated though). ➢ Immunomodulation suggested through TLR and MYD88 signalling.	[424]
Oat β-glucan	Mice (ICR strain); DSS-induced colitis; oral administered oat β-glucans for 7 days.	➢ β-glucan ↓ clinical symptoms of colitis compared to controls. ➢ β-glucan ↓ colonic mRNA expression of IL-6, TNF-α, IL-1β and iNOS compared to controls. ➢ β-glucan ↓ colonic production of IL-6, TNF-α, IL-1β and iNOS compared to controls (assessed by IHC). ➢ Associated conclusion: anti-inflammatory properties of oat β-glucans.	[425]
Astragalus PS: backbone of α-(1,4)-glucan with branched β-1,6-D-galactose and β-(1,6)-D-xylose residues.	Chickens control feed of or regular feed + APS; and challenged with intraperitoneal LPS or saline control.	➢ ↓ jejunum mucosal tissue mRNA expression of IL-6, NF-κB, TLR4, and IL-1β after LPS-challenge at day 35 of feeding and compared to controls. ➢ Associated conclusion: attenuation of LPS-induced immune stress by dietary APS.	[426]
Pectin-type PS from *Citrus unshiu* peel (for full structure see [427])	Oral administration of pectin to C3H/He mice (5 – 21 days).	➢ ↑ IL-6 and GM-CSF in culture supernatants of isolated and 5-day-cultured PPs (*ex vivo*) in mice orally supplemented with pectin compared to control mice.	[427]
Fucoidan (Maritech Synergy [contains phenols], depyrogenated fucoidan [purified fucoidan])	C57BL/6 Mice with acute DSS-induced colitis supplemented with 3 fucoidans daily for 7 days. Intraperitoneal	➢ Oral fucoidans ↓ clinical signs and symptoms of colitis compared to controls (e.g. immune cell infiltration and histology scores). ➢ Some fucoidans that were fed to mice ↓ colonic tissue (*ex vivo*, 24 hr culture) supernatant levels of IL-1β (both fucoidans), IL-10 and TNF-α (Synergy) and GM-CSF (both fucoidans) among others	[428]

	injection was also tested.	(measured in cultured supernatants).	
Guar gum (partially hydrolysed)	C57BL/6 mice fed diets containing guar gum or control for 2 weeks prior to TNBS-induced colitis	➢ Guar gum ↓ clinical symptoms of colitis (e.g. histological scores) compared to controls. ➢ ↓ colonic mucosal mRNA expression and production TNF-α, compared to controls. ➢ Associated conclusion: amelioration of intestinal inflammation by chronic guar gum intake possibly through microbiota changes and SCFA production.	429
Bletilla striata PS (contains mannose and glucose; for more details on structure, see [430] and [431].	Rat model of thioacetamide (TAA)-induced cirrhosis (intraperitoneal). N=10. Mice fed PS 15, 30 or 60mg/kg daily.	➢ Decreased cytokines TNF-α and IL-6 in ieum. ➢ Increased intestinal tight junction protein expression of ZO-1 and occludidn in ileum. ➢ Decreased ileal histology scores.	[431]

Legend: *if structure was reported in study. APS, astragalus polysaccharide. DSS, dioctyl sodium sulfosiccinate. IHC, Immunohistochemical analysis. IL, interleukin. iNOS, nitric oxide synthase. LPS, lipopolysaccharide. Monocyte chemoattractant protein-1.NO, nitric oxide. TGF, transforming growth factor beta 1 TNBS, 2,4,6-trinitrobenzene sulphonic acid. TLR, toll-like receptor.

1.3.1.1. Inulin

The fructan inulin as a common dietary fibre has received a lot of attention recently for its immunomodulatory properties including its ability to induce beneficial effects via the gut microbiota[74,157,158,432]. Notably, a comprehensive review by Vogt and colleagues (2015) describe many studies that investigate the immunomodulatory effects of dietary fructans including inulins[74]. However, the underlying mechanisms for these and other immunomodulatory PS are unclear but are suggested to involve changes in the gut microbiota and their secreted metabolites or direct interaction with immune cell PRRs such as TLRs, Dectin-1 or the MR[74,158,433-435].

Inulin is reported as a prebiotic and has been shown to modulate immune system function. For example, an inulin/oligofructose mix improved gut histology scores, and reduced IL-1β and elevated TGF-β levels in the caecum of rats with pathogen-induced colitis[436]. Further, inulin/oligofructose orally-administered to rats increased PP IL-10 and caecal secretory IgA[437]. In the same study, other prebiotic effects were observed in rats receiving combinations of probiotic bacteria, probiotics, inulin and oligofructose[437]. Recently, it was shown that dietary supplementation with long chain inulin improved clinical GI symptoms and modulated immune function in the intestine of mice subjected to caerulein-induced acute pancreatitis[438]. Long-chain but not short-chain inulin improved intestinal barrier function and histology scores in the colon[438]. It was found that long-chain inulin decreased the amount of infiltrating

neutrophils and macrophages in the colon (and in the pancreas)[438]. Further, both long-chain and short-chain inulins decreased and increased serum IL-1β and IL-10, respectively; decreased IL-1β and TNF-α and increased IL-10 in colonic tissue[438]. Interestingly, a recent comprehensive study showed both gut microbiota-dependent and -independent mechanisms of immune modulation by β-(2,1) fructans[432]. For example, they found that oral intake of inulin influenced PP DC marker expression and the numbers of B cells in the MLN in germ free mice *in vivo*[432]. Some of the immunomodulatory effects were dependent on fructan chain-length[432]. In addition to microbiota-dependent immunomodulatory effects (not discussed here), this study demonstrated that β-(2,1) fructans can directly modulate immune system function.

In vitro, inulin-type fructans stimulated both pro- and anti-inflammatory cytokines including IL-6 and IL-10, respectively, in human blood mononuclear cells[435]. These effects were found to be chain-length dependent; and the use of reporter cells revealed that inulin-type fructans interacted with TLR2 as well as TLR4, 5, 7 and 8[435]. Further, inulin-type β-2,1 fructans were shown to improve intestinal barrier integrity using T84 (human intestinal cell line) monolayers[439]. This was shown to be through interaction with TLR2 and was dependent on fructan chain-length[439]. Further, using reporter cells, it was shown that inulin-type β-2,1 fructans could bind to TLR2 directly[439]. In line with this study, it was reported that inulin improved intestinal barrier function in Caco-2 cell monolayers following pathogenic challenge through protein kinase C δ[440]. Overall, these studies demonstrated that inulin can interact with TLRs and improve intestinal permeability *in vitro*.

1.3.1.2. Glucans

A number of mechanisms have been reported underpinning the role of β-glucans in modulating immune function including via interaction with immune cell receptors such as Dectin-1 (see 1.2.5.2.3.) which recognises β-1,3-glucans[162,352,441]. Examples of the some reported immunomodulatory properties of glucans *in vitro* or using dietary animal models are shown in Table 1 and 2, respectively. For a review, see [3].

In vitro, the PS extract from the edible mushroom *Dictyophora indusiate* upregulated cytokines IL-6, IL-1β and TNF-α by RAW264.7 macrophages through TLR4[442]. The study accounted for endotoxin contamination with < 0.01 ng/ml LPS per 25 μg/ml of PS. A similar study showed that PS extract from *D. indusiate* increased phagocytic function of macrophages and their production of TNF-α and IL1-β. These effects

were impaired after treatment with anti-Dectin-1 antibodies, suggesting Dectin-1 interaction as an immunomodulatory mechanism in addition to TLR4[433].

1.3.1.3. Other polysaccharides

Many non-glucan PS have been reported to be immunostimulatory in non-clinical experimental models. For example, *in vitro*, β-(1,4)-linked mannans from *Dioscorea batatas* (yam) induced TNF-α production by mouse J774A.1 macrophages through TLR4-associated downstream signalling kinases including p38 mitogen-activated protein kinase[443]. Further, a PS extract from *Actinidia eriantha* comprising mostly galactose, arabinose and fucose as well as xylose, rhamnose, glucose and mannose in small quantities, induced TNF-α, IL-1β, IL-6 and IL-10 by murine RAW 264.7 macrophages through TLRs and NF-κB[444]. Further, fucoidan from brown algae showed induction of IL-6, IL-12, TNF-α and IL-1β production in mouse BMDCs and BMDMs *in vitro*[445]. Moreover, modifications to fucoidans including their "hyposulphation" and a lowering the number of acetyl groups reduced these effects suggesting that sulphate and acetyl groups on fucoidans are critical to their immunomodulatory function *in vitro*[445]. Mulberry leaf PS have also been shown to stimulate proinflammatory cytokines IL-12 and TNF-α in BMDCs[446]. Further, in another study using human monocyte-derived DCs, galactomannan from *Caesalpinia spinose* induced TNF-α, IL-8, IL-6, IL-1β and IL-12 p70 production and mRNA expression[447].

PS have also been shown to activate SYK which is associated with CLR signalling[328,329,448,449]. Recently, Meijerink and colleagues (2018) tested the immunomodulatory activity of 44 dietary fibres using TLR4 and TLR2 double KO mice[450]. Firstly, they demonstrated that many fibres could bind to several TLRs including TLR4 and TLR2[450]. They also showed that some fibres stimulated the production of several cytokines by BMDCs including TNF-α, IL-6, IL-12 and monocyte chemoattractant protein 1 (MCP-1) [450]. Arabinan and pectin induced potent immunostimulatory effects such as induction of cytokines by immune cells particularly with their particulate fractions, suggesting that stimulation of cytokines *in vitro* requires PS immobilisation which has also been shown using particulate β-glucans[364,450]. Moreover, branched arabinan was less potent at inducing cytokine production than linear mannan. Further, the effects of both arabinans did not depend on Dectin-1 but were dependent on SYK which may suggest the involvement of other CLRs that can activate SYK such as Dectin-2 [450].

Although many studies report the induction of proinflammatory cytokines, anti-inflammatory effects of PS have also been reported. IL-10 is a cytokine that exerts anti-inflammatory effects including through dampening the immune response after infection preventing further immune system damage to the host[451]. It also has a immunoregulatory role in intestinal immunity [452,453]. IL-10 responses have been shown to be induced by some PS *in vitro/ex vivo*[418,444]. For example, FOS and galactooligosaccharides stimulated IL-10 production by human immature monocyte-derived DCs[454]. The inhibition of proinflammatory cytokines by PS has also been reported. For example, *Astragalus* PS (APS) have been shown to inhibit TNF-α and IL-1β production and mRNA expression by THP-1 macrophages following LPS-challenge *in vitro*[455] (for a review of APS structure see [423]). This was suggested to be through suppression of NF-κB activation[455]. Similarly, studies using APS or chitosan were shown to reduce cytokines and chemokines in IEC lines[237,238,456]. Suppression of cytokine production or expression in tissues, including intestinal, by orally administered PS has also been observed *in vivo* (Table 3)[425,426,428,429,431,457].

The epithelial layer of the intestine comprising many types of IECs is an important structure of the GI immune system (1.2.3.)[165], playing a key role in maintaining intestinal immune homeostasis. Disruption of this barrier leads to intestinal immune dysregulation[165,458]. As mentioned above, inulin and other PS have been shown to improve gut barrier function[440]. PS are now being investigated for their ability to modulate secretion of inflammatory cytokines and chemokines from IECs[237,238]. For example, extracts from Sijunzi (a mixture of herbs) primarily comprising ~71% PS improved barrier permeability and decreased TNF-α, IL-8 and IL-6 production in Caco-2 cells[458]. It should be noted that the sugar composition of these PS was not determined[458]. Interestingly, zymosan and curdlan induced CCL2 and IL-8 production in SW480 and HT-29 IEC lines[368]. Further, Dectin-1 expression was evident in IEC surgical isolates and these cell lines[368]. Moreover, Dectin-1 and SYK inhibition suppressed IL-8 and CCL2 production in β-glucan-stimulated IEC lines[368]. Overall, there is accumulating evidence that other PS in addition to glucans and fructans can modulate immune function *in vitro*.

1.3.2. Immunomodulatory properties of polysaccharides from microbes

Many PS structures found in microbes are important immunomodulatory molecules[1,24,78,459]. They are often associated with initiating an immune response to pathogens and are recognised by PRRs on immune or epithelial cells[117,118,121,354,395].

Pathogen-derived PS are known as pathogen-associated molecular patterns (PAMPs) and include LPS, lipoteichoic acid, and peptidoglycan found in bacteria, or mannoproteins or β-glucans present in microbial fungi[78,117,460,461]. Figure 12 shows examples of PAMPs found in pathogenic microbial fungi and their reported PRRs. However, non-pathogenic microbes also contain similar structures such as LPS, therefore, the term microbe-associated molecular patterns (MAMPs) has been proposed[24,462]. However, the role for MAMPs from non-pathogenic microbes such as gut commensals and their interaction with the mammalian intestinal immune system remains underexplored[1,24].

1.3.2.1. Peptidoglycan

Peptidoglycan PGN is an important cell wall PAMP/MAMP for the immune response against bacterial pathogens[460]. During bacterial division, little PGN is released, however, upon infection, pathogen-derived PGN is greatly increased[24]. PGN is recognised by NOD-like receptors 1 and 2 and upon its immune cell activation there is induction of proinflammatory cytokines[125,460]. The interaction of PGN with TLR2 is controversial and has been reviewed elsewhere [460].

1.3.2.2. Lipopolysaccharide

LPS O-antigen is reported to be important in immune system evasion[82]. For example, stalling epithelial cell activation including internalisation and recognition of LPS from *Salmonella Thyphinium*[82,463]. O-antigen also plays a role in bacterial colonisation during infection and in antibody-mediated immune responses[464,465]. However, lipid A is primarily responsible for the immunogenicity of LPS generating both poor or strong host immune responses depending on its structure[131]. Lipid A structures can also have no effect or even halt proinflammatory responses[131]. Nevertheless, LPS is mostly known for its ability to initiate proinflammatory responses by the innate arm of the immune system which helps fight bacterial infection[466]. The recognition of LPS by the innate immune cell receptor TLR4 and its role in intestinal immunity is discussed in 1.2.5.1.

1.3.2.3. Fungal mannans and glucans

α-mannans and β-glucans can induce pro- or anti-inflammatory cytokines in myeloid-derived immune cells and/or epithelial cells through the CLR Dectin-2 and Dectin-1 respectively. The recognition and immune response to α-mannan, β-glucan and LPS by immune cell receptors are discussed in section 1.2.5.

In vivo, Rice and colleagues (2005) detected scleroglucan, laminarin and glucan phosphate (β-glucans) in serum after oral administration in rats[467]. Further, glucan phosphate could bind and was internalised by murine IEC independent of Dectin-1[467]. Together, these findings suggest that glucans are absorbed through IECs and can reach circulation. In the same study, mice treated with oral glucan phosphate led to improvements in overall survival following pathogenic challenge[467].

Further, β-glucan's structure may influence its immunomodulatory effects *in vitro*[162]. For example, recently Elder and colleagues (2017) found that high molecular-weight β-glucans were more effective at inducing proinflammatory cytokines IL-23, IL-6 and IL-1β by human monocyte-derived DCs than low molecular weight β-glucans[365]. Further, Goodridge and colleagues (2011) reported Dectin-1 signalling and TNF-α production in bone marrow-derived macrophages (BMDMs) by β-glucans required β-glucan to be in particulate form (a particle of β-glucan derived from *S. cerevisiae*[363]), as none of these effects were observed using soluble β-glucans[364]. Notably, they showed that soluble β-glucan (a soluble derivative from particulate β-glucan[363,364]) could bind to Dectin-1 on BMDMs but did not induce cellular activation, however (culture) plate-immobilised soluble β-glucan induced TNF-α production by BMDCs[364]. These findings suggest that the structure and form of β-glucans are important for their immunostimulatory properties.

Knowledge is limited on the role of other PS particularly from commensals and their impact on the immune system[24]. Nevertheless, the evidence for commensal PS and their immunomodulatory potential is attracting attention[24,81]. For example, α-glucan or pullulan, can be found on non-pathogenic fungi such as *Aureobasidium pullulans* and it has shown to induce the production of pro-inflammatory cytokines including IL-6 and TNF-α and IL-8 in whole blood of humans *ex vivo*[468].

1.3.2.4. Zwitterionic polysaccharides

There is emerging evidence that microbial PS may serve anti-inflammatory and immunoregulatory roles[80]. Zwitterionic PS (ZPS), a capsular PS found on both pathogenic and commensal bacteria (also see 1.1.3.2.3.), have shown to modulate T cell functions and have demonstrated anti-inflammatory effects[80,190,469]. T cell regulation is critical for intestinal immune homeostasis (see Figure 10 and 1.2.4.2.)[190]. ZPS have both negative and positive charges and can influence CD4+ T cell populations; these charges are crucial for their immunomodulatory activities [80,470]. ZPS from pathogenic bacteria including *Staphylococcus aureus* and *Strepptococcus*

pneumonia have shown to be important for the recognition and activation of immune cells[80,470,471]. Further, ZPS on the O-antigen of another commensal bacteria such as *Morganella morgani* was shown to be important for microbial T cell recognition[472]. PSA from *B. fragilis* is an example of ZPS reported for its anti-inflammatory properties and its role in bacterial colonisation and intestinal immune regulation[306,473,474]. This includes its ability to protect against opportunistic pathogen- and 2,4,6-trinitrobenezene sulphonic acid-mediated intestinal inflammation through direct induction of IL-10 producing T reg cells[80,267,306]. Further, it was shown that PSA directly interacts with TLR2 on Foxp3 T reg cells to induce immune tolerance that helps *B. fragilis* colonisation[473]. Recently, it was also shown that a PS from another commensal bacteria *Helicobacter hepaticus* (a non-pathogenic bacteria in WT mice under steady state conditions) could directly promote anti-inflammatory responses including TLR2-mediated induction of IL-10 production by intestinal macrophages[475].

1.3.2.5 Levan

In vivo, dietary levan has been shown to increase expression of proinflammatory cytokines IL-1β, TNF-α and IL-12 in fish liver, kidney, gills and intestine[476]. In contrast to increased cytokine levels, oral administration of levan in pigs decreased serum TNF-α and IL-6 following LPS-challenge[477]. Other benefits included improved digestive capability and increased populations of commensal *Lactobacillus spp.* in faeces[477]. These findings suggest that levan's immunomodulatory properties may occur via an indirect mechanism through modulation of the gut microbiota. In this regard, using fructosyltransferase (ftf) KO (knockout) *L. reuteri* strain which cannot produce levan, Sims and colleagues found that a diminished ability of the ftf mutant strain to colonise the gut of rats when exposed to competition using the wildtype (WT)[91]. This study also showed levan's ability to modulate T cell responses, as the WT but not ftf *L. reuteri* strains increased splenic Foxp3+ CD4+ regulatory T cell cells[91]. Levan's ability to modulate immune function *in vivo* after oral administration has also been demonstrated in other species. For example, Xu and colleagues (2006) showed that oral administration of levan in mice decreased ovalbumin-induced serum IgE and Th2 responses and suggested its use as a potential anti-allergy agent[26]. Further, in *Cyprinus carpio* (common carp fish), oral supplementation with 0.5% levan led to a higher respiratory burst by plasma phagocytes, increased serum lysozyme function and other physiological effects[478]. Further, dietary supplementation with levan (0.2, 0.4 and 1%) improved the survival of fish following pathogenic challenge compared to controls[478].

There is limited evidence for the induction of cytokine production or other immune molecules by levan. However, *in vitro*, levan has been reported to induce IgA production in isolated mouse PPs[479]. Levan was also shown to induce TNF-α production in murine splenocytes[480]. In line with this, Xu and colleagues (2006) reported that levan induced TNF-α and IL-12 p40 in monocyte/macrophage cell lines[26]. The secretion of IL-12 p40 was not due to LPS since IL-12 p40 was not dampened using an LPS inhibitor, polymyxin B[26]. Further, levan induced TNF-α and IL-12 p40 production by peritoneal and splenic murine primary macrophages, respectively[26]. Using TLR4 and TLR2 KO mice, levan induced TNF-α production in peritoneal cells in a TLR4-dependent and partial TLR2-dependent manner. Using TLR4 reporter cells, levan was shown to bind to TLR4 and this effect was not reduced using polymyxin B[26]. Taken together, the study showed that levan's activation of immune cells was mediated through recognition by TLR4.

In addition, levan has been shown to possess marginal anti-oxidant[481] and anti-inflammatory effects[482], improved macrophage proliferation and phagocytic activity[70], and anti-tumour and anti-cancer effects *in vitro*[71,95,100,483].

We are only beginning to understand the immunomodulatory effects of PS from commensals in the intestinal enviromnent[1,24]. Promising results from the literature, including those previously described, justifies further investigation into the immunomodulatory role of microbial PS particularly in the intestine where commensal microbes are abundant.

1.4. Aims and objectives

The overall aim of this work was to test the hypothesis that the interaction of food and microbial PS with CLRs contribute to the mechanisms underpinning their immunomodulatory properties.

We first screened food and microbial PS for their binding to Dectin-1, Dectin-2 and SIGNR1 using BWZ.36 reporter cell assays. Further, we carried out purification of microbial levan and assessed levan's interaction with CLRs. We then tested the immunomodulatory effects of purified microbial levan *in vitro* using murine BMDCs and human IECs with a focus on cytokine production.

Chapter 2: Materials and Methods

2.1. Materials

2.1.1. Cell lines

Plat-E cells were provided by Dr T. Kitamura (University of Tokyo, Japan). Parental BWZ.36 cells and Dectin-2 reporter cells were provided by Dr N. Shastri (University of California, Berkeley, CA, USA). Dectin-1, Dectin-2-QPD and mock-transfectant (mock) reporter cells (BWZ.36 parenteral cells harbouring the pMXs-IRES-GFP-CD3ζ-Ly49 (pMXs-IG) vector excluding the CLR extracellular domain sequence) were established in the Kawasaki Lab by Dr Alexandra Wittmann and Dr Norihito Kawasaki (Quadram Institute Bioscience, Norwich Research Park, UK). HEK-Blue™ human TLR4 reporter cells (#hkb-htlr4, Invivogen, USA) were a gift from Dr J.S Frick (University of Tübingen, Germany). Caco-2 cells were a gift from Dr Stephanie Schuller (University of East Anglia, Norwich, UK).

2.1.2. Bone marrow-derived dendritic cells

TLR4 KO BMDCs were provided by J.S Frick, University of Tubingen, Germany[394].

2.1.3. Mice

All C57BL6/6J WT mice and Dectin-2 KO mice were maintained at the University of East Anglia specific pathogen-free animal facility. Use of animals in this thesis was performed in accordance with the UK Home Office guidelines[394].

2.1.4. Strains and culture conditions

B. subtilis 168 was kindly provided by Professor Harry Gilbert (University of Newcastle, Newcastle, UK).

Lactobacillus semi-defined medium II (LDM2)[484] (5% sucrose) and lysogeny broth (LB) was produced in house at the Quadram Institute Bioscience, Norwich, UK (Appendix 1 and 2, respectively).

2.1.5. Antibodies

Anti-mouse Dectin-2-Alexa 647 and anti-rat IgG2a isotype-Alexa 647 (IgG isotype-Alexa 647) antibodies were provided and established by Dr Norihito Kawasaki as described in [394].

Anti-mouse SIGNR1-Alexa 647 (#MCA2394A647) was purchased from AbD Serotec. Bio-Rad, USA. Anti-rat IgM-Alexa 647 isotype control (#400813) (IgM isotype-Alexa 647) was purchased from Biolegend, UK. For use with SIGNR1

reporter assays, anti-mouse SIGNR1 functional grade antibody was purchased from eBioscience Ltd (#16-2093-82).

2.1.6. Plasmids, primers and gene synthesis

Full length *Mus musculus* CD209b (SIGNR1) cDNA was purchased from Sinobiological (#MG50486-M). SIGNR1 primers were purchased and synthesised by Sigma-Aldrich, UK (Table 4). The pBluescript II KS+ vector was obtained from Dr Norihito Kawasaki. The pMXs-IRES-EGFP-CD3 (cluster of differentiation 3)ζ-Ly49 (pMXs-IG) vector was provided by Dr T. Kitamura (University of Tokyo, Tokyo, Japan)[394,485]. HpaI-SIGNR1-QPD-NotI DNA sequence was synthesised and incorporated into a Pu57 vector by Genescript®, USA (Appendix 3). M13 forward and reverse primers were a gift from Dr Arnoud van Vliet (Institute of Food Research, Norwich, Norwich Research Park, UK).

Table 4. Sequences for SIGNR1 forward and reverse primers, and HpaI and NotI restriction enzymes

Sequence Type	Sequence
CD209b (SIGNR1) Forward Primer	5'… agttaactccaaaaccccaaataccga…3'
CD209b (SIGNR1) Reverse Primer	5'… tgcggccgcctagccttcagtgcatgggg…3'
HpaI Restriction Enzyme	5'… gtt^{v}aac…3'
NotI Restriction Enzyme	5'… gc^{v}ggccgc…3'

5', 5' prime end. 3', 3' prime end. v, site of cleavage. Sequences were constructed using ApE-A Plasmid Editor v2.0.47.

2.1.7. Polysaccharides/glycans

Details of PS or glycoconjugates used in this work are listed in Table 5. All saccharides were dissolved in sterile USP WFI bulk sterile filtered H_20 (sterile filtered H_20) (#LZBE17-724Q, Lonza, Switzerland) and concentrations were determined by weight. Typically, stock concentrations were 2 – 10 mg/ml and PS used for CLR screening - excluding all levans, all oligosaccharides, *Hafnia alvei* LPS (Hafnia-LPS), Scleroglucan, α-mannan, α-glucan and inulin from *Jerusalem artichoke* - were sterile filtered using a Minisart® High Flow Syringe 0.2 μm Polythersulfone Filter (#16532, Sartorius, Germany). Psyllium gum was suspended in NaOH and heated 70 - 80°C for up to 5 hr. Gum Karaya was heated in at 70-80°C stirred using a magnetic stirrer

for up to 5 hr. Gellan gum was heated and stirred at 70 - 80°C for 1 hr to dissolve. Typically, *E. herbicola* levan was heated at 60 – 70°C in a water bath for 5 – 20 min and vortexed to ensure all contents were dissolved. All PS were stored in 1.5 ml Eppendorf tube aliquots at -20°C.

Table 5. Composition and source of PS or glycans used for CLR screening

PS/glycan	General saccharide composition	Source**	Company/Acquisition (Product No***)	Reference ****
Acemannan	β-1,4 D-mannose polymer (partially O-acetylated)	*Plant (Aloe Vera)*	Elicityl (#MAN801)	[47]
α-mannan	α-1,6 and α-1,2-linked mannose residues with α-2,6-linked branching (Characterised in this thesis, see Chapter 3)	Yeast *(Saccharomyces cerevisiae)*	Sigma Aldrich (#M3640)	[a]
α-glucan	α-1,4 D-glucose backbone with α-1,6 branching points	*Streptomyces venezuelae*	Provided by Dr Stephen Borenmann (John Innes Centre, UK).	[486]
Arabinan	α-1,5-linked arabinose backbone which is branched with α-1,3-linked or α-1,2-linked arabinose units.	Plant (sugar beet)	Megazyme (P-ARAB)	[27,487,488]
Duphalac®	See OsLu	See reference	Provided by Mar Vilamiel, b Instituto de Investigación en Ciencias de la Alimentación, CIAL (CSIC-UAM), Spain.	[489]
E. herbicola levan	β-2,6 fructofuranose polymer that can contain β-2,1 branching. Full characterisation is described in this thesis (see Chapter 4).	*Erwinia herbicola*	Sigma Aldrich, UK.	[72,490]
Enzymatically synthesised levan	β-2,6 fructofuranose polymer that can contain β-2,1 branching. Characterised in this thesis by NMR and GPC. Full characterisation is	Recombinant levansucrase (EC. 2.4.1.10) from *Pseudomonas syringae pv. tomato*	Provided by Associate Professor Tiina Almäe, Institute of Molecular and Cell Biology, University of Tartu, Estonia.	[72,491,492]

	described in this thesis (see Chapter 4).			
Fucus Fucoidan	α-linked L-fucose polymer consisting of α-1,3-linked L-fucose linear chains with alternating α-1,3 and α-1,4-linked L-fucose units. This polymer may be sulphated or acetylated and/or contain branching consisting of other sugar units including glucuronic acid, arabinose, xylose or galactose.	Brown marine algae	Glycomix Ltd/Carbosynth*	[60,493]
Galactan	β-1,4-linked D-galactose polymer. Also contains arabinose, rhamnose, xylose and other sugars according to manufacturers.	Plant (Lupin)	Megazyme (P-GGMMV)	[76]
Gellan gum	Repeating unit of α-L-rhamnose, β-D-glucose and β-D-glucuronate and is partially acetylated.	Microbial (*Pseudomonas elodea*)	Glycomix Ltd/Carbosynth* (YG153497)	[88,494,495]
Guar Galactomannan	β-1,4-linked D-mannose with α-1,6-linked galactose side units.	Plant (Guar gum).	Megazyme (P-GALLU)	[496]
Gum karaya	Linear chain of α-1,4-linked L-rhamnose, α-1,2-linked D-galactose with α-1,4-linked D-galactose and β-1,3-linked D-glucuronic acid single side units (full structure is still not known). This polyaccharide is partially acetylated.	Plant (*Sterculia urens*)	Glycomix Ltd/Carbosynth* (YG58642).	[27]
Hafnia alvei LPS	Lipopolysaccharide containing repeated units of α-1,3-linked and α-1,2-linked mannose in its O-antigen.	*Hafnia alvei* PCM 1223	Provided by Dr Ewa Katzenellenbogen (Ludwik Hirszfeld Institute of Immunology and Experimental Therapy, Wroclaw, Poland.	[394,497]

Inulin (Glycomix Ltd)	β-2,1-linked fructose polymer generally capped with β-1,2-linked D-glucose units.	Plant (chicory root or jerusalem artichoke)	Glycomix Ltd/Carbosynth*	498
Inulin (screening label: JA Inulin)	β-2,1-linked fructose polymer generally capped with β-1,2-linked D-glucose units.	Plant *(Jerusalem artichoke)*	Sigma Aldrich	498
Konjac glucomannan	β-1,4-linked D-glucose and D-mannose polymer with partial acetylation.	Plant (tubers of *Amorphophallus konjac* or Konnyaku root)	Glycomix Ltd/Carbosynth* (PSn8/YK1033)	499-501
OsLu	Lactulose (Duphalac® [1,4-linked β-D-galactose-D-fructose disaccharide])-derived non-digestible galactooligosaccharides].	See reference	Provided by Mar Vilamiel, Instituto de Investigación en Ciencias de la Alimentación, CIAL (CSIC-UAM), Spain.	489
Pectin	Highly complex polymer consisting of D-galacturonic acid-derived polymers that can include homogalacturonan, rhamnogalatoronan I and II and xylogalacturonan.	Not attainable	Glycomix Ltd/Carbosynth*	51
Pullulan	α-1,6 D-glucose polymer that may comprise α-1,4-linked D-glucose units.	Fungal (e.g. *Aureobasisium pullulans*)	Glycomix Ltd/Carbosynth* (PSn12/YP07957)	502
Psyllium seed gum	Proposed structure: repeating β-1,4 (and 1,3-linked) D-xylose backbone linked to side chains of β-1,3-linked D-xylose, α-1,3-linked L-arabinose, or disaccharide aldobiuronic acid (1,2-linked D-galacturonic acid and L-rhamnose) linked to the xylan backbone.	Plant (*Plantago sp* genus)	Glycomix Ltd/Carbosynth* (YP58645)	43
Scleroglucan	β-1,3-linked D-glucose polymer with β-1,6 side chains every three units.	*Fungal (Sclerotium rolfsii)*	Elicityl (#GLU700)	503

Vivinal®	Commercially-available galactooligosaccharide syrup.	See reference	Obtained from Friesland Campina Domo, Hanzeplein, The Netherlands	[489]
Xyloglucan	β-1,4-linked D-glucose polymer linear chain with α-1,6-linked xylose side units which can be also attached to β-1,2-linked-D-galactose.	Plant: (Taramind)	Megazyme (P-XYGLN)	[36,37]

Glycomix are now owned by Carbosynth Ltd. The information on the source and code of the PS are based on the best available information from Carbosynth Ltd, as information on the original Glycomix is no longer available.**Information on the source is based on the best available information from Carbosynth Ltd. For PS acquired from Megazyme or Sigma Aldrich, the source is based on information on the data sheets. ***Product numbers are stated if known; or for Glycomix PS, they are based on best available information including from the Carbosynth catalogue.*, generic reference including information on PS structure. a, characterised in this thesis by Gas chromatography-mass spectrometry (GC-MS) linkage analysis (see Chapter 4). GPC, gel permeation chromatography.***

2.2. Methods

2.2.1. Cell culture

2.2.1.1. Cell culture maintenance

2.2.1.1.1. Plat E cells

Plat-E cells were grown and maintained using 100 (diameter) x 20 (height) mm or 100 (diameter) x 20 (height) mm culture plates (Starstedt; #83.3902, TC Dish 100, Standard or #83.390, TC 150 Dish, Standard, respectively) in D10 media: Dulbecco's modified Eagle medium (with 25 mM HEPES and 4.5 g/L glucose) (#LZBE12-614F, Lonza, Switzerland) supplemented with 10,000 Units/ml Penicillin/Streptomycin, 1X MEM Non-essential amino acids (#BE13-114E, Lonza, Switzerland) 4 mM L-glutamine, 10 μg/ml blastomycin, 1 μg/m puromycin and 10% FBS. Medium was changed every 2-3 days. Plat-E cells were passaged before reaching 70 - 80% confluency, the supernatant was removed, and the cells were washed with sterile Phosphate buffered saline (PBS [#BE17-512F, Lonza, Switzerland]). Adherent cells were released by adding 2 – 4 ml trypsin-EDTA (Ethylenediaminetetraacetic acid) (0.05%) (#25300054, Gibco™ [Life Technologies], ThermoFisher Scientific, USA) for 3 – 8 min in an incubator at 37°C and 5% CO_2. Culture medium was added to trypsinised cells and the suspension centrifuged at 250 g for 5 min. Cells were then resuspended in D10 medium, added to culture plates, and supplemented with 10 μg/ml blastomycin and 1 μg/ml puromycin.

2.2.1.1.2. BWZ.36 cells

BWZ.36 cells including parental and reporter cells were grown and cultured using 100 (diameter) x 20 (height) mm or 100 (diameter) x 20 (height) mm culture plates (Starstedt; #83.3902, TC Dish 100, Standard or #83.390, TC 150 Dish, Standard, respectively) and in R10 media: RPMI-1640 media (25 mM HEPES and L-glutamine) (#LZBE12-115, Lonza, Switzerland), supplemented with 10,000 Units/ml Penicillin/Streptomycin (#LZDE17-602E, Lonza, Switzerland), 50 mM 2-mercaptoethanol (#21985-023, Gibco™ [Life Technologies], ThermoFisher Scientific, USA) 2 mM L-glutamine (#LZBE17-605E, Lonza, Switzerland) and 10% heat-inactivated foetal bovine serum (FBS) (#10082147, Gibco™ [Life Technologies], ThermoFisher Scientific, USA).

Cells were prepared from frozen stocks by thawing in a heating bath at 37°C for 1 - 2 min, then gently transferred to R10 media in 15 ml conical tubes. Cells were then centrifuged at 570 g for 5 min, the supernatant discarded, resuspended in R10 and cultured in culture plates as previously described.

Typically, cells were passaged every 2 - 3 days when grown to 70 – 80% confluency. Briefly, non-adherent cells were harvested and placed in a 15 ml or 50 ml conical tube. Adherent cells were then treated with 1 – 4 ml PBS-EDTA for 2 – 5 min in an incubator at 37°C and 5% CO_2. Adherent cells were detached by light tapping and the cell suspension added to the non-adherent cells. The cell suspension was centrifuged at 270 g for 5 min, the supernatant discarded, and cells resuspended in R10 media generally using a 1:10 or 1:20 dilution and maintained described above.

For Dectin-1 reporter cell culture, cells were supplemented with 8.6 μM kifunensine (#109944-15-2, Cayman Chemical Company, USA).

2.2.1.1.3. TLR4 reporter cells

TLR4 reporter cells (Invivogen, USA) were cultured, grown, and maintained using 100 (diameter) x 20 (height) mm or 100 (diameter) x 20 (height) mm culture plates (Starstedt; #83.3902, TC Dish 100, Standard or #83.390, TC 150 Dish, Standard, respectively) and in D10 media. Cells were prepared from frozen stocks by thawing in a heating bath at 37°C for 1 - 2 min, then gently transferred to D10 media in 15 ml conical tubes. Cells were then centrifuged at 570 g for 5 min, the supernatant discarded, resuspended in D10 and cultured in culture plates supplemented with 1X HEK-Blue™ selection marker (#hb-sel, Invivogen, USA) with the media changed twice a week. For cell use or passaging, cells were harvested before reaching 80% confluency. The supernatant was removed from the culture plates, and cells were

washed with sterile PBS. Adherent cells were released by incubating with trypsin-EDTA (0.05%) for 2 – 3 min at 37°C and 5% CO_2. Culture media was added to trypsinised cells and the cell suspension centrifuged at 250 g for 5 min, resuspended in D10 media and added to culture plates supplemented with 1X HEK-Blue™ selection marker. Cells were then added to culture plates using an appropriate dilution (for example, 1 : 10) and incubated at 37°C and 5% CO_2. The media was changed twice a week.

2.2.1.1.4. Caco-2 cells

2.2.1.1.4.1. Maintenance of Caco-2 cells

Caco-2 cells were maintained in C2 medium: high glucose (4500 mg/L) DMEM (#5671, Sigma Aldrich, UK) supplemented with 200 mM L-glutamine, 10,000 Units/ml Penicillin/Streptomycin, 1 mM NEAA (#M7145, Sigma Aldrich, UK) and 10% heat-inactivated FBS (#F0804, Sigma Aldrich, UK) [Caco-2 media]. For thawing and initial passaging, cells were gently heated in a water bath at 37°C and transferred to a new tube containing C2 media. The cell suspension was centrifuged at 200 g for 4 min, the supernatant discarded, and the cells resuspended in C2 media. Cells were transferred to T75 culture flasks and the media was changed every 3 - 4 days. All cells were used for experiments between passages 19 and 30.

2.2.1.1.4.2. Transwell culture

For culture on transwells, a protocol previously established by our group was used. Briefly, Caco-2 cells were maintained in T57 flasks as described above. Cell supernatants were discarded, and the cells washed with PBS. Cells were treated with trypsin-EDTA (0.05%) (Sigma Aldrich, UK) and incubated for 2 - 5 min at 37°C and 5% CO_2. C2 medium was then added to the cells and the suspension centrifuged 200 g for 4 min. The cells were then resuspended in C2 medium and counted using a haemocytometer (Bright-Line™). Cells were seeded at $3x10^4$ on the apical side in 100 µl C2 medium in Transwell®-clear 0.4 mm pore cell culture inserts (#734-1581; Corning®, USA). 600 µl medium was then added to the basolateral side and left for 21 days in an incubator at 37°C and 5% CO_2 with the media changed every 3 – 4 days.

2.2.1.2. Cell storage and thawing

BWZ.36 cells, Plat E cells, TLR4 reporter cells, and WT and Dectin-2 KO BMDCs were stored in cell freezing solution (10% sterile dimethyl sulfoxide [DMSO] in FBS and stored at -80°C. Caco-2 cells were stored in C2 medium containing 10% DMSO.

For the thawing of all cells used in this thesis prior to initial culture, cells were gently heated in a water bath at 37°C for 1 – 2 min and transferred to a new tube of media for subsequent culture (described in 2.2.1.1.).

2.2.2. Generation and culture of bone marrow-derived dendritic cells

2.2.2.1. Isolation of murine bone marrow cells

The femur bones of mice (from C57BL6/6J WT or Dectin-2 KO mice) were isolated and cleaned with ethanol in tissue culture plates. Bones were then placed in a new tube and washed with Hanks's balanced saline solution (HBSS, Lonza, Switzerland) supplemented with 3% FBS. Bones were crushed using a mortar and pestle suspended in HBSS 3% FBS. The supernatant was transferred into a collection tube using a cell Falcon® 40 μm strainer. HBSS supplemented 3% FBS (2 – 5 ml) was then added and the crushing of bones was repeated followed by transfer to the same collection tube, as previously described. The cell suspension was centrifuged at 270 g for 10 min, the supernatant removed, and the cells dispersed by gently tapping the tube. 3 ml of 1 X red cell lysis buffer (Ammonium chloride lysis buffer [8.02 g Ammonium chloride, 0.84 g sodium bicarbonate, 0.37 g EDTA disodium dissolved in 100 ml sterile filtered H_20 for a 10X stock concentration]) was added to cells and left at room temperature (R.T) for 5 min. The solution was centrifuged at 270 g for 10 min, the cell pellet resuspended in HBSS 3% FBS and passed through a Falcon® 40 μm cell strainer. The cell suspension was again centrifuged at 270 g for 10 min, resuspended in HBSS 3% FBS and cells were counted using a haemocytometer. Cells were resuspended in cell freezing solution as described above and added to cryogenic freezing vials (#10344691, Nalgene™, Thermo Fisher Scientific, USA) at $1x10^7$ cells per vial and stored at -80°C.

2.2.2.2. In vitro generation of bone marrow-derived dendritic cells

Mouse WT or Dectin-2 KO BMDCs were generated *in vitro* from isolated bone marrow cells as described above[394,504]. Briefly, bone marrow cells were thawed 1 - 2 min in a heating bath at 37°C. Cells were gently transferred into a new tube containing M10 media (R10 media supplemented with 1 mM non-essential amino acids [#M7145, Sigma Aldrich, UK] and 1 mM sodium pyruvate [#BE13-115E, Lonza, Switzerland]). The cells were centrifuged at 270 g for 10 min, resuspended in M10 medium and cells were counted using a haemocytometer. Typically, cells were added to 10 cm culture plates at $3x10^6$ cells per dish. Generally, for older cell stocks (> 3 - 5 months), cells were added at $5x10^6$ or $10x10^6$ cells per dish. 20 ng/ml of

granulocyte-macrophage colony stimulating factor[505] (GM-CSF) (#315-03, Peprotech, UK) was added to the culture plates and cells were left for 6 days at 37°C 5% CO_2[394]. Adherent cells were used for all BMDC experiments.

2.2.3. Flow Cytometry

2.2.3.1. Flow cytometer settings

For lazer and collection filter settings see Appendix 4.

2.2.3.2. Assessment of cell surface expression

2.2.3.2.1. BWZ.36 reporter cells

BWZ.36 cells were maintained as previously described in 2.2.1.1.2. Non-adherent SIGNR1, SIGNR1-QPD, Dectin-2 or Dectin-2-QPD cells were transferred to 15 ml or 50 ml conical tubes. Adherent cells were treated with PBS-EDTA (#BE02-017F, Lonza, Switzerland) and incubated at 37°C and 5% CO_2 for 2 – 3 min. Wells were gently tapped by hand to remove any remaining adherent cells. Adherent cells were added to the 15 ml conical tube of non-adherent cells and centrifuged at 270 g for 5 min. The supernatant was discarded, and the pellet dispersed gently by tapping the tube and then cells were resuspended in R10 media. Typically, 200 μl cell suspension ($5x10^5$ cells) was transferred into separate wells of a round-bottomed 96-well plate (#83.3924.005, TC Plate 96 Well, Standard, Starstedt, UK,). Cells were centrifuged at 510 g for 3 min, the supernatant discarded and the plate briefly vortexed. 40 μl IgM isotype-Alexa 647 control or anti-mouse SIGNR1-Alexa 647 were added to SIGNR1 or SIGNR1-QPD cells at a final concentration of 10 μg/ml in FACS buffer (HBSS [#BE10-527F, Lonza, Switzerland] supplemented with 0.1% FBS and 2 mM EDTA [#15575-038, Invitrogen™ Life Technologies, ThermoFisher Scientific, USA]). Anti-mouse Dectin-2-Alexa 647 and IgG2a isotype-Alexa 647 and were added to cells at a final concentration of 2.6 μg/ml in FACS buffer. For all experiments (excluding Appendix 5 and Appendix 7), 1 μl mouse-fc block (#101320, TruStain FcX™, anti-mouse CD16/32, Biolegend, UK) was immediately added and cells were left on ice in the dark for 30 min. Cells were washed using 200 μl FACS buffer and centrifugation at 510 g for 3 min. FACS buffer (200 μl) was then added to cells and transferred to FACS tubes. Propidium iodide (PI [a fluorescent intercalating agent used to stain for dead cells[394]]) was added to cells at a final concentration of 0.33 μg/ml. PI-stained unlabelled cells (additional control) and Non-PI-stained unlabelled cells were also prepared for compensation protocols. Compensation was performed as described in 2.2.3.2.3. Cell surface expression analysis of all BWZ.36 cells were

performed using a LSR Fortessa flow cytometer (BD Biosciences) and the data analysed in FlowJo, version 10 (TreeStar, USA).

2.2.3.2.2. Bone marrow-derived dendritic cells

For detection of Dectin-2 cell surface expression, BMDCs were generated and maintained as previously described in 2.2.2. Non-adherent BMDCs cells were discarded and adherent cells were washed with PBS. Adherent cells were treated with PBS-EDTA and kept in an incubator at 37°C and 5% CO_2 for 10 - 15 min. Adherent cells were removed using a sterile cell scraper. Cells were centrifuged at 270 g for 5 min and resuspended in M10 medium. 200 μl cell suspension ($1x10^6$ cells per well) was added to 96-well round bottom plates (#83.3924.005, Starstedt, UK). The cells were centrifuged at 510 g for 3 min, the supernatant removed and briefly vortexed. Anti-Dectin-2 and IgG isotype antibodies were added to the cells at a final concentration of 2.6 μg/ml in FACS buffer, and 1 μl mouse Fc block (#101320, TruStain FcX™, anti-mouse CD16/32, Biolegend, UK) was immediately added. Cells were immediately incubated on ice for 30 min. Cells were then washed using 200 μl FACS buffer and centrifuged at 510 g for 3 min and the supernatant removed. 200 μl FACS buffer was added to the cells and the suspension transferred to FACS tubes. PI was added to cells at a final concentration of 0.33 μg/ml. PI-stained unlabelled cells (additional control) and Non-PI-stained unlabelled cells were also prepared for compensation protocols. Compensation was performed as described in 2.2.3.2.3. Analysis was performed using a LSR Fortessa flow cytometer (BD Biosciences) and BD software (BD FACSDiva Version 7.0).

2.2.3.2.3. Compensation

Comp Beads anti-rat Ig κ and negative control compensation particle sets (#552845, BD Biosciences, USA) were used for compensation in all BWZ.36 cells or BMDC flow cytometry experiments unless otherwise stated in Figure legends. Briefly, 10 μl anti-rat Ig κ and 10 μl negative control were incubated with 100 μl FACS for 10 - 15 min in the dark and 1 μl fluorescently-labelled rat IgM isotype-Alexa 647 (for SIGNR1 and SIGNR1-QPD reporter cells) or rat IgG2a isotype-Alexa 647 [for Dectin-2 or Dectin-2-QPD, or reported cells or BMDCs) was added for another 10 – 15 min with the tube protected from light. PI and non-PI stained cells were also prepared for analysis. Compensation was applied using the standard procedure provided by the BD software (BD FACSDiva version 7.0, BD Sciences, USA).

2.2.3.3. Cell Sorting GFP-positive BWZ.36-transfected cells and following cell culture

GFP-positive-transfected BWZ.36 cells were isolated using a Sony SH800 Cell Sorter. Briefly, transfected-cells were resuspended in sterile FACS buffer supplemented with 0.33 μg/ml PI and transferred through a 40 μm cell strainer into a FACS tube. Cells were sorted using a Sony SH800 Cell Sorter and collected in 15 ml tubes containing FBS and prepared for culture as described in 2.2.4.3.

2.2.3.4. Analysis of Caco-2 cell death and apoptosis.

Caco-2 cells were prepared and maintained as described in 2.2.1.4.1. The cell supernatant was removed and replaced with C2 medium without phenol red (C2 medium composition [section] but using DMEM high glucose, no phenol red, no glutamine [#31053028, Gibco™, ThermoFisher Scientific, UK] at least 4 days prior to any sample treatment. Cells were grown to reach 70 – 80% confluency and the supernatant was removed, and adherent cells were washed with sterile PBS. Cells were removed by adding trypsin-EDTA (0.05%) (Sigma Aldrich, UK) and incubated for 2 - 5 min at 37°C and 5% CO_2. C2 medium was then added to the cells and the suspension centrifuged 200 g for 4 min. The cells were then resuspended in C2 medium and counted using a haemocytometer. $5x10^4$ cells were added to individual wells of a 96 well flat-bottomed plate (#83.3924, Sarstedt, UK).

For treatment of the cells, cells were incubated with 1 mg/ml LPS from *E. coli* 0111:B4 (#L2630, Sigma Aldrich, UK), 10 or 100 ng/ml TNF-α (#300-01A, Peprotech EC Ltd, UK) or 200 μg/ml ES levan or C2 medium alone (control) in a total volume of 200 μl per well. for 24 hr incubation at 37°C and 5% CO_2. For positive controls, 1 μM staurosporine (apoptosis control [#ab120056, Abcam Ltd, UK]) and 1% Triton™ X-100 (dead cell control [#T8787, Sigma Aldrich, UK]) were added to the cells and incubated for 4 hr and 30 min, respectively.

Analysis of cell death/apoptosis was performed using a Dead Cell Apoptosis Kit with Annexin V FITC and PI for Flow Cytometry (#10267392, Invitrogen™, Life Technologies, ThermoFisher Scientific, USA) following the manufacturer's instructions with adaptions. Briefly, treated-cells were centrifuged at 510 g for 3 min and the supernatant discarded. The cell pellet was washed with sterile PBS and centrifuged at 510 g for 3 min and resuspended in annexin-binding buffer (in the kit supplied by Invitrogen™, Life Technologies, ThermoFisher Scientific, USA). Cells were gently mixed by pipetting up and down. 1 μl of PI working solution (100 μg/ml) and 5 μl of FITC Annexin (in the kit supplied by Invitrogen™, Life Technologies,

ThermoFisher Scientific, USA) were added to the cells and kept in the dark at R.T for 15 min. Cells were kept on ice and analysed using a LSR Fortessa flow cytometer (BD Biosciences) and BD software (BD FACSDiva Version 7.0).

2.2.4 Construction of BWZ.36 SIGNR1 and SIGNR1-QPD reporter cells

2.2.4.1. Cloning of SIGNR1

2.2.4.1.1. PCR amplification of SIGNR1.

SIGNR1 primers were designed to amplify the extracellular domain of SIGNR1 containing a HpaI restriction site before the domain and a NotI restriction site after the stop codon. Further, the first two amino acids of the extracellular domain of SIGNR1 were omitted to ensure that the transmembrane region was completely absent.

The extracellular domain of SIGNR1 from SIGNR1 cDNA was amplified by PCR using Phusion® High-Fidelity DNA Polymerase (#M0530S, New England Biolabs, UK). Briefly, the following was added at final concentrations into a PCR reaction tube: 5 μM SIGNR1 forward primer, 5 μM SIGNR1 forward primer, 10 ng SIGNR1 template cDNA, 0.2 mM deoxynucleotide (dNTP) solution mix (#10297018, Invitrogen™, Thermo Fisher Scientific, UK), 1X Phusion HF buffer (#M0530S, New England Biolabs Ltd, UK), 1 unit/50 μl Phusion DNA Polymerase, and sterile filtered H_20 (#BE17-724Q, Lonza, Switzerland) in a total reaction volume of 100 μl. The reaction mix was subjected to stepwise heating using a thermocycler (Techne® Prime, Techne, UK) set at 4 stages: stage 1, 1 cycle at 98°C for 30 sec; stage 2, 20 cycles of 98°C for 10 sec, 65°C for 30 sec and 72°C for 30 sec; stage 3, 98°C for 30 sec, 50°C for 20 sec and 72°C for 30 sec; and stage 4, 72°C for 5 min.

2.2.4.1.2. Gel electrophoresis and isolation of SIGNR1 DNA

PCR products were subjected to aragose gel electrophoresis and imaged by fluorescence. Briefly, a 1% aragose solution was prepared in Tris acetate-EDTA (TAE) buffer (#T9650, Sigma Aldrich, UK) in a conical flask and microwaved for 1 – 2 min and gently stirred until completely dissolved. The mixture was placed in a casting tray with the well comb in place and left to set for 20 min. The set gel was transferred into a gel box and moved into an electrophoresis apparatus (#G9-2500, Mupid-ONE, Geneflow Ltd, UK). 1X loading dye was added to each PCR sample and the solution was loaded into wells (15 μl – 50 μl total volume depending on the comb used). A 100 base pair (bp) DNA ladder (#G2101, Promega™, UK), ranging from

100 bp to 1500 bp was used for size determination. Electrophoresis was performed typically at 100 v for 20 min. The gel was then transferred into a tray and incubated in an ethidium bromide solution for 20 min, washed in H_20 and imaged using a fluorescence imager (Alphaimager®, Alpha Innotech, USA).

The extracellular domain (missing the first two amino acids) of SIGNR1 (Ser76 – Gly324[212]) is 753 bp and the restriction enzyme sequences NotI and HpaI are 8 and 6 bp's, respectively. The 767 bp PCR product corresponding to HpaI-SIGNR1-NotI was cut from the aragose gel using a sterile scalpel and transferred into 1.5 ml Eppendorf tubes.

2.2.4.1.3. Extraction and quantification of SIGNR1 DNA

SINGR1 DNA was extracted using a GeneJET Gel extraction kit (#K0691, ThermoFisher Scientific, UK) following the manufacturer's instructions. Total DNA was quantified using a NanoDrop™ 2000 Spectrophotometer (ThermoFisher Scientific, UK).

2.2.4.1.4. Ligation of SIGNR1 DNA into pBluescript II KS+ vector using T4 DNA ligase

A pBluescript II KS linear vector previously digested with restriction enzyme SmaI (#R0141S, New England Biolabs, USA) and dephosphorylated on the 5' prime end using shrimp alkaline phosphatase (#04898133001, Roche, Germany) was obtained from the Kawasaki group (Institute of Food Research, Norwich, Norwich Research Park, UK). The HpaI-SIGNR1-NotI PCR product was incubated with pBluescript II KS and T4 DNA ligase (#M0202T, New England Biolabs, USA), as described below. Briefly, 50 ng of pBluescript II KS was incubated with T4 DNA ligase reaction buffer, T4 DNA ligase, and sterile filtered H_20 with 62.75 ng Hpa1-SIGNR1-Not1 in PCR tubes in a total reaction volume of 15 μl at 16°C for 1 hr. A 5:1 Hpa1-SIGNR1-Not1 (764 bp) to pBluescript II KS (~3000 bp) ratio was used for the reaction.

2.2.4.1.5. Transformation of competent *E. coli*

The ligation mixture was used to transform competent *E. coli* DH5α (*E. coli* DH5α) (#C2987H, New England Biolabs, USA). Briefly, *E. coli* DH5α was thawed on ice for 10 min. 1 μl of ligation mix was added to 25 μl *E. coli* DH5α in 1.5. ml Eppendorf tubes, gently mixed and left on ice for 15 min. *E. coli* DH5α were heat-shocked by incubating in a water bath at 42°C for 30 sec. Tubes were then placed on ice for 3 min. 300 μl of SOC medium (to obtain optimal transformation efficiency ([#S1797, Sigma Aldrich, UK]) was added to each tube. The 1.5. ml tubes (containing the SOC medium, *E. coli* and ligation mix) were placed into 50 ml centrifuge tubes and left in

a shaking incubator at 37°C, 250 rpm for 30 min. The bacterial suspension (150 μl) was spread onto across LB-carbenicillin agar plates agar plates until fully incorporated using a sterile spreader. The agar plates were then incubated overnight at 37°C until bacterial colonies were visible and were kept at 4°C.

2.2.4.1.6. Colony PCR

Colony PCR was performed using Taq DNA polymerase to identify colonies containing pBluescript II KS+-SIGNR1. Briefly, 1X PCR reaction buffer (#11271318001, Roche, Germany), dNTP solution (#10297018, Invitrogen™, USA), M13 forward/reverse primers and Taq DNA polymerase (#11146173001, Roche, Germany) were added to PCR tubes of final concentrations/units of 200 μM, 0.5 μM, 0.5 μM and 1.25 units respectively in sterile filtered H_20 in a final reaction volume of 25 μl. Selected colonies were added to the PCR mix using a sterile pipette tip and subjected to PCR using a thermocycler set at the following; denaturing, 1 cycle at 94°C for 30 sec; amplification, 35 cycles of 94°C for 30 sec, 55°C for 30 sec and 72°C for 1 min 46 sec; and a final extension, 72°C for 5 min. In absence of the insert, the product of the reaction is expected to be ~50 - 200 bp while the size of the recombinant plasmid containing Hpa1-SIGNR1-Not1 would be ~817 - 967 bp. Aragose gel electrophoresis of the colony PCR was performed and imaged as described in 2.2.4.1.2. A 1 kb DNA ladder (#N3232S, New England BioLabs, USA) was used for size determination.

2.2.4.1.7. Amplification and purification of the pBluescript II KS+-SIGNR1 recombinant vector

Positive colonies were cultured in 10 ml Lysogeny broth (LB) media in a 50 ml tube supplemented with 50 μg/ml carbenicillin in a shaker incubator overnight at 37°C at 250 rpm. pBluescript II KS-SIGNR1 plasmids were isolated from overnight liquid cultures using a QIAprep® Spin Miniprep Kit (#27104, Qiagen, USA) following the manufacturer's instructions. Vector DNA was quantified by a NanoDrop™ 2000 Spectrophotometer (ThermoFisher Scientific, USA). pBluescript II KS+-SIGNR1 plasmid was sequenced by Eurofins using a SmartSeq Kit according to manufacturer's instructions and ApE-A plasmid Editor v2.0.47.

2.2.4.1.8. Digestion of pBluescript II KS+-SIGNR1 using HpaI and NotI restriction enzymes.

pBluescript II KS-SIGNR1 was digested by restriction enzymes HpaI (#R0105S, New England Biolabs, USA) and NotI High Fidelity HF™ (#R3189S, New England Biolabs, USA). Briefly, the following were added into a PCR tube: 5 μg pBluescript II KS-

SIGNR1 plasmid, 1X CutSmart® buffer (#B7204S, New England Biolabs, USA), 5 units of HpaI and 5 units NotI enzymes and sterile filtered H_20 in a total reaction volume of 25 μl. Mixtures were incubated at 37°C for 1 hr and subjected to gel electrophoresis and imaged as described previously. A 1kb DNA ladder (#N3232S, New England BioLabs, USA) was used for size determination. The Hpa1-SIGNR1-Not1 insert was extracted from the gel using a sterile scalpel and purified and quantified as described in 2.2.4.1.3.

2.2.4.1.9. Cloning SIGNR1 into pMXs-IG-CD3ζ-Ly49

pMXs-IG contains the intracellular (CD3ζ) and transmembrane (Ly49) fusion DNA sequence (423 bp) required for ligation with the CLR extracellular domain sequence. This plasmid also contains the sequence for enhanced green fluorescent protein (EGFP). A pMXs-IG vector previously dephosphorylated on the 5' prime end and digested by HpaI and NotI was obtained from the Kawasaki group. A ligation reaction with HpaI-SIGNR1-NotI into pMXs-IG vector was performed using T4 DNA ligase and used to transform *E. coli* DH5α, as described in 2.2.4.1.4 and 2.2.4.1.5 (with equivalent pMXs-IG and SIGNR1 DNA).

Colony PCR (see 2.2.4.1.6.) was used to identify colonies containing the pMXs-IG-SIGNR1 vector. CD3ζ-Ly49 contains 423 bp and SIGNR1 ~762 bp. M13 primers start ~50 – 200 bp upstream. Therefore, a band of ~1232 – 1382 bp indicates the pMXs-IG-SIGNR1 vector. A 100 bp DNA ladder was used for bp size determination.

Selected colonies were cultured and the pMXs-IG-SIGNR1 vector DNA was isolated and purified using a QIAprep® Spin Miniprep Kit (Qiagen, USA) according to the manufacturer's instructions. The isolated DNA was then quantified by a NanoDrop™ 2000 spectrophotometer (Thermo Scientific, USA).

2.2.4.2. Cloning of SIGNR1-QPD

The CRD of mannose-specific lectins including SIGNR1 contain an EPN (Glutamic acid, Proline and Asparagine) amino acid motif[334]. SIGNR1 CRD-mutant cells were established by switching the EPN amino acid motif to galactose-specific QPD (Glutamine, Proline and Aspartic acid) when designing the SIGNR1 extracellular domain sequence (2 mutations: E285 – Q; D287 - N)[212]. SIGNR1-QPD reporter cells control for carbohydrate-specific ligand-binding through the CRD.

Establishment of SIGNR1-QPD mutant reporter cells was similar to the procedure with SIGNR1 WT reporter cells. Briefly, the Pu57-HpaI-SIGNR1-QPD-NotI recombinant vector was digested by HpaI and NotI and subjected to aragose gel

electrophoresis and fluorescent imaging and the DNA isolated and quantified as described in 2.2.4.1.8. Ligation of SIGNR1-QPD to linearised pMXs-IG was performed using the T4 DNA ligase protocol as described in 2.2.4.1.4 (with equivalent pMXs-IG and SIGNR1-QPD). Transformation with the SIGNR1-QPD recombinant vector into *E. coli* DH5α, colony PCR, gel electrophoresis and fluorescent imaging of the gel were used to identify colonies positive for SIGNR1-QPD as described in 2.2.4.1.5., 2.2.4.1.6. and 2.2.4.1.2. (with equivalent pMXs-IG-SIGNR1-QPD). Positive colonies for containing the SIGNR1-QPD recombinant vector were cultured overnight in 50 ml tubes in LB medium and the vector DNA was extracted using Gene JET Gel extraction kit (#K0691, ThermoFisher Scientific, UK) according to the manufacturer's instructions. The DNA sequence was confirmed using a Eurofins SmartSeq kit according to the manufacturer's instructions and ApE-A plasmid Editor v2.0.47.

2.2.4.3. Transfection of SIGNR1 and SIGNR1-QPD recombinant vectors in BWZ.36 parental cells

Retroviral vectors are an effective method to insert genes directly into a cell's genome[506]. The package cell line Plat-E, contains an envelope protein gene[507]. pMXs-IG-CLR containing an envelope protein gene can be transfected into Plat-E cells resulting in the production of efficient retroviruses containing the selected vector DNA which are unable to replicate[507]. The isolated retrovirus is then incubated with BWZ.36 cells ultimately leading to infection and incorporation of the plasmid DNA into the genome of the cells.

For transfection of pMXs-IG-SIGNR1 or pMXs-IG-SIGNR1-QPD vector DNA to Plat-E cells, cells were grown to ~70 - 80% confluency and maintained as described in 2.2.1.1.1. Plat-E cells were counted using a haemocytometer (Bright-Line™, Cambridge Instruments Ltd, UK) and cells were resuspended in D10 medium added to flat 6-well plates (#83.3920, Sarstedt, UK) at $1x10^6$ cells per well. Cells were left overnight at 37°C 5% CO_2. Transfection into Plat E cells was performed using Lipofectamine® 2000 Transfection Reagent (#11668027, Thermo Fisher Scientific, UK) in line with manufacturer's instructions. Briefly, a solution was made adding 7.4 μl (5 μg) of pMXs-IG-SIGNR1 vector DNA to 250 μl Opti-MEM™ (Gibco®, ThermoFisher Scientific, UK) in a 1.5 ml Eppendorf tube and left at R.T for 5 min. In a separate tube, a lipofectamine solution was made by adding 1 ml Opti-MEM™ (Gibco™, ThermoFisher Scientific, USA) to 40 μl Lipofectamine® 2000 transfection reagent, briefly vortexed, and left at R.T for 5 min. The DNA solution was added to

the lipofectamine solution and incubated for 10 min at R.T 500 μl solution was then carefully added to Plate E cells. Following 2-day incubation at 37°C and 5% CO_2, Plat E supernatants were harvested in a 15 ml conical tube and centrifuged at 270 g for 5 min to separate the cells from the virus ready to be added to BWZ.36 parenteral cells which were maintained and prepared as described in 2.2.1.1.2. Upon reaching 70 – 90% confluency, BWZ.36 cells were seeded in 6-well plates at $1x10^5$ cells per well (3 ml volume). Plat E supernatant (2 ml) was transferred to BWZ.36 parenteral cells and 8 μg/ml Polybrene (#TR-1003-G, Sigma Aldrich, UK) was added, and the cells incubated for 2 days in at 37°C and 5% CO_2. Non-adherent cells were then harvested to a 15 ml conical tube and adherent cells were treated with 0.5 ml PBS-EDTA to released cells. These cells were then added to the non-adherent cells and the cell suspension centrifuged at 270 g for 5 min. Cells were resuspended in R10 media and maintained as described in 2.2.1.1.2 in 6-well plates. The SIGNR1 WT cells were assessed for SIGNR1 expression (WT only) by flow cytometry as described in 2.2.3.2.1 (compensation not included) to assess if transfection occurred.

After cell sorting transfected-BWZ.36 SIGNR1 or SIGNR1-QPD reported cells, cells were expanded to make cell stocks. Sorted cells (in FBS) were centrifuged 270 g for 5 min, resuspended in 2 ml R10 medium and added to flat-bottom 24 well plates (#CLS3527, Corning® Costar® TC-Treated Multiple 24-Well Plates) and left in an incubator at 37°C and 5% CO_2 for 2 – 3 days. Cells were then maintained as previously described in 2.2.1.1.2 and passaged/expanded using 24 well, 6 well, 100 mm and 150 mm culture plates to make more cell stock. Cells were stored as described in 2.2.1.2.

2.2.5. Reporter cell assays

2.2.5.1. BWZ.36 reporter cell assay

PS, glycoconjugates, oligosaccharides or SIGNR1 functional grade antibody were prepared in sterile coating buffer (8.4 g sodium bicarbonate (#S5761, Sigma Aldrich, UK), 3.56 g sodium carbonate (#S7795, Sigma Aldrich, UK) in 1l deionized water, pH 9.5) and coated onto a flat-bottom 96-well ELISA plate (#10547781, Immuno Maxisorp, ThermoFisher Scientific™, USA) overnight at 4°C. Final concentrations are described in Figure legends.

BWZ.36 reporter cells, including SIGNR1, SIGNR1-QPD, Dectin-2, Dectin-2-QPD, Dectin-1 and mock cells, were prepared from frozen stocks and maintained as described in 2.2.1.1.2. Cells were typically grown to 70 – 90% for reporter assay experiments. Briefly, non-adherent cells were harvested and transferred into a

separate 15 or 50 ml conical tube. Adherent cells were treated with 1 – 4 ml PBS-EDTA for 2 – 5 min in an incubator at 37°C and 5% CO_2. Adherent cells were then harvested and added to the non-adherent cells. The cell suspension was centrifuged at 270 g for 5 min, the supernatant discarded, and cells resuspended in R10 media. Cells were then counted using a haemocytometer and diluted to obtain 5 x 10^5 cells/ml.

The 96 well plates incubated with PS coating buffer solutions were removed from the wells using an aspirator pump and sterile glass pipette. Wells were then washed once with 200 µl PBS, and PBS was discarded. 200 µl of cell suspension was then added to each PS-coated or control-coated (coating buffer alone) wells at 1x10^5 cells per well. Cells were incubated at 37°C at 5% CO^2 overnight for 18 hr. The next day, cells were centrifuged at 510 g for 3 min, the supernatant discarded, and the cells briefly vortexed. 100 µl chlorophenol red-β-D-galactopyranoside (CPRG) working solution (100 mM 2-Mercaptoethanol [#M6250, Sigma Aldrich, UK] 0.125 % Triton X-100 [#T8787, Sigma Aldrich, UK] in PBS) containing 1.5 µM CPRG (#10884308001, Roche, Switzerland) was then added to cells. β-galactosidase activity was assessed by measuring absorbance at 570 nm and subtracted from 630 nm reference using a microplate reader (Benchmark Plus™, Bio-Rad, UK) using the Bio-Rad Microplate Manager software version 5.2.1.

2.2.5.2. TLR4 reporter cell assay

Binding to HEK hTLR4 reporter cells activates the NFkB pathway producing secreted embryonic alkaline phosphatase (SEAP) [under control of the IL-12 p40 promoter] which is detected in a colorimetric assay by the addition of HEK-Blue™Detection medium (#hb-det2, Invivogen, USA)[394].

TLR4 reporter cells were maintained as described in 2.2.1.1.3. TLR4 reporter assays were performed using HEK-Blue™ detection medium and following the manufacturer's instructions with minor modifications. Typically, cells were grown to 50 – 80% confluency, the supernatant discarded, and the cells were washed with PBS. Cells were incubated with PBS for 5 – 10 min in an incubator at 37°C and 5% CO_2 and gently tapped to remove adherent cells and harvested into a 15 or 50 ml tube. Cells were centrifuged at 250 g for 5 min, resuspended in D10 media and counted using a haemocytometer. Cells were then centrifuged at 250 g for 5 min, resuspended in appropriate volumes of HEK-Blue™ detection medium and 2.5 x 10^4 cells were added to each well of a flat-bottomed 96 well plate (#83.3924, Sarstedt, UK). All treatments were prepared in HEK-Blue™ detection medium which was

added to wells containing the cells in a total volume of 200 μl. Hafnia-LPS (see Table 5) was used as a positive control in all TLR4 reporter assay. Final concentrations of all treatments are outlined in the Figure legends. Treated-cells were incubated for 16 – 24 hr at 37°C and 5% CO_2. Absorbance was read at 655 nm using a microplate reader (Benchmark Plus™, Bio-Rad, UK).

2.2.6. Cytokine/chemokine analysis

2.2.6.1. Enzyme-linked immunosorbent assay

2.2.6.1.1. Analysis of bone marrow-derived dendritic cell supernatants by Enzyme-linked immunosorbent assay

Concentrations of TNF-α, IL-6 or IL10 in supernatants were determined by Enzyme-linked immunosorbent assay (ELISA) (mouse TNF-α [#430901], IL-6 [#431301] or IL10 [431411] ELISA MAX™, Biolegend™, UK) following the manufacturer's instructions. Briefly, TNF-α and IL-6 capture antibodies diluted in assay diluent (1% BSA in PBS) and IL-10 antibodies were diluted in PBS. 100 μl capture antibodies were coated overnight in the wells of flat-bottom 96-well ELISA plates (#10547781, Immuno Maxisorp, ThermoFisher Scientific™, USA) at 4°C. The next day, the capture antibody solutions were discarded, and the plates were washed 4 times with 300 μl wash buffer (PBS in 0.05% Tween-20) and the wells blocked by adding assay diluent and the plate sealed for 1 hr at R.T. The wells were then washed as previously described. 100 μl of levan or peptidoglycan (in assay diluent) and serial standard dilutions (in assay diluent) were added to wells for 2 hr at R.T with the plate sealed. Plates were then washed as described above. 100 μl detection antibody was then added to wells and the plates sealed at R.T for 1 hr. Plates were then washed as previously described and 100 μl of Avidin-horse radish peroxidase solution was added and incubated at R.T for 30 min. Plates were then washed as previously described with an additional wash step. Tetramethylbenzidine (TMB) (Biolegend, UK) was added to wells and the plates were kept in the dark until a colour change developed. Absorbance was read at 450 nm subtracted from 570 nm using a microplate reader (Benchmark Plus™, Bio-Rad, UK). For all tests, cytokine concentrations were quantified from absorbance values interpolated from non-linear standard curves using a 3-parameter logistic regression which was generated in GraphPad Prism (V 6.05).

2.2.6.1.2. Quantification of IL-8 in TNF-α-induced Caco-2 cells

Caco-2 monolayers were prepared as previously described in 2.2.1.1.4.1 and treated with media alone, or 10 or 100 ng/ml TNF-α on the apical side only or both apical

and basolateral sides. Final volumes were 100 μl and 600 μl for apical and basolateral compartments, respectively. IL-8 was measured by ELISA (Human IL-8 ELISA MAX™ Standard MAX™, Biolgend, UK) using the protocol described in 2.2.6.1.1. Of note, IL-8 capture antibody was diluted in assay diluent, as per manufacturer's instructions.

2.2.6.2. Screening of cytokine production by Caco-2 cells using 2.6.2.1. Meso Scale Discovery®

Caco-2 monolayers were cultured and maintained as previously described in 2.2.1.1.4.1.

For the levan treatment, cells were pre-incubated with levan (190 μg/ml) or media (control) on both apical and basolateral sides for 24 hr followed by TNF-α challenge (10 or 100 μg/ml) or media control for another 24 hr. For the simultaneous treatment, cells were incubated with levan (200 μg/ml) or media (control) on both apical and basolateral sides and immediately followed by TNF-α challenge (10 or 100 μg/ml) or media control for 24 hr. Final volumes across treatments were 100 μl and 600 μl for apical and basolateral compartments, respectively. Apical and basolateral supernatants in each well were transferred to new tubes. Cytokine analysis of cell supernatants was performed using a custom Meso Scale Discovery® (MSD) U-PLEX® Multiplex Assay (#K15067L-1 Biomarker Group 1 plate: U-PLEX Human IFN-γ U-PLEX Human IL-1β U-PLEX Human IL-6 U-PLEX Human IL-8 U-PLEX Human IL-10 U-PLEX Human MCP-1 U-PLEX Human MIF U-PLEX Human TNF-α U-PLEX Human TSLP; and TGF-β plate [#K151XWK-1], Meso Scale Diagnostics, USA) with assay procedures performed in accordance with manufacturer's instructions. Results were obtained by measuring electrochemiluminescence using an Meso™ QuickPlex SQ120. For all tests, cytokines and chemokines were quantified from absorbance values interpolated from non-linear standard curves using a 4-parameter logistic regression which was generated by the Discovery Workbench software version 4.

2.2.7. Bone marrow-derived dendritic cell treatments

2.2.7.1. Non-plate-immobilised ligand procedure

BMDCs were generated and maintained as described in 2.2.2. Non-adherent BMDCs cells were discarded and adherent cells were washed with PBS. Adherent cells were treated with PBS-EDTA and kept in an incubator at 37°C and 5% CO_2 for 10 - 15 min. Adherent cells were removed using a sterile cell scraper. Cells were centrifuged at 270 g for 5 min and resuspended in M10 medium and counted using a

haemocytometer. Levans or positive control peptidoglycan were diluted in M10 media added to round bottomed 96-well plates (#83.3925, Sarstedt, UK) containing $1x10^6$ BMDCs per well in a total volume of 200 μl for 18 hr. Final concentrations of levan or ligands are provided in the Figure legends. 96-well plates were centrifuged 510 g for 3 min and the supernatant transferred into new 96-well plates. TNF-α, IL-6 or IL10 in cell supernatants were measured by ELISA (see 2.2.6.1.1).

2.2.7.2. Plate-immobilised ligand procedure

Plate-immobilisation of ligands or levan was performed as per the coating of PS in the BWZ.36 reporter cell assay as described in 2.2.5.1. Coating buffer alone was used as a negative control (including for cells alone with medium). BMDCs were prepared as previously described for the non-plate-immobilised procedure where $1x10^6$ cells were added to PS-coated wells in 96-well plates in a total volume of 200 μl. TNF-α, IL-6 or IL10 in cell supernatants were measured by ELISA (see 2.2.6.1.1).

2.2.7.3. Inhibition assay

BMDCs were generated and maintained and prepared as described in 2.2.2. Non-plate-immobilised or plate-immobilised levan/control was performed as described above. For LPS-challenge after 3, 6, 12 or 24 hr of levan/control incubation, BMDCs were treated with 20 ng/ml *E. coli* K12 LPS (#TLR-PEKLPS, Ultrapure, Invivogen, UK) or M10 media (negative control stimulus) for 24 hr. Final volumes across all treatments in the 96-wells were kept at 250 μl following LPS-challenge. Levan pre-treatment/incubation times are indicated in the Figure legends. TNF-α, IL-6 or IL10 in cell supernatants were measured by ELISA (see 2.2.6.1.1).

2.2.8. Measurement of monolayer barrier integrity

Caco-2 cells monolayers were maintained and prepared as described in 2.2.1.1.4.2.

For the LPS treatment, cell supernatants were removed and both apical and basolateral compartments were washed with C2 media. Cells were then pre-treated 200 μg/ml ES levan or media (control) on the apical side or both apical and basolateral sides for 2 or 24 hr followed by the addition of 1 mg/ml *E. coli* 0111:B4 LPS. For TNF-α experiments, all treatments are described in 2.2.6.1.2 and 2.2.6.2.

Prior to the addition of FITC-dextran, cells were washed with C2 media on both apical and basolateral sides. 100 μl 1 mg/ml of FITC-dextran (Sigma Aldrich, UK) was added to apical compartments and 600 μl C10 was added to basolateral compartments and incubated for 4 hr. Following incubation, the basolateral

supernatant was collected. In addition, after this collection, 600 μl C2 media was also added to the basolateral compartment and discarded (wash). Another 600 μl C2 media was added to the basolateral side and incubated for another 24 hr followed by collection of the basolateral supernatant.

2-fold serial dilutions FITC dextran standards were prepared in C2 medium. Basolateral supernatants were then transferred to a 96-well plate (Black Nunc-Immuno™ MicroWell™, Nunclon®, ThermoFisher Scientific, UK) and FITC-dextran content was analysed fluorometrically using a microplate reader (ClarioStar, USA) at excitation 485 nm and emission 520 nm. A linear standard curve generated in Microsoft Excel was used to interpolate fluorescence values to FITC-dextran concentrations.

2.2.9. Characterisation of levans

2.2.9.1. Gel permeation chromatography

E. herbicola levan fractions were separated by size exclusion using a Superose™ 6 Increase 10/300 GL prepacked column for high-performance size exclusion chromatography (#29091596, GE Healthcare Life Sciences, USA). For *E. herbicola* levan collection, fractions were collected using a gel permeation chromatography (GPC) system and refractive index detector (Precision instruments, UK), and Trilution® Software (Version 3.0.26.0). All levan fractions were weighed and resuspended in sterile filtered H_20. For GPC analysis, dextrans and levans were analysed using a GPC system and refractive index detector (Series 200, PerkinElmer, USA), and the Chomera software (PerkinElmer, USA). Dextran standards were derived from *Leuconostoc mesenteroides* of 5 kDa, 12 kDa, 25 kDa, 50 kDa, 150 kDa, 270 kDa, 410 kDa, and 1400 kDa (#31417, #31418, #31419, #31420, #31421, #31422, #31423, #31424, and #49297 respectively, Fluka, Sigma Aldrich, UK). The column was kept and utilised at R.T, all injection volumes were 1 ml, and a constant flow rate of 0.5 ml/min was used for all experiments. Concentrations for collection of *E. herbicola* levan were 5 mg/ml per injection. Concentrations for the analysis of *E. herbicola* levan, ES levan and all dextrans were 5 mg/ml, 1 mg/ml and 1 mg/ml, respectively. A 4-parameter logistic curve of approximate peak elution times against voltage peaks for each dextran standard was generated in GraphPad Prism version 6.05.

2.2.9.2. Gas chromatography-mass spectrometry (GC-MS) linkage analysis

This work was carried out by the Chemical Sciences, Geosciences and Biosciences Division, Office of Basic Energy Sciences, U.S. Department of Energy grant (DE-

SC0015662) to Parastoo Azadi at the Complex Carbohydrate Research Center, Athens, GA, USA by Ian Black.

For glycosyl linkage analysis, the samples were permethylated, depolymerized, reduced, depolymerized again, reduced again, and acetylated; and the resultant partially methylated alditol acetates (PMAAs) were analysed by GC-MS as described by Heiss and colleagues[508].

For analysis of crude and purified *E. herbicola* levan, the two-step hydrolysis procedure and a spitless injections was performed. The spitless injection (as opposed to a split injection) in GC-MS analysis allows for greater sensitivity to determine the presence of trace analytes. GC-MS linkage analysis for crude and purified *E. herbicola* levan was performed using the split injection method. Of note, the experimental procedure was modified to include an initial mild hydrolysis step and reduction to prevent further degradation of fructose[509]. The initial reduction generated reduced fructose to prevent interconversion to glucose/mannose under acidic conditions[510]. The initial hydrolysis and reduction was followed by a more aggressive hydrolysis step and a second reduction to allow for the detection of any less labile substituents (e.g. α-mannan). To determine the sensitivity of the detection for mannose residues, the two-step hydrolysis of 1, 5 and 25 μg α-mannan from *S. cerevisiae* (Sigma Aldrich, UK) was used. Similarly, the sensitivity for fructose was also evaluated using 1, 5 and 25 μg of *E. herbicola* levan subjected to GPC and LRA treatment.

2.2.9.3. Nuclear magnetic resonance analysis

NMR experiments and analyses were carried out by Dr Gwenaelle Le Gall and Dr Sergey Nepogodiev (Quadram Institute, Norwich Research Park, UK). NMR analyses of levan extracts or controls were performed on a 600MHz Bruker Avance spectrometer fitted with a 5 mm TCI cryoprobe and controlled by Topspin 2.0 software. 1H NMR spectra were recorded in D2O at 300 K and consisted of 64 scans of 65,536 complex data points with a spectral width of 12.3 ppm. The NOESYPR1D presaturation sequence was used to suppress the residual water signal with low power selective irradiation at the water frequency during the recycle delay (D1 = 3 s) and mixing time (D8 = 0.01 s). Spectra were transformed with 0.3 Hz line broadening and zero filling, manually phased, and baseline corrected using the TOPSPIN 2.0 processed using Mnova 12.0 software. Interpretation of 1D spectra was assisted by use of 2D methods including COSY and HSQC.

2.2.9.4. Protein analysis

2.2.9.4.1 Bradford assay

Briefly, 2-fold standard dilutions from 1.4 to 0.1 mg/ml of bovine serum albumin (BSA) (#A7906, Sigma Aldrich, UK) were prepared in sterile filtered H_20. 5 µl of standards, *E. herbicola* crude levan (≥ 3 mg/ml) or sterile filtered H_20 (blank) were added to polystyrene flat-bottomed 96-well plates (Starstedt, UK) in duplicate. 250 µl Bradford reagent (#B6916, Sigma Aldrich, UK) was then added to wells containing the samples and standards and incubated on a UltraRocker™ Rocking Platform (BIO-Rad, UK) for 30 sec. Samples were incubated at R.T for 45 min. Absorbance was measured at 595 nm using a microplate reader (Benchmark Plus™, Bio-Rad, UK). Detection of protein in levan was assessed using a standard linear curve generated in Excel.

2.2.9.4.2. Sodium dodecyl sulphate polyacrylamide gel electrophoresis

BSA standards (dilutions from 32 ng to 0.25 [or 20 ng only] of BSA were prepared by serial dilution of BSA in sterile filtered H_20]). 6.5 µl BSA standard(s) or *E. herbicola* crude levan (4 mg/ml) or *E. herbicola* levan F1 (post GPC [3.2 mg/ml]) were added to 2.5 µl 4X lithium dodecyl sulphate (LDS) buffer (#NP0007, ThermoFischer Scientific, UK) and 1 µl (100 mM) dithiothreitol (DTT) (#D6052, Sigma Aldrich, UK) and the solution heated for 10 min at 70°C. Standards or levan samples (10 µl) were loaded into a pre-made 4 – 12% Bi-TRIS NuPAGE polyacrylamide gel (#NP0323BOX, Novex®, ThermoFischer Scientific, UK). 5 µl of protein marker (#12949, Cell Signalling Technology, USA) was also loaded in separate wells. Electrophoresis was performed using a Novex XCell SureLock™ apparatus typically at 200 V (constant), 350 mA for 35 – 45 min. The gel was stained using SPYRO® Ruby protein gel stain (#S12000, ThermoFischer Scientific, UK) according to manufacturer's instructions. Briefly, the gel was placed in a container and fixed by adding 100 ml of fix solution (50% methanol and 7% acetic acid in H_20) and left on an orbital shaker for 30 min and the fix solution discarded. This process was then repeated. The gel was then incubated with 60 ml of SPYRO® Ruby protein gel stain overnight at R.T on an orbital shaker. The gel was then transferred into a new container and incubated in 100 ml wash solution (10% methanol and 7% acetic acid) for 30 min. The gel was then rinsed in H_20 for 5 min at least twice and visualised by a Pharos-FX™ Plus molecular imager (Bio-Rad, UK) using the pre-made setting for SPYRO® Ruby protein gel stain on the Bio-Rad software (excitation and emission wavelengths at 280 and 450/610 nm, respectively).

2.2.10. Detection and removal of lipopolysaccharide

2.2.10.1. Quantification of lipopolysaccharide using Endozyme recombinant factor C assay

LPS in all levan samples was quantified using the Endozyme Recombinant Factor C (RFC) assay (Kits I and II, Hyglos, Germany) and the assay procedure was carried out following the manufacturer's instructions. RFC is a zymogen/proenzyme (precursor protease) and it is activated by LPS[511]. Addition of a fluorescent substrate with LPS-activated RFC leads to substrate cleavage and fluorescence can be measured[511,512]. Briefly, an LPS standard was reconstituted in Endozyme endotoxin-free H_20 and standard dilutions were prepared from 0.005 Endotoxin unit (EU)/ml to 50 EU/ml (0.5 pg/ml to 5000 pg/ml by weight; 100 pg represents 1 EU in the Hyglos LPS standard). 100 µl of standards or samples were added to the wells of a 96-well plate (#P8741-50EABlack Nunc-Immuno™ MicroWell™, Nunclon®, ThermoFisher Scientific, UK). 100 µl of Endozyme reaction mix (substrate, enzyme and assay buffer [volume ratio: 8:1:1]) was added. The plate was placed in a microplate reader pre-heated at 37°C and baseline fluorescence was measured at excitation 380 nm and emission 445 nm using a microplate reader (ClarioStar, BMG LABTECH, USA). The plate was incubated at 37°C for 60 or 90 min in the plate reader and fluorescence was measured again at excitation 380 nm and emission 445 nm. For all tests, LPS was quantified from absorbance values interpolated from a standard curve using a 4-parameter logistic regression, as per the manufacturer's instructions, and was generated in GraphPad Prism (V 6.05).

2.2.10.2. Lipopolysaccharide removal

2.2.10.2.1. Calcium silicate treatment

Following size exclusion chromatography, *E. herbicola* levan was purified using Lipid Removal Agent (LRA) (#13358, Sigma Aldrich, UK); a calcium silicate hydrate with a high affinity of lipids[513]. The LRA protocol was based on the procedure by Zhang and colleagues[513]. Briefly, 20 g/l LRA (by volume) was added to 4 mg/ml levan and supplemented with 20 mM sodium chloride. The solution was incubated for 4 hr on a rotary wheel at 4°C and then centrifuged at 3000 rpm for 10 min and the supernatant removed. This process was repeated and left overnight at 4°C. The supernatant was lyophilised and resuspended in sterile H_20.

2.2.10.2.2. Alkali treatment

E. herbicola levan 2 or crude enzymatically synthesised (ES) levan was lyophilised and resuspended in 0.9 M NaOH for 48 hr in a 15 ml conical tube at a concentration

of 4 mg/ml. Samples were vortexed at least twice each day for 1 - 2 min. Samples were dialysed in 4 l ultra-filtered H_20 for 2 days using a 10 kDa molecular weight cut off (MWCO) 22 mm x 35 feet dry diameter dialysis membrane (#68100, SnakeSkin® Dialysis Tubing, ThermoFisher Scientific, USA) and the H_20 was changed at least twice per day. Levan samples were harvested, freeze-dried and the dry product was resuspended in sterile filtered H_20. Of note, the alkali treatment was repeated for *E. herbicola* levan 2.

2.2.10.2.3. Thin layer chromatography (TLC) of alkali-treated levan

TLC of alkali-treated levan (while still in NaOH) was performed. The samples tested were as follows: Fructose (in H_20 and/or NaOH), crude levans and alkali-treated (purified) levans. The latter 2 samples were spiked with fructose as a control. Typically, 1 μl of *E. herbicola* levan or ES levan was placed on a TLC plate and heated until dry. This was repeated at least 5 times. Chloromethane, ethyl acetate, 2-Propanol (Isopropanol) and H_20 were mixed in a ratio of 85: 20: 50: 50, respectively, as the solvent mixture for the mobile phase. The solvent mixture was added to a TLC chamber for 30 min covered with a lid. The TLC plate was added to the chamber and left partially upright for 20 – 30 min. Following migration of the samples, the TLC plate was left to dry, briefly heated and stained with orcinol (5-Methylresorcinol) using a spray apparatus and left to dry. The plate was heated using heat gun until orange spots were clearly observed.

2.2.11. Production of levan from B. subtilis 168

The levan production protocol was based on work by Sims et al[91] and Shi et al[25] with modifications. Briefly, *B. subtilis* 168 was cultured overnight at 180 RPM at 37°C in a shaking incubator in sterile 50 ml tubes. Sterile 250 ml conical flasks (no baffles) containing 100 ml to LB or LDM2 media were inoculated with 2% vol *B. subtilis culture* for 24 hr at 180 rpm at 37°C in a shaking incubator. LB and LDM2 5% sucrose alone containing no bacteria were used as controls and subjected to the same treatment as bacterial cultures. All samples were centrifuged at 6000 g and the supernatant placed into sterile flasks. Ice-cold ethanol (1.5 vol) was added to supernatants and mixed by mechanical shaking and vortexing for 2 – 5 min. Samples were placed on an Ultra Rocker (Bio-Rad) at full speed at 4°C for at least 2 hr. Samples were harvested into 50 ml tubes and centrifuged at 12,000 g for 15 min and the supernatant discarded. Sterile filtered H_20 was added to the pellet, vortexed 2 - 5 min, and heated at 60 - 70°C. Samples were dialysed in 4 l ultra-filtered H_20 for 2

days using a 10 kDa dialysis membrane and H_20 was changed three times per day. Samples were freeze-dried, weighed and sterile filtered H_20 was added.

2.2.12. Treatment of E. herbicola levan and α-mannan with ion-exchange resin

Dowex® 50W8X, 200-400 mesh, ion-exchange resin (#335355000, Acros Organics™, Belgium) was added into a sterile 1.5 ml Eppendorf tube. The resin was washed by adding 1 ml sterile filtered H_20 and removing H_20 after using a pipette and sterile pipette tips. This was repeated 10 times and 1 ml sterile filtered H_20. *E. herbicola* levan was treated with alkali as described in 2.2.10.2.2 to remove LPS (purified *E. herbicola* levan). 400 μl of the purified *E. herbicola* levan or α-mannan was added to 200 μl of the washed resin in a separate sterile 1.5 ml Eppendorf tube. Tubes were placed on rotator for 10 min at medium speed. The resin was left to settle upright at R.T. After gravity-separation of the resin, the supernatant was collected and added to a new sterile 1.5 ml tube, freeze-dried. The samples were then weighed and resuspended in sterile filtered H_20.

2.2.13. Atomic force microscopy (AFM)

All AFM experiments were carried out by Dr Patrick Gunning (Quadram Institute Bioscience, Norwich Research Park, UK).

2.2.13.1. Tip functionalisation

Silicon nitride AFM tips (PNP-TR, Nanoworld AG, Neuchâtel, Switzerland) were functionalised using a two-step procedure (carried out at 21◦C): the first step involved incubation in a 2% solution of 3-mercaptopropyltrimethoxy silane (#175617, MTS, Sigma–Aldrich, Poole, Dorset, UK) in toluene (Sigma–Aldrich, UK) (dried over a 4Å molecular sieve) for 2 hr, followed by washing with toluene and then chloroform. In the second step, the silanised tips were incubated for 1 h in a 1 mg/ml solution of a heterobifunctional linker: MAL-PEG-SCM (binds amines for Dectin-2), 2 kD (Creative PEGWorks, Chapel Hill, NC, USA) in chloroform. The tips were rinsed with chloroform and then dried with argon and transferred into a clean gel pack. 0.5 mg/ml of proteins in PBS (#1525-DC [mouse Dectin-2], #3114-DC [human Dectin-2], R&D Systems, USA) were added onto the tips and incubated at 4 °C overnight. 50 μl (20 mg/ml) of glycine (to reduce unspecific covalent binding) was added for 2 hr and then rinsed with PBS.

2.2.13.2. Functionalisation of PS to glass slides

Silanised glass slides were incubated in 2 mM MPBH (#22305, 4-(4-N-maleimidophenyl) butyric acid hydrazide) (Thermo Fisher Scientific, Waltham, MA, USA) in ethanol for 1 hr. The tips and slides were rinsed with chloroform/ethanol, respectively, and then dried with argon. Covalent attachment of α-mannan or levans were incubated as 100 μl of 1 mg/ml solutions of the PS in PBS at pH 7.4 overnight at 4 °C followed by a PBS washing step the next day. Slides in an 18 mg/ml solution of glucose in PBS to 'sugar'-cap any unreacted hydrazide groups, followed by washing in PBS.

2.2.13.3. Force spectroscopy

Binding measurements were carried out in PBS using a MFP3D BIO AFM (Asylum Research Inc., Santa Barbara, CA, USA). Software Asylum MFP3D program. The experimental data were captured in 'force-volume' (FV) mode at a rate of 2 µm/sec in the Z direction and at a scan rate of 1 Hz and a maximum load force of 300 pN (pixel density of 32 × 32). The spring constant, k, of the cantilevers was determined by fitting the thermal noise spectra[514], yielding typical values in the range 0.03 – 0.06 N/m. Adhesion in the force spectra was quantified using a bespoke Excel macro[515] which fits a straight line to the baseline of the retract portion of the force-distance data. To explore the specificity of the control mannan binding interactions, the force measurements for mannan were repeated after addition of 100 mM mannose to the liquid cell.

2.2.14. Statistics and graphical programs

All graphs were constructed in Graph Pad prism 6 unless otherwise stated in Figure legends. Figures were adapted in Adobe Illustrator 6 or Microsoft PowerPoint. Cartoons were made in Adobe Illustrator 6 or Microsoft PowerPoint. Vector NTI v11.5.4 was used for the vector illustration. All statistical analyses including one way and two-way ANOVA were performed in Graph Pad Prism 6. A p value < 0.05 was considered as statistically significant. Statistical tests are indicated in the Figure legends.

Chapter 3: Construction and use of C-type lectin reporter cells to screen for novel carbohydrate ligands

3.1. Introduction

Many PS including edible PS from plants and fungi, or microbes have been shown to modulate immune function in animals including humans[3,162]. These immunomodulatory PS have sometimes led to the development of commercial dietary products for promoting immune health[144,155,516,517]. However, the molecular mechanisms underpinning the immunomodulatory properties of PS remain unclear[3].

CLR Dectin-1, Dectin-2 or DC-SIGN, are transmembrane carbohydrate-binding proteins expressed by a variety of innate immune cells including those of myeloid-origin such as DC, and are well-known for their role in antifungal and anti-mycobacterial immunity[118,328]. These CLRs can induce an immune response by binding to carbohydrate structures located on the cell-surface of pathogenic or opportunistic microbes[346,394,395]. Upon carbohydrate ligand binding, these receptors elicit cellular activation and initiate an immune response providing protection to the host[328]. Dectin-1, Dectin-2, and SIGNR1 (mouse homolog of human DC-SIGN), have a high-affinity for α-mannans, β-glucans, and both high-mannose and –fucose structures, respectively[338,518,519] while the mechanism of β-glucan recognition by Dectin-1 is not yet fully elucidated[329].

Dectin-2 and SIGNR1's binding specificity for high-mannose (and fucose for SIGNR1) is achieved through a conserved EPN amino acid sequence motif located in the CRD of their CTLD (and putatively) in the presence of Ca^{2+}[334]. In contrast, galactose-binding lectins contain a QPD motif in their CRD[334,520].

Here, we aim to investigate the interaction of a range of carbohydrate structures including immunomodulatory PS with CLRs as a potential mechanism underpinning their function. To test this, we will use Dectin-1, Dectin-2 and Dectin-2-QPD reporter cells and construct SIGNR1 and mutant SIGNR1-QPD BWZ.36 reporter cells. BWZ.36 cells are mouse T cell hybrids that harbour a NFAT-lacZ construct[521], a vector containing the lacZ (lac operon Z) gene fused to the minimal promotor of the human IL-2 gene[522,523]. Upon NFAT activation with a ligand, NFAT binds to the IL-2 promotor region and subsequently induces β-galactosidase production via lacZ[521,523,524]. To express CLRs at the cell surface of the cells, BWZ.36 cells are transduced with a pMXs-IG vector containing a fusion protein sequence comprising a CLR extracellular domain, a Ly49 transmembrane domain - a type II NK cell receptor integral membrane protein[525] - and a CD3ζ intracellular domain (Figure 19) resulting in the expression of CLR fusion proteins on the cell surface. Thus, ligand-

binding to the CLR extracellular domain on BWZ.36 CLR reporter cells results in CD3ζ-mediated activation of NFAT and induction of the IL-2 promoter/lacZ, and β-galactosidase can be measured in a colorimetric assay in the presence of a CPRG, a substrate for β-galactosidase (Figure 20) (see 2.2.5.1.).

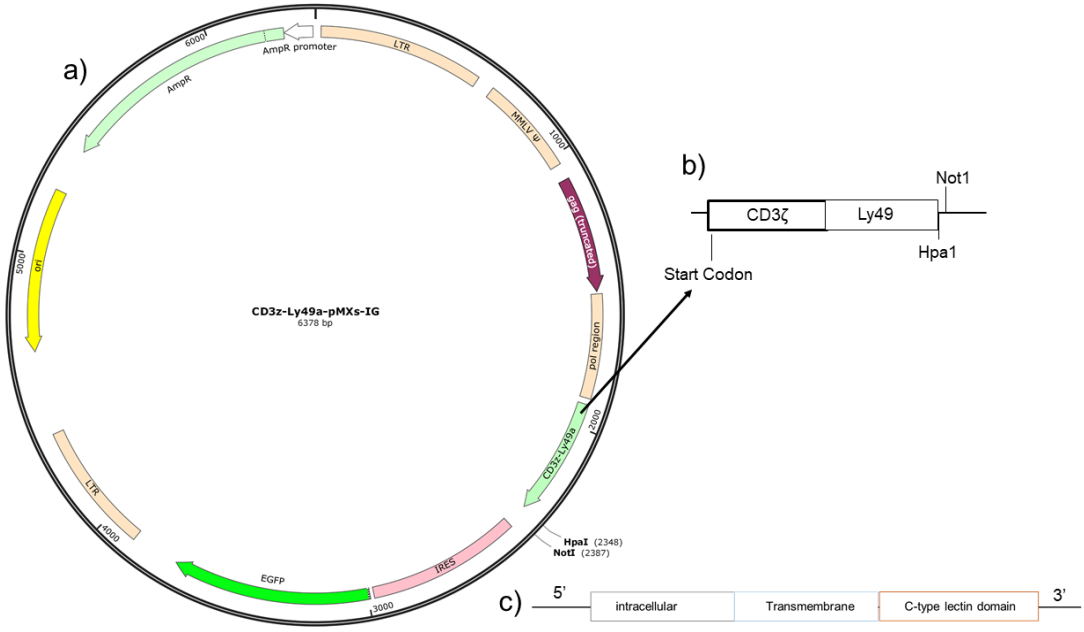

Figure 19. Schematic representation of the pMXs-IRES-EGFP-CD3ζ-Ly49 (pMXs-IG) and CD3ζ-Ly49-CLR fusion protein sequence for transfection into BWZ.36 reporter cells.

(a) and (b) the pMXs-IG retroviral vector construct contains a CD3ζ-Ly49 sequence in its multiple cloning site (MCS) and includes sequences for HpaI and NotI (restriction enzymes). The CLR ectodomain domain (labelled C-type lectin domain) sequence can be inserted adjacent to Ly49 (transmembrane) and CD3ζ (intracellular) resulting in the construction of a CD3ζ-Ly49-CLR fusion protein sequence. The pMXs-IG-CD3ζ-Ly49-CLR (pMXs-IG-CLR) is then used for transfection into BWZ.36 cells. The vector illustration was constructed using Vector NTI version 11.5.4.

For this study, the CLR BWZ.36 reporter assay allows a relatively high-throughput method to screen for carbohydrate ligand candidates. BWZ.36 reporter cells were used to screen a range of PS found in plants, mushrooms, algae and microbes for their binding to SIGNR1, Dectin-1 and Dectin-2.

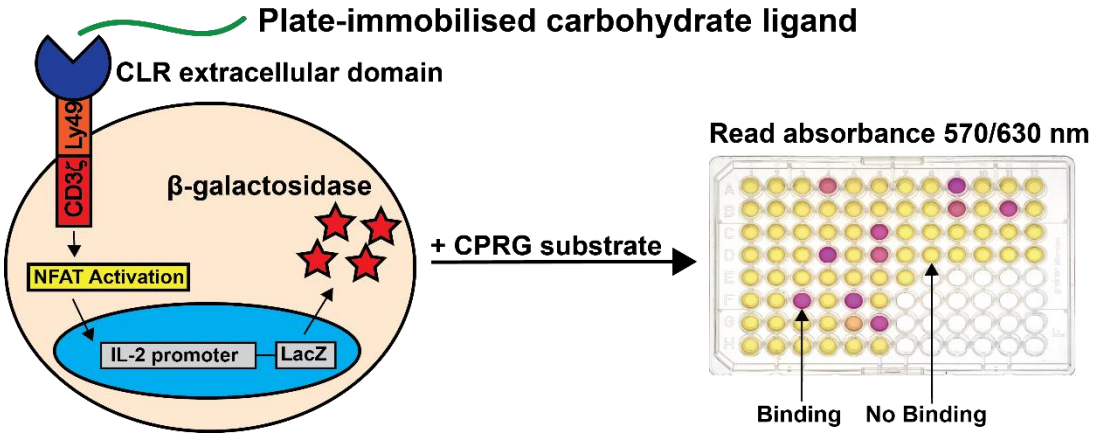

Figure 20. Schematic representation of BWZ.36 CLR reporter cell function in a colorimetric assay.

CLR BWZ.36 reporter cells are incubated with immobilised carbohydrate ligands using a 96 well plate. Binding to the CLR ectodomain induces the LacZ gene producing β-galactosidase which can be measured in a colorimetric assay by adding chlorophenol red-β-D-galactopyranoside (CPRG) and reading 570/630 nm absorbance. Ly49 and CD3ζ are transmembrane and intracellular regions, respectively. IL, interleukin. LacZ, lac operon Z.

3.2 Results

3.2.1. Establishment of BWZ.36 SIGNR1 reporter cells

3.2.1.1. Cloning of SIGNR1

For the construction of SIGNR1 reporter cells, the murine SIGNR1 DNA sequence was amplified from a SIGNR1 ectodomain template plasmid cDNA by PCR using forward and reverse SIGNR1 primers (see 2.2.4.1.). Figure 21 shows DNA bands on an aragose gel of the PCR-amplified product corresponding to the size of the SIGNR1 ectodomain (753 bp including stop codon).

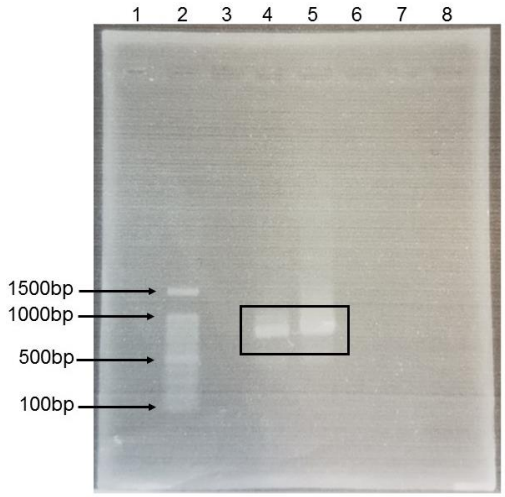

Figure 21. Electrophoresis of the SIGNR1 ectodomain after PCR amplification of SIGNR1 cDNA using SIGNR1 forward and reverse primers.

Following electrophoresis, the aragose gel (1%) was stained with ethidium bromide and visualised fluorometrically by exposure to ultraviolet light. Lane 2, DNA Ladder. Lanes 4 and 5, SIGNR1 ectodomain PCR products (duplicate). SIGNR1 ectodomain PCR products are highlighted in the black box. All other lanes are blank. Bp sizes are indicated by arrows.

The SINGR1 ectodomain PCR product was then cloned into a SmaI-digested pBluescript II KS vector following transformation in *E. coli* (see 2.2.4.1). Colony PCR identified colonies (C#2, C#6 and C#8) showing bands corresponding to the size of the SIGNR1 ectodomain within the vector (817 – 967 bp) (Figure 22). Sequencing confirmed that colonies C#6 and C#8 contained the SIGNR1-pBluescript II KS vector.

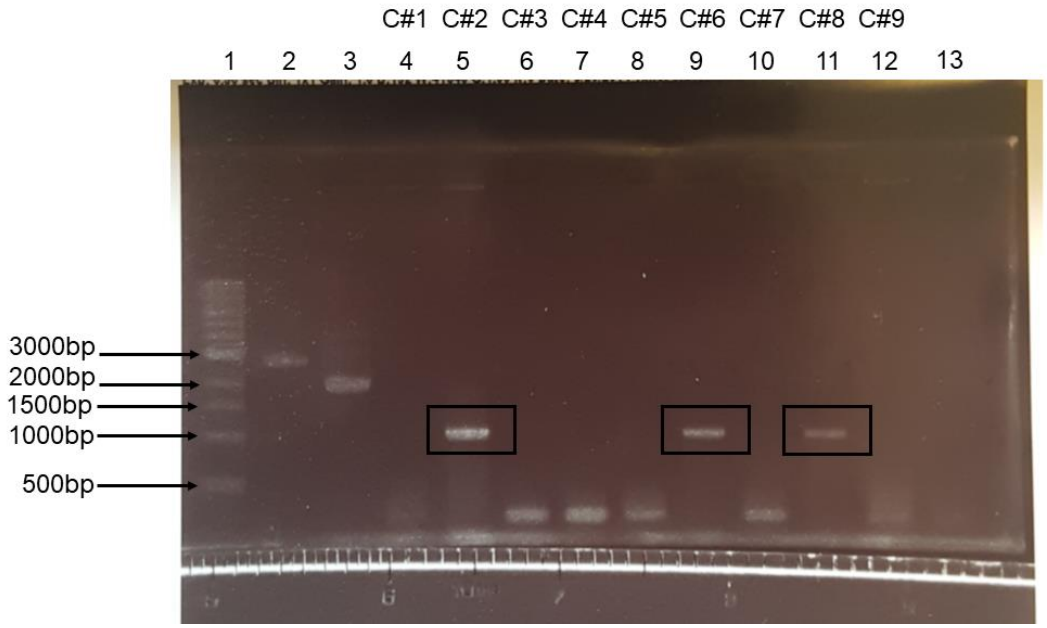

Figure 22. Electrophoresis of colony PCR products identifying colonies positive for SIGNR1.

Following electrophoresis, the aragose gel (1%) was stained with ethidium bromide and visualised fluorometrically by exposure to ultraviolet light. Lane 1, DNA ladder. Lane 2, Sma1-digested pBluescript II KS vector. Lane 3, undigested pBluescript II KS. Lanes 4 -12, colonies C#1 – C#9. Lane 13, blank. Colonies containing the recombinant SIGNR1 vector are shown in the black boxes (lane 5, 9 and 11).

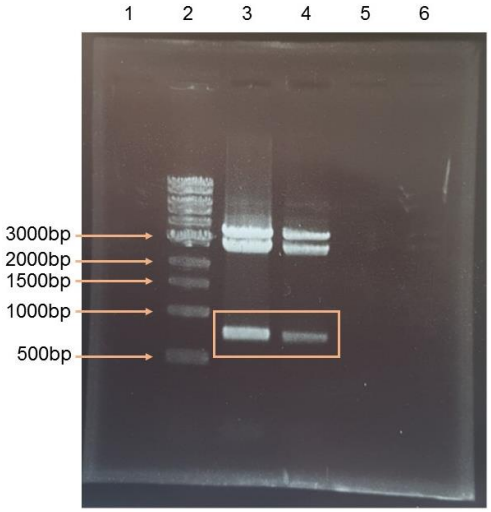

Figure 23 Electrophoresis of the SIGNR1 pBluescript II KS recombinant vector after digestion by NotI and HpaI restriction enzymes.

Following electrophoresis, the aragose gel (1%) was stained with ethidium bromide and visualised fluorometrically by exposure to ultraviolet light. Lane 2, DNA ladder. Lane 3, colony C#6. Lane 4, colony C#8 (from Figure 22). All other lanes were blank. The orange box highlights the digested products corresponding to the SIGNR1 sequence.

3.2.1.2. Expression of SIGNR1 in BWZ.36 reporter cells

The SIGNR1-pBluescript II KS recombinant vector was further amplified by culturing positive colonies (containing the recombinant vector), and the recombinant vector was then purified (see 2.2.4.1.7.). The SIGNR1 DNA sequence was cut from the vector using NotI and Hpa1 restriction enzymes (see 2.2.4.1.8.). Gel electrophoresis was used to verify the size of the digested product. Figure 23 shows bands in lanes 3 (C#6) and 4 (C#8) between 500 and 1000 bp corresponding to the size of the SIGNR1 ectodomain sequence (767 bp including digested HpaI and NotI sequences). SIGNR1 was then cut from the gel and purified.

Next, the purified SIGNR1 ectodomain sequence was inserted upstream of the CD3ζ-Ly49 sequence in a pMXs-IG vector following digestion with Not1 and HpaI (see 2.2.4.1.9). Following transformation into *E. coli*, colonies containing the recombinant SIGNR1 pMXs-IG vector were identified by PCR. Three colonies (C#1, C#2 and C#3) contained the recombinant SIGNR1 pMXs-IG vector with bands between 1000 and 1500 bp corresponding to its predicted size (~1232 – 1382 bp) (Figure 24). The recombinant SIGNR1 pMXs-IG vector was purified and isolated from colonies C#1 and C#3.

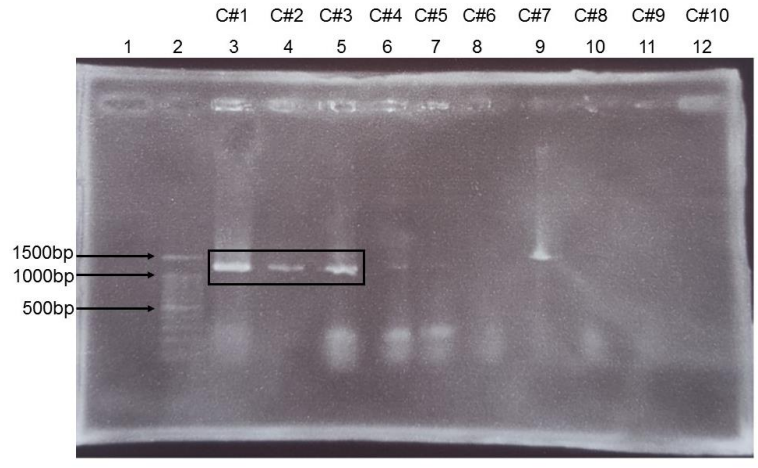

Figure 24. Electrophoresis of colony PCR products to identify colonies containing pMXs-IG-SIGNR1.

Following electrophoresis, the aragose gel (1%) was stained with ethidium bromide and visualised fluorometrically by exposure to ultraviolet light. Lane 2, DNA ladder. Lane 3 – 12, colonies C#1 – C#10. Lane 1 was blank. Colonies containing pMXs-IG-SIGNR1 are shown in black boxes.

The purified recombinant SIGNR1 pMXs-IG vector was transfected into the Plat E retrovirus packaging cell line and subsequently BWZ.36 cells were transfected with the resulting retrovirus containing the CD3ζ-Ly49-SIGNR1 sequence (see 2.2.4.3.).

Next, we confirmed the expression CD3ζ-Ly49-SIGNR1 fusion proteins on the cell surface of transfected BWZ.36 cells. The cells were analysed by flow cytometry following incubation with antibodies anti-mouse SIGNR1 Alexa 647 or rat IgM isotype-Alexa 647 control, which emits red fluorescence upon excitation. Further, as the pMXs-IG vector sequence also contains enhanced green fluorescent protein (EGFP), which emits a green fluorescence[526], this was used to identify and distinguish between transfected and non-transfected cells.

We found cells positive for both GFP and Alexa 647 fluorescence, indicating that in this population, transfection occurred and SIGNR1 was expressed on these cells (Figure 25a, Q2) (for gating strategy see Appendix 6). Non-GFP-positive cells showed negligible SIGNR1 expression (Figure 25a, Q1). Isotype controls are fluorescently-labelled antibodies that are not specific for the target antigen of interest and are used to identify unspecific binding. In contrast to the binding of anti-mouse SIGNR1-Alexa 647 shown in Figure 25a, cells labelled with IgM isotype-Alexa 647 showed negligible amounts of cells positive for Alexa 647, yet did show GFP-positive populations (Figure 25b), confirming that the binding of anti-mouse SIGNR1-Alexa 647 was specific. Of note, Alexa 647 fluorescence was initially identified using the allophycocyanin (APC) emission detection range, as APC emission is similar to Alexa 647.

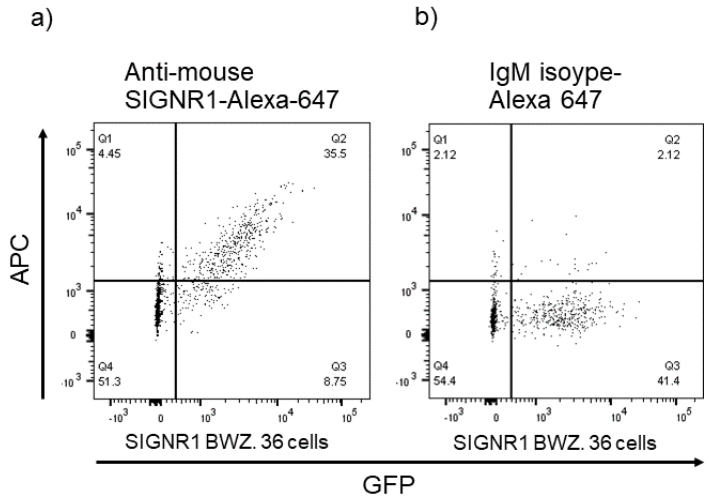

Figure 25. Analysis of SIGNR1 expression on transfected unsorted BWZ.36 cells by flow cytometry.

(a) and (b), dot plots illustrate individual cell events. The number of cell events are shown as a percentage in each of the quadrants relative to total events, Q1, Q2, Q3 and Q4. Cells were labelled with (a) anti-mouse SIGNR1-Alexa 647 or (b) IgM isotype-Alexa 647 control. Analysis was performed after initial pre-gating of cells which exclude doublet cells and dead cells (for gating strategy see Appendix 5. Q1, Q2, Q3 and Q4 split cell populations into discrete subpopulations for illustrative purposes to help clarify fluorescent and non-fluorescent cell populations. Numbers in each quadrant represent the percentage of total sample cell populations in that quadrant. Axis: APC (allophycocyanin) was used to detect Alexa 647 fluorescence, as it has a similar emission spectrum, and GFP (green fluorescent protein) is detection of GFP fluorescence. Data were generated in FlowJo® v10.0.8.

Next, the transfection of BWZ.36 cells with the recombinant SIGNR1 pMXs-IG vector was repeated as previously described. This time, GFP-positive BWZ.36 cells were isolated using a Sony SH800 flow cytometer cell sorter (see Appendix 6). To verify SIGNR1 expression on these cells, the cells were labelled with anti-mouse SIGNR1-Alexa 647 or IgM isotype-Alexa 647 and analysed by flow cytometry as previously described. We found that most cells were positive for both GFP and Alexa 647 fluorescence confirming that the cell population was primarily SIGNR1 reporter cells (Figure 26a, Q2). There were negligible amounts of cells negative for GFP highlighting the usefulness of the cell sorting (Figure 26a, Q1 and Q4). Cells labelled with IgM isotype-Alexa 647 control showed mostly GFP-positive cells and negligible cell populations positive for Alexa 647 (Figure 26b) confirming the binding specificity of anti-mouse SIGNR1-Alexa 674. Clear shifts in Alexa 647 fluorescence of anti-mouse SIGNR1-Alexa 647-treated cells compared to isotype and unlabelled controls are shown in Figure 26d, confirming SIGNR1 expression on the reporter cells. For gating strategy see Appendix 5. Another experiment also confirmed SIGNR1 expression on these reporter cells (Appendix 8).

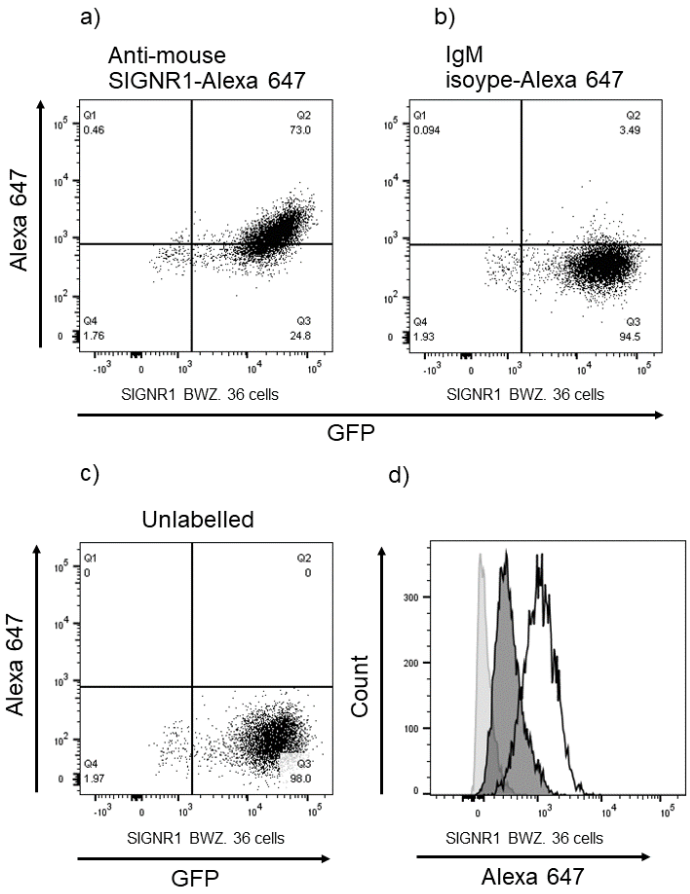

Figure 26. Analysis of SIGNR1 expression on sorted SIGNR1 reporter cells by flow cytometry

(a), (b) and (c), dot plots illustrate individual cell events. The number of cell events are shown as a percentage in each of the quadrants relative to total events, Q1, Q2, Q3 and Q4 for (a) (b) and (c). Cells were labelled with (a) anti-mouse SIGNR1-Alexa 647, (b) IgM isotype-Alexa 647 control or were (c) unlabelled (cells with PI). Analysis was performed after initial pre-gating of cells which exclude doublet cells and dead cells (for gating strategy see Appendix 6). Q1, Q2, Q3 and Q4 split populations into discrete subpopulations for illustrative purposes to help clarify fluorescent and non-fluorescent cell populations. Numbers in each quadrant represent the percentage of total sample cell populations in that quadrant. d) Histogram directly compares anti-mouse SIGNR1-Alexa 647-labelled (black outline); IgM isotype-Alexa 647-labelled (grey shading with black outline); and unlabelled cells (cells with PI only) (light grey, no black outline). Axis labels: Alexa 647 label represents detection of Alexa Fluor 647 fluorescence and GFP is represents detection of GFP fluorescence. Data were generated using FlowJo® v10.0.8.

3.2.2. Establishment of BWZ.36 SIGNR1-QPD mutant reporter cells

The CLR binding domain of mannose-specific lectins contain an EPN (Glutamic acid, Proline and Asparagine) amino acid motif[334]. SIGNR1 cells with a mutated carbohydrate-binding domain were established by introducing a galactose-specific QPD (Glutamine, Proline and Aspartic acid) amino acid motif in place of mannose-specific EPN when designing the SIGNR1 ectodomain sequence.

To construct SIGNR1-QPD reporter cells, a similar procedure to SIGNR1 was followed. Briefly, the mutant SIGNR1-QPD (ectodomain) sequence was synthesised and incorporated into a Pu57 vector commercially, and then digested by HpaI and Not1 restriction enzymes. A band corresponding to the size of the SIGNR1-QPD sequence (753 bp) was identified by aragose gel electrophoresis (Figure 27).

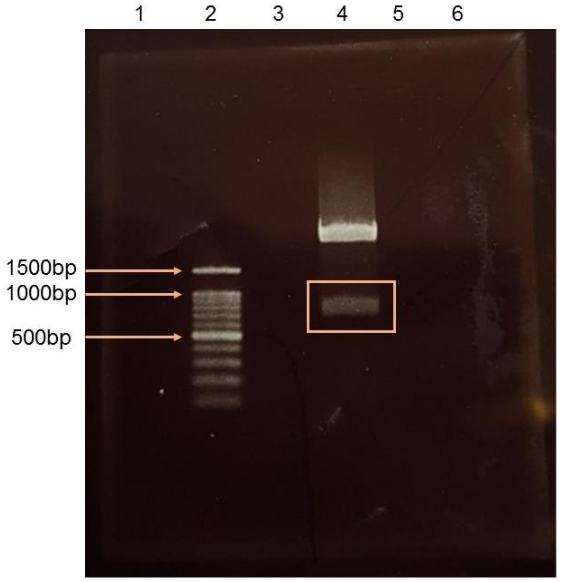

Figure 27. Electrophoresis of the SIGNR1-QPD recombinant vector after digestion by HpaI and Not1 restriction enzymes

Following electrophoresis, the aragose gel was stained with ethidium bromide and visualised fluorometrically by exposure to ultraviolet light. Image shows an 1% aragose gel subjected to electrophoresis. Lane 2, DNA ladder. Lane 3, blank. Lane 4, PCR products of SIGNR1-QPD recombinant vector after digestion by restriction enzymes. The orange box highlights the SIGNR1-QPD ectodomain sequence. All other lanes were blank.

The purified SIGNR1-QPD ectodomain sequence was inserted upstream of CD3ζ-Ly49 following digestion by HpaI and NotI and cloning into pMXs-IG vector (see 2.2.4.2.). Following transformation in *E. coli*, colonies containing the recombinant SIGNR1-QPD vector were identified by PCR. Figure 28 shows four colonies corresponding to the size of the recombinant SIGNR1-QPD vector (~1232 – 1382 bps); C#5, C#8, C#9 and C#10.

Colonies containing pMXs-IG-SIGNR1-QPD were cultured and the DNA was isolated and purified (see 2.2.4.2.). Sequencing confirmed that colonies C#5 and C#9 contained the recombinant vector comprising the SIGNR1-QPD ectodomain sequence. The recombinant SIGNR1-QPD vector was purified and transfected into

BWZ.36 cells, and GFP-positive BWZ.36 cells were isolated using a cell sorter (see 2.2.3.3.and 2.2.4.2).

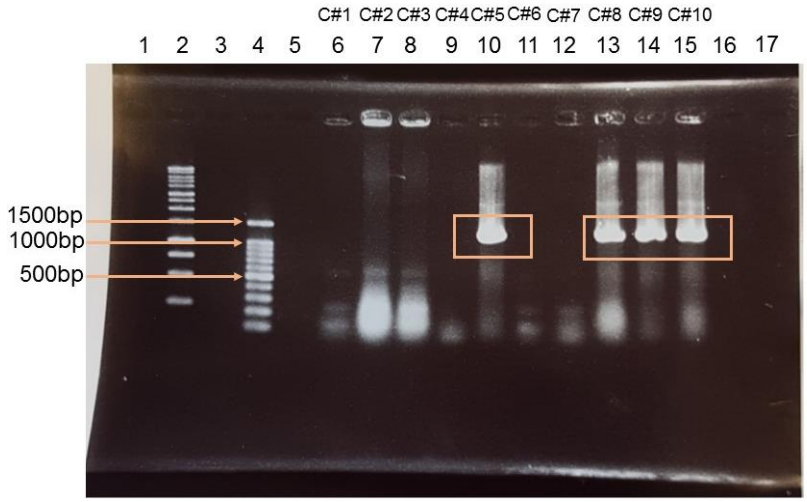

Figure 28. Electrophoresis of colony PCR products to identify colonies containing the recombinant SIGNR1-QPD vector.

Following electrophoresis, the aragose gel was stained with ethidium bromide and visualised fluorometrically by exposure to ultraviolet light. Lane 2; unused DNA ladder. Lane 4, DNA Ladder indicated. Lane 6 - 15; colonies C#1 – C#10. Colonies containing the recombinant SIGNR1-QPD vector are shown in the orange boxes. All other lanes were blank.

3.2.2.1. Expression of SIGNR1 in SIGNR1-QPD BWZ.36 reporter cells

SIGNR1 expression in BWZ.36 SIGNR1-QPD reporter cells was verified using fluorescently-labelled antibodies anti-mouse SIGNR1-Alexa 647 or IgM isotype-Alex 647 and flow cytometry as above. Anti-mouse SIGNR1-Alexa 647 could bind to SIGNR1-QPD mutant reporter cells. Most cells were positive for both GFP and Alexa 647, suggesting that in this population, transfection led to successful SIGNR1 expression in cells (Figure 29a, Q2). Further, non-GFP-positive cells showed negligible SIGNR1 expression (Figure 29a, Q3). In addition, cells labelled with IgM isotype-Alexa 647 showed negligible amounts of cells positive for Alexa 647 fluorescence, yet did show GFP-positive populations, confirming that the binding was specific to SIGNR1 (Figure 29b). Figure 29d shows clear shifts in Alexa 647 fluorescence of anti-mouse SIGNR1-Alexa 647-treated cells compared to isotype and unlabelled controls, further confirming SIGNR1 expression in the SIGNR1-QPD reporter cells. For gating strategy of Figure 29 see Appendix 9. An independent experiment confirmed SIGNR1 expression on SIGNR1-QPD reporter cells (Appendix 10).

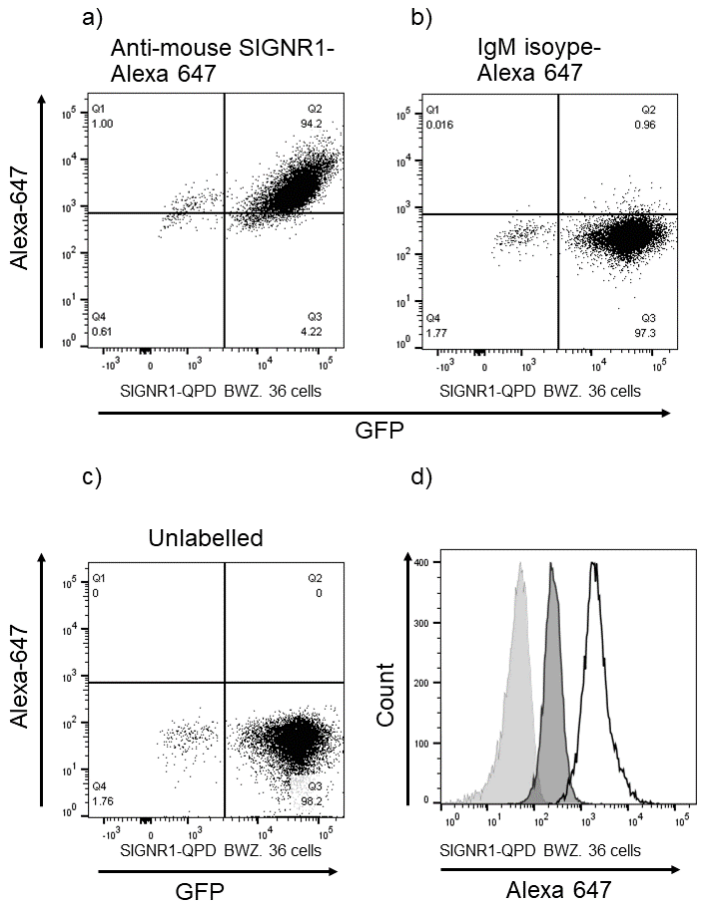

Figure 29. Analysis of SIGNR1 expression on SIGNR1-QPD reporter cells by flow cytometry.

(a), (b) and (c), dot plots illustrate individual cell events. The number of cell events are shown as a percentage in each of the quadrants relative to total events, Q1, Q2, Q3 and Q4. Cells were labelled with (a) anti-mouse SIGNR1-Alexa 647, (b) IgM isotype-Alexa 647 control or were c) unlabelled (cells with PI only). Analysis was performed after initial pre-gating of cells which exclude doublet cells and dead cells (for gating strategy see Appendix 9). Q1, Q2, Q3 and Q4 split cell populations into discrete subpopulations for illustrative purposes to help clarify fluorescent and non-fluorescent cell populations. Numbers in each quadrant represent the percentage of total sample cell populations in that quadrant. d) Histogram directly compares anti-mouse SIGNR1-Alexa 647-labelled (black outline); IgM isotype-Alexa 647-labelled (grey shading with black outline); and unlabelled cells (Cells with PI) (light grey, no black outline). Axis labels: Alexa 647 label represents Alexa Fluor 647 fluorescence and GFP (green fluorescent protein) is represents detection of GFP fluorescence. For repeated independent experiment see Appendix 10. Data were generated using FlowJo® v10.0.

3.2.2.2. Reporter assay using SIGNR1-QPD and SIGNR1 WT BWZ.36 reporter cells.

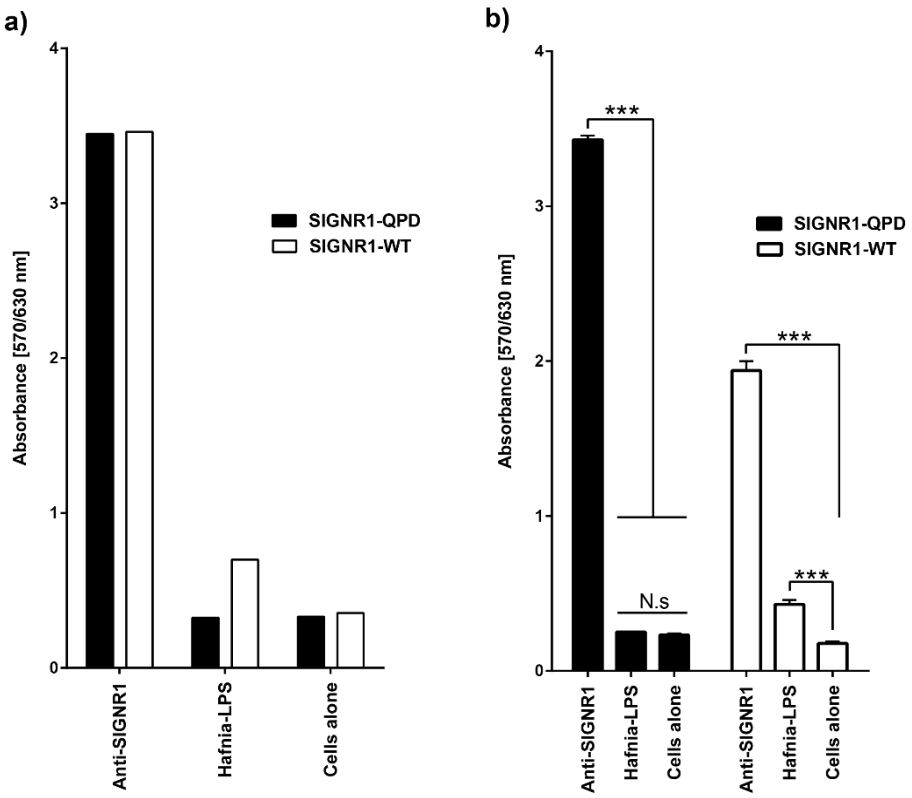

Figure 30. Interaction of SIGNR1 ligands with SIGNR1 WT and SIGNR1-QPD BWZ reporter cells.

Carbohydrate binding to CLR BWZ.36 reporter cells induces β-galactosidase production within the cell which can be measured in a colorimetric assay: CLR BWZ.36 reporter cells were incubated with immobilised carbohydrate ligands using a 96 well plate; a substrate, Chlorophenol red-β-D-galactopyranoside (CPRG), was added to cells and absorbance values were read at 570/630 nm. SINGR1 and SIGNR1-QPD BWZ reporter cell assay using anti-mouse SIGNR1 functional grade antibody (see 2.1.5.) and Hafnia-LPS. Concentrations in (a) were 20 μg/ml for anti-mouse SIGNR1 functional grade antibody and 30 μg/ml for Hafnia-LPS. Concentrations in (b) were 20 μg/ml anti-mouse SIGNR1 functional grade antibody and 10 μg/ml Hafnia-LPS. Experiments were performed in singlicate (a) or in triplicate (b). Error bars, ± SD. Statistical analysis was performed using one-way ANOVA followed by tukey's test (b). ***, p < 0.001. N.s., not statistically significant.

SIGNR1-QPD cells can be used to decipher if ligand binding is through the CRD of SIGNR1. Anti-mouse SIGNR1 functional grade antibody (see 2.1.5.) were used as a positive control to bind to SIGNR1-QPD fusion proteins expressed on reporter cells to assess the functionality of the SIGNR1-QPD mutant reporter cells. We showed that anti-SIGNR1 induced β-galactosidase production in SIGNR1-QPD reporter cells and in SIGNR1 WT reporter cells (Figure 30a). A second independent experiment was performed in triplicate confirming that the anti-mouse SIGNR1 functional grade antibody was able to induce β-galactosidase production in both SIGNR1-QPD and

SIGNR1 WT reporter cells (Figure 30 b). Further, we found that a mannan-linked lipopolysaccharide from *Hafnia alvei* PCM 1223 (Hafnia-LPS)[527] was able to bind to SIGNR1 but not SIGNR1-QPD, suggesting that Hafnia-LPS was recognised by SIGNR1 through its CRD. These findings were further confirmed in our published work where Hafnia-LPS was used as a control for binding experiments with bacterial adhesins[212].

3.2.3. Screening for novel SIGNR1 carbohydrate ligands

The BWZ.36 SIGNR1 reporter cells were used to screen for binding of various food and microbial PS to SIGNR1 in a bioassay (Figure 20). Mock cells containing a transfected pMXs-IG vector not harbouring a CLR ectodomain sequence were used as a negative control. These cells were previously established by the Kawasaki group (Quadram Institute, Norwich Research Park, Norwich, UK). Here, we carried out screening of Hafnia-LPS, α-mannan, scleroglucan, acemannan, xyloglucan, pectin, fucoidan and inulin (see 2.1.7.).

The results of the screening at 3 different concentrations of PS showed binding of Hafnia-LPS (Figure 31a [and Figure 30]) and α-mannan from *S. cerevisiae* to SIGNR1 as compared to mock cells (Figure 31a). Binding was assessed by comparing to unstimulated cells treated with PS coating buffer only (cells alone). The binding of Hafnia-LPS, α-mannan and acemannan to SIGNR1 reporter cells was repeated in triplicate confirming binding of Hafnia-LPS and α-mannan to SIGNR1 compared to cells alone (Figure 31b). Hafnia-LPS, α-mannan and acemannan were also incubated with mock cells where negligible absorbance was observed (see Appendix 11).

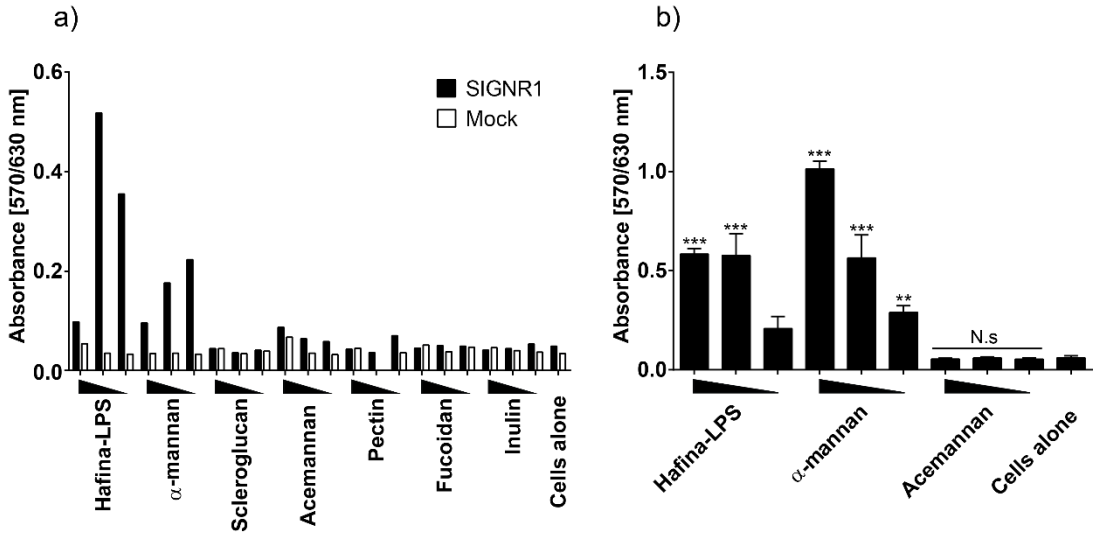

Figure 31. Screening of PS to SIGNR1 reporter cells.

Carbohydrate binding to CLR BWZ.36 reporter cells induces β-galactosidase production within the cell which can be measured in a colorimetric assay: CLR BWZ.36 reporter cells were incubated with immobilised carbohydrate ligands using a 96 well plate; a substrate, Chlorophenol red-β-D-galactopyranoside (CPRG), was added to cells and absorbance values were read at 570/630 nm. (a) Reporter assay was performed with both SIGNR1 and mock reporter cells. PS concentrations were 10, 4 and 0.2 μg/ml. (b) Second independent experiment with SIGNR1 reporter cells. Inulin (Glycomix). Data in (b) were performed in triplicate. PS concentrations were 1, 0.3 and 0.1 μg/ml. Error bars, ± SD. Statistical analysis was performed using one-way ANOVA followed by tukey's test (b). ***, p < 0.001 compared to cells alone. N.s., not statistically significant compared to cells alone.

Hafnia-LPS was then used as a positive control to screen other carbohydrate ligands including α-glucan from *Streptomyces venezuelae* which was shown to bind to SIGNR1 (Figure 32 and Appendix 12).

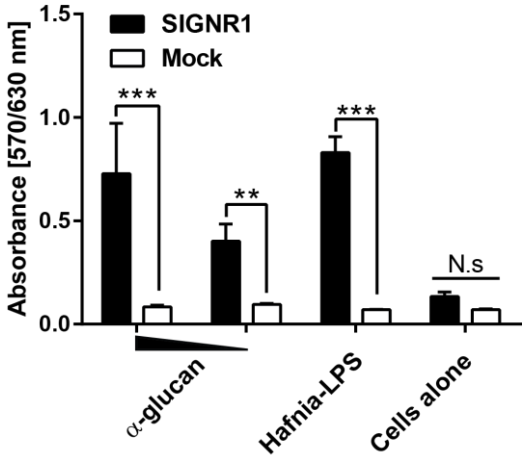

Figure 32. Interaction of α-glucan from Streptomyces venezuelae with SINGR1 and mock reporter cells.

Carbohydrate binding to CLR BWZ.36 reporter cells induces β-galactosidase production within the cell which can be measured in a colorimetric assay: CLR BWZ.36 reporter cells were incubated with immobilised carbohydrate ligands using a 96 well plate; a substrate, Chlorophenol red-β-D-galactopyranoside (CPRG), was added to cells and absorbance values were read at 570/630 nm. α-glucan was used at 100 μg/ml and 10 μg/ml and Hafnia-LPS at 10 μg/ml (positive control). All experiments were performed in triplicate. Error bars, ± SD. Statistical analysis was performed using one-way ANOVA followed by tukey's test (b). ***, p < .001 and **, p < 0.001, as indicated. N.s with straight line, not statistically significant. For repeated independent experiment see Appendix 12.

Taken together, the results of PS screening with BWZ.36 SIGNR1 reporter cells indicate that Hafnia-LPS and α-glucan are likely novel ligands of SIGNR1.

3.2.4. Screening for novel Dectin-1 and Dectin-2 carbohydrate ligands

Dectin-2 WT reporter cells were kindly provided by Dr N. Shastri (University of California Berkeley, CA, USA). Dectin-1 reporter cells and Dectin-2 QPD cells were established by Alexandra Wittmann and Norihito Kawasaki (Quadram Institute, Norwich, UK). Dectin-1 and Dectin-2 expression on reporter cells were verified previously by the Kawasaki group[394]. In addition, expression of Dectin-2 on Dectin-2 and Dectin-2-QPD reporter cells are shown in Appendix 13. Here, we screened a diverse range of food as well as microbial glycans including Hafnia-LPS, α-mannan, scleroglucan, acemannan, pectin, fucoidan, inulins, pullulan, konjac mannan, galactan, galactomannan, glucomannan, gum karaya, xyloglucan, arabinan, psyllium gum and lactulose- and lactose-derived prebiotic galactooligosaccharides. See 2.1.7. for further details of food and microbial glycans used in this study.

3.2.4.1. BWZ.36 Dectin-1 reporter cell screening

Among all PS tested, only scleroglucan, a β-(1,3) glucan[128], was found to bind to Dectin-1 and not to mock cells (Figure 33a), as also confirmed in a second independent experiment in triplicate (Figure 33b).

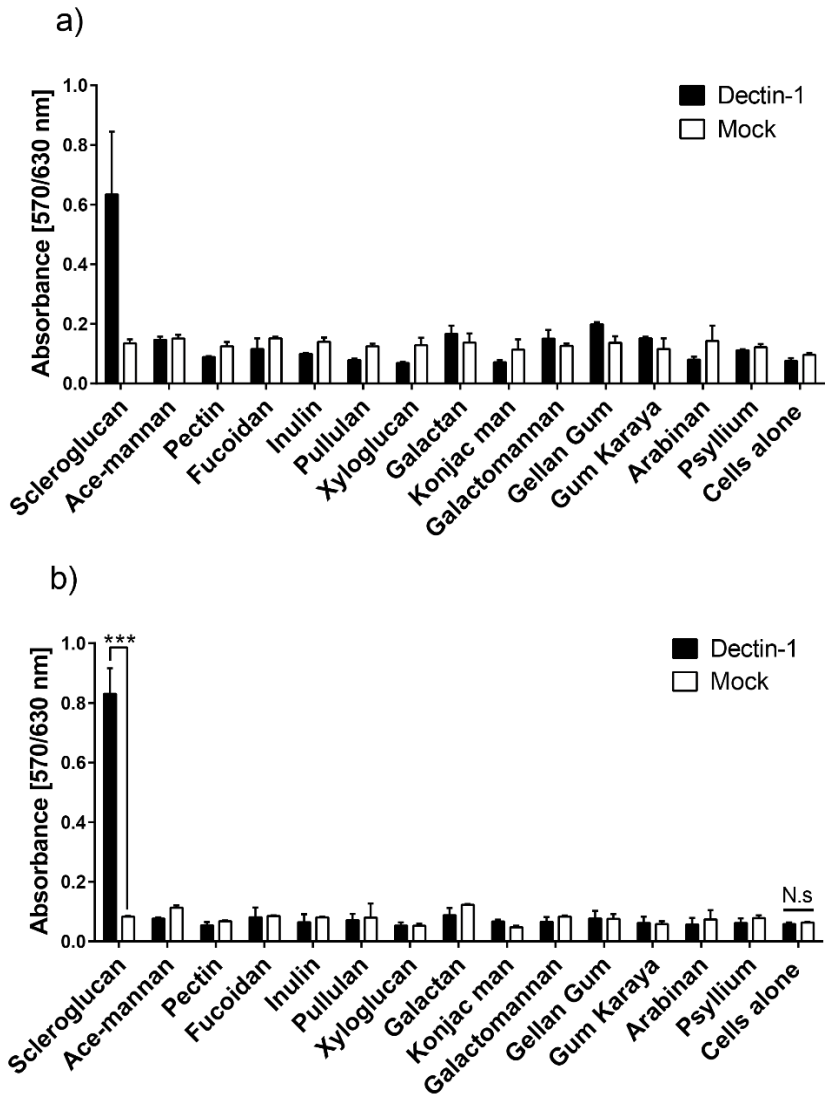

Figure 33. Screening of PS to Dectin-1 reporter cells.

Carbohydrate binding to CLR BWZ.36 reporter cells induces β-galactosidase production within the cell which can be measured in a colorimetric assay: CLR BWZ.36 reporter cells were incubated with immobilised carbohydrate ligands using a 96 well plate; a substrate, Chlorophenol red-β-D-galactopyranoside (CPRG), was added to cells and absorbance values were read at 570/630 nm. Reporter assays were performed with both Dectin-1 reporter cells and mock cells. Experiments were performed in (a) duplicate and (b) in triplicate. All PS concentrations were 1 μg/ml. Error bars, ±SD. Statistical analyses were performed by one-way ANOVA followed by Tukey's test. ***, p < 0.001. N.s., not statistically significant.

3.2.4.2. BWZ.36 Dectin-2 reporter cell screening

The initial screening of PS to Dectin-2 reporter cells in two independent experiments showed that Hafnia-LPS and α-mannan (from *S. cerevisiae)* could bind to Dectin-2 (Figure 34 and Appendix 14), with no binding seen with mock cells. No binding to Dectin-2 was observed with the other PS tested. α-mannan, a known Dectin-2 ligand[339], was also shown to bind to Dectin-2 and was used as a positive control for subsequent Dectin-2 reporter assays.

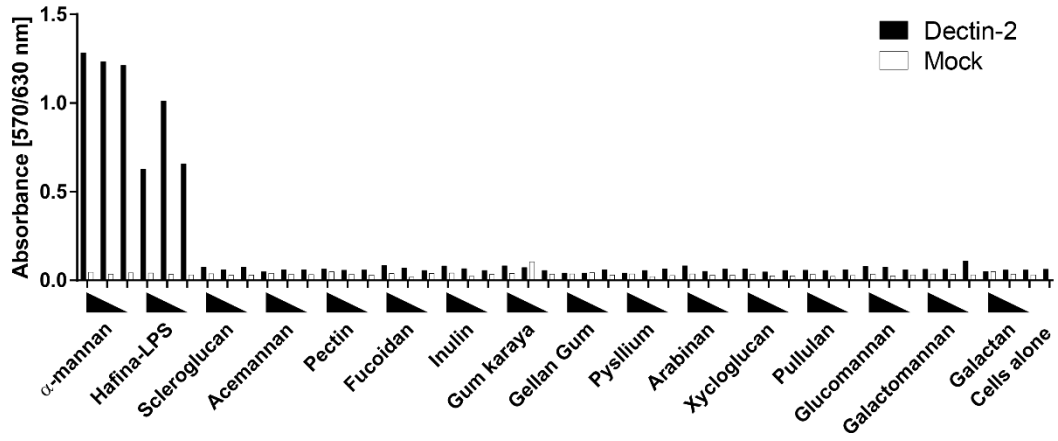

Figure 34. Screening of PS to Dectin-2 reporter cells.

Carbohydrate binding to CLR BWZ.36 reporter cells induces β-galactosidase production within the cell which can be measured in a colorimetric assay: CLR BWZ.36 reporter cells were incubated with immobilised carbohydrate ligands using a 96 well plate; a substrate, Chlorophenol red-β-D-galactopyranoside (CPRG), was added to cells and absorbance values were read at 570/630 nm. Reporter assays were performed using Dectin-2 and mock reporter cells using PS concentrations of 10, 2 and 0.4 μg/ml. For repeated independent experiment see Appendix 14.

Prebiotic galactooligosaccharides (GOS) were also tested for their binding to Dectin-2 using reporter cells[489]. Oligosaccharide OsLu is a prebiotic GOS derived from lactulose and is synthesised using *Aspergillus oryzae*-derived β-galactosidase and commercial lactulose (Duphalac®)[528] (Figure 35 and Appendix 16). OsLu mixtures were initially purified by fermentation with *S. cerevisiae* (OsLu-Sc) or activated charcoal (OsLu-ActC)[489,529] (Figure 34).

OsLu-Sc but not OsLu-ActC bound to Dectin-2 reporter cells, but not to mock or Dectin-2 QPD suggesting that binding of OsLu-Sc occurred through the CRD (Figure 36a). Further, commercial GOS Duphalac® and Vivinal® did not bind to Dectin-2 compared with OsLu-Sc (Figure 36b). These data suggest that purification of OsLu with *S. cerevisiae* conferred OsLu the ability to interact with Dectin-2. These findings

were also shown in repeated experiments (Appendix 15). We hypothesised that *S. cerevisiae*-derived mannoproteins were introduced through purification. OsLu-Sc was fractionated by ultrafiltration, resulting in compounds > 10 kDa (Retentate; OsLu-Sc-R) or > 10 kDa (Permeate; OsLu-Sc-P); and precipitated with 87% ethanol, resulting in a precipitate (OsLu-Sc-Pp) and supernatant fraction (OsLu-Sc-S) (Figure 35). The carbohydrate composition and protein content are shown in Appendix 16. We found that OsLu-Sc-R and OsLu-Sc-Pp could bind to Dectin-2 but not OsLu-Sc-P (Figure 36a). This was also found in repeated experiment (Appendix 15). The protein content of all samples was generally low, however appreciable amounts were found in OsLu-Sc, OsLu-Sc-R and OsLu-Sc-Pp (Appendix 16). The binding of OsLu-Sc-R and OsLu-Sc-Pp (but not OsLu-Sc-P) to Dectin-2 suggest that the protein content in these samples may be responsible for Dectin-2 binding to OsLu-Sc. Further proteomic analysis performed by our collaborators of OsLu-Sc-R and OsLu-Sc-Pp, identified 119 and 89 proteins, respectively, and confirmed the presence of mannoproteins in these samples including Hsp150[530] and invertase[531] (most abundant) from *S. cerevisiae*[489]. As mannan is the only sugar moiety attached to fungal proteins, all *S. cerevisiae*-derived glycoproteins contain mannan[532]. Further, the mannan attachment sequence N-X-S/T is strongly identifiable in the protein list constructed by our collaborators[489]. Overall, these data suggest that the observed binding to Dectin-2 by OsLu-Sc was mediated by mannoproteins introduced during the purification process with *S. cerevisiae*. For further information about this study see[489].

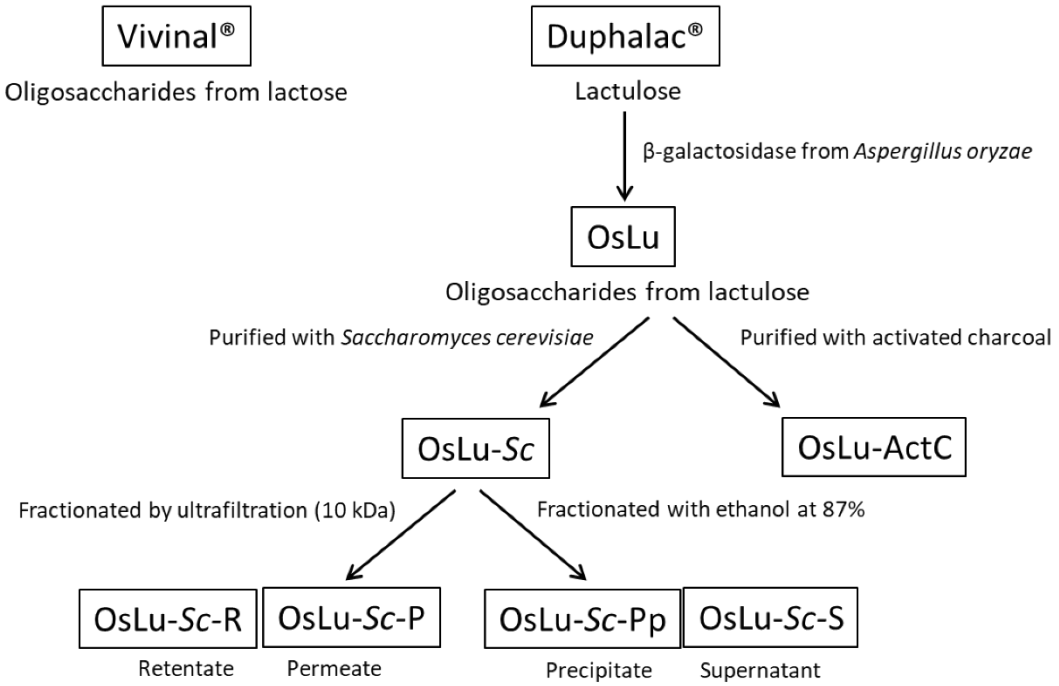

Figure 35. Basic schematic of the production and purification of prebiotic galactooligosaccharide OsLu.

Samples used for testing interaction with Dectin-2 are shown. Taken from [489]. Permission is not required for authors to use this Figure as stated by the Copyright Clearance Centre.

a)

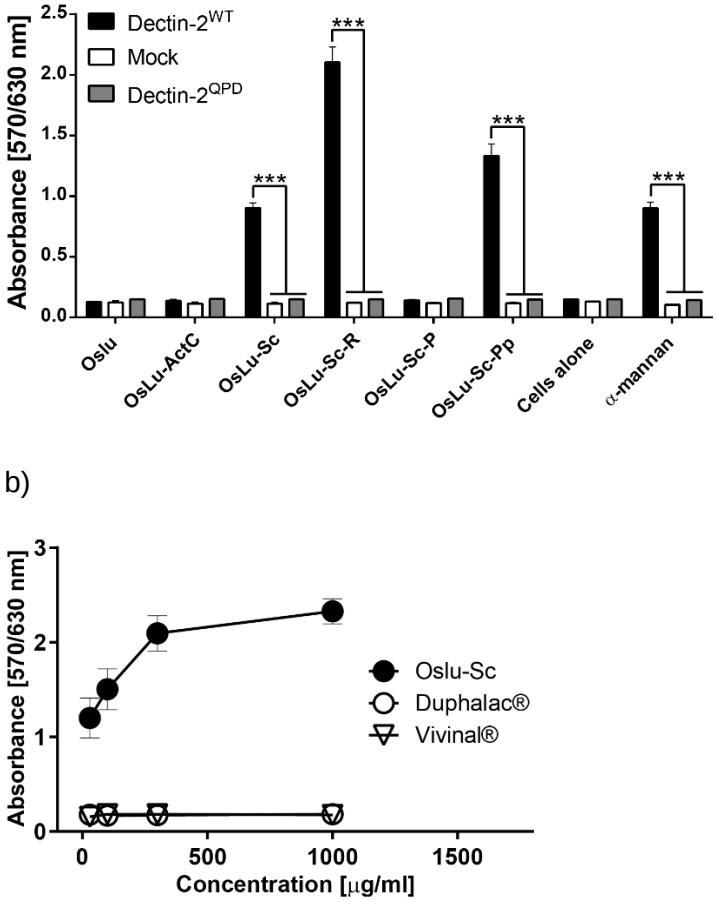

Figure 36. Interaction of OsLu preparations and other prebiotic oligosaccharides with Dectin-2 using reporter cells.

Carbohydrate binding to CLR BWZ.36 reporter cells induces β-galactosidase production within the cell which can be measured in a colorimetric assay: CLR BWZ.36 reporter cells were incubated with immobilised carbohydrate ligands using a 96 well plate; a substrate, Chlorophenol red-β-D-galactopyranoside (CPRG), was added to cells and absorbance values were read at 570/630 nm. (a) Dectin-2, Dectin-2-QPD and mock reporter cell assay of different preparations of OsLu (see Figure 35). All OsLu concentrations were used at 50μg and α-mannan at 1 μg/ml (b) Dectin-2 reporter assay with OsLu and commercial prebiotic galactooligosaccharides. Concentrations are as indicated. Data are means of triplicate values ±SD (error bars). Statistical analyses were performed by one-way ANOVA followed by Tukey's test. ***, p < 0.001 as indicated. For repeated independent experiments see Appendix 15.

Interestingly, a levan-type fructan from *E. herbicola*, a high molecular weight fructose polymer, bound to Dectin-2 and not Dectin-2-QPD or mock cells suggesting that binding was through the CRD (Figure 37 and Appendix 17). This was unexpected, as Dectin-2 so far has been reported to be highly specific for α-mannan structures.

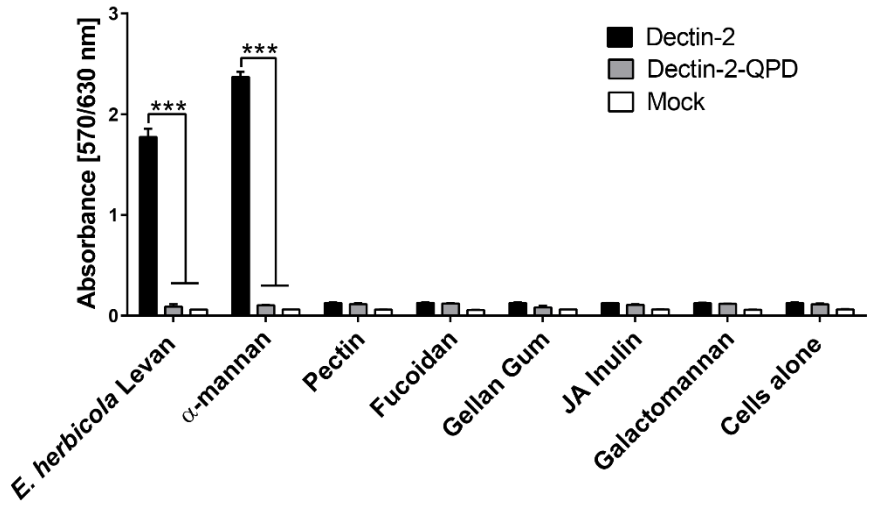

Figure 37. Screening of PS to Dectin-2 and Dectin-2-QPD reporter cells.

Carbohydrate binding to CLR BWZ.36 reporter cells induces β-galactosidase production within the cell which can be measured in a colorimetric assay: CLR BWZ.36 reporter cells were incubated with immobilised carbohydrate ligands using a 96 well plate; a substrate, Chlorophenol red-β-D-galactopyranoside (CPRG), was added to cells and absorbance values were read at 570/630 nm. Reporter assay using Dectin-2, Dectin-2-QPD and mock reporter cells. All PS concentrations were 20 μg/ml. JA, Jerusalem artichoke. Data are means of triplicate values ±SD (error bars). Statistical analyses were performed by one-way ANOVA followed by Tukey's test. ***, p < 0.001. For repeated independent experiment see Appendix 17.

3.3. Summary and Discussion

In this study, we screened for new carbohydrate ligands through the construction and use of BWZ.36 CLR reporter cells. Among all food oligosaccharides/PS or microbial glycans tested, several ligands were identified as discussed below.

Scleroglucan is a high molecular weight β-glucan comprising a β-1,3 backbone with β-1,6 linked branch points and is produced by *Sclerotium* fungi[128]. Here, scleroglucan was shown to bind to Dectin-1 using reporter cells. This result is in line with previous studies showing that scleroglucan can confer the ability of mouse DCs through Dectin-1-activation to differentiate CD4+ T cells into Th9 cells, a T cell subset reported to be involved in autoimmune disease, antitumor immunity and allergy[533]. Further, scleroglucan has been shown to bind to mouse recombinant Dectin-1 using surface plasmon resonance competition assays[534].

We found that Hafnia-LPS, an α-mannan-linked LPS from strain *Hafnia alvei* PCM 1223 strain[527], was recognised by SIGNR1. The binding was confirmed to be through the CRD since no binding was observed to SIGNR1-QPD reported cells. SIGNR1 and SIGNR1-QPD reporter cells were also used by our group which found that SIGNR1 recognises gut commensal bacteria *Lactobacillus reuteri* mucus adhesin

(MUB)[212]. Interestingly, we showed that SIGNR1 bound to an α-glucan from *S. venezuelae*. The α-glucan structure is similar to glycogen and contains an α-1,4 backbone with α-1,6 branching points[486]. Interestingly, a mycobacterial CPS, α-glucan, has previously been reported to bind to DC-SIGN, the human homolog of mouse SIGNR1, which is in line with our findings[535].

Here, we showed that Hafnia-LPS was also recognised by Dectin-2. Hafnia-LPS contains mannose residues in its O-antigen[527] which would contribute to the reporter cell binding, as Dectin-2 is known to recognise high-mannose structures[339]. It was also reported by the Kawasaki group that Hafnia-LPS interaction with Dectin-2 augments Toll-like receptor 4 (TLR4) activation in BMDC[394]. Furthermore, our data also showed that α-mannan from *S. cerevisiae* was recognised by Dectin-2 but did not bind Dectin-2-QPD reporter cells, confirming that α-mannan-binding to Dectin-2 is through the CRD.

Moreover, using Dectin-2 reporter cells, we showed that prebiotic oligosaccharide OsLu purified using *S. cerevisiae* and not OsLu purified by active charcoal or other prebiotics Duphalac® and Vivinal® could bind to Dectin-2[489]. During purification of OsLu, our data suggest that the introduction of mannoproteins from yeast was responsible for the observed binding to Dectin-2, highlighting the importance of the method used for purification of prebiotic GOS. The mechanisms for OsLu's reported immunomodulatory effects *in vivo* are not fully verified, however, this capacity to bind to an immune cell receptor warrants further investigation[536].

Strikingly, we found that microbial levan PS bound to Dectin-2 through the CRD. The binding of this commercial fructofuranose EPS to Dectin-2 was unexpected, as to date, α-mannans and other high-mannose structures are the only reported ligands of Dectin-2[339]. Levan is a fructan that is produced by both plants and bacteria[70,72,537]. Microbial levan is generally of higher molecular weight than levans produced in plants[538]. Microbial levans are large β-(2,6) fructofuranose polymers which can possess β-(2,1) branch points[72] and are generally > 500 kDa in molecular weight, however microbial levans lower in molecular weight including < 50 kDa have been reported[104]. Levan is synthesised by many bacteria[538] including *B. polymyxa*[539] and *M. laevanformans*[101] *B. subtilis*[25], *Z. mobilis*[95], *p. syringae pv*[540] *and E. herbicola*[97] through the action of levansucrase (EC 2.4.1.10)[72]. Levan is also produced by *Streptococcus mutans* found in human oral cavities[541] and *Lactobacillus reuteri*, a commensal microbe found in the gut[91]. Low molecular weight levan-type fructans are also produced and present in a few plant species such as *Curcuma kwangsiensis*[70],

Pachysandra terminalis[69] and *Agropyron cristatum*[68] as a non-structural storage carbohydrate located in leaf and stem sheaths[70-73]. Further, levan can also be found in fermented foods[26,537]. The molecular weight of levan can vary depending on the bacterial species and production method used[71,72,102,542,543]. Moreover, the structural features of levan may be important, as they may have an impact on levan's bioactivity including its anti-tumour effects[95,100]. In addition, similar structure-function relationships are suggested for other immunomodulatory PS including another fructose polymer, inulin[162,359,432].

Interestingly, levan has shown to elicit immunomodulatory and anti-tumour effects both *in vivo* and *in vitro*[26,70,91,95,482,544,545], yet the molecular mechanisms underpinning these effects remain unclear. Moreover, it has been suggested that levan may interact with immune cell receptor TLR4 expressed by innate immune cells[26]. Interestingly, inulin from Jerusalem artichoke, another fructose polymer comprising β-2,1 backbone[65] did not bind to Dectin-2. Therefore, our data suggest a possible preference of Dectin-2 for β-2,6 fructofuranose linkages. Levan's interaction with Dectin-2 may thus contribute to the reported immunomodulatory effects of levan[26,72,91].

Overall, several interactions of PS and CLRs SIGNR1, Dectin-1 and Dectin-2 were identified using the BWZ.36 CLR reporter cell assays. The next chapter will investigate the purification and characterisation of levan and will further assess its interaction with Dectin-2.

Chapter 4: Interaction of crude and purified levan with Dectin-2 and TLR4

4.1. Introduction

In the previous chapter, commercial microbial levan from *E. herbicola* was found to bind to Dectin-2 through the CRD using a cell reporter assay. The binding of microbial levan to Dectin-2 was unexpected, as levan is a fructofuranose polymer[72]. *E. herbicola* is a gram-negative bacterium that resides in various environments including soil, aquaculture and on the surface of plants, and is suggested as an opportunistic pathogen in animals including humans[546,547]. Levan can also be derived from commensal bacteria including *B. subtilis* and *L. reuteri* and can be found in fermented food[25,26,91,92].

Recognition of PS structures by CLR including Dectin-2 is well known, however, most reports are based on the study of opportunistic or pathogenic microbes[328,394]. Dectin-2 is a CLR found on a variety of myeloid cells including DC and macrophages and plays a role particularly in antimycobacterial and antifungal immunity[121,328,548]. Dectin-2 has a high specificity for α-mannan structures which can be found on the surfaces of pathogenic fungi and mycobacteria[120,395,549]. Carbohydrate recognition by Dectin-2 can lead to immune cell responses providing protection for the host[120,391,548].

The aim of this chapter is to purify and characterise commercial *E. herbicola* levan and test the interaction of crude and purified levan with Dectin-2 using BWZ.36 reporter cells and assess the direct binding with Dectin-2 protein using atomic force spectroscopy. Lastly, the interaction of crude or purified levan with TLR4 using HEK 293 reporter cells was investigated.

4.2. Results

4.2.1. Purification of E. herbicola levan

E. herbicola levan was first purified using gel permeation chromatography (GPC) resulting in 5 main elution fractions (Figure 38). F1 was the most abundant fraction with a yield of ~53% by overall weight. Analysis of the identifiable peak elution times for 5 kDa, 12 kDa, 25 kDa, 50 kDa, 80 kDa, 150 kDa, 270 kDa, 410 kDa, and 1400 kDa commercial dextran standards was performed to use for investigation of levan's size (see Appendix 18). As dextran is a compositionally- and structurally-different PS from levan, the approach provides apparent molecular weights. It should be noted that no levan size standards are commercially available and dextrans > 1400 kDa were not obtainable. Therefore, the abundant F1 fraction of *E. herbicola* was estimated to be $\geq$ 1400 kDa (Figure 38), which is in line with previous reports[97,490].

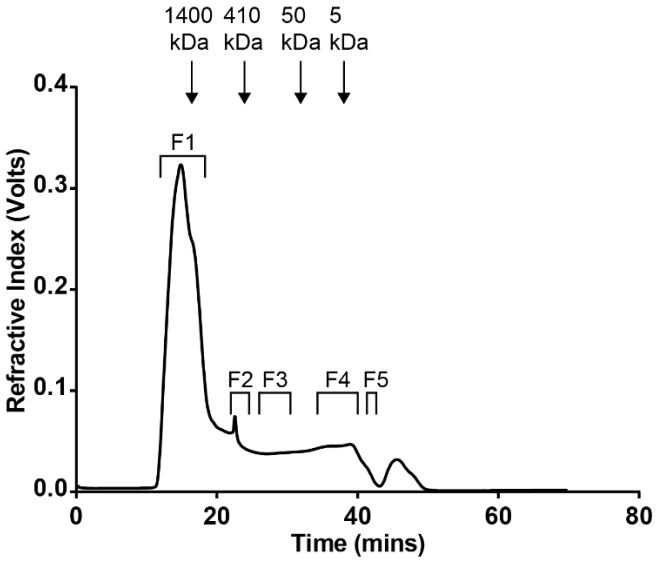

Figure 38. Representative fractionation and molecular weight determination of E. herbicola levan by gel permeation chromatography.

Arrows on the chromatograph show the apparent molecular weights of E. herbicola levan fractions F1, F2, F3, F4 and F5 based on commercial Dextran standards (see Appendix 18). The graph was constructed in GraphPad Prism after exporting data from the gel permeation chromatography (GPC) system and Microsoft Excel.

No protein content $\geq$ 33.4 μg per mg of levan was detected in *E. herbicola* crude levan by Bradford (Appendix 19). For higher sensitivity, we used SDS PAGE and stained gels with Spyro™ Ruby reagent. No proteins $\geq$ 0.3 μg per mg of levan were

detected in *E. herbicola* levan crude, or ≥ 0.38 μg per mg of the *E. herbicola* levan F1 fraction (*E. herbicola* levan 1) (Appendix 20).

Most gram-negative bacteria including *E. herbicola* harbour LPS[550,551], a potent immune cell-stimulator and PRR ligand[275]. Therefore, we quantified LPS in *E. herbicola* crude levan using the EndoZyme® recombinant Factor C Assay. Our analysis showed that levan contained 8.2 ng/mg (ng of LPS per mg of levan; average of 4 independent tests; SD, ± 1.4). After GPC, *E. herbicola* levan 1 LPS levels increased ~3-fold to 23.8 ng/mg (average of 2 independent tests; SD = 0.7). To remove LPS from *E. herbicola* levan 1, two methods were employed (Figure 39). Initially, commercial LRA was used on *E. herbicola* levan 1 (see 2.2.10.2.1.) leading to a ~4.3-fold decrease from 23.8 ng/mg to 5.5 ng/mg (average of three independent tests; SD = 1.8). LPS is reported to elicit immunostimulatory effects on human-derived DCs *in vitro* at concentrations as low as 0.002 - 0.2 ng/ml including the induction of pro-inflammatory cytokines (≥ 0.02 ng/ml)[411]. Therefore, a method to degrade LPS chemically using sodium hydroxide (alkali-treatment) was developed (see 2.2.10.2.2. and Figure 40) which further reduced LPS concentrations to ≤ 7.8 pg/mg ([*E. herbicola* levan 3] Figure 39). Further, we confirmed that no smaller oligosaccharides or monosaccharides were released as a result of the treatment with sodium hydroxide, as shown by thin layer chromatography (TLC) (Appendix 21).

Taken together, *E. herbicola* crude levan was purified using GPC, LRA and alkali treatment to reduce LPS content to a concentration which is likely below the reported immunostimulatory levels on DCs *in vitro*[411].

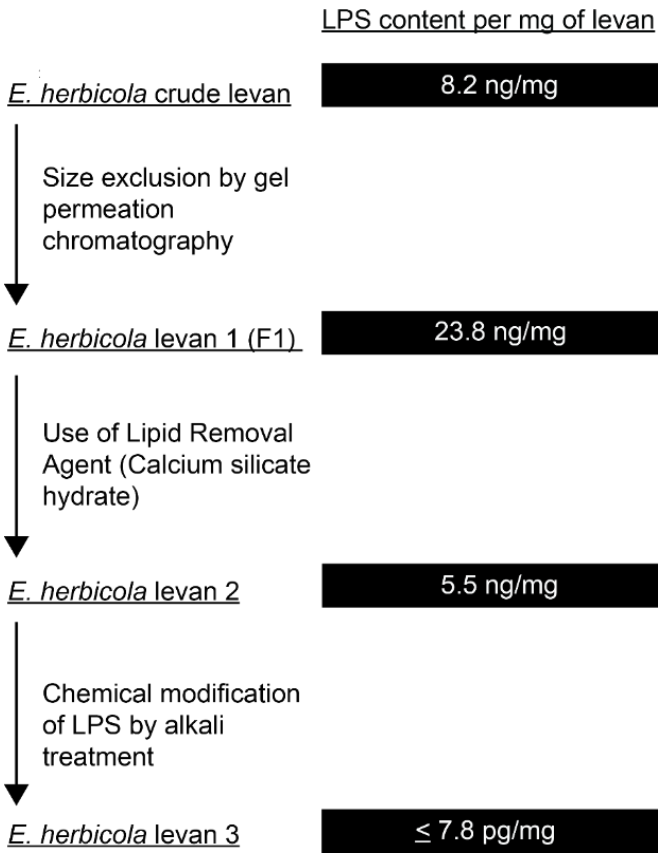

Figure 39. Graphical representation of the purification of E. herbicola levan and removal of LPS. F1, fraction 1 from Figure 40 (E. herbicola levan 1).

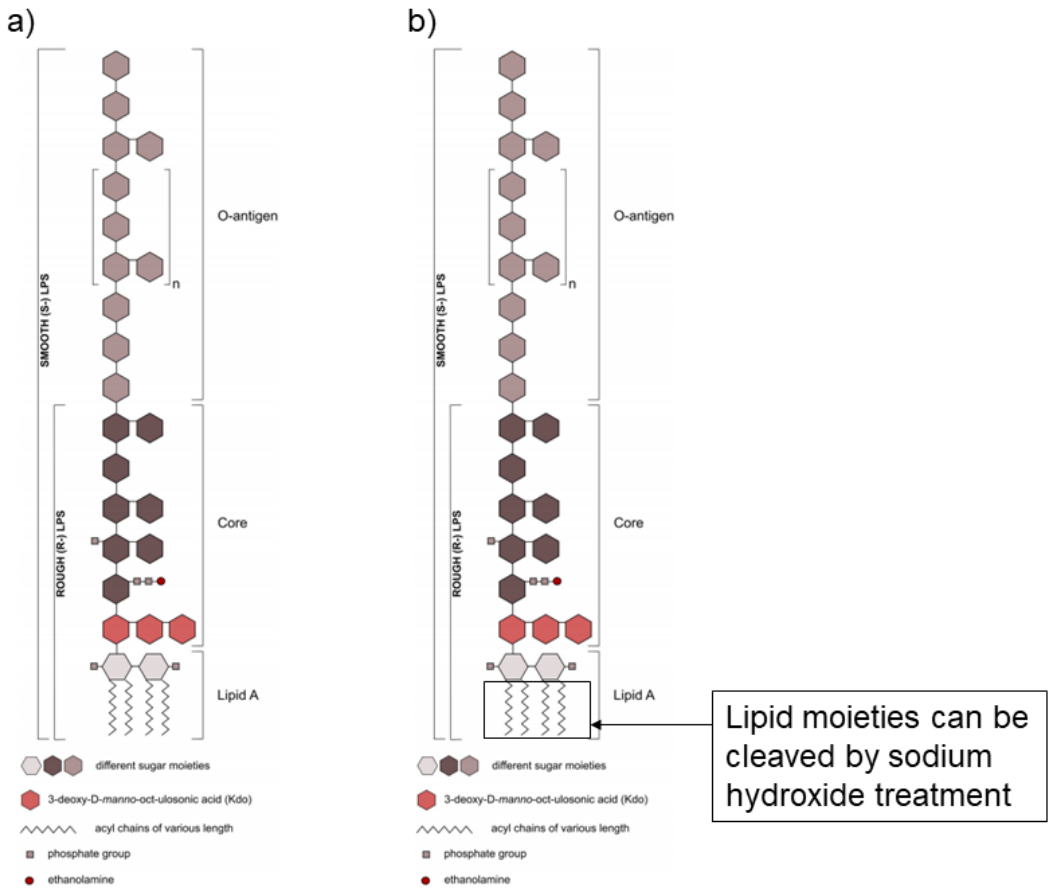

Figure 40. Structure of LPS and its chemical modification by alkali treatment.

(a) basic structure of LPS containing an oligosaccharide core, Lipid A (made up of lipids linked to sugar moieties), and a variable O-antigen region. (b) region of LPS (black box) that is cleaved and released from the core and O-antigen region when treated with sodium hydroxide. Taken from [131] with minor adaptions. Article is under the Creative Commons Attribution-Non-commercial-No Derivatives License (CC BY NC ND). Image licence: https://creativecommons.org/licenses/by-nc-nd/4.0/legalcode.

4.2.2. Characterisation of crude and purified E. herbicola levan

4.2.2.1. NMR analysis

Structural characterisation of crude and purified levan from *E. herbicola* was performed by NMR spectroscopy. ^{1}H NMR spectra of both crude and purified *E. herbicola* levan 3 showed identical spectra in the carbohydrate region (3-5 ppm) that confirmed that levan's structure was unaffected by the purification procedure (Figure 41a and 41b). Furthermore, ^{1}H NMR spectra profiles of both levan samples were similar to published ^{1}H NMR spectra of known levans to that of previously reported *L. reuteri* levan[91] (Figure 41c). Further, a sample of *E. herbicola* levan 3 was analysed

by 2D COSY and $^{1}H,^{13}C$ HSQC technique (Figure 41d and 41e, respectively) which allowed to assign its chemical shifts as listed in Table 6. ^{13}C NMR chemical shifts for *E. herbicola* levan 3 were similar to published values, see [71] (Appendix 22). Taken together, our NMR analysis confirmed the characterisation of *E. herbicola* crude levan and its purified form *E. herbicola* levan 3 as β-(2,6) fructans.

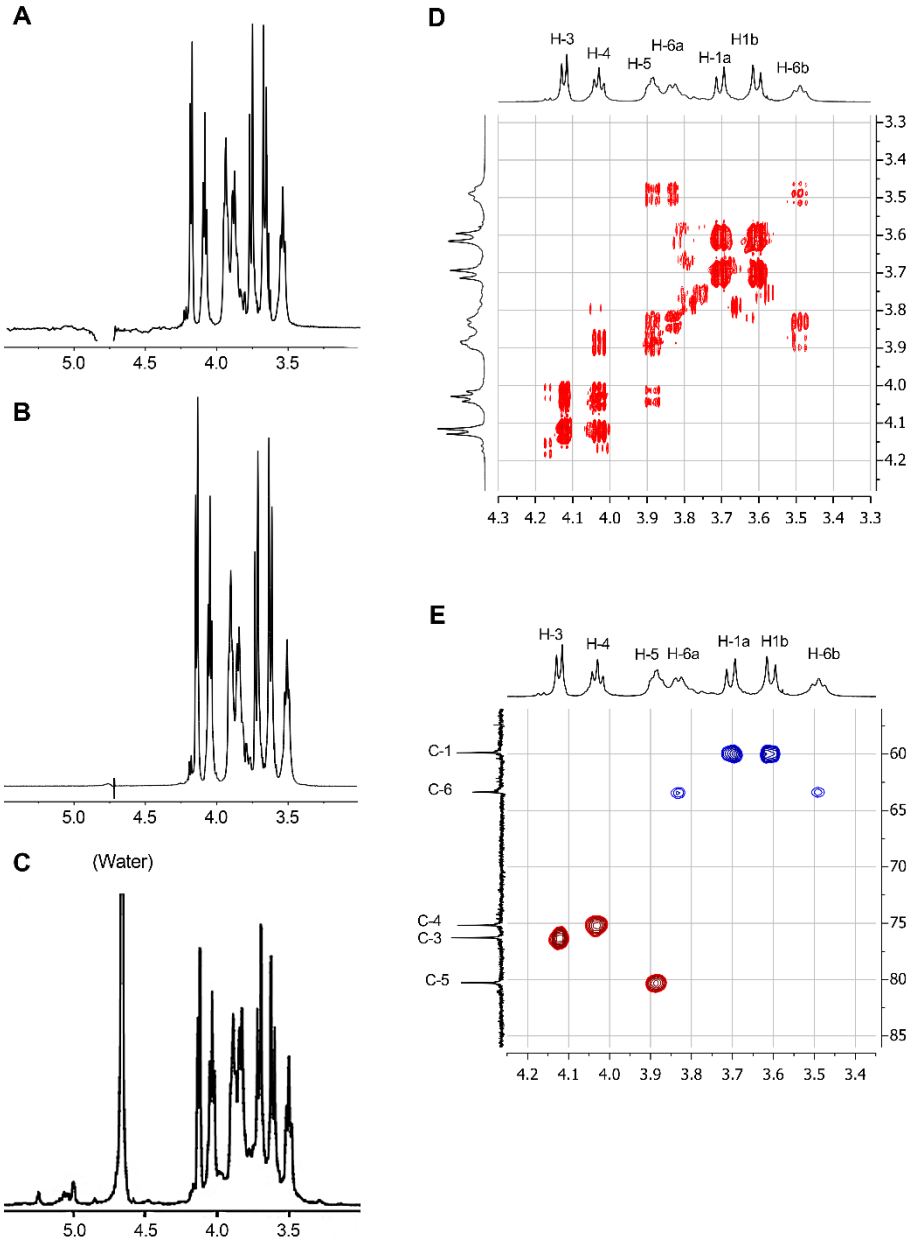

Figure 41. NMR spectra of levans.

(a) Carbohydrate region of ^{1}H NMR of E. herbicola levan crude as compared to (b) purified E. herbicola levan 3 and (c) ^{1}H NMR of L. reuteri levan as adapted from Ref.[91]; (d) COSY 2D NMR of purified E. herbicola levan 3; (e) $^{1}H,^{13}C$ HSQC 2D NMR of purified 3 with proton carbon signals assignment shown on projections. NMR: 600 MHz, D_2O, 300 K. (c) was taken from [91] with permission from Springer Nature and the Copyright Clearance Center. NMR analysis was performed by Sergey Nepogodiev and Gwenaelle Le Gall.

Table 6. Chemical shifts for E. herbicola levan 3 in ^{1}H and ^{13}C NMR spectra.

H-1a	***H-1b***	***H-3***	***H-4***	***H-5***	***H6a***	***H-6b***
3.71	3.61	4.12	4.02	3.89	3.71	3.49
C-1	***C-2***	***C-3***	***C-4***	***C-5***	***C-6***	
59.89	104.20	76.28	75.19	80.28	63.4	

Legend: H, hydrogen. C, Carbon. NMR analysis was performed by Sergey Nepogodiev and Gwenaelle Le Gall.

4.2.2.2. Glycosyl linkage analysis by gas chromatography-mass spectrometry

α-mannan is a potent Dectin-2 ligand found on the cell-surface of some pathogenic fungi and bacteria[489]. To characterise the carbohydrate linkage of crude and purified *E. herbicola* levan and confirm that no mannose residues were present, glycosyl linkage analysis using partially methylated alditol acetates and GC-MS was used. The sensitivity of the method allowed the detection of 1 - 5 μg of mannose or fructose residues in α-mannan from *S. cerevisiae* or *E. herbicola* levan 2, respectively (Appendix 23 and 24).

E. herbicola crude levan and *E. herbicola* levan 3 had similar GC-MS profiles showing predominant β-(2,6) fructose linkages (see Appendix 25 for GC-MS data). Table 8 shows the relative percentage (area) of GC profile peaks for each levan sample; the 2,6-linked fructose residues (6-Fructose), representing β-(2,6) linkages, accounted for 86.1% and 81.3% of total residues for *E. herbicola* crude levan and *E. herbicola* levan 3, respectively. Importantly, no mannose residues were detected.

Table 7. Relative percentage of each detected peak in E. herbicola 3 and E. herbicola crude levan.

Peak	***E. herbicola* levan 3 (%)**	***E. herbicola* crude levan (%)**
Terminal Fructose Residue #1 (t-Fruc)	2.0	2.2
Terminal Fructose Residue #2 (t-Fruc)	3.8	4.0
Terminal Glucopyranosyl residue (t-Glc)	0.5	0
2,6 linked Fructose residue #1 (6-Fructose)	37.0	46.2
2,6 linked Fructose residue #2 (6-Fructose)	44.8	39.9
1,4 linked Glucopyranosyl residue (4-Glc)	0.9	0.1
2,4,6 linked Fructose residue #1 (4,6-Fructose)	0.3	0.0
2,4,6 linked Fructose residue #2 (4,6-Fructose)	0.2	0.0
1,2,6 linked Fructose residue #1 (1,6-Fructose)	4.1	2.7
1,2,6 linked Fructose residue #2 (1,6-Fructose)	6.4	4.8

GC-MS linkage analysis was performed by Ian Black.

1,2,6-linked fructose residues (1-6-Fructose), representing β-(2,1) branching points, accounted for 7.5% and 10.5% of linkage residues for *E. herbicola* crude levan and *E. herbicola* levan 3, respectively. Terminal fructose (t-Fructose) residues (2 peaks)

accounted for (in total) 6.2% and 5.8% for *E. herbicola* crude levan and *E. herbicola* levan 3, respectively. A small amount of a terminal glucopyranosyl residue (0.5%) was detected in *E. herbicola* crude levan, but not in *E. herbicola* levan 3. The low amount of 2,4,6-linked fructose residues (4,6-Fructose) may be as a result of undermethylation, which has been described as a common difficultly of this method[509]. 1,4-linked glucopyranosyl residues accounted for 0.9% and 0.1% in *E. herbicola* crude levan and in *E. herbicola* levan 3, respectively. This may be due to capped glucose residues[72] or due to small contaminants such as cellulose.

Taken together, our data show that *E. herbicola* crude levan and *E. herbicola* levan 3 were fructofuranose polymers comprising a predominant linear chain of β-(2,6)-linked fructose with β-(2,1) branching points which is in line with previous reports[71,490].

4.2.3. Dectin-2 interaction with crude and purified E. herbicola levan using BWZ.36 reporter cells.

To test the binding of crude and purified *E. herbicola* levan to Dectin-2, Dectin-2 BWZ.36 reporter cells were used in a cell bioassay (see Figure 20)[394,489].

The carbohydrate-binding domain of mannose-specific lectins including Dectin-2 contain an EPN (Glutamic acid, Proline and Asparagine) amino acid motif[334]. Dectin-2-QPD cells were established by our group harbouring a mutated carbohydrate-binding domain through introduction of a galactose-specific QPD (Glutamine, Proline and Aspartic acid) amino acid motif in place of a mannose-specific EPN motif[394] allowing a control for CRD-specific binding. Further, mock cells, which are BWZ.36 parental cells that do not express a CLR ectodomain, were used as another control.

After initial purification by GPC, all *E. herbicola* levan fractions showed observable binding to Dectin-2 (Figure 42a). The positive control α-mannan bound to Dectin-2, but not to mock cells (Figure 42b). Further, in the same experiment, no binding was observed to mock cells using the highest concentration (Appendix 26).

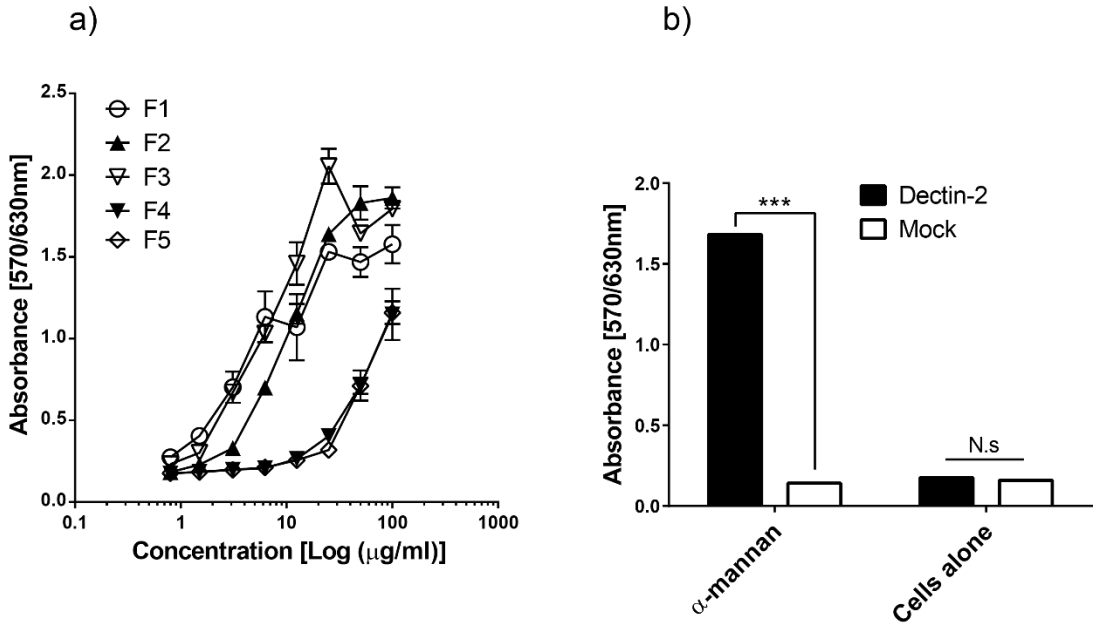

Figure 42. Interaction of E. herbicola levan fractions and Dectin-2 using Dectin-2 and mock reporter cells.

Carbohydrate binding to CLR BWZ.36 reporter cells induces β-galactosidase production within the cell which can be measured in a colorimetric assay: CLR BWZ.36 reporter cells were incubated with immobilised carbohydrate ligands using a 96 well plate; a substrate, Chlorophenol red-β-D-galactopyranoside (CPRG), was added to cells and absorbance values were read at 570/630 nm. (a) E. herbicola levan fractions and Dectin-2 reporter cells. (b) Controls α-mannan and cells alone with Dectin-2 and mock reporter cells used in the same experiment as a). F1, F2, F3, F4 and F5 represent collected fractions of E. herbicola levan after GPC (see Figure 38). The concentration of positive control α-mannan was 1.5 μg/ml. The experiment was performed in triplicate. Error bars, ± SD. Statistical analysis for was performed using one-way ANOVA followed by tukey's test (b). ***, p < 0.001. N.s., not statistically significant.

As *E. herbicola* levan 1 was shown to bind to Dectin-2 in the screening assay (Figure 42a), Dectin-2 and Dectin-2-QPD mutant reporter cells were used to confirm binding and to determine if the interaction was through the CRD. *E. herbicola* levan 1 bound to Dectin-2 and not to mock cells confirming binding (Figure 43 and Appendix 27). The absorbance values for *E. herbicola* levan 1 were significantly lower in Dectin-2-QPD cells than Dectin-2 WT, suggesting that binding is likely through the CRD. Similar results were observed for positive control α-mannan (Figure 43).

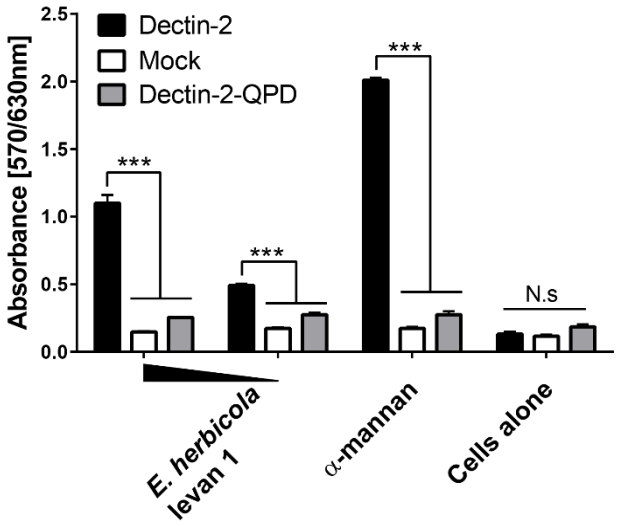

Figure 43. Interaction of E. herbicola levan 1 with Dectin-2 and its CRD using Dectin-2, Dectin-2-QPD and mock reporter cells.

Carbohydrate binding to CLR BWZ.36 reporter cells induces β-galactosidase production within the cell which can be measured in a colorimetric assay: CLR BWZ.36 reporter cells were incubated with immobilised carbohydrate ligands using a 96 well plate; a substrate, Chlorophenol red-β-D-galactopyranoside (CPRG), was added to cells and absorbance values were read at 570/630 nm. E. herbicola levan was used at 25 μg/ml and 5 μg/ml, positive control α-mannan at 1 μg/ml. Experiment was performed in triplicate. Error bars, ± SD. Statistical analysis was performed using one-way ANOVA followed by tukey's test (b). ***, p < 0.001. N.s with straight line, not statistically significant. For repeated independent experiment see Appendix 27.

Following LPS removal (Figure 39), Dectin-2-binding to *E. herbicola* levan 2 and *E. herbicola* levan 3 was found to be greatly reduced compared *E. herbicola* crude levan (Figure 44). Two further independent experiments confirmed that Dectin-2 binding by *E. herbicola* levan 2 and *E. herbicola* levan 3 was significantly reduced compared to *E. herbicola* crude levan (Appendix 28). Taken together, these data showed that LPS is likely to be an important contributor of *E. herbicola* crude levan's ability to bind to Dectin-2.

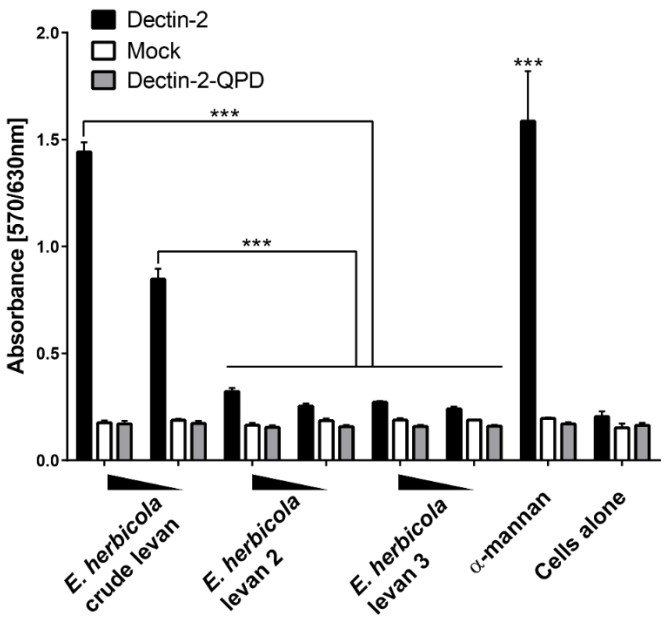

Figure 44. Comparative binding of E. herbicola crude levan, E. herbicola levan 2 and E. herbicola levan 3 to Dectin-2 and its CRD using Dectin-2, Dectin-2-QPD and mock reporter cells.

Carbohydrate binding to CLR BWZ.36 reporter cells induces β-galactosidase production within the cell which can be measured in a colorimetric assay: CLR BWZ.36 reporter cells were incubated with immobilised carbohydrate ligands using a 96 well plate; a substrate, Chlorophenol red-β-D-galactopyranoside (CPRG), was added to cells and absorbance values were read at 570/630 nm. All levans were used at 200 and 20 μg/ml, and positive control α-mannan at 1 μg/ml. Experiment was performed with n = 6. Error bars, ± SD. Statistical analysis was performed using one-way ANOVA followed by tukey's test (b). ***, p < 0.001. For repeated independent experiments see Appendix 28.

4.2.4. Production and characterisation of B. subtilis levan

As *E. herbicola* is a gram-negative bacterium, it is possible that the source of LPS bound to levan comes from the bacteria. To further investigate levan's interaction with Dectin-2, the gram-positive bacterium *B. subtilis* 168 was used to produce levan in-house. Here, two culture media were tested; Lysogeny Broth (LB) which is widely used for bacterial culture[552]; and minimal media *Lactobacillus* defined medium II (LDM2) which is used for the growth of *L. reuteri* strains[212,484].

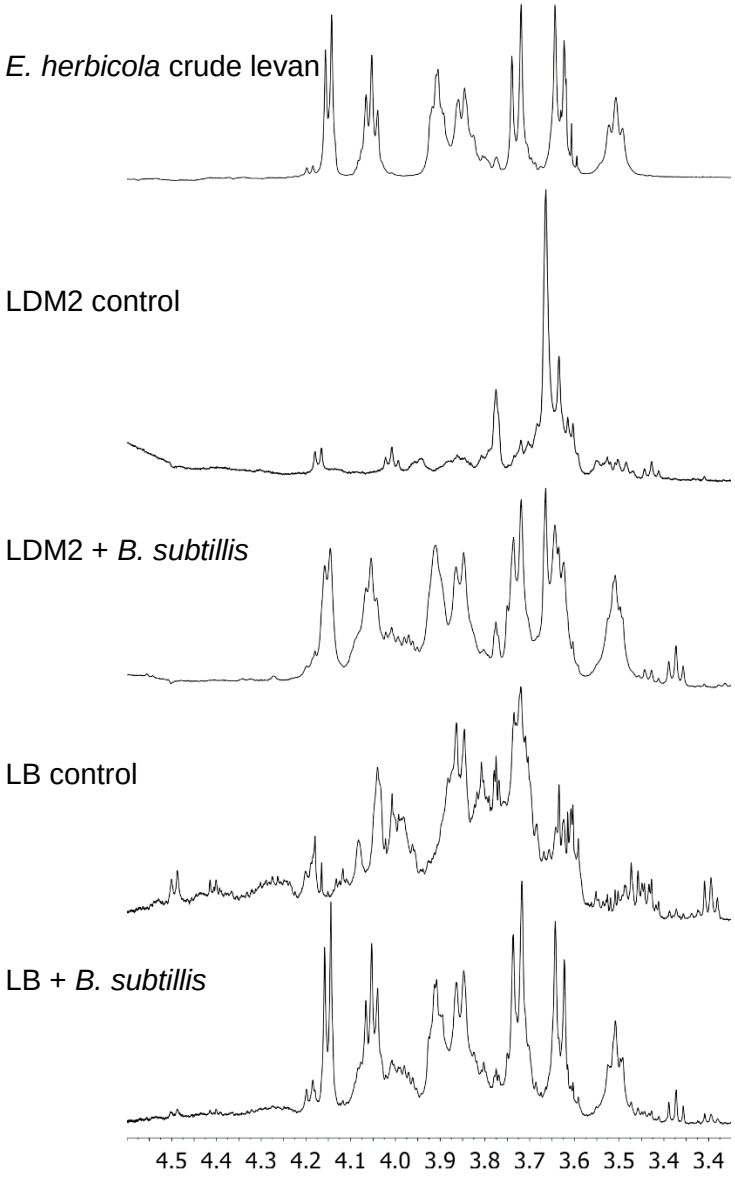

Figure 45. NMR analysis of levan-producing B. subtilis 168 culture extracts and media-only controls.

Stacked ^{1}H NMR spectra show the region characteristic for signals of levan protons. LB, lysogeny broth. LDM2, Lactobacillus semi-defined medium II. NMR analysis was performed by Sergey Nepogodiev and Gwenaelle Le Gall.

B. subtilis levan and controls were characterised by 2D ^{1}H NMR. The production of levan in both LB and LDM2 *B. subtilis* cultures produced similar NMR spectra to that of *E. herbicola* crude levan used as a standard (Figure 45). Levan was not detected in the ^{1}H NMR spectrum of LB and LDM2 media-only controls (Figure 45).

Taken together, the NMR analysis demonstrated that levan was effectively produced by *B. subtilis* in both LB and LDM2 media.

4.2.5. Dectin-2 interaction with B. subtilis levan using BWZ.36 reporter cells

The rationale for the use of LDM2 to produce levan is that LB but not LDM2 comprises yeast extract which contains α-mannans[91]; and we found that LB but not LDM2 media could bind to Dectin-2 in the reporter assay (Figure 46 and Appendix 29). Many studies of levan production using culture-based methods have been reported to use yeast or yeast extract in some form during the process[99,490,553-557]. Therefore, both LB (with yeast extract) and LDM2 (no yeast extract) containing no bacteria were also subjected to the levan production process as controls.

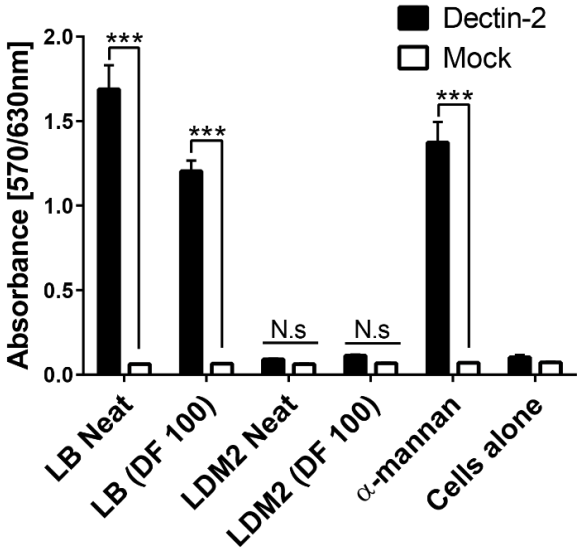

Figure 46. Interaction of LB and LDM2 culture media with Dectin-2 using Dectin-2 and mock reporter cells.

Carbohydrate binding to CLR BWZ.36 reporter cells induces β-galactosidase production within the cell which can be measured in a colorimetric assay: CLR BWZ.36 reporter cells were incubated with immobilised carbohydrate ligands using a 96 well plate; a substrate, Chlorophenol red-β-D-galactopyranoside (CPRG), was added to cells and absorbance values were read at 570/630 nm. DF 100 (of LB or LDM2) represent their dilution by a factor of 100 in sterile H_20. Error bars, ± SD. The experiment was performed in triplicate. Statistical analysis was performed using one-way ANOVA followed by tukey's test. ***, p < 0.001, as indicated. N.s. with straight line, not statistically significant compared to cells alone and across the indicated treatments. For repeated independent experiments see Appendix 29.

To determine if *B. subtilis* levan could bind to Dectin-2, Dectin-2, Dectin-2-QPD and mock reporter cells were used as previously described. Levan produced in LB or LDM2 bound to Dectin-2 cells but not Dectin-2-QPD (Figure 47), suggesting that binding occurs via the CRD, with LB-produced *B. subtilis* levan showing more pronounced binding. However, the medium-only controls also bound to Dectin-2 and

with higher binding observed with LB *B. subtilis* levan, suggesting other factors in the media may induce Dectin-2 reporter cells, hampering the use of this material to assess the immunomodulatory properties of levan *in vitro*. CRD-dependent Dectin-2 binding of levan made in LB or LDM2, and LB and LDM2 controls, was further confirmed in an independent experiment (Appendix 30).

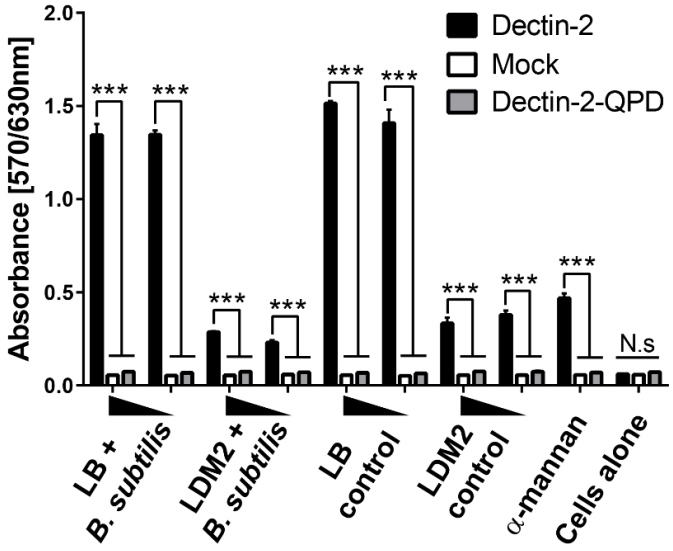

Figure 47. Interaction of B. subtilis levan and media-only controls with Dectin-2 using Dectin-2, Dectin-2-QPD and mock reporter cells.

Carbohydrate binding to CLR BWZ.36 reporter cells induces β-galactosidase production within the cell which can be measured in a colorimetric assay: CLR BWZ.36 reporter cells were incubated with immobilised carbohydrate ligands using a 96 well plate; a substrate, Chlorophenol red-β-D-galactopyranoside (CPRG), was added to cells and absorbance values were read at 570/630 nm. B. subtilis levan and medium-only controls were used at 100 μg/ml and 10 μg/ml and positive control α-mannan at 1 μg/ml. The experiment were performed in triplicate. Error bars, ± SD. Statistical analysis was performed using one-way ANOVA followed by tukey's test (b). ***, p < 0.001, as indicated. N.s, with straight line, not statistically significant. For repeated independent experiment see Appendix 30.

4.2.6. Purification and characterisation of enzymatically synthesised levan

Enzymatically synthesised (ES) levan derived from recombinant levansucrase Lsc3 from *Pseudomonas syringae pv* tomato was obtained from Tiina Almae (University of Tartu)[491,492] and characterised here by GPC analysis. The analysis revealed that the predominant fraction has a high molecular weight, ≥1400 kD (Figure 48), in line with previous reports[558]. A small peak at 40 min was also observed in water, which may be due to contamination in the GPC system. ES levan showed a very low LPS content (compared to *E. herbicola* crude levan and *E. herbicola* levan 1 and 2) of ~88 pg/mg (SD = 0.003 [average of two independent tests]). After alkali treatment (see

2.2.10.2.2.), the LPS content in ES levan was further reduced to ≤ 2 pg/mg (two independent tests). The GPC profile for ES levan post alkali-treatment (purified ES levan) was similar to ES levan prior to treatment (ES levan) (Figure 48) both showing molecular weights ≥ 1400 kDa. Repeat runs of these samples using GPC confirmed the similar profiles between ES levan and purified ES levan and the high molecular weights of the predominant fractions (Appendix 31).

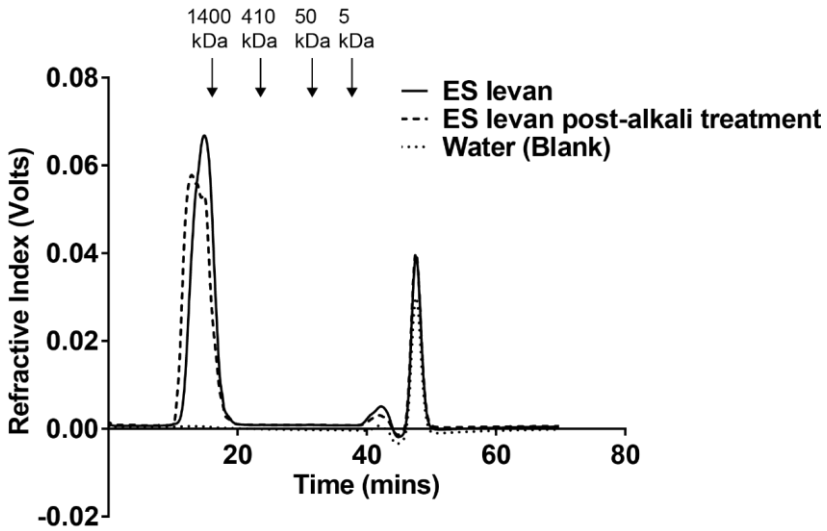

Figure 48. GPC profile of ES levan pre- and post-LPS alkali treatment.

Purified ES levan (ES levan post-alkali treatment) is after treatment with sodium hydroxide to inactivate LPS (see 2.2.10.2.2.). Water (blank) was used as a control for known system contaminants. The graph was constructed in GraphPad Prism after exporting data from the GPC system and Microsoft Excel.

In addition, ES levan pre- and post-alkali treatment showed similar ^{1}H NMR spectra and peak distribution as *E. herbicola* crude levan (Figure 49). Taken together, these data confirmed the integrity of ES levan.

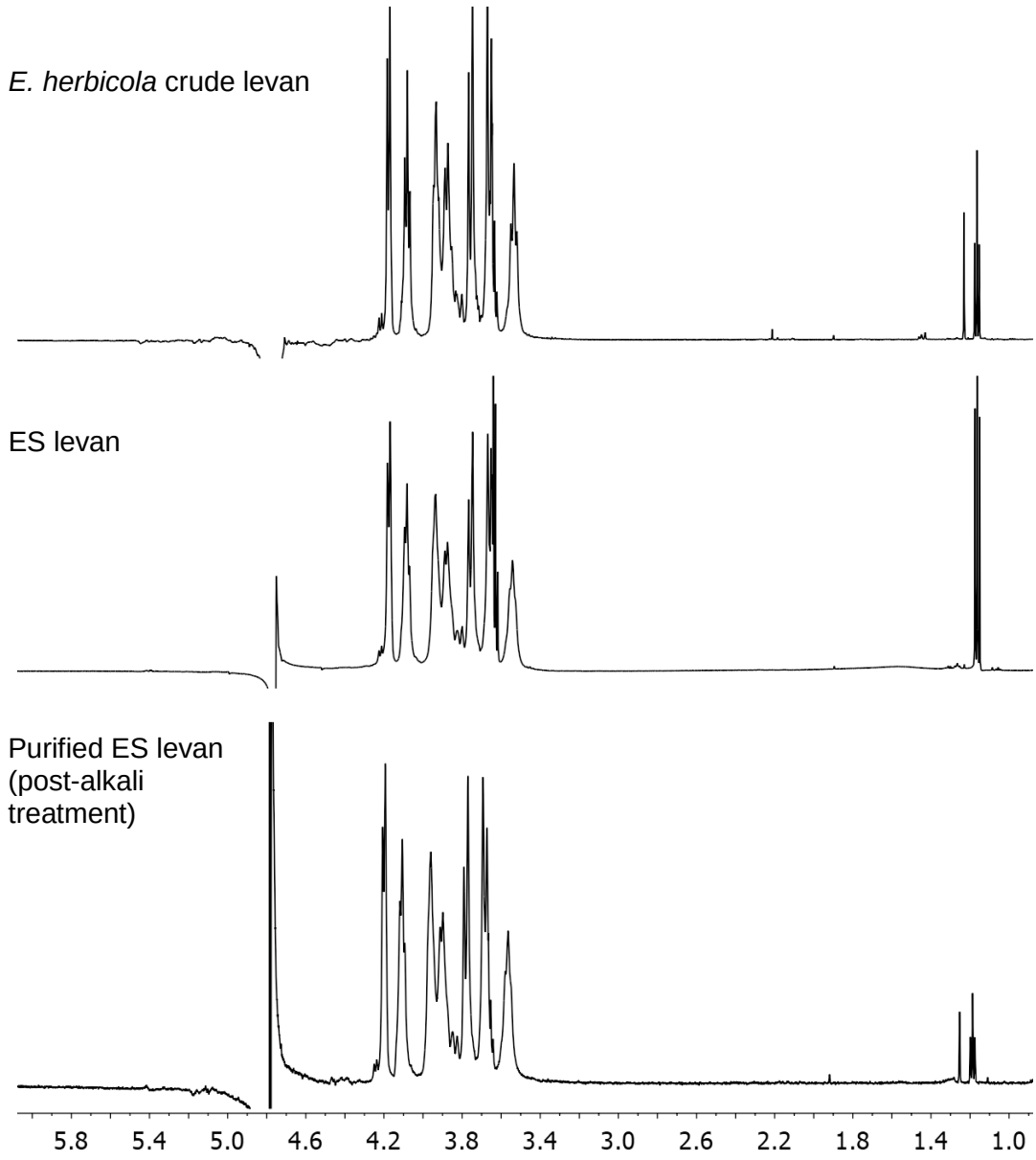

Figure 49. ^{1}H NMR spectra of ES levan before and after alkali treatment.

NMR spectra of ES levans are shown in comparison to ^{1}H NMR of E. herbicola crude levan. ES levan (crude) and purified ES levan (treated with alkali). NMR analysis was performed by Sergey Nepogodiev and Gwenaelle Le Gall.

4.2.7. Dectin-2 interaction with enzymatically synthesised levan using BWZ.36 reporter cells

The interaction of Dectin-2 and ES levan was tested using Dectin-2, Dectin-2-QPD and mock reporter cells. In one experiment, although the α-mannan control bound to Dectin-2, but not to mock or Dectin-2-QPD cells (Figure 50), there was no binding to ES levan, showing that high-purity ES levan synthesised by recombinant levansucrase Lsc3 does not interact with Dectin-2. Two further independent

experiments confirmed that ES levan did not bind to Dectin-2 using reporter cells (Appendix 32).

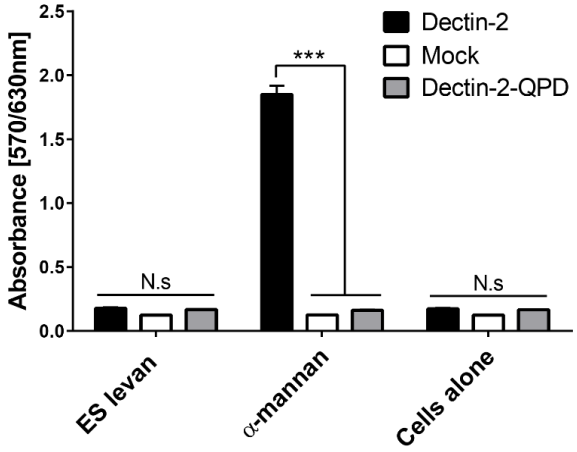

Figure 50. Interaction of ES levan with Dectin-2 using Dectin-2, Dectin-2-QPD and mock reporter cells.

Carbohydrate binding to CLR BWZ.36 reporter cells induces β-galactosidase production within the cell which can be measured in a colorimetric assay: CLR BWZ.36 reporter cells were incubated with immobilised carbohydrate ligands using a 96 well plate; a substrate, Chlorophenol red-β-D-galactopyranoside (CPRG), was added to cells and absorbance values were read at 570/630 nm. ES levan was used at 100 μg/ml, positive control α-mannan at 1 μg/ml. The experiment was performed in triplicate. Error bars, ± SD. Statistical analysis was performed using one-way ANOVA followed by tukey's test (b). ***, p < 0.001, as indicated. N.s with straight line, not statistically significant. For repeated independent experiments see Appendix 32.

4.2.8. Interaction of crude E. herbicola levan and enzymatically synthesised levan with Dectin-2 recombinant protein using atomic force spectroscopy

To assess the direct interaction of levan to Dectin-2, ES levan and *E. herbicola* levan, immobilised on glass slides, were tested for specific adhesion to Dectin-2 recombinant protein-functionalised atomic force microscopy (AFM) tips (see Materials and Methods). Interaction between ES levan and mouse Dectin-2 protein was not observed, however, a modest interaction was observed with *E. herbicola* crude levan (Figure 51). A high number of specific adhesions were seen with the positive control α-mannan (Figure 52), in line with the reporter cell results. When using mannose as an inhibitor, the frequency of specific adhesions for α-mannan was reduced (Figure 52c). These data showed that Dectin-2 directly interacts with α-mannan, and to a lesser extent with *E. herbicola* crude levan, but not with ES levan, and therefore supports our previous findings using reporter cells.

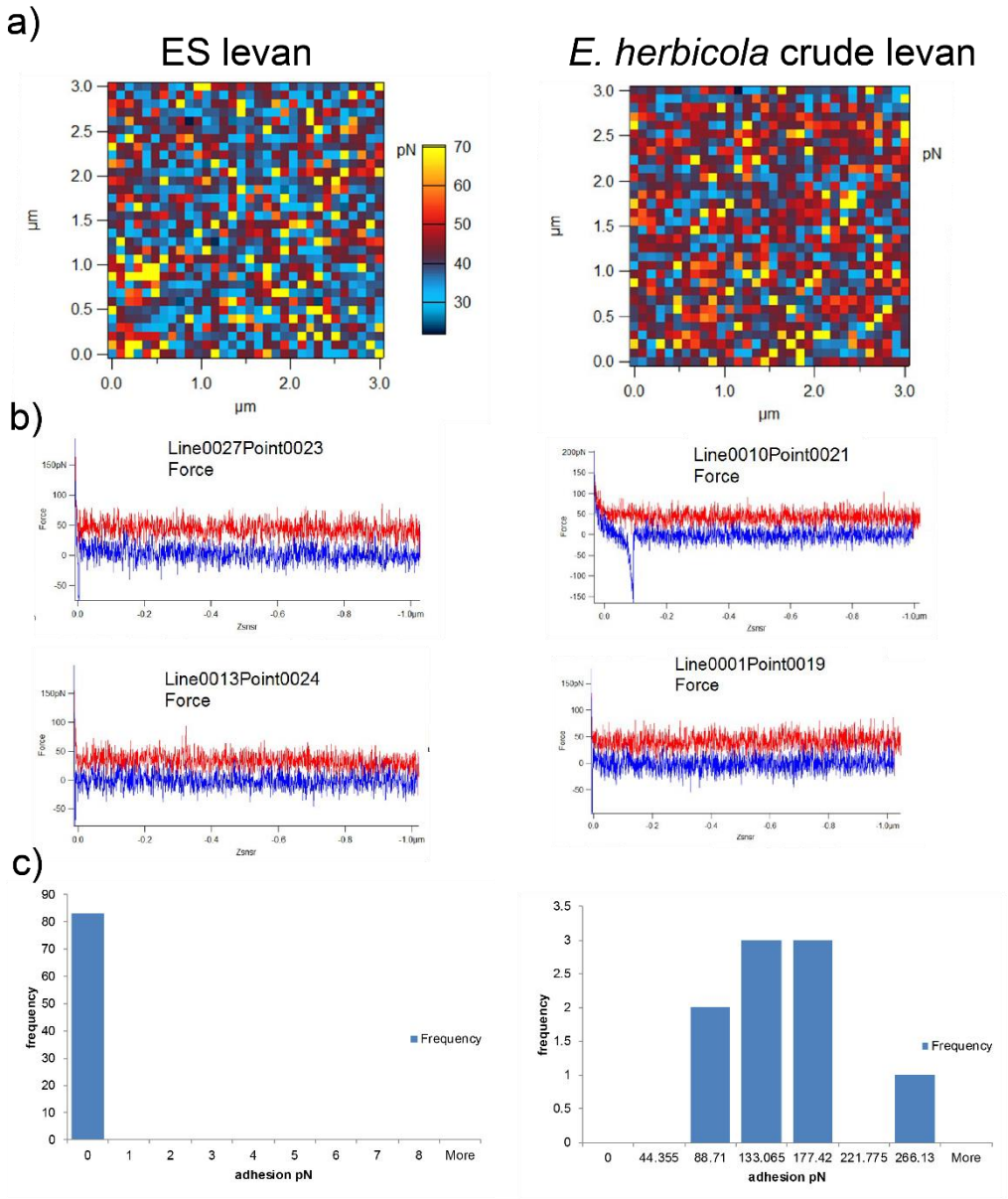

Figure 51. Forces spectroscopy measurements showing interaction of ES levan and E. herbicola crude levan with AFM tips functionalised with recombinant mouse Dectin-2 protein.

Force curves allow the characteristic detection of specific interactions between an AFM functionalised tip (attached to a cantilever) and ligand attached on a glass slide by measuring changes in force per interaction. (a) Adhesion maps show a collection of individual AFM Dectin-2 protein-functionalised tip-surface force map curves (both retraction and extending) at many separate points (2D scan) on across the glass slides containing levan [559,560]. Each square represents force spectroscopy curves (b) showing characteristic specific (top right), or non-specific or no adhesions (shown by characteristic changes in force) between the sample on the surface of the glass slides and the Dectin-2 protein-functionalised tip. Y axis, Force (pN). (c) Adhesion (pN) histograms showing the frequency of any specific interactions. AFM, atomic force microscopy. AFM was performed by Allan Patrick Gunning.

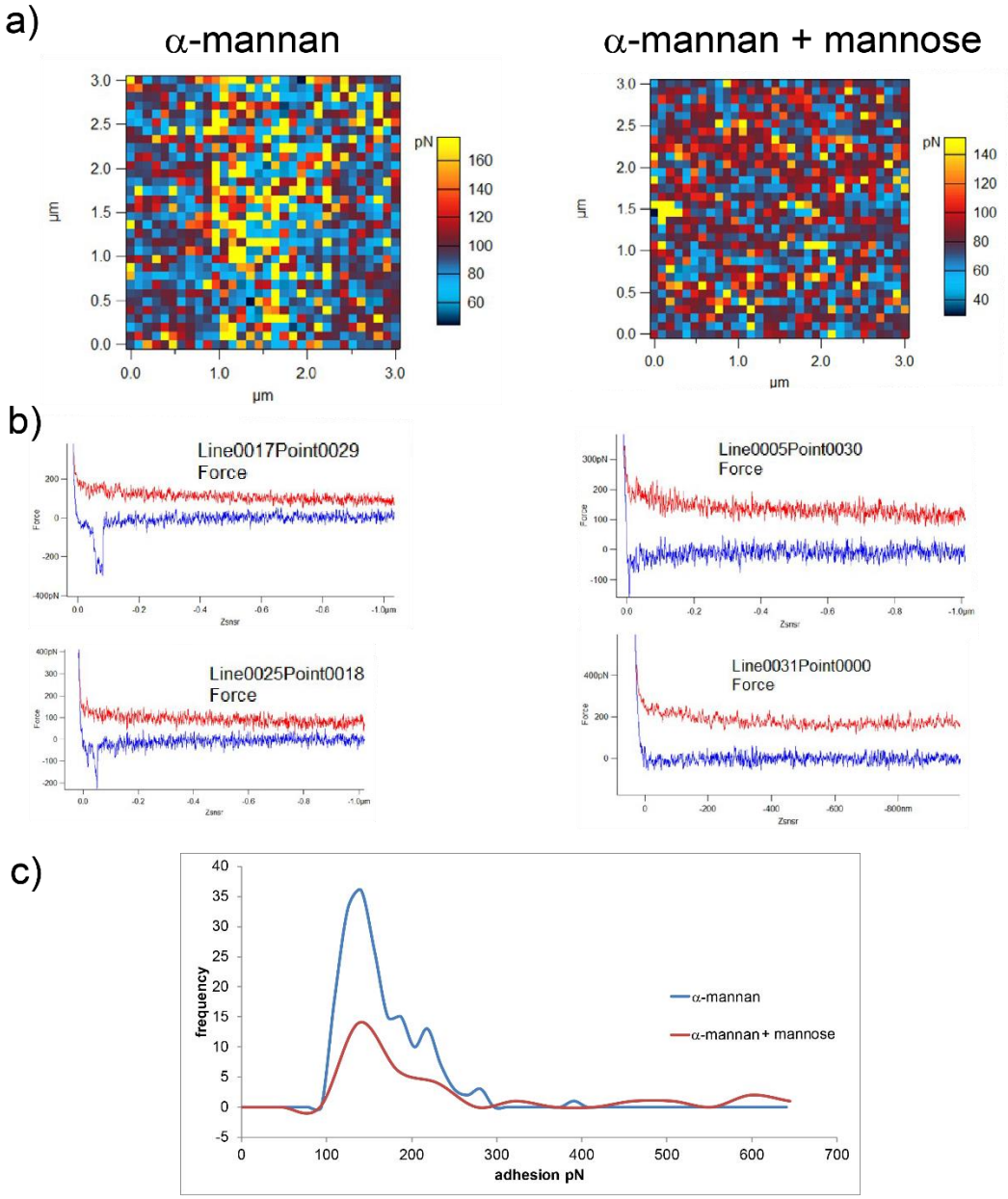

Figure 52. Forces spectroscopy measurements showing interaction of α-mannan with α-mannan + mannose with AFM tips functionalised with recombinant mouse Dectin-2 protein.

Force curves allow the characteristic detection of specific interactions between an AFM functionalised tip (attached to a cantilever) and ligand attached on a glass slide by measuring changes in force per interaction. (a) Adhesion maps show a collection of individual AFM Dectin-2 protein-functionalised tip-surface force map curves (both retraction and extending) at many separate points (2D scan) on across the glass slides containing mannan or mannan with mannose [559,560]. Each square represents force spectroscopy curves (b) showing characteristic specific (top right), or non-specific or no adhesions (shown by characteristic changes in force) between the sample on the surface of the glass slides and the Dectin-2 protein-functionalised tip. X axis, Zsnsr. Y axis, Force (pN). (c) Adhesion (pN) histograms showing frequency of any specific interactions comparing α-mannan with α-mannan + mannose. AFM was performed by Allan Patrick Gunning.

The binding of ES levan and *E. herbicola* crude levan was also tested to human Dectin-2 recombinant protein. ES levan showed negligible specific adhesions to human Dectin-2 protein while *E. herbicola* crude levan showed a higher frequency of specific adhesions (Figure 53). Again, a high number of specific adhesions were seen using the positive control α-mannan (Figure 54). Interestingly, with or without mannose as an inhibitor, the frequency of specific adhesions were similar (Figure 54c), which was not observed using mouse Dectin-2 protein. A summary of the adhesion histograms for all force spectroscopy measurements comparing the interaction of levans to mouse or human Dectin-2 recombinant proteins is shown in Figure 55.

Taken together, the force spectroscopy data showed that human and mouse Dectin-2 recombinant proteins directly interact with α-mannan, and to a lesser extent *E. herbicola* crude levan, but not to ES levan.

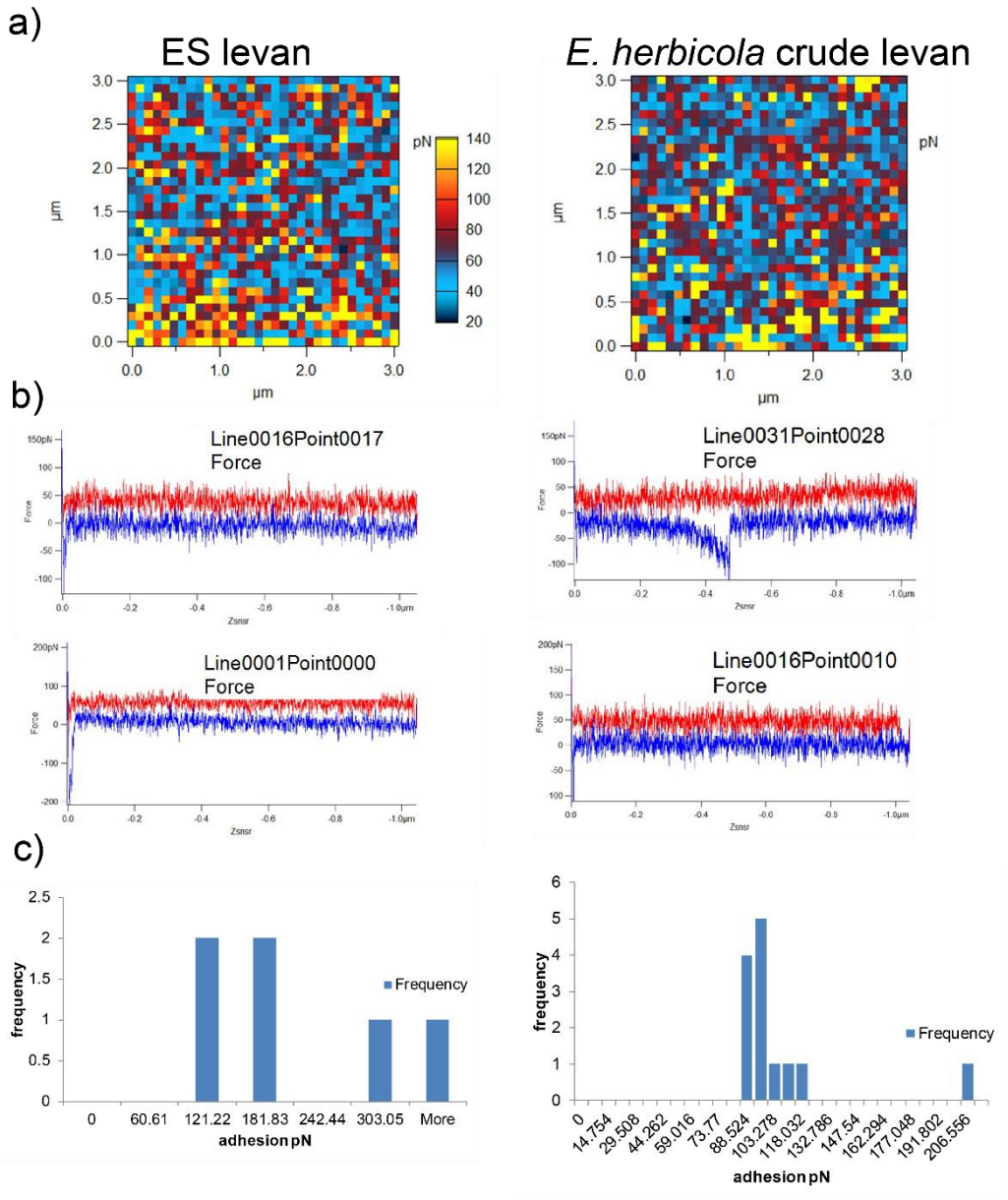

Figure 53. Forces spectroscopy measurements showing interaction of ES levan and E. herbicola crude levan with AFM tips functionalised with recombinant human Dectin-2 protein.

Force curves allow the characteristic detection of specific interactions between an AFM functionalised tip (attached to a cantilever) and ligand attached on a glass slide by measuring changes in force per interaction. (a) Adhesion maps show a collection of individual AFM Dectin-2 protein-functionalised tip-surface force map curves (both retraction and extending) at many separate points (2D scan) on across the glass slides containing levan [559,560]. Each square represents force spectroscopy curves (b) showing characteristic specific (top right), or non-specific or no adhesions (shown by characteristic changes in force) between the sample on the surface of the glass slides and the Dectin-2 protein-functionalised tip. X axis, Zsnsr. Y axis, Force (pN). (c) Adhesion (pN) histograms showing frequency of any specific interactions comparing α-mannan with α-mannan + mannose. AFM was performed by Allan Patrick Gunning.

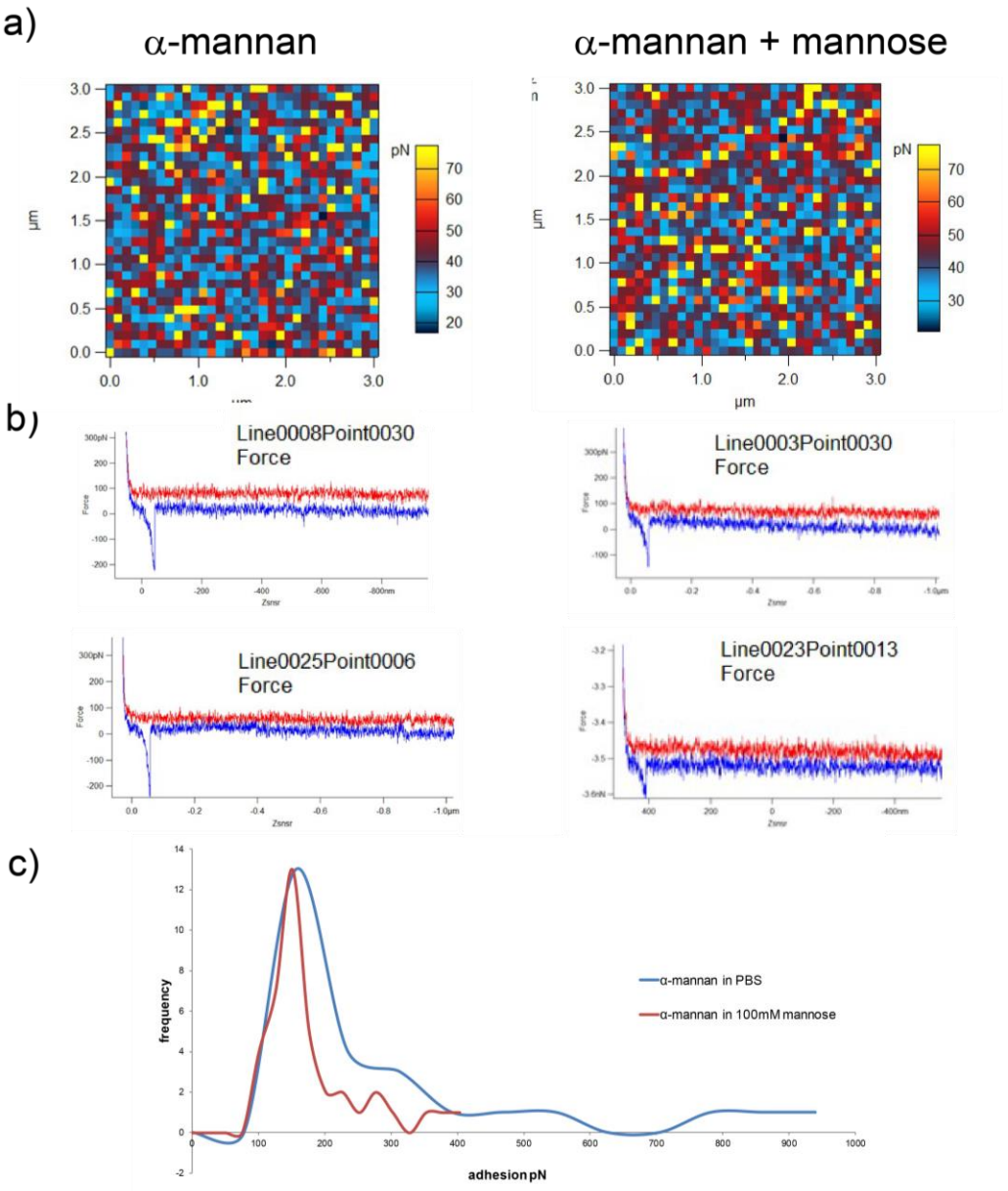

Figure 54. Forces spectroscopy measurements showing interaction of α-mannan with α-mannan + mannose with AFM tips functionalised with recombinant human Dectin-2 protein.

Force curves allow the characteristic detection of specific interactions between an AFM functionalised tip (attached to a cantilever) and ligand attached on a glass slide by measuring changes in force per interaction. (a) Adhesion maps show a collection of individual AFM Dectin-2 protein-functionalised tip-surface force map curves (both retraction and extending) at many separate points (2D scan) on across the glass slides containing mannan or mannan with mannose [559,560]. Each square represents force spectroscopy curves (b) showing characteristic specific (top right), or non-specific or no adhesions (shown by characteristic changes in force) between the sample on the surface of the glass slides and the Dectin-2 protein-functionalised tip.X axis, Zsnsr. Y axis, Force (pN). (c) Adhesion (pN) histograms showing frequency of any specific interactions comparing α-mannan with α-mannan + mannose. AFM was performed by Allan Patrick Gunning.

a)

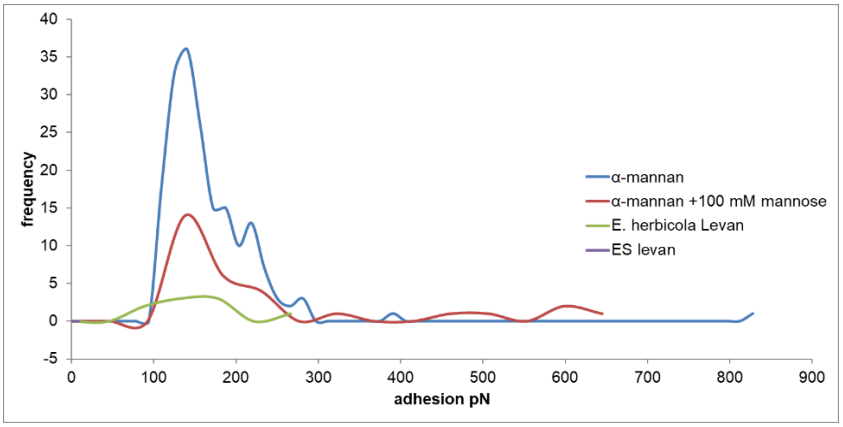

b)

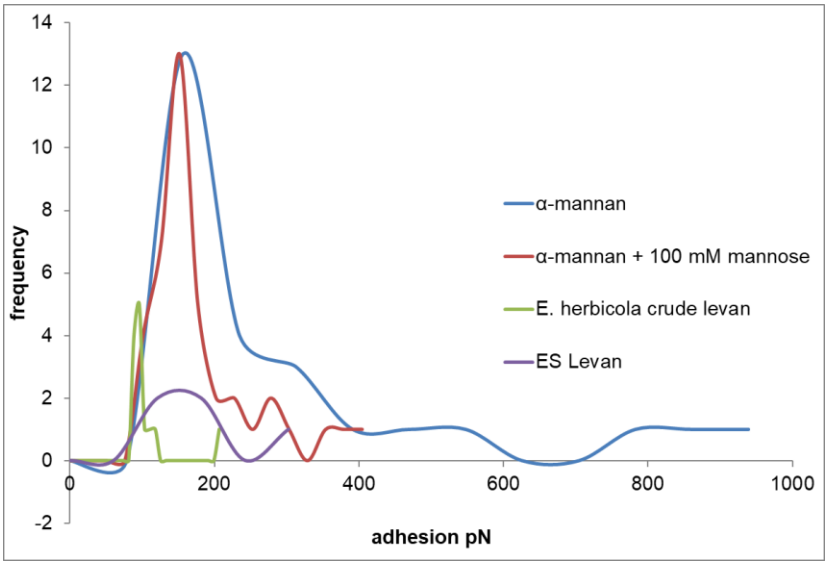

Figure 55. Summary of the adhesion histograms for all force spectroscopy measurements comparing interaction of levan and Dectin-2 recombinant proteins.

(a) Adhesion histogram of ES levan, E. herbicola crude levan, α-mannan and α-mannan + mannose showing specific adhesions with mouse Dectin-2 protein. (b) Adhesion histogram of ES levan, E. herbicola crude levan, α-mannan and α-mannan + mannose showing specific adhesions with human Dectin-2 protein. AFM was performed by Allan Patrick Gunning.

4.2.9. Interaction of crude and purified E. herbicola levan and enzymatically synthesised levan with Toll-like receptor 4 using HEK 293 reporter cells.

It was previously reported that levan interacts with TLR4 and can elicit immunostimulatory effects *in vitro*[26]. Here we showed that LPS was an important contributor of *E. herbicola* levan's ability to bind to Dectin-2. Since LPS is a TLR4

ligand that initiates a potent immune response[314,411,561], HEK 293 TLR4 reporter cells were used to assess TLR4 interaction with *E. herbicola* crude and purified levans. Using this approach, *E. herbicola* crude levan and *E. herbicola* levan 2 both showed significant binding to TLR4 when compared to cells alone (Figure 56 and Appendix 33). However, *E. herbicola* levan 3, which had negligible LPS concentrations, showed no binding to TLR4 (Figure 56 and Appendix 33). These data suggest that removal of LPS impairs the ability of *E. herbicola* levan to interact with TLR4.

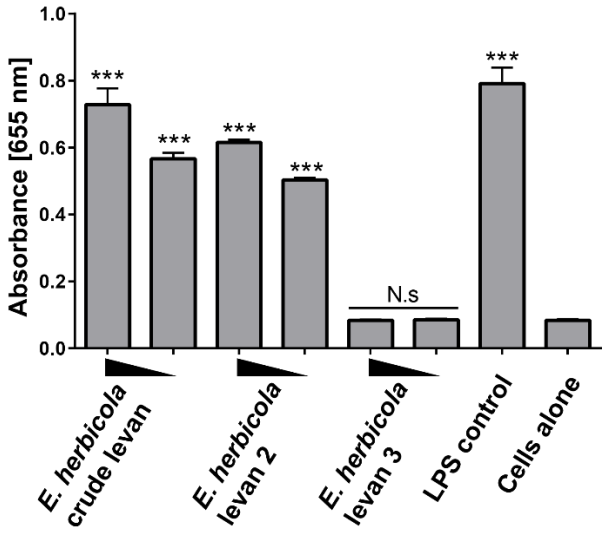

Figure 56. Interaction of TLR4 with crude and purified E. herbicola levans using TLR4 reporter cells.

Ligand binding to TLR4 reporter cells results in the production of secreted embryonic alkaline phosphatase (SEAP) which can be measured in a colorimetric assay: TLR4 reporter cells were incubated with carbohydrate ligands or control (LPS) in HEK blue medium[394] using a 96 well plate; and absorbance values were read at 655 nm. The experiment was performed in triplicate. E. herbicola levans were used at 100 μg/ml and 50 μg/ml and positive control LPS at 0.1μg/ml. Error bars, ± SD. Statistical analysis was performed using one-way ANOVA followed by tukey's test (b). ***, p < 0.001 compared to cells alone. N.s with straight line, not statistically significant compared to cells alone. For repeated experiments see Appendix 33a and Appendix 33b.

Next, we tested the ability of ES levan to interact with TLR4. As mentioned previously, ES levan contained very small amounts of LPS (~88 pg/mg, SD = 0.003 [2 independent tests]) which were reduced to ≤ 2 pg/mg after alkali treatment (purified ES levan). ES levan was found to bind to TLR4 compared to cells alone (Figure 57a and Appendix 34a). In addition, purified ES levan failed to bind to TLR4 when compared to cells alone, where ES levan and LPS control bound to TLR4 significantly (Figure 57b and (Appendix 34b and Appendix 34c). In support, *B. subtilis* levan produced in minimal media LDM2 (to overcome the presence of yeast components in LB) failed to bind to TLR4 (Figure 57c and Appendix 34d).

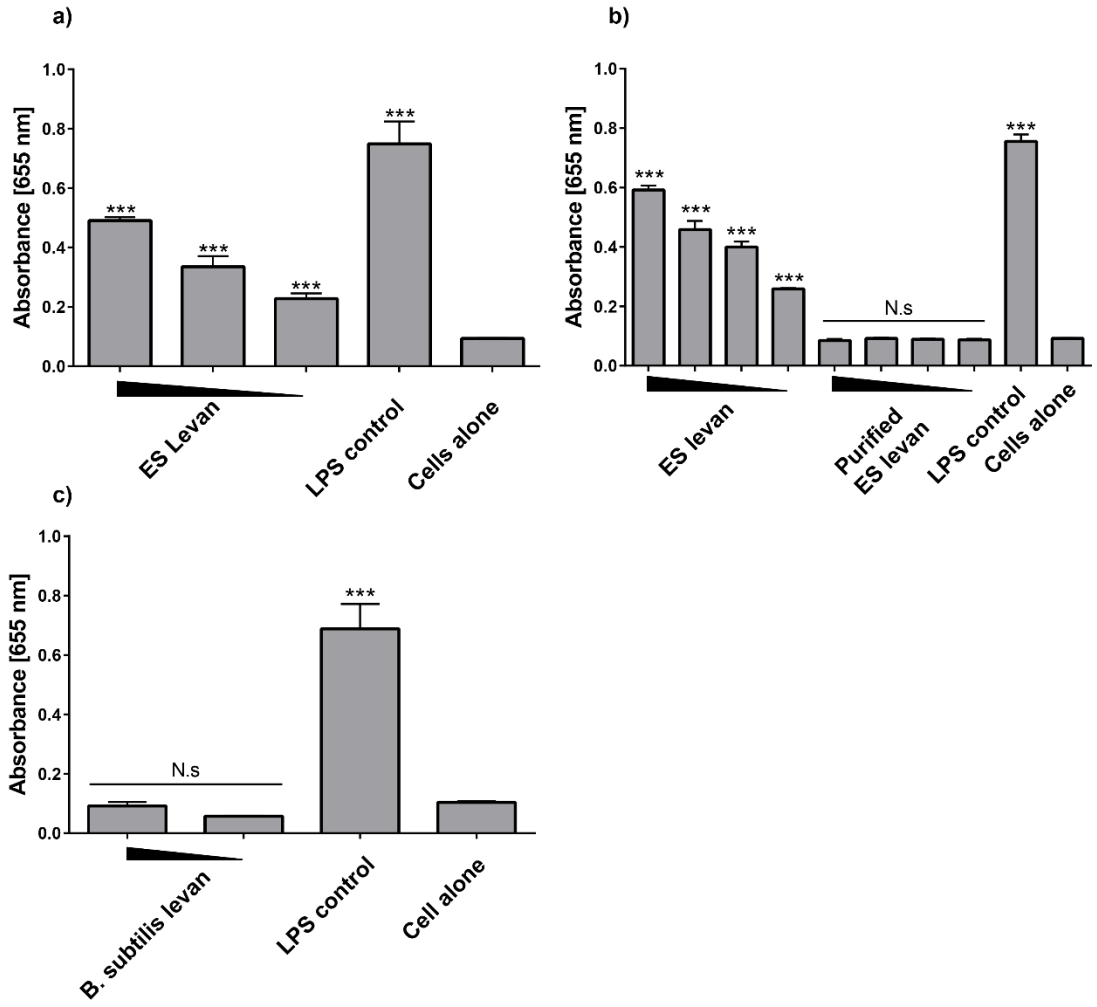

Figure 57. Interaction of TLR4 with crude and purified ES levan and B. subtilis levan using TLR4 reporter cells.

Ligand binding to TLR4 reporter cells results in the production of secreted embryonic alkaline phosphatase (SEAP) which can be measured in a colorimetric assay: TLR4 reporter cells were incubated with carbohydrate ligands or control (LPS) in HEK blue medium[394] using a 96 well plate; and absorbance values were read at 655 nm. (a) TLR4 binding to ES levan compared to cells alone. ES levans were used at 100 μg/ml, 50 μg/ml and 25 μg/ml and positive control LPS at 1 μg/ml. b) TLR4 binding to ES levan (crude) compared to purified ES levan (ES levan treated with alkali). c) TLR4 reporter assay with gram-positive B. subtilis levan compared to controls. All experiments shown were performed in triplicate. Error bars, ± SD. Statistical analysis was performed using one-way ANOVA followed by tukey's test. ***, p < 0.001 compared to cells alone. N.s., not statistically significant compared to cells alone. For repeated independent experiment(s) from (a) see Appendix 34a, from (b) see Appendix 34b and 34c, and from (c) see Appendix 34d.

To exclude the possibility that the alkali treatment used to remove LPS had an impact on *E. herbicola* crude levan's ability to bind to TLR4 through the potential formation of salts, *E. herbicola* crude levan was directly subjected to alkali treatment (Purified ES levan) and subsequently treated with an anion exchange resin in an attempt to

remove any potential salts. Non-TLR4 ligand α-mannan was also treated with the anion exchange resin as a control, as LPS or other components capable of binding to TLR4, may be acquired through exposure to non-sterile resin. It was found that purified *E. herbicola* levan subjected to alkali and treated with or without the resin failed to bind to TLR4 and no difference was seen between treatments (Figure 58 and Appendix 35). The positive controls, LPS and *E. herbicola* crude levan, did significantly bind to TLR4. These data demonstrate that the alkali treatment did not interfere with the ability of *E. herbicola* levan to bind to TLR4.

Overall, LPS was shown to be an important contributor to the TLR4-binding ability of crude levans.

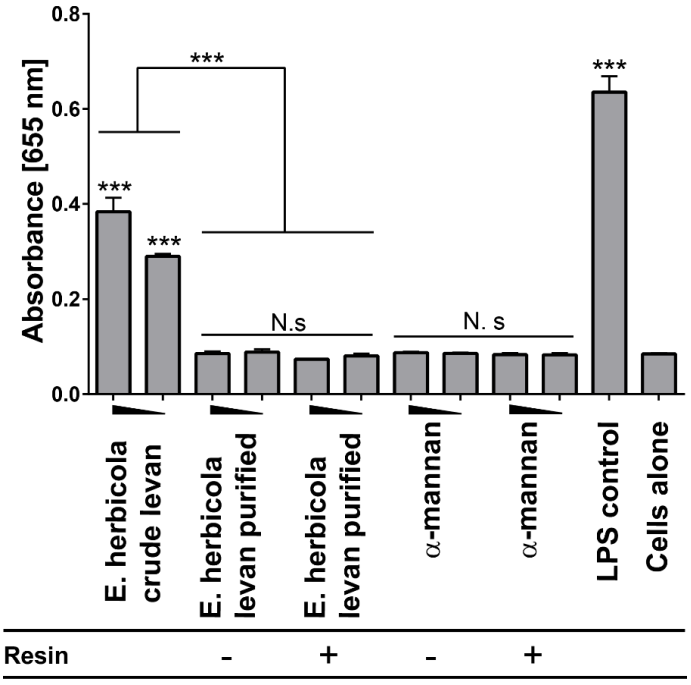

Figure 58. Interaction of TLR4 with E. herbicola levan and α-mannan treated with or without anion exchange resin using HEK293 TLR4 reporter cells.

Ligand binding to TLR4 reporter cells results in the production of secreted embryonic alkaline phosphatase (SEAP) which can be measured in a colorimetric assay: TLR4 reporter cells were incubated with carbohydrate ligands or control (LPS) in HEK blue medium[394] using a 96 well plate; and absorbance values were read at 655 nm. All levans and α-mannan were used at 100 μg/ml and 50 μg/ml, and LPS control at 1 μg/ml. E. herbicola levan purified, E. herbicola crude levan directly treated with alkali to remove LPS. The experiment was performed in triplicate. Error bars, ± SD. Statistical analysis was performed using one-way ANOVA followed by tukey's test. ***, p < 0.001 as indicated or compared to cells alone. N.s with straight line, not statistically significant across treatments or all compared to cells alone. For repeated independent experiment see Appendix 35.

4.3. Summary and Discussion

In this chapter, we investigated the interaction of microbial fructan levan with immune cell receptor Dectin-2. Levan has been reported to modulate immune function *in vitro* and *in vivo*[26,71,72,91], yet the molecular mechanisms remain unclear. We found that commercial crude *E. herbicola* levan could interact with immune cell PRR and CLR Dectin-2 which is the first report of a fructan interacting with a CLR. We then developed a robust process to purify and inactivate LPS found in levan. Importantly, Dectin-2 binding of purified *E. herbicola* levan was significantly reduced suggesting that LPS was a key contributor towards the ability of commercial *E. herbicola* crude levan to bind to Dectin-2.

Using TLR4 reporter cells, we also showed that crude *E. herbicola* levan could interact with TLR4 *in vitro*, however, purified *E. herbicola* or ES levan did not bind to TLR4 suggesting LPS was responsible for crude levan's ability to bind to TLR4. Interestingly, it has been reported that TLRs including TLR4 interact with plant and microbial fructans[26,439,562]. For example, the immunomodulatory properties and protective effect on the epithelial barrier by β-(2,1) fructose polymer inulin *in vitro* is reported to involve TLR4[563] and TLR2[439], respectively. Further, β-(2,1) fructans have been shown to increase cytokine expression in human peripheral blood mononuclear cells[435], and using TLR reporter cells, these β-(2,1) fructans were found to bind to TLR2 but also other TLRs including TLR4, suggesting that the immunomodulatory properties of fructans may involve interaction with TLRs[435]. More relevantly, the immunomodulatory properties (cytokine production by isolated peritoneal cells) of β-(2,6) fructan levan from *B. subtilis* natto were shown to be dependent on TLR4, where they also found that levan activated TLR4 reporter cells *in vitro* [26]. In contrast to our findings, the contribution of LPS to TLR4 binding by levan was ruled out due to the use of i) gram-positive-derived levan and ii) use of polymyxin B (LPS inhibitor) which reduced TLR4 binding (on TLR4 reporter cells) by LPS but not levan[26].

LPS is recognised by TLR4 through involvement of extracellular proteins including CD14 and MD-2 and is important for the host immune response against pathogens including the induction of proinflammatory cytokines by immune cells[275,309,314]. LPS is derived from gram-negative bacteria and comprises 3 basic parts; lipid A, a core oligosaccharide region, and an O-antigen PS which is highly variable among bacterial species and usually comprises up to 5 different sugar residues[131,132]. Lipid A is important for TLR4-mediated recognition of LPS[131]. In this work, degradation of lipid A using alkali treatment may explain why the TLR4-binding of levan was

abolished. It is unlikely that the core oligosaccharide and O-antigen was degraded, as no free monosaccharides were observed in post-alkali-treatment TLC analysis. The exact role of the variable O-antigen structure of LPS in immune function including pattern recognition is unclear[394], however it is known to be important for the adaptive immune response against some pathogenic/opportunistic bacteria[564,565]. Interestingly, it was recently shown that α–mannan-linked O-antigen of LPS from *Hafnia alvei* PCM 1223 but not galactose-linked LPS from *Salmonella enterica* 066 was recognised by Dectin-2 which influenced cellular activation of BMDCs[394]. The glycan composition of LPS found in *E. herbicola* levan may be important for the binding of crude levan to Dectin-2. Other bacterial strains including *Rahnella aquatilis* 3-95 and *Klebsiella pneumoniae* O3 and O5 have been reported to possess LPS structures containing α-mannan residues in their O-antigen[566-568]. Further work is required to isolate and characterise the glycan structures of *E. herbicola* LPS and investigate its potential interaction with Dectin-2. This perhaps highlights a future area for investigation focused on deciphering the LPS O-antigen structures of other bacterial strains and their interaction with CLRs.

E. herbicola levan (before and after purification) was characterised by GC-MS linkage analysis and NMR. GC-MS linkage analysis showed a predominant linear chain of β-(2,6) fructosyl residues containing 8 – 10% β-(2,1) branching which is higher than previously reported for *E. herbicola* levan (5%) by NMR[92,490]. However, higher degrees of branching up to 12% and 12.9% and have been reported using methylation analysis in levans from *B. polymyxa*[539] and *M. laevanformans*[101], respectively. There are limited reports of microbial levan's branching structure using GC-MS linkage analysis. Further, the sensitivity for GC-MS linkage analysis for mannose and fructose residues from α-mannan and levan, respectively, was only 1 μg - 5 μg, therefore other glycans present in levan including LPS could only be detected at these limits or above. These factors are important to consider when assessing immunomodulatory PS *in vitro* where bioactive carbohydrate-derived contaminants at trace levels may be present[3,411-413,415].

Overall, we showed that LPS was an important contributor to levan's ability to bind to Dectin-2 and TLR4. This was established through the development of an effective method to inactivate LPS allowing purified samples for further testing levan's immunomodulatory properties *in vitro*.

Chapter 5: Interaction of crude and purified levan with dendritic cells and intestinal epithelial cells

5.1. Introduction

TLRs and CLRs are important for pathogen recognition of MAMPs and initiation of the immune response in mammalian species, and are primarily expressed in myeloid APC including DCs and macrophages, amongst other cell types[312,392,569]. APCs including DCs are found in GALT and can elicit an immune response or induce tolerance depending on the antigen it encounters[259]. APCs are proposed to encounter antigen either by extension of their dendrites into the lumen or through M-cell transport across the epithelial layer[268,297]. Notably, TLRs are also expressed by IECs[313]. The epithelium contains several multi-functional IECs including enterocytes which can elicit an immune response upon exposure to antigen, such as secretion of cytokines and chemokines, similarly to APCs[19,191,230]. LPS is a typical MAMP found on gram-negative bacteria that can bind to TLR4/MD-2 and induce the production of cytokines by immune cells[131]. Likewise, Dectin-2 is a CLR that binds to high-mannose MAMPs which elicits cellular activation inducing cytokine production by APCs including DCs and macrophages[121,391]. In chapter 4, LPS was found to be a contributor to crude levan's ability to bind to TLR4 and Dectin-2.

The aim of this chapter is to investigate the immunomodulatory properties of crude or purified levan *in vitro* using immune cells and IECs. Primary murine BMDCs produced *in vitro* are an effective model to test for immunomodulatory properties of PS including assessment of the induction of pro- and anti-inflammatory cytokines[394,446,570]. Here, we used WT, TLR4 KO or Dectin-2 KO BMDCs derived from mouse models to test the ability of levan to induce cytokine production. Further, we investigated whether levan could modulate cytokine production in BMDCs following an inflammatory challenge. Finally, we assessed levan's immunomodulatory effects on epithelial cells *in vitro* using Caco-2 cells.

5.2. Results

5.2.1. Impact of crude and purified E. herbicola levan on cytokine production by WT, Dectin-2 knockout and TLR4 knockout bone marrow-derived dendritic cells

To assess the impact of levan on cytokine production, BMDCs were generated *in vitro* from WT, Dectin-2 KO and TLRK KO mice bone marrow cells. Although these have been suggested to comprise a heterogenous population of macrophages and DCs[505], we refer to these cells in this thesis as BMDCs.

5.2.1.1. Detection of Dectin-2 expression on WT, TLR4 knockout and Dectin-2 knockout bone marrow-derived dendritic cells

Dectin-2 expression on WT, Dectin-2 KO or TLR4 KO BMDCs was analysed by flow cytometry using Alexa 647-labelled antibodies anti-mouse Dectin-2-Alexa 647 (see section 2.1.5.) and rat isotype control IgG isotype-Alexa 647 (see section 2.1.5.)[394]. Gating strategies for all experiments are shown and described in Appendix 36 (for data in Figure 59) or Appendix 38 (for data in Appendix 37).

Figure 59a (and Appendix 37a) shows expression of Dectin-2 on WT BMDCs represented by a notable shift change in Alexa 647 fluorescence compared to isotype and unlabelled controls. A small second peak with no shift difference in Alexa 647 fluorescence was also detected (Figure 59a), suggesting that a population of WT cells (~5 %) in these preparations may not express Dectin-2 as shown in Appendix 36d. In addition, no notable shift in Alexa Fluor 647 fluorescence was detected in Dectin-2 KO BMDCs compared to isotype and unlabelled controls (Figure 59b and Appendix S 37d), confirming that Dectin-2 KO BMDCs did not express Dectin-2.

Further, we assessed Dectin-2 expression on TLR4 KO BMDCs. Figure 59c shows a shift change in Alexa 647 fluorescence compared to isotype and unlabelled controls indicating expression of Dectin-2 on TLR4 KO BMDCs but a second peak with no notable shift difference in Alexa 647 fluorescence was also observed, suggesting that ~50 % of cells in this population expressed Dectin-2 as shown in Appendix 36e. A second independent experiment also showed expression of Dectin-2 on WT and TLR4 KO BMDCs (Appendix 37a and Appendix S37b, respectively) with ~86 % of cells in both these populations expressing Dectin-2 (Appendix 37e and Appendix 37f respectively).

Of note, we did not check TLR4 expression on WT BMDCs, as TLR4 KO BMDCs were obtained and previously characterised by J.S Frick, University of Tubingen, Germany and were not responsive to LPS, as shown in a recent publication by the Kawasaki group[394].

Overall, we confirmed that Dectin-2 was expressed in cell populations of WT and TLR4 KO BMDCs and was not expressed by Dectin-2 KOs.

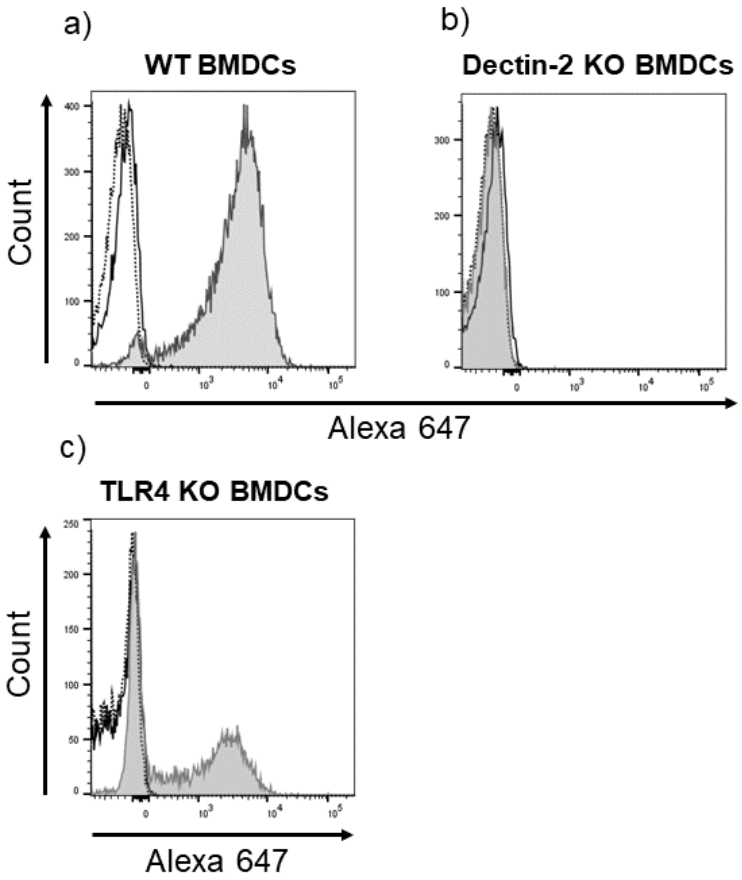

Figure 59. Expression of Dectin-2 on WT, Dectin-2 KO and TLR4 KO BMDCs using flow cytometry.

Bone marrow cells isolated from wild type, Dectin-2 KO or TLR4 KO mice were differentiated into BMDCs and analysed for Dectin-2 expression by flow cytometry using fluorescently-labelled (Alexa Fluor 647) anti-mouse Dectin-2 antibodies. Histograms show fluorescence of cell populations after cell labelling and initial pre-gating of cells which exclude doublet cells and dead cells (for gating strategy see Appendix 36). (a) WT BMDCs (b) Dectin-2 KO BMDCs and (c) TLR4 KO BMDCs labelled with anti-mouse Dectin-2-Alexa 647 (grey shading with dark grey outline), IgG isotype-Alexa 647 (black outline) or unlabelled (cells with PI) (dotted black outline). Data were analysed using FlowJo® v10.0.8.

5.2.1.2. Impact of E. herbicola levan crude, E. herbicola levan 2 and E. herbicola levan 3 on cytokine production by bone marrow-derived dendritic cells

Next, we assessed the impact of levan on cytokine production by BMDCs using *E. herbicola* crude levan, *E. herbicola* levan 2 and *E. herbicola* levan 3 from (see Figure 39) containing 8.2 ng/ml, 5.5 ng/ml and $\leq$ 7.8 pg/ml of LPS respectively. In three independent experiments, we showed that *E. herbicola* crude levan stimulated IL-6, TNF-α and IL-10 production but purified *E. herbicola* levan 3 did not (Figure 60 and Appendix 39 and Appendix 40). *E. herbicola* levan 2 also stimulated IL-6 and TNF-α (Figure 60a and 60b; and Appendix 39a and Appendix 39b; and Appendix 40a and 40b). A statistically significant induction of IL-10 in WT BMDCs by *E. herbicola* levan 2 was only observed in one independent experiment (Appendix 40c [also see Appendix 39c and Figure 60c]). Peptidoglycan was used as a positive control and induced IL-6, TNF-α and IL-10 in all experiments (Figure 60 and Appendix 39 and Appendix 40).

We also assessed differences in cytokine production between WT and Dectin-2 KO cells by *E. herbicola* levan. We observed a statistically significant reduction of IL-6 and TNF-α production by Dectin-2 KO BMDCs compared to WT BMDCs using *E. herbicola* crude levan in all three independent experiments (Figure 60a and 60b; Appendix 39a and Appendix 39b; and Appendix 40a and Appendix 40b). A statistically significant reduction of IL-10 production by Dectin-2 KO BMDCs compared to WT BMDCs using *E. herbicola* crude levan was only seen in one experiment (Appendix 40 [also see Figure 60c and Appendix 39c]). Moreover, a statistically significant reduction of IL-6 production by Dectin-2 KO BMDCs compared to WT BMDCs using *E. herbicola* levan 2 was only observed in one independent experiment (Appendix 40a [also see Figure 60a and Appendix 39a]).

Taken together, *E. herbicola* levan crude induced IL-6, TNF-α and IL-10 production in both WT and Dectin-2 KO BMDCs, with the induction of TNF-α and IL-6 by *E. herbicola* levan crude being partly dependent on Dectin-2. Importantly, data from 3 independent experiments showed that purified *E. herbicola* levan 3 did not induce IL-6, TNF-α or IL-10 production by WT, Dectin-2 KO or TLR4 KO BMDCs, suggesting that LPS is responsible for these effects.

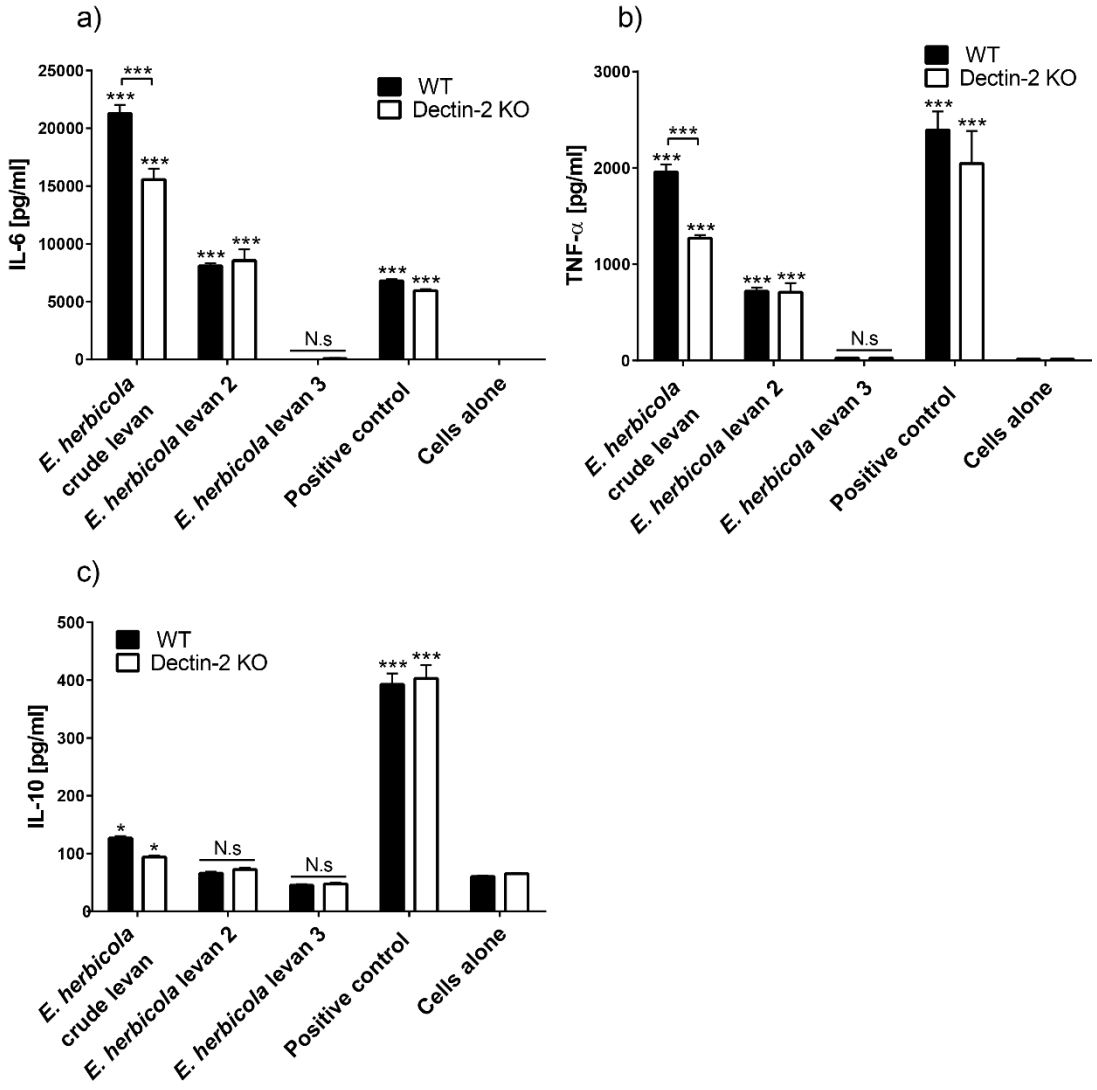

Figure 60. Induction of cytokine production in WT and Dectin-2 KO BMDCs by crude and purified E. herbicola levan.

BMDCs were incubated with E. herbicola levans or a positive control using a 96 well plate; and cytokine production in the supernatant was measured by ELISA. Data show (a) IL-6, (b) TNF-α, and (c) IL-10 production in BMDCs by crude and purified E. herbicola levan. E. herbicola levan was used at 250 μg/ml and peptidoglycan at 100 μg/ml as a positive control. All experiments were performed in triplicate. Error bars, ± SD. Statistical analysis was performed using one-way ANOVA followed by tukey's test. ***, p<0.001. **, p<0.01. *, p < 0.05 compared to cells alone. N.s. with straight line, not statistically significant compared to cells alone. Statistically significant differences between treatments are marked as indicated (comparative line; ***, p < 0.001. **, p < 0.01. *, p < 0.05). For repeated independent experiments see Appendix 39 and Appendix 40.

Next, the impact of levan on cytokine production was tested using BMDCs derived from WT or TLR4 KO mice. Peptidoglycan, used as a positive control, showed that WT and TLR4 KO cells produced IL-6, TNF-α and IL-10 in two independent experiments (Figure 61 and Appendix 41). We showed induction of IL-6 production by *E. herbicola* crude levan in WT BMDCs while IL-6 production was significantly reduced or absent in TLR4 KOs (Figure 61a and Appendix 41a). *E. herbicola* levan

2 also induced IL-6 production in WT BMDCs while no induction of IL-6 in TLR4 KOs was observed (Figure 61a and Appendix 41a). Importantly, there was no induction of IL-6 in WT or TLR4 KO BMDCs by purified *E. herbicola* levan 3 (Figure 61a and Appendix 41a). Further, TNF-α production by BMDCs using *E. herbicola* crude levan and *E. herbicola* levan 2 was also TLR4-dependent, as induction of TNF-α was observed in WT BMDCs but not TLR4 KOs (Figure 61b and Appendix 41b). Importantly, induction of TNF-α by purified *E. herbicola* levan 3 was not observed in WT or TLR4 KOs (Figure 61b and Appendix 41). *E. herbicola* crude levan induced IL-10 production by WT BMDCs in one experiment only while no statistically significant induction of IL-10 was observed in TLR4 KO cells (Appendix 41c and Figure 61c). Importantly, no induction of IL-10 production by *E. herbicola* levan 2 or purified *E. herbicola* levan 3 compared to cells alone was observed in the WT or TLR4 KO BMDCs (Figure 61c and Appendix 41c).

Taken together, these data showed that the induction of cytokines IL-6 and TNF-α by BMDCs using *E. herbicola* crude levan was strongly dependent on TLR4. Further, there was no induction of IL-6 or TNF-α or IL-10 by purified *E. herbicola* levan 3, suggesting that LPS is primarily responsible for the cytokine responses *in vitro*.

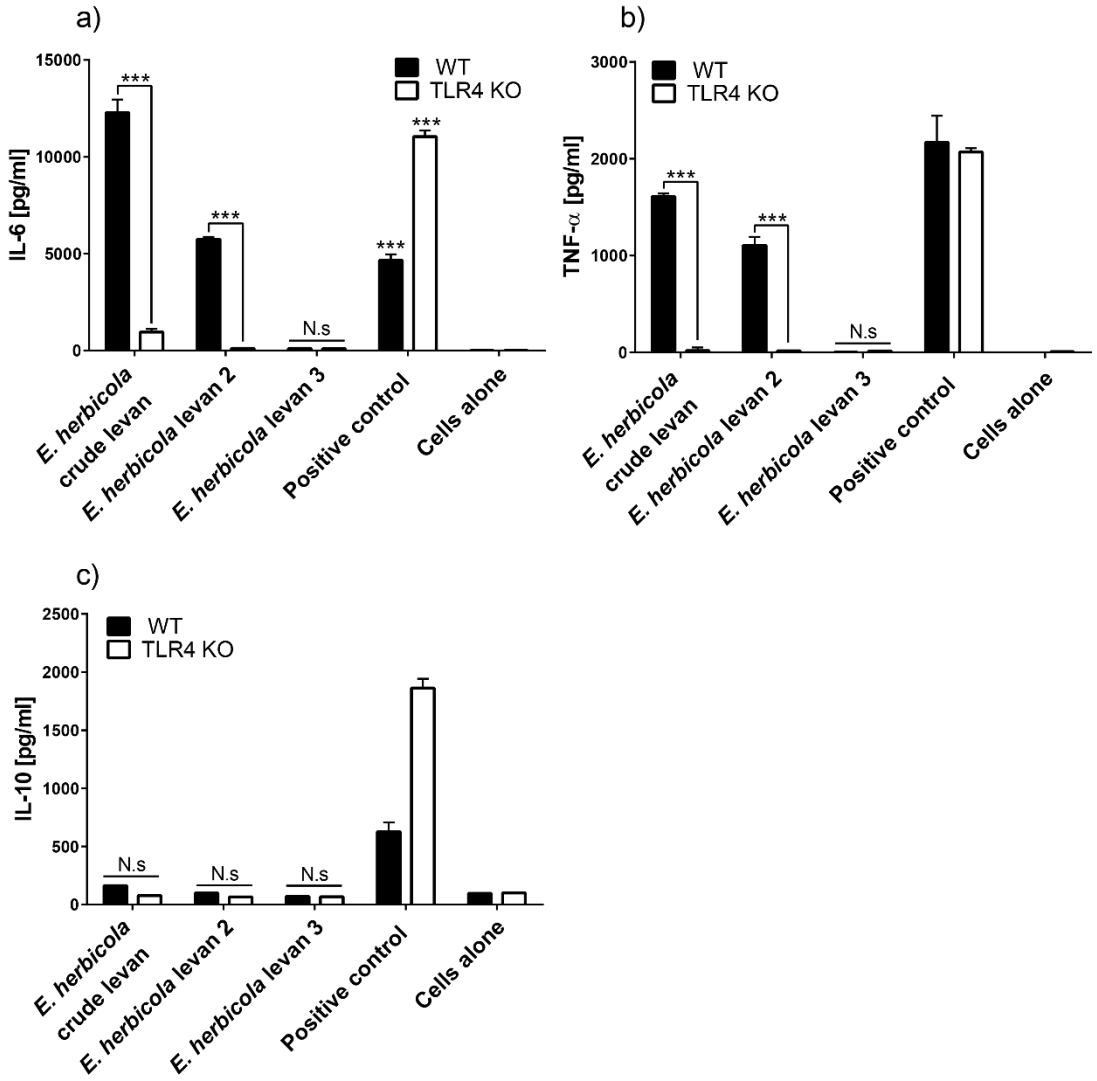

Figure 61. Induction of cytokine production in WT and TLR4 KO BMDCs by crude and purified E. herbicola levan.

BMDCs were incubated with E. herbicola levans or a positive control using a 96 well plate; and cytokine production in the supernatant was measured by ELISA. Data show (a) IL-6, (b) TNF-α, and (c) IL-10 production in BMDCs by crude and purified E. herbicola levan. E. herbicola levan was used at 250 μg/ml and peptidoglycan at 100 μg/ml as a positive control. All experiments were performed in triplicate. Error bars, ± SD. Statistical analysis was performed using one-way ANOVA followed by tukey's test. ***, p < 0.001. **, p<0.01. *, p < 0.05 compared to cells alone. N.s. with straight line, not statistically significant compared to cells alone. Differences between treatments are marked as indicated (comparative line; ***, p < 0.001. **, p < 0.01. *, p < 0.05). For repeated independent experiment see Appendix 41.

5.2.2. Impact of crude and purified enzymatically synthesised levan on the induction of cytokine production by WT bone-marrow-derived dendritic cells

In order to validate the results obtained with purified *E. herbicola* levan and BMDCs, we used crude ES levan containing ~88 pg/mg (SD = 0.003) LPS and alkali-treated

ES levan (Purified ES levan) with $\leq$ 2 pg/mg LPS, therefore, considered below the reported levels of LPS-induced induction of cytokine production by dendritic cells *in vitro*[411].

To verify previous results with purified *E. herbicola* levan 3, we first investigated the stimulatory effects of crude and purified ES levan on WT BMDCs using two approaches. Previously, we added *E. herbicola* crude levan freely (non-plate immobilised) to the cells. Using this approach, we found that co-incubation of (non-plate-immobilised) *E. herbicola* levan but not crude or purified ES levan induced IL-6 (Figure 62a and Appendix 42a) and TNF-α production (Figure 62b and Appendix 42b) in WT compared to cells alone. Further, induction of IL-10 by *E. herbicola* crude levan was observed at 125 and 250 μg/ml whereas there was no induction of IL-10 production by ES levan or purified ES at 62.5, 125 or 250 μg/ml (Figure 62c and Appendix 42c). Taken together, these data confirmed that non-immobilised ES levan did not induce production of cytokines in WT BMDCs, as shown for *E. herbicola* levan 3.

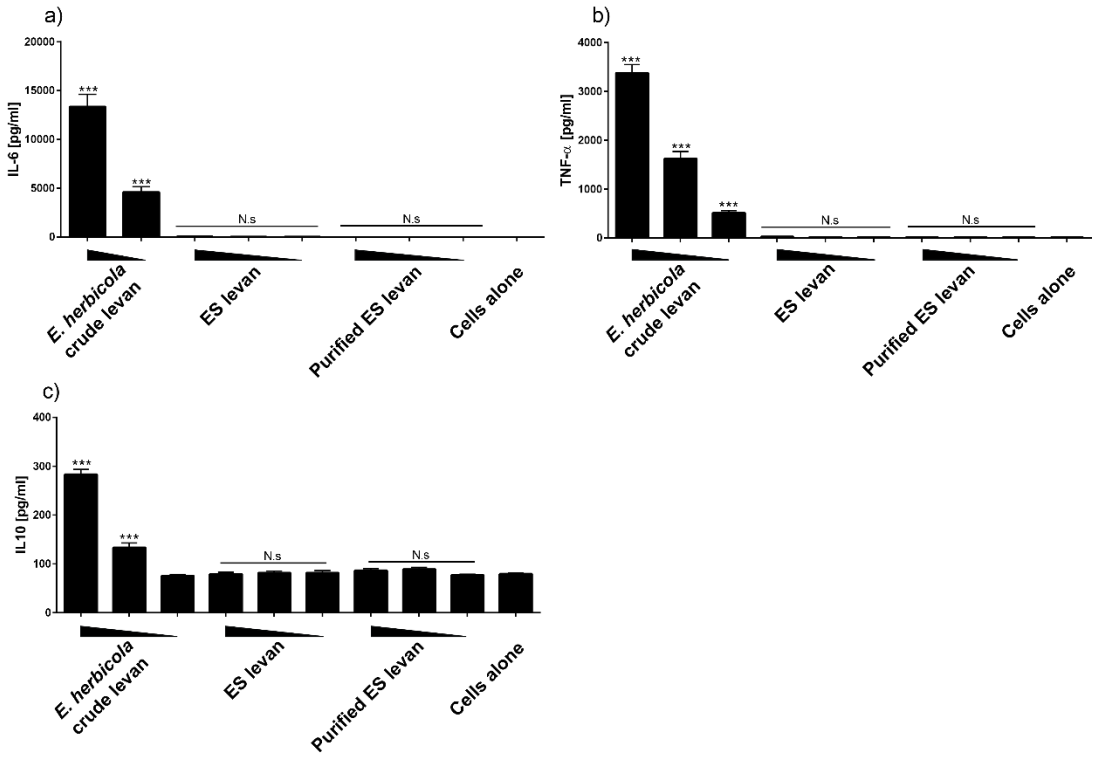

Figure 62. Induction of cytokine production in WT BMDCs by non-immobilised crude or purified ES levan and E. herbicola crude levan.

BMDCs were incubated with ES levan, purified ES levan or E. herbicola crude levan (positive control) using a 96 well plate; and cytokine production in the supernatant was measured by ELISA. Data show a) IL-6, b) TNF-α, and c) IL-10 production in BMDCs by non-plate-immobilised E. herbicola crude, ES levan (crude) and purified ES levan (post alkali treatment). In a), all ES levan concentrations were 250, 125 and 62.5 μg/ml and E. herbicola levan 125 and 62.5 μg/ml. For b) and c), all levan concentrations were 250, 125 and 62.5 μg/ml. All experiments were performed in triplicate. Error bars, ± SD. Statistical analysis was performed using one-way ANOVA followed by tukey's test (b). ***, p < 0.001 compared to cells alone. N.s. with straight line, all not statistically significant compared to cells alone. For repeated independent experiment see Appendix 42.

It was previously reported that Dectin-1-activation and the induction of TNF-α in murine BMDCs required immobilisation of soluble β-glucan or for β-glucan to be in particulate form *in vitro*[364] (also see 1.3.2.3.).

Therefore, we tested whether plate-immobilised *E. herbicola* crude levan and crude or purified ES levan could stimulate pro- or anti-inflammatory cytokine production in BMDCs. We found that plate-immobilised *E. herbicola* crude levan co-incubated with WT BMDCs led to the induction of IL-6, TNF-α and IL-10 at 62.5, 125 and 250 μg/ml but this was not seen using ES levan or purified ES levan (Figure 63 and Appendix 43).

Taken together, these data confirmed that plate-immobilised crude or purified ES levan was not able to induce the production of cytokines in BMDCs, as shown for *E. herbicola* levan 3.

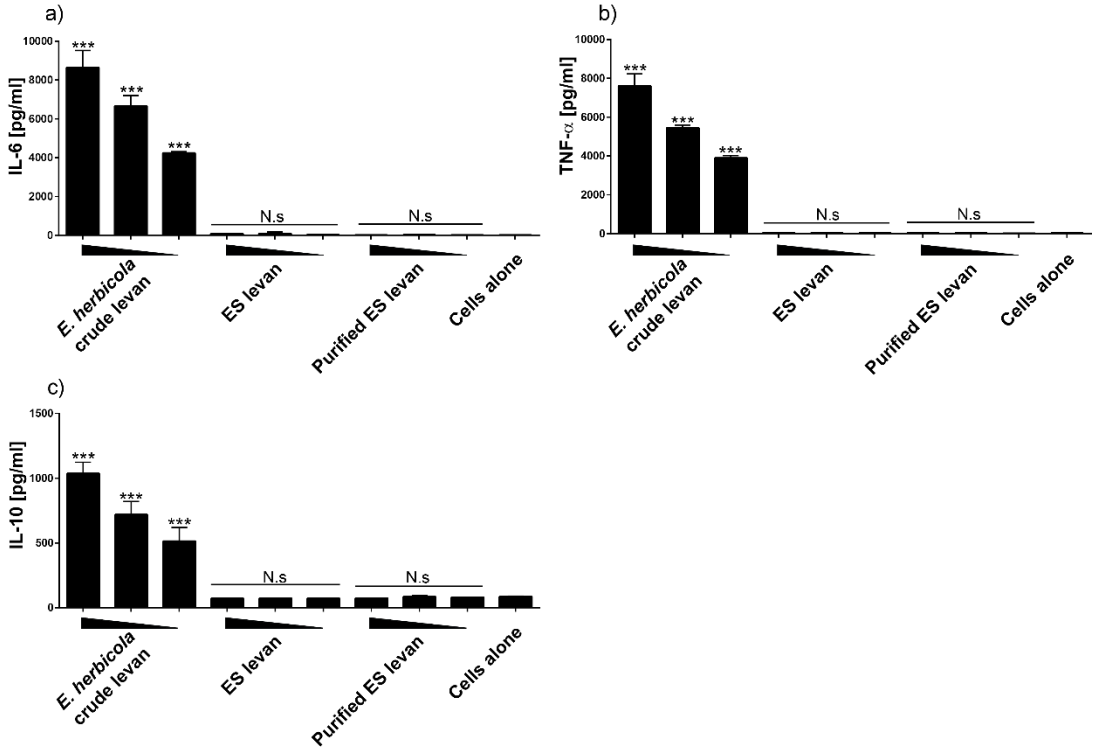

Figure 63. Induction of cytokine production in WT BMDCs by plate-immobilised crude or purified ES levan and E. herbicola crude levan.

BMDCs were incubated with ES levan, purified ES levan or E. herbicola crude levan (positive control) using a 96 well plate; and cytokine production in the supernatant was measured by ELISA. Data show a) IL-6, b) TNF-α, and c) IL-10 production in BMDCs by plate-immobilised E. herbicola crude, enzymatically synthesised (ES) levan (crude) and purified ES levan (post alkali treatment). All levan concentrations were 250, 125 and 62.5 μg/ml. All experiments were performed in triplicate. Error bars, ± SD. Statistical analysis was performed using one-way ANOVA followed by tukey's test (b). ***, p < 0.001 compared to cells alone. N.s. with straight line, not statistically significant compared to cells alone. For repeated independent experiment see Appendix 43.

5.2.3. Modulation of cytokine production in LPS-induced bone marrow-derived dendritic cells by purified enzymatically synthesised levan.

Here, we explored the inhibitory effects of levan on proinflammatory cytokine production using LPS-treated BMDCs.

Our preliminary results showed that simultaneous co-incubation of purified ES levan and LPS did not inhibit cytokine production in BMDCs (Appendix 44). Next, we assessed LPS-induced cytokine production following pre-treatment of BMDCs with purified ES levan for 3, 6, 12 and 24 hr (Figure 64). A statistically significant ~1.3-fold reduction of IL-6 production (at 12 hr) was observed using both 50 and 200 μg/ml plate-immobilised purified ES levan when compared to cells treated with LPS alone (Figure 64a). In contrast, no decrease in IL-6 production was detected using non-plate-immobilised purified ES levan (Figure 64c). There was no inhibitory effect on TNF-α using non-plate-immobilised or plate-immobilised ES levan (Figure 64b and 64d).

Immobilised

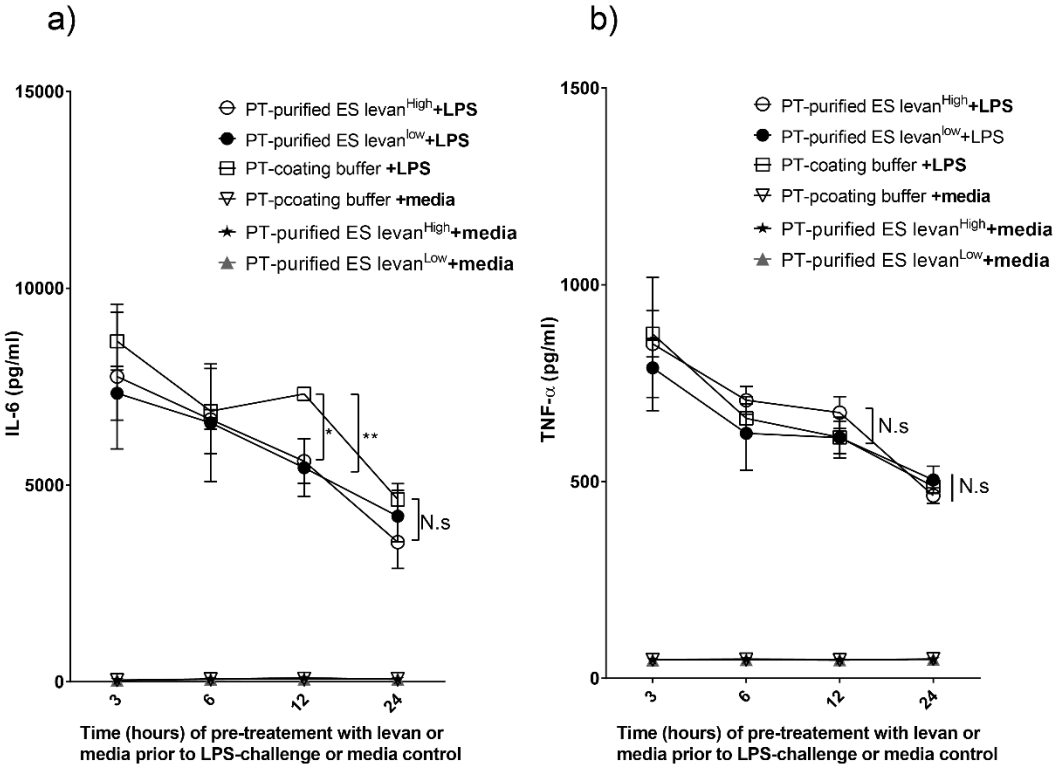

non-immobilised

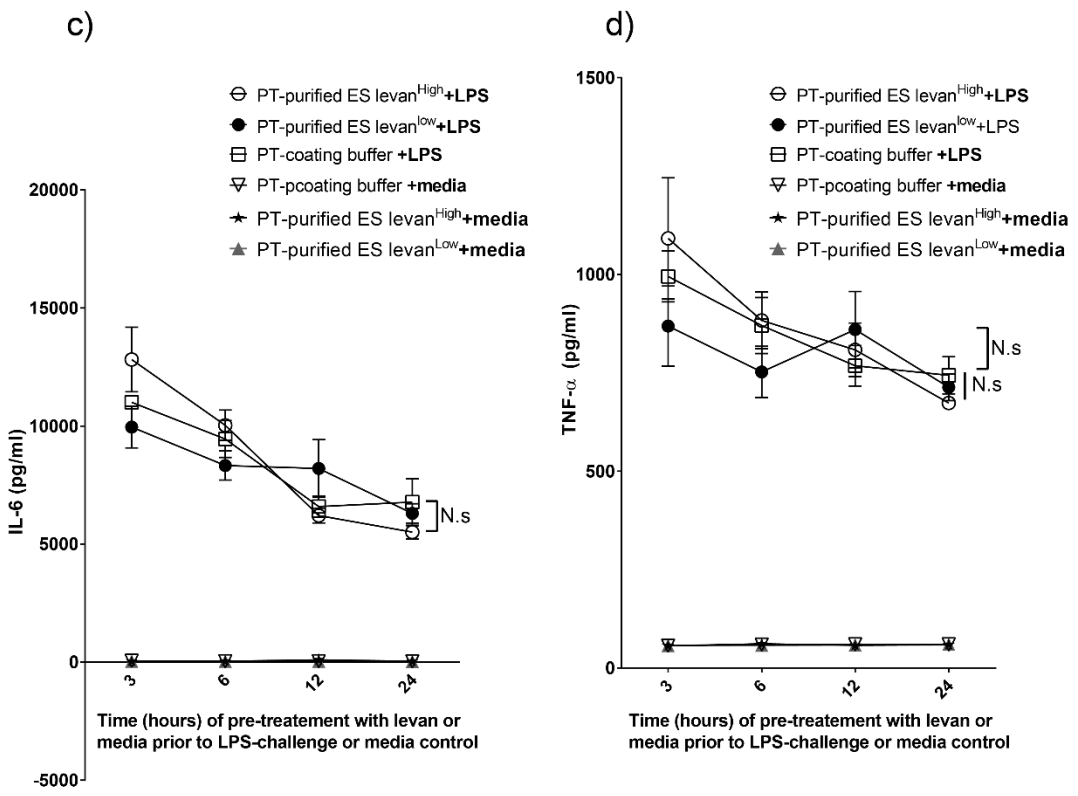

Immobilised

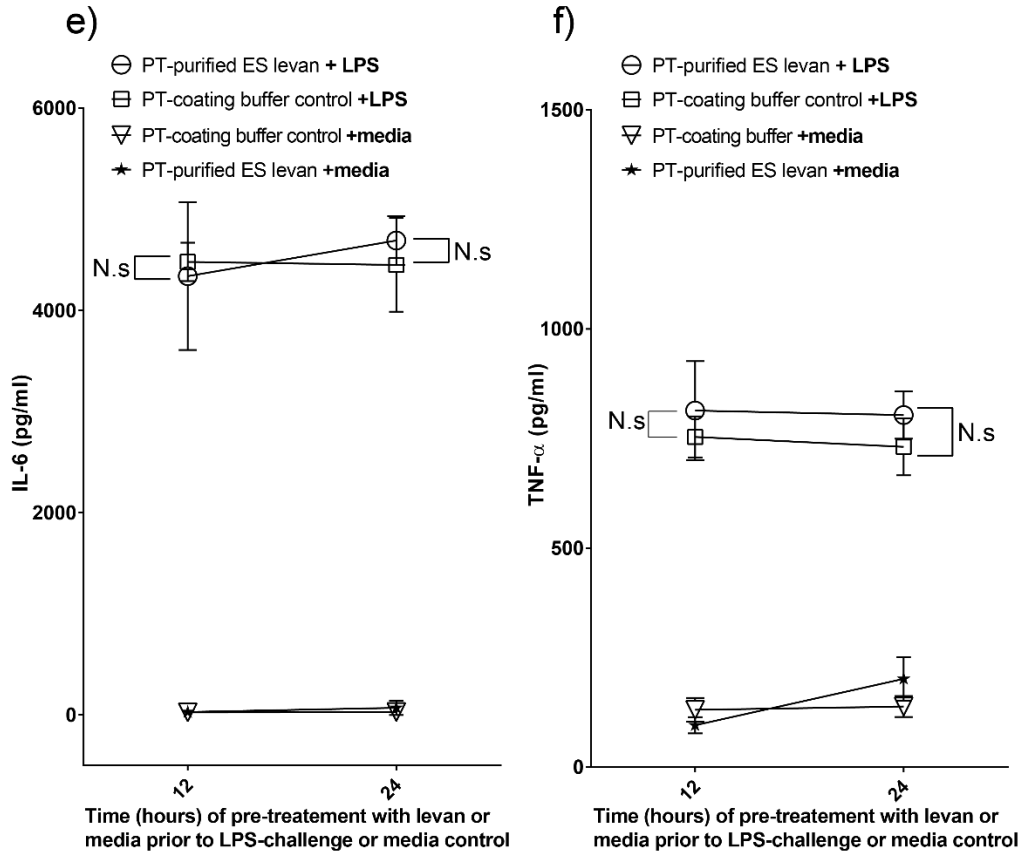

non-immobilised

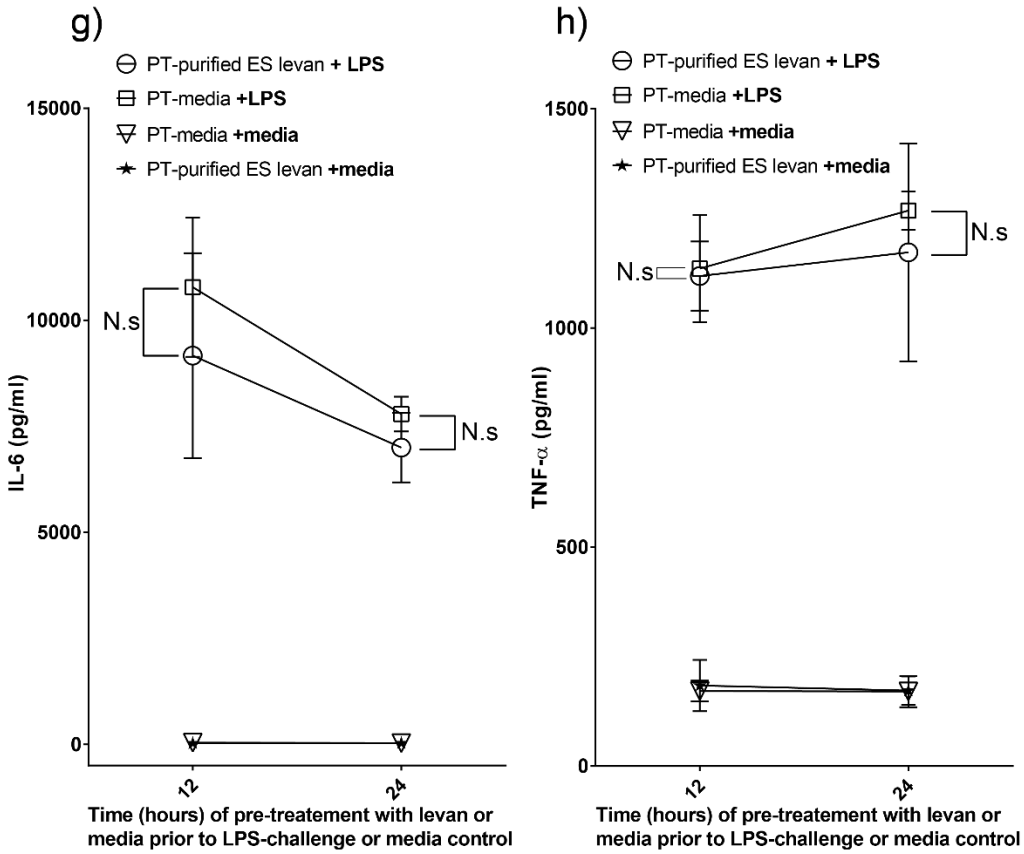

Figure 64. Modulation of cytokine production in LPS-challenged BMDCs pre-treated with purified ES levan.

BMDCs were pre-incubated with purified ES levan or media control and then challenged with LPS or media control using a 96 well plate; and cytokine production in the supernatant was measured by ELISA. X axis; time of BMDC pre-incubation with purified ES levan, PS coating buffer (for coating levan) or media alone (control) prior to challenge with LPS or media (control). PT, pre-treatment. +LPS (LPS challenge). +media (challenge control). First experiment using plate-immobilised [(a) and (b)] and non-plate-immobilised [(c) and (d)] pre-treatment of levan at 3, 6, 12 and 24 hr prior to LPS challenge (see 2.2.7.3). Second experiment using plate-immobilised [(e) and (f]) and non-plate-immobilised [(g) and (h)] pre-treatment of levan at 12 and 24 hr prior to LPS challenge. Purified ES levan^{High}, ES levan^{Low} and LPS (E. coli K12) concentrations were 200 μg/ml, 50 μg/ml and 20 ng/ml respectively. Experiments (a) to (d) were performed in triplicate. Experiments from (e) to (h) were performed with n = 6. Error bars, ± SD. Statistical analysis was performed using two-way ANOVA followed by tukey's test (b). p < 0.05 was considered statistically significant. N.s., not statistically significant as indicated. N.s. (straight line), not statistically significant across indicated treatments.

For further validation of these results, experiments were repeated at 12 and 24 hr pre-incubation with purified ES levan, with replicates increased to n = 6. No statistically significant inhibition of TNF-α or IL-6 production was observed under these conditions (Figure 64e to 64h).

5.2.4. Impact of purified enzymatically synthesised levan on Caco-2 cells.

5.2.4.1. Impact of purified enzymatically synthesised levan on monolayer permeability.

Here, we investigated whether levan could improve intestinal barrier function *in vitro* using LPS-challenged Caco-2 monolayers. Caco-2 cells were grown for 21 days in transwell culture plates resulting in differentiated Caco-2 monolayers. Purified ES levan was used in this study, as it was the purest levan available. Apical or both apical and basolateral compartments were treated with levan alone, cells alone, levan and LPS or LPS alone. Levan pre-treatment was carried out for 2hr ('2 hr pre-treatment experiment') or 24 hr ('24 hr pre-treatment experiment') before LPS-challenge. FITC-dextran was applied to the apical compartment and monolayer permeability was assessed by measuring basolateral supernatant concentrations of FITC[440]. High concentrations of LPS (1 mg/ml) were used to disrupt Caco-2 monolayers, as previously reported[571].

As expected, LPS treatment disrupted Caco-2 monolayer integrity. In the 24 hr pre-treatment experiment with cells simultaneously stimulated in apical and basolateral compartments, significantly higher concentrations [means] of FITC dextran were found in basolateral supernatants of cells treated with LPS alone (48.43 μg/ml, SD ±

6.68) or LPS + levan (52.58 μg/ml, SD ± 17.53) compared to levan alone (0.8 μg/ml, SD ± 0.05) and cells alone (0.65 μg/ml, SD ± 0.04) (Figure 65d). Similarly, in the 2 hr pre-treatment experiment with cells simultaneously stimulated in apical and basolateral compartments, significantly higher concentrations of FITC dextran were observed in basolateral supernatants of cells treated with LPS alone (37.8 μg/ml, SD ± 14.9) or LPS + levan (37.6 μg/ml, SD ± 12.75) compared to levan alone (0.79 μg/ml, SD ± 0.06) and cells alone (0.69 μg/ml, SD ± 0.03) (Figure 65c).

In the 24 hr pre-treatment experiment with cells simultaneously stimulated in apical compartments only, significantly higher concentrations of FITC dextran were found in basolateral supernatants of cells treated with LPS alone (12.73 μg/ml, SD ± 3.58) or LPS + levan (19.92 μg/ml, SD ± 5) compared to levan alone (0.78 μg/ml, SD ± 0.08) and cells alone (0.78 μg/ml, SD ± 0.04) (Figure 65b). In the 2 hr pre-treatment experiment with cells simultaneously stimulated in apical compartments only, no statistically significant differences were observed (Figure 65b).

In addition, no statistically significant differences in basolateral FITC-dextran concentration between cells treated with LPS only or both LPS and levan were observed (Figure 65). Further, treatment with levan only did not differ significantly in FITC-dextran concentrations compared to cells alone (Figure 65).

Taken together, these experiments indicate that levan did not improve Caco-2 monolayer permeability in response to high-dose LPS treatment, and levan treatment alone did not disrupt barrier integrity.

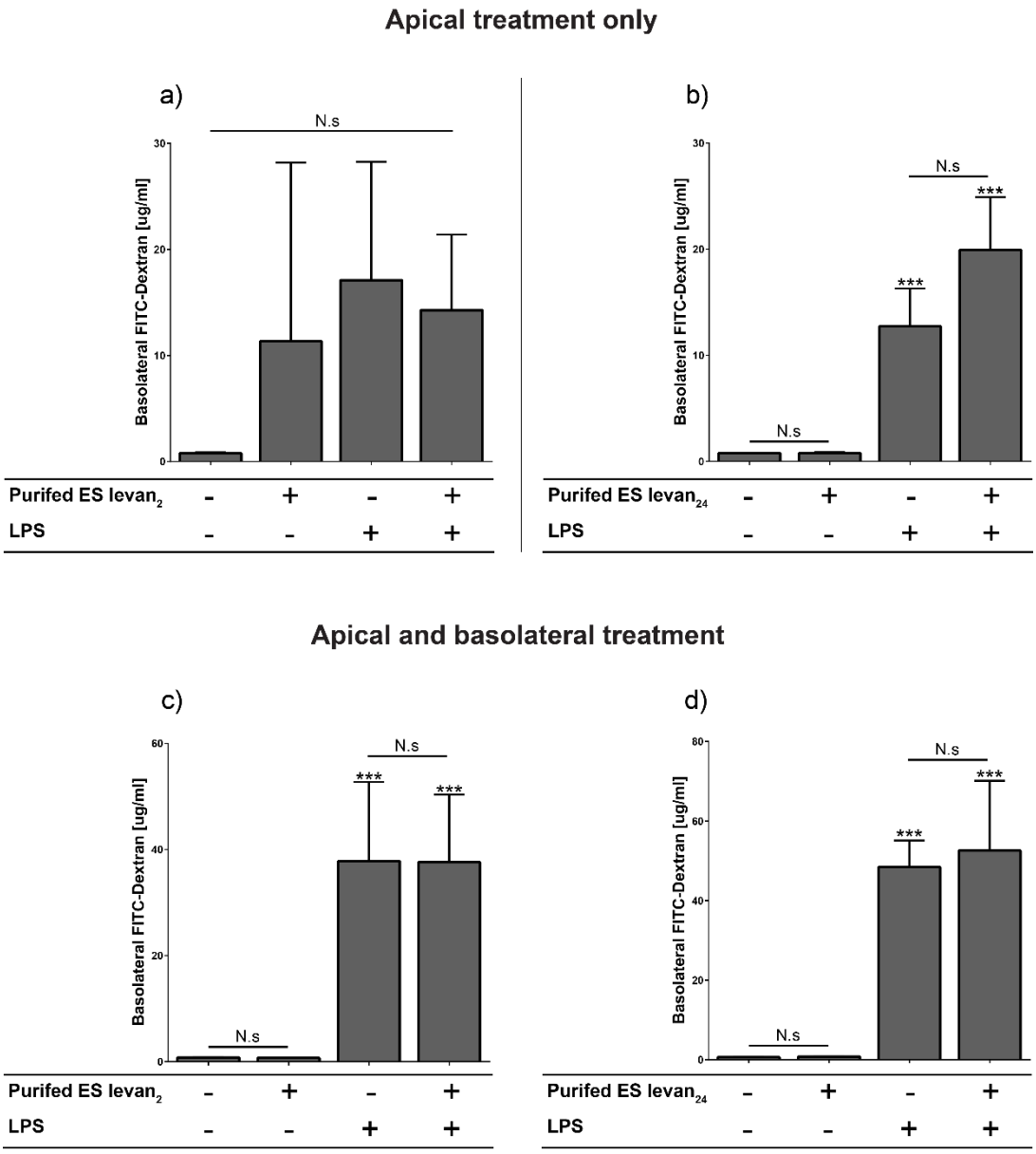

Figure 65. Impact of purified ES levan on Caco-2 monolayer permeability following LPS-challenge.

Caco-2 cell monolayers were prepared after 21 days using transwell culture plates. Monolayers were pre-treated with purified ES levan for 2 or 24 hrs and subsequently challenged with LPS on apical sides only or on both apical and basolateral sides. After washing, FITC-dextran was added to apical compartments and FITC concentrations were measured on the basolateral side.

Data show FITC dextran concentrations in the basolateral compartment after application of 1 mg/ml FITC-dextran on the apical side. Cells were pre-treated with 200 μg/ml purified ES levan. LPS (E. coli 0111:B4) was added at 1 mg/ml. (b) and (d) purified ES levan$_{24}$; cells pre-treated for 24 hr before LPS/media control stimulation. (a) and (c) purified ES levan$_2$; cells pre-treated for 2 hr before LPS stimulation. 'Apical treatment only' ([a] and [b]) and or 'apical and basolateral treatment' ([c] and [d]) refers to mode of application for both LPS and levan treatments. Experiment was performed in triplicate. Error bars, ± SD. Statistical analysis was performed using one-way ANOVA followed by tukey's test (b). ***, p < 0.001. compared to cells alone control (no levan and no LPS treatment). p < 0.05 was considered statistically significant. N.s., (straight line) not statistically between or across treatments indicated.

5.2.4.2. Impact of purified enzymatically synthesised levan on cytokine and chemokine production by Caco-2 cell monolayers.

Preliminary work in our group showed that high doses of LPS (1 mg/ml) were ineffective at stimulating cytokine production in our Caco-2 cell lines, in line with some previous reports[572,573]. Further, using flow cytometry, we found that 1 mg/ml of LPS induced a trend of apoptosis/necrosis in undifferentiated Caco-2 cells compared to media alone (Appendix 45), as previously reported[571,572], suggesting that LPS was not suitable for modulation of cytokine/chemokine production.

In contrast, it is reported that TNF-α elicits an immune response in Caco-2 cells at lower concentrations (10 – 100 ng/ml)[574]. Therefore, IL-8 production was determined in TNF-α-induced Caco-2 monolayers to assess the suitability of TNF-α. We found that simultaneous stimulation of both apical and basolateral compartments with 100 ng/ml and 10 ng/ml TNF-α induced IL-8 production in apical supernatants (Figure 66a). This effect was less pronounced or absent in basolateral supernatants (Figure 66b). We also showed in a preliminary experiment that 100 ng/ml of TNF-α and 1mg/ml LPS induced a trend of apoptosis/necrosis in undifferentiated Caco-2 cells as compared to cells treated with media control as well as levan alone (Appendix 46). In contrast to 1 mg/ml LPS, TNF-α at 100 ng/ml did not appear to disrupt Caco-2 monolayer permeability compared to cells alone at 4 hr basolateral collection (Appendix 47). As a result, TNF-α rather than LPS was used in the rest of the study.

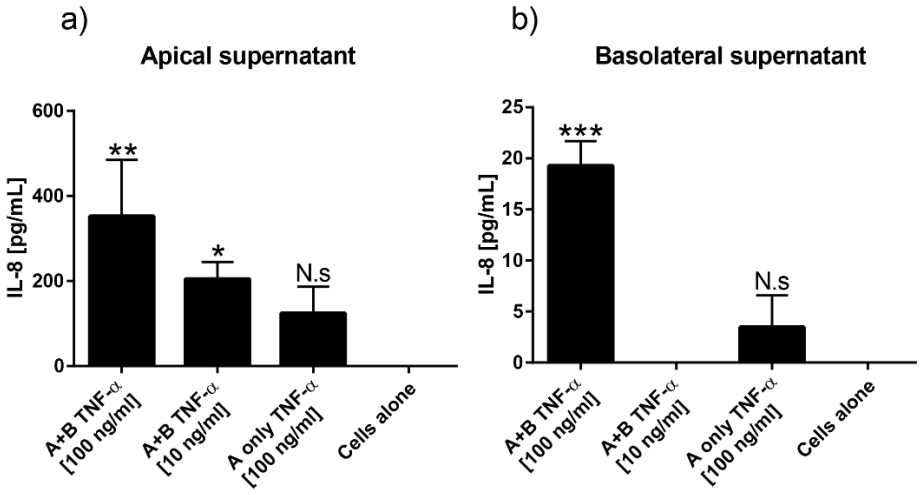

Figure 66. IL-8 production by TNF-α-induced Caco-2 cell monolayers.

Caco-2 cell monolayers were prepared after 21 days using transwell culture plates. Monolayers were treated with TNF-α on apical sides only or on both apical and basolateral sides; and supernatant concentrations of IL-8 were determined by ELISA. Data shows IL-8 production in (a) apical supernatants and (b) basolateral supernatants. A+B; simultaneous apical and basolateral TNF-α treatment. A only; apical TNF-α treatment only. All concentrations are as indicated. Experiments were performed in triplicate. Error bars, ± SD. Statistical analysis was performed using one-way ANOVA followed by tukey's test (b). ***, p < 0.001; **, p < 0.01; and *, p < 0.05 compared to cells alone. N.s., not statistically significant compared to cells alone.

In order to investigate if purified ES levan could modulate or induce cytokine production in epithelial cells, Caco-2 monolayers were subjected to treatment on both the apical and basolateral side with TNF-α alone, TNF-α and levan, levan alone or medium alone (see 2.2.6.2.). Cells with levan/media treatments were either added simultaneously ('simultaneous experiment') with TNF-α/medium control or were pre-treated with levan for 24 hr ('pre-treatment experiment') prior to stimulation with TNF-α or medium control. Concentrations for pre- or simultaneous treatment with levan were 190 μg/ml and 200 μg/ml, respectively, and either 10 ng/ml or 100 ng/ml was used for TNF-α treatments. Analysis using FITC dextran permeability assay (as previously described using LPS) showed no increase in monolayer permeability after TNF-α or other treatments compared to cells treated with media alone at 4 hr or 24 hr (LPS experiment was 4 hr only) (Appendix 48). Next, cytokine and chemokine production was determined using a Meso Scale Discovery (MSD) analyte screening platform.

5.2.4.2.1. Cytokine and chemokine production in apical supernatants

Here, we showed that in the simultaneous experiment, 100 ng/ml of TNF-α induced IL-6 (13.78 pg/ml, SD ± 2.46), IL-8 (489.24 pg/ml, SD ± 98.34), MCP-1 (79.43 pg/ml, SD ± 17.86) and IL-1-β (2.37 pg/ml, SD ± 0.39) production by Caco-2 cells compared

to cells alone in apical supernatants (Figure 67a, 67b, 67c and 67d, respectively). In line with this, treatment with both TNF-α (100 ng/ml) and levan also induced production of these cytokines. However, no statistically significant differences in the production of these cytokines or chemokines by Caco-2 cells in apical supernatants was found between cells treated with 100 ng/ml TNF-α alone or with both TNF-α (100 ng/ml) and levan (200 μg/ml). In the same experiment, 10 ng/ml of TNF-α induced IL-6 (7.91 pg/ml, SD ± 2.9), MCP-1 (79.77 pg/ml, SD ± 9.12) production by Caco-2 cells compared to cells alone (Figure 67a and 67c). In cells treated with both TNF-α (10 ng/ml) and levan (200 μg/ml), only a statistically significant induction of IL-6 was observed, however there was no statistically significant difference in IL-6 production in apical supernatants between cells treated with TNF-α alone (10 ng/ml) or with both TNF-α (10 ng/ml) and levan (200 μg/ml) (Figure 67a).

In the levan pre-treatment experiment assessing apical supernatants, cells treated with TNF-α alone (100 ng/ml) or with both TNF-α (100 ng/ml) and levan (190 μg/ml) induced IL-8 production by Caco-2 cells (Figure 67j). In cells treated with TNF-α (100 ng/ml) and levan (190 μg/ml) but not 100 ng/ml TNF-α alone, a statistically significant induction of IL-6 and MCP-1 was observed by Caco-2 cells in apical supernatants (compared to cells alone) (Figure 67i and 67k, respectively). Here, no difference was observed for IL-6 and MCP-1 production between cells treated with TNF-α alone (100 ng/ml) or with both TNF-α (100 ng/ml) and levan (190 μg/ml).

Further, in both simultaneous and levan pre-treatment experiments, TNF-α had no impact on the production of transforming growth factor beta (TGF-β), TSLP, Macrophage migration inhibitory factor (MIF), IL-10 and IFN-γ by Caco-2 cells in apical supernatants (Figure 67e to 67p). Further, no induction or modulation of any cytokines or chemokines were observed by purified ES levan alone in the pre-treatment or simultaneous experiments (Figure 67).

5.2.4.2.2. Cytokine and chemokine production in basolateral supernatants

Next, cytokine and chemokine production by Caco-2 cells in basolateral supernatants was assessed (Figure 68). In the simultaneous experiment, TNF-α (100 ng/ml) significantly induced IL-6 (0.82 pg/ml, SD ± 0.13), IL-8 (97.99 pg/ml, SD ± 2.09), MCP-1 (20.126 pg/ml, SD ± 2.32) and IL-1-β (0.384 pg/ml, SD ± 0.003) production by Caco-2 cells compared to cells alone in basolateral supernatants (Figure 68a, 70b, 70c and 70d, respectively). Further, cells treated with both TNF-α (100 ng/ml) and levan (200 μg/ml) induced these cytokines. However, no statistically significant

differences in the production of these cytokines or chemokines were found between cells treated with 100 ng/ml TNF-α alone or with both TNF-α (100 ng/ml) and levan (200 μg/ml). 10 ng/ml of TNF-α induced IL-6 (0.430 pg/ml, SD ± 0.06), IL-8 (28.85 pg/ml, SD ± 1.61), MCP-1 (9.5 pg/ml, SD ± 0.75) and IL-1-β (0.1 pg/ml, SD ± 0.017) production by Caco-2 cells compared to cells alone in basolateral supernatants (Figure 68a, 68b, 68c and 68d, respectively). The TNF-α (10 ng/ml) and levan (200 μg/ml) treatment group also showed induction of these cytokines and chemokines. However, no statistically significant differences in these cytokines or chemokines produced by Caco-2 cells in basolateral supernatants were found between cells treated with TNF-α alone (10 ng/ml) or with both TNF-α (10 ng/ml) and levan (200 μg/ml).

In the pre-treatment experiment, cells treated with TNF-α alone (100 ng/ml) or with both TNF-α (100 ng/ml) and levan (190 μg/ml) induced IL-8 and MCP-1 production by Caco-2 cells in basolateral supernatants, however no statistically significant differences between IL-8 and MCP-1 production was observed between these treatments (Figure 68k and 68l, respectively). In both simultaneous and levan pre-treatment experiments assessing basolateral supernatants, TNF-α had no impact on the production of TGF-β, TSLP, MIF and IL-10 by Caco-2 cells. Further, no induction or modulation of any cytokines or chemokines was observed by purified ES levan alone in the pre-treatment or simultaneous experiments in basolateral supernatants (Figure 68). The induction of IFN-γ production by Caco-2 cells in the basolateral supernatant was only observed in cells treated with both TNF-α (10 ng/ml) and levan (190 μg/ml), but not by other treatment groups in the pre-treatment experiment and no differences were evident between groups (Figure 68o). Moreover, no statistically significant increase in basolateral supernatant IFN-γ was observed in the simultaneous experiment.

In summary, purified ES levan did not modulate cytokine or chemokine production by Caco-2 cell monolayers following TNF-α challenge. Further, levan alone did not stimulate any cytokine or chemokine production in these cells.

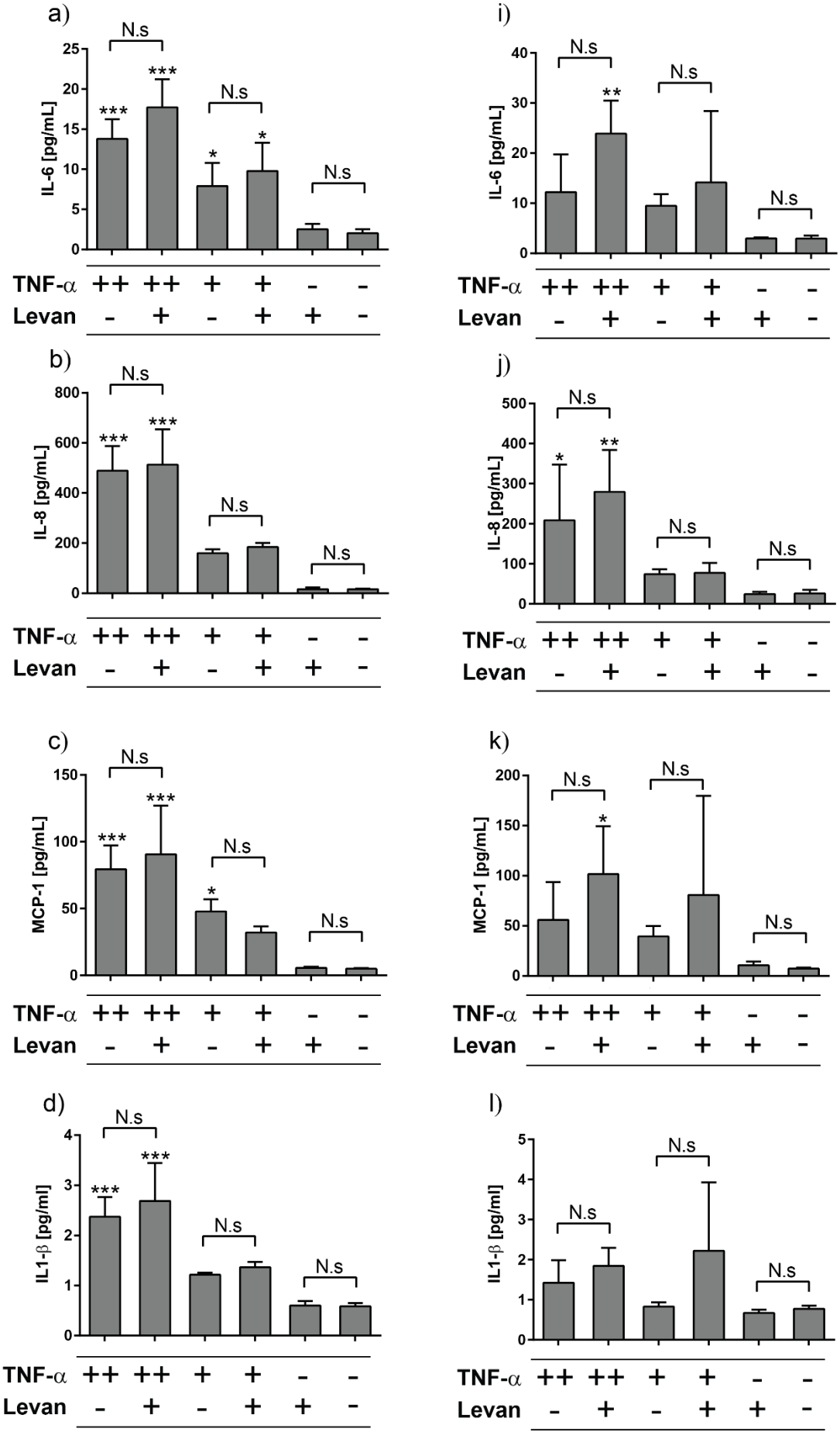
a)
IL-6 [pg/mL]
N.s
***
*
TNF-α ++ ++ + + - -
Levan - + - + + -
i)
IL-6 [pg/mL]
N.s
**
TNF-α ++ ++ + + - -
Levan - + - + + -
b)
IL-8 [pg/mL]
N.s
***
TNF-α ++ ++ + + - -
Levan - + - + + -
j)
IL-8 [pg/mL]
N.s
*
**
TNF-α ++ ++ + + - -
Levan - + - + + -
c)
MCP-1 [pg/mL]
N.s
***
*
TNF-α ++ ++ + + - -
Levan - + - + + -
k)
MCP-1 [pg/mL]
N.s
*
TNF-α ++ ++ + + - -
Levan - + - + + -
d)
IL1-β [pg/ml]
N.s
***
TNF-α ++ ++ + + - -
Levan - + - + + -
l)
IL1-β [pg/ml]
N.s
TNF-α ++ ++ + + - -
Levan - + - + + -

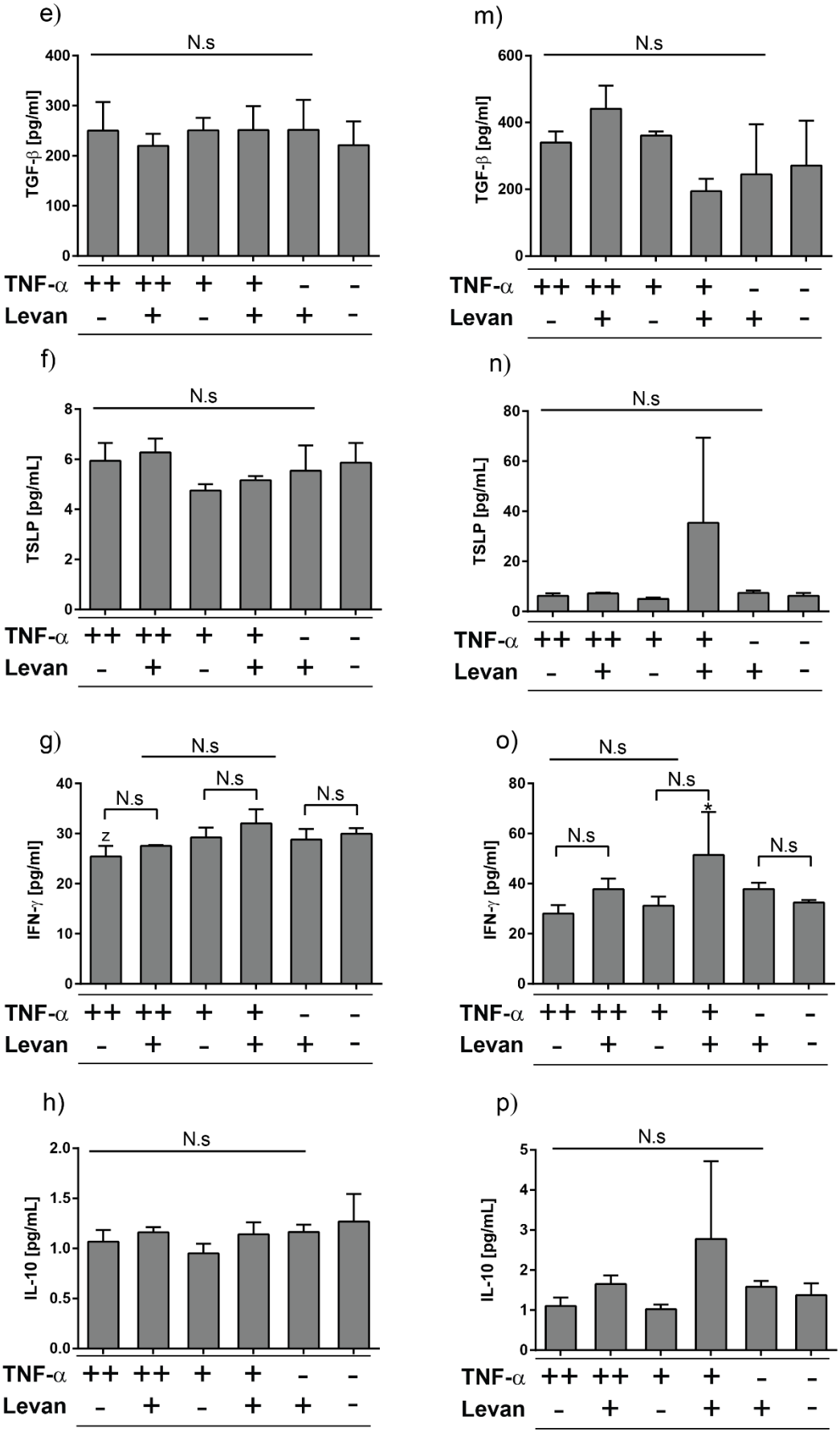
e)
N.s
TGF-β [pg/ml]
400
300
200
100
0
TNF-α ++ ++ + + - -
Levan - + - + + -
m)
N.s
TGF-β [pg/ml]
600
400
200
0
TNF-α ++ ++ + + - -
Levan - + - + + -
f)
N.s
TSLP [pg/mL]
8
6
4
2
0
TNF-α ++ ++ + + - -
Levan - + - + + -
n)
N.s
TSLP [pg/mL]
80
60
40
20
0
TNF-α ++ ++ + + - -
Levan - + - + + -
g)
N.s
N.s
N.s
N.s
z
IFN-γ [pg/ml]
40
30
20
10
0
TNF-α ++ ++ + + - -
Levan - + - + + -
o)
N.s
N.s
N.s
N.s
*
IFN-γ [pg/ml]
80
60
40
20
0
TNF-α ++ ++ + + - -
Levan - + - + + -
h)
N.s
IL-10 [pg/mL]
2.0
1.5
1.0
0.5
0.0
TNF-α ++ ++ + + - -
Levan - + - + + -
p)
N.s
IL-10 [pg/mL]
5
4
3
2
1
0
TNF-α ++ ++ + + - -
Levan - + - + + -

Figure 67. Impact of purified ES levan on the production of cytokines/chemokines by Caco-2 monolayers on the apical compartment.

Caco-2 cell monolayers were prepared after 21 days using transwell culture plates. Monolayers were either pre-treated with purified ES levan for 24 hours and challenged with TNF-α, or purified ES levan was added simultaneously with TNF-α, on both apical and basolateral sides; and apical supernatant concentrations of cytokines and chemokines were determined by Meso Scale Discovery. Data show IL-6, IL-8, MCP-1, IL1-b, TGF-β, TSLP, IFN-γ and IL-10 production by Caco-2 monolayers secreted into apical compartments. Simultaneous treatment with TNF-α and purified ES levan (a – h). 24 hr pre-treatment with purified ES levan prior to TNF-α challenge (i – p). ++ 100 μg/ml TNF-α. +, 10 μg/ml TNF-α. Simultaneous treatment with levan was 200 μg/ml (final concentration). Purified ES levan pre-treatment concentrations were 190 μg/ml. Error bars, + SD. Statistical analysis was performed using one-way ANOVA followed by tukey's test (b). ***, p<0.001; **, p<0.01; and *, p < 0.05 compared to cells alone (- -). N.s. (comparative line), not statistically significant between indicated treatments. N.s. (straight line), not statistically significant compared to cells alone. Z, p < 0.05 (lower than cells alone) The few values below fit curve range of the Meso Scale Discovery system analysis were considered as zero. N = 3 for IL-10 analysis for TNF-α 10 ng/ml + purified ES levan treatment (excluded a 262-fold outlier compared to average of n = 3). N = 4 for all other treatments.

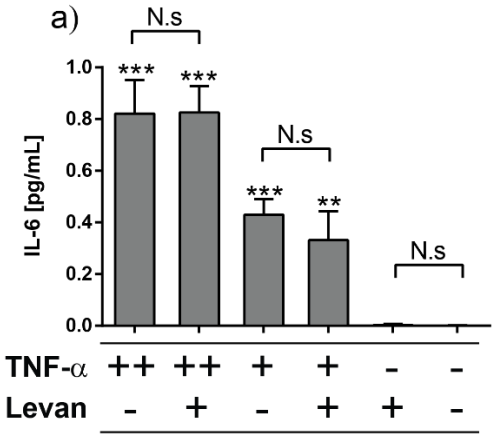
a)
N.s
***
***
N.s
***
**
N.s
1.0
0.8
0.6
0.4
0.2
0.0
IL-6 [pg/mL]
TNF-α ++ ++ + + - -
Levan - + - + + -

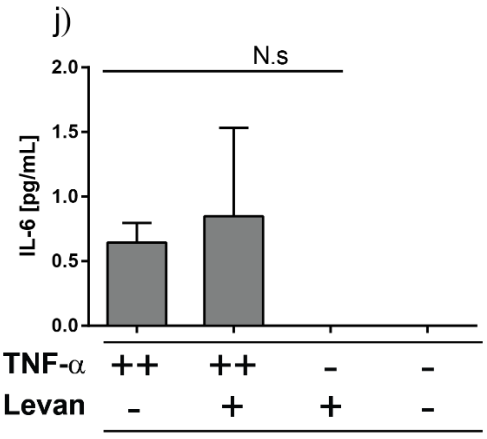
j)
N.s
2.0
1.5
1.0
0.5
0.0
IL-6 [pg/mL]
TNF-α ++ ++ - -
Levan - + + -

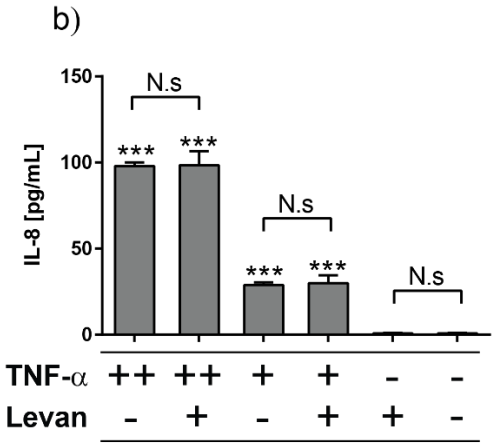
b)
N.s
***
***
N.s
***
***
N.s
150
100
50
0
IL-8 [pg/mL]
TNF-α ++ ++ + + - -
Levan - + - + + -

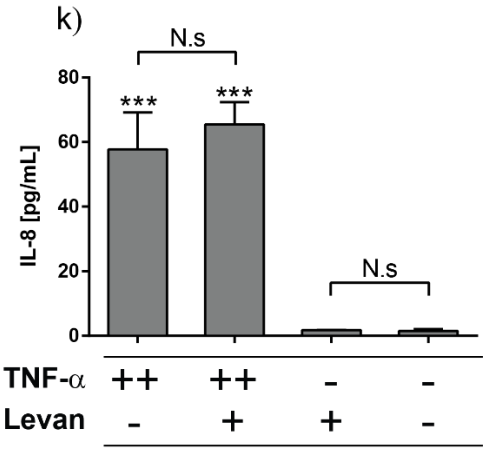
k)
N.s
***
***
N.s
80
60
40
20
0
IL-8 [pg/mL]
TNF-α ++ ++ - -
Levan - + + -

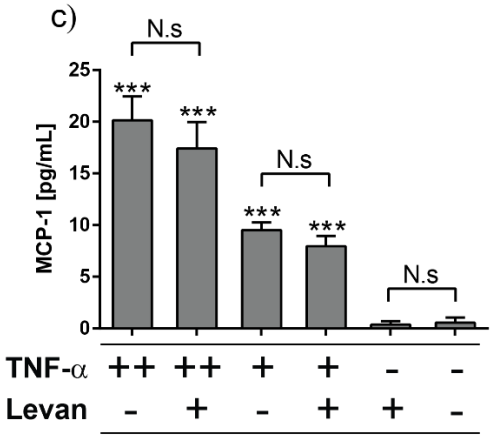
c)
N.s
***
***
N.s
***
***
N.s
25
20
15
10
5
0
MCP-1 [pg/mL]
TNF-α ++ ++ + + - -
Levan - + - + + -

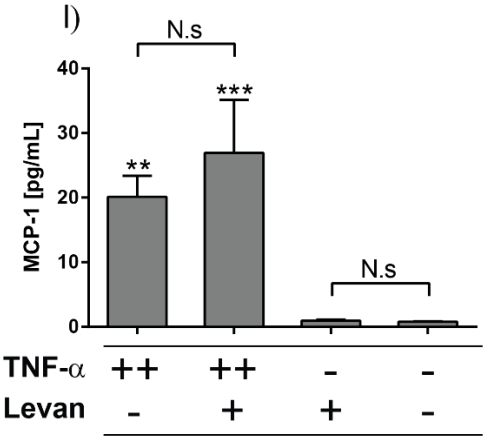
l)
N.s
**
***
N.s
40
30
20
10
0
MCP-1 [pg/mL]
TNF-α ++ ++ - -
Levan - + + -

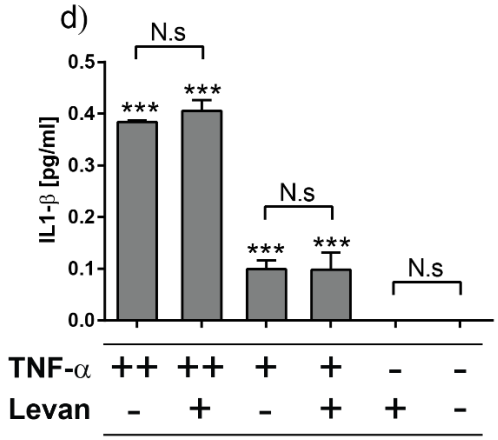
d)
N.s
***
***
N.s
***
***
N.s
0.5
0.4
0.3
0.2
0.1
0.0
IL1-β [pg/ml]
TNF-α ++ ++ + + - -
Levan - + - + + -

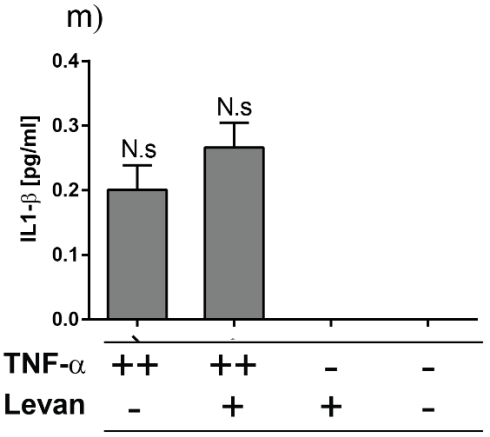
m)
N.s
N.s
0.4
0.3
0.2
0.1
0.0
IL1-β [pg/ml]
TNF-α ++ ++ - -
Levan - + + -

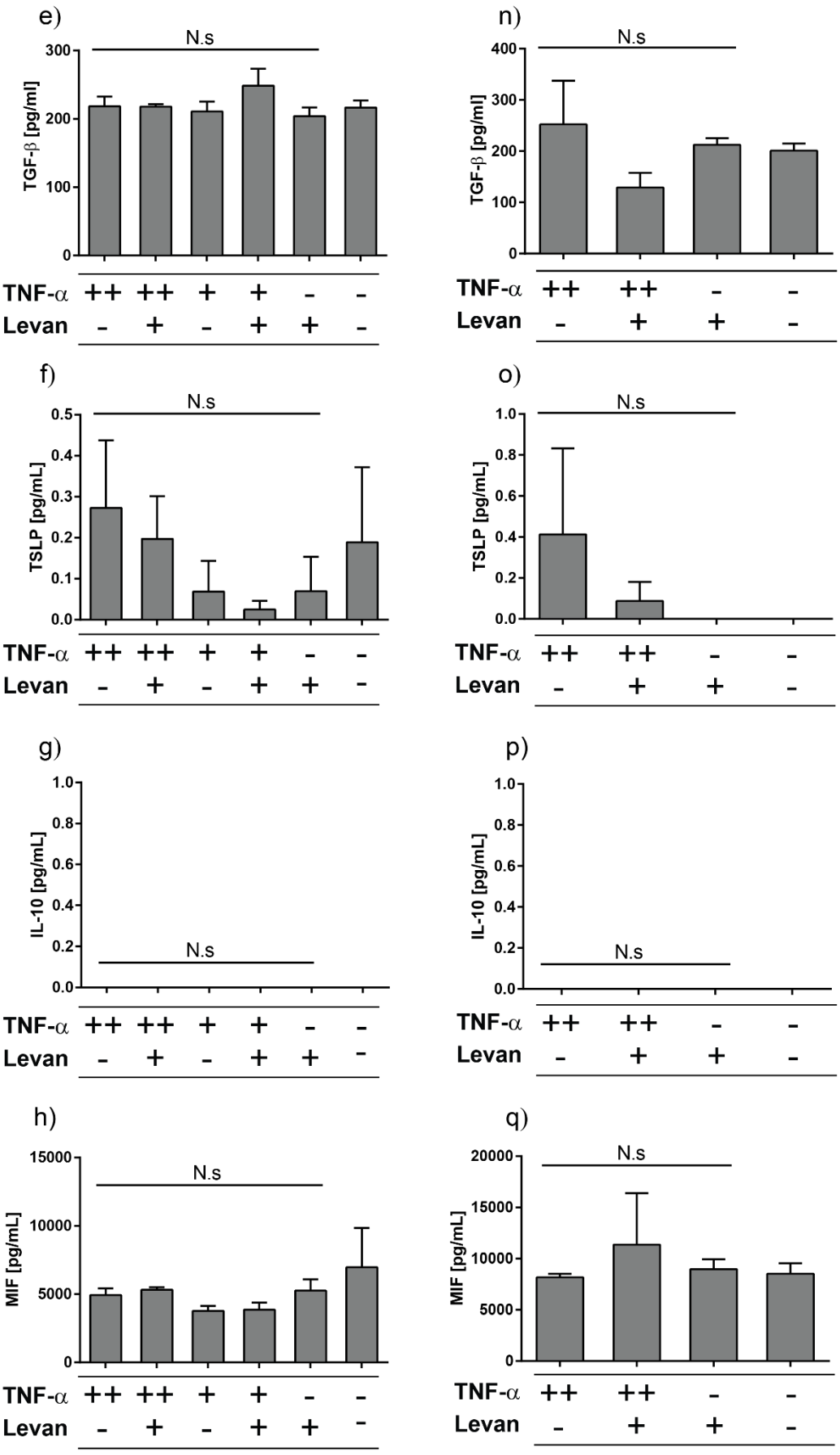
e)
N.s
TGF-β [pg/ml]
300
200
100
0
TNF-α ++ ++ + + - -
Levan - + - + + -
n)
N.s
TGF-β [pg/ml]
400
300
200
100
0
TNF-α ++ ++ - -
Levan - + + -
f)
N.s
TSLP [pg/mL]
0.5
0.4
0.3
0.2
0.1
0.0
TNF-α ++ ++ + + - -
Levan - + - + + -
o)
N.s
TSLP [pg/mL]
1.0
0.8
0.6
0.4
0.2
0.0
TNF-α ++ ++ - -
Levan - + + -
g)
IL-10 [pg/mL]
1.0
0.8
0.6
0.4
0.2
0.0
N.s
TNF-α ++ ++ + + - -
Levan - + - + + -
p)
IL-10 [pg/mL]
1.0
0.8
0.6
0.4
0.2
0.0
N.s
TNF-α ++ ++ - -
Levan - + + -
h)
MIF [pg/mL]
15000
10000
5000
0
N.s
TNF-α ++ ++ + + - -
Levan - + - + + -
q)
MIF [pg/mL]
20000
15000
10000
5000
0
N.s
TNF-α ++ ++ - -
Levan - + + -

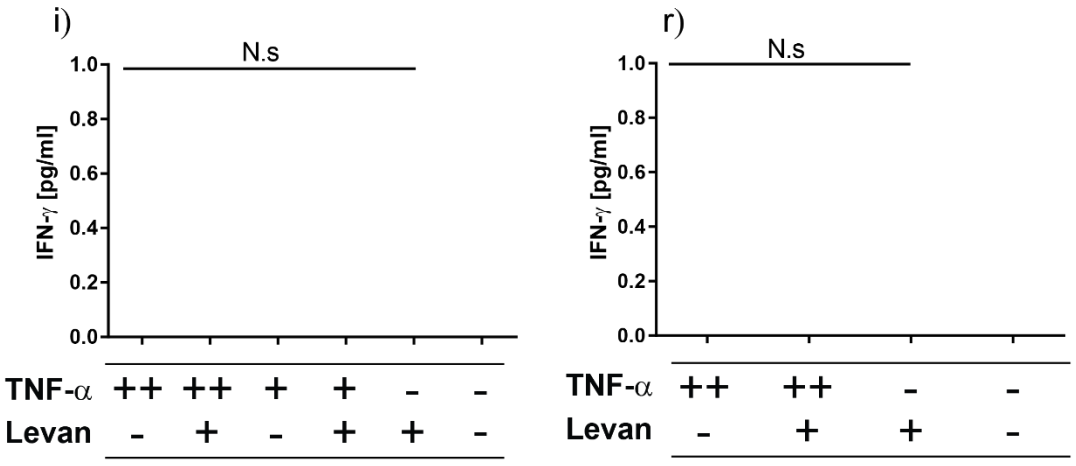

Figure 68. Impact of purified ES levan on the production of cytokines/chemokines by Caco-2 monolayers on the basolateral compartment.

Caco-2 cell monolayers were prepared after 21 days using transwell culture plates. Monolayers were either pre-treated with purified ES levan for 24 hours and challenged with TNF-α, or purified ES levan was added simultaneously with TNF-α, on both apical and basolateral sides; and basolateral supernatant concentrations of cytokines and chemokines were determined by Meso Scale Discovery. Data show IL-6, IL-8, MCP-1, IL1-b, TGF-β, TSLP, IL-10, MIF and IFN-γ and production by Caco-2 monolayers secreted into basolateral compartments. Simultaneous treatment with TNF-α and purified ES levan (a – i). 24 hr pre-treatment with purified ES levan prior to TNF-α challenge (j – r). ++ 100 μg/ml TNF-α. +, 10 μg/ml TNF-α. Simultaneous treatment with purified ES levan was 200 μg/ml (final concentration). Purified ES levan pre-treatment concentrations were 190 μg/ml. Error bars, + SD. Statistical analysis was performed using one-way ANOVA followed by tukey's test (b). ***, p < 0.001; **, p < 0.01 and *, p < 0.05 compared to cells alone. N.s. (comparative line), not statistically significant between indicated treatments. N.s. (straight line), not statistically significant compared to cells alone (- -). Any values below fit curve range of the Meso Scale Discovery system analysis were considered as zero. N = 3 for all treatments.

5.3. Summary and Discussion

Here, we studied the impact of crude and purified *E. herbicola* levan on cytokine production by murine-derived BMDCs. Crude *E. herbicola* levan induced IL-6 and TNF-α production primarily through TLR4, in line with results using TLR4 reporter cells described in Chapter 4. As LPS is a primary ligand for TLR4-MD-2[461], this may explain the strong dependency on TLR4 for the induction of cytokines in BMDCs by *E. herbicola* crude levan. We also showed that induction of TNF-α and IL-6 production in BMDCs by *E. herbicola* crude levan was partly Dectin-2 dependent which may be due to the presence of α-mannan in *E. herbicola* levan samples, as this sugar has been reported in structurally characterised LPS[527,566,575-577]. Further investigation into the structure of LPS bound to levan is required to confirm its interaction with TLR4 and/or Dectin-2 on BMDCs. Induction of IL-10 in BMDCS by crude *E. herbicola* levan was shown, however, it should also be noted that a second independent experiment comparing WT and TLR4 KOs showed no statistically significant induction of IL-10 production.

Importantly, purified *E. herbicola* levan as well as non-plate- or plate-immobilised ES purified did not induce TNF-α, IL-6 or IL-10 production by BMDCs suggesting that LPS was a key contributor to these effects. In contrast, Xu et al (2006) showed that levan isolated from *B. subtilis* natto mucilage induced TNF-α and IL-12 p40 by macrophage cell lines *in vitro*[26]. In this study, polymyxin B inhibited LPS-induced IL-12 production by J774.1 macrophages but not levan-treated cells[26]. Using TLR4 reporter cells and TLR4 KO mice, they showed binding of TLR4 to levan and TLR4-dependent induction of TNF-α by adherent peritoneal cells *in vitro* further supporting that levan's immunomodulatory properties on cells occurred via recognition by TLR4, which was shown here using crude *E. herbicola* levan but not using purified levans.

The ability of levan to inhibit cytokine production in BMDCs after LPS-challenge was also explored. Such approaches have been used with other PS such as astragalus PS (APS), heteropolysaccharides that are largely heterogenous in structure, for a review see [423]. APS was shown to reduce inflammation *in vitro* by inhibiting both the expression and production of IL-6, IL-8 and TNF-α in LPS-induced H9c2 cardiomyoblasts[578]. More relevantly, it was reported that APS inhibited cytokine expression and production including TNF-α by LPS-induced human THP-1 macrophages through suppression of NF-kB- and JNK-associated pathways[455] which are important activation pathways for the induction of proinflammatory cytokines including TNF-α and IL-6 by DCs[411] and IL-8 by epithelial cells[579],

respectively. In contrast, we showed that levan had no inhibitory effect on TNF-α or IL-6 production by BMDCs following LPS-challenge.

To explore alternative mechanisms underpinning the reported immunomodulatory properties of levan, levan's (purified ES levan) interaction with the gut epithelium was investigated using Caco-2 cells. Caco-2 monolayers are frequently used for assessing intestinal barrier function *in vitro*[107,580]. It has been reported that PS including inulin could improve monolayer integrity following LPS or bacterial-challenge *in vitro*[237,440]. Levan was also suggested to marginally improve Caco-2 monolayer permeability compared to medium-treatment alone as assessed by transepithelial electrical resistance[107]. Variable doses of LPS can be required for disruption of Caco-2 cell monolayers[581,582], due to variability in the LPS structure or potency, or the reported morphological or growth characteristic differences between Caco-2 cell clones[583] which may extend to other biological differences such as location (apical or basolateral sides) and abundance of receptor expression. Here, we showed that that levan had no improvement in monolayer permeability when Caco-2 cells were pre-exposed to 1 mg/ml LPS.

We also investigated whether levan (purified ES levan) could stimulate or inhibit cytokine production in Caco-2 cells following an inflammatory challenge, as Caco-2 cells are known to produce cytokines[580] modulated by PS[237,238]. For example, a study by Wang and colleagues (2013) showed that Caco-2 cells pre-treated with APS prior to LPS challenge or treated simultaneously with APS LPS downregulated expression of TNF-α, IL-8 and IL-1β as well as improved monolayer integrity in response to disruption by LPS treatment *in vitro*[237]. A similar study using Caco-2 cells challenged with LPS showed that sulphated APS were more effective at downregulating expression of these cytokines[456]. Further, chitosan nanoparticles were shown to inhibit MCP-1, MIF, TNF-α and IL-8 production by Caco-2 cells following LPS challenge[238]. The authors concluded that this was due to improvements in monolayer barrier integrity and partly through modulation of NF-κB[238], a transcription factor responsible for induction of cytokines by immune cells[584]. Further, low-molecular weight fucoidan from brown seaweed significantly reduced IL1-β and TNF-α production and increased IL-10 and IFN-γ production in Caco-2 cells[585]. These studies highlight the potential for the immunomodulatory effects of PS on epithelial cells *in vitro*. To the best of our knowledge no study has investigated the ability of levan to modulate cytokine or chemokine production in IEC *in vitro*. Using purified ES levan, we monitored the production of IL-6, IL-8, MCP-1, IL-1-β, TGF-β, TSLP,

MIF, IL-10 or IFN-γ by Caco-2 monolayers in either apical or basolateral supernatants following TNF-α challenge. However, purified ES levan did not induce production of these analytes. TGF-β and TSLP were screened due to their suggested role in intestinal immune regulation including being produced by IECs in response to microbial stimulation *in vitro* and steering intestinal DCs and macrophages towards a more tolerogenic phenotype[191,241,326]. Further, oral administration of brown rice-derived PS to mice increased TGF-β production in isolated PPs[586].

Overall, we showed that LPS bound to crude levan was a key contributor to the induction of cytokine production by BMDC *in vitro*. Purified ES levan did not impact on cytokine or chemokine production by BMDCs or Caco-2 monolayers, or Caco-2 membrane permeability following inflammatory challenge.

Chapter 6: General discussion, perspectives and concluding remarks

In this work, we investigated the interaction of PS from plants, fungi, algae and microbes with CLRs as a potential mechanism underpinning their immunomodulatory properties. We first used a semi high-throughput screen to identify novel interactions of PS with CLR Dectin-1, Dectin-2 and SIGNR1. The use of CRD-modified mutant cells (QPD) allowed to control for carbohydrate-specific binding. Using this approach, we identified several novel interactions with CLRs including α-glucan and Hafnia-LPS with SIGNR1, and microbial levan with Dectin-2. Another screening platform that is commonly used to investigate carbohydrate-protein interactions are glycan or lectin microarrays[587-590]. Our reporter cell assay allows to identify the interaction between PS with extracellular CLR protein domains on a cell surface, leading to intracellular signalling as opposed to a direct biochemical PS-protein interaction. Use of complementary biochemical-based approaches are, therefore, important to verify novel ligand interactions. Here, we confirmed the interaction between levan and Dectin-2 protein using AFM.

Most knowledge on cell surface CLRs and their pattern recognition is based on the studies of opportunistic/pathogenic microbes, or viruses[117,125,309]. The best studied examples include, α-mannan and Dectin-2[120,121,402], β-glucan and Dectin-1[359,549], and DC-SIGN and hepatitis C or HIV glycoproteins[591,592]. However, recently, the immunomodulatory properties of a food PS, arabinan, was shown to be through signalling molecule SYK *in vitro*, suggesting that CLRs may interact with carbohydrates found in the gut[450]. Reports have shown that Dectin-2 is expressed in mouse intestine *in vivo*[392], and Dectin-1 expression was reported in human IECs *ex vivo*[368]. There is also evidence that CLRs influence intestinal immune homeostasis[366]. For example, one study reported that Dectin-1 KO mice were resistant to experimentally-induced colitis through microbiota-mediated induction of colonic LP T reg cells[369]. A contrasting study showed that Dectin-1 KO mice harbouring opportunistic fungi were more susceptible to experimentally-induced colitis[593]. Investigation into CLR expression patterns in the gut is warranted to further explore their potential immunomodulatory functions with regards to PS from food and microbes.

When assessing the immunomodulatory properties of PS *in vitro*, it is essential to take into account the steps leading to their purification. Unexpectedly, we showed that growth media could also bind to Dectin-2. This was in part to the presence of yeast extract in the medium containing mannoproteins[91,117,594]. Interestingly, we also showed that purification of GOS OsLu by *S. cerevisiae* conferred the ability of OsLu to bind to Dectin-2[489], suggesting that the use of yeast in the production method for

carbohydrates may influence bioactivity *in vitro*. It may also influence the immunomodulatory properties of OsLu in rats *in vivo* including modulation of cytokines and chemokines in colonic tissue after oral administration[536]. However, OsLu also modulated gut microbial composition[536], therefore further research is required to investigate the contribution of OsLu interaction with Dectin-2[489]. Exploring other growth media or purification methods to produce high-purity PS is warranted to study PS immunomodulatory properties *in vitro*.

Importantly, we showed that LPS in crude *E. herbicola* levan was primarily responsible for cytokine production by BMDCs. The structure of LPS can influence the strength of a cellular immune response including cytokine production[131,595]. LPS has been reported to stimulate IL-6 and IL-8 production in BMDCs at only 20 pg/ml, and TNF-α production was also induced in the same cells at 200 pg/ml LPS[412]. In another study, 10 pg/ml and 20 pg/ml of LPS led to the induction of TNF-α and IL-6 by BMDCs, respectively[414]. These studies demonstrate the high sensitivity of LPS stimulating host immune responses *in vitro*. Interestingly, LPS has also been reported to contribute to the immunomodulatory effects of other compounds. For example, LPS was attributable to the immunomodulatory properties of food proteins *in vitro* including the induction of cytokines by THP-1 macrophages and an ability to activate TLR4 reporter cells[596]. Similarly, LPS contributed to IL-8 production in HT-29 cells by β-glucans[597]. Moreover, a recent study showed that pullulan - treated with polymyxin B (aragose) to remove LPS from 210 ng/ml to 10 ng/ml - induced production of pro-inflammatory cytokines including IL-6, TNF-α and IL-8 in whole blood of humans, *ex vivo*[468]. However, as mentioned above, LPS may be immunostimulatory at these low levels[411,414]. Further, one study demonstrated that cytokine production by LPS-treated BMDCs was only significantly reduced by incubating with polymyxin B if LPS concentrations of $\leq$ 20 ng/ml were used[414]. In addition, since polymyxin B was shown to be cytotoxic at concentrations > 10 μg/ml, polymyxin B may not be suitable for *in vitro* studies of immunomodulatory PS, and highlights the need for more sensitive and effective methods to remove LPS.

Here we first used GPC and LRA[513] for LPS removal, however these methods failed to reduce LPS to below immunostimulatory levels[411,414], which prompted the development of a new method to inactivate LPS in levan. Importantly, the purification process did not alter levan's structure as was shown by GC-MS linkage analysis and NMR. Other reports of LPS removal include the use of Triton-X-114 which has been shown to be effective for removing LPS from food protein preparations[596]. Another

study proposed a combination of alkali, ethanol and heat treatment for 5 hr followed by the addition of acid (neutralisation) to inactivate LPS in PS samples but reported some PS degradation during this treatment[412].

It may also be important to address both LPS and other MAMPs in PS samples when assessing the immunomodulatory properties of PS *in vitro*. This could be done through the use of BMDCs generated from transgenic mice, for example double TLR2 and TLR4 KO mice as shown by Meijerink and colleagues (2018)[450]. A more extensive approach was applied by Danne and colleagues (2017) that used BMMs generated *in vitro* from a variety of PRR KO mice including TLR, NOD-2 and CLR KOs in order to assess the immunomodulatory properties of a PS isolated from gut-resident *Helicobacter hepaticus*[475].

In addition to LPS, other factors may contribute to the immunomodulatory properties of PS[3]. Recently, a review by Han (2018) commented on the lack of standardisation across studies regarding the production and characterisation of PS extracts[415]. For example, different characterisation or production methods across studies for producing PS result in a lack of reproducible results regarding PS composition[415]. This is further complicated by the fact that many PS are carbohydrate mixtures and separating these PS, such as by GPC, may not always yield the same PS structures, as the conditions may vary across studies including the type of column, flow rate and detection instrument used[415]. Further, crude extracts may also contain other bioactive compounds e.g. flavonoids and terpenoids found in mushroom PS extracts that may influence the bioactivity of the PS[3,156,405,415]. Generally, the field requires technological advancements in order to produce high-purity or synthesised PS that are well-characterised that can be used to assess or screen for their immunomodulatory properties *in vitro*.

We then tested the potential role of levan in reinforcing barrier integrity or modulating IEC cytokine production. There is evidence that PS can improve membrane barrier integrity *in vitro*[439,440,598]; and improvements in IEC barrier integrity *in vivo* have been observed with dietary inulin, rhamnogalacturonan or *Bletilla striata* PS[431,438,598]. It is important to note that in physiological conditions *in vivo*, dietary PS would need to penetrate through the mucus layer to interact directly with the epithelium or be metabolised by gut bacteria in the lumen which can produce metabolites influencing gut barrier function as shown with butyrate[209,210,599,600]. The mechanisms for the promotion of barrier integrity by PS may involve TLR, for example, fructans have shown to aid in IEC barrier protection through interaction with TLR *in vitro*[439]. PS,

particularly APS, have been reported to modulate IEC anti-inflammatory cytokine responses *in vitro*[237,456,598]. However, it has been shown that dietary APS increased serum proinflammatory cytokine levels in experimental mouse models[424], possibly through their interaction with TLR4. TLR expression varies along the SI and LI and from the apical and basolateral sides as shown in mouse intestine[313]. However, it is unclear whether TLR expression in cell lines reflects TLR pattern expression *in vivo*[313]. Further work is warranted to assess the interaction of dietary PS with TLRs across different areas of the GI tract *in vivo*.

It may be that dietary PS can progress beyond the epithelium. For example, Rice and colleagues (2005) showed that orally-administered glucans were absorbed into circulation in rats, and glucans could be internalised by murine IEC *in vitro*[467]. Moreover, Wang and colleagues (2017) recently showed that orally-administered PS from *Angelica sinensis* were absorbed through the GI tract and entered the blood stream and other organs[601]. They also found that these PS were internalised and were transported through Caco-2 cell monolayers[601]. Interestingly, minor intestinal absorption of orally-administered fucoidan has been reported in rats *in vivo*[602]. This study also showed fucoidan-positive (internalised) cells in the mucosa of the SI and also reported that fucoidan uptake may also be evident in GALT macrophages[602]. Taken together, these studies suggest that PS may be able to breach the mucus and epithelial layer and reach GALT immune cells or other tissues in the body. It may also be possible that luminal sampling by APCs[165,259] is involved with this process.

In this work, we used BMDCs to assess the immunomodulatory properties of levan. It is important to consider that BMDCs are a basic *in vitro* model for testing the immunomodulatory properties of PS *in vitro* and their use may not reflect the full characteristics of DC subsets found in the gut or in other tissues *in vivo*[570], for example receptor expression[270]. Further, depending on the method used for *in vitro*-generation of BMDCs, cells may comprise different cell types and cell surface markers, as reported recently[570,603]. Although we observed no immunomodulatory effects on BMDCs by purified levan, we cannot rule out that levan does not interact with (i) other immune cells or (ii) other receptors not present on *in vitro*-generated BMDCs that may be present on gut immune cells *in vivo*.

In contrast to invasive microbial pathogens that penetrate the mucus layer and can reach the epithelium, commensal bacteria are generally confined to the lumen or mucus layer[184,462]. A growing body of literature describes a role for commensal microbes in intestinal immune homeostasis[462,604], particularly it has been shown that

gut commensal-derived molecules are involved in immune regulation in the gut, for example, through production of SCFAs[20,261,604]. However, the role of commensal-derived PS in intestinal immune regulation is less understood[24]. Many commensal bacteria produce EPS, which is gaining more attention due to reports of their immunomodulatory properties[1,81,83]. For example, Sims and colleagues (2012) found that colonisation of of *L. reuteri* 100-23 mutant strains (incapable of producing EPS levan) induce significantly lower Foxp3 T reg cell numbers in the spleen compared to WT strains, suggesting that levan production was responsible for this immunomodulatory activity[91]. It may also be that EPS modulate cytokine production. For example, a mutant strain of *B. longum* (incapable of EPS production) was shown to have significantly larger effects on the production of proinflammatory cytokines by human PMBCs than the *B. longum* 35624 WT strain (capable of producing EPS) *in vitro*/*ex vivo*. Further, addition of *B. longum* EPS to mutant strains incubated with PBMCs significantly reduced IFN-γ and IL-12 production compared to the same bacteria not supplemented with EPS[605]. In line with this, it has also been shown that EPS isolated from *L. johnsonii* induced production of IL-12 as well as IL-10 in BMDCs[606]. Moreover, induction of cytokines in RAW 264.7 cells including TNF-α and IL-6 by EPS from probiotic-associated strains *L. paracasei* and *L. plantarum* has also been reported[607]. The mechanisms for these effects may involve PRRs including TLRs as shown in the examples below. Danne and colleagues (2017) reported that a crude PS isolated from the culture supernatants of *Helicobacter hepaticus* (a non-pathogenic bacterium in WT mice under steady state conditions) induced IL-10 production in BMMs *in vitro* in a Myd88 (an important adapter molecule for TLR signalling[608]) and TLR2-dependent manner[475]. Further, zwitterionic CPS PSA from gut commensal *B. fragilis* induced TNF-α and IL-12p40 production by BMDCs through TLR2, and induced IL-8 production by HEK293 cells expressing TLR2 *in vitro*[609]. Further, Round and colleagues (2011) showed that PSA from *B. fragilis* induced IL-10 production both in BMDCs (*in vitro)* and isolated CD4+ T cells (*ex vivo*) in a TLR2-dependent manner[473]. Another study, *in vivo*, found that PSA administered orally to mice ameliorated experimentally induced colitis, however this effect was not observed in TLR2 KO mice[267]. Further, IL-10 expression was increased in the MLNs of WT mice fed PSA compared to PBS controls (and with experimentally-induced colitis) but this effect was absent in TLR2 KO mice; and IL-17 expression in the MLNs of TLR2 KO mice fed PSA also increased compared to PBS control but this effect was not observed in WT mice[267]. These studies suggest commensal PS may exert their immunomodulatory effects via TLR2 interaction in the gut.

We are only just beginning to address the role of dietary and commensal PS in the complex environment of the GI tract. Evidence clearly suggests that PS from food and commensal microbes possess immunomodulatory potential *in vitro* which may involve direct interaction with immune cell receptors; however, these interactions *in vivo* clearly require further research which will be important for unravelling the role of PS in GI health and disease in the exciting area of gut immunity.

References

1 Porter, N. T. & Martens, E. C. The Critical Roles of Polysaccharides in Gut Microbial Ecology and Physiology. *Annu. Rev. Microbiol.* **71**, 349-369 (2017).

2 Kamerling, J. Basics Concepts and Nomenclature Recommendations in Carbohydrate Chemistry. (2007).

3 Ramberg, J. E., Nelson, E. D. & Sinnott, R. A. Immunomodulatory dietary polysaccharides: a systematic review of the literature. *Nutr J* **9**, 1-22 (2010).

4 Ghazarian, H., Idoni, B. & Oppenheimer, S. B. A glycobiology review: carbohydrates, lectins and implications in cancer therapeutics. *Acta histochemica* **113**, 236-247 (2011).

5 van Kooyk, Y., Kalay, H. & Garcia-Vallejo, J. J. Analytical Tools for the Study of Cellular Glycosylation in the Immune System. *Frontiers in Immunology* **4**, 451 (2013).

6 Prestegard, J. H., Liu, J. & Widmalm, G. Oligosaccharides and Polysaccharides. (2017).

7 Cosgrove, D. J. Growth of the plant cell wall. *Nature Reviews Molecular Cell Biology* **6**, 850 (2005).

8 Makki, K., Deehan, E. C., Walter, J. & Backhed, F. The Impact of Dietary Fiber on Gut Microbiota in Host Health and Disease. *Cell Host Microbe* **23**, 705-715 (2018).

9 Zhou, J. Y., Oswald, D. M., Oliva, K. D., Kreisman, L. S. C. & Cobb, B. A. The Glycoscience of Immunity. *Trends Immunol.* **39**, 523-535 (2018).

10 Lovegrove, A., Edwards, C. H., De Noni, I., Patel, H., El, S. N., Grassby, T., Zielke, C., Ulmius, M., Nilsson, L., Butterworth, P. J., Ellis, P. R. & Shewry, P. R. Role of polysaccharides in food, digestion, and health. *Crit. Rev. Food Sci. Nutr.* **57**, 237-253 (2017).

11 Stephen, A. M., Champ, M. M. J., Cloran, S. J., Fleith, M., van Lieshout, L., Mejborn, H. & Burley, V. J. Dietary fibre in Europe: current state of knowledge on definitions, sources, recommendations, intakes and relationships to health. *Nutrition Research Reviews* **30**, 149-190 (2017).

12 Nie, Y., Lin, Q. & Luo, F. Effects of Non-Starch Polysaccharides on Inflammatory Bowel Disease. *International Journal of Molecular Sciences* **18**, 1372 (2017).

13 Fuller, S., Beck, E., Salman, H. & Tapsell, L. New Horizons for the Study of Dietary Fiber and Health: A Review. *Plant Foods for Human Nutrition* **71**, 1-12 (2016).

14 Thursby, E. & Juge, N. Introduction to the human gut microbiota. *Biochem. J.* **474**, 1823-1836 (2017).

15 Jones, J. M. CODEX-aligned dietary fiber definitions help to bridge the 'fiber gap'. *Nutrition Journal* **13**, 34 (2014).

16 Huang, T., Xu, M., Lee, A., Cho, S. & Qi, L. Consumption of whole grains and cereal fiber and total and cause-specific mortality: prospective analysis of 367,442 individuals. *BMC Medicine* **13**, 59 (2015).

17 Saeed, F., Pasha, I., Arshad, M. U., Muhammad Anjum, F., Hussain, S., Rasheed, R., Nasir, M. A. & Shafique, B. Physiological and Nutraceutical Perspectives of Fructan. *Int. J. Food Prop.* **18**, 1895-1904 (2015).

18 Wood, P. J. Cereal β-glucans in diet and health. *Journal of Cereal Science* **46**, 230-238 (2007).

19 Allaire, J. M., Crowley, S. M., Law, H. T., Chang, S. Y., Ko, H. J. & Vallance, B. A. The Intestinal Epithelium: Central Coordinator of Mucosal Immunity. *Trends Immunol.* **39**, 677-696 (2018).

20 Corrêa-Oliveira, R., Fachi, J. L., Vieira, A., Sato, F. T. & Vinolo, M. A. R. Regulation of immune cell function by short-chain fatty acids. *Clinical & Translational Immunology* **5**, e73 (2016).
21 Krumbeck, J. A., Maldonado-Gomez, M. X., Ramer-Tait, A. E. & Hutkins, R. W. Prebiotics and synbiotics: dietary strategies for improving gut health. *Current opinion in gastroenterology* **32**, 110-119 (2016).
22 Gibson, G. R., Hutkins, R., Sanders, M. E., Prescott, S. L., Reimer, R. A., Salminen, S. J., Scott, K., Stanton, C., Swanson, K. S., Cani, P. D., Verbeke, K. & Reid, G. Expert consensus document: The International Scientific Association for Probiotics and Prebiotics (ISAPP) consensus statement on the definition and scope of prebiotics. *Nature Reviews Gastroenterology &Amp; Hepatology* **14**, 491 (2017).
23 Shoaib, M., Shehzad, A., Omar, M., Rakha, A., Raza, H., Sharif, H. R., Shakeel, A., Ansari, A. & Niazi, S. Inulin: Properties, health benefits and food applications. *Carbohydrate Polymers* **147**, 444-454 (2016).
24 Patten, D. A. & Collett, A. Exploring the immunomodulatory potential of microbial-associated molecular patterns derived from the enteric bacterial microbiota. *Microbiology* **159**, 1535-1544 (2013).
25 Shih, I. L., Yu, Y. T., Shieh, C. J. & Hsieh, C. Y. selective production and characterization of levan by Bacillus subtilis (Natto) Takahashi. *J. Agric. Food Chem.* **53**, 8211-8215 (2005).
26 Xu, Q., Yajima, T., Li, W., Saito, K., Ohshima, Y. & Yoshikai, Y. Levan (beta-2, 6-fructan), a major fraction of fermented soybean mucilage, displays immunostimulating properties via Toll-like receptor 4 signalling: induction of interleukin-12 production and suppression of T-helper type 2 response and immunoglobulin E production. *Clin. Exp. Allergy* **36**, 94-101 (2006).
27 Stephen, A. M. & Phillips, G. O. *Food polysaccharides and their applications*. (CRC press, 2006).
28 Zhu, F., Du, B. & Xu, B. A critical review on production and industrial applications of beta-glucans. *Food Hydrocolloids* **52**, 275-288 (2016).
29 Regand, A., Chowdhury, Z., Tosh, S. M., Wolever, T. M. S. & Wood, P. The molecular weight, solubility and viscosity of oat beta-glucan affect human glycemic response by modifying starch digestibility. *Food Chem.* **129**, 297-304 (2011).
30 Burton, R. A. & Fincher, G. B. (1,3;1,4)-β-D-Glucans in Cell Walls of the Poaceae, Lower Plants, and Fungi: A Tale of Two Linkages. *Molecular Plant* **2**, 873-882 (2009).
31 Lei, N., Wang, M., Zhang, L., Xiao, S., Fei, C., Wang, X., Zhang, K., Zheng, W., Wang, C., Yang, R. & Xue, F. Effects of Low Molecular Weight Yeast β-Glucan on Antioxidant and Immunological Activities in Mice. *International Journal of Molecular Sciences* **16**, 21575-21590 (2015).
32 Giavasis, I. Bioactive fungal polysaccharides as potential functional ingredients in food and nutraceuticals. *Curr. Opin. Biotechnol.* **26**, 162-173 (2014).
33 Othman, R. A., Moghadasian, M. H. & Jones, P. J. Cholesterol-lowering effects of oat beta-glucan. *Nutr. Rev.* **69**, 299-309 (2011).
34 Scheller, H. V. & Ulvskov, P. Hemicelluloses. *Annu. Rev. Plant Biol.* **61**, 263-289 (2010).
35 Zabotina, O. A. Xyloglucan and Its Biosynthesis. *Frontiers in Plant Science* **3**, 134 (2012).
36 Kozioł, A., Cybulska, J., Pieczywek, P. M. & Zdunek, A. Evaluation of Structure and Assembly of Xyloglucan from Tamarind Seed (Tamarindus indica L.) with Atomic Force Microscopy. *Food Biophysics* **10**, 396-402 (2015).

37 Hayashi, T. & Kaida, R. Functions of Xyloglucan in Plant Cells. *Molecular Plant* **4**, 17-24 (2011).
38 Ozcan, E., Sun, J., Rowley, D. C. & Sela, D. A. A human gut commensal ferments cranberry carbohydrates to produce formate. *Appl. Environ. Microbiol.* (2017).
39 Nishinari, K., Takemasa, M., Osaka, J. H. Z. & Takahashi, R. 2.19 Storage Plant Polysaccharides: Xyloglucans, Galactomannans, Glucomannans. (2007).
40 Fry, S. C., Mohler, K. E., Nesselrode, B. H. W. A. & Franková, L. Mixed-linkage β-glucan : xyloglucan endotransglucosylase, a novel wall-remodelling enzyme from Equisetum (horsetails) and charophytic algae. *The Plant Journal* **55**, 240-252 (2008).
41 Qaisrani, T. B., Qaisrani, M. M. & Qaisrani, T. M. Arabinoxylans from psyllium husk: A review. *J. Environ. Agri. Sci* **6**, 33-39 (2016).
42 Gharibzahedi, S. M. T., Razavi, S. H. & Mousavi, S. M. Psyllium husk gum: An attractive carbohydrate biopolymer for the production of stable canthaxanthin emulsions. *Carbohydrate Polymers* **92**, 2002-2011 (2013).
43 Madgulkar, A. R., Rao, M. R. & Warrier, D. in *Polysaccharides* 1-17 (Springer, 2014).
44 Vega-Lopez, S., Freake, H. C. & Fernandez, M. L. Sex and hormonal status modulate the effects of psyllium on plasma lipids and monocyte gene expression in humans. *J. Nutr.* **133**, 67-70 (2003).
45 Tester, R. F. & Al-Ghazzewi, F. H. Mannans and health, with a special focus on glucomannans. *Food Res. Int.* **50**, 384-391 (2013).
46 Ishii, J., Okazaki, F., Djohan, A. C., Hara, K. Y., Asai-Nakashima, N., Teramura, H., Andriani, A., Tominaga, M., Wakai, S., Kahar, P., Yopi, Prasetya, B., Ogino, C. & Kondo, A. From mannan to bioethanol: cell surface co-display of β-mannanase and β-mannosidase on yeast Saccharomyces cerevisiae. *Biotechnology for Biofuels* **9**, 188 (2016).
47 Femenia, A., García-Pascual, P., Simal, S. & Rosselló, C. Effects of heat treatment and dehydration on bioactive polysaccharide acemannan and cell wall polymers from Aloe barbadensis Miller. *Carbohydrate Polymers* **51**, 397-405 (2003).
48 May, C. D. Industrial pectins: Sources, production and applications. *Carbohydrate Polymers* **12**, 79-99 (1990).
49 BAKER, R. A. Reassessment of Some Fruit and Vegetable Pectin Levels. *J. Food Sci.* **62**, 225-229 (1997).
50 Chapman, H. D., Morris, V. J., Selvendran, R. R. & O'Neill, M. A. Static and dynamic light-scattering studies of pectic polysaccharides from the middle lamellae and primary cell walls of cider apples. *Carbohydrate Research* **165**, 53-68 (1987).
51 Mohnen, D. Pectin structure and biosynthesis. *Curr. Opin. Plant Biol.* **11**, 266-277 (2008).
52 Naqash, F., Masoodi, F. A., Rather, S. A., Wani, S. M. & Gani, A. Emerging concepts in the nutraceutical and functional properties of pectin—A Review. *Carbohydrate Polymers* **168**, 227-239 (2017).
53 Atmodjo, M. A., Hao, Z. & Mohnen, D. Evolving views of pectin biosynthesis. *Annu. Rev. Plant Biol.* **64**, 747-779 (2013).
54 Bergman, M., Djaldetti, M., Salman, H. & Bessler, H. Effect of citrus pectin on malignant cell proliferation. *Biomedicine & pharmacotherapy = Biomedecine & pharmacotherapie* **64**, 44-47 (2010).
55 Liu, Y., Dong, M., Yang, Z. & Pan, S. Anti-diabetic effect of citrus pectin in diabetic rats and potential mechanism via PI3K/Akt signaling pathway. *International Journal of Biological Macromolecules* **89**, 484-488 (2016).

56 Mortensen, A., Aguilar, F., Crebelli, R., Di Domenico, A., Frutos, M. J., Galtier, P., Gott, D., Gundert-Remy, U., Lambré, C., Leblanc, J.-C., Lindtner, O., Moldeus, P., Mosesso, P., Oskarsson, A., Parent-Massin, D., Stankovic, I., Waalkens-Berendsen, I., Woutersen, R. A., Wright, M., Younes, M., Brimer, L., Peters, P., Wiesner, J., Christodoulidou, A., Lodi, F., Tard, A. & Dusemund, B. Re-evaluation of karaya gum (E 416) as a food additive. *EFSA Journal* **14**, e04598 (2016).

57 Stevens, B. J. H. & Selvendran, R. R. Structural investigation of an arabinan from cabbage (Brassica oleracea var. capitata). *Phytochemistry* **19**, 559-561 (1980).

58 Li, B., Lu, F., Wei, X. & Zhao, R. Fucoidan: Structure and Bioactivity. *Molecules (Basel, Switzerland)* **13**, 1671 (2008).

59 Ale, M. T., Mikkelsen, J. D. & Meyer, A. S. Important Determinants for Fucoidan Bioactivity: A Critical Review of Structure-Function Relations and Extraction Methods for Fucose-Containing Sulfated Polysaccharides from Brown Seaweeds. *Mar. Drugs* **9**, 2106 (2011).

60 Fitton, J., Stringer, D. & Karpiniec, S. Therapies from Fucoidan: An Update. *Mar. Drugs* **13**, 5920 (2015).

61 Peukert, M., Thiel, J., Mock, H.-P., Marko, D., Weschke, W. & Matros, A. Spatiotemporal Dynamics of Oligofructan Metabolism and Suggested Functions in Developing Cereal Grains. *Frontiers in Plant Science* **6** (2016).

62 Apolinário, A. C., de Lima Damasceno, B. P. G., de Macêdo Beltrão, N. E., Pessoa, A., Converti, A. & da Silva, J. A. Inulin-type fructans: a review on different aspects of biochemical and pharmaceutical technology. *Carbohydrate polymers* **101**, 368-378 (2014).

63 Saarela, M. *Functional foods: Concept to product*. (Elsevier, 2011).

64 Cimini, S., Locato, V., Vergauwen, R., Paradiso, A., Cecchini, C., Vandenpoel, L., Verspreet, J., Courtin, C. M., D'Egidio, M. G., Van den Ende, W. & De Gara, L. Fructan biosynthesis and degradation as part of plant metabolism controlling sugar fluxes during durum wheat kernel maturation. *Frontiers in Plant Science* **6**, 89 (2015).

65 Versluys, M., Tarkowski, Ł. P. & Van den Ende, W. Fructans as DAMPs or MAMPs: evolutionary prospects, cross-tolerance, and multistress resistance potential. *Frontiers in plant science* **7**, 2061 (2017).

66 Livingston, D. P., Hincha, D. K. & Heyer, A. G. Fructan and its relationship to abiotic stress tolerance in plants. *Cell. Mol. Life Sci.* **66**, 2007-2023 (2009).

67 Baumgartner, S., Dax, T. G., Praznik, W. & Falk, H. Characterisation of the high-molecular weight fructan isolated from garlic (Allium sativum L.). *Carbohydrate research* **328**, 177-183 (2000).

68 Kawakami, A. & Yoshida, M. Fructan:fructan 1-fructosyltransferase, a key enzyme for biosynthesis of graminan oligomers in hardened wheat. *Planta* **223**, 90 (2005).

69 Van den Ende, W., Coopman, M., Clerens, S., Vergauwen, R., Le Roy, K., Lammens, W. & Van Laere, A. Unexpected Presence of Graminan- and Levan-Type Fructans in the Evergreen Frost-Hardy Eudicot Pachysandra terminalis (Buxaceae): Purification, Cloning, and Functional Analysis of a 6-SST/6-SFT Enzyme. *Plant Physiol.* **155**, 603-614 (2011).

70 Dong, C.-X., Zhang, L.-J., Xu, R., Zhang, G., Zhou, Y.-B., Han, X.-Q., Zhang, Y. & Sun, Y.-X. Structural characterization and immunostimulating activity of a levan-type fructan from Curcuma kwangsiensis. *International Journal of Biological Macromolecules* **77**, 99-104 (2015).

71 Srikanth, R., Reddy, C. H. S., Siddartha, G., Ramaiah, M. J. & Uppuluri, K. B. Review on production, characterization and applications of microbial levan. *Carbohydrate polymers* **120**, 102-114 (2015).

72 Öner, E. T., Hernández, L. & Combie, J. Review of Levan polysaccharide: From a century of past experiences to future prospects. *Biotechnol. Adv.* **34**, 827-844 (2016).
73 Gupta, S., Das, P., Singh, S., Akhtar, M., Meena, D. & Mandal, S. Microbial levari, an ideal prebiotic and immunonutrient in aquaculture. *World Aquacult.* **42**, 61 (2011).
74 Vogt, L., Meyer, D., Pullens, G., Faas, M., Smelt, M., Venema, K., Ramasamy, U., Schols, H. A. & De Vos, P. Immunological properties of inulin-type fructans. *Crit. Rev. Food Sci. Nutr.* **55**, 414-436 (2015).
75 Delattre, C., Fenoradosoa, T. A. & Michaud, P. Galactans: an overview of their most important sourcing and applications as natural polysaccharides. *Brazilian Archives of Biology and Technology* **54**, 1075-1092 (2011).
76 Chavan, R. R., Fahey, L. M. & Harris, P. J. Quantification of (1→4)-β-d-Galactans in Compression Wood Using an Immuno-Dot Assay. *Plants* **4**, 29-43 (2015).
77 Wijesekara, I., Pangestuti, R. & Kim, S.-K. Biological activities and potential health benefits of sulfated polysaccharides derived from marine algae. *Carbohydrate polymers* **84**, 14-21 (2011).
78 Cress, B. F., Englaender, J. A., He, W., Kasper, D., Linhardt, R. J. & Koffas, M. A. Masquerading microbial pathogens: capsular polysaccharides mimic host-tissue molecules. *FEMS Microbiol. Rev.* **38**, 660-697 (2014).
79 Ahmad, N. H., Mustafa, S. & Che Man, Y. B. Microbial Polysaccharides and Their Modification Approaches: A Review. *Int. J. Food Prop.* **18**, 332-347 (2015).
80 Neff, C. P., Rhodes, M. E., Arnolds, K. L., Collins, C. B., Donnelly, J., Nusbacher, N., Jedlicka, P., Schneider, J. M., McCarter, M. D., Shaffer, M., Mazmanian, S. K., Palmer, B. E. & Lozupone, C. A. Diverse intestinal bacteria contain putative zwitterionic capsular polysaccharides with anti-inflammatory properties. *Cell host & microbe* **20**, 535-547 (2016).
81 Castro-Bravo, N., Wells, J. M., Margolles, A. & Ruas-Madiedo, P. Interactions of Surface Exopolysaccharides From Bifidobacterium and Lactobacillus Within the Intestinal Environment. *Frontiers in Microbiology* **9** (2018).
82 Maldonado, R. F., Sá-Correia, I. & Valvano, M. A. Lipopolysaccharide modification in Gram-negative bacteria during chronic infection. *FEMS Microbiol. Rev.* **40**, 480-493 (2016).
83 Laino, J., Villena, J., Kanmani, P. & Kitazawa, H. Immunoregulatory Effects Triggered by Lactic Acid Bacteria Exopolysaccharides: New Insights into Molecular Interactions with Host Cells. *Microorganisms* **4** (2016).
84 Yildiz, H. & Karatas, N. Microbial exopolysaccharides: Resources and bioactive properties. *Process Biochem.* **72**, 41-46 (2018).
85 Freitas, F., Alves, V. D. & Reis, M. A. M. Advances in bacterial exopolysaccharides: from production to biotechnological applications. *Trends Biotechnol.* **29**, 388-398 (2011).
86 K.R, S. & V, P. Review on production, downstream processing and characterization of microbial pullulan. *Carbohydrate Polymers* **173**, 573-591 (2017).
87 Dionísio, M., Braz, L., Corvo, M., Lourenço, J. P., Grenha, A. & Rosa da Costa, A. M. Charged pullulan derivatives for the development of nanocarriers by polyelectrolyte complexation. *International Journal of Biological Macromolecules* **86**, 129-138 (2016).
88 Osmałek, T., Froelich, A. & Tasarek, S. Application of gellan gum in pharmacy and medicine. *Int. J. Pharm.* **466**, 328-340 (2014).
89 Dhaneshwar, S. S., Mini, K., Gairola, N. & Kadam, S. Dextran: A promising macromolecular drug carrier. *Indian journal of pharmaceutical sciences* **68**, 705 (2006).

90 Runyon, J. R., Nilsson, L., Ulmius, M., Castro, A., Ionescu, R., Andersson, C. & Schmidt, C. Characterizing changes in levan physicochemical properties in different pH environments using asymmetric flow field-flow fractionation. *Anal. Bioanal. Chem.* **406**, 1597-1605 (2014).
91 Sims, I. M., Frese, S. A., Walter, J., Loach, D., Wilson, M., Appleyard, K., Eason, J., Livingston, M., Baird, M., Cook, G. & Tannock, G. W. Structure and functions of exopolysaccharide produced by gut commensal Lactobacillus reuteri 100-23. *The ISME journal* **5**, 1115-1124 (2011).
92 Cuskin, F., Flint, J. E., Gloster, T. M., Morland, C., Baslé, A., Henrissat, B., Coutinho, P. M., Strazzulli, A., Solovyova, A. S. & Davies, G. J. How nature can exploit nonspecific catalytic and carbohydrate binding modules to create enzymatic specificity. *Proceedings of the National Academy of Sciences* **109**, 20889-20894 (2012).
93 Feng, J., Gu, Y., Quan, Y., Zhang, W., Cao, M., Gao, W., Song, C., Yang, C. & Wang, S. Recruiting a new strategy to improve levan production in Bacillus amyloliquefaciens. *Scientific Reports* **5**, 13814 (2015).
94 Han, J., Xu, X., Gao, C., Liu, Z. & Wu, Z. Levan-Producing Leuconostoc citreum Strain BD1707 and Its Growth in Tomato Juice Supplemented with Sucrose. *Appl. Environ. Microbiol.* **82**, 1383-1390 (2016).
95 Calazans, G. c. M. T., Lima, R. C., de França, F. P. & Lopes, C. E. Molecular weight and antitumour activity of Zymomonas mobilis levans. *International Journal of Biological Macromolecules* **27**, 245-247 (2000).
96 Laue, H., Schenk, A., Li, H., Lambertsen, L., Neu, T. R., Molin, S. & Ullrich, M. S. Contribution of alginate and levan production to biofilm formation by Pseudomonas syringae. *Microbiology* **152**, 2909-2918 (2006).
97 Keith, J., Wiley, B., Ball, D., Arcidiacono, S., Zorfass, D., Mayer, J. & Kaplan, D. Continuous culture system for production of biopolymer levan using erwinia herbicola. *Biotechnol. Bioeng.* **38**, 557-560 (1991).
98 KOJIMA, I., SAITO, T., IIZUKA, M., MINAMIURA, N. & ONO, S. Characterization of Levan Produced by Serratia sp. *J. Ferment. Bioeng.* **75**, 9-12 (1993).
99 Franken, J., Brandt, B. A., Tai, S. L. & Bauer, F. F. Biosynthesis of levan, a bacterial extracellular polysaccharide, in the yeast Saccharomyces cerevisiae. *PLoS One* **8**, e77499 (2013).
100 Yoon, E. J., Yoo, S.-H., Cha, J. & Gyu Lee, H. Effect of levan's branching structure on antitumor activity. *International Journal of Biological Macromolecules* **34**, 191-194 (2004).
101 Oh, I.-K., Yoo, S.-H., Bae, I.-Y., Cha, J.-H. & Lee, H.-G. Effects of Microbacterium laevaniformans Levans molecular weight on cytotoxicity. *Journal of microbiology and biotechnology* **14**, 985-990 (2004).
102 Jakob, F., Pfaff, A., Novoa-Carballal, R., Rubsam, H., Becker, T. & Vogel, R. F. Structural analysis of fructans produced by acetic acid bacteria reveals a relation to hydrocolloid function. *Carbohydr Polym* **92**, 1234-1242 (2013).
103 Shih, I.-L., Chen, L.-D., Wang, T.-C., Wu, J.-Y. & Liaw, K.-S. Tandem production of levan and ethanol by microbial fermentation. *Green Chemistry* **12**, 1242-1247 (2010).
104 Dos Santos, L. F., Martins Paiva, W., Borsato, D., MDL, C. C. D. S. & Celligoi, P. C. Characterization and optimization of levan production by Bacillus subtilis NATTO. *Rom Biotechnol Lett* **18**, 8413-8422 (2013).
105 Raga-Carbajal, E., Carrillo-Nava, E., Costas, M., Porras-Dominguez, J., López-Munguía, A. & Olvera, C. Size product modulation by enzyme concentration reveals two distinct levan elongation mechanisms in Bacillus subtilis levansucrase. *Glycobiology* **26**, 377-385 (2016).

106 Visnapuu, T., Mardo, K. & Alamäe, T. Levansucrases of a Pseudomonas syringae pathovar as catalysts for the synthesis of potentially prebiotic oligo- and polysaccharides. *New Biotechnology* **32**, 597-605 (2015).
107 Bondarenko, O. M., Ivask, A., Kahru, A., Vija, H., Titma, T., Visnapuu, M., Joost, U., Pudova, K., Adamberg, S., Visnapuu, T. & Alamäe, T. Bacterial polysaccharide levan as stabilizing, non-toxic and functional coating material for microelement-nanoparticles. *Carbohydrate Polymers* **136**, 710-720 (2016).
108 Jakob, F., Steger, S. & Vogel, R. F. Influence of novel fructans produced by selected acetic acid bacteria on the volume and texture of wheat breads. *Eur. Food Res. Technol.* **234**, 493-499 (2012).
109 Byun, B. Y., Lee, S.-J. & Mah, J.-H. Antipathogenic activity and preservative effect of levan (β-2,6-fructan), a multifunctional polysaccharide. *Int. J. Food Sci. Tech.* **49**, 238-245 (2014).
110 Sezer, A. D., Kazak Sarılmışer, H., Rayaman, E., Çevikbaş, A., Öner, E. T. & Akbuğa, J. Development and characterization of vancomycin-loaded levan-based microparticular system for drug delivery. *Pharm. Dev. Technol.* **22**, 627-634 (2017).
111 Dahech, I., Belghith, K. S., Hamden, K., Feki, A., Belghith, H. & Mejdoub, H. Oral administration of levan polysaccharide reduces the alloxan-induced oxidative stress in rats. *Int J Biol Macromol* **49**, 942-947 (2011).
112 Kang, S.-A., Hong, K.-H., Jang, K.-H., Kim, S.-H., Lee, K.-H., Chang, B.-I., Kim, C.-H. & Choue, R.-W. Anti-obesity and hypolipidemic effects of dietary levan in high fat diet-induced obese rats. *Journal of microbiology and biotechnology* **14**, 796-804 (2004).
113 Adamberg, K., Tomson, K., Talve, T., Pudova, K., Puurand, M., Visnapuu, T., Alamäe, T. & Adamberg, S. Levan Enhances Associated Growth of Bacteroides, Escherichia, Streptococcus and Faecalibacterium in Fecal Microbiota. *PLOS ONE* **10**, e0144042 (2015).
114 Arrizon, J., Hernández-Moedano, A., Oner, E. T. & González-Avila, M. In vitro prebiotic activity of fructans with different fructosyl linkage for symbiotics elaboration. *International Journal of Probiotics & Prebiotics* **9**, 69 (2014).
115 Sonnenburg, E. D., Zheng, H., Joglekar, P., Higginbottom, S. K., Firbank, S. J., Bolam, D. N. & Sonnenburg, J. L. Specificity of Polysaccharide Use in Intestinal Bacteroides Species Determines Diet-Induced Microbiota Alterations. *Cell* **141**, 1241-1252 (2010).
116 Adnan, H. A., Jabbar, F. & Mahdi, S. Bioactivity of Bacillus Species Isolated from Human Feces. *JURNAL OF MADENAT ALELEM COLLEGE* **4**, 50-61 (2012).
117 Erwig, L. P. & Gow, N. A. R. Interactions of fungal pathogens with phagocytes. *Nature Reviews Microbiology* **14**, 163 (2016).
118 Marakalala, M. J. & Ndlovu, H. Signaling C-type lectin receptors in antimycobacterial immunity. *PLoS Path.* **13**, e1006333 (2017).
119 Ma, L., Chen, Z., Huang, D. W., Kutty, G., Ishihara, M., Wang, H., Abouelleil, A., Bishop, L., Davey, E., Deng, R., Deng, X., Fan, L., Fantoni, G., Fitzgerald, M., Gogineni, E., Goldberg, J. M., Handley, G., Hu, X., Huber, C., Jiao, X., Jones, K., Levin, J. Z., Liu, Y., Macdonald, P., Melnikov, A., Raley, C., Sassi, M., Sherman, B. T., Song, X., Sykes, S., Tran, B., Walsh, L., Xia, Y., Yang, J., Young, S., Zeng, Q., Zheng, X., Stephens, R., Nusbaum, C., Birren, B. W., Azadi, P., Lempicki, R. A., Cuomo, C. A. & Kovacs, J. A. Genome analysis of three Pneumocystis species reveals adaptation mechanisms to life exclusively in mammalian hosts. *Nature Communications* **7**, 10740 (2016).
120 Saijo, S., Ikeda, S., Yamabe, K., Kakuta, S., Ishigame, H., Akitsu, A., Fujikado, N., Kusaka, T., Kubo, S., Chung, S.-h., Komatsu, R., Miura, N., Adachi, Y., Ohno, N., Shibuya, K., Yamamoto, N., Kawakami, K., Yamasaki,

S., Saito, T., Akira, S. & Iwakura, Y. Dectin-2 Recognition of α-Mannans and Induction of Th17 Cell Differentiation Is Essential for Host Defense against Candida albicans. *Immunity* **32**, 681-691 (2010).

121 Yonekawa, A., Saijo, S., Hoshino, Y., Miyake, Y., Ishikawa, E., Suzukawa, M., Inoue, H., Tanaka, M., Yoneyama, M. & Oh-hora, M. Dectin-2 is a direct receptor for mannose-capped lipoarabinomannan of mycobacteria. *Immunity* **41**, 402-413 (2014).

122 Horwath, M. C., Fecher, R. A. & Deepe, G. S. Histoplasma capsulatum, lung infection and immunity. *Future microbiology* **10**, 967-975 (2015).

123 Zhang, M. X., Brandhorst, T. T., Kozel, T. R. & Klein, B. S. Role of Glucan and Surface Protein BAD1 in Complement Activation by Blastomyces dermatitidisYeast. *Infect. Immun.* **69**, 7559-7564 (2001).

124 Rappleye, C. A., Eissenberg, L. G. & Goldman, W. E. Histoplasma capsulatum [alpha]-(1,3)-glucan blocks innate immune recognition by the [beta]-glucan receptor. *Proc. Natl Acad. Sci. USA* **104**, 1366-1370 (2007).

125 Mahla, R., Reddy, C., Prasad, D. & Kumar, H. Sweeten PAMPs: Role of sugar complexed PAMPs in innate immunity and vaccine biology. *Frontiers in Immunology* **4** (2013).

126 Plato, A., Hardison, S. E. & Brown, G. D. Pattern recognition receptors in antifungal immunity. *Seminars in Immunopathology* **37**, 97-106 (2015).

127 Viñarta, S. C., Molina, O. E., Figueroa, L. I. C. & Fariña, J. I. A further insight into the practical applications of exopolysaccharides from Sclerotium rolfsii. *Food Hydrocolloids* **20**, 619-629 (2006).

128 Castillo, N. A., Valdez, A. L. & Fariña, J. I. Microbial production of scleroglucan and downstream processing. *Frontiers in microbiology* **6** (2015).

129 Punja, Z. & Damiani, A. Comparative growth, morphology, and physiology of three Sclerotium species. *Mycologia*, 694-706 (1996).

130 Farina, J. I., Vinarta, S. C., Cattaneo, M. & Figueroa, L. I. Structural stability of Sclerotium rolfsii ATCC 201126 beta-glucan with fermentation time: a chemical, infrared spectroscopic and enzymatic approach. *J. Appl. Microbiol.* **106**, 221-232 (2009).

131 Steimle, A., Autenrieth, I. B. & Frick, J. S. Structure and function: Lipid A modifications in commensals and pathogens. *Int. J. Med. Microbiol.* **306**, 290-301 (2016).

132 Ranf, S. Immune Sensing of Lipopolysaccharide in Plants and Animals: Same but Different. *PLoS Path.* **12**, e1005596 (2016).

133 Berry, M. C., McGhee, G. C., Zhao, Y. & Sundin, G. W. Effect of a waaL mutation on lipopolysaccharide composition, oxidative stress survival, and virulence in Erwinia amylovora. *FEMS Microbiol. Lett.* **291**, 80-87 (2009).

134 Bertsche, U., Mayer, C., Götz, F. & Gust, A. A. Peptidoglycan perception—Sensing bacteria by their common envelope structure. *Int. J. Med. Microbiol.* **305**, 217-223 (2015).

135 Hsu, Y. P., Meng, X. & VanNieuwenhze, M. S. in *Methods in Microbiology* Vol. 43 (eds Colin Harwood & Grant J. Jensen) 3-48 (Academic Press, 2016).

136 Jennings, H. J., Bhauacharjee, A. K., Bundle, D. R., Paul Kenny, C., Martin, A. & Smith, I. C. P. Structures of the Capsular Polysaccharides of Neisseria meningitidis as Determined by 13C-Nuclear Magnetic Resonance Spectroscopy. *The Journal of Infectious Diseases* **136**, S78-S83 (1977).

137 Willis, L. M. & Whitfield, C. Structure, biosynthesis, and function of bacterial capsular polysaccharides synthesized by ABC transporter-dependent pathways. *Carbohydr Res* **378**, 35-44 (2013).

138 Crisel, R., Baker, R. S. & Dorman, D. E. Capsular polymer of Haemophilus influenzae, type b. I. Structural characterization of the capsular polymer of strain Eagan. *J. Biol. Chem.* **250**, 4926-4930 (1975).

139 Lobo, L. A., Benjamim, C. F. & Oliveira, A. C. The interplay between microbiota and inflammation: lessons from peritonitis and sepsis. *Clin Transl Immunology* **5**, e90 (2016).
140 Coyne, M. J., Weinacht, K. G., Krinos, C. M. & Comstock, L. E. Mpi recombinase globally modulates the surface architecture of a human commensal bacterium. *Proceedings of the National Academy of Sciences of the United States of America* **100**, 10446-10451 (2003).
141 Bloem, K., Garcia-Vallejo, J. J., Vuist, I. M., Cobb, B. A., van Vliet, S. J. & van Kooyk, Y. Interaction of the Capsular Polysaccharide A from Bacteroides fragilis with DC-SIGN on Human Dendritic Cells is Necessary for Its Processing and Presentation to T Cells. *Front Immunol* **4**, 103 (2013).
142 Tzianabos, A. O., Pantosti, A., Baumann, H., Brisson, J. R., Jennings, H. J. & Kasper, D. L. The capsular polysaccharide of Bacteroides fragilis comprises two ionically linked polysaccharides. *J. Biol. Chem.* **267**, 18230-18235 (1992).
143 Stier, H., Ebbeskotte, V. & Gruenwald, J. Immune-modulatory effects of dietary Yeast Beta-1,3/1,6-D-glucan. *Nutrition Journal* **13**, 38-38 (2014).
144 Schnaar, R. L. & Freeze, H. H. A "glyconutrient sham". *Glycobiology* **18**, 652-657 (2008).
145 Stier, H., Ebbeskotte, V. & Gruenwald, J. Immune-modulatory effects of dietary Yeast Beta-1, 3/1, 6-D-glucan. *Nutrition journal* **13**, 38 (2014).
146 McElhaney, J. E., Goel, V., Toane, B., Hooten, J. & Shan, J. J. Efficacy of COLD-fX in the prevention of respiratory symptoms in community-dwelling adults: a randomized, double-blinded, placebo controlled trial. *Journal of Alternative & Complementary Medicine* **12**, 153-157 (2006).
147 Udani, J. K. Immunomodulatory effects of ResistAid™: A randomized, double-blind, placebo-controlled, multidose study. *Journal of the American College of Nutrition* **32**, 331-338 (2013).
148 Fuller, R., Moore, M. V., Lewith, G., Stuart, B. L., Ormiston, R. V., Fisk, H. L., Noakes, P. S. & Calder, P. C. Yeast-derived β-1,3/1,6 glucan, upper respiratory tract infection and innate immunity in older adults. *Nutrition* **39-40**, 30-35 (2017).
149 Rincão, V. P., Yamamoto, K. A., Silva Ricardo, N. M. P., Soares, S. A., Paccola Meirelles, L. D., Nozawa, C. & Carvalho Linhares, R. E. Polysaccharide and extracts from Lentinula edodes: structural features and antiviral activity. *Virology Journal* **9**, 37-37 (2012).
150 Dai, X., Stanilka, J. M., Rowe, C. A., Esteves, E. A., Nieves, C., Spaiser, S. J., Christman, M. C., Langkamp-Henken, B. & Percival, S. S. Consuming Lentinula edodes (Shiitake) Mushrooms Daily Improves Human Immunity: A Randomized Dietary Intervention in Healthy Young Adults. *Journal of the American College of Nutrition* **34**, 478-487 (2015).
151 Ji, L., Jie, Z., Ying, X., Yue, Q., Zhou, Y. & Sun, L. Structural characterization of alkali-soluble polysaccharides from Panax ginseng C. A. Meyer. *Royal Society Open Science* **5** (2018).
152 Cho, Y.-J., Son, H.-J. & Kim, K.-S. A 14-week randomized, placebo-controlled, double-blind clinical trial to evaluate the efficacy and safety of ginseng polysaccharide (Y-75). *Journal of Translational Medicine* **12**, 283 (2014).
153 Clarke, S. T., Green-Johnson, J. M., Brooks, S. P. J., Ramdath, D. D., Bercik, P., Avila, C., Inglis, G. D., Green, J., Yanke, L. J., Selinger, L. B. & Kalmokoff, M. β2-1 Fructan supplementation alters host immune responses in a manner consistent with increased exposure to microbial components: results from a double-blinded, randomised, cross-over study in healthy adults. *British Journal of Nutrition* **115**, 1748-1759 (2016).

154 Dehghan, P., Farhangi, M. A., Tavakoli, F., Aliasgarzadeh, A. & Akbari, A. M. Impact of prebiotic supplementation on T-cell subsets and their related cytokines, anthropometric features and blood pressure in patients with type 2 diabetes mellitus: A randomized placebo-controlled Trial. *Complementary Therapies in Medicine* **24**, 96-102 (2016).
155 Samuelsen, A. B. C., Schrezenmeir, J. & Knutsen, S. H. Effects of orally administered yeast-derived beta-glucans: A review. *Mol. Nutr. Food Res.* **58**, 183-193 (2014).
156 Martel, J., Ko, Y.-F., Ojcius, D. M., Lu, C.-C., Chang, C.-J., Lin, C.-S., Lai, H.-C. & Young, J. D. Immunomodulatory Properties of Plants and Mushrooms. *Trends Pharmacol. Sci.* **38**, 967-981 (2017).
157 Franco-Robles, E. & López, M. G. Implication of Fructans in Health: Immunomodulatory and Antioxidant Mechanisms. *The Scientific World Journal* **2015**, 289267 (2015).
158 Peshev, D. & Van den Ende, W. Fructans: Prebiotics and immunomodulators. *Journal of Functional Foods* **8**, 348-357 (2014).
159 Lecerf, J.-M., Dépeint, F., Clerc, E., Dugenet, Y., Niamba, C. N., Rhazi, L., Cayzeele, A., Abdelnour, G., Jaruga, A., Younes, H., Jacobs, H., Lambrey, G., Abdelnour, A. M. & Pouillart, P. R. Xylo-oligosaccharide (XOS) in combination with inulin modulates both the intestinal environment and immune status in healthy subjects, while XOS alone only shows prebiotic properties. *British Journal of Nutrition* **108**, 1847-1858 (2012).
160 Dehghan, P., Pourghassem Gargari, B. & Asghari Jafar-abadi, M. Oligofructose-enriched inulin improves some inflammatory markers and metabolic endotoxemia in women with type 2 diabetes mellitus: A randomized controlled clinical trial. *Nutrition* **30**, 418-423 (2014).
161 Fernandes, R., do Rosario, V. A., Mocellin, M. C., Kuntz, M. G. F. & Trindade, E. B. S. M. Effects of inulin-type fructans, galacto-oligosaccharides and related synbiotics on inflammatory markers in adult patients with overweight or obesity: A systematic review. *Clin. Nutr.* **36**, 1197-1206 (2017).
162 Ferreira, S. S., Passos, C. P., Madureira, P., Vilanova, M. & Coimbra, M. A. Structure–function relationships of immunostimulatory polysaccharides: A review. *Carbohydrate Polymers* **132**, 378-396 (2015).
163 Niv, E., Shapira, Y., Akiva, I., Rokhkind, E., Naor, E., Arbiv, M. & Vaisman, N. Effect of levan supplement in orange juice on weight, gastrointestinal symptoms and metabolic profile of healthy subjects: results of an 8-week clinical trial. *Nutrients* **4**, 638-647 (2012).
164 Welcome, M. O. in *Gastrointestinal Physiology: Development, Principles and Mechanisms of Regulation* 53-106 (Springer International Publishing, 2018).
165 Mowat, A. M. & Agace, W. W. Regional specialization within the intestinal immune system. *Nature Reviews Immunology* **14**, 667 (2014).
166 Martins dos Santos, V., Müller, M. & de Vos, W. M. Systems biology of the gut: the interplay of food, microbiota and host at the mucosal interface. *Curr. Opin. Biotechnol.* **21**, 539-550 (2010).
167 Iliev, I. D. Dectin-1 exerts dual control in the gut. *Cell host & microbe* **18**, 139-141 (2015).
168 Oh, J., Byrd, Allyson L., Park, M., Kong, Heidi H. & Segre, Julia A. Temporal Stability of the Human Skin Microbiome. *Cell* **165**, 854-866 (2016).
169 Huffnagle, G. B., Dickson, R. P. & Lukacs, N. W. The respiratory tract microbiome and lung inflammation: a two-way street. *Mucosal Immunol* **10**, 299-306 (2017).
170 Gottschick, C., Deng, Z.-L., Vital, M., Masur, C., Abels, C., Pieper, D. H. & Wagner-Döbler, I. The urinary microbiota of men and women and its changes

in women during bacterial vaginosis and antibiotic treatment. *Microbiome* **5**, 99 (2017).

171 Valdes, A. M., Walter, J., Segal, E. & Spector, T. D. Role of the gut microbiota in nutrition and health. *BMJ* **361** (2018).

172 Sender, R., Fuchs, S. & Milo, R. Revised Estimates for the Number of Human and Bacteria Cells in the Body. *PLoS Biol.* **14**, e1002533 (2016).

173 Young, V. B. The role of the microbiome in human health and disease: an introduction for clinicians. *BMJ* **356** (2017).

174 The Human Microbiome Project, C., Huttenhower, C., Gevers, D., Knight, R., Abubucker, S., Badger, J. H., Chinwalla, A. T., Creasy, H. H., Earl, A. M., FitzGerald, M. G., Fulton, R. S., Giglio, M. G., Hallsworth-Pepin, K., Lobos, E. A., Madupu, R., Magrini, V., Martin, J. C., Mitreva, M., Muzny, D. M., Sodergren, E. J., Versalovic, J., Wollam, A. M., Worley, K. C., Wortman, J. R., Young, S. K., Zeng, Q., Aagaard, K. M., Abolude, O. O., Allen-Vercoe, E., Alm, E. J., Alvarado, L., Andersen, G. L., Anderson, S., Appelbaum, E., Arachchi, H. M., Armitage, G., Arze, C. A., Ayvaz, T., Baker, C. C., Begg, L., Belachew, T., Bhonagiri, V., Bihan, M., Blaser, M. J., Bloom, T., Bonazzi, V., Paul Brooks, J., Buck, G. A., Buhay, C. J., Busam, D. A., Campbell, J. L., Canon, S. R., Cantarel, B. L., Chain, P. S. G., Chen, I. M. A., Chen, L., Chhibba, S., Chu, K., Ciulla, D. M., Clemente, J. C., Clifton, S. W., Conlan, S., Crabtree, J., Cutting, M. A., Davidovics, N. J., Davis, C. C., DeSantis, T. Z., Deal, C., Delehaunty, K. D., Dewhirst, F. E., Deych, E., Ding, Y., Dooling, D. J., Dugan, S. P., Michael Dunne, W., Scott Durkin, A., Edgar, R. C., Erlich, R. L., Farmer, C. N., Farrell, R. M., Faust, K., Feldgarden, M., Felix, V. M., Fisher, S., Fodor, A. A., Forney, L. J., Foster, L., Di Francesco, V., Friedman, J., Friedrich, D. C., Fronick, C. C., Fulton, L. L., Gao, H., Garcia, N., Giannoukos, G., Giblin, C., Giovanni, M. Y., Goldberg, J. M., Goll, J., Gonzalez, A., Griggs, A., Gujja, S., Kinder Haake, S., Haas, B. J., Hamilton, H. A., Harris, E. L., Hepburn, T. A., Herter, B., Hoffmann, D. E., Holder, M. E., Howarth, C., Huang, K. H., Huse, S. M., Izard, J., Jansson, J. K., Jiang, H., Jordan, C., Joshi, V., Katancik, J. A., Keitel, W. A., Kelley, S. T., Kells, C., King, N. B., Knights, D., Kong, H. H., Koren, O., Koren, S., Kota, K. C., Kovar, C. L., Kyrpides, N. C., La Rosa, P. S., Lee, S. L., Lemon, K. P., Lennon, N., Lewis, C. M., Lewis, L., Ley, R. E., Li, K., Liolios, K., Liu, B., Liu, Y., Lo, C.-C., Lozupone, C. A., Dwayne Lunsford, R., Madden, T., Mahurkar, A. A., Mannon, P. J., Mardis, E. R., Markowitz, V. M., Mavromatis, K., McCorrison, J. M., McDonald, D., McEwen, J., McGuire, A. L., McInnes, P., Mehta, T., Mihindukulasuriya, K. A., Miller, J. R., Minx, P. J., Newsham, I., Nusbaum, C., O'Laughlin, M., Orvis, J., Pagani, I., Palaniappan, K., Patel, S. M., Pearson, M., Peterson, J., Podar, M., Pohl, C., Pollard, K. S., Pop, M., Priest, M. E., Proctor, L. M., Qin, X., Raes, J., Ravel, J., Reid, J. G., Rho, M., Rhodes, R., Riehle, K. P., Rivera, M. C., Rodriguez-Mueller, B., Rogers, Y.-H., Ross, M. C., Russ, C., Sanka, R. K., Sankar, P., Fah Sathirapongsasuti, J., Schloss, J. A., Schloss, P. D., Schmidt, T. M., Scholz, M., Schriml, L., Schubert, A. M., Segata, N., Segre, J. A., Shannon, W. D., Sharp, R. R., Sharpton, T. J., Shenoy, N., Sheth, N. U., Simone, G. A., Singh, I., Smillie, C. S., Sobel, J. D., Sommer, D. D., Spicer, P., Sutton, G. G., Sykes, S. M., Tabbaa, D. G., Thiagarajan, M., Tomlinson, C. M., Torralba, M., Treangen, T. J., Truty, R. M., Vishnivetskaya, T. A., Walker, J., Wang, L., Wang, Z., Ward, D. V., Warren, W., Watson, M. A., Wellington, C., Wetterstrand, K. A., White, J. R., Wilczek-Boney, K., Wu, Y., Wylie, K. M., Wylie, T., Yandava, C., Ye, L., Ye, Y., Yooseph, S., Youmans, B. P., Zhang, L., Zhou, Y., Zhu, Y., Zoloth, L., Zucker, J. D., Birren, B. W., Gibbs, R. A., Highlander, S. K., Methé, B. A., Nelson, K. E., Petrosino, J. F., Weinstock, G. M., Wilson, R. K. & White, O.

Structure, function and diversity of the healthy human microbiome. *Nature* **486**, 207 (2012).

175 Qin, J., Li, R., Raes, J., Arumugam, M., Burgdorf, K. S., Manichanh, C., Nielsen, T., Pons, N., Levenez, F., Yamada, T., Mende, D. R., Li, J., Xu, J., Li, S., Li, D., Cao, J., Wang, B., Liang, H., Zheng, H., Xie, Y., Tap, J., Lepage, P., Bertalan, M., Batto, J.-M., Hansen, T., Le Paslier, D., Linneberg, A., Nielsen, H. B., Pelletier, E., Renault, P., Sicheritz-Ponten, T., Turner, K., Zhu, H., Yu, C., Li, S., Jian, M., Zhou, Y., Li, Y., Zhang, X., Li, S., Qin, N., Yang, H., Wang, J., Brunak, S., Doré, J., Guarner, F., Kristiansen, K., Pedersen, O., Parkhill, J., Weissenbach, J., Meta, H. I. T. C., Antolin, M., Artiguenave, F., Blottiere, H., Borruel, N., Bruls, T., Casellas, F., Chervaux, C., Cultrone, A., Delorme, C., Denariaz, G., Dervyn, R., Forte, M., Friss, C., van de Guchte, M., Guedon, E., Haimet, F., Jamet, A., Juste, C., Kaci, G., Kleerebezem, M., Knol, J., Kristensen, M., Layec, S., Le Roux, K., Leclerc, M., Maguin, E., Melo Minardi, R., Oozeer, R., Rescigno, M., Sanchez, N., Tims, S., Torrejon, T., Varela, E., de Vos, W., Winogradsky, Y., Zoetendal, E., Bork, P., Ehrlich, S. D. & Wang, J. A human gut microbial gene catalogue established by metagenomic sequencing. *Nature* **464**, 59 (2010).

176 Ignacio, A., Morales, C. I., Câmara, N. O. S. & Almeida, R. R. Innate Sensing of the Gut Microbiota: Modulation of Inflammatory and Autoimmune Diseases. *Frontiers in Immunology* **7**, 54 (2016).

177 Bäckhed, F., Ley, R. E., Sonnenburg, J. L., Peterson, D. A. & Gordon, J. I. Host-Bacterial Mutualism in the Human Intestine. *Science* **307**, 1915-1920 (2005).

178 Rowland, I., Gibson, G., Heinken, A., Scott, K., Swann, J., Thiele, I. & Tuohy, K. Gut microbiota functions: metabolism of nutrients and other food components. *European Journal of Nutrition* **57**, 1-24 (2018).

179 Pompei, A., Cordisco, L., Amaretti, A., Zanoni, S., Matteuzzi, D. & Rossi, M. Folate Production by Bifidobacteria as a Potential Probiotic Property. *Appl. Environ. Microbiol.* **73**, 179-185 (2007).

180 Albert, M. J., Mathan, V. I. & Baker, S. J. Vitamin B12 synthesis by human small intestinal bacteria. *Nature* **283**, 781 (1980).

181 Cooke, G., Behan, J. & Costello, M. Newly identified vitamin K-producing bacteria isolated from the neonatal faecal flora. *Microb. Ecol. Health Dis.* **18**, 133-138 (2006).

182 Masuda, M., Ide, M., Utsumi, H., Niiro, T., Shimamura, Y. & Murata, M. Production Potency of Folate, Vitamin B12, and Thiamine by Lactic Acid Bacteria Isolated from Japanese Pickles. *Biosci., Biotechnol., Biochem.* **76**, 2061-2067 (2012).

183 Li, J., Jia, H., Cai, X., Zhong, H., Feng, Q., Sunagawa, S., Arumugam, M., Kultima, J. R., Prifti, E., Nielsen, T., Juncker, A. S., Manichanh, C., Chen, B., Zhang, W., Levenez, F., Wang, J., Xu, X., Xiao, L., Liang, S., Zhang, D., Zhang, Z., Chen, W., Zhao, H., Al-Aama, J. Y., Edris, S., Yang, H., Wang, J., Hansen, T., Nielsen, H. B., Brunak, S., Kristiansen, K., Guarner, F., Pedersen, O., Dore, J., Ehrlich, S. D., Bork, P. & Wang, J. An integrated catalog of reference genes in the human gut microbiome. *Nat. Biotechnol.* **32**, 834-841 (2014).

184 Donaldson, G. P., Lee, S. M. & Mazmanian, S. K. Gut biogeography of the bacterial microbiota. *Nature Reviews Microbiology* **14**, 20 (2015).

185 den Bogert, B. v., Erkus, O., Boekhorst, J., Goffau, M. d., Smid, E. J., Zoetendal, E. G. & Kleerebezem, M. Diversity of human small intestinal Streptococcus and Veillonella populations. *FEMS Microbiol. Ecol.* **85**, 376-388 (2013).

186 Gu, S., Chen, D., Zhang, J.-N., Lv, X., Wang, K., Duan, L.-P., Nie, Y. & Wu, X.-L. Bacterial Community Mapping of the Mouse Gastrointestinal Tract. *PLOS ONE* **8**, e74957 (2013).
187 Li, H., Limenitakis, J. P., Fuhrer, T., Geuking, M. B., Lawson, M. A., Wyss, M., Brugiroux, S., Keller, I., Macpherson, J. A., Rupp, S., Stolp, B., Stein, J. V., Stecher, B., Sauer, U., McCoy, K. D. & Macpherson, A. J. The outer mucus layer hosts a distinct intestinal microbial niche. *Nature Communications* **6**, 8292 (2015).
188 Lee, S. M., Donaldson, G. P., Mikulski, Z., Boyajian, S., Ley, K. & Mazmanian, S. K. Bacterial colonization factors control specificity and stability of the gut microbiota. *Nature* **501**, 426 (2013).
189 Tropini, C., Earle, K. A., Huang, K. C. & Sonnenburg, J. L. The Gut Microbiome: Connecting Spatial Organization to Function. *Cell Host Microbe* **21**, 433-442 (2017).
190 Mazmanian, S. K. & Lee, Y. K. Interplay between Intestinal Microbiota and Host Immune System. *J Bacteriol Virol* **44**, 1-9 (2014).
191 Peterson, L. W. & Artis, D. Intestinal epithelial cells: regulators of barrier function and immune homeostasis. *Nat. Rev. Immunol.* **14**, 141-153 (2014).
192 Wilson, C. L., Ouellette, A. J., Satchell, D. P., Ayabe, T., López-Boado, Y. S., Stratman, J. L., Hultgren, S. J., Matrisian, L. M. & Parks, W. C. Regulation of Intestinal α-Defensin Activation by the Metalloproteinase Matrilysin in Innate Host Defense. *Science* **286**, 113-117 (1999).
193 Brandl, K., Plitas, G., Schnabl, B., DeMatteo, R. P. & Pamer, E. G. MyD88-mediated signals induce the bactericidal lectin RegIII gamma and protect mice against intestinal Listeria monocytogenes infection. *J. Exp. Med.* **204**, 1891-1900 (2007).
194 den Hartog, G., Chattopadhyay, R., Ablack, A., Hall, E. H., Butcher, L. D., Bhattacharyya, A., Eckmann, L., Harris, P. R., Das, S., Ernst, P. B. & Crowe, S. E. Regulation of Rac1 and Reactive Oxygen Species Production in Response to Infection of Gastrointestinal Epithelia. *PLoS Path.* **12**, e1005382 (2016).
195 Rogier, E., Frantz, A., Bruno, M. & Kaetzel, C. Secretory IgA is Concentrated in the Outer Layer of Colonic Mucus along with Gut Bacteria. *Pathogens* **3**, 390 (2014).
196 Gutzeit, C., Magri, G. & Cerutti, A. Intestinal IgA production and its role in host-microbe interaction. *Immunol. Rev.* **260**, 76-85 (2014).
197 Mantis, N. J., Rol, N. & Corthésy, B. Secretory IgA's complex roles in immunity and mucosal homeostasis in the gut. *Mucosal immunology* **4**, 603-611 (2011).
198 Ost, K. S. & Round, J. L. Communication Between the Microbiota and Mammalian Immunity. *Annu. Rev. Microbiol.* **72**, 399-422 (2018).
199 Wu, G. D., Chen, J., Hoffmann, C., Bittinger, K., Chen, Y.-Y., Keilbaugh, S. A., Bewtra, M., Knights, D., Walters, W. A., Knight, R., Sinha, R., Gilroy, E., Gupta, K., Baldassano, R., Nessel, L., Li, H., Bushman, F. D. & Lewis, J. D. Linking Long-Term Dietary Patterns with Gut Microbial Enterotypes. *Science (New York, N.y.)* **334**, 105-108 (2011).
200 David, L. A., Maurice, C. F., Carmody, R. N., Gootenberg, D. B., Button, J. E., Wolfe, B. E., Ling, A. V., Devlin, A. S., Varma, Y., Fischbach, M. A., Biddinger, S. B., Dutton, R. J. & Turnbaugh, P. J. Diet rapidly and reproducibly alters the human gut microbiome. *Nature* **505**, 559-563 (2014).
201 Round, J. L. & Mazmanian, S. K. The gut microbiota shapes intestinal immune responses during health and disease. *Nature Reviews Immunology* **9**, 313 (2009).
202 Walker, A. W., Ince, J., Duncan, S. H., Webster, L. M., Holtrop, G., Ze, X., Brown, D., Stares, M. D., Scott, P., Bergerat, A., Louis, P., McIntosh, F.,

Johnstone, A. M., Lobley, G. E., Parkhill, J. & Flint, H. J. Dominant and diet-responsive groups of bacteria within the human colonic microbiota. *The ISME journal* **5**, 220 (2010).

203 Cheng, W., Lu, J., Li, B., Lin, W., Zhang, Z., Wei, X., Sun, C., Chi, M., Bi, W., Yang, B., Jiang, A. & Yuan, J. Effect of Functional Oligosaccharides and Ordinary Dietary Fiber on Intestinal Microbiota Diversity. *Frontiers in Microbiology* **8** (2017).

204 Chassaing, B., Koren, O., Goodrich, J. K., Poole, A. C., Srinivasan, S., Ley, R. E. & Gewirtz, A. T. Dietary emulsifiers impact the mouse gut microbiota promoting colitis and metabolic syndrome. *Nature* **519**, 92-96 (2015).

205 Jandhyala, S. M., Talukdar, R., Subramanyam, C., Vuyyuru, H., Sasikala, M. & Reddy, D. N. Role of the normal gut microbiota. *World Journal of Gastroenterology : WJG* **21**, 8787-8803 (2015).

206 Biedermann, L., Zeitz, J., Mwinyi, J., Sutter-Minder, E., Rehman, A., Ott, S. J., Steurer-Stey, C., Frei, A., Frei, P., Scharl, M., Loessner, M. J., Vavricka, S. R., Fried, M., Schreiber, S., Schuppler, M. & Rogler, G. Smoking Cessation Induces Profound Changes in the Composition of the Intestinal Microbiota in Humans. *PLOS ONE* **8**, e59260 (2013).

207 Chang, P. V., Hao, L., Offermanns, S. & Medzhitov, R. The microbial metabolite butyrate regulates intestinal macrophage function via histone deacetylase inhibition. *Proceedings of the National Academy of Sciences* **111**, 2247-2252 (2014).

208 Siregar, C., Wasito, E. B. & Sudiana, I. K. Effect of Butyric Acid on p53 Expression and Apoptosis in Colon Epithelial Cells in Mice after Treated with 9,10-dimethyl-1,2-benz(a)anthracene. *Procedia Chemistry* **18**, 141-146 (2016).

209 Kelly, C. J., Zheng, L., Campbell, E. L., Saeedi, B., Scholz, C. C., Bayless, A. J., Wilson, K. E., Glover, L. E., Kominsky, D. J., Magnuson, A., Weir, T. L., Ehrentraut, S. F., Pickel, C., Kuhn, K. A., Lanis, J. M., Nguyen, V., Taylor, C. T. & Colgan, S. P. Crosstalk between Microbiota-Derived Short-Chain Fatty Acids and Intestinal Epithelial HIF Augments Tissue Barrier Function. *Cell Host Microbe* **17**, 662-671 (2015).

210 Peng, L., Li, Z.-R., Green, R. S., Holzman, I. R. & Lin, J. Butyrate Enhances the Intestinal Barrier by Facilitating Tight Junction Assembly via Activation of AMP-Activated Protein Kinase in Caco-2 Cell Monolayers. *The Journal of Nutrition* **139**, 1619-1625 (2009).

211 Tailford, L. E., Owen, C. D., Walshaw, J., Crost, E. H., Hardy-Goddard, J., Le Gall, G., de Vos, W. M., Taylor, G. L. & Juge, N. Discovery of intramolecular trans-sialidases in human gut microbiota suggests novel mechanisms of mucosal adaptation. *Nature Communications* **6**, 7624 (2015).

212 Bene, K. P., Kavanaugh, D. W., Leclaire, C., Gunning, A. P., MacKenzie, D. A., Wittmann, A., Young, I. D., Kawasaki, N., Rajnavolgyi, E. & Juge, N. Lactobacillus reuteri Surface Mucus Adhesins Upregulate Inflammatory Responses Through Interactions With Innate C-Type Lectin Receptors. *Frontiers in Microbiology* **8** (2017).

213 Kravtsov, E. G., Yermolayev, A. V., Anokhina, I. V., Yashina, N. V., Chesnokova, V. L. & Dalin, M. V. Adhesion characteristics of lactobacillus is a criterion of the probiotic choice. *Bulletin of Experimental Biology and Medicine* **145**, 232-234 (2008).

214 Sun, J. & Chang, E. B. Exploring gut microbes in human health and disease: Pushing the envelope. *Genes & Diseases* **1**, 132-139 (2014).

215 de Lange, K. M., Moutsianas, L., Lee, J. C., Lamb, C. A., Luo, Y., Kennedy, N. A., Jostins, L., Rice, D. L., Gutierrez-Achury, J., Ji, S.-G., Heap, G., Nimmo, E. R., Edwards, C., Henderson, P., Mowat, C., Sanderson, J., Satsangi, J., Simmons, A., Wilson, D. C., Tremelling, M., Hart, A., Mathew,

C. G., Newman, W. G., Parkes, M., Lees, C. W., Uhlig, H., Hawkey, C., Prescott, N. J., Ahmad, T., Mansfield, J. C., Anderson, C. A. & Barrett, J. C. Genome-wide association study implicates immune activation of multiple integrin genes in inflammatory bowel disease. *Nat. Genet.* **49**, 256 (2017).

216 Ananthakrishnan, A. N. Environmental Risk Factors for Inflammatory Bowel Disease. *Gastroenterology & Hepatology* **9**, 367-374 (2013).

217 Levy, M., Kolodziejczyk, A. A., Thaiss, C. A. & Elinav, E. Dysbiosis and the immune system. *Nat. Rev. Immunol.* **17**, 219-232 (2017).

218 Yatsunenko, T., Rey, F. E., Manary, M. J., Trehan, I., Dominguez-Bello, M. G., Contreras, M., Magris, M., Hidalgo, G., Baldassano, R. N., Anokhin, A. P., Heath, A. C., Warner, B., Reeder, J., Kuczynski, J., Caporaso, J. G., Lozupone, C. A., Lauber, C., Clemente, J. C., Knights, D., Knight, R. & Gordon, J. I. Human gut microbiome viewed across age and geography. *Nature* **486**, 222 (2012).

219 Wu, G. D. & Lewis, J. D. Analysis of the Human Gut Microbiome and Association With Disease. *Clinical Gastroenterology and Hepatology* **11**, 774-777 (2013).

220 Agace, W. W. & McCoy, K. D. Regionalized development and maintenance of the intestinal adaptive immune landscape. *Immunity* **46**, 532-548 (2017).

221 De Santis, S., Cavalcanti, E., Mastronardi, M., Jirillo, E. & Chieppa, M. Nutritional Keys for Intestinal Barrier Modulation. *Frontiers in Immunology* **6**, 612 (2015).

222 Okumura, R. & Takeda, K. Roles of intestinal epithelial cells in the maintenance of gut homeostasis. *Experimental & molecular medicine* **49**, e338 (2017).

223 Helander, H. F. & Fändriks, L. Surface area of the digestive tract – revisited. *Scandinavian Journal of Gastroenterology* **49**, 681-689 (2014).

224 Ermund, A., Schütte, A., Johansson, M. E. V., Gustafsson, J. K. & Hansson, G. C. Studies of mucus in mouse stomach, small intestine, and colon. I. Gastrointestinal mucus layers have different properties depending on location as well as over the Peyer's patches. *American Journal of Physiology - Gastrointestinal and Liver Physiology* **305**, G341-G347 (2013).

225 Johansson, M. E., Sjövall, H. & Hansson, G. C. The gastrointestinal mucus system in health and disease. *Nature Reviews Gastroenterology and Hepatology* **10**, 352 (2013).

226 Johansson, M. E., Larsson, J. M. & Hansson, G. C. The two mucus layers of colon are organized by the MUC2 mucin, whereas the outer layer is a legislator of host-microbial interactions. *Proceedings of the National Academy of Sciences of the United States of America* **108 Suppl 1**, 4659-4665 (2011).

227 Johansson, M. E. V., Phillipson, M., Petersson, J., Velcich, A., Holm, L. & Hansson, G. C. The inner of the two Muc2 mucin-dependent mucus layers in colon is devoid of bacteria. *Proceedings of the National Academy of Sciences* **105**, 15064-15069 (2008).

228 Cornick, S., Tawiah, A. & Chadee, K. Roles and regulation of the mucus barrier in the gut. *Tissue barriers* **3**, e982426 (2015).

229 Lei, Y. M. K., Nair, L. & Alegre, M.-L. The interplay between the intestinal microbiota and the immune system. *Clinics and Research in Hepatology and Gastroenterology* **39**, 9-19 (2015).

230 Kagnoff, M. F. The intestinal epithelium is an integral component of a communications network. *The Journal of Clinical Investigation* **124**, 2841-2843 (2014).

231 Andrews, C., McLean, M. H. & Durum, S. K. Cytokine Tuning of Intestinal Epithelial Function. *Frontiers in immunology* **9**, 1270-1270 (2018).

232 Flannigan, K. L., Geem, D., Harusato, A. & Denning, T. L. Intestinal Antigen-Presenting Cells: Key Regulators of Immune Homeostasis and Inflammation. *The American Journal of Pathology* **185**, 1809-1819 (2015).
233 Lee, N. & Kim, W.-U. Microbiota in T-cell homeostasis and inflammatory diseases. *Experimental & molecular medicine* **49**, e340-e340 (2017).
234 Wang, H., Rogers, T. J., Paton, J. C. & Paton, A. W. Differential effects of Escherichia coli subtilase cytotoxin and Shiga toxin 2 on chemokine and proinflammatory cytokine expression in human macrophage, colonic epithelial, and brain microvascular endothelial cell lines. *Infect. Immun.* **82**, 3567-3579 (2014).
235 Knodler, L. A., Crowley, S. M., Sham, H. P., Yang, H., Wrande, M., Ma, C., Ernst, R. K., Steele-Mortimer, O., Celli, J. & Vallance, B. A. Noncanonical inflammasome activation of caspase-4/caspase-11 mediates epithelial defenses against enteric bacterial pathogens. *Cell Host Microbe* **16**, 249-256 (2014).
236 Fiorentino, M., Levine, M. M., Sztein, M. B. & Fasano, A. Effect of Wild-Type Shigella Species and Attenuated Shigella Vaccine Candidates on Small Intestinal Barrier Function, Antigen Trafficking, and Cytokine Release. *PLOS ONE* **9**, e85211 (2014).
237 Wang, X., Li, Y., Yang, X. & Yao, J. Astragalus polysaccharide reduces inflammatory response by decreasing permeability of LPS-infected Caco2 cells. *Int J Biol Macromol* **61**, 347-352 (2013).
238 Tu, J., Xu, Y., Xu, J., Ling, Y. & Cai, Y. Chitosan nanoparticles reduce LPS-induced inflammatory reaction via inhibition of NF-κB pathway in Caco-2 cells. *International Journal of Biological Macromolecules* **86**, 848-856 (2016).
239 Huang, Y., Li, N., Liboni, K. & Neu, J. Glutamine decreases lipopolysaccharide-induced IL-8 production in Caco-2 cells through a non-NF-kappaB p50 mechanism. *Cytokine* **22**, 77-83 (2003).
240 Ke, X., Hu, G., Fang, W., Chen, J., Zhang, X., Yang, C., Peng, J., Chen, Y. & Sferra, T. J. Qing Hua Chang Yin inhibits the LPS-induced activation of the IL-6/STAT3 signaling pathway in human intestinal Caco-2 cells. *Int. J. Mol. Med.* **35**, 1133-1137 (2015).
241 Zeuthen, L. H., Fink, L. N. & Frokiaer, H. Epithelial cells prime the immune response to an array of gut-derived commensals towards a tolerogenic phenotype through distinct actions of thymic stromal lymphopoietin and transforming growth factor-β. *Immunology* **123**, 197-208 (2008).
242 Tian, Z., Liu, X., Dai, R., Xiao, Y., Wang, X., Bi, D. & Shi, D. Enterococcus faecium HDRsEf1 protects the intestinal epithelium and attenuates ETEC-induced IL-8 secretion in enterocytes. *Mediators of Inflammation* **2016** (2016).
243 Welcome, M. O. in *Gastrointestinal Physiology: Development, Principles and Mechanisms of Regulation* 685-771 (Springer International Publishing, 2018).
244 Brandtzaeg, P., Kiyono, H., Pabst, R. & Russell, M. W. Terminology: nomenclature of mucosa-associated lymphoid tissue. *Mucosal Immunol* **1**, 31-37 (2008).
245 Bharhani, M. S., Borojevic, R., Basak, S., Ho, E., Zhou, P. & Croitoru, K. IL-10 protects mouse intestinal epithelial cells from Fas-induced apoptosis via modulating Fas expression and altering caspase-8 and FLIP expression. *American journal of physiology. Gastrointestinal and liver physiology* **291**, G820-829 (2006).
246 Tinoco-Veras, C. M., Santos, A. A. Q. A., Stipursky, J., Meloni, M., Araujo, A. P. B., Foschetti, D. A., López-Ureña, D., Quesada-Gómez, C., Leitão, R. F. C., Gomes, F. C. A. & Brito, G. A. d. C. Transforming Growth Factor β1/SMAD Signaling Pathway Activation Protects the Intestinal Epithelium from <span

class="named-content genus-species" id="named-content-1">Clostridium difficile Toxin A-Induced Damage. *Infect. Immun.* **85** (2017).

247 Grabinger, T., Bode, K. J., Demgenski, J., Seitz, C., Delgado, M. E., Kostadinova, F., Reinhold, C., Etemadi, N., Wilhelm, S., Schweinlin, M., Hänggi, K., Knop, J., Hauck, C., Walles, H., Silke, J., Wajant, H., Nachbur, U., W. Wei-Lynn, W. & Brunner, T. Inhibitor of Apoptosis Protein-1 Regulates Tumor Necrosis Factor–Mediated Destruction of Intestinal Epithelial Cells. *Gastroenterology* **152**, 867-879 (2017).

248 Ma, T. Y., Boivin, M. A., Ye, D., Pedram, A. & Said, H. M. Mechanism of TNF-{alpha} modulation of Caco-2 intestinal epithelial tight junction barrier: role of myosin light-chain kinase protein expression. *American journal of physiology. Gastrointestinal and liver physiology* **288**, G422-430 (2005).

249 Wang, Q., Guo, X. L., Wells-Byrum, D., Noel, G., Pritts, T. A. & Ogle, C. K. Cytokine-induced epithelial permeability changes are regulated by the activation of the p38 mitogen-activated protein kinase pathway in cultured Caco-2 cells. *Shock* **29**, 531-537 (2008).

250 Sappington, P. L., Han, X., Delude, R. L. & Fink, M. P. Pro-inflammatory cytokines decrease the expression of tight junction proteins in Caco-2 intestinal epithelial cells through a process that is dependent on peroxynitrite formation and PARP activation. *Critical Care* **6**, P102-P102 (2002).

251 West, C. E., Renz, H., Jenmalm, M. C., Kozyrskyj, A. L., Allen, K. J., Vuillermin, P., Prescott, S. L., MacKay, C., Salminen, S., Wong, G., Sinn, J., Stokholm, J., Bisgaard, H., Pawankar, R., Noakes, P., Kesper, D. & Tulic, M. The gut microbiota and inflammatory noncommunicable diseases: Associations and potentials for gut microbiota therapies. *J. Allergy Clin. Immunol.* **135**, 3-13 (2015).

252 Corr, S. C., Gahan, C. C. & Hill, C. M-cells: origin, morphology and role in mucosal immunity and microbial pathogenesis. *FEMS Immunol. Med. Microbiol.* **52**, 2-12 (2008).

253 Lorenz, R. G. & Newberry, R. D. Isolated lymphoid follicles can function as sites for induction of mucosal immune responses. *Ann. N. Y. Acad. Sci.* **1029**, 44-57 (2004).

254 Baptista, A. P., Olivier, B. J., Goverse, G., Greuter, M., Knippenberg, M., Kusser, K., Domingues, R. G., Veiga-Fernandes, H., Luster, A. D., Lugering, A., Randall, T. D., Cupedo, T. & Mebius, R. E. Colonic patch and colonic SILT development are independent and differentially regulated events. *Mucosal Immunology* **6**, 511 (2012).

255 Ruddle, N. H. & Akirav, E. M. Secondary Lymphoid Organs: Responding to Genetic and Environmental Cues in Ontogeny and the Immune Response. *The Journal of Immunology* **183**, 2205-2212 (2009).

256 Jung, C., Hugot, J.-P. & Barreau, F. Peyer's Patches: The Immune Sensors of the Intestine. *International Journal of Inflammation* **2010**, 823710 (2010).

257 Cornes, J. S. Number, size, and distribution of Peyer's patches in the human small intestine: Part I The development of Peyer's patches. *Gut* **6**, 225-229 (1965).

258 Fagarasan, S. & Honjo, T. Intestinal IgA synthesis: regulation of front-line body defences. *Nature Reviews Immunology* **3**, 63 (2003).

259 Mowat, A. M. To respond or not to respond - a personal perspective of intestinal tolerance. *Nat. Rev. Immunol.* **18**, 405-415 (2018).

260 van Wijk, F. & Cheroutre, H. Mucosal T cells in gut homeostasis and inflammation. *Expert review of clinical immunology* **6**, 559-566 (2010).

261 Kamada, N., Seo, S.-U., Chen, G. Y. & Núñez, G. Role of the gut microbiota in immunity and inflammatory disease. *Nature Reviews Immunology* **13**, 321-335 (2013).

262 Atarashi, K., Tanoue, T. & Honda, K. Induction of lamina propria Th17 cells by intestinal commensal bacteria. *Vaccine* **28**, 8036-8038 (2010).
263 Shale, M., Schiering, C. & Powrie, F. CD4(+) T-cell subsets in intestinal inflammation. *Immunol. Rev.* **252**, 164-182 (2013).
264 Ni, J., Wu, G. D., Albenberg, L. & Tomov, V. T. Gut microbiota and IBD: causation or correlation? *Nature reviews. Gastroenterology & hepatology* **14**, 573-584 (2017).
265 Belkaid, Y. & Hand, Timothy W. Role of the Microbiota in Immunity and Inflammation. *Cell* **157**, 121-141 (2014).
266 Geuking, Markus B., Cahenzli, J., Lawson, Melissa A. E., Ng, Derek C. K., Slack, E., Hapfelmeier, S., McCoy, Kathy D. & Macpherson, Andrew J. Intestinal Bacterial Colonization Induces Mutualistic Regulatory T Cell Responses. *Immunity* **34**, 794-806 (2011).
267 Round, J. L. & Mazmanian, S. K. Inducible Foxp3⁺ regulatory T-cell development by a commensal bacterium of the intestinal microbiota. *Proceedings of the National Academy of Sciences* **107**, 12204-12209 (2010).
268 Gross, M., Salame, T.-M. & Jung, S. Guardians of the Gut – Murine Intestinal Macrophages and Dendritic Cells. *Frontiers in Immunology* **6**, 254 (2015).
269 Bernardo, D., Chaparro, M. & Gisbert, J. P. Human Intestinal Dendritic Cells in Inflammatory Bowel Diseases. *Mol. Nutr. Food Res.* **62**, 1700931 (2018).
270 Joeris, T., Muller-Luda, K., Agace, W. W. & Mowat, A. M. Diversity and functions of intestinal mononuclear phagocytes. *Mucosal Immunol* **10**, 845-864 (2017).
271 Lee, S. H., Starkey, P. M. & Gordon, S. Quantitative analysis of total macrophage content in adult mouse tissues. Immunochemical studies with monoclonal antibody F4/80. *J. Exp. Med.* **161**, 475-489 (1985).
272 Gautier, E. L., Shay, T., Miller, J., Greter, M., Jakubzick, C., Ivanov, S., Helft, J., Chow, A., Elpek, K. G., Gordonov, S., Mazloom, A. R., Ma'ayan, A., Chua, W.-J., Hansen, T. H., Turley, S. J., Merad, M., Randolph, G. J., the Immunological Genome, C., Gautier, E. L., Jakubzick, C., Randolph, G. J., Best, A. J., Knell, J., Goldrath, A., Miller, J., Brown, B., Merad, M., Jojic, V., Koller, D., Cohen, N., Brennan, P., Brenner, M., Shay, T., Regev, A., Fletcher, A., Elpek, K., Bellemare-Pelletier, A., Malhotra, D., Turley, S., Jianu, R., Laidlaw, D., Collins, J., Narayan, K., Sylvia, K., Kang, J., Gazit, R., Garrison, B. S., Rossi, D. J., Kim, F., Rao, T. N., Wagers, A., Shinton, S. A., Hardy, R. R., Monach, P., Bezman, N. A., Sun, J. C., Kim, C. C., Lanier, L. L., Heng, T., Kreslavsky, T., Painter, M., Ericson, J., Davis, S., Mathis, D. & Benoist, C. Gene-expression profiles and transcriptional regulatory pathways that underlie the identity and diversity of mouse tissue macrophages. *Nat. Immunol.* **13**, 1118 (2012).
273 Smythies, L. E., Sellers, M., Clements, R. H., Mosteller-Barnum, M., Meng, G., Benjamin, W. H., Orenstein, J. M. & Smith, P. D. Human intestinal macrophages display profound inflammatory anergy despite avid phagocytic and bacteriocidal activity. *The Journal of Clinical Investigation* **115**, 66-75 (2005).
274 Rivollier, A., He, J., Kole, A., Valatas, V. & Kelsall, B. L. Inflammation switches the differentiation program of Ly6Chi monocytes from antiinflammatory macrophages to inflammatory dendritic cells in the colon. *J. Exp. Med.* **209**, 139-155 (2012).
275 Park, B. S. & Lee, J. O. Recognition of lipopolysaccharide pattern by TLR4 complexes. *Experimental & molecular medicine* **45**, e66 (2013).
276 Mowat, A. M. & Bain, C. C. Mucosal Macrophages in Intestinal Homeostasis and Inflammation. *Journal of Innate Immunity* **3**, 550-564 (2011).
277 Zigmond, E., Bernshtein, B., Friedlander, G., Walker, Catherine R., Yona, S., Kim, K.-W., Brenner, O., Krauthgamer, R., Varol, C., Müller, W. & Jung, S.

Macrophage-Restricted Interleukin-10 Receptor Deficiency, but Not IL-10 Deficiency, Causes Severe Spontaneous Colitis. *Immunity* **40**, 720-733 (2014).

278 Murai, M., Turovskaya, O., Kim, G., Madan, R., Karp, C. L., Cheroutre, H. & Kronenberg, M. Interleukin 10 acts on regulatory T cells to maintain expression of the transcription factor Foxp3 and suppressive function in mice with colitis. *Nat. Immunol.* **10**, 1178 (2009).

279 Hadis, U., Wahl, B., Schulz, O., Hardtke-Wolenski, M., Schippers, A., Wagner, N., Müller, W., Sparwasser, T., Förster, R. & Pabst, O. Intestinal Tolerance Requires Gut Homing and Expansion of FoxP3+ Regulatory T Cells in the Lamina Propria. *Immunity* **34**, 237-246 (2011).

280 Zigmond, E., Varol, C., Farache, J., Elmaliah, E., Satpathy, Ansuman T., Friedlander, G., Mack, M., Shpigel, N., Boneca, Ivo G., Murphy, Kenneth M., Shakhar, G., Halpern, Z. & Jung, S. Ly6Chi Monocytes in the Inflamed Colon Give Rise to Proinflammatory Effector Cells and Migratory Antigen-Presenting Cells. *Immunity* **37**, 1076-1090 (2012).

281 Kassiotis, G. & Kollias, G. Uncoupling the proinflammatory from the immunosuppressive properties of tumor necrosis factor (TNF) at the p55 TNF receptor level: implications for pathogenesis and therapy of autoimmune demyelination. *J. Exp. Med.* **193**, 427-434 (2001).

282 Artis, D. Epithelial-cell recognition of commensal bacteria and maintenance of immune homeostasis in the gut. *Nat. Rev. Immunol.* **8**, 411-420 (2008).

283 Vallon-Eberhard, A., Landsman, L., Yogev, N., Verrier, B. & Jung, S. Transepithelial Pathogen Uptake into the Small Intestinal Lamina Propria. *The Journal of Immunology* **176**, 2465-2469 (2006).

284 Rescigno, M., Urbano, M., Valzasina, B., Francolini, M., Rotta, G., Bonasio, R., Granucci, F., Kraehenbuhl, J.-P. & Ricciardi-Castagnoli, P. Dendritic cells express tight junction proteins and penetrate gut epithelial monolayers to sample bacteria. *Nat. Immunol.* **2**, 361 (2001).

285 Niess, J. H., Brand, S., Gu, X., Landsman, L., Jung, S., McCormick, B. A., Vyas, J. M., Boes, M., Ploegh, H. L., Fox, J. G., Littman, D. R. & Reinecker, H.-C. CX₃CR1-Mediated Dendritic Cell Access to the Intestinal Lumen and Bacterial Clearance. *Science* **307**, 254-258 (2005).

286 Diehl, G. E., Longman, R. S., Zhang, J. X., Breart, B., Galan, C., Cuesta, A., Schwab, S. R. & Littman, D. R. Microbiota restricts trafficking of bacteria to mesenteric lymph nodes by CX(3)CR1(hi) cells. *Nature* **494**, 116-120 (2013).

287 Du Plessis, J., Vanheel, H., Janssen, C. E. I., Roos, L., Slavik, T., Stivaktas, P. I., Nieuwoudt, M., van Wyk, S. G., Vieira, W., Pretorius, E., Beukes, M., Farré, R., Tack, J., Laleman, W., Fevery, J., Nevens, F., Roskams, T. & Van der Merwe, S. W. Activated intestinal macrophages in patients with cirrhosis release NO and IL-6 that may disrupt intestinal barrier function. *Journal of Hepatology* **58**, 1125-1132 (2013).

288 Al-Ghadban, S., Kaissi, S., Homaidan, F. R., Naim, H. Y. & El-Sabban, M. E. Cross-talk between intestinal epithelial cells and immune cells in inflammatory bowel disease. *Scientific Reports* **6**, 29783 (2016).

289 Han, D., Walsh, Matthew C., Cejas, Pedro J., Dang, Nicholas N., Kim, Youngmi F., Kim, J., Charrier-Hisamuddin, L., Chau, L., Zhang, Q., Bittinger, K., Bushman, Frederic D., Turka, Laurence A., Shen, H., Reizis, B., DeFranco, Anthony L., Wu, Gary D. & Choi, Y. Dendritic Cell Expression of the Signaling Molecule TRAF6 Is Critical for Gut Microbiota-Dependent Immune Tolerance. *Immunity* **38**, 1211-1222 (2013).

290 Rigby, R. J., Knight, S. C., Kamm, M. A. & Stagg, A. J. Production of interleukin (IL)-10 and IL-12 by murine colonic dendritic cells in response to microbial stimuli. *Clin. Exp. Immunol.* **139**, 245-256 (2005).

291 Schlitzer, A., McGovern, N., Teo, P., Zelante, T., Atarashi, K., Low, D., Ho, Adrian W. S., See, P., Shin, A., Wasan, Pavandip S., Hoeffel, G., Malleret, B., Heiseke, A., Chew, S., Jardine, L., Purvis, Harriet A., Hilkens, Catharien M. U., Tam, J., Poidinger, M., Stanley, E. R., Krug, Anne B., Renia, L., Sivasankar, B., Ng, Lai G., Collin, M., Ricciardi-Castagnoli, P., Honda, K., Haniffa, M. & Ginhoux, F. IRF4 Transcription Factor-Dependent CD11b+ Dendritic Cells in Human and Mouse Control Mucosal IL-17 Cytokine Responses. *Immunity* **38**, 970-983 (2013).

292 Edelson, B. T., Kc, W., Juang, R., Kohyama, M., Benoit, L. A., Klekotka, P. A., Moon, C., Albring, J. C., Ise, W., Michael, D. G., Bhattacharya, D., Stappenbeck, T. S., Holtzman, M. J., Sung, S.-S. J., Murphy, T. L., Hildner, K. & Murphy, K. M. Peripheral CD103(+) dendritic cells form a unified subset developmentally related to CD8α(+) conventional dendritic cells. *The Journal of Experimental Medicine* **207**, 823-836 (2010).

293 Cecchini, M. G., Dominguez, M. G., Mocci, S., Wetterwald, A., Felix, R., Fleisch, H., Chisholm, O., Hofstetter, W., Pollard, J. W. & Stanley, E. R. Role of colony stimulating factor-1 in the establishment and regulation of tissue macrophages during postnatal development of the mouse. *Development* **120**, 1357-1372 (1994).

294 Hiemstra, I. H., Beijer, M. R., Veninga, H., Vrijland, K., Borg, E. G. F., Olivier, B. J., Mebius, R. E., Kraal, G. & den Haan, J. M. M. The identification and developmental requirements of colonic CD169(+) macrophages. *Immunology* **142**, 269-278 (2014).

295 Watchmaker, P. B., Lahl, K., Lee, M., Baumjohann, D., Morton, J., Kim, S. J., Zeng, R., Dent, A., Ansel, K. M., Diamond, B., Hadeiba, H. & Butcher, E. C. Comparative transcriptional and functional profiling defines conserved programs of intestinal DC differentiation in humans and mice. *Nat. Immunol.* **15**, 98-108 (2014).

296 Schiavi, E., Smolinska, S. & O'Mahony, L. Intestinal dendritic cells. *Current opinion in gastroenterology* **31**, 98-103 (2015).

297 Mabbott, N. A., Donaldson, D. S., Ohno, H., Williams, I. R. & Mahajan, A. Microfold (M) cells: important immunosurveillance posts in the intestinal epithelium. *Mucosal Immunology* **6**, 666 (2013).

298 McDole, J. R., Wheeler, L. W., McDonald, K. G., Wang, B., Konjufca, V., Knoop, K. A., Newberry, R. D. & Miller, M. J. Goblet cells deliver luminal antigen to CD103+ dendritic cells in the small intestine. *Nature* **483**, 345-349 (2012).

299 Farache, J., Koren, I., Milo, I., Gurevich, I., Kim, K.-W., Zigmond, E., Furtado, Glaucia C., Lira, Sergio A. & Shakhar, G. Luminal Bacteria Recruit CD103+ Dendritic Cells into the Intestinal Epithelium to Sample Bacterial Antigens for Presentation. *Immunity* **38**, 581-595 (2013).

300 Sun, C. M., Hall, J. A., Blank, R. B., Bouladoux, N., Oukka, M., Mora, J. R. & Belkaid, Y. Small intestine lamina propria dendritic cells promote de novo generation of Foxp3 T reg cells via retinoic acid. *J. Exp. Med.* **204**, 1775-1785 (2007).

301 Ng, S. C., Benjamin, J. L., McCarthy, N. E., Hedin, C. R. H., Koutsoumpas, A., Plamondon, S., Price, C. L., Hart, A. L., Kamm, M. A., Forbes, A., Knight, S. C., Lindsay, J. O., Whelan, K. & Stagg, A. J. Relationship between human intestinal dendritic cells, gut microbiota, and disease activity in Crohn's disease. *Inflammatory Bowel Diseases* **17**, 2027-2037 (2011).

302 Munoz, L., Jose Borrero, M., Ubeda, M., Lario, M., Diaz, D., Frances, R., Monserrat, J., Pastor, O., Aguado-Fraile, E., Such, J., Alvarez-Mon, M. & Albillos, A. Interaction between intestinal dendritic cells and bacteria translocated from the gut in rats with cirrhosis. *Hepatology (Baltimore, Md.)* **56**, 1861-1869 (2012).

303 Neurath, M. F. Cytokines in inflammatory bowel disease. *Nature Reviews Immunology* **14**, 329 (2014).
304 Coombes, J. L. & Powrie, F. Dendritic cells in intestinal immune regulation. *Nature Reviews Immunology* **8**, 435 (2008).
305 Kaisar, M. M. M., Pelgrom, L. R., van der Ham, A. J., Yazdanbakhsh, M. & Everts, B. Butyrate Conditions Human Dendritic Cells to Prime Type 1 Regulatory T Cells via both Histone Deacetylase Inhibition and G Protein-Coupled Receptor 109A Signaling. *Frontiers in Immunology* **8** (2017).
306 Mazmanian, S. K., Round, J. L. & Kasper, D. L. A microbial symbiosis factor prevents intestinal inflammatory disease. *Nature* **453**, 620-625 (2008).
307 Tezuka, H., Abe, Y., Asano, J., Sato, T., Liu, J., Iwata, M. & Ohteki, T. Prominent Role for Plasmacytoid Dendritic Cells in Mucosal T Cell-Independent IgA Induction. *Immunity* **34**, 247-257 (2011).
308 Tezuka, H., Abe, Y., Iwata, M., Takeuchi, H., Ishikawa, H., Matsushita, M., Shiohara, T., Akira, S. & Ohteki, T. Regulation of IgA production by naturally occurring TNF/iNOS-producing dendritic cells. *Nature* **448**, 929 (2007).
309 Brubaker, S. W., Bonham, K. S., Zanoni, I. & Kagan, J. C. Innate immune pattern recognition: a cell biological perspective. *Annu. Rev. Immunol.* **33**, 257-290 (2015).
310 Oliveira-Nascimento, L., Massari, P. & Wetzler, L. M. The Role of TLR2 in Infection and Immunity. *Frontiers in immunology* **3**, 79-79 (2012).
311 Kawasaki, T. & Kawai, T. Toll-like receptor signaling pathways. *Frontiers in immunology* **5**, 461-461 (2014).
312 Vaure, C. & Liu, Y. A comparative review of toll-like receptor 4 expression and functionality in different animal species. *Frontiers in immunology* **5**, 316 (2014).
313 Price, A. E., Shamardani, K., Lugo, K. A., Deguine, J., Roberts, A. W., Lee, B. L. & Barton, G. M. A Map of Toll-like Receptor Expression in the Intestinal Epithelium Reveals Distinct Spatial, Cell Type-Specific, and Temporal Patterns. *Immunity* **49**, 560-575.e566 (2018).
314 Park, B. S., Song, D. H., Kim, H. M., Choi, B.-S., Lee, H. & Lee, J.-O. The structural basis of lipopolysaccharide recognition by the TLR4–MD-2 complex. *Nature* **458**, 1191 (2009).
315 Hansen, G. H., Rasmussen, K., Niels-Christiansen, L.-L. & Danielsen, E. M. Lipopolysaccharide-binding protein: localization in secretory granules of Paneth cells in the mouse small intestine. *Histochemistry and Cell Biology* **131**, 727-732 (2009).
316 Lizundia, R., Sauter, K.-S., Taylor, G. & Werling, D. Host species-specific usage of the TLR4-LPS receptor complex. *Innate Immunity* **14**, 223-231 (2008).
317 Stamatos, N. M., Carubelli, I., van de Vlekkert, D., Bonten, E. J., Papini, N., Feng, C., Venerando, B., d'Azzo, A., Cross, A. S., Wang, L.-X. & Gomatos, P. J. LPS-induced cytokine production in human dendritic cells is regulated by sialidase activity. *J. Leukocyte Biol.* **88**, 1227-1239 (2010).
318 Chow, J. C., Young, D. W., Golenbock, D. T., Christ, W. J. & Gusovsky, F. Toll-like receptor-4 mediates lipopolysaccharide-induced signal transduction. *J. Biol. Chem.* **274**, 10689-10692 (1999).
319 Gronbach, K., Flade, I., Holst, O., Lindner, B., Ruscheweyh, H. J., Wittmann, A., Menz, S., Schwiertz, A., Adam, P., Stecher, B., Josenhans, C., Suerbaum, S., Gruber, A. D., Kulik, A., Huson, D., Autenrieth, I. B. & Frick, J.-S. Endotoxicity of Lipopolysaccharide as a Determinant of T-Cell−Mediated Colitis Induction in Mice. *Gastroenterology* **146**, 765-775 (2014).
320 Hacini-Rachinel, F., Gomez de Aguero, M., Kanjarawi, R., Moro-Sibilot, L., Le Luduec, J. B., Macari, C., Boschetti, G., Bardel, E., Langella, P., Dubois, B. & Kaiserlian, D. Intestinal dendritic cell licensing through Toll-like receptor

4 is required for oral tolerance in allergic contact dermatitis. *J. Allergy Clin. Immunol.* **141**, 163-170 (2018).
321 Janelsins, B. M., Lu, M. & Datta, S. K. Altered inactivation of commensal LPS due to acyloxyacyl hydrolase deficiency in colonic dendritic cells impairs mucosal Th17 immunity. *Proceedings of the National Academy of Sciences* **111**, 373-378 (2014).
322 Medvedev, A. E., Lentschat, A., Wahl, L. M., Golenbock, D. T. & Vogel, S. N. Dysregulation of LPS-Induced Toll-Like Receptor 4-MyD88 Complex Formation and IL-1 Receptor-Associated Kinase 1 Activation in Endotoxin-Tolerant Cells. *The Journal of Immunology* **169**, 5209-5216 (2002).
323 Sodhi, C., Levy, R., Gill, R., Neal, M. D., Richardson, W., Branca, M., Russo, A., Prindle, T., Billiar, T. R. & Hackam, D. J. DNA attenuates enterocyte Toll-like receptor 4-mediated intestinal mucosal injury after remote trauma. *American Journal of Physiology - Gastrointestinal and Liver Physiology* **300**, G862-G873 (2011).
324 de Kivit, S., Tobin, M. C., Forsyth, C. B., Keshavarzian, A. & Landay, A. L. Regulation of Intestinal Immune Responses through TLR Activation: Implications for Pro- and Prebiotics. *Frontiers in Immunology* **5**, 60 (2014).
325 Guo, S., Al-Sadi, R., Said, H. M. & Ma, T. Y. Lipopolysaccharide Causes an Increase in Intestinal Tight Junction Permeability in Vitro and in Vivo by Inducing Enterocyte Membrane Expression and Localization of TLR-4 and CD14. *The American Journal of Pathology* **182**, 375-387 (2013).
326 Abreu, M. T. Toll-like receptor signalling in the intestinal epithelium: how bacterial recognition shapes intestinal function. *Nature Reviews Immunology* **10**, 131 (2010).
327 Yoon, S.-i., Kurnasov, O., Natarajan, V., Hong, M., Gudkov, A. V., Osterman, A. L. & Wilson, I. A. Structural basis of TLR5-flagellin recognition and signaling. *Science (New York, N.Y.)* **335**, 859-864 (2012).
328 Brown, G. D., Willment, J. A. & Whitehead, L. C-type lectins in immunity and homeostasis. *Nature Reviews Immunology* (2018).
329 Dambuza, I. M. & Brown, G. D. C-type lectins in immunity: recent developments. *Curr. Opin. Immunol.* **32**, 21-27 (2015).
330 Llera, A. S., Viedma, F., Sánchez-Madrid, F. & Tormo, J. Crystal Structure of the C-type Lectin-like Domain from the Human Hematopoietic Cell Receptor CD69. *J. Biol. Chem.* **276**, 7312-7319 (2001).
331 Mayer, S., Raulf, M.-K. & Lepenies, B. C-type lectins: their network and roles in pathogen recognition and immunity. *Histochemistry and Cell Biology* **147**, 223-237 (2017).
332 Drickamer, K. C-type lectin-like domains. *Curr. Opin. Struct. Biol.* **9**, 585-590 (1999).
333 Zelensky, A. N. & Gready, J. E. The C-type lectin-like domain superfamily. *FEBS J.* **272**, 6179-6217 (2005).
334 Drickamer, K. Engineering galactose-binding activity into a C-type mannose-binding protein. *Nature* **360**, 183-186 (1992).
335 Tang, J., Lin, G., Langdon, W. Y., Tao, L. & Zhang, J. Regulation of C-type Lectin Receptor-mediated Anti-Fungal Immunity. *Frontiers in immunology* **9**, 123 (2018).
336 Weis, W. I. & Drickamer, K. Structural basis of lectin-carbohydrate recognition. *Annu. Rev. Biochem.* **65**, 441-473 (1996).
337 Plato, A., Willment, J. A. & Brown, G. D. C-type lectin-like receptors of the dectin-1 cluster: ligands and signaling pathways. *International reviews of immunology* **32**, 134-156 (2013).
338 McGreal, E. P., Rosas, M., Brown, G. D., Zamze, S., Wong, S. Y., Gordon, S., Martinez-Pomares, L. & Taylor, P. R. The carbohydrate-recognition

domain of Dectin-2 is a C-type lectin with specificity for high mannose. *Glycobiology* **16**, 422-430 (2006).
339 Feinberg, H., Jegouzo, S. A. F., Rex, M. J., Drickamer, K., Weis, W. I. & Taylor, M. E. Mechanism of pathogen recognition by human dectin-2. *J. Biol. Chem.* **292**, 13402-13414 (2017).
340 Brown, J., O'Callaghan, C. A., Marshall, A. S., Gilbert, R. J., Siebold, C., Gordon, S., Brown, G. D. & Jones, E. Y. Structure of the fungal β-glucan-binding immune receptor dectin-1: Implications for function. *Protein Sci.* **16**, 1042-1052 (2007).
341 Palma, A. S., Feizi, T., Zhang, Y., Stoll, M. S., Lawson, A. M., Díaz-Rodríguez, E., Campanero-Rhodes, M. A., Costa, J., Gordon, S. & Brown, G. D. Ligands for the β-glucan receptor, Dectin-1, assigned using "designer" microarrays of oligosaccharide probes (neoglycolipids) generated from glucan polysaccharides. *J. Biol. Chem.* **281**, 5771-5779 (2006).
342 Love, P. E. & Hayes, S. M. ITAM-mediated signaling by the T-cell antigen receptor. *Cold Spring Harbor perspectives in biology* **2**, a002485-a002485 (2010).
343 Hoving, J. C., Wilson, G. J. & Brown, G. D. Signalling C-Type lectin receptors, microbial recognition and immunity. *Cell. Microbiol.* **16**, 185-194 (2014).
344 del Fresno, C., Iborra, S., Saz-Leal, P., Martínez-López, M. & Sancho, D. Flexible signaling of myeloid C-type lectin receptors in immunity and inflammation. *Frontiers in immunology* **9** (2018).
345 Osorio, F. & e Sousa, C. R. Myeloid C-type lectin receptors in pathogen recognition and host defense. *Immunity* **34**, 651-664 (2011).
346 Geijtenbeek, T. B. & Gringhuis, S. I. Signalling through C-type lectin receptors: shaping immune responses. *Nature Reviews Immunology* **9**, 465-479 (2009).
347 Tang, J., Lin, G., Langdon, W. Y., Tao, L. & Zhang, J. Regulation of C-Type Lectin Receptor-Mediated Antifungal Immunity. *Frontiers in Immunology* **9**, 123 (2018).
348 Tsang, E., Giannetti, A. M., Shaw, D., Dinh, M., Joyce, K., Gandhi, S., Ho, H., Wang, S., Papp, E. & Bradshaw, J. M. Molecular mechanism of the Syk activation switch. *J. Biol. Chem.* **283**, 32650-32659 (2008).
349 Asamaphan, P., Willment, J. A. & Brown, G. D. in *C-Type Lectin Receptors in Immunity* (ed Sho Yamasaki) 51-63 (Springer Japan, 2016).
350 Joo, H., Upchurch, K., Zhang, W., Ni, L., Li, D., Xue, Y., Li, X.-H., Hori, T., Zurawski, S., Liu, Y.-J., Zurawski, G. & Oh, S. Opposing roles of Dectin-1 expressed on human pDCs and mDCs in Th2 polarization. *Journal of immunology (Baltimore, Md. : 1950)* **195**, 1723-1731 (2015).
351 Serezani, C. H., Kane, S., Collins, L., Morato-Marques, M., Osterholzer, J. J. & Peters-Golden, M. Macrophage Dectin-1 Expression Is Controlled by Leukotriene B₄ via a GM-CSF/PU.1 Axis. *The Journal of Immunology* **189**, 906-915 (2012).
352 Taylor, P. R., Brown, G. D., Reid, D. M., Willment, J. A., Martinez-Pomares, L., Gordon, S. & Wong, S. Y. The β-glucan receptor, dectin-1, is predominantly expressed on the surface of cells of the monocyte/macrophage and neutrophil lineages. *The Journal of immunology* **169**, 3876-3882 (2002).
353 Shah, V. B., Huang, Y., Keshwara, R., Ozment-Skelton, T., Williams, D. L. & Keshvara, L. β-Glucan Activates Microglia without Inducing Cytokine Production in Dectin-1-Dependent Manner. *The Journal of Immunology* **180**, 2777-2785 (2008).
354 Chen, S. M., Shen, H., Zhang, T., Huang, X., Liu, X. Q., Guo, S. Y., Zhao, J. J., Wang, C. F., Yan, L., Xu, G. T., Jiang, Y. Y. & An, M. M. Dectin-1 plays an

important role in host defense against systemic Candida glabrata infection. *Virulence* **8**, 1643-1656 (2017).

355 Leibundgut-Landmann, S. SYK- and CARD9-dependent coupling of innate immunity to the induction of T helper cells that produce interleukin 17. *Nature Immunol.* **8**, 630-638 (2007).

356 Takano, T., Motozono, C., Imai, T., Sonoda, K. H., Nakanishi, Y. & Yamasaki, S. Dectin-1 intracellular domain determines species-specific ligand spectrum by modulating receptor sensitivity. *J. Biol. Chem.* **292**, 16933-16941 (2017).

357 Brown, G. D., Taylor, P. R., Reid, D. M., Willment, J. A., Williams, D. L., Martinez-Pomares, L., Wong, S. Y. & Gordon, S. Dectin-1 is a major β-glucan receptor on macrophages. *The Journal of experimental medicine* **196**, 407-412 (2002).

358 Inoue, M. & Shinohara, M. L. Clustering of Pattern Recognition Receptors for Fungal Detection. *PLoS Path.* **10**, e1003873 (2014).

359 Elder, M. J., Webster, S. J., Chee, R., Williams, D. L., Hill Gaston, J. S. & Goodall, J. C. β-Glucan Size Controls Dectin-1-Mediated Immune Responses in Human Dendritic Cells by Regulating IL-1β Production. *Frontiers in Immunology* **8**, 791 (2017).

360 Strasser, D., Neumann, K., Bergmann, H., Marakalala, M. J., Guler, R., Rojowska, A., Hopfner, K. P., Brombacher, F., Urlaub, H., Baier, G., Brown, G. D., Leitges, M. & Ruland, J. Syk kinase-coupled C-type lectin receptors engage protein kinase C-sigma to elicit Card9 adaptor-mediated innate immunity. *Immunity* **36**, 32-42 (2012).

361 Drummond, R. A., Franco, L. M. & Lionakis, M. S. Human CARD9: A Critical Molecule of Fungal Immune Surveillance. *Frontiers in Immunology* **9** (2018).

362 Liu, T., Zhang, L., Joo, D. & Sun, S.-C. NF-κB signaling in inflammation. *Signal transduction and targeted therapy* **2**, 17023 (2017).

363 Qi, C., Cai, Y., Gunn, L., Ding, C., Li, B., Kloecker, G., Qian, K., Vasilakos, J., Saijo, S., Iwakura, Y., Yannelli, J. R. & Yan, J. Differential pathways regulating innate and adaptive anti-tumor immune responses by particulate and soluble yeast-derived β-glucans. *Blood* (2011).

364 Goodridge, H. S., Reyes, C. N., Becker, C. A., Katsumoto, T. R., Ma, J., Wolf, A. J., Bose, N., Chan, A. S. H., Magee, A. S., Danielson, M. E., Weiss, A., Vasilakos, J. P. & Underhill, D. M. Activation of the innate immune receptor Dectin-1 upon formation of a "phagocytic synapse". *Nature* **472**, 471-475 (2011).

365 Elder, M. J., Webster, S. J., Chee, R., Williams, D. L., Gaston, J. & Goodall, J. C. β-glucan size controls dectin-1 mediated immune responses in human dendritic cells by regulating IL-1β production. *Frontiers in Immunology* **8**, 791 (2017).

366 Hernandez-Santos, N. & Klein, B. S. Through the Scope Darkly: The Gut Mycobiome Comes into Focus. *Cell Host Microbe* **22**, 728-729 (2017).

367 Rochereau, N., Drocourt, D., Perouzel, E., Pavot, V., Redelinghuys, P., Brown, G. D., Tiraby, G., Roblin, X., Verrier, B., Genin, C., Corthésy, B. & Paul, S. Dectin-1 Is Essential for Reverse Transcytosis of Glycosylated SIgA-Antigen Complexes by Intestinal M Cells. *PLoS Biol.* **11**, e1001658 (2013).

368 Cohen-Kedar, S., Baram, L., Elad, H., Brazowski, E., Guzner-Gur, H. & Dotan, I. Human intestinal epithelial cells respond to beta-glucans via Dectin-1 and Syk. *Eur. J. Immunol.* **44**, 3729-3740 (2014).

369 Tang, C., Kamiya, T., Liu, Y., Kadoki, M., Kakuta, S., Oshima, K., Hattori, M., Takeshita, K., Kanai, T., Saijo, S., Ohno, N. & Iwakura, Y. Inhibition of Dectin-1 Signaling Ameliorates Colitis by Inducing Lactobacillus-Mediated Regulatory T Cell Expansion in the Intestine. *Cell Host Microbe* **18**, 183-197 (2015).

370 Zhou, T., Chen, Y., Hao, L. & Zhang, Y. DC-SIGN and immunoregulation. *Cell Mol Immunol* **3**, 279-283 (2006).
371 Sprokholt, J. K., Overmars, R. J. & Geijtenbeek, T. B. H. in *C-Type Lectin Receptors in Immunity* (ed Sho Yamasaki) 129-150 (Springer Japan, 2016).
372 Engering, A., van Vliet, S. J., Geijtenbeek, T. B. H. & van Kooyk, Y. Subset of DC-SIGN⁺ dendritic cells in human blood transmits HIV-1 to T lymphocytes. *Blood* **100**, 1780-1786 (2002).
373 Granelli-Piperno, A., Pritsker, A., Pack, M., Shimeliovich, I., Arrighi, J. F., Park, C. G., Trumpfheller, C., Piguet, V., Moran, T. M. & Steinman, R. M. Dendritic cell-specific intercellular adhesion molecule 3-grabbing nonintegrin/CD209 is abundant on macrophages in the normal human lymph node and is not required for dendritic cell stimulation of the mixed leukocyte reaction. *J. Immunol.* **175**, 4265-4273 (2005).
374 Jameson, B., Baribaud, F., Pohlmann, S., Ghavimi, D., Mortari, F., Doms, R. W. & Iwasaki, A. Expression of DC-SIGN by dendritic cells of intestinal and genital mucosae in humans and rhesus macaques. *J. Virol.* **76**, 1866-1875 (2002).
375 Soilleux, E. J., Morris, L. S., Leslie, G., Chehimi, J., Luo, Q., Levroney, E., Trowsdale, J., Montaner, L. J., Doms, R. W., Weissman, D., Coleman, N. & Lee, B. Constitutive and induced expression of DC-SIGN on dendritic cell and macrophage subpopulations in situ and in vitro. *J Leukoc Biol* **71**, 445-457 (2002).
376 Appelmelk, B. J., van Die, I., van Vliet, S. J., Vandenbroucke-Grauls, C. M. J. E., Geijtenbeek, T. B. H. & van Kooyk, Y. Cutting Edge: Carbohydrate Profiling Identifies New Pathogens That Interact with Dendritic Cell-Specific ICAM-3-Grabbing Nonintegrin on Dendritic Cells. *The Journal of Immunology* **170**, 1635-1639 (2003).
377 Steeghs, L., van Vliet, S. J., Uronen-Hansson, H., van Mourik, A., Engering, A., Sanchez-Hernandez, M., Klein, N., Callard, R., van Putten, J. P., van der Ley, P., van Kooyk, Y. & van de Winkel, J. G. Neisseria meningitidis expressing lgtB lipopolysaccharide targets DC-SIGN and modulates dendritic cell function. *Cell. Microbiol.* **8**, 316-325 (2006).
378 Park, C. G., Takahara, K., Umemoto, E., Yashima, Y., Matsubara, K., Matsuda, Y., Clausen, B. E., Inaba, K. & Steinman, R. M. Five mouse homologues of the human dendritic cell C-type lectin, DC-SIGN. *Int. Immunol.* **13**, 1283-1290 (2001).
379 Parent, S. A., Zhang, T., Chrebet, G., Clemas, J. A., Figueroa, D. J., Ky, B., Blevins, R. A., Austin, C. P. & Rosen, H. Molecular characterization of the murine SIGNR1 gene encoding a C-type lectin homologous to human DC-SIGN and DC-SIGNR. *Gene* **293**, 33-46 (2002).
380 Takahara, K., Arita, T., Tokieda, S., Shibata, N., Okawa, Y., Tateno, H., Hirabayashi, J. & Inaba, K. Difference in fine specificity to polysaccharides of Candida albicans mannoprotein between mouse SIGNR1 and human DC-SIGN. *Infect. Immun.* **80**, 1699-1706 (2012).
381 Prabagar, M., Do, Y., Ryu, S., Park, J., Choi, H., Choi, W., Yun, T., Moon, J., Choi, I. & Ko, K. SIGN-R1, a C-type lectin, enhances apoptotic cell clearance through the complement deposition pathway by interacting with C1q in the spleen. *Cell Death & Differentiation* **20**, 535-545 (2013).
382 Geijtenbeek, T. B., Groot, P. C., Nolte, M. A., van Vliet, S. J., Gangaram-Panday, S. T., van Duijnhoven, G. C., Kraal, G., van Oosterhout, A. J. & van Kooyk, Y. Marginal zone macrophages express a murine homologue of DC-SIGN that captures blood-borne antigens in vivo. *Blood* **100**, 2908-2916 (2002).
383 Kang, Y. S., Yamazaki, S., Iyoda, T., Pack, M., Bruening, S. A., Kim, J. Y., Takahara, K., Inaba, K., Steinman, R. M. & Park, C. G. SIGN-R1, a novel C-

type lectin expressed by marginal zone macrophages in spleen, mediates uptake of the polysaccharide dextran. *Int. Immunol.* **15**, 177-186 (2003).

384 Rabinovich, G. A. A sweet path toward tolerance in the gut. *Nat. Med.* **16**, 1076-1077 (2010).

385 Diana, J., Moura, I. C., Vaugier, C., Gestin, A., Tissandie, E., Beaudoin, L., Corthésy, B., Hocini, H., Lehuen, A. & Monteiro, R. C. Secretory IgA Induces Tolerogenic Dendritic Cells through SIGNR1 Dampening Autoimmunity in Mice. *The Journal of Immunology* **191**, 2335-2343 (2013).

386 Kang, Y.-S., Kim, J. Y., Bruening, S. A., Pack, M., Charalambous, A., Pritsker, A., Moran, T. M., Loeffler, J. M., Steinman, R. M. & Park, C. G. The C-type lectin SIGN-R1 mediates uptake of the capsular polysaccharide of Streptococcus pneumoniae in the marginal zone of mouse spleen. *Proceedings of the National Academy of Sciences* **101**, 215-220 (2004).

387 Nagaoka, K., Takahara, K., Tanaka, K., Yoshida, H., Steinman, R. M., Saitoh, S., Akashi-Takamura, S., Miyake, K., Kang, Y. S., Park, C. G. & Inaba, K. Association of SIGNR1 with TLR4-MD-2 enhances signal transduction by recognition of LPS in gram-negative bacteria. *Int. Immunol.* **17**, 827-836 (2005).

388 Saunders, S. P., Barlow, J. L., Walsh, C. M., Bellsoi, A., Smith, P., McKenzie, A. N. & Fallon, P. G. C-type lectin SIGN-R1 has a role in experimental colitis and responsiveness to lipopolysaccharide. *J. Immunol.* **184**, 2627-2637 (2010).

389 Zhou, Y., Kawasaki, H., Hsu, S.-C., Lee, R. T., Yao, X., Plunkett, B., Fu, J., Yang, K., Lee, Y. C. & Huang, S.-K. Oral tolerance to food-induced systemic anaphylaxis mediated by the C-type lectin SIGNR1. *Nat. Med.* **16**, 1128-1133 (2010).

390 Ifrim, D. C., Bain, J. M., Reid, D. M., Oosting, M., Verschueren, I., Gow, N. A. R., van Krieken, J. H., Brown, G. D., Kullberg, B.-J., Joosten, L. A. B., van der Meer, J. W. M., Koentgen, F., Erwig, L. P., Quintin, J. & Netea, M. G. Role of Dectin-2 for Host Defense against Systemic Infection with Candida glabrata. *Infect. Immun.* **82**, 1064-1073 (2014).

391 Yabe, R. & Saijo, S. in *C-Type Lectin Receptors in Immunity* 3-13 (Springer, 2016).

392 Taylor, P. R., Reid, D. M., Heinsbroek, S. E., Brown, G. D., Gordon, S. & Wong, S. Y. Dectin-2 is predominantly myeloid restricted and exhibits unique activation-dependent expression on maturing inflammatory monocytes elicited in vivo. *Eur. J. Immunol.* **35**, 2163-2174 (2005).

393 McDonald, J. U., Rosas, M., Brown, G. D., Jones, S. A. & Taylor, P. R. Differential dependencies of monocytes and neutrophils on dectin-1, dectin-2 and complement for the recognition of fungal particles in inflammation. *PLoS One* **7**, e45781 (2012).

394 Wittmann, A., Lamprinaki, D., Bowles, K. M., Katzenellenbogen, E., Knirel, Y. A., Whitfield, C., Nishimura, T., Matsumoto, N., Yamamoto, K. & Iwakura, Y. Dectin-2 Recognizes Mannosylated O-antigens of Human Opportunistic Pathogens and Augments Lipopolysaccharide Activation of Myeloid Cells. *J. Biol. Chem.* **291**, 17629-17638 (2016).

395 Ishikawa, T., Itoh, F., Yoshida, S., Saijo, S., Matsuzawa, T., Gonoi, T., Saito, T., Okawa, Y., Shibata, N., Miyamoto, T. & Yamasaki, S. Identification of Distinct Ligands for the C-type Lectin Receptors Mincle and Dectin-2 in the Pathogenic Fungus Malassezia. *Cell Host & Microbe* **13**, 477-488 (2013).

396 Mori, D., Shibata, K. & Yamasaki, S. C-type lectin receptor dectin-2 binds to an endogenous protein β-glucuronidase on dendritic cells. *PloS one* **12**, e0169562 (2017).
397 Saijo, S. & Iwakura, Y. Dectin-1 and Dectin-2 in innate immunity against fungi. *Int. Immunol.*, dxr046 (2011).
398 Sato, K., Yang, X.-l., Yudate, T., Chung, J.-S., Wu, J., Luby-Phelps, K., Kimberly, R. P., Underhill, D., Cruz, P. D. & Ariizumi, K. Dectin-2 is a pattern recognition receptor for fungi that couples with the Fc receptor γ chain to induce innate immune responses. *J. Biol. Chem.* **281**, 38854-38866 (2006).
399 LeibundGut-Landmann, S., Groß, O., Robinson, M. J., Osorio, F., Slack, E. C., Tsoni, S. V., Schweighoffer, E., Tybulewicz, V., Brown, G. D., Ruland, J. & Reis e Sousa, C. Syk- and CARD9-dependent coupling of innate immunity to the induction of T helper cells that produce interleukin 17. *Nat. Immunol.* **8**, 630 (2007).
400 Chang, T.-H., Huang, J.-H., Lin, H.-C., Chen, W.-Y., Lee, Y.-H., Hsu, L.-C., Netea, M. G., Ting, J. P. Y. & Wu-Hsieh, B. A. Dectin-2 is a primary receptor for NLRP3 inflammasome activation in dendritic cell response to Histoplasma capsulatum. *PLoS Path.* **13**, e1006485 (2017).
401 Whitmarsh, A. J. Regulation of gene transcription by mitogen-activated protein kinase signaling pathways. *Biochim. Biophys. Acta* **1773**, 1285-1298 (2007).
402 Robinson, M. J., Osorio, F., Rosas, M., Freitas, R. P., Schweighoffer, E., Groß, O., Verbeek, J. S., Ruland, J., Tybulewicz, V. & Brown, G. D. Dectin-2 is a Syk-coupled pattern recognition receptor crucial for Th17 responses to fungal infection. *The Journal of experimental medicine* **206**, 2037-2051 (2009).
403 Karin, M., Liu, Z. & Zandi, E. AP-1 function and regulation. *Curr. Opin. Cell Biol.* **9**, 240-246 (1997).
404 Vannucci, L., Krizan, J., Sima, P., Stakheev, D., Caja, F., Rajsiglova, L., Horak, V. & Saieh, M. Immunostimulatory properties and antitumor activities of glucans. *Int. J. Oncol.* **43**, 357-364 (2013).
405 El Enshasy, H. A. & Hatti-Kaul, R. Mushroom immunomodulators: unique molecules with unlimited applications. *Trends Biotechnol.* **31**, 668-677 (2013).
406 Xu, X., Xu, P., Ma, C., Tang, J. & Zhang, X. Gut microbiota, host health, and polysaccharides. *Biotechnol. Adv.* **31**, 318-337 (2013).
407 Okolie, C. L., C. K. Rajendran, S. R., Udenigwe, C. C., Aryee, A. N. A. & Mason, B. Prospects of brown seaweed polysaccharides (BSP) as prebiotics and potential immunomodulators. *J. Food Biochem.* **41**, e12392 (2017).
408 Jantan, I., Ahmad, W. & Bukhari, S. N. A. Plant-derived immunomodulators: an insight on their preclinical evaluation and clinical trials. *Frontiers in Plant Science* **6**, 655 (2015).
409 Cai, H.-l., Huang, X.-j., Nie, S.-p., Xie, M.-y., Phillips, G. O. & Cui, S. W. Study on Dendrobium officinale O-acetyl-glucomannan (Dendronan®): Part III–Immunomodulatory activity in vitro. *Bioactive Carbohydrates and Dietary Fibre* **5**, 99-105 (2015).
410 Xu, D., Wang, H., Zheng, W., Gao, Y., Wang, M., Zhang, Y. & Gao, Q. Charaterization and immunomodulatory activities of polysaccharide isolated from Pleurotus eryngii. *International Journal of Biological Macromolecules* **92**, 30-36 (2016).
411 Schwarz, H., Schmittner, M., Duschl, A. & Horejs-Hoeck, J. Residual endotoxin contaminations in recombinant proteins are sufficient to activate human CD1c+ dendritic cells. *PloS one* **9**, e113840 (2014).
412 Govers, C., Tomassen, M. M. M., Rieder, A., Ballance, S., Knutsen, S. H. & Mes, J. J. Lipopolysaccharide quantification and alkali-based inactivation in

polysaccharide preparations to enable in vitro immune modulatory studies. *Bioactive Carbohydrates and Dietary Fibre* **8**, 15-25 (2016).

413 Gertsch, J., Viveros-Paredes, J. M. & Taylor, P. Plant immunostimulants--scientific paradigm or myth? *J. Ethnopharmacol.* **136**, 385-391 (2011).

414 Tynan, G. A., McNaughton, A., Jarnicki, A., Tsuji, T. & Lavelle, E. C. Polymyxin B inadequately quenches the effects of contaminating lipopolysaccharide on murine dendritic cells. *PloS one* **7**, e37261 (2012).

415 Han, Q.-B. Critical Problems Stalling Progress in Natural Bioactive Polysaccharide Research and Development. *J. Agric. Food Chem.* **66**, 4581-4583 (2018).

416 Xing, X., Cui, S. W., Nie, S., Phillips, G. O., Goff, H. D. & Wang, Q. Study on Dendrobium officinale O-acetyl-glucomannan (Dendronan(R)): part II. Fine structures of O-acetylated residues. *Carbohydr Polym* **117**, 422-433 (2015).

417 Smiderle, F. R., Alquini, G., Tadra-Sfeir, M. Z., Iacomini, M., Wichers, H. J. & Van Griensven, L. J. L. D. Agaricus bisporus and Agaricus brasiliensis (1→6)-β-d-glucans show immunostimulatory activity on human THP-1 derived macrophages. *Carbohydrate Polymers* **94**, 91-99 (2013).

418 Yermak, I. M., Barabanova, A. O., Aminin, D. L., Davydova, V. N., Sokolova, E. V., Solov'eva, T. F., Kim, Y. H. & Shin, K. S. Effects of structural peculiarities of carrageenans on their immunomodulatory and anticoagulant activities. *Carbohydrate Polymers* **87**, 713-720 (2012).

419 Perera, N., Yang, F. L., Lu, Y. T., Li, L. H., Hua, K. F. & Wu, S. H. Antrodia cinnamomea Galactomannan Elicits Immuno-stimulatory Activity Through Toll-like Receptor 4. *International journal of biological sciences* **14**, 1378-1388 (2018).

420 Heinsbroek, S. E. M., Williams, D. L., Welting, O., Meijer, S. L., Gordon, S. & de Jonge, W. J. Orally delivered β-glucans aggravate dextran sulfate sodium (DSS)-induced intestinal inflammation. *Nutrition Research* **35**, 1106-1112 (2015).

421 Sweeney, T., Collins, C. B., Reilly, P., Pierce, K. M., Ryan, M. & O'Doherty, J. V. Effect of purified β-glucans derived from Laminaria digitata, Laminaria hyperborea and Saccharomyces cerevisiae on piglet performance, selected bacterial populations, volatile fatty acids and pro-inflammatory cytokines in the gastrointestinal tract of pigs. *British Journal of Nutrition* **108**, 1226-1234 (2012).

422 Ryan, M. T., O'Shea, C. J., Collins, C. B., O'Doherty, J. V. & Sweeney, T. Effects of dietary supplementation with Laminaria hyperborea, Laminaria digitata, and Saccharomyces cerevisiae on the IL-17 pathway in the porcine colon. *J. Anim. Sci.* **90**, 263-265 (2012).

423 Jin, M., Zhao, K., Huang, Q. & Shang, P. Structural features and biological activities of the polysaccharides from Astragalus membranaceus. *International Journal of Biological Macromolecules* **64**, 257-266 (2014).

424 Zhou, L., Liu, Z., Wang, Z., Yu, S., Long, T., Zhou, X. & Bao, Y. Astragalus polysaccharides exerts immunomodulatory effects via TLR4-mediated MyD88-dependent signaling pathway in vitro and in vivo. *Scientific Reports* **7**, 44822 (2017).

425 Liu, B., Lin, Q., Yang, T., Zeng, L., Shi, L., Chen, Y. & Luo, F. Oat β-glucan ameliorates dextran sulfate sodium (DSS)-induced ulcerative colitis in mice. *Food & function* **6**, 3454-3463 (2015).

426 Liu, L., Shen, J., Zhao, C., Wang, X., Yao, J., Gong, Y. & Yang, X. Dietary Astragalus polysaccharide alleviated immunological stress in broilers exposed to lipopolysaccharide. *International Journal of Biological Macromolecules* **72**, 624-632 (2015).

427 Suh, H.-J., Yang, H.-S., Ra, K.-S., Noh, D.-O., Kwon, K.-H., Hwang, J.-H. & Yu, K.-W. Peyer's patch-mediated intestinal immune system modulating activity of pectic-type polysaccharide from peel of Citrus unshiu. *Food Chem.* **138**, 1079-1086 (2013).
428 Lean, Q. Y., Eri, R. D., Fitton, J. H., Patel, R. P. & Gueven, N. Fucoidan Extracts Ameliorate Acute Colitis. *PLOS ONE* **10**, e0128453 (2015).
429 Takagi, T., Naito, Y., Higashimura, Y., Ushiroda, C., Mizushima, K., Ohashi, Y., Yasukawa, Z., Ozeki, M., Tokunaga, M., Okubo, T., Katada, K., Kamada, K., Uchiyama, K., Handa, O., Itoh, Y. & Yoshikawa, T. Partially hydrolysed guar gum ameliorates murine intestinal inflammation in association with modulating luminal microbiota and SCFA. *The British journal of nutrition* **116**, 1199-1205 (2016).
430 Wang, Y., Liu, J., Li, Q., Wang, Y. & Wang, C. Two natural glucomannan polymers, from Konjac and Bletilla, as bioactive materials for pharmaceutical applications. *Biotechnol. Lett.* **37**, 1-8 (2015).
431 Luo, L., Zhou, Z., Xue, J., Wang, Y., Zhang, J., Cai, X., Liu, Y. & Yang, F. Bletilla striata polysaccharide has a protective effect on intestinal epithelial barrier disruption in TAA-induced cirrhotic rats. *Experimental and therapeutic medicine* **16**, 1715-1722 (2018).
432 Fransen, F., Sahasrabudhe, N. M., Elderman, M., Bosveld, M., El Aidy, S., Hugenholtz, F., Borghuis, T., Kousemaker, B., Winkel, S., van der Gaast-de Jongh, C., de Jonge, M. I., Boekschoten, M. V., Smidt, H., Schols, H. A. & de Vos, P. β2→1-Fructans Modulate the Immune System In Vivo in a Microbiota-Dependent and -Independent Fashion. *Frontiers in Immunology* **8** (2017).
433 Deng, C., Fu, H., Shang, J., Chen, J. & Xu, X. Dectin-1 mediates the immunoenhancement effect of the polysaccharide from Dictyophora indusiata. *International Journal of Biological Macromolecules* **109**, 369-374 (2018).
434 Karaca, K., Sharma, J. M. & Nordgren, R. Nitric oxide production by chicken macrophages activated by acemannan, a complex carbohydrate extracted from Aloe Vera. *Int. J. Immunopharmacol.* **17**, 183-188 (1995).
435 Vogt, L., Ramasamy, U., Meyer, D., Pullens, G., Venema, K., Faas, M. M., Schols, H. A. & de Vos, P. Immune Modulation by Different Types of β2→1-Fructans Is Toll-Like Receptor Dependent. *PLOS ONE* **8**, e68367 (2013).
436 Hoentjen, F., Welling, G. W., Harmsen, H. J., Zhang, X., Snart, J., Tannock, G. W., Lien, K., Churchill, T. A., Lupicki, M. & Dieleman, L. A. Reduction of colitis by prebiotics in HLA-B27 transgenic rats is associated with microflora changes and immunomodulation. *Inflammatory bowel diseases* **11**, 977-985 (2005).
437 Roller, M., Rechkemmer, G. & Watzl, B. Prebiotic inulin enriched with oligofructose in combination with the probiotics Lactobacillus rhamnosus and Bifidobacterium lactis modulates intestinal immune functions in rats. *The journal of Nutrition* **134**, 153-156 (2004).
438 He, Y., Wu, C., Li, J., Li, H., Sun, Z., Zhang, H., de Vos, P., Pan, L.-L. & Sun, J. Inulin-Type Fructans Modulates Pancreatic–Gut Innate Immune Responses and Gut Barrier Integrity during Experimental Acute Pancreatitis in a Chain Length-Dependent Manner. *Frontiers in Immunology* **8** (2017).
439 Vogt, L. M., Meyer, D., Pullens, G., Faas, M. M., Venema, K., Ramasamy, U., Schols, H. A. & de Vos, P. Toll-like receptor 2 activation by beta2-->1-fructans protects barrier function of T84 human intestinal epithelial cells in a chain length-dependent manner. *J. Nutr.* **144**, 1002-1008 (2014).
440 Wu, R. Y., Abdullah, M., Määttänen, P., Pilar, A. V. C., Scruten, E., Johnson-Henry, K. C., Napper, S., O'Brien, C., Jones, N. L. & Sherman, P. M. Protein

kinase C δ signaling is required for dietary prebiotic-induced strengthening of intestinal epithelial barrier function. *Scientific Reports* **7**, 40820 (2017).

441 Cheung, P. C. K. Mini-review on edible mushrooms as source of dietary fiber: Preparation and health benefits. *Food Science and Human Wellness* **2**, 162-166 (2013).

442 Deng, C., Shang, J., Fu, H., Chen, J., Liu, H. & Chen, J. Mechanism of the immunostimulatory activity by a polysaccharide from Dictyophora indusiata. *International Journal of Biological Macromolecules* **91**, 752-759 (2016).

443 Liu, J.-Y., Yang, F.-L., Lu, C.-P., Yang, Y.-L., Wen, C.-L., Hua, K.-F. & Wu, S.-H. Polysaccharides from Dioscorea batatas Induce Tumor Necrosis Factor-α Secretion via Toll-like Receptor 4-Mediated Protein Kinase Signaling Pathways. *J. Agric. Food Chem.* **56**, 9892-9898 (2008).

444 Sun, H., Zhang, J., Chen, F., Chen, X., Zhou, Z. & Wang, H. Activation of RAW264.7 macrophages by the polysaccharide from the roots of Actinidia eriantha and its molecular mechanisms. *Carbohydr Polym* **121**, 388-402 (2015).

445 Khil'chenko, S. R., Zaporozhets, T. S., Shevchenko, N. M., Zvyagintseva, T. N., Vogel, U., Seeberger, P. & Lepenies, B. Immunostimulatory activity of fucoidan from the brown alga Fucus evanescens: Role of sulfates and acetates. *J. Carbohydr. Chem.* **30**, 291-305 (2011).

446 Xue, M., Sun, H., Cao, Y., Wang, G., Meng, Y., Wang, D. & Hong, Y. Mulberry leaf polysaccharides modulate murine bone-marrow-derived dendritic cell maturation. *Human vaccines & immunotherapeutics* **11**, 946-950 (2015).

447 Santander, S. P., Aoki, M., Hernandez, J. F., Pombo, M., Moins-Teisserenc, H., Mooney, N. & Fiorentino, S. Galactomannan from Caesalpinia spinosa induces phenotypic and functional maturation of human dendritic cells. *Int. Immunopharmacol.* **11**, 652-660 (2011).

448 Ostrop, J. & Lang, R. Contact, Collaboration, and Conflict: Signal Integration of Syk-Coupled C-Type Lectin Receptors. *The Journal of Immunology* **198**, 1403-1414 (2017).

449 Gringhuis, S. I., den Dunnen, J., Litjens, M., van der Vlist, M., Wevers, B., Bruijns, S. C. & Geijtenbeek, T. B. Dectin-1 directs T helper cell differentiation by controlling noncanonical NF-kappaB activation through Raf-1 and Syk. *Nat. Immunol.* **10**, 203-213 (2009).

450 Meijerink, M., Rösch, C., Taverne, N., Venema, K., Gruppen, H., Schols, H. A. & Wells, J. M. Structure Dependent-Immunomodulation by Sugar Beet Arabinans via a SYK Tyrosine Kinase-Dependent Signaling Pathway. *Frontiers in Immunology* **9** (2018).

451 Saraiva, M. & O'Garra, A. The regulation of IL-10 production by immune cells. *Nature Reviews Immunology* **10**, 170 (2010).

452 Kole, A. & Maloy, K. J. Control of intestinal inflammation by interleukin-10. *Curr. Top. Microbiol. Immunol.* **380**, 19-38 (2014).

453 Mantovani, A. & Marchesi, F. IL-10 and macrophages orchestrate gut homeostasis. *Immunity* **40**, 637-639 (2014).

454 Lehmann, S., Hiller, J., van Bergenhenegouwen, J., Knippels, L. M. J., Garssen, J. & Traidl-Hoffmann, C. In Vitro Evidence for Immune-Modulatory Properties of Non-Digestible Oligosaccharides: Direct Effect on Human Monocyte Derived Dendritic Cells. *PLoS ONE* **10**, e0132304 (2015).

455 He, X., Shu, J., Xu, L., Lu, C. & Lu, A. Inhibitory effect of Astragalus polysaccharides on lipopolysaccharide-induced TNF-a and IL-1beta production in THP-1 cells. *Molecules (Basel, Switzerland)* **17**, 3155-3164 (2012).

456 Wang, X., Wang, S., Li, Y., Wang, F., Yang, X. & Yao, J. Sulfated Astragalus polysaccharide can regulate the inflammatory reaction induced by LPS in Caco2 cells. *Int J Biol Macromol* **60**, 248-252 (2013).

457 Yin, G., Huang, J., Ma, M., Suo, X. & Huang, Z. Oyster crude polysaccharides attenuates lipopolysaccharide-induced cytokines production and PPARγ expression in weanling piglets. *SpringerPlus* **5**, 677 (2016).
458 Lu, Y., Li, L., Zhang, J. W., Zhong, X. Q., Wei, J. A. & Han, L. Total polysaccharides of the Sijunzi decoction attenuate tumor necrosis factor-alpha-induced damage to the barrier function of a Caco-2 cell monolayer via the nuclear factor-kappaB-myosin light chain kinase-myosin light chain pathway. *World journal of gastroenterology* **24**, 2867-2877 (2018).
459 Mazmanian, S. K. & Kasper, D. L. The love–hate relationship between bacterial polysaccharides and the host immune system. *Nature Reviews Immunology* **6**, 849-858 (2006).
460 Wolf, A. J. & Underhill, D. M. Peptidoglycan recognition by the innate immune system. *Nat. Rev. Immunol.* **18**, 243-254 (2018).
461 Bryant, C. E., Spring, D. R., Gangloff, M. & Gay, N. J. The molecular basis of the host response to lipopolysaccharide. *Nat. Rev. Microbiol.* **8**, 8-14 (2010).
462 Martens, E. C., Neumann, M. & Desai, M. S. Interactions of commensal and pathogenic microorganisms with the intestinal mucosal barrier. *Nat. Rev. Microbiol.* (2018).
463 Duerr, C. U., Zenk, S. F., Chassin, C., Pott, J., Gütle, D., Hensel, M. & Hornef, M. W. O-Antigen Delays Lipopolysaccharide Recognition and Impairs Antibacterial Host Defense in Murine Intestinal Epithelial Cells. *PLoS Path.* **5**, e1000567 (2009).
464 Lerouge, I. & Vanderleyden, J. O-antigen structural variation: mechanisms and possible roles in animal/plant–microbe interactions. *FEMS Microbiol. Rev.* **26**, 17-47 (2002).
465 Zhang, X., Goebel, E. M., Rodríguez, M. E., Preston, A. & Harvill, E. T. The O Antigen Is a Critical Antigen for the Development of a Protective Immune Response to Bordetella parapertussis. *Infect. Immun.* **77**, 5050-5058 (2009).
466 Zenhom, M., Hyder, A., de Vrese, M., Heller, K. J., Roeder, T. & Schrezenmeir, J. Prebiotic oligosaccharides reduce proinflammatory cytokines in intestinal Caco-2 cells via activation of PPARgamma and peptidoglycan recognition protein 3. *J. Nutr.* **141**, 971-977 (2011).
467 Rice, P. J., Adams, E. L., Ozment-Skelton, T., Gonzalez, A. J., Goldman, M. P., Lockhart, B. E., Barker, L. A., Breuel, K. F., Deponti, W. K., Kalbfleisch, J. H., Ensley, H. E., Brown, G. D., Gordon, S. & Williams, D. L. Oral delivery and gastrointestinal absorption of soluble glucans stimulate increased resistance to infectious challenge. *J. Pharmacol. Exp. Ther.* **314**, 1079-1086 (2005).
468 Noss, I., Doekes, G., Thorne, P. S., Heederik, D. J. & Wouters, I. M. Comparison of the potency of a variety of β-glucans to induce cytokine production in human whole blood. *Innate Immunity* **19**, 10-19 (2013).
469 Stephen, T. L., Groneck, L. & Kalka-Moll, W. M. The modulation of adaptive immune responses by bacterial zwitterionic polysaccharides. *International journal of microbiology* **2010** (2010).
470 Tzianabos, A., Onderdonk, A., Rosner, B., Cisneros, R. & Kasper, D. Structural features of polysaccharides that induce intra-abdominal abscesses. *Science* **262**, 416-419 (1993).
471 Tzianabos, A. O., Wang, J. Y. & Lee, J. C. Structural rationale for the modulation of abscess formation by Staphylococcus aureus capsular polysaccharides. *Proceedings of the National Academy of Sciences of the United States of America* **98**, 9365-9370 (2001).
472 Young, N. M., Kreisman, L. S., Stupak, J., MacLean, L. L., Cobb, B. A. & Richards, J. C. Structural characterization and MHCII-dependent

immunological properties of the zwitterionic O-chain antigen of Morganella morganii. *Glycobiology* **21**, 1266-1276 (2011).

473 Round, J. L., Lee, S. M., Li, J., Tran, G., Jabri, B., Chatila, T. A. & Mazmanian, S. K. The Toll-like receptor 2 pathway establishes colonization by a commensal of the human microbiota. *Science* **332**, 974-977 (2011).

474 Mazmanian, S. K., Liu, C. H., Tzianabos, A. O. & Kasper, D. L. An Immunomodulatory Molecule of Symbiotic Bacteria Directs Maturation of the Host Immune System. *Cell* **122**, 107-118 (2005).

475 Danne, C., Ryzhakov, G., Martinez-Lopez, M., Ilott, N. E., Franchini, F., Cuskin, F., Lowe, E. C., Bullers, S. J., Arthur, J. S. C. & Powrie, F. A Large Polysaccharide Produced by Helicobacter hepaticus Induces an Anti-inflammatory Gene Signature in Macrophages. *Cell Host Microbe* **22**, 733-745.e735 (2017).

476 Gupta, S. K., Sarkar, B., Bhattacharjee, S., Kumar, N., Naskar, S. & Uppuluri, K. B. Modulation of cytokine expression by dietary levan in the pathogen aggravated rohu, Labeo rohita fingerlings. *Aquaculture* **495**, 496-505 (2018).

477 Li, J. & Kim, I. H. Effects of levan-type fructan supplementation on growth performance, digestibility, blood profile, fecal microbiota, and immune responses after lipopolysaccharide challenge in growing pigs. *J. Anim. Sci.* **91**, 5336-5343 (2013).

478 Rairakhwada, D., Pal, A. K., Bhathena, Z. P., Sahu, N. P., Jha, A. & Mukherjee, S. C. Dietary microbial levan enhances cellular non-specific immunity and survival of common carp (Cyprinus carpio) juveniles. *Fish Shellfish Immunol.* **22**, 477-486 (2007).

479 Ishida, R., Sakaguchi, K., Matsuzaki, C., Katoh, T., Ishida, N., Yamamoto, K. & Hisa, K. Levansucrase from Leuconostoc mesenteroides NTM048 produces a levan exopolysaccharide with immunomodulating activity. *Biotechnol. Lett.* **38**, 681-687 (2016).

480 Xu, X., Gao, C., Liu, Z., Wu, J., Han, J., Yan, M. & Wu, Z. Characterization of the levan produced by Paenibacillus bovis sp. nov BD3526 and its immunological activity. *Carbohydrate Polymers* **144**, 178-186 (2016).

481 Liu, J., Luo, J., Ye, H. & Zeng, X. Preparation, antioxidant and antitumor activities in vitro of different derivatives of levan from endophytic bacterium Paenibacillus polymyxa EJS-3. *Food Chem. Toxicol.* **50**, 767-772 (2012).

482 Srikanth, R., Siddartha, G., Sundhar Reddy, C. H. S. S., Harish, B. S., Janaki Ramaiah, M. & Uppuluri, K. B. Antioxidant and anti-inflammatory levan produced from Acetobacter xylinum NCIM2526 and its statistical optimization. *Carbohydrate Polymers* **123**, 8-16 (2015).

483 Esawy, M. A., Amer, H., Gamal-Eldeen, A. M., El Enshasy, H. A., Helmy, W. A., Abo-Zeid, M. A. M., Malek, R., Ahmed, E. F. & Awad, G. E. A. Scaling up, characterization of levan and its inhibitory role in carcinogenesis initiation stage'. *Carbohydrate polymers* **95**, 578-587 (2013).

484 Kotarski, S. F. & Savage, D. C. Models for Study of the Specificity by Which Indigenous Lactobacilli Adhere to Murine Gastric Epithelia. *Infect. Immun.* **26**, 966-975 (1979).

485 Akatsuka, A., Ito, M., Yamauchi, C., Ochiai, A., Yamamoto, K. & Matsumoto, N. Tumor cells of non-hematopoietic and hematopoietic origins express activation-induced C-type lectin, the ligand for killer cell lectin-like receptor F1. *Int. Immunol.* **22**, 783-790 (2010).

486 Rashid, A. M., Batey, S. F. D., Syson, K., Koliwer-Brandl, H., Miah, F., Barclay, J. E., Findlay, K. C., Nartowski, K. P., Khimyak, Y. Z., Kalscheuer, R. & Bornemann, S. Assembly of α-Glucan by GlgE and GlgB in Mycobacteria and Streptomycetes. *Biochemistry* **55**, 3270-3284 (2016).

487 Verhertbruggen, Y., Marcus, S. E., Haeger, A., Verhoef, R., Schols, H. A., McCleary, B. V., McKee, L., Gilbert, H. J. & Paul Knox, J. Developmental

complexity of arabinan polysaccharides and their processing in plant cell walls. *The Plant Journal* **59**, 413-425 (2009).

488 Kim, Y.-S., Lim, Y.-R. & Oh, D.-K. l-Arabinose production from sugar beet arabinan by immobilized endo- and exo-arabinanases from Caldicellulosiruptor saccharolyticus in a packed-bed reactor. *J. Biosci. Bioeng.* **113**, 239-241 (2012).

489 Young, I. D., Montilla, A., Olano, A., Wittmann, A., Kawasaki, N. & Villamiel, M. Effect of purification of galactooligosaccharides derived from lactulose with Saccharomyces cerevisiae on their capacity to bind immune cell receptor Dectin-2. *Food Res. Int.* (2018).

490 Blake, J., Clarke, M., Jansson, P. & McNeil, K. Fructan from Erwinia herbicola. *J. Bacteriol.* **151**, 1595-1597 (1982).

491 Visnapuu, T., Mardo, K., Mosoarca, C., Zamfir, A. D., Vigants, A. & Alamäe, T. Levansucrases from Pseudomonas syringae pv. tomato and P. chlororaphis subsp. aurantiaca: Substrate specificity, polymerizing properties and usage of different acceptors for fructosylation. *J. Biotechnol.* **155**, 338-349 (2011).

492 Adamberg, S., Tomson, K., Vija, H., Puurand, M., Kabanova, N., Visnapuu, T., Jõgi, E., Alamäe, T. & Adamberg, K. Degradation of Fructans and Production of Propionic Acid by Bacteroides thetaiotaomicron are Enhanced by the Shortage of Amino Acids. *Frontiers in Nutrition* **1** (2014).

493 Ale, M. T. & Meyer, A. S. Fucoidans from brown seaweeds: An update on structures, extraction techniques and use of enzymes as tools for structural elucidation. *RSC Advances* **3**, 8131-8141 (2013).

494 Gong, Y., Wang, C., Lai, R. C., Su, K., Zhang, F. & Wang, D.-a. An improved injectable polysaccharide hydrogel: modified gellan gum for long-term cartilage regeneration in vitro. *Journal of Materials Chemistry* **19**, 1968-1977 (2009).

495 Cui, S. W., Wu, Y. & Ding, H. in *Fibre-Rich and Wholegrain Foods* (eds Jan A. Delcour & Kaisa Poutanen) 96-119 (Woodhead Publishing, 2013).

496 Mahammad, S., Comfort, D. A., Kelly, R. M. & Khan, S. A. Rheological properties of guar galactomannan solutions during hydrolysis with galactomannanase and α-galactosidase enzyme mixtures. *Biomacromolecules* **8**, 949-956 (2007).

497 Katzenellenbogen, E., Kocharova, N. A., Zatonsky, G. V., Kübler-Kiełb, J., Gamian, A., Shashkov, A. S., Knirel, Y. A. & Romanowska, E. Structural and serological studies on Hafnia alvei O-specific polysaccharide of α-d-mannan type isolated from the lipopolysaccharide of strain PCM 1223. *FEMS Immunology & Medical Microbiology* **30**, 223-227 (2001).

498 Mensink, M. A., Frijlink, H. W., van der Voort Maarschalk, K. & Hinrichs, W. L. J. Inulin, a flexible oligosaccharide I: Review of its physicochemical characteristics. *Carbohydrate Polymers* **130**, 405-419 (2015).

499 Abdelhameed, A. S., Ang, S., Morris, G. A., Smith, I., Lawson, C., Gahler, R., Wood, S. & Harding, S. E. An analytical ultracentrifuge study on ternary mixtures of konjac glucomannan supplemented with sodium alginate and xanthan gum. *Carbohydrate Polymers* **81**, 145-148 (2010).

500 Behera, S. S. & Ray, R. C. Konjac glucomannan, a promising polysaccharide of Amorphophallus konjac K. Koch in health care. *International Journal of Biological Macromolecules* **92**, 942-956 (2016).

501 Davé, V. & McCarthy, S. P. Review of konjac glucomannan. *J. Environ. Polymer Degradation* **5**, 237 (1997).

502 Singh, R. S., Kaur, N. & Kennedy, J. F. Pullulan and pullulan derivatives as promising biomolecules for drug and gene targeting. *Carbohydrate Polymers* **123**, 190-207 (2015).

503 Coviello, T., Palleschi, A., Grassi, M., Matricardi, P., Bocchinfuso, G. & Alhaique, F. Scleroglucan: A Versatile Polysaccharide for Modified Drug Delivery. *Molecules (Basel, Switzerland)* **10**, 6 (2005).
504 Lutz, M. B., Kukutsch, N., Ogilvie, A. L., Rossner, S., Koch, F., Romani, N. & Schuler, G. An advanced culture method for generating large quantities of highly pure dendritic cells from mouse bone marrow. *J. Immunol. Methods* **223**, 77-92 (1999).
505 Helft, J., Bottcher, J., Chakravarty, P., Zelenay, S., Huotari, J., Schraml, B. U., Goubau, D. & Reis e Sousa, C. GM-CSF Mouse Bone Marrow Cultures Comprise a Heterogeneous Population of CD11c(+)MHCII(+) Macrophages and Dendritic Cells. *Immunity* **42**, 1197-1211 (2015).
506 Kitamura, T., Koshino, Y., Shibata, F., Oki, T., Nakajima, H., Nosaka, T. & Kumagai, H. Retrovirus-mediated gene transfer and expression cloning: powerful tools in functional genomics. *Experimental hematology* **31**, 1007-1014 (2003).
507 Morita, S., Kojima, T. & Kitamura, T. Plat-E: an efficient and stable system for transient packaging of retroviruses. *Gene Ther.* **7**, 1063 (2000).
508 Heiss, C., Klutts, J. S., Wang, Z., Doering, T. L. & Azadi, P. The structure of Cryptococcus neoformans galactoxylomannan contains beta-D-glucuronic acid. *Carbohydr Res* **344**, 915-920 (2009).
509 Kamerling, J. P. & Boons, G.-J. *Comprehensive glycoscience: from chemistry to systems biology*. (Elsevier, 2007).
510 Harris, D. W. & Feather, M. S. Mechanism of the interconversion of D-glucose, D-mannose, and D-fructose in acid solution. *J. Am. Chem. Soc.* **97**, 178-181 (1975).
511 Ding, J. L. & Ho, B. Endotoxin detection--from limulus amebocyte lysate to recombinant factor C. *Sub-cellular biochemistry* **53**, 187-208 (2010).
512 Inoue, K. Y., Ino, K., Shiku, H. & Matsue, T. Electrochemical detection of endotoxin using recombinant factor C zymogen. *Electrochemistry Communications* **12**, 1066-1069 (2010).
513 Zhang, J. P., Wang, Q., Smith, T. R., Hurst, W. E. & Sulpizio, T. Endotoxin removal using a synthetic adsorbent of crystalline calcium silicate hydrate. *Biotechnol. Prog.* **21**, 1220-1225 (2005).
514 Hutter, J. L. & Bechhoefer, J. Calibration of atomic-force microscope tips. *Review of Scientific Instruments* **64**, 1868-1873 (1993).
515 Gunning, A. P., Chambers, S., Pin, C., Man, A. L., Morris, V. J. & Nicoletti, C. Mapping specific adhesive interactions on living human intestinal epithelial cells with atomic force microscopy. *FASEB J.* **22**, 2331-2339 (2008).
516 Maehara, Y., Tsujitani, S., Saeki, H., Oki, E., Yoshinaga, K., Emi, Y., Morita, M., Kohnoe, S., Kakeji, Y., Yano, T. & Baba, H. Biological mechanism and clinical effect of protein-bound polysaccharide K (KRESTIN(®)): review of development and future perspectives. *Surgery today* **42**, 8-28 (2012).
517 Riede, L., Grube, B. & Gruenwald, J. Larch arabinogalactan effects on reducing incidence of upper respiratory infections. *Current Medical Research and Opinion* **29**, 251-258 (2013).
518 Taylor, P. R. Dectin-1 is required for [beta]-glucan recognition and control of fungal infection. *Nature Immunol.* **8**, 31-38 (2007).
519 Gringhuis, S. I., Kaptein, T. M., Wevers, B. A., Mesman, A. W. & Geijtenbeek, T. B. H. Fucose-specific DC-SIGN signalling directs T helper cell type-2 responses via IKKε- and CYLD-dependent Bcl3 activation. *Nature Communications* **5**, 3898 (2014).
520 Vasta, G., Ahmed, H., Nita-Lazar, M., Banerjee, A., Pasek, M., Shridhar, S., Guha, P. & Fernández-Robledo, J. Galectins as self/non-self recognition receptors in innate and adaptive immunity: an unresolved paradox. *Frontiers in Immunology* **3** (2012).

521 Sanderson, S. & Shastri, N. LacZ inducible, antigen/MHC-specific T cell hybrids. *Int. Immunol.* **6**, 369-376 (1994).
522 Pyż, E. & Brown, G. D. in *Immune Receptors: Methods and Protocols* (eds Jonathan P. Rast & James W. D. Booth) 1-19 (Humana Press, 2011).
523 Karttunen, J. & Shastri, N. Measurement of ligand-induced activation in single viable T cells using the lacZ reporter gene. *Proceedings of the National Academy of Sciences* **88**, 3972-3976 (1991).
524 Malarkannan, S., Mendoza, L. M. & Shastri, N. in *Antigen Processing and Presentation Protocols* 265-272 (Springer, 2000).
525 Berry, R., Rossjohn, J. & Brooks, A. G. The Ly49 natural killer cell receptors: a versatile tool for viral self-discrimination. *Immunol. Cell Biol.* **92**, 214 (2014).
526 Cinelli, R. A. G., Ferrari, A., Pellegrini, V., Tyagi, M., Giacca, M. & Beltram, F. The Enhanced Green Fluorescent Protein as a Tool for the Analysis of Protein Dynamics and Localization: Local Fluorescence Study at the Single-molecule Level. *Photochem. Photobiol.* **71**, 771-776 (2000).
527 Katzenellenbogen, E., Kocharova, N. A., Zatonsky, G. V., Kubler-Kielb, J., Gamian, A., Shashkov, A. S., Knirel, Y. A. & Romanowska, E. Structural and serological studies on Hafnia alvei O-specific polysaccharide of alpha-D-mannan type isolated from the lipopolysaccharide of strain PCM 1223. *FEMS Immunol. Med. Microbiol.* **30**, 223-227 (2001).
528 Cardelle-Cobas, A., Olano, A., Irazoqui, G., Giacomini, C., Batista-Viera, F., Corzo, N. & Corzo-Martínez, M. Synthesis of Oligosaccharides Derived from Lactulose (OsLu) Using Soluble and Immobilized Aspergillus oryzae β-Galactosidase. *Frontiers in Bioengineering and Biotechnology* **4**, 21 (2016).
529 Morales, V., Sanz, M. L., Olano, A. & Corzo, N. Rapid Separation on Activated Charcoal of High Oligosaccharides in Honey. *Chromatographia* **64**, 1-6 (2006).
530 Kapteyn, J. C., Van Egmond, P., Sievi, E., Van Den Ende, H., Makarow, M. & Klis, F. M. The contribution of the O-glycosylated protein Pir2p/Hsp150 to the construction of the yeast cell wall in wild-type cells and beta 1,6-glucan-deficient mutants. *Mol. Microbiol.* **31**, 1835-1844 (1999).
531 Bergh, M. L., Cepko, C. L., Wolf, D. & Robbins, P. W. Expression of the Saccharomyces cerevisiae glycoprotein invertase in mouse fibroblasts: glycosylation, secretion, and enzymatic activity. *Proceedings of the National Academy of Sciences of the United States of America* **84**, 3570-3574 (1987).
532 Striebeck, A., Robinson, D. A., Schüttelkopf, A. W. & van Aalten, D. M. Yeast Mnn9 is both a priming glycosyltransferase and an allosteric activator of mannan biosynthesis. *Open biology* **3**, 130022 (2013).
533 Zhao, Y., Chu, X., Chen, J., Wang, Y., Gao, S., Jiang, Y., Zhu, X., Tan, G., Zhao, W., Yi, H., Xu, H., Ma, X., Lu, Y., Yi, Q. & Wang, S. Dectin-1-activated dendritic cells trigger potent antitumour immunity through the induction of Th9 cells. *Nature Communications* **7**, 12368 (2016).
534 Adams, E. L., Rice, P. J., Graves, B., Ensley, H. E., Yu, H., Brown, G. D., Gordon, S., Monteiro, M. A., Papp-Szabo, E., Lowman, D. W., Power, T. D., Wempe, M. F. & Williams, D. L. Differential high-affinity interaction of dectin-1 with natural or synthetic glucans is dependent upon primary structure and is influenced by polymer chain length and side-chain branching. *J. Pharmacol. Exp. Ther.* **325**, 115-123 (2008).
535 Geurtsen, J., Chedammi, S., Mesters, J., Cot, M., Driessen, N. N., Sambou, T., Kakutani, R., Ummels, R., Maaskant, J., Takata, H., Baba, O., Terashima, T., Bovin, N., Vandenbroucke-Grauls, C. M., Nigou, J., Puzo, G., Lemassu, A., Daffe, M. & Appelmelk, B. J. Identification of mycobacterial alpha-glucan as a novel ligand for DC-SIGN: involvement of mycobacterial capsular polysaccharides in host immune modulation. *J. Immunol.* **183**, 5221-5231 (2009).

536 Algieri, F., Rodríguez-Nogales, A., Garrido-Mesa, N., Vezza, T., Garrido-Mesa, J., Utrilla, M. P., Montilla, A., Cardelle-Cobas, A., Olano, A. & Corzo, N. Intestinal anti-inflammatory effects of oligosaccharides derived from lactulose in the trinitrobenzenesulfonic acid model of rat colitis. *J. Agric. Food Chem.* **62**, 4285-4297 (2014).
537 Shih, I.-L. & Yu, Y.-T. Simultaneous and selective production of levan and poly(γ-glutamic acid) by Bacillus subtilis. *Biotechnol. Lett.* **27**, 103-106 (2005).
538 Öner, E. T., Hernández, L. & Combie, J. Review of Levan polysaccharide: From a century of past experiences to future prospects. *Biotechnol. Adv.*
539 Han, Y. W. & Clarke, M. A. Production and characterization of microbial levan. *J. Agric. Food Chem.* **38**, 393-396 (1990).
540 Kasapis, S., Morris, E. R., Gross, M. & Rudolph, K. Solution properties of levan polysaccharide from Pseudomonas syringae pv. phaseolicola, and its possible primary role as a blocker of recognition during pathogenesis. *Carbohydrate Polymers* **23**, 55-64 (1994).
541 Ogawa, A., Furukawa, S., Fujita, S., Mitobe, J., Kawarai, T., Narisawa, N., Sekizuka, T., Kuroda, M., Ochiai, K. & Ogihara, H. Inhibition of Streptococcus mutans biofilm formation by Streptococcus salivarius FruA. *Appl. Environ. Microbiol.* **77**, 1572-1580 (2011).
542 Han, Y. W. Microbial levan. *Adv. Appl. Microbiol.* **35**, 171-194 (1990).
543 González-Garcinuño, Á., Tabernero, A., Sánchez-Álvarez, J. M., Galán, M. A. & del Valle, E. M. M. Effect of bacteria type and sucrose concentration on levan yield and its molecular weight. *Microbial cell factories* **16**, 91 (2017).
544 Bayoumi, F. S., El Amir, A. M., El Deeb, S. & El Zaher, H. A. Immunomodulatory and Chemo preventive activity of Bacillus subtilis sulphated Levan. (2012).
545 Kazak Sarilmiser, H. & Toksoy Oner, E. Investigation of anti-cancer activity of linear and aldehyde-activated levan from Halomonas smyrnensis AAD6T. *Biochem. Eng. J.* **92**, 28-34 (2014).
546 Perry, K. L., Simonitch, T. A., Harrison-Lavoie, K. J. & Liu, S. T. Cloning and regulation of Erwinia herbicola pigment genes. *J. Bacteriol.* **168**, 607-612 (1986).
547 Bucher, C. & von Graevenitz, A. Evaluation of three differential media for detection of Enterobacter agglomerans (Erwinia herbicola). *J. Clin. Microbiol.* **15**, 1164-1166 (1982).
548 Taylor, P. R., Roy, S., Leal Jr, S. M., Sun, Y., Howell, S. J., Cobb, B. A., Li, X. & Pearlman, E. Activation of neutrophils by autocrine IL-17A-IL-17RC interactions during fungal infection is regulated by IL-6, IL-23, ROR [gamma] t and dectin-2. *Nat. Immunol.* **15**, 143-151 (2014).
549 Taylor, P. R., Tsoni, S. V., Willment, J. A., Dennehy, K. M., Rosas, M., Findon, H., Haynes, K., Steele, C., Botto, M. & Gordon, S. Dectin-1 is required for β-glucan recognition and control of fungal infection. *Nat. Immunol.* **8**, 31-38 (2007).
550 Dutkiewicz, J. Studies on endotoxin of Erwinia herbicola and their biological activity. *Zentralblatt fur Bakteriologie, Parasitenkunde, Infektionskrankheiten und Hygiene. Erste Abteilung Originale. Reihe A: Medizinische Mikrobiologie und Parasitologie* **236**, 487-508 (1976).
551 Wang, X. & Quinn, P. J. in *Endotoxins: Structure, Function and Recognition* (eds Xiaoyuan Wang & Peter J. Quinn) 3-25 (Springer Netherlands, 2010).
552 Choi, H., Chakraborty, S., Liu, R., Gellman, S. H. & Weisshaar, J. C. Medium effects on minimum inhibitory concentrations of nylon-3 polymers against E. coli. *PLoS One* **9**, e104500 (2014).
553 González-Garcinuño, Á., Tabernero, A., Sánchez-Álvarez, J. M., Galán, M. A. & Martin del Valle, E. M. Effect of bacteria type and sucrose concentration

on levan yield and its molecular weight. *Microbial Cell Factories* **16**, 91 (2017).

554 Abdel-Fattah, A. F., Mahmoud, D. A. R. & Esawy, M. A. T. Production of Levansucrase from Bacillus subtilis NRC 33a and Enzymic Synthesis of Levan and Fructo-Oligosaccharides. *Curr. Microbiol.* **51**, 402-407 (2005).

555 Dogsa, I., Brloznik, M., Stopar, D. & Mandic-Mulec, I. Exopolymer Diversity and the Role of Levan in Bacillus subtilis Biofilms. *PLOS ONE* **8**, e62044 (2013).

556 Liu, Q., Yu, S., Zhang, T., Jiang, B. & Mu, W. Efficient biosynthesis of levan from sucrose by a novel levansucrase from Brenneria goodwinii. *Carbohydrate Polymers* **157**, 1732-1740 (2017).

557 Ernandes, F. M. P. G. & Garcia-Cruz, C. H. Nutritional requirements of Zymomonas mobilis CCT 4494 for levan production. *Brazilian Archives of Biology and Technology* **54**, 589-600 (2011).

558 Mardo, K., Visnapuu, T., Vija, H., Aasamets, A., Viigand, K. & Alamäe, T. A Highly Active Endo-Levanase BT1760 of a Dominant Mammalian Gut Commensal Bacteroides thetaiotaomicron Cleaves Not Only Various Bacterial Levans, but Also Levan of Timothy Grass. *PLOS ONE* **12**, e0169989 (2017).

559 Green, N. H., Allen, S., Davies, M. C., Roberts, C. J., Tendler, S. J. & Williams, P. M. Force sensing and mapping by atomic force microscopy. *TrAC Trends in Analytical Chemistry* **21**, 65-74 (2002).

560 A-Hassan, E., Heinz, W. F., Antonik, M. D., D'Costa, N. P., Nageswaran, S., Schoenenberger, C.-A. & Hoh, J. H. Relative Microelastic Mapping of Living Cells by Atomic Force Microscopy. *Biophys. J.* **74**, 1564-1578 (1998).

561 Pugh, N. D., Tamta, H., Balachandran, P., Wu, X., Howell, J. L., Dayan, F. E. & Pasco, D. S. The majority of in vitro macrophage activation exhibited by extracts of some immune enhancing botanicals is due to bacterial lipoproteins and lipopolysaccharides. *Int. Immunopharmacol.* **8**, 1023-1032 (2008).

562 Zhang, X., Qi, C., Guo, Y., Zhou, W. & Zhang, Y. Toll-like receptor 4-related immunostimulatory polysaccharides: Primary structure, activity relationships, and possible interaction models. *Carbohydrate Polymers* **149**, 186-206 (2016).

563 Capitan-Canadas, F., Ortega-Gonzalez, M., Guadix, E., Zarzuelo, A., Suarez, M. D., de Medina, F. S. & Martinez-Augustin, O. Prebiotic oligosaccharides directly modulate proinflammatory cytokine production in monocytes via activation of TLR4. *Mol. Nutr. Food Res.* **58**, 1098-1110 (2014).

564 Ramachandran, G. Gram-positive and gram-negative bacterial toxins in sepsis: a brief review. *Virulence* **5**, 213-218 (2014).

565 Rollenske, T., Szijarto, V., Lukasiewicz, J., Guachalla, L. M., Stojkovic, K., Hartl, K., Stulik, L., Kocher, S., Lasitschka, F., Al-Saeedi, M., Schröder-Braunstein, J., von Frankenberg, M., Gaebelein, G., Hoffmann, P., Klein, S., Heeg, K., Nagy, E., Nagy, G. & Wardemann, H. Cross-specificity of protective human antibodies against Klebsiella pneumoniae LPS O-antigen. *Nat. Immunol.* **19**, 617-624 (2018).

566 Zdorovenko, E. L., Varbanets, L. D., Zatonsky, G. V. & Ostapchuk, A. N. Structures of two putative O-specific polysaccharides from the Rahnella aquatilis 3-95 lipopolysaccharide. *Carbohydrate Research* **341**, 164-168 (2006).

567 Vinogradov, E., Frirdich, E., MacLean, L. L., Perry, M. B., Petersen, B. O., Duus, J. Ø. & Whitfield, C. Structures of lipopolysaccharides from Klebsiella pneumoniae. Elucidation of the structure of the linkage region between core and polysaccharide O chain and identification of the residues at the non-reducing termini of the O chains. *J. Biol. Chem.* (2002).

568 Rangarajan, M., Aduse-Opoku, J., Paramonov, N., Hashim, A., Bostanci, N., Fraser, O. P., Tarelli, E. & Curtis, M. A. Identification of a second lipopolysaccharide in Porphyromonas gingivalis W50. *J. Bacteriol.* **190**, 2920-2932 (2008).
569 Kimura, Y., Inoue, A., Hangai, S., Saijo, S., Negishi, H., Nishio, J., Yamasaki, S., Iwakura, Y., Yanai, H. & Taniguchi, T. The innate immune receptor Dectin-2 mediates the phagocytosis of cancer cells by Kupffer cells for the suppression of liver metastasis. *Proceedings of the National Academy of Sciences* **113**, 14097-14102 (2016).
570 Lutz, M. B., Inaba, K., Schuler, G. & Romani, N. Still alive and kicking: in-vitro-generated GM-CSF dendritic cells! *Immunity* **44**, 1-2 (2016).
571 Lei, Q., Qiang, F., Chao, D., Di, W., Guoqian, Z., Bo, Y. & Lina, Y. Amelioration of hypoxia and LPS-induced intestinal epithelial barrier dysfunction by emodin through the suppression of the NF-kappaB and HIF-1alpha signaling pathways. *Int. J. Mol. Med.* **34**, 1629-1639 (2014).
572 Van De Walle, J., Hendrickx, A., Romier, B., Larondelle, Y. & Schneider, Y.-J. Inflammatory parameters in Caco-2 cells: Effect of stimuli nature, concentration, combination and cell differentiation. *Toxicol. In Vitro* **24**, 1441-1449 (2010).
573 Böcker, U., Yezerskyy, O., Feick, P., Manigold, T., Panja, A., Kalina, U., Herweck, F., Rossol, S. & Singer, M. V. Responsiveness of intestinal epithelial cell lines to lipopolysaccharide is correlated with Toll-like receptor 4 but not Toll-like receptor 2 or CD14 expression. *International journal of colorectal disease* **18**, 25-32 (2003).
574 Sonnier, D. I., Bailey, S. R., Schuster, R. M., Lentsch, A. B. & Pritts, T. A. TNF-alpha induces vectorial secretion of IL-8 in Caco-2 cells. *J Gastrointest Surg* **14**, 1592-1599 (2010).
575 Kocharova, N. A., Zatonsky, G. V., Bystrova, O. V., Shashkov, A. S., Knirel, Y. A., Kholodkova, E. V. & Stanislavsky, E. S. Structure of the O-specific polysaccharide of Citrobacter braakii O7a,3b,1c. *Carbohydr Res* **333**, 335-338 (2001).
576 Prehm, P., Jann, B. & Jann, K. The O9 antigen of Escherichia coli. Structure of the polysaccharide chain. *Eur. J. Biochem.* **67**, 53-56 (1976).
577 Jiang, L., Perepelov, A. V., Filatov, A. V., Liu, B., Shashkov, A. S., Senchenkova, S. y. N., Wang, L. & Knirel, Y. A. Structure and gene cluster of the O-antigen of Escherichia coli O68. *Carbohydrate Research* **397**, 27-30 (2014).
578 Ren, Q., Zhao, S., Ren, C. & Ma, Z. Astragalus polysaccharide alleviates LPS-induced inflammation injury by regulating miR-127 in H9c2 cardiomyoblasts. *Int. J. Immunopathol. Pharmacol.* **32**, 2058738418759180 (2018).
579 Hoffmann, E., Dittrich-Breiholz, O., Holtmann, H. & Kracht, M. Multiple control of interleukin-8 gene expression. *J. Leukocyte Biol.* **72**, 847-855 (2002).
580 Lea, T. in *The Impact of Food Bioactives on Health* 103-111 (Springer, 2015).
581 Hirotani, Y., Ikeda, K., Kato, R., Myotoku, M., Umeda, T., Ijiri, Y. & Tanaka, K. Protective effects of lactoferrin against intestinal mucosal damage induced by lipopolysaccharide in human intestinal Caco-2 cells. *Yakugaku zasshi : Journal of the Pharmaceutical Society of Japan* **128**, 1363-1368 (2008).
582 Mu, X., Pan, C., Zheng, S., Alhamdi, Y., Sun, B., Shi, Q., Wang, X., Sun, Z., Toh, C. & Wang, G. Protective Effects of Carbon Monoxide-Releasing Molecule-2 on the Barrier Function of Intestinal Epithelial Cells. *PLoS ONE* **9**, e104032 (2014).
583 Sambuy, Y., De Angelis, I., Ranaldi, G., Scarino, M. L., Stammati, A. & Zucco, F. The Caco-2 cell line as a model of the intestinal barrier: influence of cell

and culture-related factors on Caco-2 cell functional characteristics. *Cell Biol. Toxicol.* **21**, 1-26 (2005).
584 Zhang, Q., Lenardo, M. J. & Baltimore, D. 30 Years of NF-kappaB: A Blossoming of Relevance to Human Pathobiology. *Cell* **168**, 37-57 (2017).
585 Hwang, P. A., Phan, N. N., Lu, W. J., Ngoc Hieu, B. T. & Lin, Y. C. Low-molecular-weight fucoidan and high-stability fucoxanthin from brown seaweed exert prebiotics and anti-inflammatory activities in Caco-2 cells. *Food & nutrition research* **60**, 32033 (2016).
586 Kim, H., Lee, H. & Shin, K. S. Intestinal immunostimulatory activity of neutral polysaccharide isolated from traditionally fermented Korean brown rice vinegar. *Biosci Biotechnol Biochem* **80**, 2383-2390 (2016).
587 Taylor, M. E. & Drickamer, K. Structural insights into what glycan arrays tell us about how glycan-binding proteins interact with their ligands. *Glycobiology* **19**, 1155-1162 (2009).
588 Drickamer, K. & Taylor, M. E. Recent insights into structures and functions of C-type lectins in the immune system. *Curr. Opin. Struct. Biol.* **34**, 26-34 (2015).
589 Rillahan, C. D. & Paulson, J. C. Glycan microarrays for decoding the glycome. *Annu. Rev. Biochem.* **80**, 797-823 (2011).
590 Maglinao, M., Eriksson, M., Schlegel, M. K., Zimmermann, S., Johannssen, T., Götze, S., Seeberger, P. H. & Lepenies, B. A platform to screen for C-type lectin receptor-binding carbohydrates and their potential for cell-specific targeting and immune modulation. *J. Controlled Release* **175**, 36-42 (2014).
591 Ludwig, I. S., Lekkerkerker, A. N., Depla, E., Bosman, F., Musters, R. J. P., Depraetere, S., van Kooyk, Y. & Geijtenbeek, T. B. H. Hepatitis C Virus Targets DC-SIGN and L-SIGN To Escape Lysosomal Degradation. *J. Virol.* **78**, 8322-8332 (2004).
592 Su, S. V., Hong, P., Baik, S., Negrete, O. A., Gurney, K. B. & Lee, B. DC-SIGN Binds to HIV-1 Glycoprotein 120 in a Distinct but Overlapping Fashion Compared with ICAM-2 and ICAM-3. *J. Biol. Chem.* **279**, 19122-19132 (2004).
593 Iliev, I. D., Funari, V. A., Taylor, K. D., Nguyen, Q., Reyes, C. N., Strom, S. P., Brown, J., Becker, C. A., Fleshner, P. R., Dubinsky, M., Rotter, J. I., Wang, H. L., McGovern, D. P., Brown, G. D. & Underhill, D. M. Interactions between commensal fungi and the C-type lectin receptor Dectin-1 influence colitis. *Science* **336**, 1314-1317 (2012).
594 Li, J. & Karboune, S. A comparative study for the isolation and characterization of mannoproteins from Saccharomyces cerevisiae yeast cell wall. *Int J Biol Macromol* **119**, 654-661 (2018).
595 Rallabhandi, P., Awomoyi, A., Thomas, K. E., Phalipon, A., Fujimoto, Y., Fukase, K., Kusumoto, S., Qureshi, N., Sztein, M. B. & Vogel, S. N. Differential activation of human TLR4 by Escherichia coli and Shigella flexneri 2a lipopolysaccharide: combined effects of lipid A acylation state and TLR4 polymorphisms on signaling. *Journal of immunology (Baltimore, Md. : 1950)* **180**, 1139-1147 (2008).
596 Teodorowicz, M., Perdijk, O., Verhoek, I., Govers, C., Savelkoul, H. F., Tang, Y., Wichers, H. & Broersen, K. Optimized Triton X-114 assisted lipopolysaccharide (LPS) removal method reveals the immunomodulatory effect of food proteins. *PLoS One* **12**, e0173778 (2017).
597 Rieder, A., Grimmer, S., L. Aachmann, F., Westereng, B., Kolset, S. O. & Knutsen, S. H. Generic tools to assess genuine carbohydrate specific effects on in vitro immune modulation exemplified by β-glucans. *Carbohydrate Polymers* **92**, 2075-2083 (2013).
598 Maria-Ferreira, D., Nascimento, A. M., Cipriani, T. R., Santana-Filho, A. P., Watanabe, P. d. S., Sant´Ana, D. d. M. G., Luciano, F. B., Bocate, K. C. P.,

van den Wijngaard, R. M., Werner, M. F. d. P. & Baggio, C. H. Rhamnogalacturonan, a chemically-defined polysaccharide, improves intestinal barrier function in DSS-induced colitis in mice and human Caco-2 cells. *Scientific Reports* **8**, 12261 (2018).

599 Geirnaert, A., Calatayud, M., Grootaert, C., Laukens, D., Devriese, S., Smagghe, G., De Vos, M., Boon, N. & Van de Wiele, T. Butyrate-producing bacteria supplemented in vitro to Crohn's disease patient microbiota increased butyrate production and enhanced intestinal epithelial barrier integrity. *Scientific Reports* **7**, 11450 (2017).

600 Martin-Gallausiaux, C., Béguet-Crespel, F., Marinelli, L., Jamet, A., Ledue, F., Blottière, H. M. & Lapaque, N. Butyrate produced by gut commensal bacteria activates TGF-beta1 expression through the transcription factor SP1 in human intestinal epithelial cells. *Scientific Reports* **8**, 9742 (2018).

601 Wang, K., Cheng, F., Pan, X., Zhou, T., Liu, X., Zheng, Z., Luo, L. & Zhang, Y. Investigation of the transport and absorption of Angelica sinensis polysaccharide through gastrointestinal tract both in vitro and in vivo. *Drug Deliv.* **24**, 1360-1371 (2017).

602 Nagamine, T., Nakazato, K., Tomioka, S., Iha, M. & Nakajima, K. Intestinal Absorption of Fucoidan Extracted from the Brown Seaweed, Cladosiphon okamuranus. *Mar. Drugs* **13**, 48 (2015).

603 Helft, J., Böttcher, J., Chakravarty, P., Zelenay, S., Huotari, J., Schraml, B. U., Goubau, D. & e Sousa, C. R. GM-CSF mouse bone marrow cultures comprise a heterogeneous population of CD11c+ MHCII+ macrophages and dendritic cells. *Immunity* **42**, 1197-1211 (2015).

604 Belkaid, Y. & Harrison, O. J. Homeostatic Immunity and the Microbiota. *Immunity* **46**, 562-576 (2017).

605 Schiavi, E., Gleinser, M., Molloy, E., Groeger, D., Frei, R., Ferstl, R., Rodriguez-Perez, N., Ziegler, M., Grant, R., Moriarty, T. F., Plattner, S., Healy, S., O'Connell Motherway, M., Akdis, C. A., Roper, J., Altmann, F., van Sinderen, D. & O'Mahony, L. The Surface-Associated Exopolysaccharide of Bifidobacterium longum 35624 Plays an Essential Role in Dampening Host Proinflammatory Responses and Repressing Local T_H17 Responses. *Appl. Environ. Microbiol.* **82**, 7185-7196 (2016).

606 Gorska, S., Sandstrom, C., Wojas-Turek, J., Rossowska, J., Pajtasz-Piasecka, E., Brzozowska, E. & Gamian, A. Structural and immunomodulatory differences among lactobacilli exopolysaccharides isolated from intestines of mice with experimentally induced inflammatory bowel disease. *Sci Rep* **6**, 37613 (2016).

607 Liu, C. F., Tseng, K. C., Chiang, S. S., Lee, B. H., Hsu, W. H. & Pan, T. M. Immunomodulatory and antioxidant potential of Lactobacillus exopolysaccharides. *J. Sci. Food Agric.* **91**, 2284-2291 (2011).

608 Warner, N. & Núñez, G. MyD88: A Critical Adaptor Protein in Innate Immunity Signal Transduction. *The Journal of Immunology* **190**, 3-4 (2013).

609 Wang, Q., McLoughlin, R. M., Cobb, B. A., Charrel-Dennis, M., Zaleski, K. J., Golenbock, D., Tzianabos, A. O. & Kasper, D. L. A bacterial carbohydrate links innate and adaptive responses through Toll-like receptor 2. *The Journal of experimental medicine* **203**, 2853-2863 (2006).

610 González Flecha, F. L. & Levi, V. Determination of the molecular size of BSA by fluorescence anisotropy. *Biochemistry and Molecular Biology Education* **31**, 319-322 (2003).

Appendices

Appendix 1

INGREDIENTS		UNIT AMOUNT	AMOUNT REQUIRED	UNITS
Di Potassium Phosphate (K2HPO4)		1.5	1.5	g
Mono Potassium Phosphate (KH2PO4)		1.5	1.5	g
Vitamin free casamino acids		10	10	g
Sodium acetate		15	15	g
Sodium citrate		0.22	0.22	g
Tryptophan		50	50	mg
Asparagine		0.2	0.2	g
Cysteine HCl		0.2	0.2	g
Thiamine HCl (stock 10mg/100ml UPW)		2	2	ml
para(4)-aminobenzoic acid (stock 10mg/100ml UPW)		0.4	0.4	ml
Calcium pantothenic acid (stock 10mg/100ml UPW)		4	4	ml
Niacin (stock 20mg/100ml)		5	5	ml
Pyridoxine HCl (stock 10mg/100ml)		0.5	0.5	ml
Biotin *		5	5	µl
Folic acid **		50	50	µl
Riboflavin ***		0.5	0.5	ml
Adenine sulphate		10	10	mg
Uracil		20	20	mg
Guanine HCl		10	10	mg
Cytidine (acid)		50	50	mg
Thymidine ****		1	1	µl
Tween 80		1	1	ml
Magnesium Sulfate heptahydrate (MgSO4.7H2O)		0.163	0.163	g
Manganese Sulfate tetrahydrate (MnSO4.4H20)		23.4	23.4	mg
Iron (II) Sulfate heptahydrate (FeSO4.7H2O)		13	13	mg
Ultra Pure Water	to	950	950	ml

TECHNICAL DETAILS

FILTER STERILISE-autoclaving will cause some ingredients to degrade. Cover sterilised bottle in foil to prevent UV degradation of solution.

1/20 volume of 40% (w/v) filter-sterilised sucrose stock can be added if required

DETAILS

Date:- Name:-

Made for:-
Changes/additions:-

Autoclave temp+time:-
Successful:-

* 100x Biotin stock : 5mg in 0.5ml 10mM HCl + 1µl 95% ethanol.
** 100x Folic acid stock : 5mg in 2.5ml 1mM NaOH.
*** 10x Riboflavin stock : 4mg in 5ml 20mM acetic acid.
**** 1000x Thymidine stock : 3.2mg in 2.0ml 1M HCl.

Appendix 1. Composition of Lactobacillus semi-defined medium II (LDM2).

For levan production, 5% sucrose was also added, and the media stored and treated under sterile conditions.

Appendix 2

INGREDIENTS	UNIT AMOUNT	AMOUNT REQUIRED	UNITS
BD Tryptone (BD211705)	10	10	g
BD Yeast Extract (212720)	5	5	g
Sodium Chloride (NaCl)	10	10	g
Distilled Water	1	1	litre
Agar (if required)	15	15	g
		0	
		0	
		0	
		0	
		0	
		0	
		0	
		0	
		0	
		0	
		0	
		0	
		0	
		0	
		0	
		0	
		0	
		0	
		0	
		0	
		0	
		0	
		0	
		0	

TECHNICAL DETAILS

For overlay add Agar at 0.7%

Adjust pH for LB to 7.0
Adjust pH for LB mod to 7.5

Autoclave at 121c for 15min

DETAILS

Date:- Name:-

Made for:-
Changes/additions:-

Autoclave temp+time:-
Successful:-

Appendix 2. Composition of lysogeny broth (LB).

LB was stored and treated under sterile conditions.

Appendix 3

HpaI-SIGNR1-QPD-NotI DNA 5’ prime to 3’ prime end sequence

agttaactccaaaaccccaaataccgagaggcagaaggaacaagagaagatcctccaggaactgacccag
ctgacagatgagcttacgtccaggatccccatctcccaagggaagaatgagtccatgcaggcgaagatcactg
agcaactgatgcagctgaaaactgaactcttgtccaggattcccatcttccaggggcagaatgagtccatacaa
gagaagatctctgagcaactgatgcagctgaaggctgaacttctttccaagatctccagcttcccggtaaaggat
gattctaagcaggagaagatctaccaacagctggtacagatgaagactgaactcttccgcctgtgtcgactctgc
ccctgggactggacattcctcctaggaaattgttacttcttctccaagtcccagcggaactggaatgacgccgtca
cagcttgcaaagaagtgaaggctcaactagtcatcatcaatagtgatgaagagcagaccttcctgcagcagac
ttctaaggctaaaggaccaacctggatgggcctgtcagacctgaagaaggaggccacgtggctctgggtagat
ggttctactctgtcatccagattccagaaatattggaatagagggcagcctgacaacatcggtgaggaagactgt
gtcgaatttgctggggatggctggaatgactctaaatgtgaactcaaaaagttctggatctgcaagaagtctgca
accccatgcactgaaggctaggcggccgca

Appendix 3. SIGNR1-QPD sequence.

NotI and HpaI Restriction enzyme sequences are highlighted in light grey. The mutant QPD sequence in exchange for EPN [mutated at E285 and D287N][212] is shown in the black box. The stop codon is highlighted in dark grey. Sequences were constructed using ApE-A plasmid Editor v2.0.47.

Appendix 4

Fluorescence/Tag	Collection Filter Setting	Excitation Lazer
Alexa 647	670/14	Red (640 nm)
PI	695/40	Blue (488 nm)
FITC	530/30	Blue (488 nm)

Appendix 4. BD LSR Fortessa filter and lazer settings.

Appendix 5

IgM Isotype-Alexa 647

Anti-SIGNR1-Alexa 647

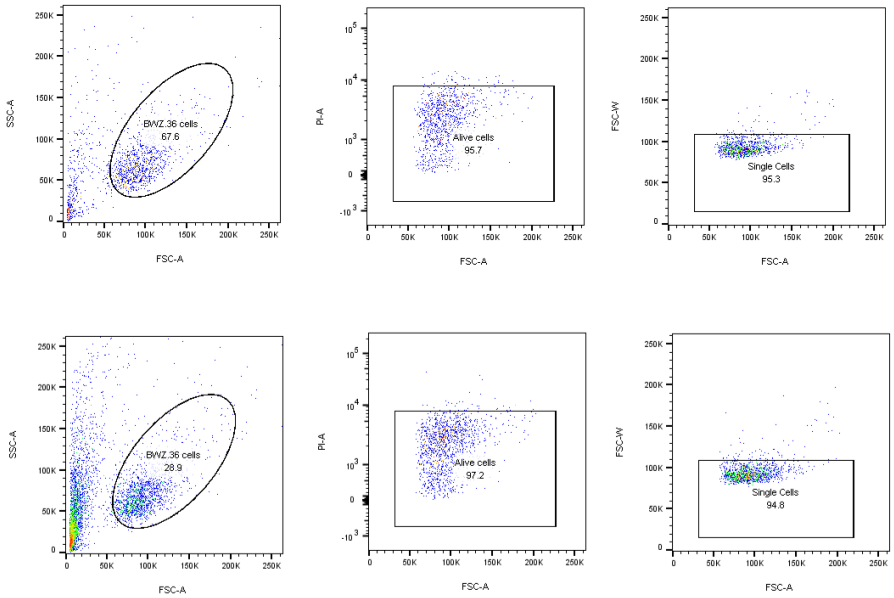

Appendix 5. Pre-gating of SIGNR1-transfected BWZ.36 cells treated with anti-mouse SIGNR1-Alexa 674 or isotype control from Figure 25.

Dot plots from left to right show initial cell population, exclusion of doublet cells and dead cells using PI staining. Compensation in this experiment was not applied. Indicated from top to bottom: cells labelled with IgM isotype-Alexa 647 or anti-mouse SIGNR1-Alexa 647. FSC-A, forward scatter area. FSC-W, forward scatter width. SSC-A, side scatter area. PI, propidium iodide.

Appendix 6

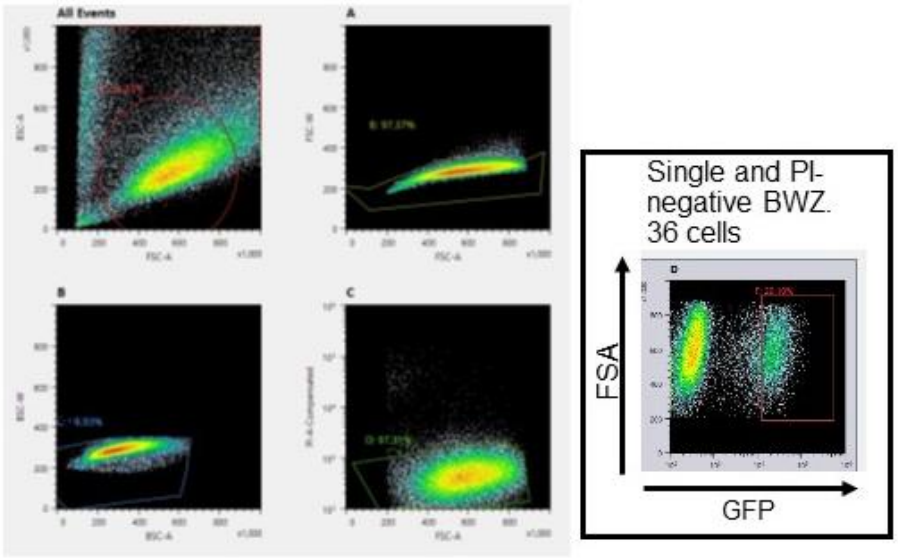

Appendix 6. Cell sorting of GFP-positive transfected BWZ.36 cells

BWZ.36 GFP-positive transfected with pMXs-IG-SIGNR1 were sorted using the Sony SH800 cell sorter. Figure shows a screenshot of gated cells (grey box shading) (dot plots). GFP-positive cells isolated and collected are shown in the red box (dot plots). FSC-A, forward scatter area. FSC-W, forward scatter width. SSC-A, side scatter area. PI, propidium iodide.

Appendix 7

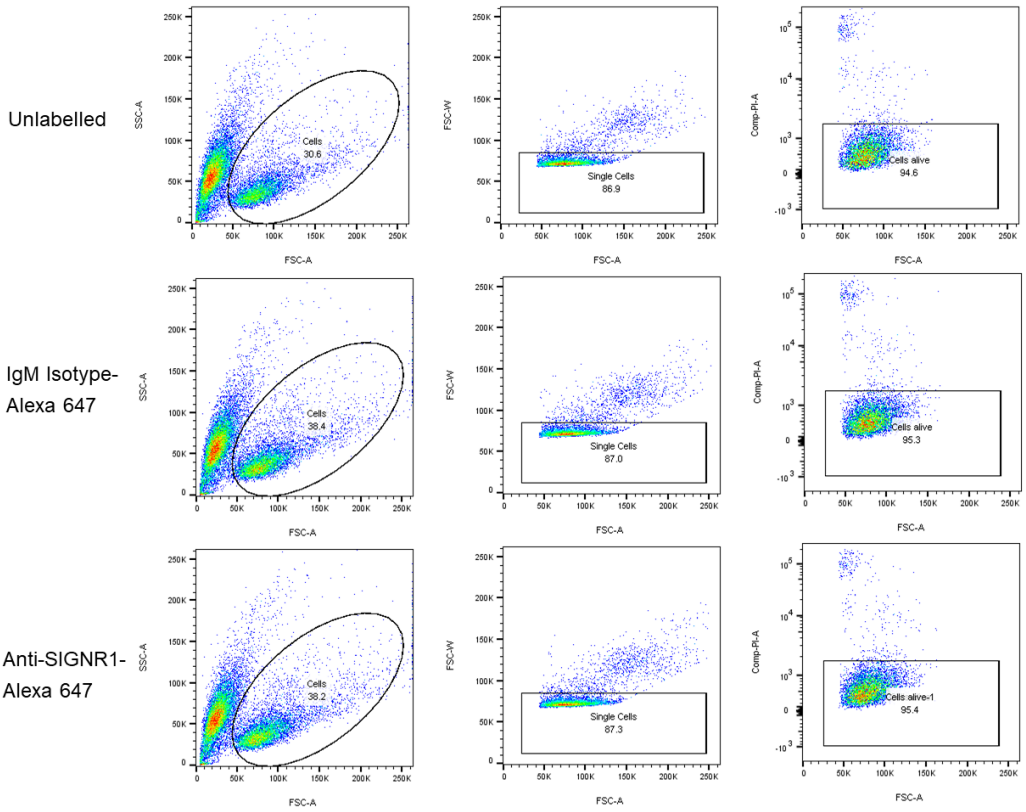

Appendix 7. Pre-gating of SIGNR1-transfected BWZ.36 cells treated with anti-mouse SIGNR1-Alexa 674 or isotype control, or unlabelled cells from Figure 26.

Dot plots from left to right show initial cell population, exclusion of doublet cells and dead cells using PI staining. Indicated from top to bottom: unlabelled cells (cells with PI), cells labelled with IgM isotype-Alexa 647 or ant-mouse Alexa 647-SIGNR1. FSC-A, forward scatter area. FSC-W, forward scatter width.SSC-A, side scatter area. Comp-PI-A, compensated propidium iodide area.

Appendix 8

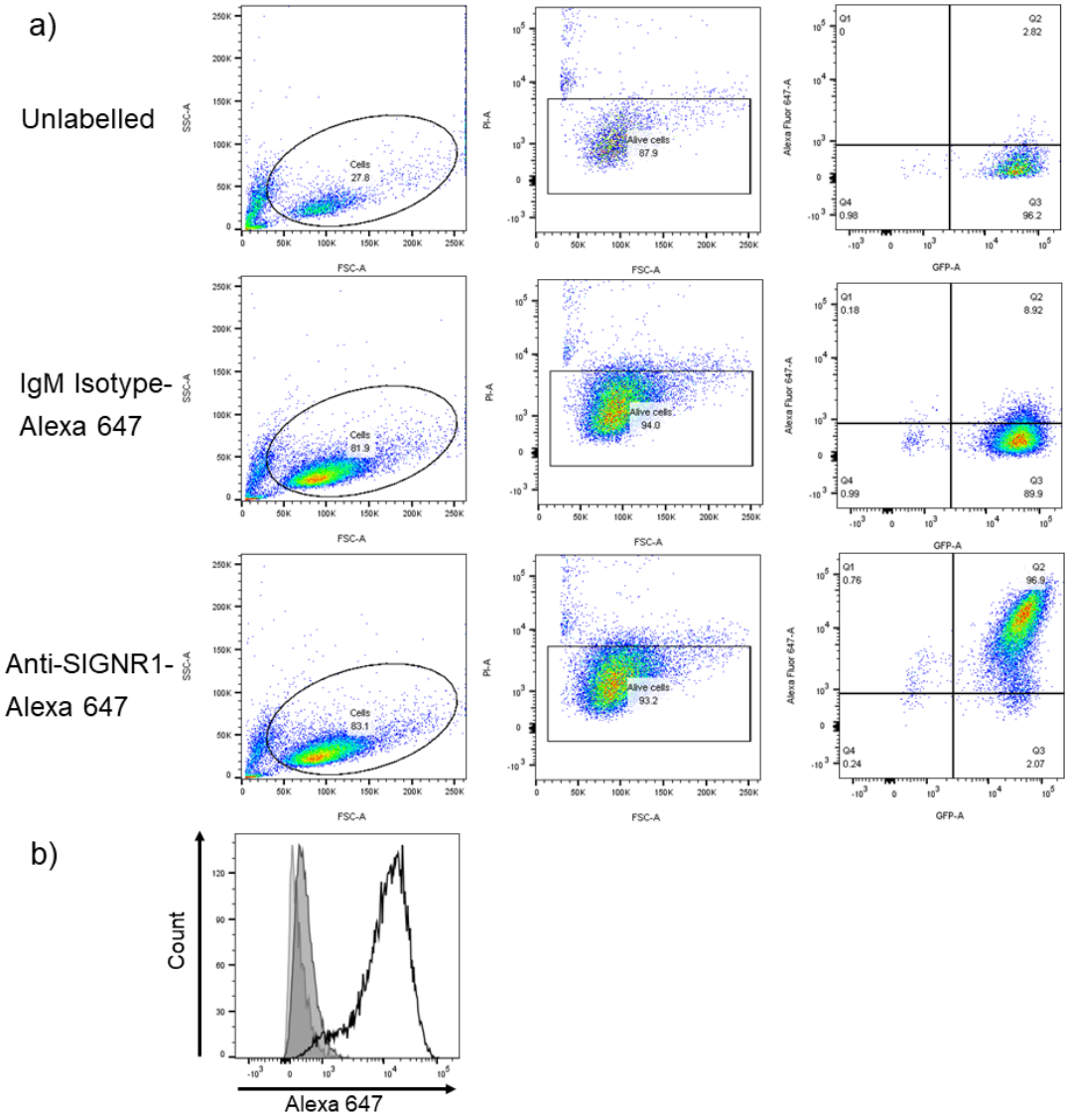

Appendix 8. Analysis of SIGNR1 expression on SIGNR1 reporter cells by flow cytometry.

This is an additional independent experiment to support data in Figure 26. (a) Dot plots illustrate individual cell events. The number of cell events are shown as a percentage in each of the quadrants relative to total events, Q1, Q2, Q3 and Q4 for (a) (b) and (c). Cells were labelled with anti-mouse SIGNR1-Alexa 647, IgM isoype-Alexa 647 control or were unlabelled (cells with PI); compensation was not performed. (a) gating strategy excluded dead cells using PI staining. Dot plots of Alexa 647 against GFP fluorescence are shown. Q1, Q2, Q3 and Q4 split populations into discrete subpopulations for illustrative purposes to help clarify fluorescent and non-fluorescent cell populations. Numbers in each quadrant represent the percentage of total sample cell populations in that quadrant. (b) Histogram directly compares anti-mouse SIGNR1-Alexa 647-labelled (black outline); IgM isotype-Alexa 647-labelled (grey shading with dark grey outline); and unlabelled cells (cells with PI) (light grey, no black outline). FSC-A, forward scatter area. SSC-A, side scatter area. PI, propidium iodide. Axis labels: Alexa 647 label represents detection of Alexa Fluor 647 fluorescence and GFP is represents detection of GFP fluorescence. Data were generated using FlowJo® v10.0.8.

Appendix 9

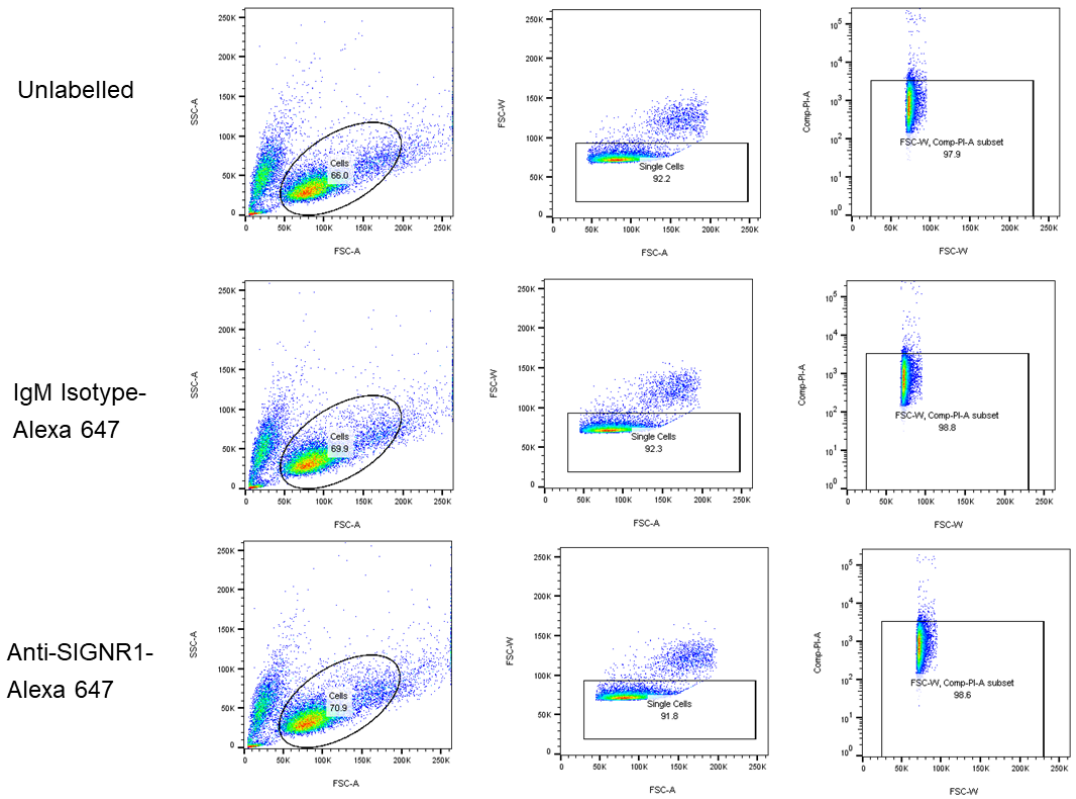

Appendix 9. Pre-gating of SIGNR1-QPD-transfected BWZ.36 cells treated with anti-mouse SIGNR1-Alexa 674 or isotype control, or unlabelled cells from Figure 29.

Dot plots from left to right show initial cell population, exclusion of doublet cells and dead cells using PI staining. Indicated from top to bottom: unlabelled cells (cells with PI), or cells labelled with IgM isotype-Alexa 647 or ant-mouse SIGNR1-Alexa 647. FSC-A, forward scatter area. FSC-W, forward scatter width. SSC-A, side scatter area. Comp-PI-A, compensated propidium iodide area.

Appendix 10

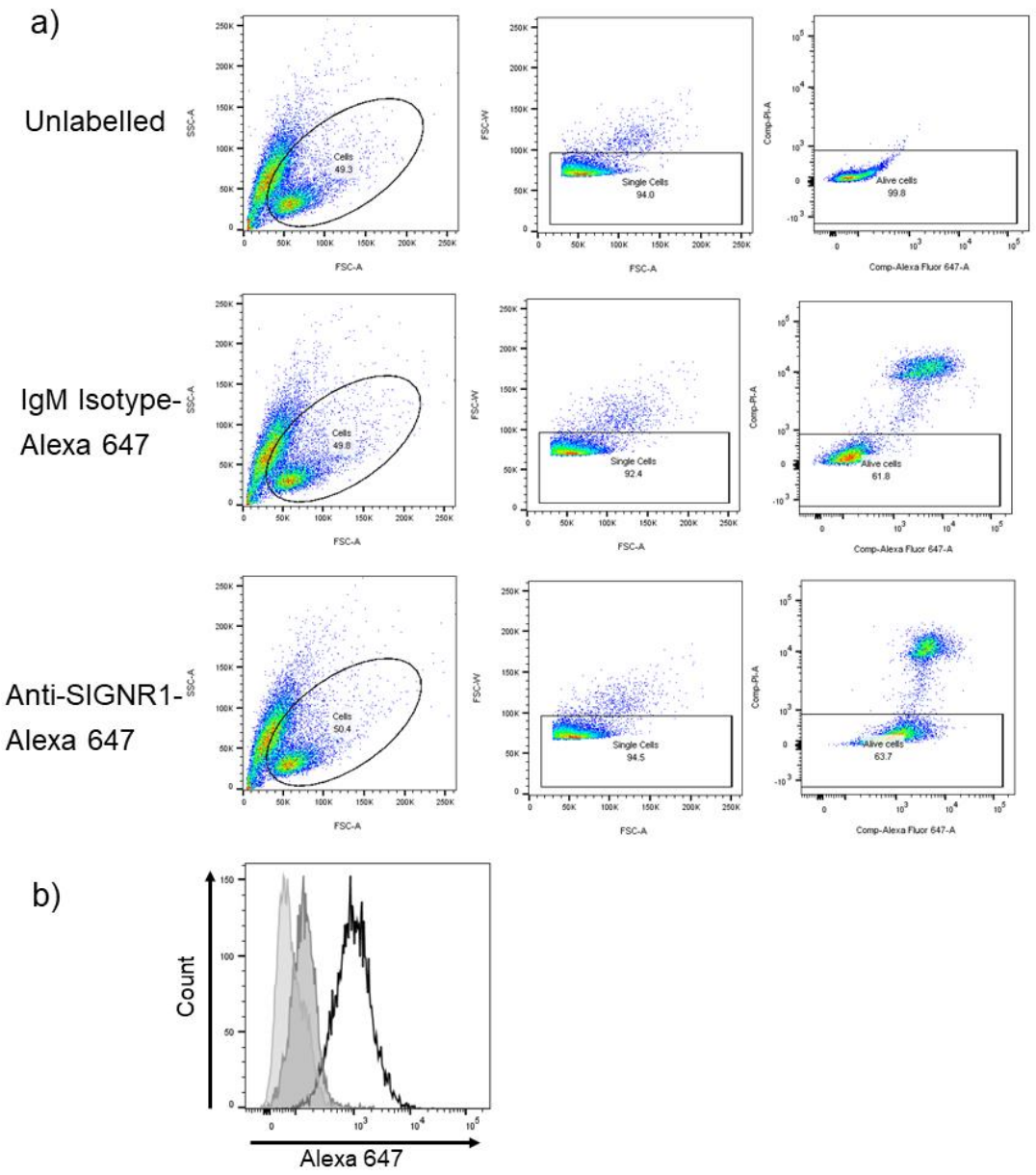

Appendix 10. Analysis of SIGNR1 expression on SIGNR1-QPD reporter cells by flow cytometry.

This is a repeated independent experiment to support data in Figure 29. Dot plots illustrate individual cell events. Cells were labelled with anti-mouse SIGNR1-Alexa 647, IgM isotype-Alexa 647 control or were unlabelled (cells with PI). (a) gating strategy excluding doublet cells, and dead cells using PI staining. (b) Histogram directly compares anti-mouse SIGNR1-Alexa 647-labelled (black outline); IgM isotype-Alexa 647-labelled (grey shading with dark grey outline); and unlabelled cells (cells with PI) (light grey, no black outline). Axis labels: Alexa 647 label represents detection of Alexa 647 fluorescence and GFP represents detection of GFP fluorescence. Data were generated using FlowJo® v10.0.8. FSC-A, forward scatter area. FSC-W, forward scatter width. SSC-A, side scatter area. Comp-PI-A, compensated propidium iodide area.

Appendix 11

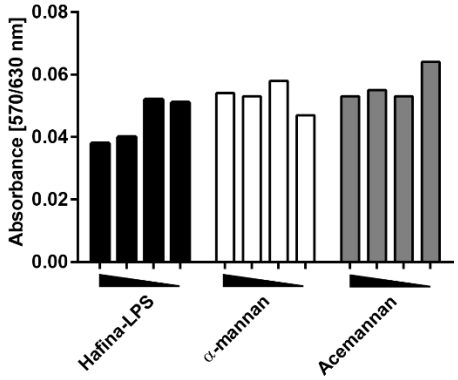

Appendix 11. Screening of Hafnia-LPS, α-mannan and acemannan to mock reporter cells.

Carbohydrate binding to CLR BWZ.36 reporter cells induces β-galactosidase production within the cell which can be measured in a colorimetric assay: CLR BWZ.36 reporter cells were incubated with immobilised carbohydrate ligands using a 96 well plate; a substrate, Chlorophenol red-β-D-galactopyranoside (CPRG), was added to cells and absorbance values were read at 570/630 nm (a) Reporter assay was performed in singlicate with mock cells. This data corresponds to those mentioned in Figure 31b. PS concentrations were 1, 0.3 and 0.1 μg/ml as in Figure 31b.

Appendix 12

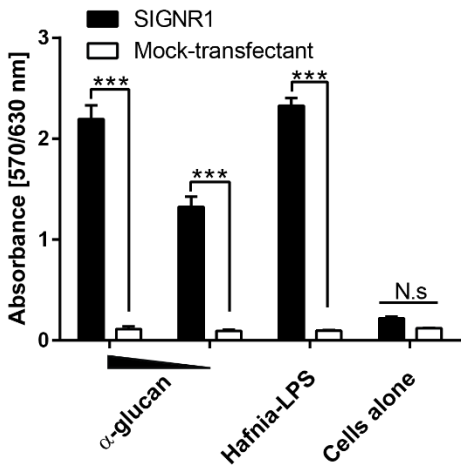

Appendix 12. Interaction of α-glucan from Streptomyces venezuelae and Hafnia-LPS with SINGR1 and mock reporter cells.

Carbohydrate binding to CLR BWZ.36 reporter cells induces β-galactosidase production within the cell which can be measured in a colorimetric assay: CLR BWZ.36 reporter cells were incubated with immobilised carbohydrate ligands using a 96 well plate; a substrate, Chlorophenol red-β-D-galactopyranoside (CPRG), was added to cells and absorbance values were read at 570/630 nm. A repeated independent experiment supporting Figure 32. Concentrations of α-glucan were 100 and 10 μg/ml, and Hafnia-LPS was 10 μg/ml (positive control). All experiments were performed in triplicate. Error bars, ± SD. Statistical analysis was performed using one-way ANOVA followed by tukey's test (b). ***, p < 0.001 and **, p < 0.001, as indicated. N.s with straight line, not statistically significant.

Appendix 13

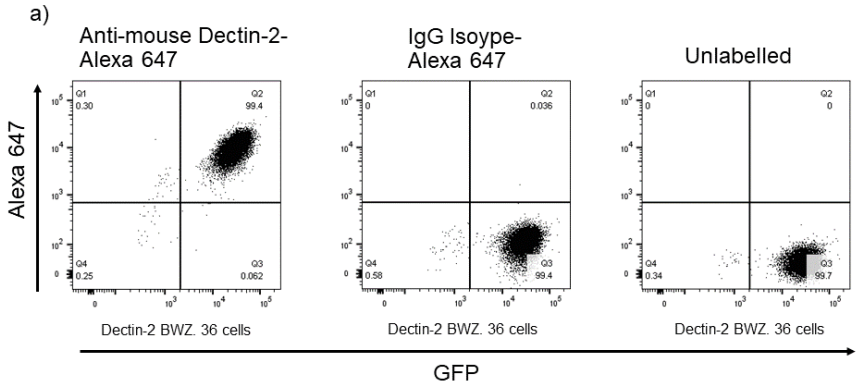
a)
Anti-mouse Dectin-2-Alexa 647
IgG Isoype-Alexa 647
Unlabelled
Alexa 647
Q1 0.30
Q2 99.4
Q4 0.25
Q3 0.062
Q1 0
Q2 0.036
Q4 0.58
Q3 99.4
Q1 0
Q2 0
Q4 0.34
Q3 99.7
Dectin-2 BWZ. 36 cells
Dectin-2 BWZ. 36 cells
Dectin-2 BWZ. 36 cells
GFP

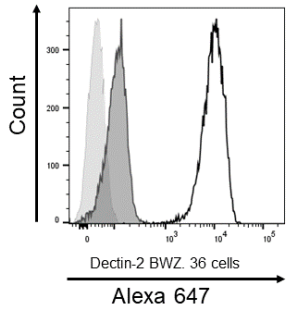
b)
Count
Dectin-2 BWZ. 36 cells
Alexa 647

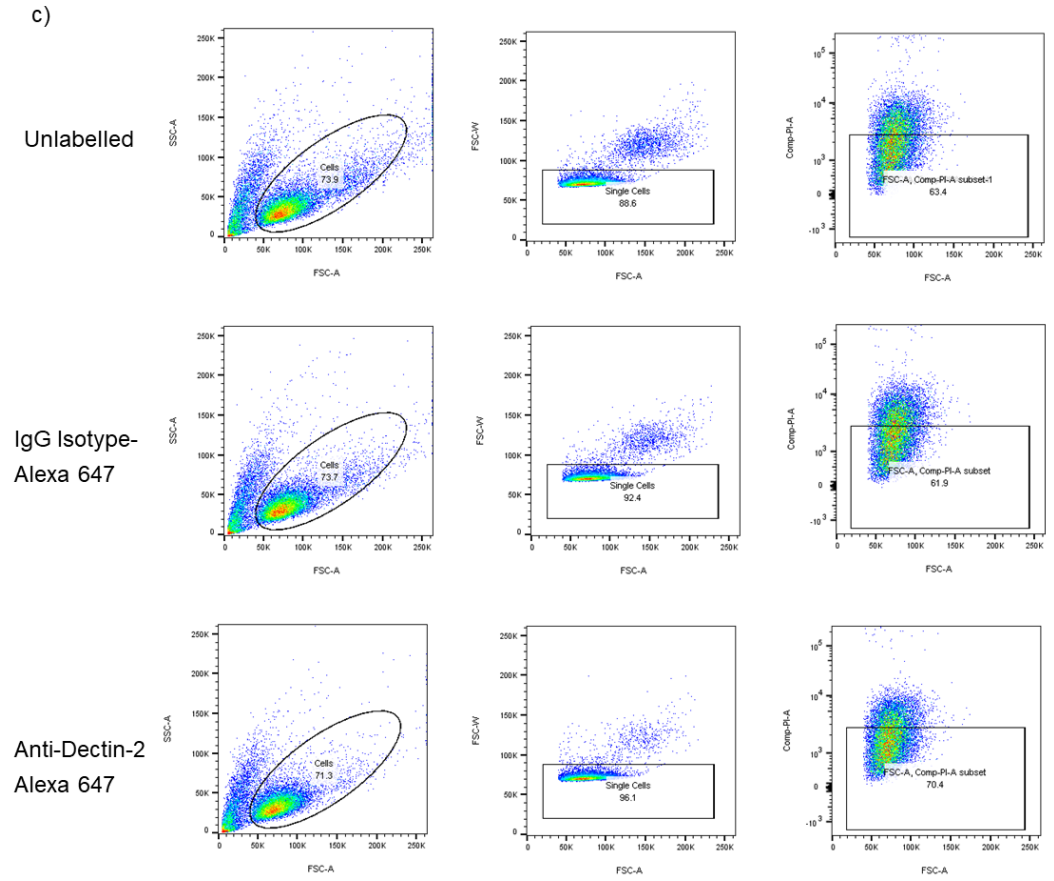
c)
Unlabelled
IgG Isotype-Alexa 647
Anti-Dectin-2 Alexa 647
SSC-A
FSC-A
Cells 73.3
FSC-W
Single Cells 88.6
Comp-PI-A
FSC-A, Comp-PI-A subset-1 63.4
Cells 73.7
Single Cells 92.4
FSC-A, Comp-PI-A subset 61.9
Cells 71.3
Single Cells 96.1
FSC-A, Comp-PI-A subset 70.4

d)

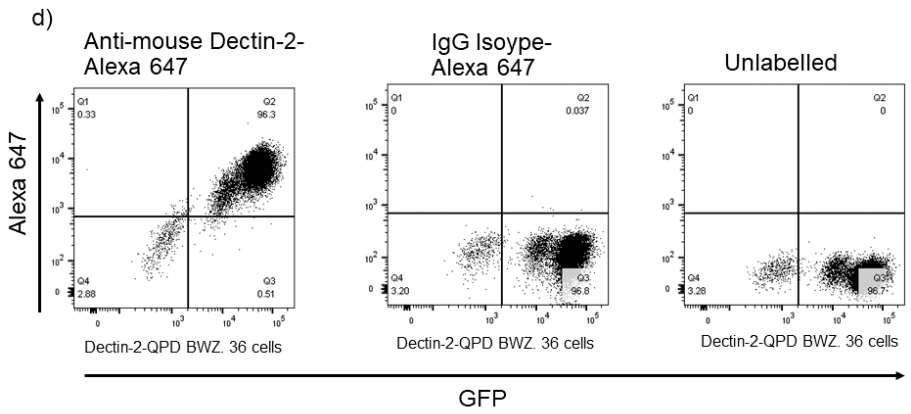
Anti-mouse Dectin-2-
Alexa 647
IgG Isoype-
Alexa 647
Unlabelled
Alexa 647
Q1
0.33
Q2
96.3
Q4
2.88
Q3
0.51
Q1
0
Q2
0.037
Q4
3.20
Q3
96.8
Q1
0
Q2
0
Q4
3.28
Q3
96.7
Dectin-2-QPD BWZ. 36 cells
Dectin-2-QPD BWZ. 36 cells
Dectin-2-QPD BWZ. 36 cells
GFP

e)

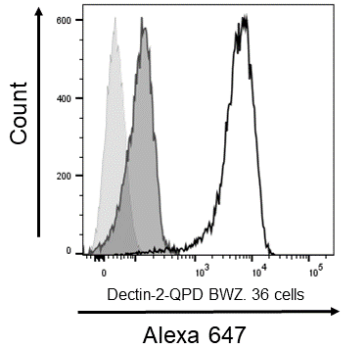
Count
600
400
200
0
Dectin-2-QPD BWZ. 36 cells
Alexa 647

f)

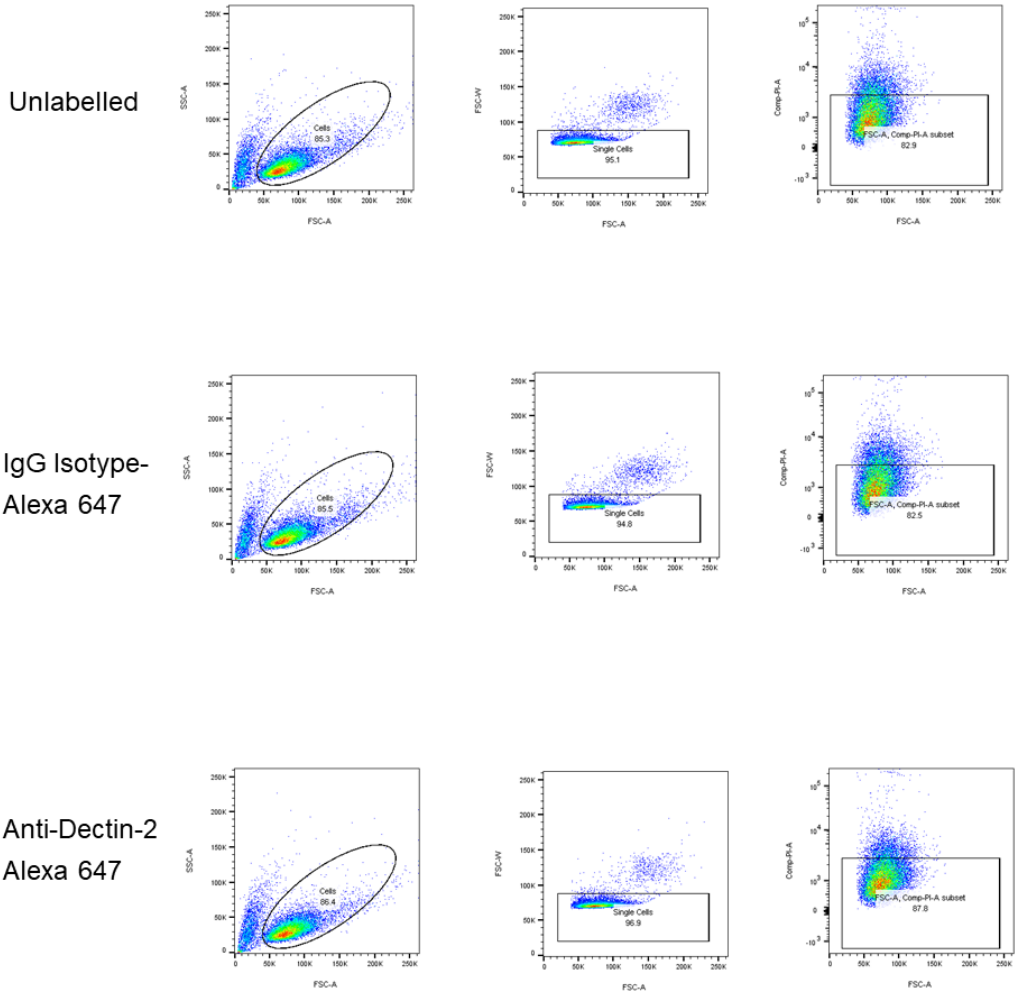
Unlabelled
IgG Isotype-
Alexa 647
Anti-Dectin-2
Alexa 647
SSC-A
FSC-A
Cells
85.3
FSC-W
Single Cells
95.1
Comp-PI-A
FSC-A, Comp-PI-A subset
82.9
Cells
85.5
Single Cells
94.8
FSC-A, Comp-PI-A subset
82.5
Cells
86.4
Single Cells
96.9
FSC-A, Comp-PI-A subset
87.8

Appendix 13. Analysis of Dectin-2 expression on Dectin-2 and Dectin-2-QPD reporter cells by flow cytometry.

(a) and (d), dot plots illustrate individual cell events. The number of cell events are shown as a percentage in each of the quadrants relative to total events, Q1, Q2, Q3 and Q4. Cells were labelled with anti-mouse Dectin-2-Alexa 647, IgG isotype-Alexa 647 control or were unlabelled (cells with PI) as indicated. Analysis was performed after initial pre-gating of cells which exclude doublet cells and dead cells. Q1, Q2, Q3 and Q4 split cell populations into discrete subpopulations for illustrative purposes to help clarify fluorescent and non-fluorescent cell populations. Numbers in each quadrant represent the percentage of total sample cell populations in that quadrant. (b) and (e) show histograms for Dectin-2 and Dectin-2-QPD reporter cells, respectively. Anti-mouse Dectin-2-Alexa 647-labelled (black outline); IgG isotype-Alexa 647-labelled (grey shading with black outline); and unlabelled cells (cells with PI) (light grey, no black outline) are as indicated. Axis labels: Alexa 647 label represents Alexa 647 fluorescence and GFP is represents detection of GFP fluorescence. (c) and (f) show the gating strategy for Dectin-2 and Dectin-2-QPD reporter cells, respectively: excluding doublet cells, and dead cells using PI staining. Data were generated using FlowJo® v10.0.8. FSC-A, forward scatter area. FSC-W, forward scatter width. SSC-A, side scatter area. Comp-PI-A, compensated propidium iodide area.

Appendix 14

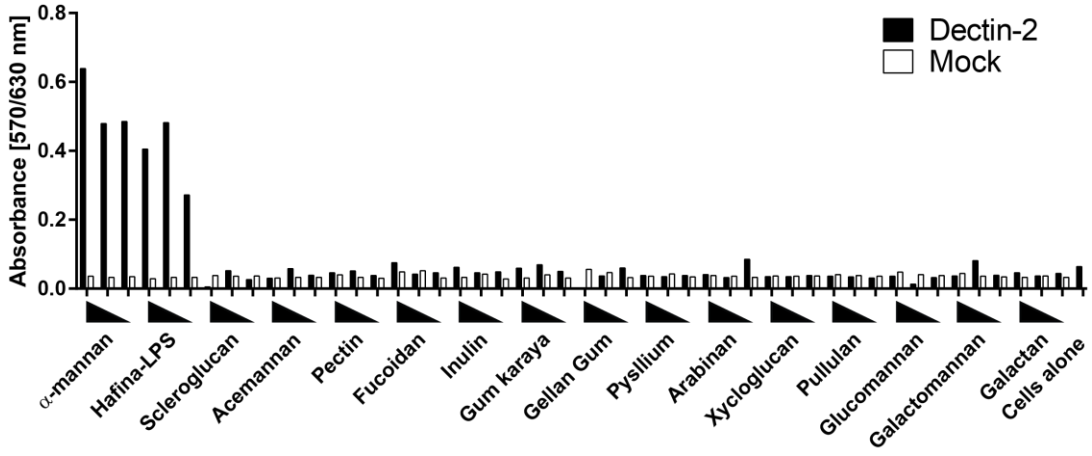

Appendix 14. Screening of PS to Dectin-2 reporter cells.

Carbohydrate binding to CLR BWZ.36 reporter cells induces β-galactosidase production within the cell which can be measured in a colorimetric assay: CLR BWZ.36 reporter cells were incubated with immobilised carbohydrate ligands using a 96 well plate; a substrate, Chlorophenol red-β-D-galactopyranoside (CPRG), was added to cells and absorbance values were read at 570/630 nm. A repeated independent experiment supporting Figure 34. Reporter assays were performed using Dectin-2 and mock reporter cells. Experiments were performed at PS concentrations 10, 2 or0.4 μg/ml.

Appendix 15

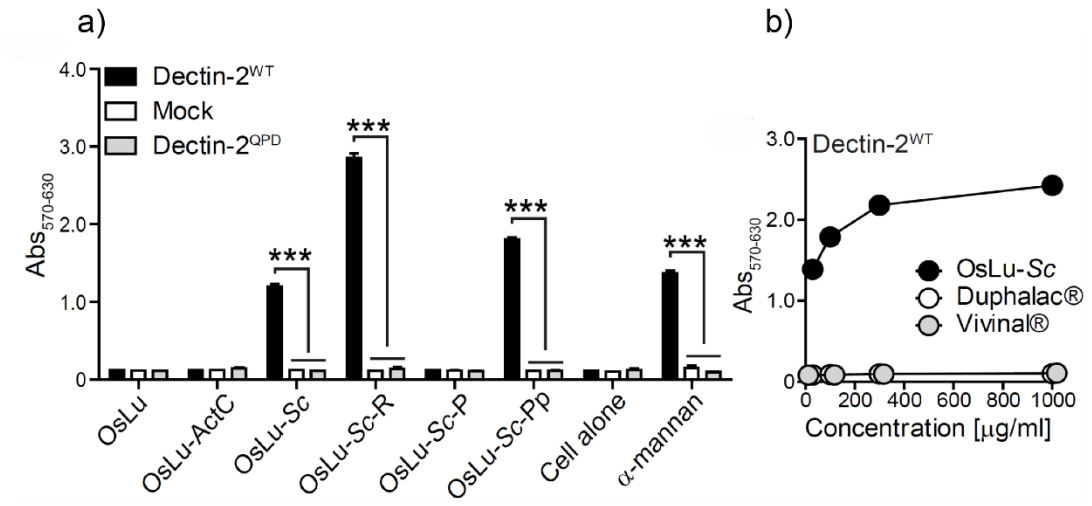

Appendix 15. Interaction of OsLu preparations and other prebiotic oligosaccharides with Dectin-2 using reporter cells.

Carbohydrate binding to CLR BWZ.36 reporter cells induces β-galactosidase production within the cell which can be measured in a colorimetric assay: CLR BWZ.36 reporter cells were incubated with immobilised carbohydrate ligands using a 96 well plate; a substrate, Chlorophenol red-β-D-galactopyranoside (CPRG), was added to cells and absorbance values were read at 570/630 nm. A repeated independent experiment supporting Figure 36 and taken from [489]. a) Dectin-2, Dectin-2-QPD and mock reporter cell assay of different preparations of OsLu (see Figure 35). All OsLu concentrations were used at 50 μg and α-mannan at 1 μg/ml. (b) Dectin-2 reporter assay with OsLu and commercial prebiotic galactooligosaccharides. Concentrations in (b) were 30, 100, 300 or 1000 μg/ml. Data are means of triplicate values ±SD (error bars). Statistical analyses were performed by one-way ANOVA followed by Tukey's test. ***, p < 0.001. Permission is not required for authors to use this Figure as stated by the Copyright Clearance Centre.

Appendix 16

Content (%) of protein and carbohydrates (mono-, di- and oligosaccharides) found in the different prebiotic samples studied.

	Protein	Fructose	Galactose	Glucose	Lactulose	Lactose	Other	Trisaccharides	Tetrasaccharides	Pentasaccharides
	%*	%**	%	%	%	%	disaccharides %	%	%	%
OsLu	0.05***	19.5	12.4	1.19	24.7	n.d.	13.6	22.6	5.42	0.65
	(0.02)	(0.01)	(0.00)	(0.00)	(0.02)		(0.01)	(0.02)	(0.55)	(0.20)
OsLu-ActC	< 0.05	1.51	0.80	0.14	10.3	n.d.	7.00	52.1	25.2	2.99
		(0.12)	(0.09)	(0.08)	(1.20)		(0.29)	(0.15)	(0.02)	(0.05)
OsLu-*Sc*	0.44	0.63	14.1	n.d.	26.2	n.d.	21.1	25.6	9.67	2.80
	(0.10)	(0.20)	(1.04)		(1.20)		(1.14)	(0.74)	(0.75)	(0.60)
OsLu-*Sc*-R	0.46	0.25	10.4	0.06	24.2	n.d.	18.9	28.2	13.8	4.33
	(0.04)	(0.01)	(0.29)	(0.01)	(0.78)		(0.55)	(0.94)	(0.44)	(0.15)
OsLu-*Sc*-P	0.05	0.30	11.3	0.78	26.6	n.d.	20.0	25.9	11.7	3.50
	(0.03)	(0.01)	(0.42)	(0.19)	(0.98)		(0.38)	(0.82)	(0.95)	(0.01)
OsLu-*Sc*-Pp	0.53	0.35	9.63	0.08	23.6	n.d.	25.2	33.6	7.20	0.77
	(0.09)	(0.19)	(0.85)	(0.03)	(0.01)		(0.03)	(0.02)	(0.05)	(0.42)
OsLu-Sc-S	< 0.05	0.94	25.8	0.07	39.0	n.d.	22.7	11.4	n.d.	n.d.
		(0.27)	(0.01)	(0.03)	(0.03)		(0.13)	(0.94)		
Duphalac®	< 0.05		7.87	0.29	88.7	3.22				
			(0.79)	(0.05)	(0.69)	(0.25)				
Vivinal®GOS	< 0.1****	–	1.41	20.7	–	18.0	20.5	21.0	13.1	5.45
			(0.11)	(2.14)		(0.29)	(0.69)	(0.79)	(0.89)	(0.66)

n.d. no detected (quantification limit 10 mg/L).
* % with respect to DM.
** % with respect to total carbohydrates.
*** Average (standard deviation).
**** Data provided by the manufacturer.

Appendix 16. Protein and carbohydrate contents in OsLu samples, and commercial prebiotic oligosaccharides.

DM, dry matter. Taken from [489]. Permission is not required for authors to use this Figure as stated by the Copyright Clearance Centre.

Appendix 17

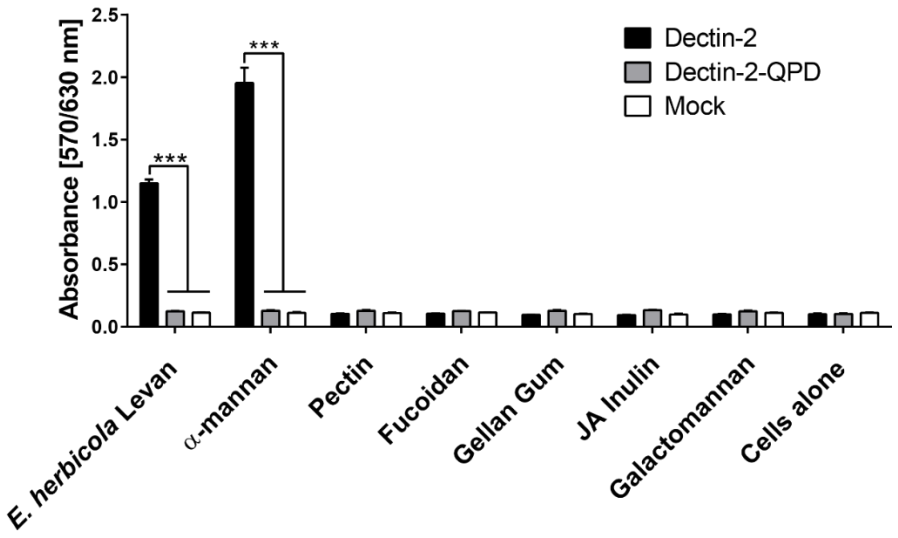

Appendix 17. Screening of PS to Dectin-2 and Dectin-2-QPD reporter cells.

Carbohydrate binding to CLR BWZ.36 reporter cells induces β-galactosidase production within the cell which can be measured in a colorimetric assay: CLR BWZ.36 reporter cells were incubated with immobilised carbohydrate ligands using a 96 well plate; a substrate, Chlorophenol red-β-D-galactopyranoside (CPRG), was added to cells and absorbance values were read at 570/630 nm. Reporter assay using Dectin-2, Dectin-2-QPD and mock reporter cells. A repeated independent experiment supporting Figure 37. All PS concentrations were 20 μg/ml. JA, Jerusalem artichoke. Data are means of triplicate values ±SD (error bars). Statistical analyses were performed by one-way ANOVA followed by Tukey's test. ***, p < 0.001.

Appendix 18

a)

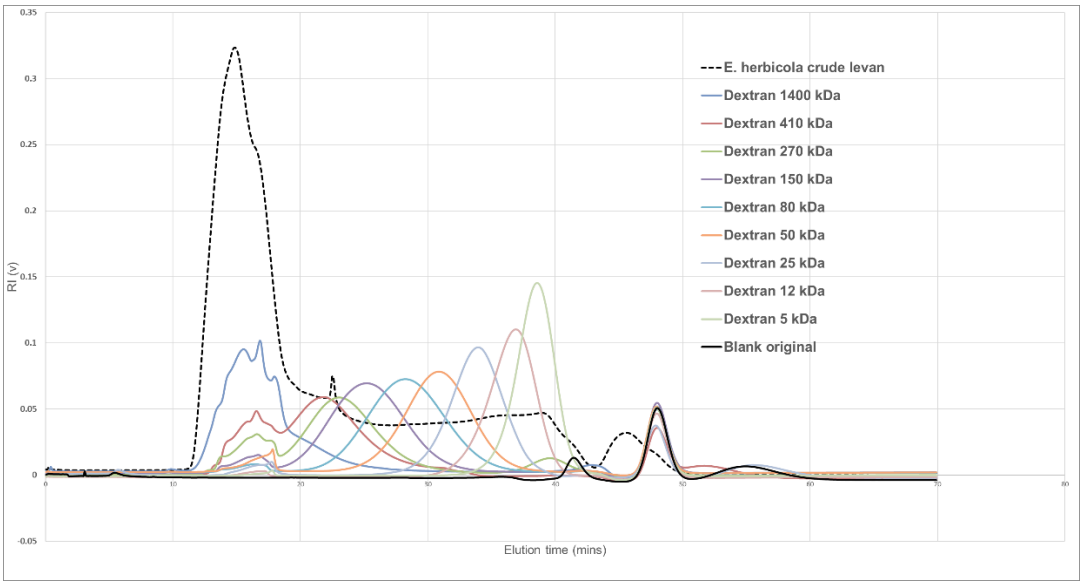

b)

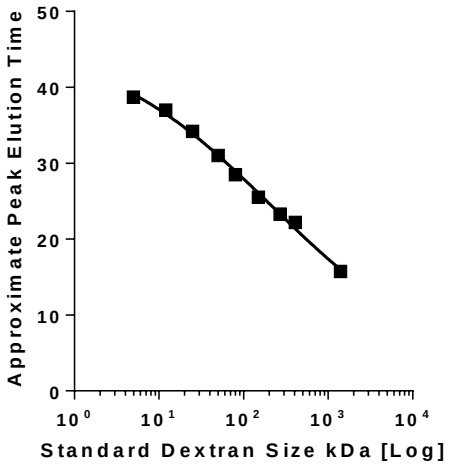

Appendix 18. Analysis of dextran standards using size exclusion chromatography.

Gel permeation chromatography profile of dextran standards. Peak elution times for 5 kDa, 12kDa, 25 kda, 50 kDa, 80 kDa, 150 kDa, 270 kDa, 410 kDa, and 1400 kDa dextran standards are shown. Predominant peaks identified the dextran standards. The peak for 1400 kDa was assumed as the first clearly identifiable peak. The main elution peak for E. herbicola crude levan was observed upstream of the 1400 kDa dextran standard. A non-linear calibration curve (4-parameter logistic regression; R2 = 0.996 and adjusted R2 = 0.994) using approximate peak elution times is shown in (b) and constructed in GraphPad Prism. Data in (a) was extracted from the Chromera software (Perkin Elmer) and analysis was performed in Excel.

Appendix 19

a)

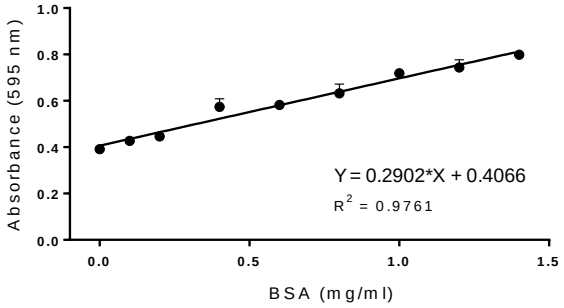

b)

mg/ml	BSA STND	BSA STND	Levan	Levan	5	6	7	8	9	10	11	12	
1.4	0.804	0.794	0.394	0.354	0.042	0.038	0.037	0.037	0.038	0.038	0.038	0.049	
1.2	0.767	0.72	0.04	0.039	0.039	0.047	0.037	0.037	0.037	0.037	0.041	0.038	
1	0.721	0.716	0.038	0.037	0.058	0.037	0.037	0.037	0.038	0.037	0.038	0.037	
0.8	0.604	0.661	0.037	0.037	0.037	0.037	0.038	0.038	0.039	0.038	0.037	0.037	
0.6	0.578	0.586	0.038	0.038	0.037	0.043	0.037	0.037	0.038	0.041	0.044	0.044	
0.4	0.549	0.599	0.04	0.039	0.038	0.045	0.037	0.037	0.039	0.037	0.038	0.042	
0.2	0.46	0.432	0.038	0.039	0.039	0.037	0.038	0.038	0.039	0.044	0.045	0.046	
0.1	0.417	0.437	0.039	0.038	0.038	0.038	0.037	0.037	0.04	0.043	0.397	0.386	Blanks
	Average Absorbance												
Levan	**0.374**	**< blank**											
Blank	**0.392**												

Appendix 19. Quantification of protein content in E. herbicola crude levan by Bradford assay.

Protein content was determined using a Bradford assay. (a) Linear standard curve shows absorbance values (595 nm) of BSA standards. (b) Raw absorbance values including blank and E. herbicola crude levan (in duplicate) are represented in the Table. Average absorbance for E. herbicola crude levan was below the blank value (bottom left of the grid).

Appendix 20

a)

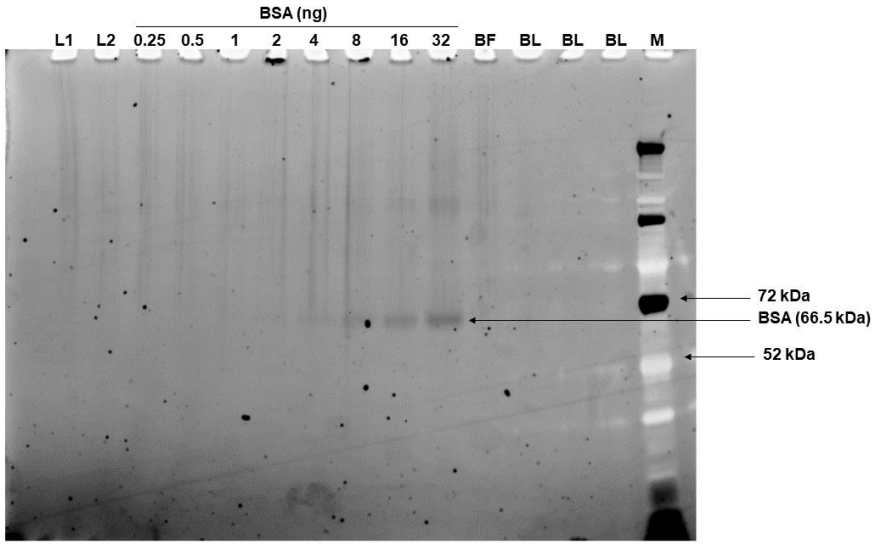

b)

c)

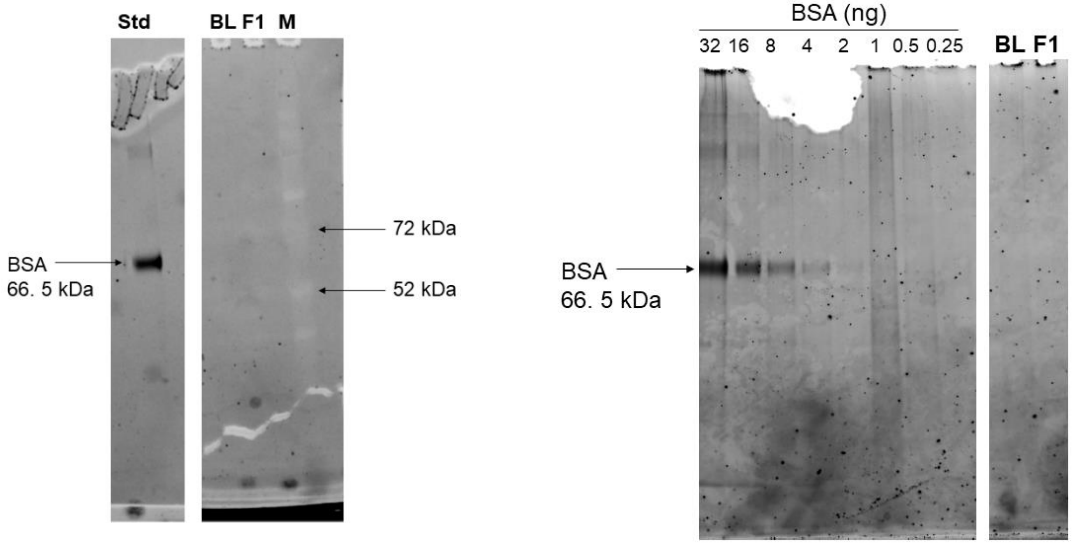

Appendix 20. Detection of proteins in E. herbicola crude levan and E. herbicola levan Fractions 1, 2 ,3 and 4 (post-GPC) by SDS page and Spyro™ Ruby gel staining.

(a) L1, E. herbicola crude levan. L2, E. herbicola crude levan (duplicate). BF, buffer alone. BL, blank lane. M, marker (a). BSA concentrations are as indicated. (b) F1, E. herbicola crude levan fraction 1 post-size exclusion. BL, blank lane. M, protein marker. Std, BSA standard. 20 ng of BSA was used (indicated by arrow). In the marker lane, arrows show proteins at 52 and 72 kDa. BSA is 66.5 kDa[610]. (c) Repeat of F1, E. herbicola crude levan fraction 1 post-size exclusion. BSA concentrations are as indicated. Images were acquired and prepared using Bio-Rad Quantity One software and Image Lab™. Images from (a) (b) and (c) were then prepared and labelled using Microsoft PowerPoint.

Appendix 21

a)

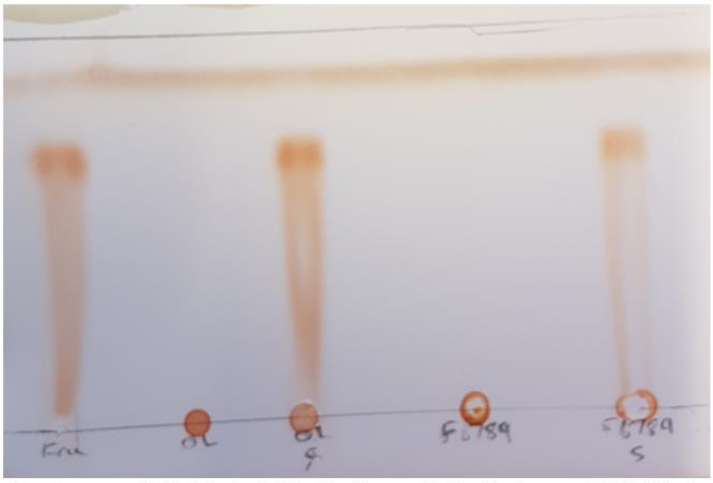

b)

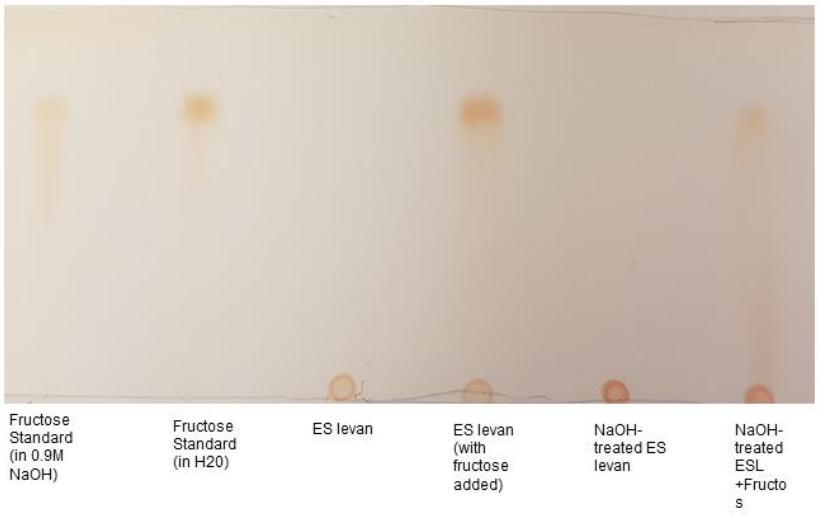

Appendix 21. Thin layer chromatography (followed by orcinol staining) of levans treated with sodium hydroxide.

(a) TLC of E. herbicola levan 2 (post-GPC and post-LRA) treated with sodium hydroxide (NaOH) prior to dialysis. 'E. herbicola levan 2' represents E. herbicola after NaOH treatment. A fructose standard was tested with or without levan, as indicated. (b) TLC of ES levan treated with NaOH prior to dialysis. A fructose standard was tested and without levan, as indicated. Fructose was also tested in 0.9 M NaOH.

Appendix 22

Table 2
Chemical shifts of microbial Levan.

Carbon atom	Chemical shifts of Levan [^{13}C NMR (ppm)]				
	P. fluorescens (Jathore et al., 2012)	*Z. mobilis* (Jathore et al., 2012)	*L. reuteri 100-23* (Sims et al., 2011)	*B.subtilis (natto)* (Shih et al., 2005)	*B.polymyxa* (Shih et al., 2005)
C-1	60.435	60.761	61.4	60.1	60.7
C-2	104.696	104.641	105.6	104.4	104.2
C-3	76.770	77.683	77.8	76.5	77.0
C-4	75.783	75.754	76.7	75.4	75.7
C-5	80.880	80.783	81.7	80.5	80.5
C-6	63.978	63.957	64.8	63.6	63.6

Appendix 22. ^{13}C NMR chemical shifts of levan.

Taken from [71] with permission from Elsevier and Copyright Clearance Center.

Appendix 23

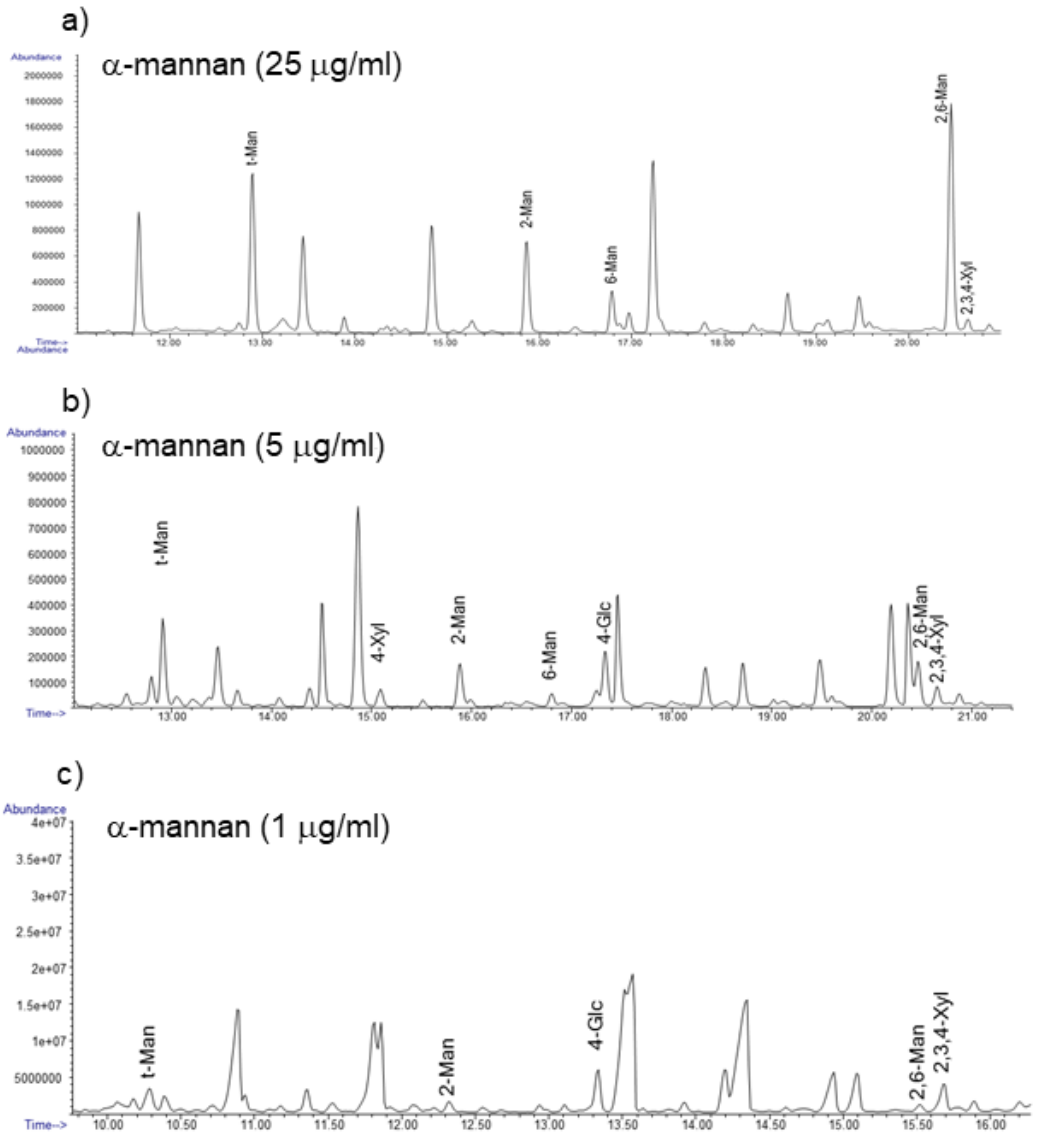

Appendix 23. Glucosyl linkage analysis of α-mannan from Saccharomyces cerevisiae used in this study

Labelling is based on a 1-linkage for aldose sugars and a 2-linkage for ketose sugars e.g. 2-Man is a mannose residue linked at carbon 2 representing an α-(1,2) linkage, and 2-,6-Man is a mannose residue linked at carbon 2 and representing both α-(1,2) and α-(1,6) links indicating a branching point. t-, terminal. Glc, glucopyranosyl. Xyl, xylose. Man, mannose. GC-MS linkage analysis was performed by Ian Black.

Appendix 24

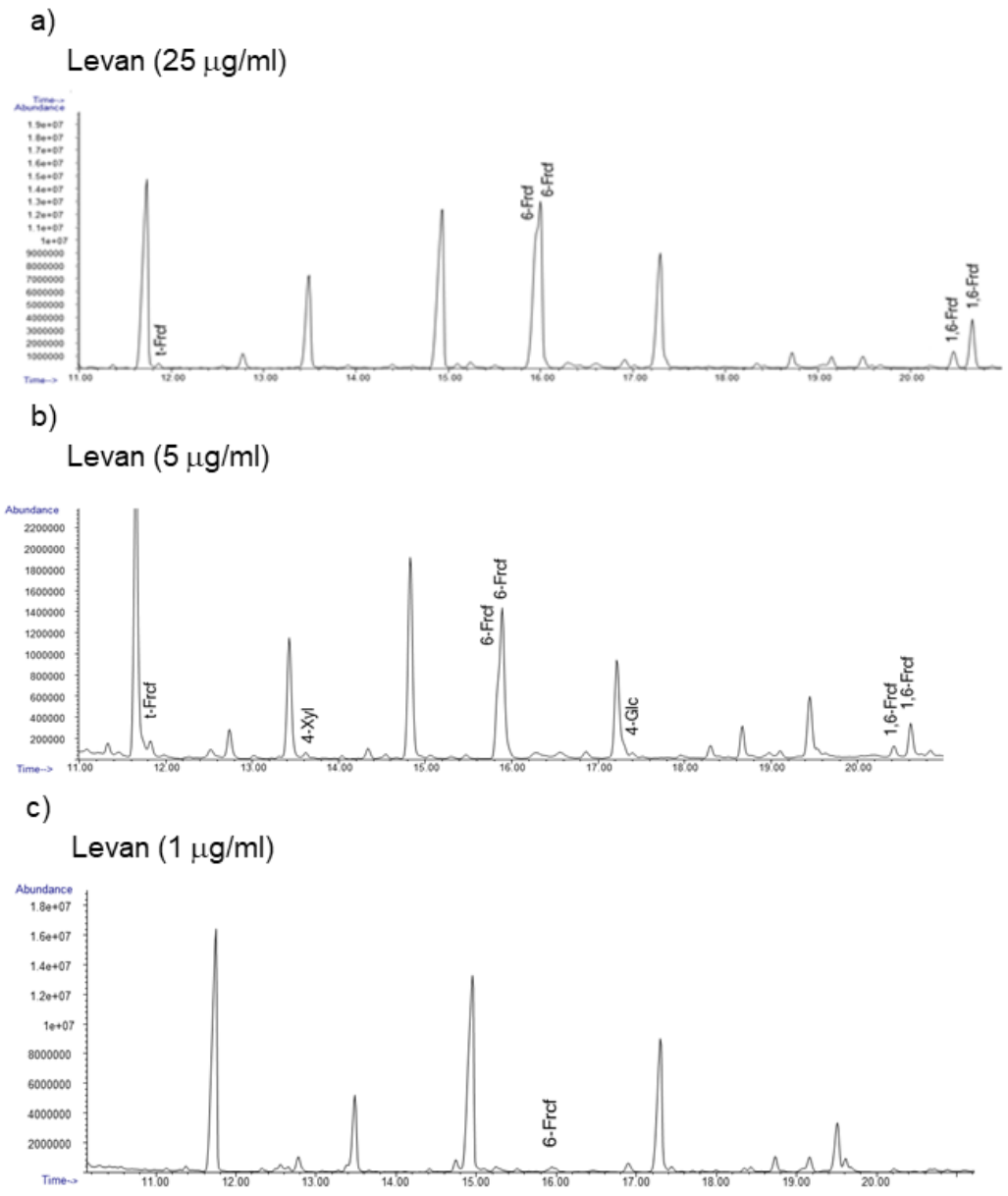

Appendix 24. Glucosyl linkage analysis of E. herbicola levan 2 used in this study.

Labelling is based on a 1-linkage for aldose sugars and a 2-linkage for ketose sugars e.g. 6-Frct is a fructose residue linked at carbon 6 representing a β-(2,6) linkage. 1,6-Frct indicates β-(2,1) branching. Frct, Fructofuranosyl. t-, terminal. Glc, glucopyranosyl. Xyl, xylose. GC-MS linkage analysis was performed by Ian Black.

Appendix 25

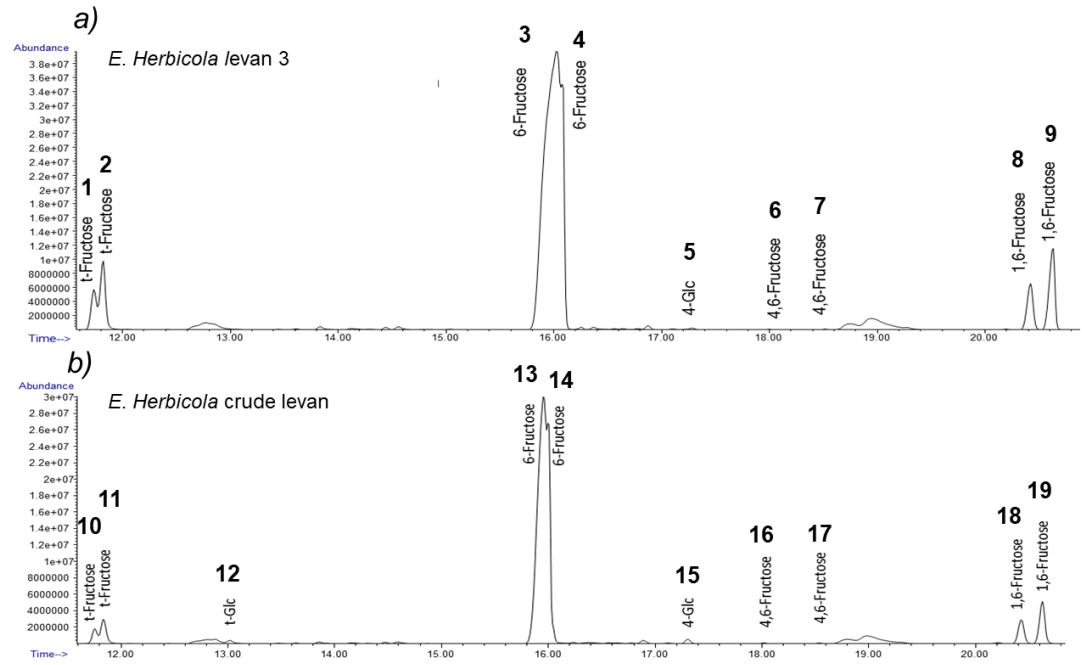

c)

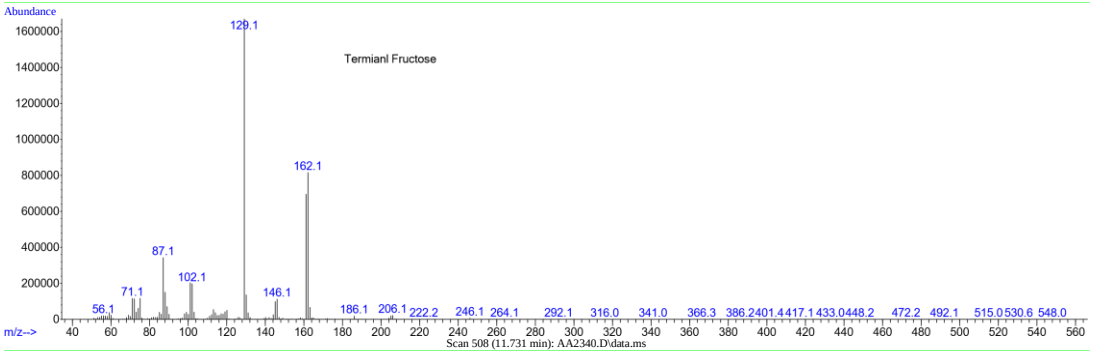

d)

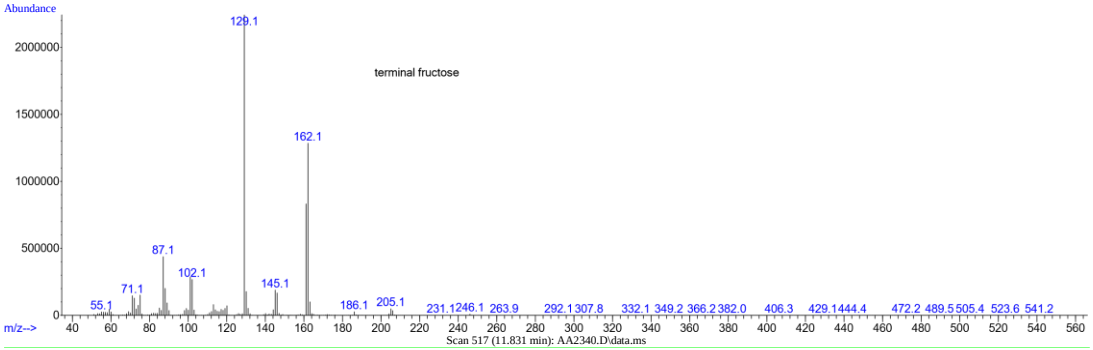

e)

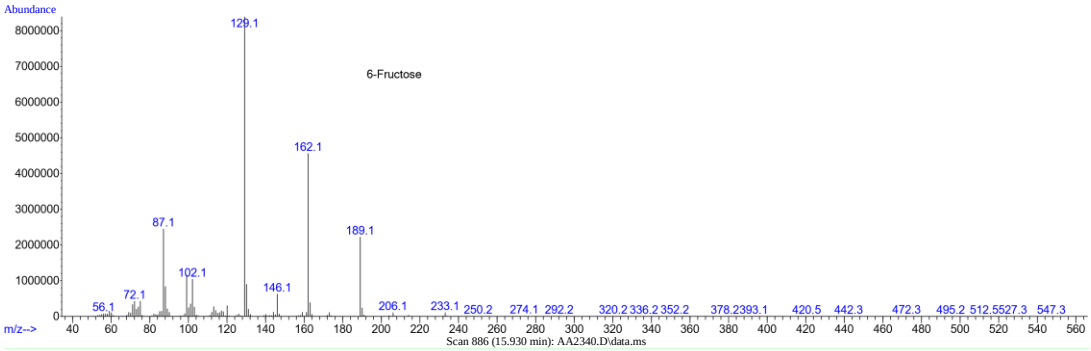
Abundance
129.1
6-Fructose
162.1
87.1
189.1
102.1
146.1
72.1
56.1
206.1
233.1
m/z-->
Scan 886 (15.930 min): AA2340.D\data.ms

f)

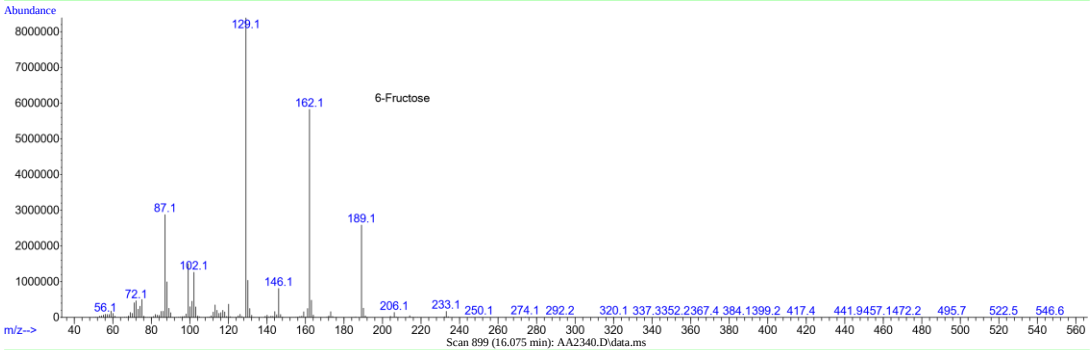
Abundance
129.1
6-Fructose
162.1
87.1
189.1
102.1
146.1
72.1
56.1
206.1
233.1
m/z-->
Scan 899 (16.075 min): AA2340.D\data.ms

g)

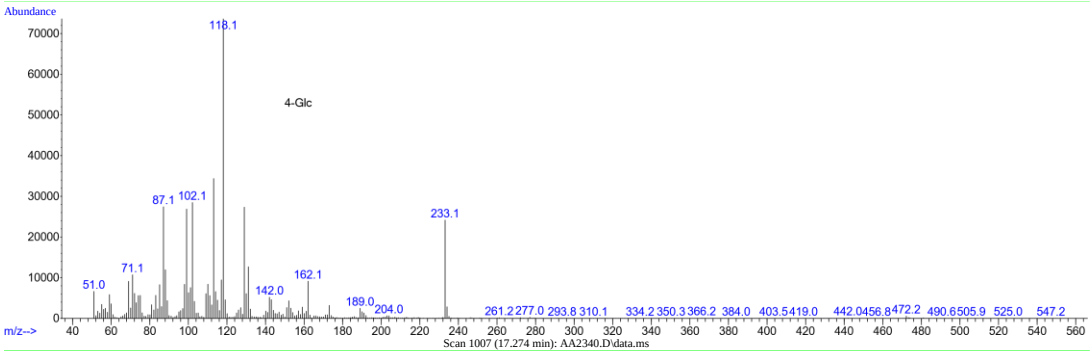
Abundance
118.1
4-Glc
87.1
102.1
233.1
71.1
51.0
162.1
142.0
189.0
204.0
m/z-->
Scan 1007 (17.274 min): AA2340.D\data.ms

h)

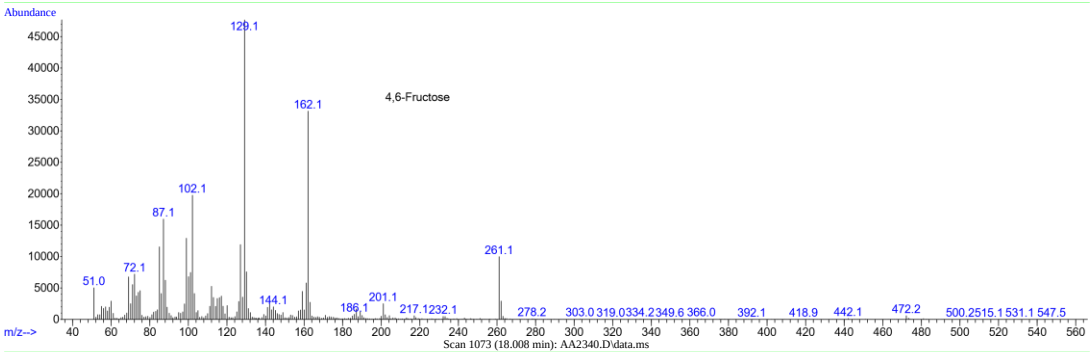
Abundance
129.1
162.1
4,6-Fructose
102.1
87.1
261.1
72.1
51.0
144.1
186.1
201.1
217.1232.1
278.2
303.0 319.0334.2349.6 366.0
392.1
418.9
442.1
472.2
500.2515.1 531.1 547.5
m/z-->
Scan 1073 (18.008 min): AA2340.D\data.ms

i)

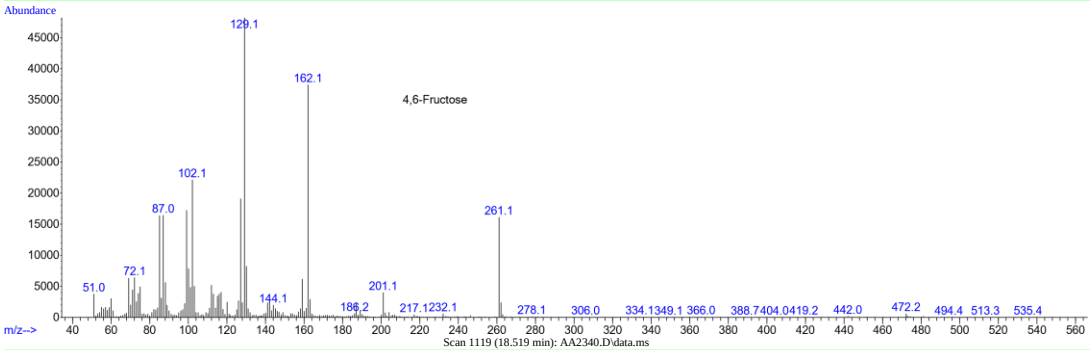
Abundance
129.1
162.1
4,6-Fructose
102.1
87.0
261.1
72.1
51.0
201.1
144.1
186.2
217.1232.1
278.1
306.0
334.1349.1 366.0
388.7404.0419.2
442.0
472.2
494.4
513.3
535.4
m/z-->
Scan 1119 (18.519 min): AA2340.D\data.ms

j)

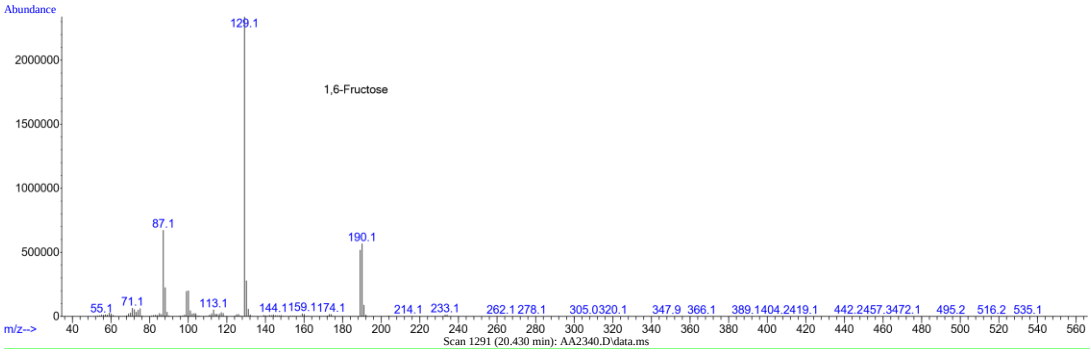
Abundance
129.1
1,6-Fructose
87.1
190.1
55.1
71.1
113.1
144.1159.1174.1
214.1
233.1
262.1 278.1
305.0320.1
347.9
366.1
389.1404.2419.1
442.2457.3472.1
495.2
516.2
535.1
m/z-->
Scan 1291 (20.430 min): AA2340.D\data.ms

k)

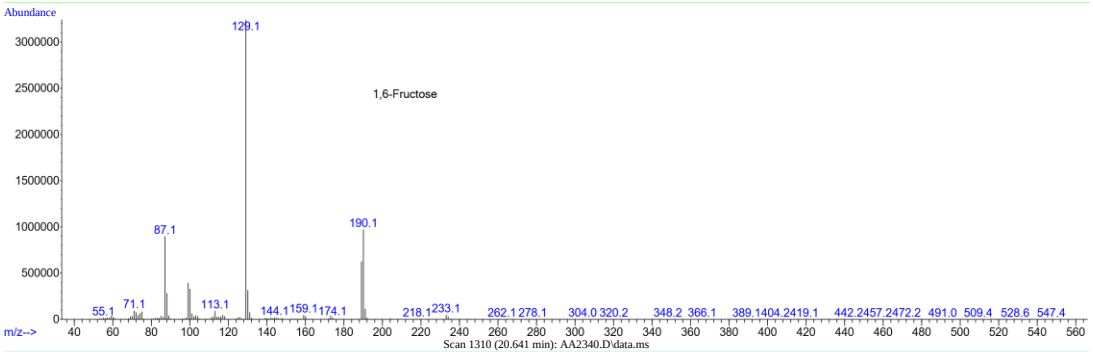
Abundance
1,6-Fructose
m/z-->
Scan 1310 (20.641 min): AA2340.D\data.ms

l)

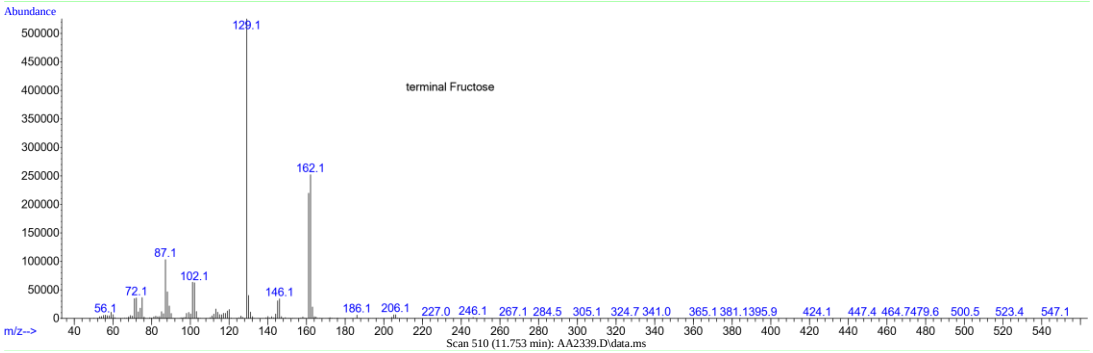
Abundance
terminal Fructose
m/z-->
Scan 510 (11.753 min): AA2339.D\data.ms

m)

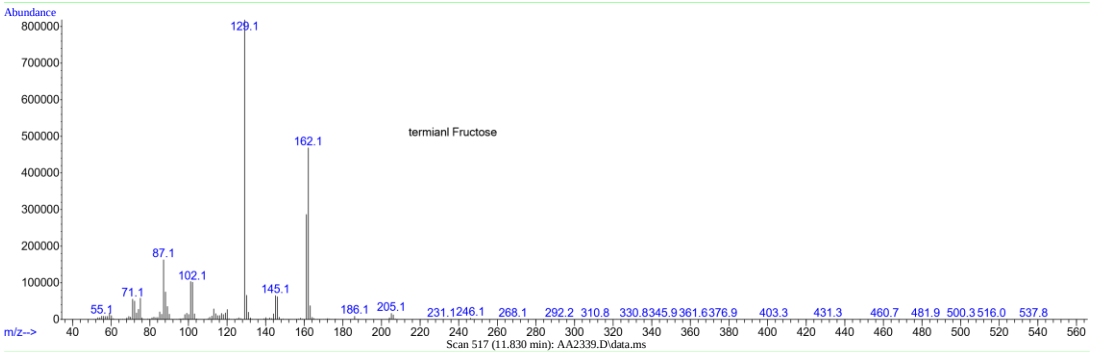
Abundance
termianl Fructose
m/z-->
Scan 517 (11.830 min): AA2339.D\data.ms

n)

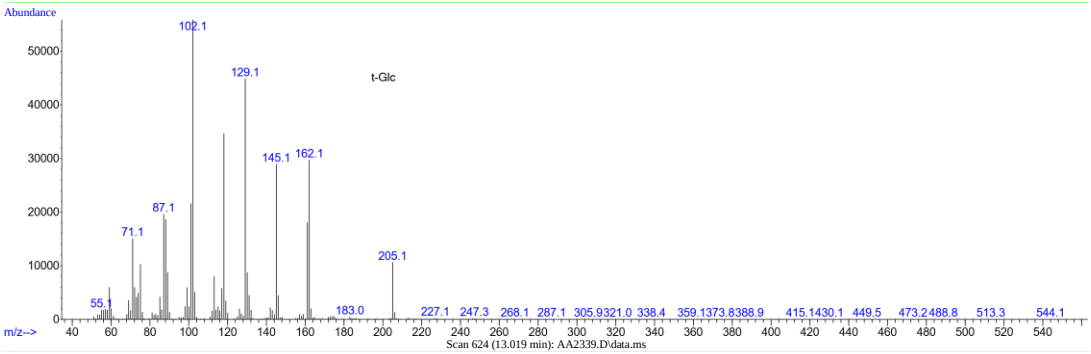
Abundance
102.1
129.1
t-Glc
145.1
162.1
87.1
71.1
205.1
55.1
183.0
227.1
247.3
268.1
287.1
305.9
321.0
338.4
359.1
373.8
388.9
415.1
430.1
449.5
473.2
488.8
513.3
544.1
m/z-->
Scan 624 (13.019 min): AA2339.D\data.ms

o)

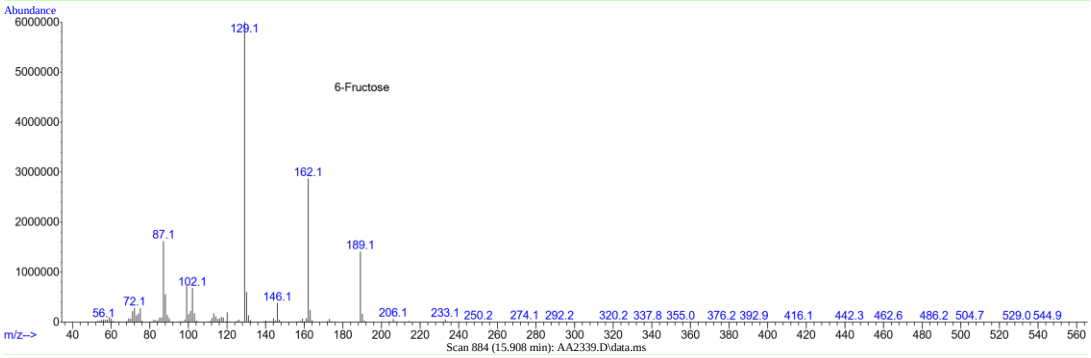
Abundance
129.1
6-Fructose
162.1
87.1
189.1
102.1
146.1
72.1
56.1
206.1
233.1
250.2
274.1
292.2
320.2
337.8
355.0
376.2
392.9
416.1
442.3
462.6
486.2
504.7
529.0
544.9
m/z-->
Scan 884 (15.908 min): AA2339.D\data.ms

p)

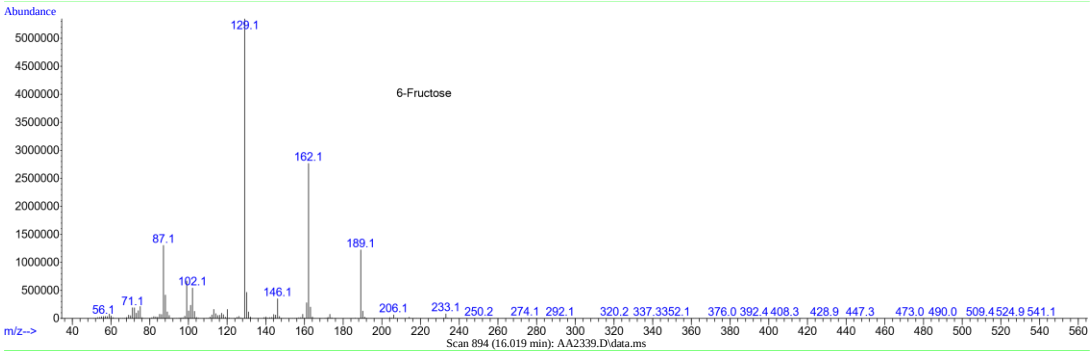
Abundance
129.1
6-Fructose
162.1
87.1
189.1
102.1
146.1
71.1
56.1
206.1
233.1
250.2
274.1
292.1
320.2
337.3
352.1
376.0
392.4
408.3
428.9
447.3
473.0
490.0
509.4
524.9
541.1
m/z-->
Scan 894 (16.019 min): AA2339.D\data.ms

q)

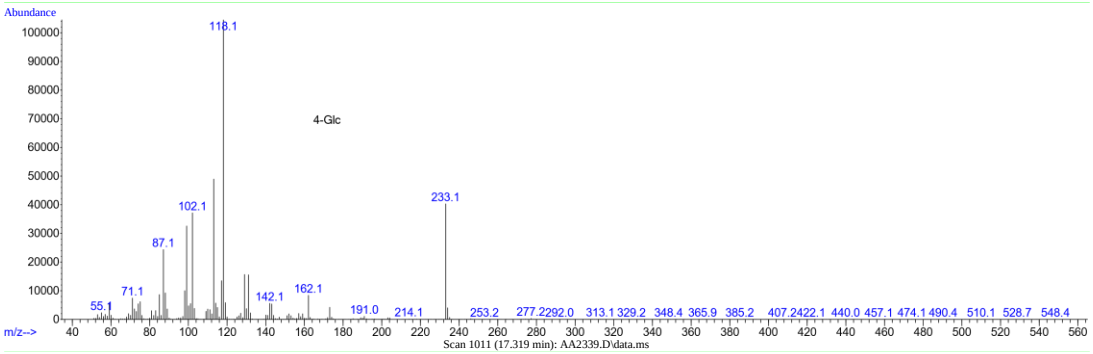
Abundance
4-Glc
m/z-->
Scan 1011 (17.319 min): AA2339.D\data.ms

r)

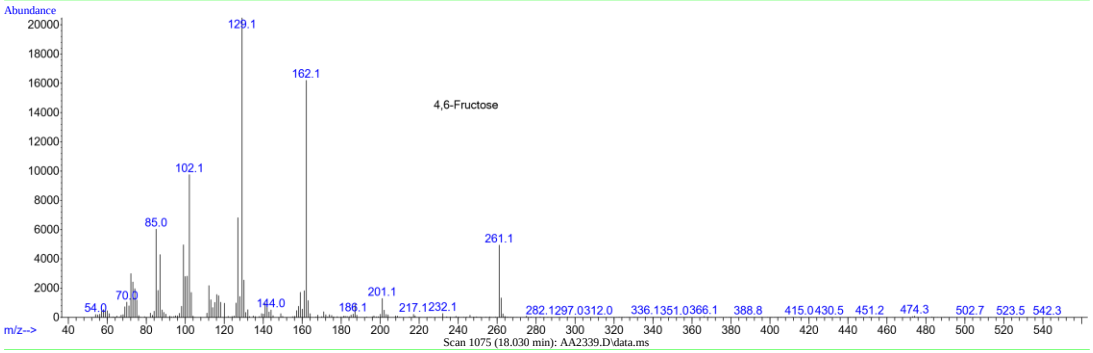
Abundance
4,6-Fructose
m/z-->
Scan 1075 (18.030 min): AA2339.D\data.ms

s)

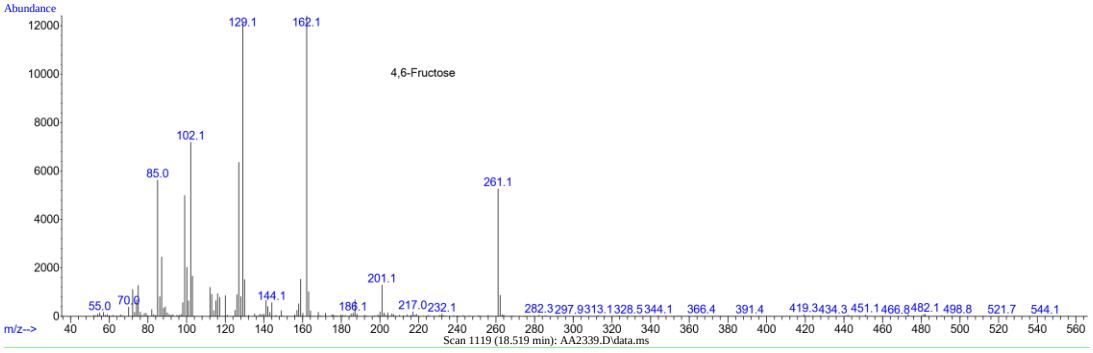
Abundance
4,6-Fructose
m/z-->
Scan 1119 (18.519 min): AA2339.D\data.ms

t)

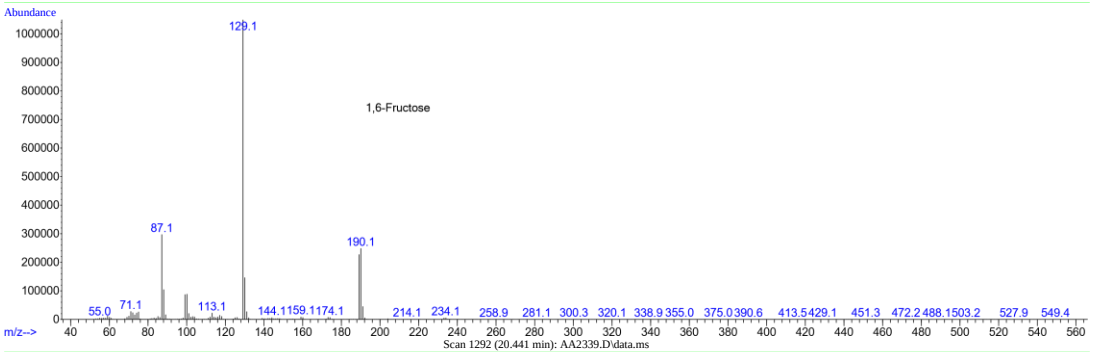

u)

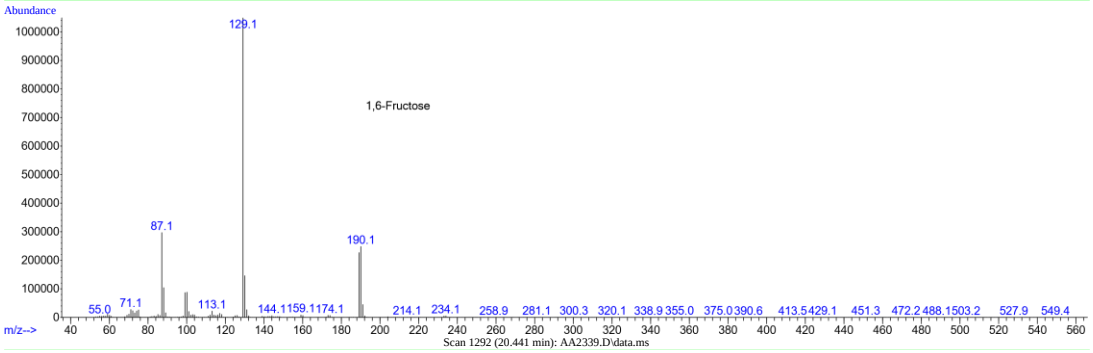

Appendix 25. GC profile and MS data of partially methylated alditol acetate derivatives showing glycosyl linkage analysis of E. herbicola Levan 3 and E. herbicola crude levan.

Supplementary information supporting Table 7. GC profile of E. herbicola levan 3 (purified) (a) and E. herbicola crude levan (b). Mass spectrum for each identified GC peak are shown for E. herbicola levan 3 (c – k) and E. herbicola crude levan (l – u) as indicated. The numbers (1 – 19) on the GPC chromatogram per peak correspond to the MS data as follows: 1-c, 2-d, 3-e, 4-f, 5-g, 6-h, 7-i, 8-j, 9-k, 10-l, 11-m, 12-n, 13-o, 14-p, 15-q, 16-r, 17-s, 18-t, and 19-u. Additionally, GPC chromatogram labelling is based on 1-linkage for aldose sugars and the 2-linkage for ketose sugars e.g. 6-frct is a fructose residue linked at carbons 2 and 6. 1,6-Frct indicates β-(2,1) branching. 't', terminal. Glc, glucopyranosyl. GC-MS linkage analysis was performed by Ian Black.

Appendix 26

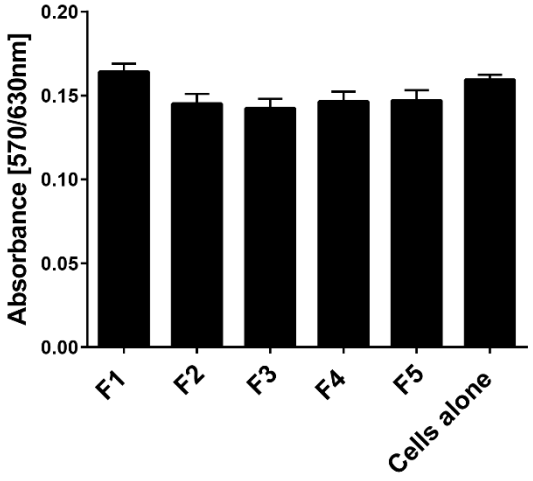

Appendix 26. Reporter cell assay of E. herbicola levan fractions using mock reporter cells; an additional control corresponding to Figure 42.

Carbohydrate binding to CLR BWZ.36 reporter cells induces β-galactosidase production within the cell which can be measured in a colorimetric assay: CLR BWZ.36 reporter cells were incubated with immobilised carbohydrate ligands using a 96 well plate; a substrate, Chlorophenol red-β-D-galactopyranoside (CPRG), was added to cells and absorbance values were read at 570/630 nmF1, F2, F3, F4 and F5 are E. herbicola levan fractions post-GPC. All concentrations were 100 μg/ml. Experiments were performed in triplicate. Error bars, ± SD.

Appendix 27

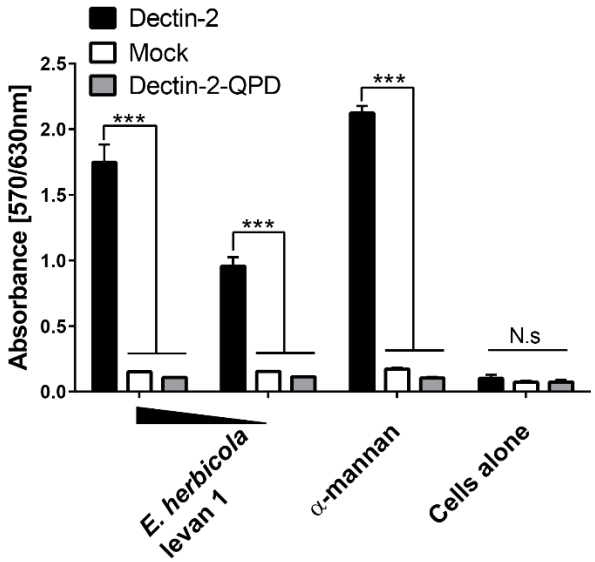

Appendix 27. Reporter cell assay of E. herbicola levan 1 with Dectin-2 and its CRD using Dectin-2, Dectin-2-QPD and mock reporter cells.

Carbohydrate binding to CLR BWZ.36 reporter cells induces β-galactosidase production within the cell which can be measured in a colorimetric assay: CLR BWZ.36 reporter cells were incubated with immobilised carbohydrate ligands using a 96 well plate; a substrate, Chlorophenol red-β-D-galactopyranoside (CPRG), was added to cells and absorbance values were read at 570/630 nm. Experiment is an independent repeat of Figure 43. E. herbicola levan was used at 25 μg/ml and 5 μg/ml, positive control α-mannan at 1 μg/ml. Experiments were performed in triplicate. Error bars, ± SD. Statistical analysis was performed using one-way ANOVA followed by tukey's test (b). ***, p < 0.001. N.s with straight line, not statistically significant.

Appendix 28

a)

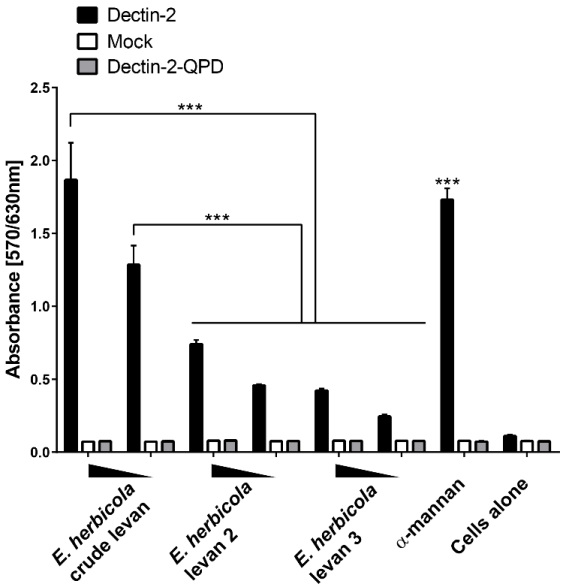

b)

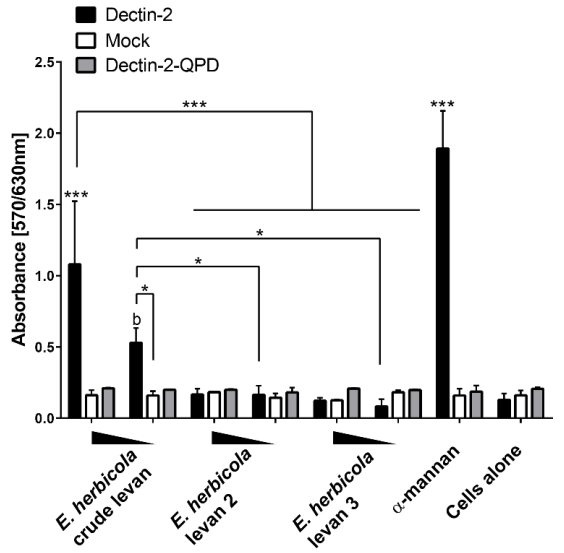

Appendix 28. Comparative binding of E. herbicola crude levan, E. herbicola levan 2 and E. herbicola levan 3 to Dectin-2 and its CRD using Dectin-2, Dectin-2-QPD and mock reporter cells.

Carbohydrate binding to CLR BWZ.36 reporter cells induces β-galactosidase production within the cell which can be measured in a colorimetric assay: CLR BWZ.36 reporter cells were incubated with immobilised carbohydrate ligands using a 96 well plate; a substrate, Chlorophenol red-β-D-galactopyranoside (CPRG), was added to cells and absorbance values were read at 570/630 nm. Two repeated independent experiments of Figure 44 are shown in (a) and (b). All levan concentrations were used at 200 μg/ml and 20 μg/ml, and positive control α-mannan at 1 μg/ml. All experiments shown in (a) and (b) were performed in triplicate. Error bars, ± SD. Statistical analysis was performed using one-way ANOVA followed by tukey's test (b). ***, p < 0.001. *, p < 0.05 compared to cells alone. Statistically significant differences between treatments are marked as indicated (comparative line; ***, p < 0.001. **, p < 0.01. *, p < 0.05). b, p < 0.05 compared to WT and mock cells alone.

Appendix 29

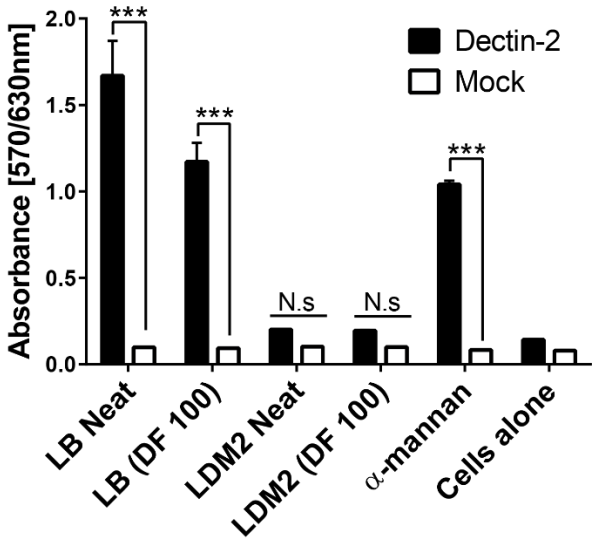

Appendix 29. Reporter cell assay of LB and LDM2 culture media using Dectin-2 and mock reporter cells.

Carbohydrate binding to CLR BWZ.36 reporter cells induces β-galactosidase production within the cell which can be measured in a colorimetric assay: CLR BWZ.36 reporter cells were incubated with immobilised carbohydrate ligands using a 96 well plate; a substrate, Chlorophenol red-β-D-galactopyranoside (CPRG), was added to cells and absorbance values were read at 570/630 nm. Experiment is an independent repeat of Figure 46. Experiments was performed in triplicate. DF 100, LB or LDM2 diluted by a factor of 100 in sterile H_20. Error bars, ± SD. Statistical analysis was performed using one-way ANOVA followed by tukey's test (b). ***, p < 0.001, as indicated. N.s. with straight line, not statistically significant compared to cells alone and across the indicated treatments.

Appendix 30

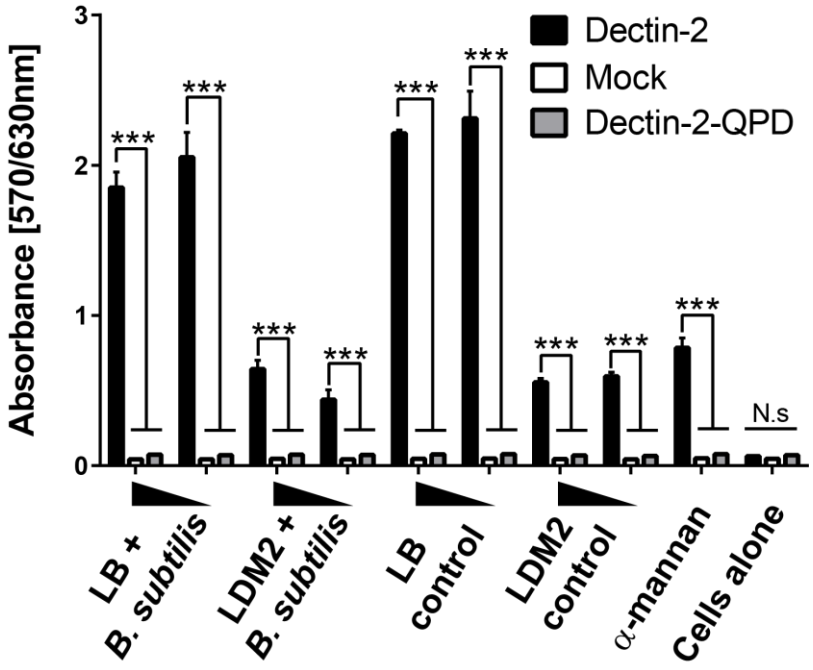

Appendix 30. Reporter cell assay of B. subtilis levan and medium-only controls using Dectin-2, Dectin-2-QPD and mock reporter cells.

Carbohydrate binding to CLR BWZ.36 reporter cells induces β-galactosidase production within the cell which can be measured in a colorimetric assay: CLR BWZ.36 reporter cells were incubated with immobilised carbohydrate ligands using a 96 well plate; a substrate, Chlorophenol red-β-D-galactopyranoside (CPRG), was added to cells and absorbance values were read at 570/630 nm. Experiment is an independent repeat of Figure 47. B. subtilis levan and media-only controls were used at 100μg/ml and 10 μg/ml, and positive control α-mannan at 1 μg/ml. The experiments were performed in triplicate. Error bars, ± SD. Statistical analysis was performed using one-way ANOVA followed by tukey's test (b). ***, p < 0.001. N.s, with straight line, not statistically significant.

Appendix 31

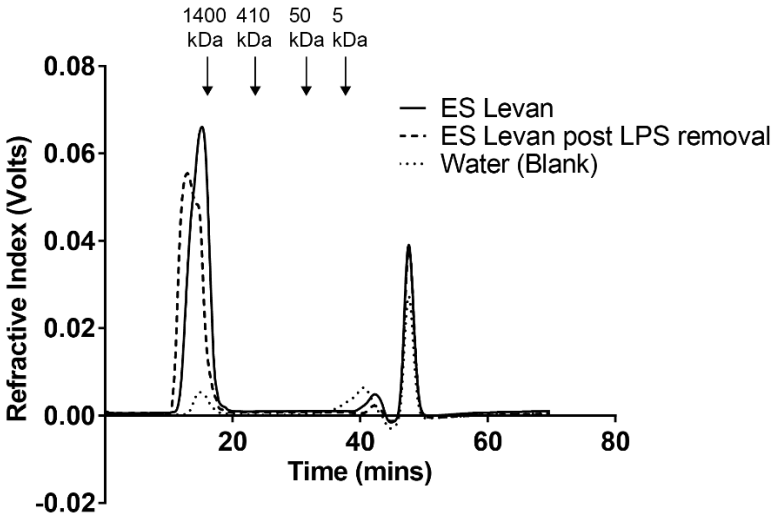

Appendix 31. Gel permeation chromatography profile of ES levan pre- and post-LPS alkali treatment.

Repeated independent GPC runs for ES levan and purified ES levan from Figure 48. Samples for purified ES levan (ES Levan post LPS removal is after LPS inactivation by alkali treatment. Water (blank) was used as a control. The graph was constructed in GraphPad Prism.

Appendix 32

a)

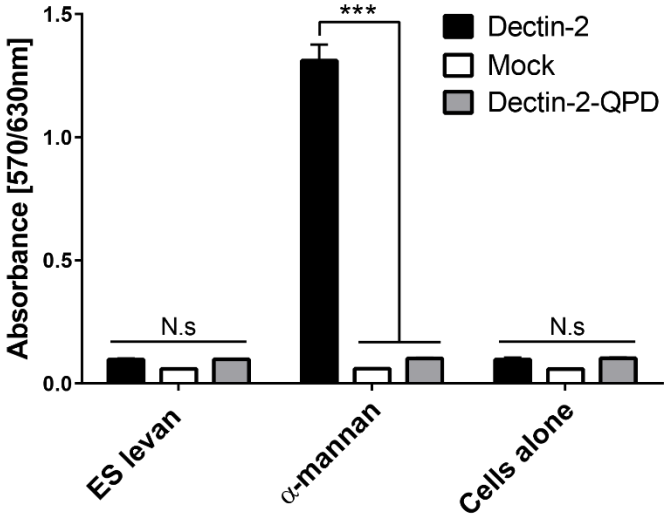

b)

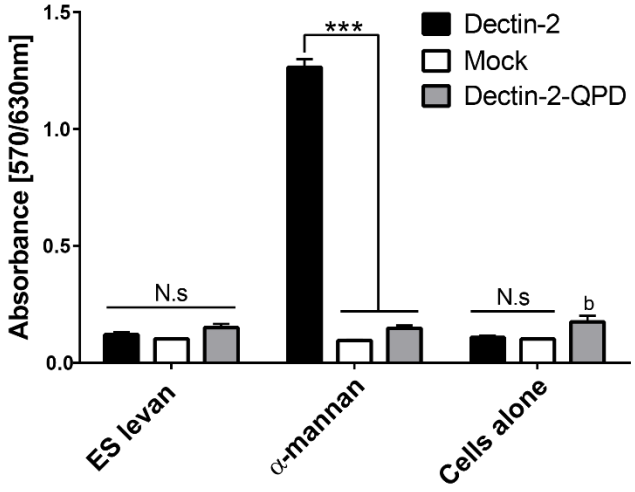

Appendix 32. Reporter cell assay of ES levan using Dectin-2, Dectin-2-QPD and mock reporter cells.

Carbohydrate binding to CLR BWZ.36 reporter cells induces β-galactosidase production within the cell which can be measured in a colorimetric assay: CLR BWZ.36 reporter cells were incubated with immobilised carbohydrate ligands using a 96 well plate; a substrate, Chlorophenol red-β-D-galactopyranoside (CPRG), was added to cells and absorbance values were read at 570/630 nm. Two repeated independent experiments of Figure 50 are shown in (a) and (b). ES levan was used at 100 μg/ml, and positive control α-mannan at 1 μg/ml. All experiments were performed in triplicate. Error bars, ± SD. Statistical analysis was performed using one-way ANOVA followed by tukey's test (b). ***, p < 0.001, as indicated. b (on cells alone Dectin-2 QPD), we additionally noted an increase in QPD compared to WT cells alone (p < 0.01) and to mock cells (p < 0.001). N.s with straight line, not statistically significant

Appendix 33

a)

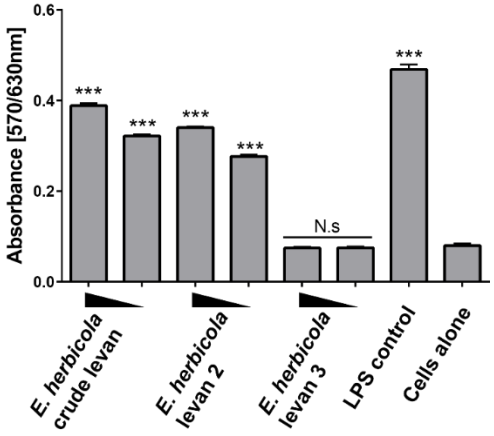

b)

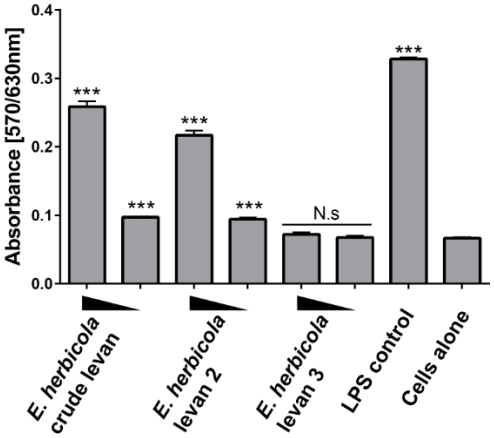

Appendix 33. Reporter cell assay of crude and purified E. herbicola levans using TLR4 reporter cells.

Ligand binding to TLR4 reporter cells results in the production of secreted embryonic alkaline phosphatase (SEAP) which can be measured in a colorimetric assay: TLR4 reporter cells were incubated with carbohydrate ligands or control (LPS) in HEK blue medium[394] using a 96 well plate; and absorbance values were read at 655 nm. Repeat separate experiments of Figure 56 using levan concentrations of (a) 50 μg/ml and 100 μg/ml or (b) 10 μg/ml and 100 μg/ml. All experiments were performed in triplicate. Concentration of positive control LPS was 0.1μg/ml. Error bars, ± SD. Statistical analysis was performed using one-way ANOVA followed by tukey's test (b). ***, p < 0.001 compared to cells alone. N.s with straight line, not statistically significant compared to cells alone.

Appendix 34

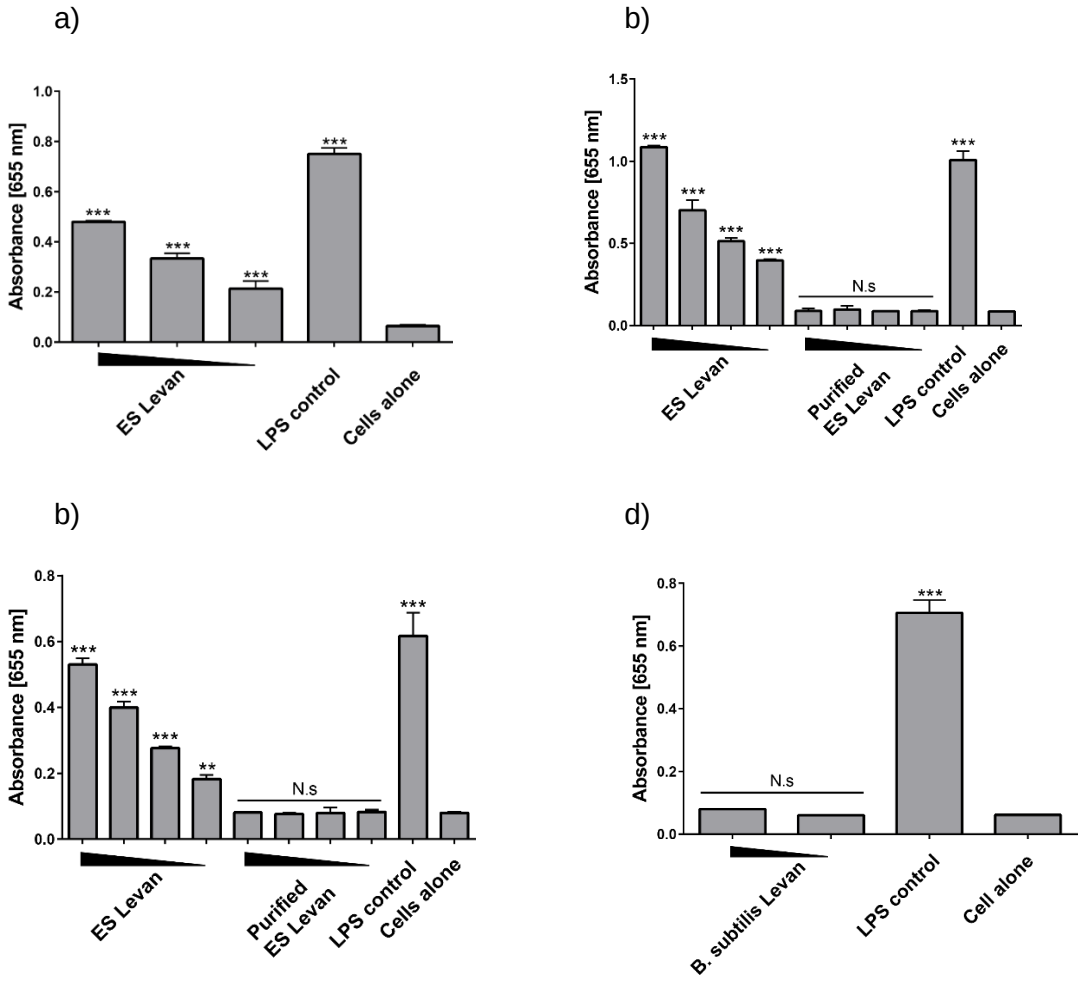

Appendix 34. Reporter cell assay of ES levan, or B. subtilis levan made in LDM2 minimal media, using TLR4 reporter cells.

Ligand binding to TLR4 reporter cells results in the production of secreted embryonic alkaline phosphatase (SEAP) which can be measured in a colorimetric assay: TLR4 reporter cells were incubated with carbohydrate ligands or control (LPS) in HEK blue medium[394] using a 96 well plate; and absorbance values were read at 655 nm. (a) Repeated independent experiment of Figure 57a showing TLR4 binding to ES levan compared to cells alone. ES levan concentrations are 100 μg/ml, 50 μg/ml and 25 μg/ml and positive control LPS at 1 μg/ml. Two repeated independent experiments of Figure 57b are presented in (b) and (c) showing TLR4 binding to ES levan compared to Purified ES levan (ES levan treated with alkali). (d) Repeated independent experiment of Figure 57c showing TLR4 reporter assay and B. subtilis levan (made using minimal media LDM2) compared to controls. All experiments were performed in triplicate. Error bars, ± SD. Statistical analysis was performed using one-way ANOVA followed by tukey's test. ***, p < 0.001 compared to cells alone. N.s with straight line, not statistically significant compared to cells alone.

Appendix 35

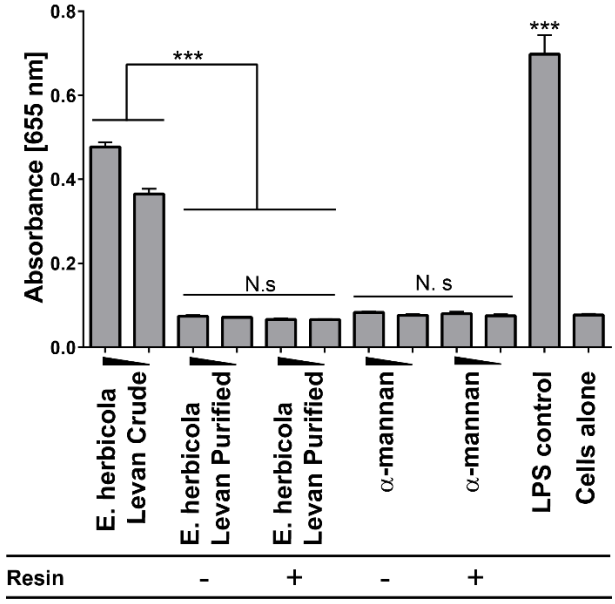

Appendix 35. Interaction of TLR4 with E. herbicola levan and α-mannan treated with or without anion exchange resin using HEK293 TLR4 reporter cells.

Ligand binding to TLR4 reporter cells results in the production of secreted embryonic alkaline phosphatase (SEAP) which can be measured in a colorimetric assay: TLR4 reporter cells were incubated with carbohydrate ligands or control (LPS) in HEK blue medium[394] using a 96 well plate; and absorbance values were read at 655 nm. Experiment is an independent repeat of Figure 58. All levans and α-mannan were used at 100 μg/ml and 50 μg/ml, and LPS control at 0.1 μg/ml. The experiment was performed in triplicate. E. herbicola levan purified, E. herbicola levan directly treated with alkali. Error bars, ± SD. Statistical analysis was performed using one-way ANOVA followed by tukey's test. ***, p < 0.001 as indicated or compared to cells alone. N.s with straight line, not statistically significant across treatments or all compared to cells alone.

Appendix 36

a)

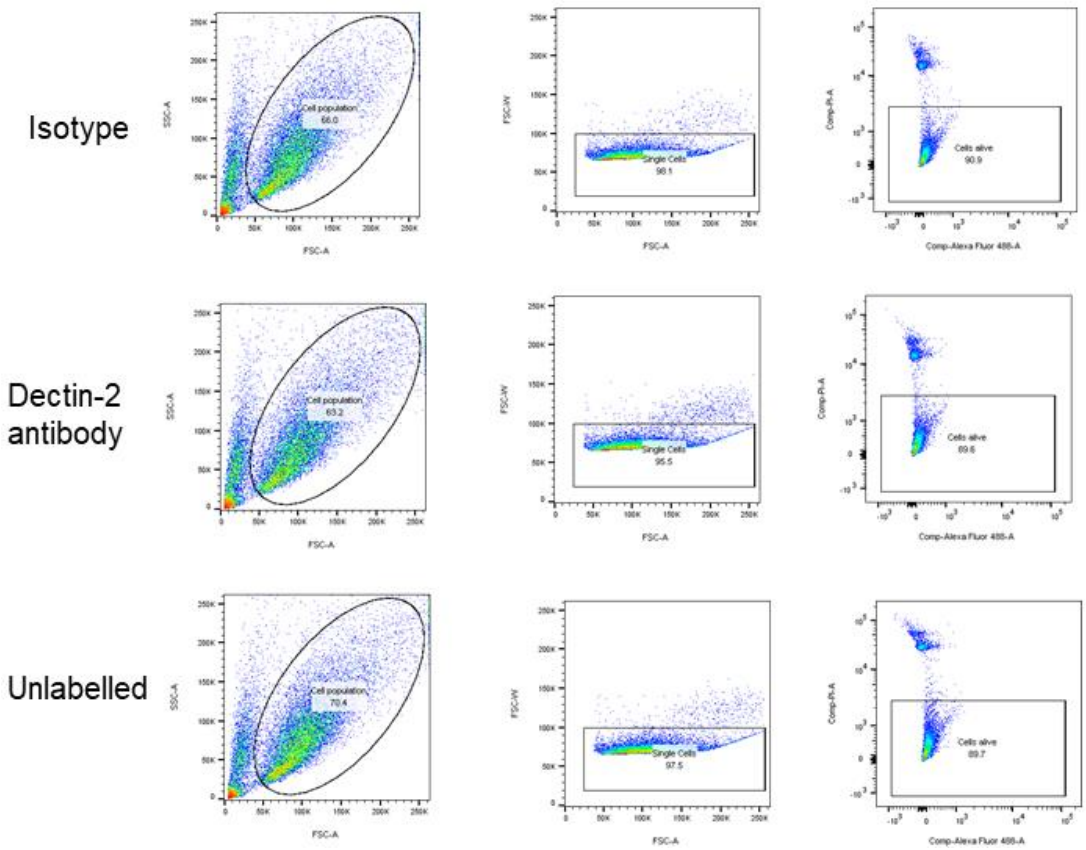

b)

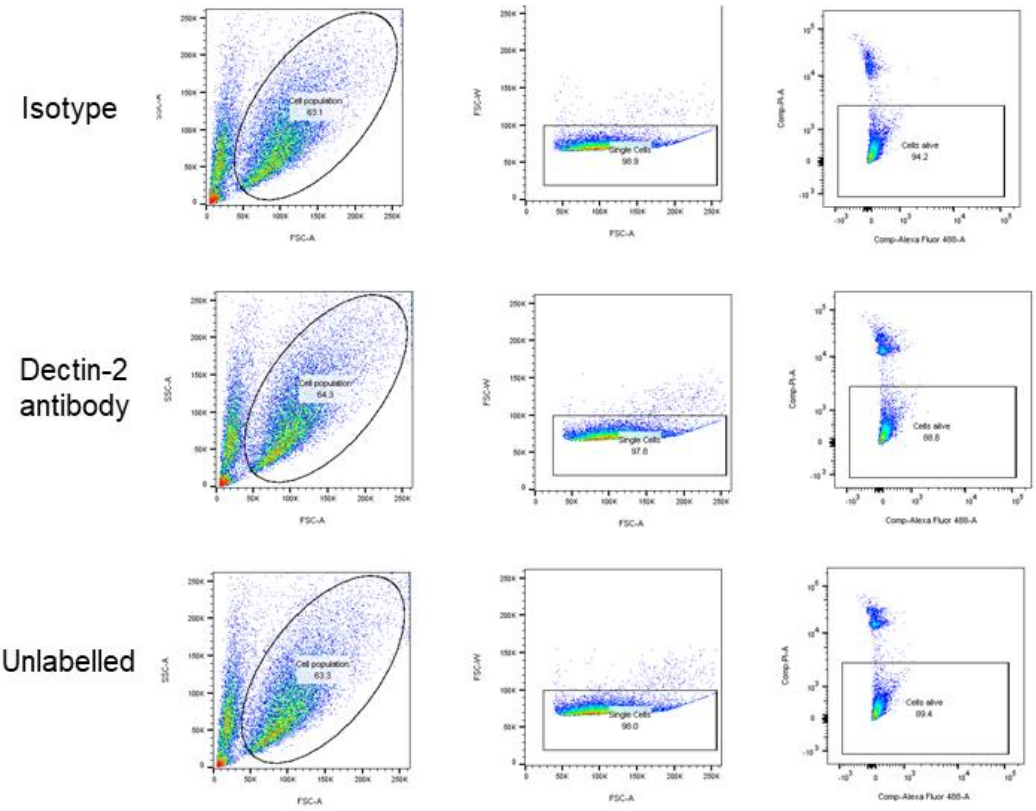
Isotype
Cell population
63.1
Single Cells
98.9
Cells alive
94.2
Dectin-2 antibody
Cell population
64.3
Single Cells
97.8
Cells alive
88.8
Unlabelled
Cell population
63.3
Single Cells
98.0
Cells alive
89.4
FSC-A
SSC-A
FSC-W
Comp-PI-A
Comp-Alexa Fluor 488-A

c)

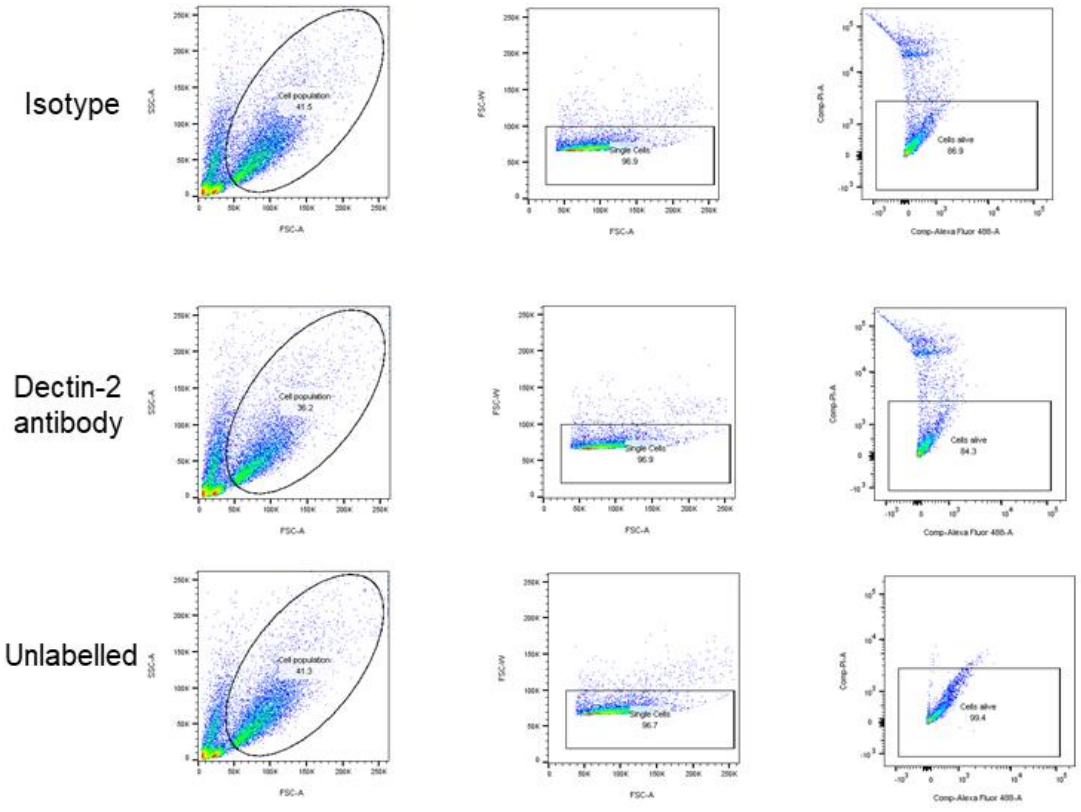
Isotype
Cell population
41.5
Single Cells
96.9
Cells alive
86.9
Dectin-2 antibody
Cell population
36.2
Single Cells
96.9
Cells alive
84.3
Unlabelled
Cell population
41.3
Single Cells
96.7
Cells alive
99.4
FSC-A
SSC-A
FSC-W
Comp-PI-A
Comp-Alexa Fluor 488-A

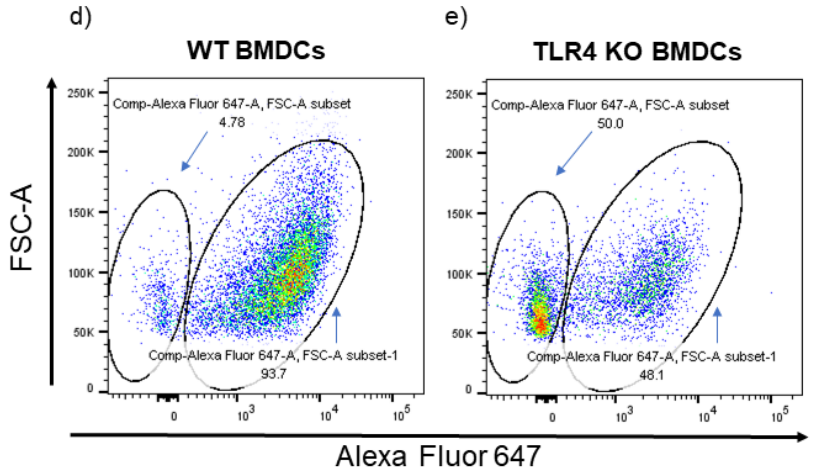

Appendix 36. Additional flow cytometry data assessing Dectin-2 expression by WT, Dectin-2 KO and TLR4 KO BMDCs corresponding to Figure 59.

Bone marrow cells isolated from wild type, Dectin-2 KO or TLR4 KO mice were differentiated into BMDCs and analysed for Dectin-2 expression by flow cytometry using fluorescently-labelled (Alexa Fluor 647) anti-mouse Dectin-2 antibodies. (a) WT BMDCs, (b) D2 KO BMDCs and (c) TLR4 KO BMDCs: data shows dot plots from left to right: initial cell population, exclusion of doublet cells and dead cells using PI staining. From top to bottom: IgG isotype-Alexa 647- and anti-mouse Dectin-2-Alexa 647-labelled cells, or unlabelled cells (cells with PI). (d) and (e), dot plots of anti-mouse Dectin-2-Alexa-labelled WT and TLR4 KO cells corresponding to Figure 59a and 59c, respectively, highlighting the percentage of cell populations positive for Alexa 647 fluorescence. FSC-A, forward scatter area. FSC-W, forward scatter width. SSC-A, side scatter area. Comp-PI-A, compensated propidium iodide area. Data was generated using FlowJo® v10.0.8

Appendix 37

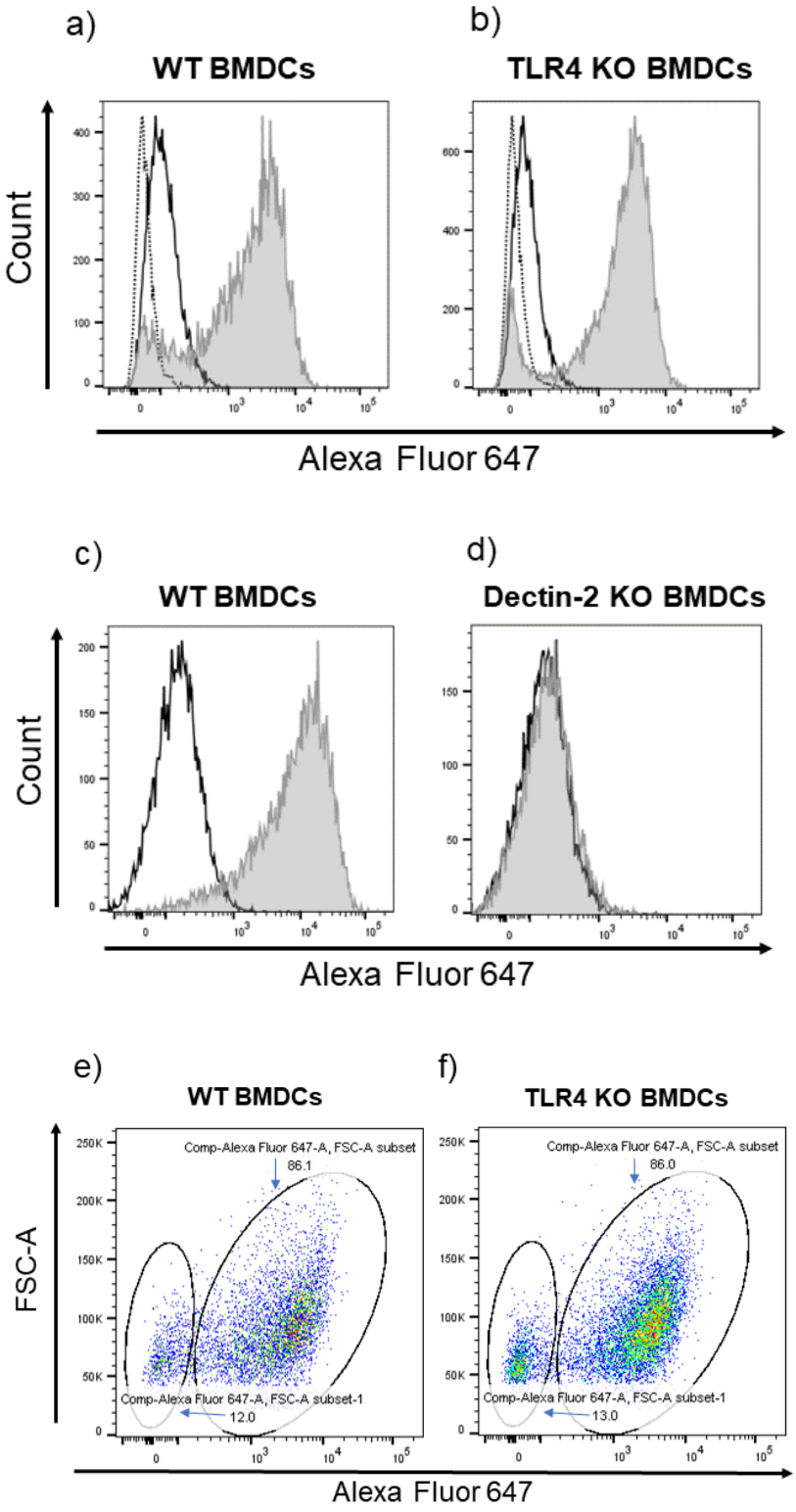
a)
WT BMDCs
b)
TLR4 KO BMDCs
Count
Alexa Fluor 647
c)
WT BMDCs
d)
Dectin-2 KO BMDCs
Count
Alexa Fluor 647
e)
WT BMDCs
Comp-Alexa Fluor 647-A, FSC-A subset
86.1
Comp-Alexa Fluor 647-A, FSC-A subset-1
12.0
f)
TLR4 KO BMDCs
Comp-Alexa Fluor 647-A, FSC-A subset
86.0
Comp-Alexa Fluor 647-A, FSC-A subset-1
13.0
FSC-A
Alexa Fluor 647

Appendix 37. Further experiments in addition to Figure 59 showing the expression of Dectin-2 on WT, Dectin-2 KO and TLR4 KO BMDCs using flow cytometry.

Bone marrow cells isolated from wild type, Dectin-2 KO or TLR4 KO mice were differentiated into BMDCs and analysed for Dectin-2 expression by flow cytometry using fluorescently-labelled (Alexa Fluor 647) anti-mouse Dectin-2 antibodies. (a) and (b); and (c) and (d) were separate experiments. (a) to (d), histograms show fluorescence of cell populations after cell labelling and initial pre-gating of cells which exclude doublet cells and dead cells (see Appendix 37 for gating strategy). Histograms are (a) WT BMDCs (b) TLR4 KO BMDCs, and (c) WT and (d) Dectin-2 KO BMDCs labelled with anti-mouse Dectin-2-Alexa 647 (grey shading with dark grey outline), IgG isotype-Alexa 647 (black outline) or unlabelled (cells with PI) (dotted black outline). Corresponding to the histograms shown in (a) and (b), (d) and (e) show dot plots of anti-mouse Dectin-2-Alexa 647-labelled WT and TLR4 KO cells, respectively, highlighting the percentage of cell populations positive for Alexa 647 fluorescence. Axis labels: Alexa 647 represents detection of Alexa 647 fluorescence. FSC-A, forward scatter area. FSC-W, forward scatter width. SSC-A, side scatter area. Comp-PI-A, compensated propidium iodide area. BMDCs, bone-marrow derived dendritic cells. TLR4, Toll-like receptor 4. KO, knockout. WT, wildtype. Data was generated using FlowJo® v10.0.8

Appendix 38

a)

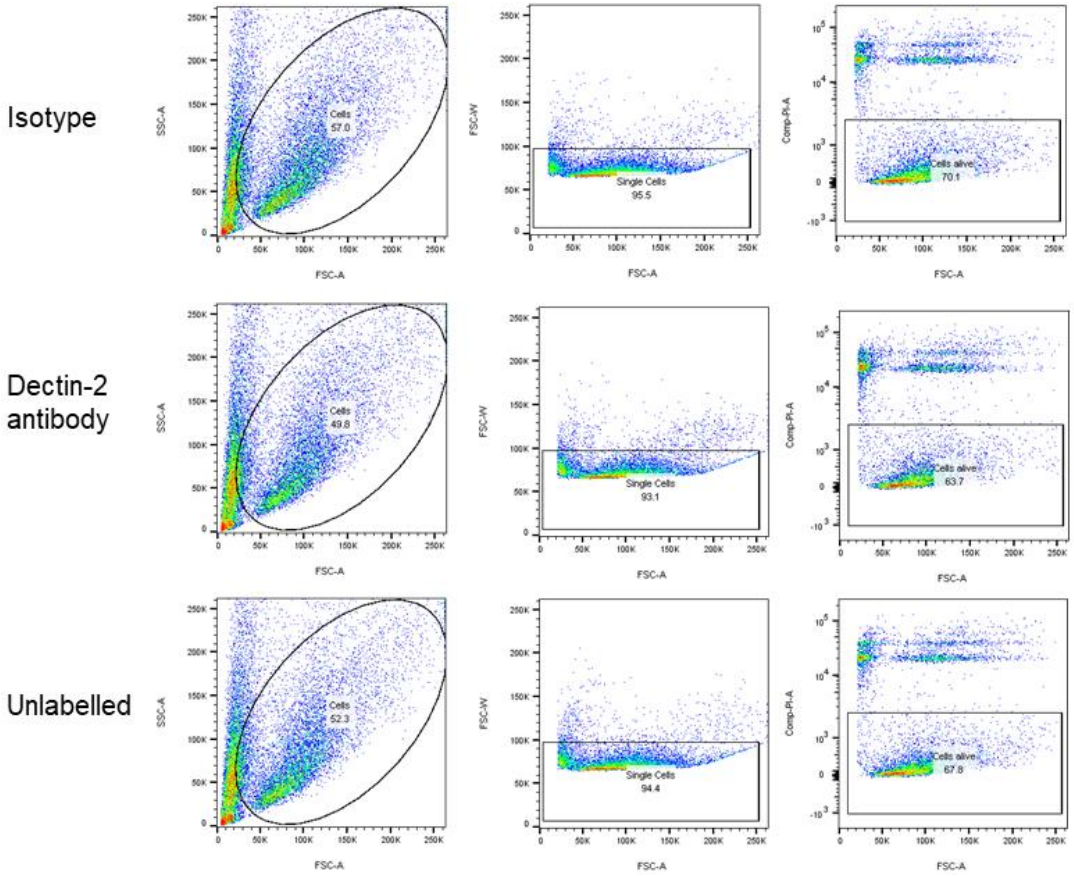

b)

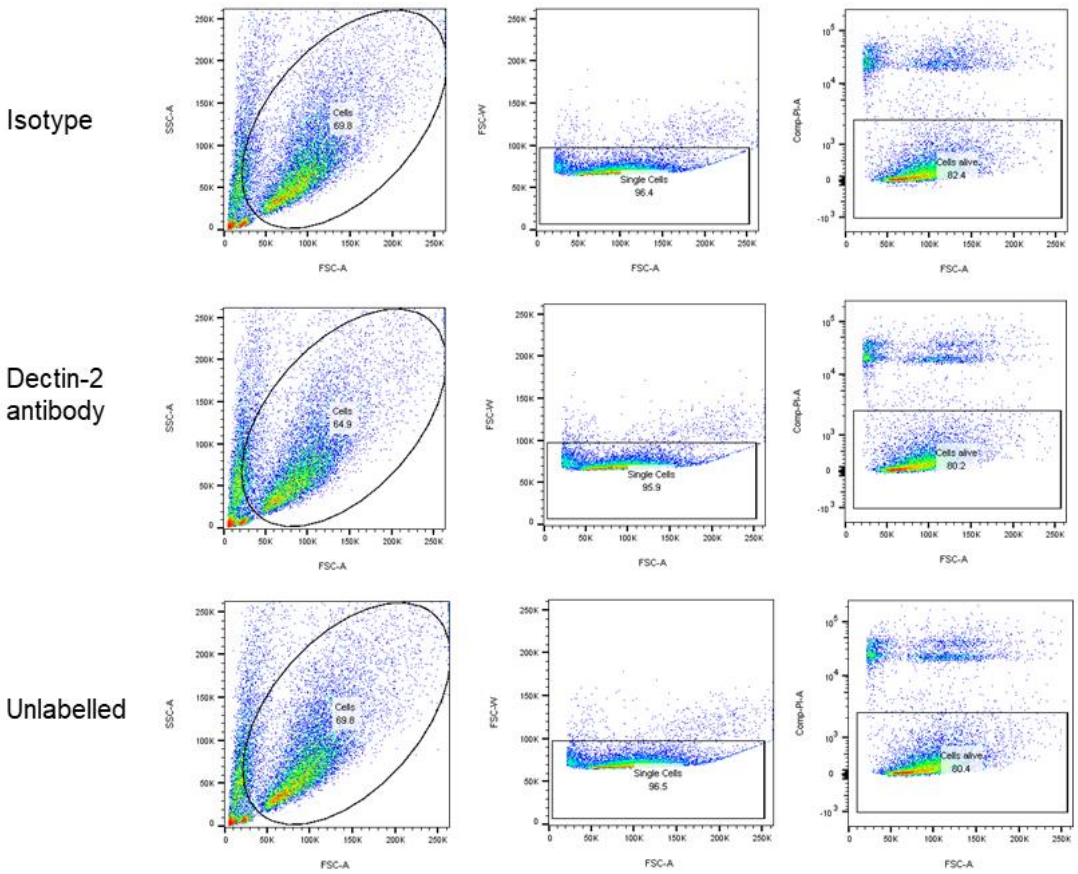
Isotype
Cells
69.8
Single Cells
96.4
Cells alive
82.4
Dectin-2 antibody
Cells
64.9
Single Cells
95.9
Cells alive
80.2
Unlabelled
Cells
69.8
Single Cells
96.5
Cells alive
80.4
SSC-A
FSC-A
FSC-W
Comp-PI-A

c)

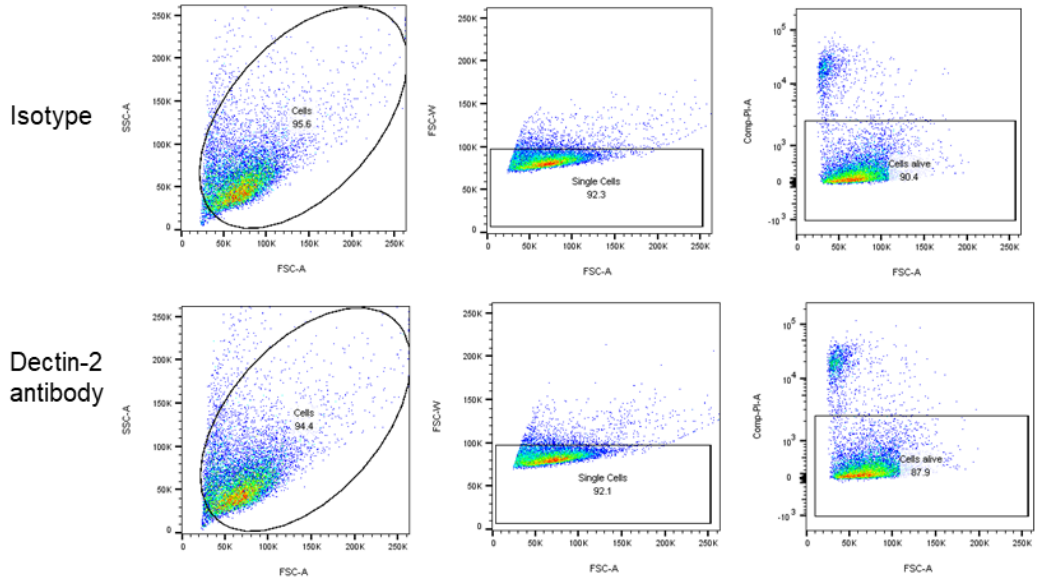
Isotype
Cells
95.6
Single Cells
92.3
Cells alive
90.4
Dectin-2 antibody
Cells
94.4
Single Cells
92.1
Cells alive
87.9
SSC-A
FSC-A
FSC-W
Comp-PI-A

d)

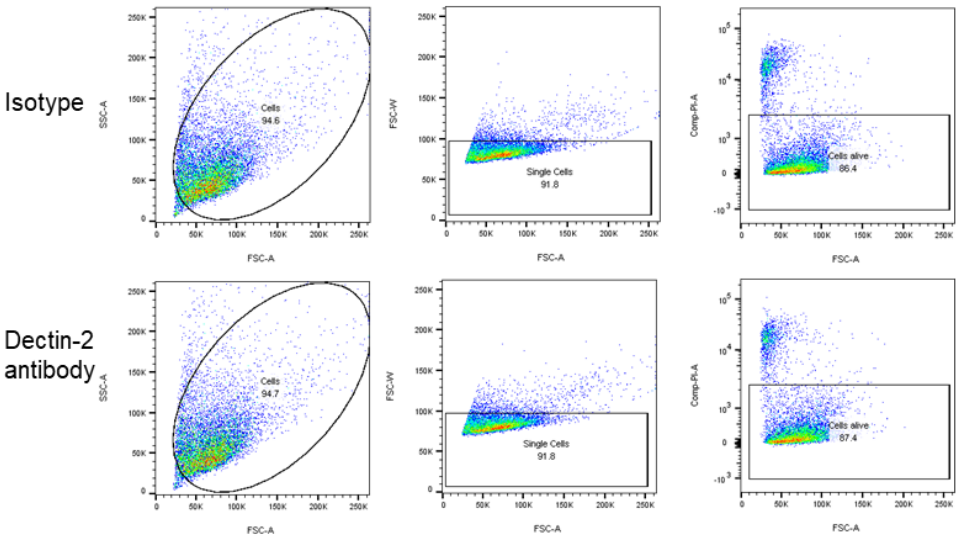

Appendix 38. Pre-gating of anti-mouse Dectin-2-Alexa 674, isotype control and unlabelled BMDCs from Appendix 37.

Bone marrow cells isolated from wild type, Dectin-2 KO or TLR4 KO mice were differentiated into BMDCs and analysed for Dectin-2 expression by flow cytometry using fluorescently-labelled (Alexa Fluor 647) anti-mouse Dectin-2 antibodies. Dot plots from left to right show initial cell population, exclusion of doublet cells and dead cells (using PI staining). Gating for experiment (a) WT and (b) TLR4 KO BMDCs are shown corresponding to S 37a and S 37b (and S 37e and S 37f), respectively. Gating for experiment of (c) WT BMDCs and (d) D2 KO BMDCs are shown corresponding to S 37c and S 37d. respectively. From top to bottom: Alexa 647 IgM isotype or Alexa 647-Dectin-2-labelled cells, and unlabelled cells (cells with PI). Axis labels: Alexa 647 represents detection of Alexa 647 fluorescence. FSC-A, forward scatter area. FSC-W, forward scatter width. SSC-A, side scatter area. Comp-PI-A, compensated propidium iodide area. Data was generated using FlowJo® v10.0.8

Appendix 39

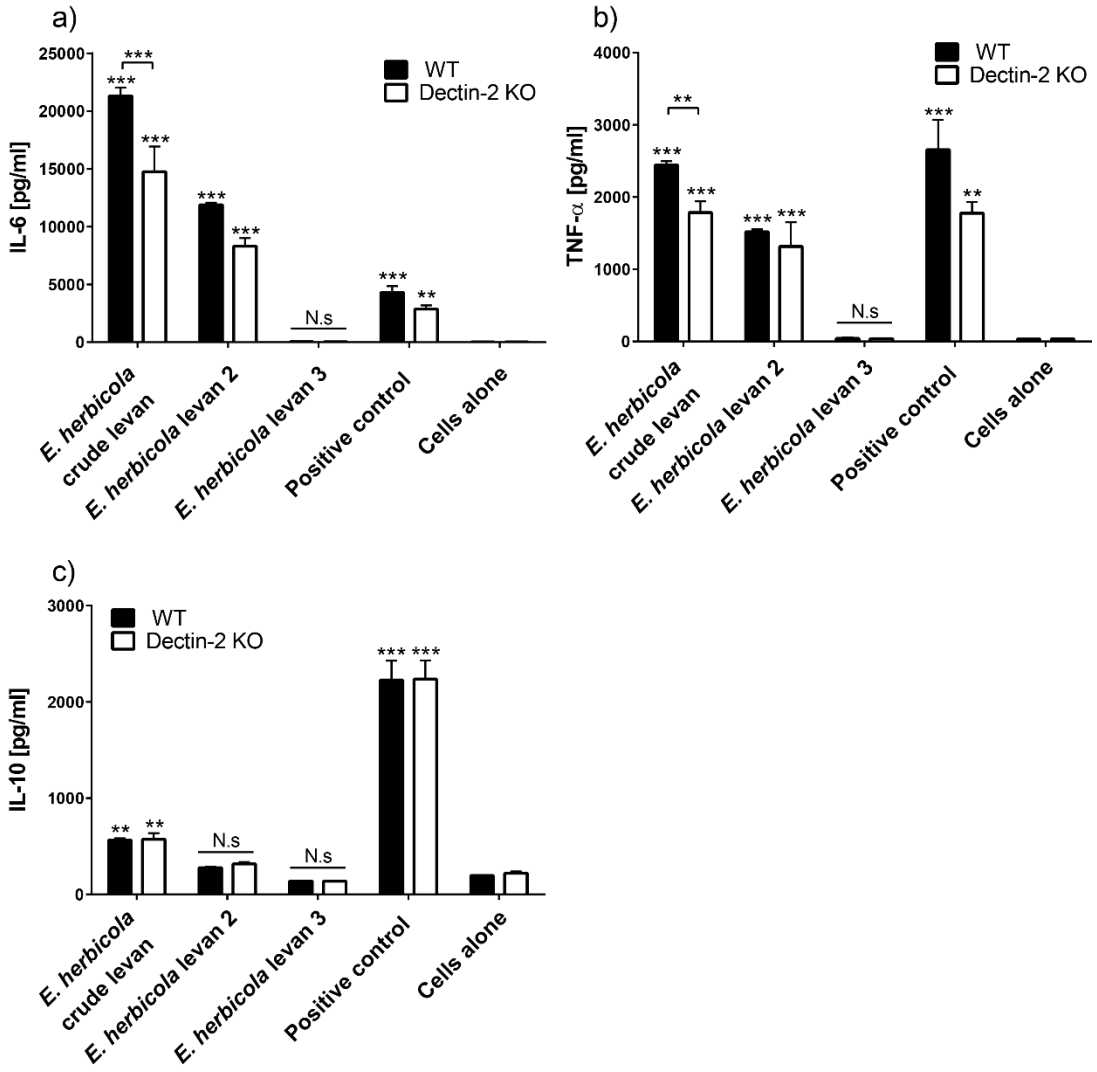

Appendix 39. Induction of cytokine production in WT and Dectin-2 KO BMDCs by crude and purified E. herbicola levan.

BMDCs were incubated with E. herbicola levans or a positive control using a 96 well plate; and cytokine production in the supernatant was measured by ELISA. Repeated independent experiment from Figure 60. Data show (a) IL-6, (b) TNF-α, and (c) IL-10 production in BMDCs by crude and purified E. herbicola levan. E. herbicola levan was used at 250 μg/ml, peptidoglycan [non-Dectin-2 ligand) was used at 100 μg/ml as a positive control. All experiments were performed in triplicate. Error bars, ± SD. Statistical analysis was performed using one-way ANOVA followed by tukey's test (b). ***, p < 0.001. **, p < 0.01. *, p < 0.05 compared to cells alone N.s., with straight line, all not statistically significant compared to cells alone. Differences between treatments are marked as indicated (comparative line).

Appendix 40

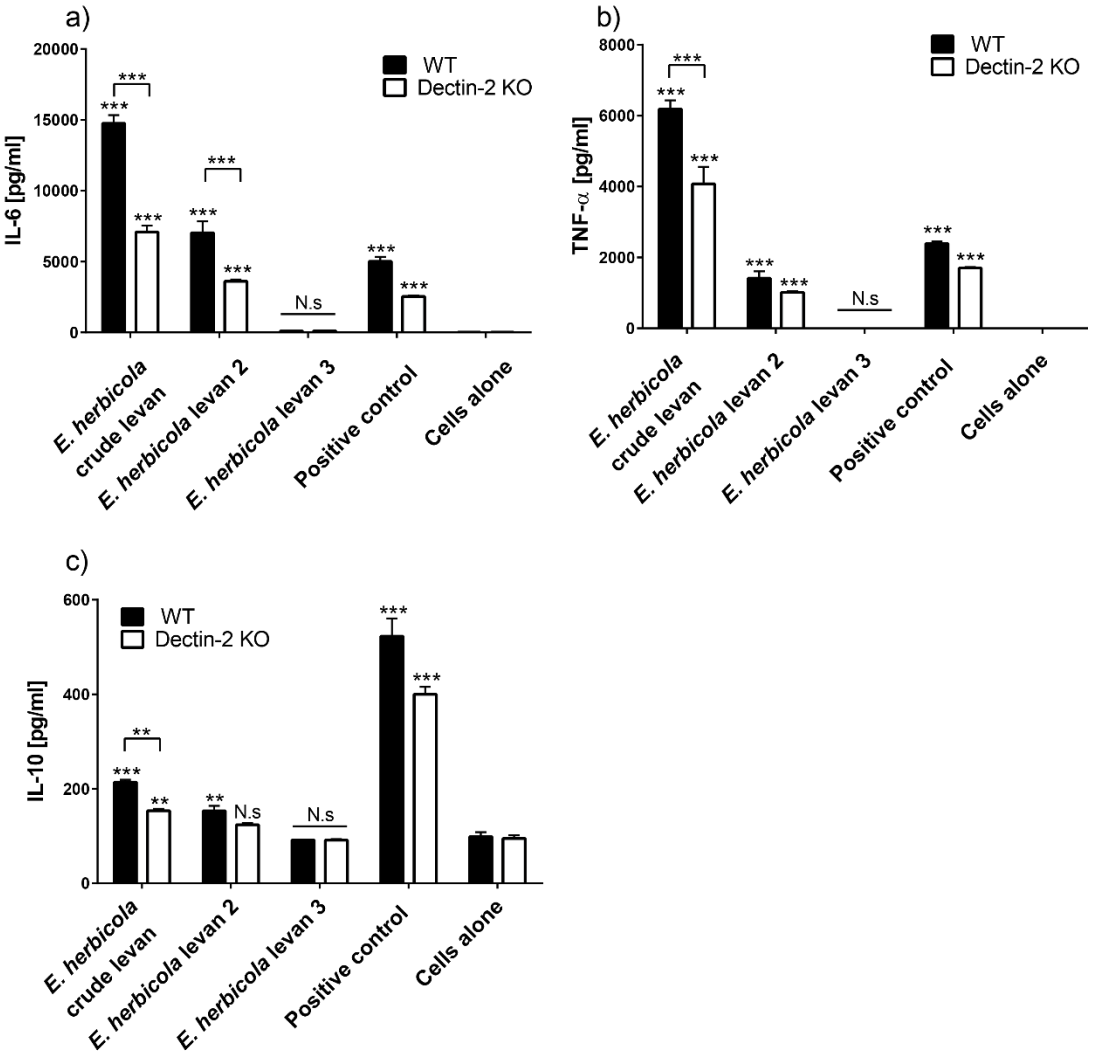

Appendix 40. Induction of cytokine production in WT and Dectin-2 KO BMDCs by crude and purified E. herbicola levan

BMDCs were incubated with E. herbicola levans or a positive control using a 96 well plate; and cytokine production in the supernatant was measured by ELISA. Repeated independent experiment from Figure 60. Data show (a) IL-6, (b) TNF-α, and (c) IL-10 production in BMDCs by crude and purified E. herbicola levan. E. herbicola levan was used at 250 μg/ml, peptidoglycan [non-Dectin-2 ligand) was used at 100 μg/ml as a positive control. All experiments were performed in triplicate. Error bars, ± SD. Statistical analysis was performed using one-way ANOVA followed by tukey's test (b). ***, p < 0.001. **, p < 0.01. *, p < 0.05 compared to cells alone. N.s., not statistically significant compared to cells alone. N.s., with straight line, all not statistically significant compared to cells alone. Differences between treatments are marked as indicated.

Appendix 41

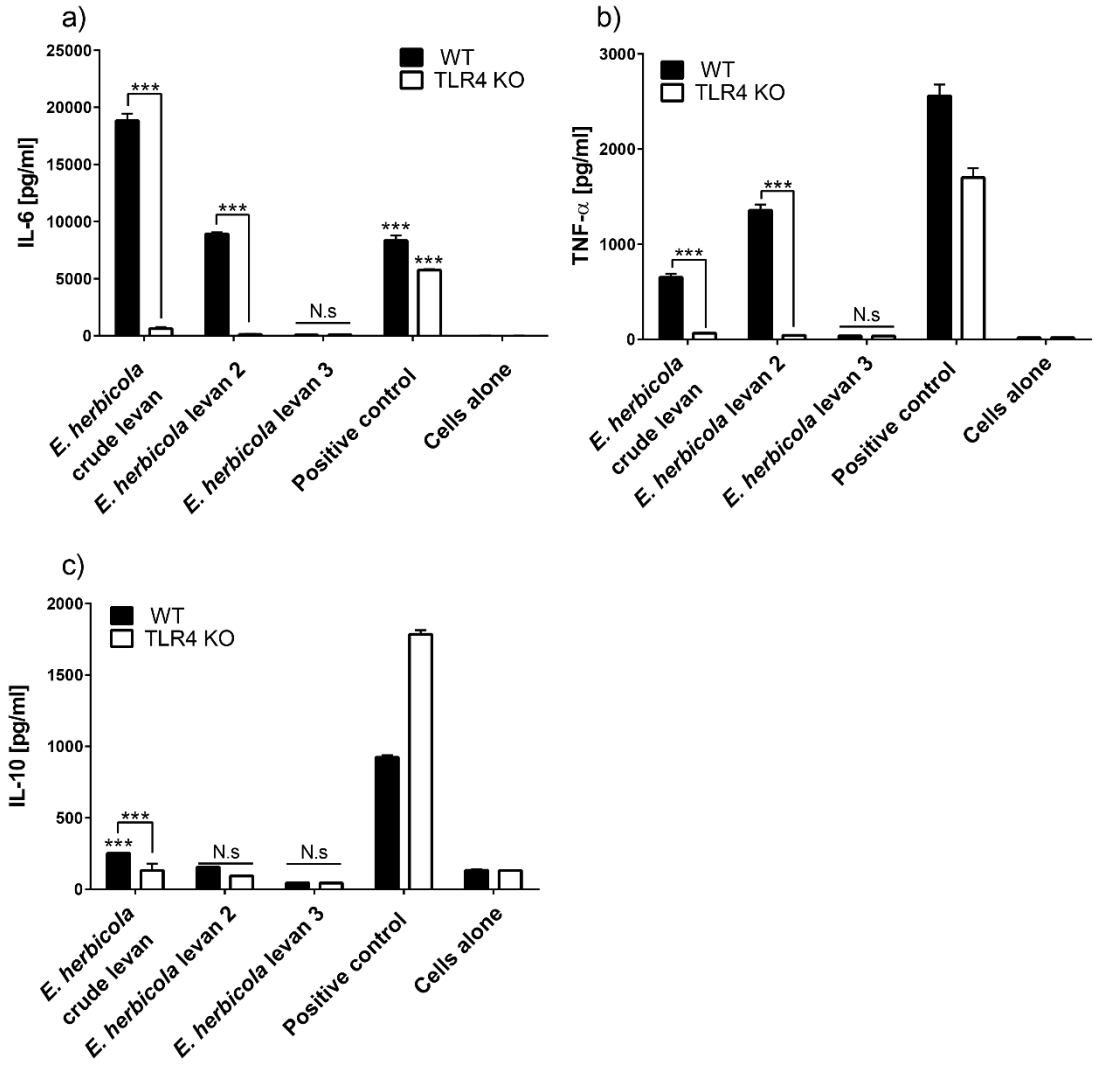

Appendix 41. Induction of cytokine production in WT and TLR4 KO BMDCs by crude and purified E. herbicola levan

BMDCs were incubated with E. herbicola levans or a positive control using a 96 well plate; and cytokine production in the supernatant was measured by ELISA. Repeated independent experiment from Figure 61. Data show (a) IL-6, (b) TNF-α, and (c) IL-10 production in BMDCs by crude and purified E. herbicola levan. E. herbicola levan was used at 250 μg/ml, peptidoglycan [non-Dectin-2 ligand) was used at 100 μg/ml as a positive control. All experiments were performed in triplicate. Error bars, ± SD. Statistical analysis was performed using one-way ANOVA followed by tukey's test (b). ***, p < 0.001. **, p < 0.01. *, p < 0.05 compared to cells alone. N.s., not statistically significant compared to cells alone. N.s., with straight line, all not statistically significant compared to cells alone. Differences between treatments are marked as indicated (comparative line).

Appendix 42

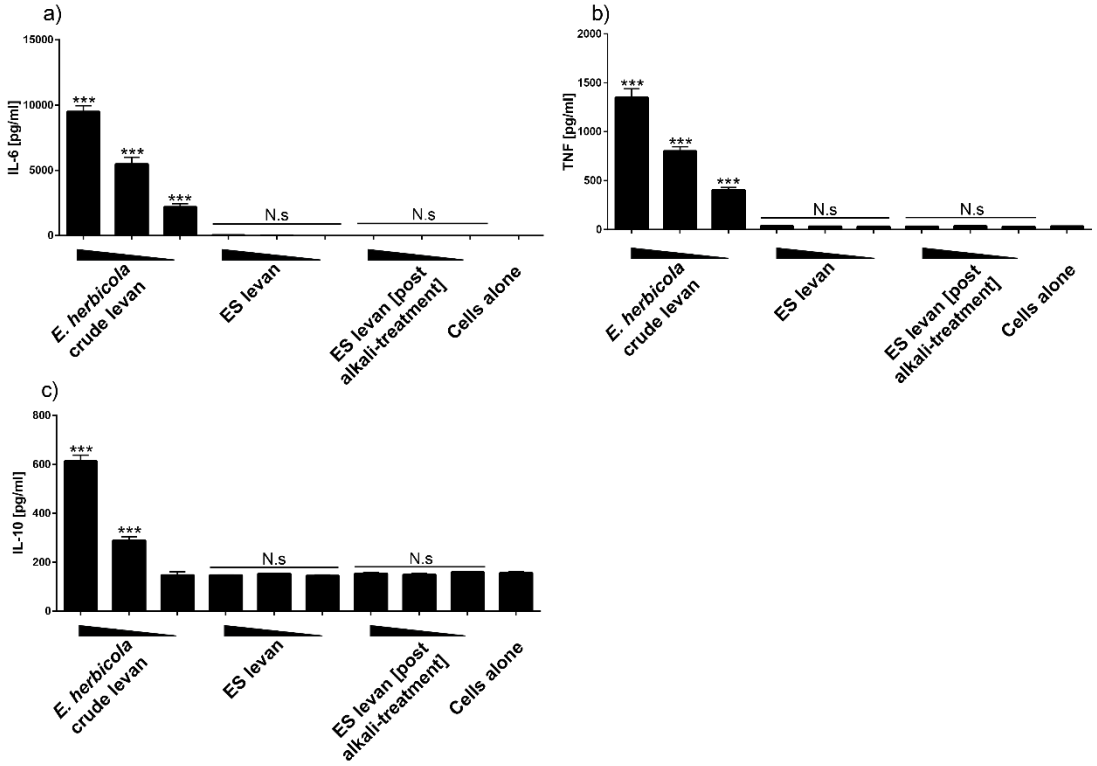

Appendix 42. Induction of cytokine production in WT BMDCs by non-immobilised crude and purified ES levan, and E. herbicola crude levan.

BMDCs were incubated with ES levan, purified ES levan or E. herbicola crude levan (positive control) using a 96 well plate; and cytokine production in the supernatant was measured by ELISA. Repeated experiment from Figure 62. Data show (a) IL-6, (b) TNF-α, and (c) IL-10 production in bone marrow-derived dendritic cells (BMDCs) by non-plate-immobilised E. herbicola crude, ES levan (crude) and purified ES levan (post alkali-treatment). In (a), all ES levan concentrations were 250 μg/ml, 125 μg/ml and 62.5 μg/ml and E. herbicola levan 125 μg/ml and 62.5 μg/ml. For (b) and (c), all levan concentrations were 250 μg/ml, 125 μg/ml and 62.5 μg/ml. All experiments were performed in triplicate. Error bars, $\pm$ SD. Statistical analysis was performed using one-way ANOVA followed by tukey's test (b). ***, p < 0.001 compared to cells alone. N.s. with straight line, all not statistically significant compared to cells alone.

Appendix 43

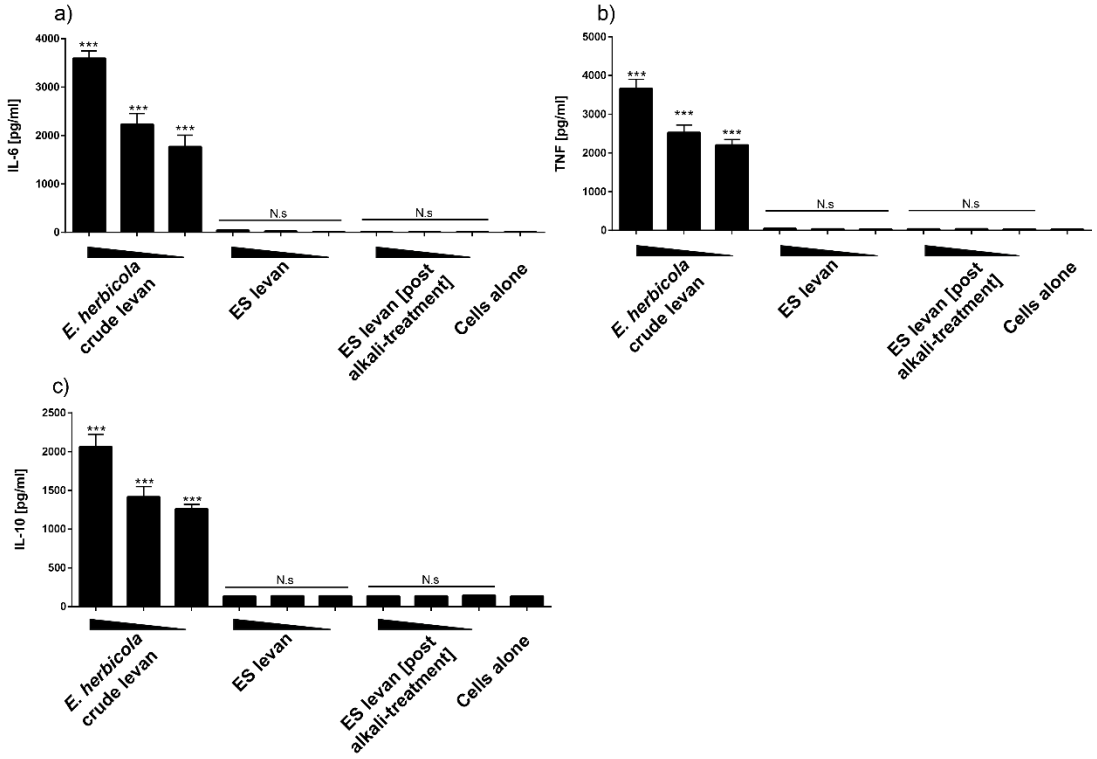

Appendix 43. Induction of cytokine production in WT BMDCs by plate-immobilised ES levan and E. herbicola crude levan.

BMDCs were incubated with ES levan, purified ES levan or E. herbicola crude levan (positive control) using a 96 well plate; and cytokine production in the supernatant was measured by ELISA. Repeated experiment from Figure 63. Data show (a) IL-6, (b) TNF-α, and (c) IL-10 production in BMDCs by non-plate-immobilised E. herbicola crude, ES levan (crude) and Purified ES levan (post alkali-treatment). All levan concentrations were 250 μg/ml, 125 μg/ml and 62.5 μg/ml. All experiments were performed in triplicate. Error bars, $\pm$ SD. Statistical analysis was performed using one-way ANOVA followed by tukey's test (b). ***, p < 0.001 compared to cells alone. N.s. with straight line, not statistically significant compared to cells alone.

Appendix 44

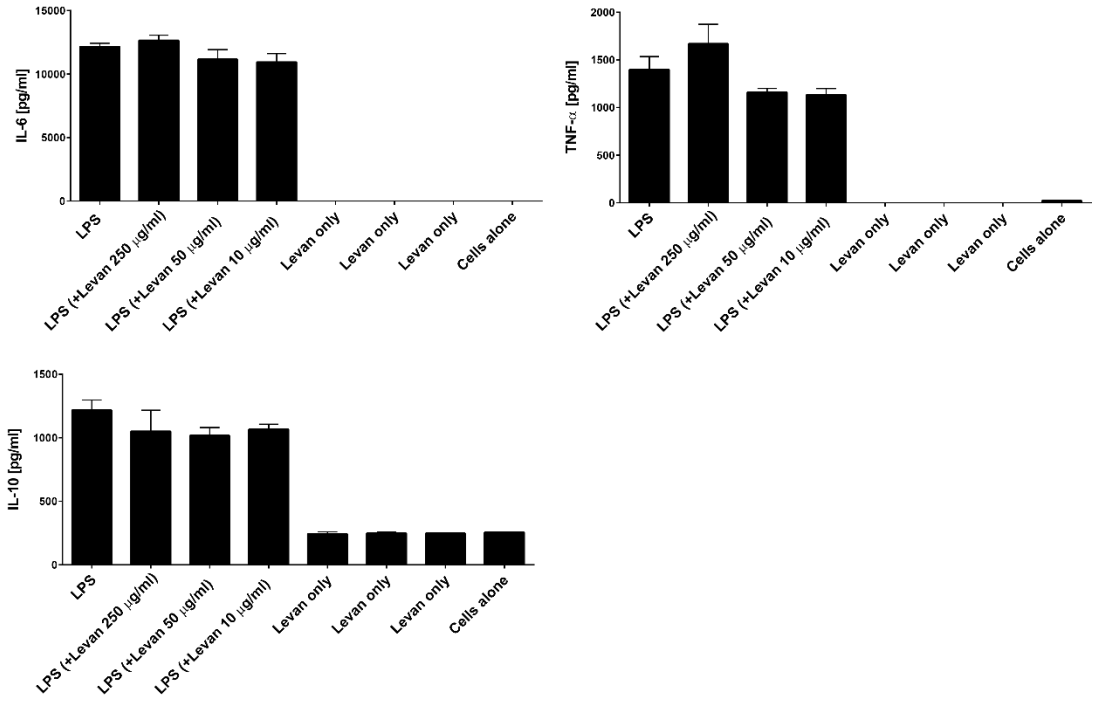

Appendix 44. Impact of purified ES levan on cytokine production by LPS-challenged BMDCs

BMDCs were incubated with ES levan alone, ES Levan + LPS, LPS alone or negative control (cells alone) using a 96 well plate; and cytokine production in the supernatant was measured by ELISA. Data show a) IL-6, b) TNF-α, and c) IL-10 production in BMDCs treated with LPS alone, Purified ES levan and LPS (E. coli K12), Purified ES levan alone or media alone. All levan concentrations were 125 μg/ml, 25 μg/ml and 5 μg/ml. LPS concentrations were 0.5 μg/ml. The experiment was performed in duplicate. Error bars, ± SD.

Appendix 45

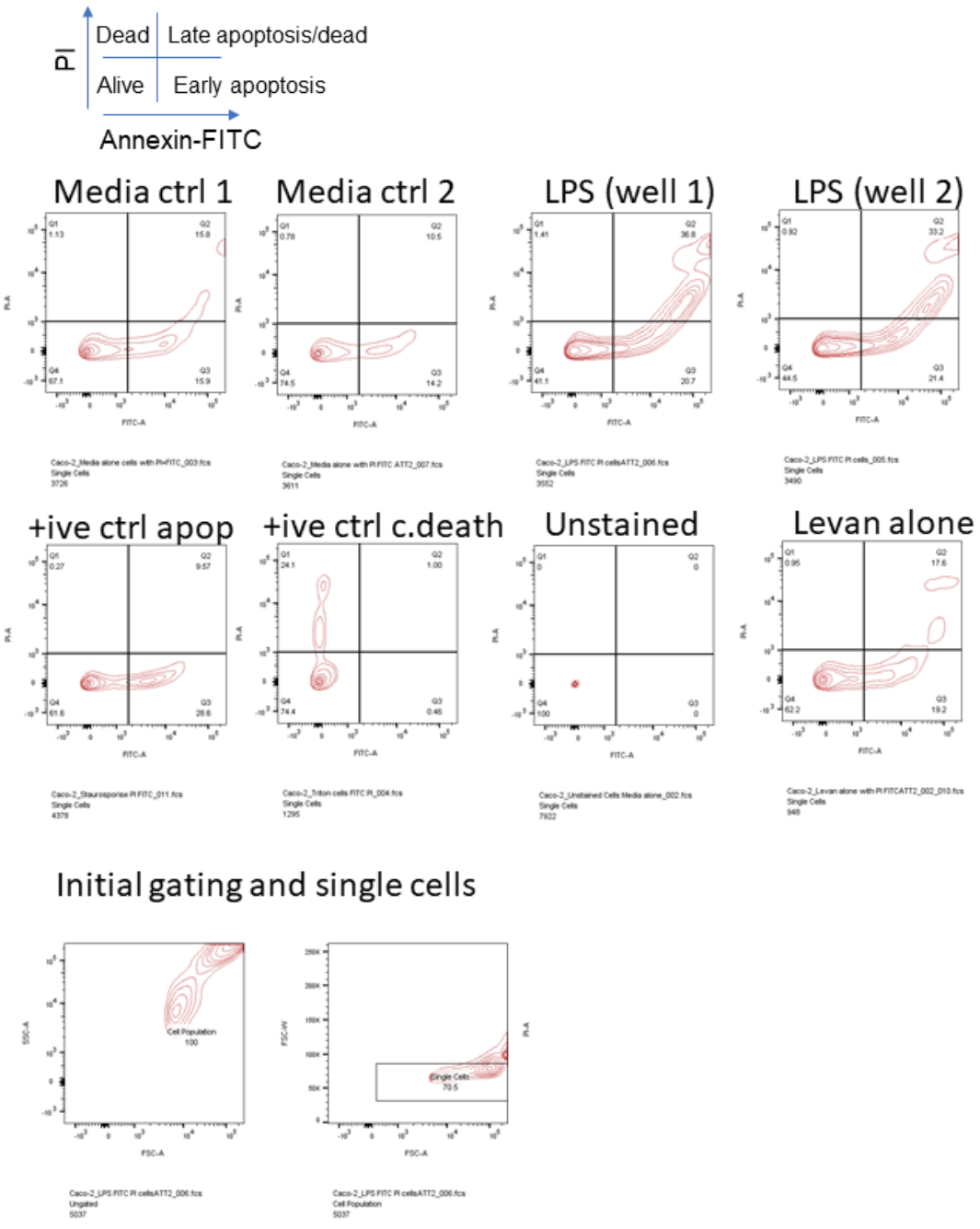

Appendix 45. Impact of LPS and purified ES levan on cell death and apoptosis of undifferentiated Caco-2 cells.

Contour plots show PI [X-axis] and annexin-FITC [Y-axis] - also indicated by the cartoon at the top. Percentages of total single cells (after gating) are indicated in the 4 quadrants. Initial gating including gating for single cells using LPS-treated cells is shown at the bottom of the figure. Treatments are as indicated. Dead cell control, 1% Triton X. Apoptosis control, 1μM staurosporine. Purified ES levan was used at 200 μg/ml and LPS at 1 mg/ml. Ctrl (control cells only [media only]). All levan; purified ES levan. Media control and LPS were performed independently in duplicate; others in singlicate.

Appendix 46

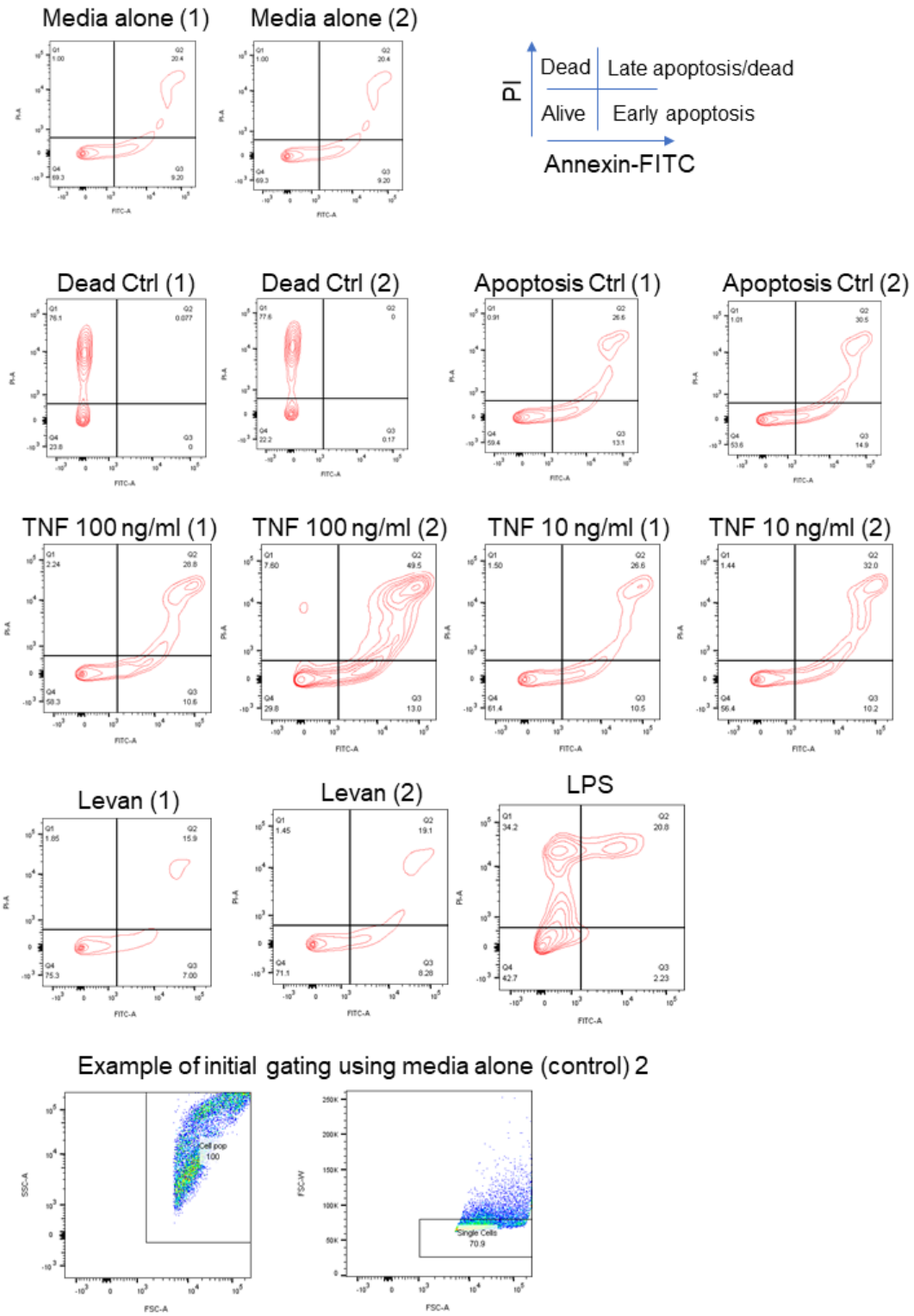
Media alone (1)
Media alone (2)
PI
Dead
Late apoptosis/dead
Alive
Early apoptosis
Annexin-FITC
Dead Ctrl (1)
Dead Ctrl (2)
Apoptosis Ctrl (1)
Apoptosis Ctrl (2)
TNF 100 ng/ml (1)
TNF 100 ng/ml (2)
TNF 10 ng/ml (1)
TNF 10 ng/ml (2)
Levan (1)
Levan (2)
LPS
Example of initial gating using media alone (control) 2
Cell pop
100
Single Cells
70.9
SSC-A
FSC-A
FSC-W

Appendix 46. Impact of TNF-α, LPS and purified ES levan on cell death and apoptosis of undifferentiated Caco-2 cells.

Contour show PI [X-axis] and annexin-FITC [Y-axis], also indicated by the cartoon at the top. Percentages of total single cells (after gating) are indicated in the 4 quadrants. An example of initial gating including gating for single cells using media-treated only cells is shown at the bottom of the figure. Treatments are as indicated. Dead cell control; 1% Triton X (apically-treated). Apoptosis control; 1μM staurosporine (apically-treated). Purified ES levan at 200 μg/ml. LPS at 1 mg/ml. TNF-α concentrations are as indicated in the figure. Ctrl (control). All levan; purified ES levan. Media control, dead cell control, apoptosis control, levan and all TNF-α treatments were performed independently in duplicate; others in singlicate. FSC-A, forward scatter area. FSC-W, forward scatter width.SSC-A, side scatter area. PI, propidium iodide.

Appendix 47

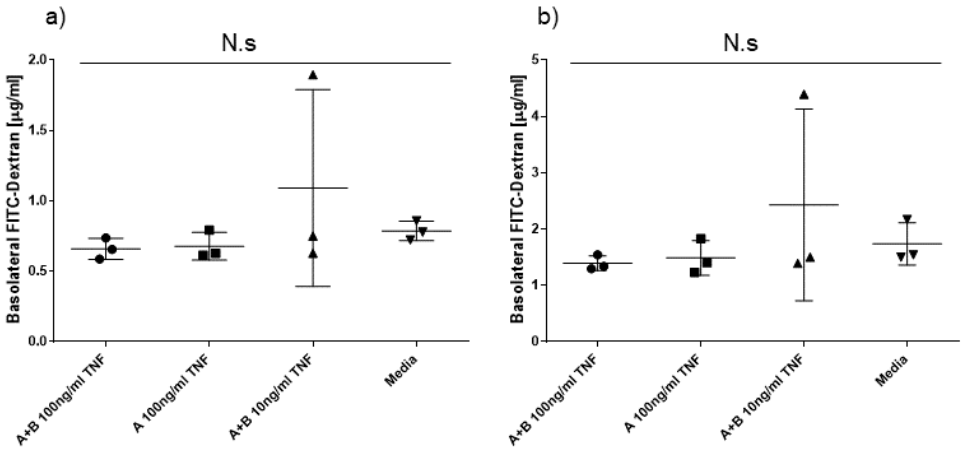

Appendix 47. Impact of TNF-α on Caco-2 monolayer permeability from experiment described in Figure 66.

Data show FITC dextran concentrations in the basolateral compartment after application of 1mg/ml FITC-dextran on the apical side. Concentrations of TNF-α are as indicated. 'A' represents treatment of the apical compartment only. 'A+B' represents simultaneous treatment on both apical and basolateral sides. (a) and (b) are 4 and 24 hr measurements of FITC-dextran, respectively. Horizontal bars indicate mean values. Error bars, $\pm$ SD. N.s. with straight line, not statistically significant across treatments. A p value of 0.05 was considered statistically significant. Experiments were performed in triplicate. TNF, tumour necrosis factor-α.

Appendix 48

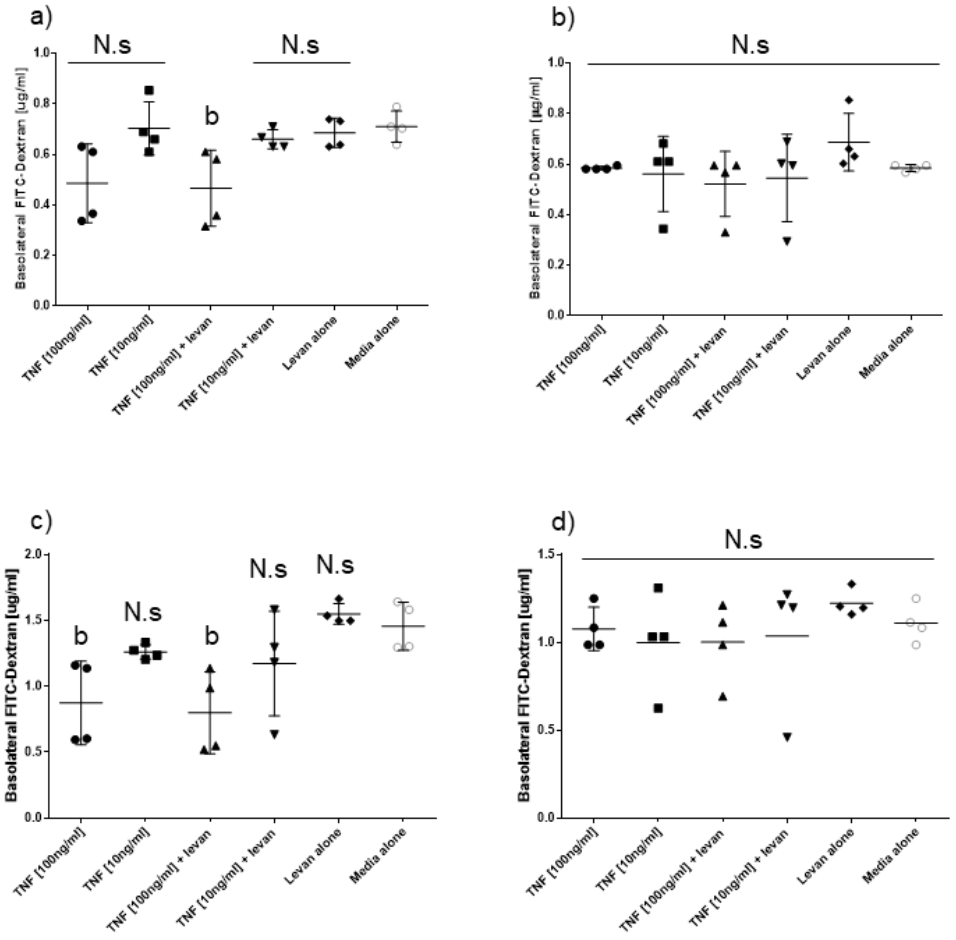

Appendix 48. Impact of purified ES levan on Caco-2 monolayer permeability following TNF-α-challenge from experiment described in Figure 67 and Figure 68.

Data show FITC dextran concentrations in the basolateral compartment after application of 1 mg/ml FITC-dextran on the apical side. (a) and (c) are simultaneous treatments; (b) and (d) are pre-treated with levan or media for 24 hr prior to stimulation with TNF-α or media control. Concentrations of purified enzymatically synthesised (ES) levan were 200 μg/ml for simultaneous treatment, 190μg/ml of 24 hr pre-treatment with levan. TNF-α are concentrations are as indicated. All treatments were applied both on apical and basolateral compartments. (a) and (b) are 4 hr; and (c) and (d) are 24 basolateral collection. N = 4 for experiment. Horizontal bars indicate mean values. Error bars, $\pm$ SD. b, p value < 0.05 statistical significant was evident but values were lower that cells alone. N.s. with straight line, not statistically significant across treatments. A p value of 0.05 was considered statistically significant.